INTERNATIONAL SYMPOSIUM

ON

APPLICATIONS OF MARINE GEODESY

JUNE 3,4,5, 1974

BATTELLE AUDITORIUM
COLUMBUS, OHIO

Co-Sponsors

- Battelle-Columbus
- Defense Mapping Agency (DMA/PR)
- National Aeronautics and Space Administration (NASA/OAI)
- National Ocean Survey of NOAA (NOAA/NOS)
- National Science Foundation (NSF)
- Office of Naval Research (ONR)

Associate Sponsors

- The American Geophysical Union (AGU)
- Institute of Navigation (ION)
- International Association of Geodesy (IAG)
- International Association of Physical Sciences for the Oceans (IAPSO)
- Marine Technology Society (MTS)
- National Security Industrial Association (NSIA)

PROCEEDINGS OF THE

INTERNATIONAL SYMPOSIUM ON

APPLICATIONS OF MARINE GEODESY

JUNE 3, 4, 5, 1974

BATTELLE MEMORIAL INSTITUTE

COLUMBUS, OHIO

This document contains only the formally-presented papers. It had been expected to include also edited transcriptions of the questions and answers following each paper and the panel discussions. However, because of difficulties in satisfying all parties on the wording of the transcriptions, those have not been included.

This publication may be obtained from the Marine Technology Society, 1730 M Street, NW, Washington, DC 20036.
Price per copy is $12.00.

Reprints of individual papers may be obtained by arrangement with the Marine Technology Society. Prices on request.

INTERNATIONAL SYMPOSIUM ON APPLICATIONS
OF MARINE GEODESY

CO-SPONSORS

Battelle-Columbus
The Defense Mapping Agency (DMA/PR)
National Aeronautics and Space Administration (NASA/OA)
National Ocean Survey of NOAA (NOAA/NOS)
National Science Foundation (NSF)
Office of Naval Research (ONR)

ASSOCIATE SPONSORS

The American Geophysical Union (AGU)
Institute of Navigation (ION)
International Association of Geodesy (IAG)
International Association for the Physical Sciences of the Oceans (IAPSO)
Marine Technology Society (MTS)
National Security Industrial Association (NSIA)

PROGRAM COMMITTEE

Helmut Moritz, cochairman — TECHNICAL UNIVERSITY OF GRAZ
A. George Mourad, cochairman — BATTELLE COLUMBUS LABORATORIES

MEMBERS

J. R. Apel (NOAA/AOML)
J. E. Bennett (ONR)
R. L. Duncombe (Naval Observatory)
C. E. Ewing (AGU)
D. M. Fubara (BCL)
J. H. Jorgenson (NSIA)
G. W. Lennon (Institute of Coastal Oceanography and Tides, England)
K. V. Mackenzie (NAVOCEANO)
J. Murphy (NASA/OA)
H. Orlin (NOAA/NOS)
R. E. Sheriff (Chevron Oil Co.)
W. E. Strange (Computer Sciences Inc)
U. A. Uotila (Ohio State Univ.)
O. W. Williams (DMA/PR)

SESSION CHAIRMEN

Session I: Requirements for Marine Geodesy (1)
F. A. Roberts — CHEVRON OIL FIELD RESEARCH COMPANY

Session II: Requirements for Marine Geodesy (2)
Dr. M. M. Macomber — DEFENSE MAPPING AGENCY

Session III: Marine Geodesy and Positioning/Navigation
K. V. Mackenzie — NAVAL OCEANOGRAPHIC OFFICE

Session IV: Marine Geodesy and Ocean Physics
Prof. I. I. Mueller — THE OHIO STATE UNIVERSITY

Session V: Satellite Altimetry and Modern Geoid Methods
Dr. G. C. Weiffenbach — SMITHSONIAN ASTROPHYSICAL OBSERVATORY

Session VI: Marine Gravity Anomalies and Geodesy
Dr. A. Malahoff — OFFICE OF NAVAL RESEARCH

BANQUET SPEAKER

Dr. Athelstan Spilhaus — NOAA

TABLE OF CONTENTS

SESSION III: MARINE GEODESY AND POSITIONING/NAVIGATION

SESSION IV: MARINE GEODESY AND OCEAN PHYSICS

CALL TO ORDER

PROF. HELMUT MORITZ, Chairman

Ladies and Gentlemen, I would like to welcome you all to the symposium on the Applications of Marine Geodesy. First, I would like to introduce myself, my name is Helmut Moritz - I am with the Technical University at Graz, Austria. Originally, I was supposed to serve as co-chairman here, the chairman of the symposium being Mr. George Mourad from Battelle; but unfortunately George has not yet completely recovered from a recent operation so he has asked me to take over the chairmanship of this symposium. Perhaps it may be well to recall the history of marine geodesy and of marine geodesy symposia. As you well know, in 1966 there was the first marine geodesy symposium here at Battelle. It was co-sponsored by Battelle and NOAA. The second one was in 1969 in New Orleans and organized by the Marine Technology Society. In 1971 at the IUGG General Assembly in Moscow, there was also a symposium on marine geodesy and now in 1974 we have a symposium that is called Applications of Marine Geodesy. So, it seems that marine geodesy has reached the stage where one can really also present applications and results. Well, this symposium will deal with these subjects. I would also like to transmit to you a message from George Mourad. He would like to extend his special thanks to the many people who made this symposium possible. In addition to the co-sponsors, associate sponsors and the committee members, a special thanks is due for two particular non-committee members for their assistance and who have been very much involved in the preparation of the symposium. These are Capt. Jane Mackenzie, Marine Consultant, and Dr. Milton Johnson of NOAA who will be speaking in Session IV. Also, from Battelle to Drs. Al Robinson and Mike Fubara, who very adequately filled in for George's absence. I would like to transmit to you the greetings from the International Association of Geodesy. You know there is a special study group within the association of geodesy of which George Mourad is Chairman. And on behalf of the International Association of Geodesy, and of the International Scientific Community, I would like to extend special thanks and appreciation to Battelle Memorial Institute for making this symposium possible by arranging it.

And now Ladies and Gentlemen, I would like to introduce Dr. John M. Batch, Director of the Columbus Division of Battelle Memorial Institute who will be our host and will then give a speech of introduction. Dr. Batch has been active in research, research management, and education since 1950. In his present position as Director, he is responsible for all research and supporting activities at the Battelle Columbus Laboratories and associated marine facilities at Long Beach, California, Daytona Beach, Florida and Duxbury, Massachusetts. Early in his career, Dr. Batch was employed by General Electric Company and later by Battelle. His main field of research and development was in the field of nuclear engineering with emphasis on heat transfer to nuclear reaction design and safety. He is author and co-author of a great number of reports and publications. Dr. Batch has also been very active in Education. He has a distinguished educational career beginning as an instructor in mechanical engineering at South Dakota State College and Purdue University and leading up to an adjunct associate professorship at the University of Washington in Washington State University during the time he was associate director of Battelle Northwest Laboratories at Richland, Washington. Well, may I ask Dr. Batch to give his address.

WELCOME

from

Dr. John M. Batch, Director
Battelle Columbus Laboratories

It gives me a great deal of pleasure to be able to welcome you to Columbus and to Battelle Columbus Laboratories on this really beautiful day. I'm very happy that the committee had foresight enough to schedule this symposium on a day when the weather was like this.

We at Battelle are indeed gratified to be able to join with the five co-sponsors and the six associate sponsors in creating this symposium on Applications of Marine Geodesy. I want to emphasize that we are only one of the co-sponsors; the co-sponsors need to be given a lot of the credit.

I would like to be able to tour you through the Battelle Facilities and show you what Battelle is all about. But we don't have time. However, I can give you a quick description of the Battelle Facilities. As most of you know, Battelle is a research organization. Our total effort in research is about 130 million dollars a year and our facilities are spread throughout the United States and also in Europe.

This symposium is being held at the Battelle Columbus facilities which house approximately 2,600 people. The Battelle Northwest Laboratories activities are very similar to Battelle Columbus research although there are variances in emphases. Northwest division has about 1,700 employees. Battelle also has two facilities in Europe which perform contract research, one in Geneva, Switzerland with 650 employees and the other at Frankfurt, Germany with 850 people.

As far as marine research is concerned, our activities are mainly concerned with marine engineering, marine biology and various aspects of marine fouling. Our marine laboratory at Duxbury, Massachusetts, which is about 40 miles south of Boston, is involved in looking at the environmental effects of plant and animal life in the ocean. Our marine laboratory at Daytona Beach, Florida, is primarily concerned with marine fouling. Ocean engineering research is performed in our Long Beach, California facilities. A fourth marine laboratory is operated by Battelle Northwest at Sequim, Washington, very close to the Pacific Ocean.

That is a very short description of Battelle, but it does give you an idea of our facilities that are specifically and directly associated with marine activities.

In all our many areas of activity, Battelle is deeply concerned with the utilization of science and engineering for the benefit of mankind. For this reason we are particularly happy to note that a large portion of the papers that will be given here will be devoted to applications--that is, current and future uses of marine geodesy for practical application.

As far as the implications of potential future uses, I would like to invite all of you to participate in a meeting which will take place tonight, which is not a part of this symposium but which you should find very interesting. Battelle is joining with the Department of Geodetic Science at the Ohio State University in a study of the future requirements of marine geodesy. Tonight at 8:00 p.m., we are jointly sponsoring an open session in the third floor auditorium at the Sheraton Columbus Hotel. At this meeting we hope to generate a very lively discussion on the future of marine geodesy. The meeting will be chaired by Professor Ivan Mueller from Ohio State University. He joins with me in hoping you will be able to attend the meeting. Along the same lines, we hope you will complete the questionnaire you received along with the conference program and return it to us sometime today.

If we can assist you in any way in making your stay here more pleasant please do not hesitate to call on us. We will be happy to arrange tours through the facilities here at Battelle Columbus if you are interested. There are a number of Battelle people who are participating in this symposium, but we also have some young ladies who are sitting out at the front desk, whom you will be able to identify easily. Ask them or ask any of us and we will do anything conceivably possible to assist you.

Thanks again and welcome to Battelle. Enjoy this symposium.

INTRODUCTION
OF

FRANK L. WILLIAMS

by

PROF. HELMUT MORITZ

Now I have the pleasure of introducing to you Dr. Frank L. Williams as representative of the Co-Sponsors. Dr. Williams is a graduate of Auburn University, Massachusetts Institute of Technology where he graduated as bachelor and master in aeronautical engineering. First, he has had a period of some seven years as an Air Force Officer and then he joined NASA. Since 1958, he has had a very distinguished career within NASA. He worked together with Verner Von Brown and since July, 1972 he has served in his present position as Director of the Special Programs Division, Office of Applications. In this position he is responsible for programs such as SEASAT and GEOS-C. So, we are very privileged to have Dr. Frank Williams talk to us now on behalf of the Co-Sponsors.

OPENING REMARKS

MR. FRANK L. WILLIAMS
Director, Special Programs Division
Office of Applications, NASA

Thank you. It is a privilege to be a representative spokesman, if you will, of the Co-Sponsors and on behalf of the Co-Sponsors which are listed in your program--The Battelle-Columbus Labs, The Defense Mapping Agency, The Office of Applications at NASA, The National Ocean Survey of NOAA, The Office of Naval Research and The National Science Foundation--as well as several Associate Sponsors. On behalf of all of us, we welcome you to the symposium.

We, as Co-Sponsors, would like to thank the Battelle-Columbus Labs for the work that they have done, and it has been quite a chore, I am sure, to make all the arrangements for this symposium. We would like to thank the Program Committee, Dr. Moritz and George Mourad. I am certainly sorry George can't be he I have had the personal pleasure of working with George over the last several years and I know how much this symposium has meant to him.

As the Sponsors and Co-Sponsors, we are pleased with the reception that the symposium has received, as is indicated by the number of representatives from various domestic user organizations, as well as foreign representatives. The subjects being covered is broad, and I think we are now really moving into the realm of the applications of ocean geoid and geodetics. The papers, of which I have been able to get an advanced copy, I have read and I am quite impressed by their quality. I think we are off to an exceptionally good start - and speaking for the Sponsors we are quite pleased.

I did want to take advantage of this opportunity to talk breifly about some of the NASA activities and how we see NASA fitting into the subject matter being discussed at the symposium.

A little over two years ago, we assembled from what was emerging in the science and early applications days the Earth and Ocean Physics Applications Program commonly known as EOPAP. This program was not defined by just NASA, and was not defined in just one meeting or over a brief period, but is one that has evolved over the years. However, finally in a very concentrated effort working with what we call our user community--which consists of other governmental agencies, industry, the academic community and in some cases foreign involvement--led to the formal definition of the EOPAP program. To put things into perspective, we set some long range objectives or goals for the EOPAP program which are shown in Figure 1.

These are the goals that we set and are related to the development and validation of methods for observing earth dynamic motion using space techniques. The first objective addresses tectonic plate motion and, in particular, earthquakes. The next two objectives relate to the oceans. Again, from a NASA standpoint, these focus on the applications of space techniques, tools, and technologies. Finally, the last objective deals

with the local geoid, and extending geodetic control to inaccessable areas; in the areas of mapping and geophysics applications - again a topic under discussion at this symposium.

We at NASA recognize that the ultimate accomplishment of these objectives is not a NASA responsibility. Ultimately, this responsibility lies with the collective user community. However, we feel that we have a role to play, a contribution to make, and can be a participant in achieveing these very worthwhile objectives. We have defined a program - again a NASA program - but defined in conperation with our user community--again, other government agencies, industry and the academic community as well as international participants. This long range plan is illustrated in Figure 2. To develop this plan we had a good heritage with which to start. The top three programs have already used space techniques to address the subject. The earth and ocean physics applications programs start with the Line Measurement Systems, Forecasting Techniques & Modeling and range to Advanced Applications Flight Experiments (AAFE) program. The remaining program, in Figure 2, are activites within NASA - with the exception, TIMATION - that are complementary or support the activities we have in the Earth and Ocean Physics Applications Program.

I don't plan to discuss all of them, but to talk about several as time permits. Measurement systems, forecasting techniques, and modeling are, to a degree, supporting research and technology activities that address the modeling and forecasting techniques that apply to marine geodesy, as well as tectonic plate motion, etc. Data analysis is an activity that is set aside specifically to analyze, utilize the data being collected for the various ground, as well as space based experiments that are underway. These are ongoing activities.

Tectonic plate motion is a new activity that is building on some past research and technology work. The San Andreas Fault experiment and the VLBI-Very Long Baseline Interferometry work address position, plate motion, UT-1 or earth rotation and polar motion.

Next are the flight experiments. GEOS-C is a research satellite that will be launched t third quarter of this year, that will carry an altimeter and, hopefully, will address--in a much more precise way, as well as on a global basis--the geoid. The altimeter will also give us the altitude from the satellite to the surface of the ocean as well as, we feel, the wave heig: so that we will be able to get sea-state information out of that system. LAGEOS is a large and very dense sphere about 2 feet in diameter that will be launched in 1976 - and will provide a permanent reference place in space and a very precise orbit for our laser ranging for geodetic work. SEASAT-A is what we at NASA feel is the first oceanographic satellite and I won't go into any more details. Walter McCandless will be giving a paper on SEASAT this afternoon. To get a better handle on the gravity field, we are planning GEOPAUSE - and GRAVSAT. SEASAT-B is planned for the early 1980's, and, being very frank, is relatively undefined at this point in time. First we want to get GEOS-C under our belt and understand how well that system is going to work and develop a firmer handle on precisely what SEASAT-A will do. SEASAT-B could be anything from an advanced research and development type system through the spectrum up to a prototype operational system, and we, NASA as well as our user community, will begin to address that in a very definitive way starting this coming year. Let us pass over Skylab since I have a little bit of data that I am going to show you in a moment. TIMATION is a Department of Defense system which provides another reference base laser ranging. The ATS-F satellite--Advanced Technology Satellite series F--was just launched last week, and is successfully in orbit. Everything is checking out and it seems to be operating quite satisfactorily. In fact, it was a flawless flight. I bring that up in that we will be using ATS-F in concert with GEOS-C, which will be launched later this year, for satellite-to-satellite tracking, GEOS-C being in low orbit and ATS-F being in a synchronous orbit. Also we will use this satellite-to-satellite data transmission on the ASTP or Apollo Soyuz Test Program--we have two experiments that will be flown in this joint U.S.-Soviet mission. Again, we will be testing satellite-to-satellite tracking but this time we will have the Apollo spacecraft tracked from the ATS-F,

so we will have a high satellite tracking a low satellite. After the docking mission is completed, we will disengage, or undock, with the docking module being disengaged from the command module to allow the two to separate. This will enable satellite-to-satellite tracking between two low-orbiting satellites - to be done in unison with ATS-F high-low tracking. The combination of high-low as well as low-low tracking, we feel will give us an awful lot of very good gravity field data. Unfortunately, it will be a short duration mission but we feel that it will give us good design criteria, hard information, for the final designs of GEOPAUSE, as well as better handle on some of the theories that exist today. Finally, when the shuttle comes along, I think we will be ready to make maximum utilization of it for the applications that we will be discussing these three days here at the symposium.

I did bring along what I think is very new data. Figure 3 shows a geoid model map of the earth. This one happens to be the Goddard Space Flight Center GEM-6 model of the geoid. Superimposed on this is the ground track of the Skylab pass number 49. During this pass number 49 we turned on the altimeter which was flying aboard the Skylab and, in essence, we have a complete altimetry map of the oceans for the complete Skylab pass. When these data were taken, we did not turn the altimeter on and let it run continually but turned it on for a while and then turned it off. I should point out that the results shown here in Figure 4 are quick look data. They have not been refined as yet, and, therefore, are subject to some modifications, but this is the geoid based on the GEM-6 model (shown as the solid line in Figure 4), and the altimetry data obtained on pass 49 starting over the Southern Atlantic proceeding just off the tip of Africa, to South of New Guinea, across the Pacific, then across U.S. and over the Caribbean. I think you will see, as I do, that particularly for quick look data, without any processing to remove potential system bias errors, that it is a rather remarkable set of data and, to my knowledge, this is the first time that we have in fact obtained, on a global scale, verification of the ocean geoid. I bring this up because I think we are really, as I said earlier, in the transition phase from science to applications. We at NASA have some new tools to bring to bear, new technologies to offer which can be used in conjunction with analytical techniques and experimental verifications to generate the type of data that will be discussed here at this symposium. I believe that, by working together, the processes required to utilize this data operationally will be developed. So, I think we can expect a lot from this symposium and a lot from you ladies and gentlemen in this field in the coming years. Thank you very much.

FIGURE 1. EARTH AND OCEAN PHYSICS APPLICATIONS PROGRAM (EOPAP) OBJECTIVES

- DEVELOPMENT AND VALIDATION OF METHODS OF OBSERVING THE EARTH'S DYNAMICAL MOTIONS USING SPACE TECHNIQUES TO MAKE UNIQUE CONTRIBUTIONS TO THE KNOWLEDGE OF EARTHQUAKE MECHANISMS AND THE DEVELOPMENT OF EARTHQUAKE PREDICTION APPROACHES.
- DEVELOPMENT AND VALIDATION OF MEANS FOR PREDICTING THE GENERAL OCEAN CIRCULATION, SURFACE CURRENTS, AND THEIR TRANSPORT OF MASS, HEAT, AND NUTRIENTS.
- DEVELOPMENT AND VALIDATION OF METHODS FOR SYNOPTIC MONITORING AND PREDICTING OF TRANSIENT SURFACE PHENOMENA, INCLUDING THE MAGNITUDES AND GEOGRAPHICAL DISTRIBUTIONS OF SEA STATE, STORM SURGES, SWELL SURFACE WINDS, ETC., WITH EMPHASIS ON IDENTIFYING EXISTING AND POTENTIAL HAZARDS.
- REFINEMENT OF THE GLOBAL GEOID, EXTENSION OF GEODETIC CONTROL TO INACCESSIBLE AREAS INCLUDING THE OCEAN FLOORS, AND IMPROVEMENT OF KNOWLEDGE OF THE GEOMAGNETIC FIELD FOR MAPPING AND GEOPHYSICAL APPLICATIONS, TO SATISFY STATED USER REQUIREMENTS.

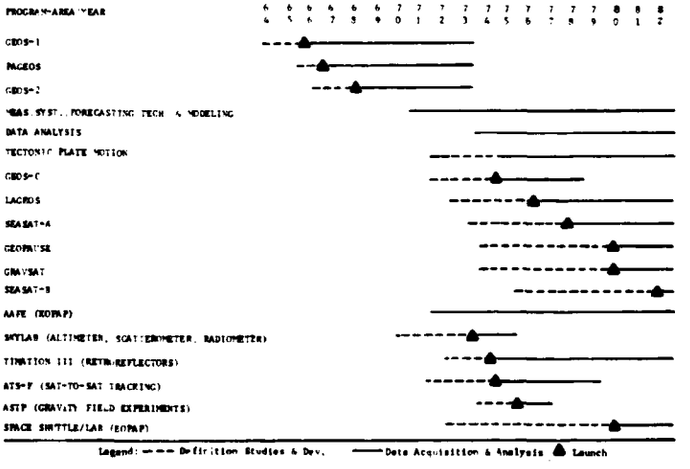

Figure 2. EARTH AND OCEAN PHYSICS APPLICATIONS PROGRAM (EOPAP) AND RELATED ACTIVITIES

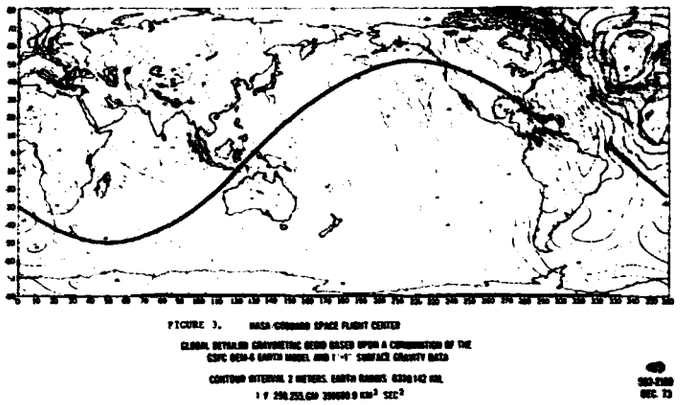

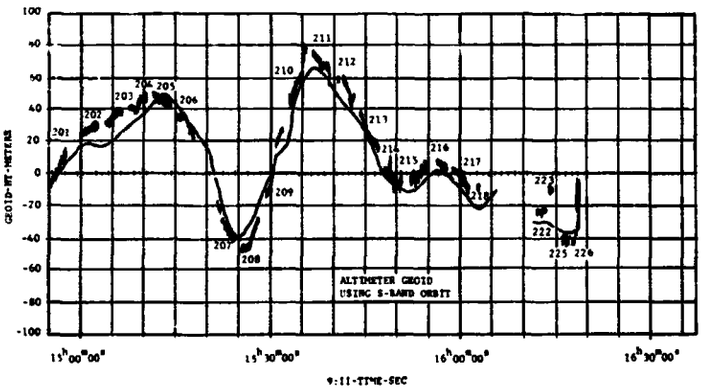

Figure 4. ALTIMETER GEOID USING S-BAND ORBIT

ECONOMIC ASPECTS OF MARINE GEODESY

K. E. McConnell
Department of Resource Economics
University of Rhode Island
Kingston, R. I.

ABSTRACT

The growth in world population and industrial output is rapidly increasing the demands for the use of the ocean as a transportation medium, source of raw materials and recreation facilities. Orderly and efficient use of the ocean requires a thorough knowledge of the ocean, and it is one of the tasks of marine geodesy to provide this knowledge. The purpose of this paper is to provide an analytical framework for dealing with the economic aspects of marine geodesy. Part I of the paper develops the concept of economic efficiency. Part II constructs a hypothetical market for the information provided by marine geodesy, and examines how this market might work without government intervention. Part III examines the rationale for government participation in the provision of information about the ocean.

EFFICIENCY IN THE ALLOCATION OF MARINE INFORMATION

This paper deals with the economic aspects of information about the physical characteristics of the ocean, information supplied by natural sciences like marine geodesy.[1] The growth in the demand for this type of information comes from two interrelated developments: (1) the rapid expansion in the commercial exploitation of the ocean and (2) the response of governmental regulation to the increasing use of the ocean.

The growth in the commercial and industrial uses of the ocean can be illustrated in many ways. A list of some of the ocean-related commercial activities is revealing: mining of oil, gas, sand, gravel, and the potential mining of manganese modules and other minerals; recreation in different forms of swimming, boating, and fishing; commercial fishing by many methods; ocean dumping; and many different types of transportation.[2] The above increase in the uses of ocean resources has occurred in part because of the rising relative prices of land-based substitutes. In addition, we have witnessed increased use of the ocean for the purposes of national defense and research and development.

It is widely recognized that the ocean and its resources are common property resources; because of their physical and biological characteristics, they cannot be privately controlled and so their ownership is vested in the community at large.

Consider, for example, the problems inherent in defining ownership rights to a fishery resource such as the tuna. Only with the recent dramatic increase in the use of the ocean has the absence of private ownership created conflicts. Governments at the national and international level are now engaged in defining more clearly the particular community to which resource rights properly belong. An example is the 200 mile limit controversy. It is both the increasing use of the ocean by private concerns and the concomitant increasing governmental regulations of the use of the ocean which has lead directly to the economic importance of marine geodesy.

The purpose of this paper is to examine the basic economic aspects of marine geodesy. Administrators and scientists are constantly making decisions concerning the allocation of research effort in marine geodesy. For example, some general issues that must be faced are: What types of technological advances should be sought? What part of the ocean should be charted? How much of the ocean should be charted and in what detail? These are economic decisions in part because they involve the allocation of scarce resources (research funds and personnel) among competing uses (research projects). And increasingly, as the Office of Management and the Budget makes decisions using benefit-cost considerations, the allocation of research funds in marine geodesy and other marine-related disciplines will have to be justified. An economic discussion of marine geodesy can therefore be useful in choosing among alternative research projects.

I. CRITERIA FOR ECONOMIC EFFICIENCY

Economic tools, if usefully applied to the development of marine resources, can provide efficient methods of exploiting marine resources. An efficient allocation of resources, in the economist's jargon, is one such that there is no possible rellocation of those resources which could increase the net output of the economy. For example, a petroleum refinery is said to be operating efficiently if it is not possible to produce more refined products with the same men, machines, and raw materials and the same technology. Another way of stating that an allocation is efficient is that it maximizes the difference between total benefits and total costs for any given project.

Efficiency is of course only a model with which real situations can be compared. Under circumstances where ownership rights are clearly defined, markets function well, benefits accrue only to consumers, and costs only to producers, resources are considered to be allocated efficiently by the private sector of our economy.

However, there are conditions when the private sector's allocation of resources will not be efficient. Resources are allocated inefficiently in the private sector if any of the following conditions hold:

1) ownership of resources is not clearly defined;
2) markets do not function competitively;
3) the benefits gained by a consumer of a good differ from benefits gained by society;
4) the costs to society of producing the good are different from the costs to the producer.

If resources are allocated inefficiently by the private sector for any of the above reasons, there is a prima facie justification for government intervention in the economy.

There are many examples of government intervention in

marine resource development on the grounds that the private sector operates inefficiently. In the exploitation of fisheries, when ownership of the exloited resource, the fish stock, is not clearly defined, there are many schemes for government regulation.[3] Another example is the use of coastal waters for waste disposal by private firms, which imposes costs on society that the firms themselves do not suffer. Such firms are being increasingly regulated.

One of the aims of this paper is to consider the appropriate mix of governmental and private enterprise which produces the efficient level of information about marine geodesy. A framework for the analysis of the efficiency of informational systems can be derived. Such a framework, when combined with data, can aid in the economic evaluation of particular projects as well as guide the efficient exploration of the oceans.

Economists derive criteria for economic efficiency by the study of the private profit-seeking economy. It is therefore fruitful to consider the enterprise of studying marine geodesy as though it were an industry. It is a useful fiction because it will enable us to analyze the production and use of the "output" of marine geodesy in a familiar framework. If we consider marine geodesy an industry, then it seems logical to let information from geodesy be the"output." Information, of course, can come in many forms: specific knowledge of the particular areas of the ocean, new technological devices such as types of radio signals, or new concepts. In general, the information provided us by the study of marine geodesy has economic value because it reduces the uncertainty of success of many ventures. The process by which information reduces uncertainty will be discussed more fully below.

II. INFORMATION ABOUT THE OCEAN: DEMAND AND SUPPLY

The demand for marine geodesy is provided by three sets of institutions: (1) industrial corporations, such as petroleum and shipping companies; (2) scientific bodies, such as universities or private research groups like the Battelle Institute; and (3) government agencies, such as the Department of Defense. These groups of institutions want information on the ocean ultimately for different reasons, but the information they want may be the same.[4]

In the case of industrial concerns, it is easy to conceptualize (though difficult to measure) the market value of information about the ocean. Reductions in uncertainty result in profits for the firm. Under certain conditions, the increases in profits are a measure of the net benefits from the information.[4] For corporation, we may think of two types of information:

1) information reducing the uncertainty concerning technological future of the company, i.e., what are its endowments and productive capabilities.

2) information reducing the uncertainty surrounding the market for its products. Such information would increase the firm's ability to predict its future prices and the future behavior of its competitors.

In the context of this paper, we are concerned only with the first kind of information--marine geodesy produces information which reduces uncertainty about the technological environment of the firm. For example, a better charting of the ocean reduces the number of shipwrecks, lowering the costs

of insurance. Information on the structure of the ocean floor decreases the uncertainty that extractive companies have concerning the profitability of exploiting the floor. Information on the structure of the ocean floor aids the firm in two ways: (1) it gives the firm some indication about whether the mineral the firm seeks exists there; and (2) it indicates to the firm something about the costs of extracting the material. More specific examples could be given. In each case, we could see that the industrial concern would be willing to pay for information derived from the study of marine geodesy because it enables the firm to calculate the expected returns from a given investment.

Scientific concerns have an interest in obtaining information about marine geodesy because they use the information as an input for further investigation. The results of further investigation can be of commercial interest to private corportations marketing the output of the ocean, or they can be simply desired for their own sake, i.e., pure research as an end activity itself. To illustrate, information to a scientific concern may come in the form of mechanical innovation which increases the accuracy of the description of the ocean floor. A scientific concern would value this innovation because (1) it would permit scientists to describe more accurately the floor in a given location, thus decreasing the uncertainty about the exploitation of that location (for example, it would permit more accurate estimates of constructing oil and gas pipelines); (2) it would give scientists better insight into the overall structure of the geoid.

Government demand for the information from marine geodesy comes from several different sources. It is an important input in providing national defense, though it is exceedingly difficult to place an economic value on national defense. Government can also use information in dealing with issues such as the controversy surrounding the 200 mile limit. Positioning and relocation will be very important in this controversy, particularly when the potential boundary crosses an oil field. Even when countries agree in principle on the location of boundaries, measurements must be sufficiently accurate to prevent disputes over the ownership of specific points. Also, assigning liabilities for pollution outfalls entails the ability to locate the results of pollution accurately. All the above indicate why the government values the information provided by marine geodesy.

On the supply side of the model, we have two institutions, private firms and government, providing information. Government information is generally provided at a zero or nominal price, while private industry generally attempts to supply information approximately at the cost of producing it. In addition, these institutions purchase the services of research concerns. The structure of the supply side of marine geodesy information market is appropriately outlined as follows:

Institutions providing information about marine geodesy

1. government agencies
    a. directly, through in-house research
    b. indirectly, by contract to research concerns
2. private concerns
    a. through in-house research
    b. by contract to other research concerns

III. MARINE GEODESY: AN EFFICIENT ALLOCATION OF RESOURCES

As it exists, our current system of producing information about marine geodesy features significant subsidies by the federal government. Therefore, individual researchers, in and out of government, need not consider whether a particular research result will be profitable to them. Researchers do not even need to consider whether the information they produce would be saleable (although it often is). In effect, we have a system whereby information is a free good, except for the transactions costs inherent in obtaining the information.

We can compare our current system with a system involving no government subsidies to gain an idea of the efficiency of such an allocation, and hence a justification for government's role in subsidizing research. With no government subsidies, private industry would supply most of our information about the ocean. In private industry, each research proposal would be subjected to the screening question, "Can the information produced by this research project be sold to interested parties for a price sufficiently high to cover the costs of producing the information?" Under those circumstances, with no government participation on the supply side, some information would be produced. From an economist's point of view, would it be the best amount (when best means most efficient)? The answer is no, the free market allocation of resources to the production of information about marine geodesy is not likely to be efficient.

The basic cause of inefficiency in the market allocation of information is that the producer cannot appropriate all of the benefits to himself, because he cannot prevent re-use of the information. Information can have externalities, or benefits which accrue to parties other than those directly engaged in the transaction. For example, suppose a private research corporation undertook a research project to chart a particular small portion of the ocean, with a view toward selling the chart to a shipping company. The research company could be assured only of reaping the benefits from the sale to the shipping company, although the chart could benefit all users of the ocean in the area in question. The information might be valued by scientists and Defense Department officials, but no market exists for its sale. In short, total social benefits exceed the private returns to the research concern for the sale of the chart. From the public's point of view engaging in a research project may be an efficient allocation of resources, even though a private concern might find that its costs for undertaking the project exceeded the appropriable returns.

Hence we have in essence the justification for government subsidy of production of information in marine geodesy. Many projects with total benefits exceeding total costs will not be undertaken in the private sector because some of the benefits, in the form of spillovers or externalities, cannot be captured by producers of information. Thus we have government subsidies for producing information as part of a program for efficient allocation of resources.

IV. LEASING POLICIES FOR OFFSHORE PETROLEUM[5]

For purposes of illustration, it is useful to consider the problem of the appropriate government policy towards leasing of offshore petroleum sites. Many are aware of the preparations now under way in the development of the Georges Bank field, off the coast of New England. Although no one knows for sure there is speculation that the Georges Bank field may be a prolific petroleum area.

It is obvious that in the bidding for leases, physical information about the ocean is extremely important. If the oil and gas are to be piped to shore, the floor must be well charted. And naturally Georges Bank must be well charted. Clearly, there is a tremendous bank of information, much of it geodetic, that the petroleum companies use in preparing their bids.

We can imagine two basic approaches by governmental agencies (specifically the Bureau of Land Management) towards gathering information about Georges Bank. On the one hand, government could let each firm interested in the bidding gather its own information. On the other hand, the government could compile all relevant data concerning Georges Bank (geologic, geodetic, and other) and make it available to all interested bidders. Which system would be more efficient, in the sense that it provides the same information at minimum costs?

It seems clear that if the information gathering on Georges Bank is left to the market as it currently exists, it will be inefficient. There are no mechanisms for the private exchange of information. Hence, when one firm gathers information, it can not sell it to another, even though both would willingly participate in such an exchange. Each firm would have to do its own exploring, and it seems quite likely that the same information could be gathered more cheaply by government provision. Gathering information for bids on Georges Bank seems clearly to be an activity which produces benefits in excess of the benefits enjoyed by the firm which gets the information. Hence it seems appropriate to consider some form of government regulation.

CONCLUSION

This paper has applied the tools of economics to an examination of marine geodesy. We have developed the idea that it is in the interests of economic efficiency to have government participate in the supplying of marine geodesy research. This paper has necessarily been an initial look at the general problem of the allocation of research effort. It is an interesting economic problem in general, and researchers and administrators have many specific problems to solve in particular, so that it seems a fruitful area for applied research.

FOOTNOTES

1. This paper is offered without any pretenses of expertise in Marine Geodesy. Basic sources on marine geodesy used in the preparation of this paper are Proceedings of the First Symposium on Marine Geodesy (7) and Marine Geodesy - A Practical View (5).

2. Statistics on the use of ocean resources are not collected in any uniform way. A useful source of data concerning energy in Kash et al., Energy Under the Oceans (4). Fisheries data is available from the Bureau of Commercial Fisheries. Little is known of the total recreational use of the ocean.

3. International schemes for the efficient use of fisheries have attempted to set quotas for each nation. Quotas have been particularly controversial and difficult to enforce.

4. Information theory is a relatively new and promising area in economics. A good introduction can be found in Hirschleifer (3).

5. Economists are giving increasing attention to leasing and

the development of offshore petroleum. The economic problem of exploratory drilling is the subject of a paper by Peterson (6). Grigalunas (2) has examined the likely impact of the development of Georges Bank on New England. The study by the Council of Environmental Quality (1) will give a detailed evaluation of Atlantic OCS petroleum.

REFERENCES

(1) Council on Environmental Quality OCS Oil and Gas - An Environmental Assessment U.S. Government Printing Office Washington, 1974.

(2) Grigalunas, Thomas A. "The Economic Impact of Potential Petroleum Development on the Atlantic Outer Continental Shelf" testimony before the National Ocean Policy Committee, U.S. Senate, April 24, 1974.

(3) Hirschleifer, Jack "Where Are We in the Theory of Information" American Economic Review, Papers and Proceedings, May, 1973 pp. 31-39.

(4) Kash, Don E., et. al. Energy Under the Oceans. University of Oklahoma Press, Norman, 1973.

(5) Marine Geodesy - A Practical View. Proceedings of Second Marine Geodesy Symposium, Marine Technology Society, Washington, 1969.

(6) Frederick M. Peterson "Two Externalities in Petroleum Exploration", Department of Economics, University of Maryland, October, 1973 (unpublished paper).

(7) Proceedings of the First Marine Geodesy Symposium. U. S. Government Printing Office, 1967.

ACCURACY REQUIREMENTS FOR CERTAIN MARINE OPERATIONS

T. K. Treadwell, Associate Professor
Department of Oceanography
Texas A&M University
College Station, Texas

ABSTRACT

Ocean scientists are concerned with geodetic positioning at sea in three different areas: The inherent requirements of the science they are doing; the legal requirements surrounding science at sea; and as a special case of safety and prudent navigation. The requirements of ocean science vary widely, from the order of tens of meters to kilometers. Repetition rate of fixing is also highly variable. A relatively new concern is the legal aspects; what was formerly a free high seas is likely to become strictly nationalized and often privately owned. Oceanographers will need to be able to know geodetic positions to respond to these new requirements in carrying out their work. Finally, since most scientists are not seamen, special attention must be given to prudent and safe scientific operations. Due to unfamiliarity and enthusiasm, work can be endangered or put in legal jeopardy. There are several distinct problems related to geodesy which concern the ocean scientist: Absolute positioning; relative positioning; navigation; tracking; and recovery. Varying amounts of progress have been made in all these fields, but in each one considerable is left to do to provide the oceanographer with reliable, precise and reasonably-priced data.

The title of this paper is vague, and deliberately so, since I will touch briefly on the needs in general, of oceanographers at sea, both for the present and the future. Some of these needs are being discussed in greater detail by other speakers at this symposium, but some are not -- perhaps because the solutions to them are far from obvious.

The needs of ocean scientists for geodetic information at sea fall into several categories, with widely varying ranges of needs as far as accuracy, frequency, and methodology are concerned. Slicing the pie in one direction, one can divide their needs as follows:

-- the demands of science, per se
-- the legal requirements
-- the requirements for safety and prudent navigation

In the first category, the needs of science itself, accuracy requirements can range from extremely loose to

extremely tight. On the one hand, many biological and chemical studies can get by with positioning accuracy even less than that needed for ordinary navigation. This is the case when one is investigating properties or phenomena which are of a broad homogeneous nature. If measurements are being made of the trace elements in sea water, for example, and these are homogeneous over rather large areas, then a scientific need for precise position location does not exist. If one is studying animal or plant populations which are scattered with little variation over broad areas, again even the most general knowledge of the ship's position is more than adequate. Many of these phenomena vary far more with depth, or with time, than they do with latitude and longitude, so those factors are the controlling ones rather than horizontal measurements.

On the other hand, many oceanic research projects require very tight accuracies. This is particularly true in the case of geological and physical investigations. Much of geological oceanography is hard to distinguish from straight bathymetric charting -- and I will avoid the semantic hang-up concerning what is "research" and what is "surveys". Perhaps the old saw, that "If it's useful, it's a survey; if it's useless, it's research" is as good as any. Gathering data in pursuit of a scientific hypothesis in research is often indistinguishable from what many of us would call surveys, and in any case, frequently grades into a problem-oriented mode as the research progresses.

In any event, doing good bathymetry demands positioning accuracies which are rather well-known and accepted. They are a function of the scale, precision of depth determination, data density, and other factors, but in any case, accuracy requirements range from moderate to very tight. It is indeed surprising, though how many reputable geological oceanographers do not recognize this fact, or at least do not give it adequate attention. It is appalling to consider how much ship-time and man-years have been absolutely wasted in the last twenty-five years in quasi-scientific bathymetric surveys. All too frequently, because of inadequate positioning, the results are not even internally consistent, much less of a quality that can be fitted with other data into a coherent composite picture.

At worst, such floating data are not only useless, but actually damaging and misleading. To take a single example, because of inconsistent bathymetric data a submarine canyon, complete with name -- Alaminos Canyon -- was for years on the charts of the northwestern Gulf of Mexico. Recent studies have shown that the area is far more complex bathymetrically; a series of hills, ridges, basins, and valleys, which were erroneously forced into the format of a submarine canyon.

In the investigation of the materials and structure of the sea-bed, also, precision is needed if a true picture is to be obtained. Here, as in many of these marine problems, one can draw a parallel with their land equivalents. Making a geological or geophysical map on land requires certain well-known standards; should we settle for less, out in the open ocean? These problems are being faced up to, I think, rather better by scientists and engineers in industry than the academic scientists. When one is considering a commitment to drill an offshore oil well, at costs in the range of tens of millions of dollars, or dredging for phosphorite or manganese nodules at a tremendous investment, there is very little margin for error.

Yet all too often the marine geologist will dredge or core or run geophysical lines at sea, doing a fine job of it except for the lack of positioning accuracy. In the early days of marine geology, this led to some startling conclusions;

according to some reports, the entire Pacific Ocean was blanketed with manganese nodules. Maybe it is, but the precision customarily associated with a land geological survey was often lacking, and some doubt persists. I am reminded of the old story of the pocket kingdom, with a smallish army, which would march its few soldiers round and round the castle, to give the impression of a large fighting force. Is it possible that we were counting the same nodules over and over again? Only by the use of adequate positioning accuracies can we determine the true extent of sea-bed resources, and I am encouraged to see that another section at this symposium is discussing this topic.

In much of physical oceanography, too, positioning is critical. The tracking of current floats; the location of the margins of water bodies; the investigation of localized phenomena such as upwelling, all require rather tight horizontal control to be meaningful.

The frequency with which accurate positions are needed also varies considerably. In the case of single-point, one-shot stations, a single fix may do the job. For most moving operations, however, one would optimally desire continuous precision, or at least a repetition rate sufficient to allow adequately precise interpolations between fixes. This is why satellite navigation, even with its high precision at any particular fix, is not suitable by itself for most oceanographic research operations. A fix interval of roughly an hour is too long for many large-scale investigations.

To summarize the scientific requirements, they are extremely variable in regard to accuracy, frequency, and method. It is entirely likely that other requirements for precise positioning at sea will be more demanding than the intrinsic needs of the science being done there.

Turning next to the legal requirements which ocean scientists (and others) face, we have an entirely different set of problems. History amply demonstrates that the face of the earth has been progressively divided up just as soon as it became worth something; as soon as it became economically and, therefore, politically desirable. First, national areas of sovereignty are established; these are subdivided into the jurisdiction of smaller political units, and (ordinarily) into individual ownership. As a result of this evolution of ownership, there are now only two areas on the globe's surface which remain unassigned: the Antarctic and the sea. If something of value were discovered in the Antarctic, I suspect that its internationality would go down the drain overnight.

In the ocean, we are already seeing the evolutionary process of jurisdiction in a rapidly-accelerating fashion. The continental shelf areas are either proven or highly-likely resource areas for both living and non-living resources, in addition to their historical significance and importance to shipping, warfare, and recreational usages. In line with this growing awareness of value, nations have already begun to extend the limits of their jurisdiction out onto the shelves and into the ocean. Traditional national seaward limits of three miles have been progressively stretched to twelve, 60, and even 200 miles.

It seems entirely likely that this trend will continue; I for one fully expect to see the demise of the concept of "Freedom of the Seas" within the next very few years. The only real question to be resolved is how this will be accomplished; what the administrative machinery will be. An earlier international convention has already given the coastal states the right to control and exploit the seabed off their coasts to a depth of 200 meters (essentially, the edge of the continental shelf),

and, as far beyond that as they have the capability of exploiting the ocean floor. While this is ambiguous at best, and stupefying if interpreted literally, it is indicative of the trend. We are in for more extension of national lines of jurisdiction, rather than less.

A group of international experts will meet this summer in South America to have a cut at the problem, and try to shape up some kind of administrative scheme that can be made to work. Regardless of what they come up with, ocean scientists are faced right now with problems involving geodetic positioning at sea in this connection -- of knowing when they are within the legal boundaries of a coastal state.

This is not an academic matter, in more ways than one; most scientists know little about international law and politics and the economic and social and military forces that drive them; and it is definitely not academic, since it is something that we must live with almost every research cruise; we must get permission from the coastal state to work near it, and must also know when we are indeed within its jurisdiction. Most states, by the way, are being very sticky about these things; requests for permission to conduct research in coastal waters must be submitted months in advance, and permission to work there almost always involves conditions such as sharing data and taking local scientists aboard.

I am not at all sure about how to handle this sort of legal positioning problem. It does not seem too practical to think of the dry-land equivalents of fences and markers; yet we must come to something of this kind of thing sooner or later. Scientists may be able to live with some looseness and ambiguity; but when the chips are down, as in the case of commercial minerals and fish, the least one can ask for is precision of positioning (both for the property lines and for the scientists or commercial operators) adequate to cope with potential cases at law.

Oceanographers in general, by the way, are fighting a desperate and doubtless losing rear-guard action to try to maintain freedom of the seas. Most of the developing countries involved in the exploitation of the seas off their coasts simply do not understand the concept of basic research; they regard the scientist as a harbinger of commercial fishing fleets and offshore drilling rigs. Unfortunately, while the link between university scientist and commercial venture is not often a strong and direct one, the basic premise is correct: Research customarily draws economic exploitation after it. Oceanographers, I am afraid, are going to be dragged kicking and screaming, into the coming system, and it may be a traumatic experience.

The final need for ocean scientists is a special case of the general requirement for positioning as a matter of safe navigation and prudent ship operations. I will not go into the general need; it is reasonably well known. What makes the case of scientists special is that they are for the most part not mariners. It may sound paradoxical to say that a man may be an excellent ocean scientist and at the same time be a poor sailor, but that is my thesis. Scientists are, with few exceptions, passengers; their training has not been in maritime affairs. Science is their first love and their driving force. It is all too tempting for them to try things that no prudent seaman would consider. They have a long history too of pressuring skippers to do unwise things; often ships personnel will go along against their better judgment because they are persuaded that the science involved justifies the hazard.

This involves positioning in many aspects. One is the possible infringement on national jurisdictions noted above; a

scientist might be prone to run close to the boundary, while a professional seaman would give it a prudently wide berth. As another case, the use of special equipment, such as research submersibles, may be operated in a marginally safe way due to carelessness or lack of knowledge about the criticality of positioning. In any case, ocean researchers will need more, rather than less, of this sort of information and assistance.

Let me turn finally to a statistical summary of the kinds of specific problems ocean scientists face, and the state of the art for coping with each.

The question of positioning is often poorly understood by oceanographers, due to the confusion of "navigation", "positioning", "tracking" and "recovery". The oceanographer, however, is involved in all of them to some extent.

Absolute Positioning, in the classic geodetic sense, involves the identification of a point in reference to geodetic coordinates of latitude, longitude, and mean sea level (or other vertical reference datum). In practice on land, this involves the establishment of a grid of a relatively few primary geodetic positions, whose location is determined to very great accuracy -- decimals of meter and better. Based on this high-precision grid are a multitude of secondary grids and offshoots, whose accuracy is of the order of a meter. Other detail, such as that shown on a topographic chart, is hung around these primary and secondary frameworks and is of accuracies of tens of meters. All primary and many secondary and tertiary points on land are carefully and permanently marked on the ground, so that one can recover them and use them as starting points for further surveys.

Following also from these precision grids are the legal surveys which delimit the land itself; establish its ownership, and that of other rights, such as minerals; mark state and national boundaries; lay out highways and railroads and pipelines and other developments.

Unfortunately, few of these exist at sea at the present, and a discussion of precise surveys, geodetic points, or legal boundaries there does not at this moment carry the same practical meaning as it does on land. Further, I am not aware of any method to achieve the same accuracy, density, and marking of points at sea as is available on land. One might conceivably improve existing electronic positioning equipment so that the required accuracy could be obtained at the sea surface; but we are then faced with the problem of permanent marking of the position. The sea-bed is the only truly permanent place to put markers, and the gap between the sea surface and sea floor has proven impossible to bridge, in the sense of transference of geodetic accuracies.

In view of these problems, activities requiring accuracy at sea have often gone to a system of relative, rather than absolute, positioning. If one needs reasonably good accuracy within a rather small area, it is possible to establish and mark a local datum. This can be actual markers, such as acoustic beacons, or the like, whose geodetic position is only known approximately. Positions of objects can be fixed relative to this local datum with fair accuracy, usually of the order of meters or tens of meters. Of course this has no accurate relationship to a world-wide geodetic datum, and two or more local datums will not necessarily match up with each other. Relative positioning may meet the needs of small, local investigations when precise latitude and longitude is not important; but it will be insufficient for establishing such things as boundaries of nations, or of mineral leases.

Navigation is simply fixing the position of a vessel or other moving object. It can range from relatively high-precision, such as satellite navigation, Loran C, and some other electronic positioning systems, down to dead reckoning or plain guessing. Accuracy at best is of the order of tens of meters, and at worst in tens of kilometers. At present, these systems are largely limited to use on the ocean's surface, and not readily transferable to the sea bed. Frequency of position-fixing is also involved; the satellite navigation system produces good accuracy, but only provides it every hour or so, which for most survey purposes leaves a lot to be desired.

Tracking is but a special case of relative positioning, in which one vehicle or fixed station keeps track of another vehicle. A typical oceanographic case is that in which a surface vessel acoustically tracks a research submarine. In tracking, since the tracking vessel is using (ordinarily) routine navigation to position itself, then it necessarily follows that the plot of the object being tracked is of considerably less precision -- a chain of progressively weak links.

Recovery (or repeatability) is another special case of relative positioning, in which the object is to simply return to a given point repeatedly, regardless of the absolute location of the homing object, or the object being homed on. This is particularly applicable in such cases as homing on oil field wellheads, or finding a distressed submarine. Obviously accuracy is either perfect or non-existent -- either you succeed or you don't -- so speculation as to precision is meaningless. Using acoustic methods, good success can be had with simple recovery problems in most cases.

I have tried to emphasize in the foregoing that from the point of view of the oceanographer, the positioning of things at sea, in whichever of the several contexts one wants to consider, is a severe and in many cases unsolved problem. We have made progress in the field of short-range, small area relative positioning, and in recovery. But in the true meaning of positioning, and in the transference of positions to the field of a sounding cone, or to the end of a wire strung with instruments, we still have a long way to go. Finally, the determination, marking, and recovery of accurate geodetic positions at sea, in the legal sense used by land geodesists, simply does not exist. We oceanographers are customers, and not specialists in this field, and hope that soon there will be reliable, precise, and cheap methods available to provide the information we need.

REQUIREMENTS AND APPLICATIONS OF MARINE GEODESY AND SATELLITE TECHNOLOGY TO OPERATIONS IN THE OCEANS

A. G. Mourad and D. M. J. Fubara
Battelle, Columbus Laboratories

ABSTRACT

This paper explores what marine geodesy has to offer, and its practical relevancy to various operations in the oceans. On the basis of several previous studies, desirable accuracy and precision are assessed for the various operations. Marine geodesy tools and techniques--and the satellite technology and classical systems required to implement these techniques--are discussed. Finally, it is shown that the practical applications of marine geodesy to operations in the oceans have many unanswered challenges that merit immediate action in view of the many practical and scientific needs for what marine geodesy has to offer.

INTRODUCTION

Marine geodesy is the branch of geodesy for determination of marine geographic positions, geodetic controls, and the geoid (the equipotential surface that can be approximated with mean sea level). Determination of these parameters is not an end in itself but a means to solving various practical problems in man's inevitable activities in the oceans, such as engineering surveying for mapping and charting, resources exploration, test range and ground truth establishment, oceanographic and other earth and ocean physics applications research, and some basic scientific objectives of geodesy and geophysics.

The accomplishment of marine geodesy objectives requires unique tools and techniques and special adaptation of proven geodetic systems such as satellite technology, electronic distance measurement (EDM), geodetic astronomy, gravimetric geodesy and the potentially usable very long baseline interferometry (VLBI). The uses of these various options are discussed briefly. Each of the marine geodesy determinations and its practical and scientific applications have different accuracy and/or precision requirements which are assessed in the paper, based on the results of several studies and publications. The assessed accuracy/precision requirements are not errorless estimates. They are greatly influenced by accuracy/precision limitations of existing systems and techniques as well as cost-benefit considerations without compromising safety in marine operations.

In order to achieve the various marine geodesy objectives and their practical/scientific applications, there are many unanswered challenges which the paper lists. It is concluded these objectives and applications are necessary for man's successful but nondestructive and systematic exploitation of the oceans--safely and with a minimum of boundary rights' conflicts. The exploitation of the oceans is, of course, an undeniable necessity.

MARINE GEODESY RELEVANCY AND ACCURACY REQUIREMENTS

Figure 1 is a summary of marine geodesy objectives and the various practical and scientific applications in the oceans to which these objectives are relevant. Table 1 shows the degree of relevancy of marine geodesy (determination of geographic positions, geodetic controls, and the geoid) to the stated practical and scientific applications areas. Detailed discussions on these issues are in References [7], [13], and [18].

First, it is necessary to point out the interdependency between determination of the geoid and establishment of geodetic controls and positions. The geoid is required for definition of the figure of the earth and the reference surface for geodetic computations, the reduction of geodetic measurements, and a reference datum for height measurements [8]. It defines a model of the earth's gravity field required for orbit computation which is necessary for the use of satellite technology for establishment of geodetic controls and positions. The earth's gravity model or geoid is needed for improved efficiency of inertial navigation systems, and also in several national defense roles. The oceanographic need to interpret sea surface departures from an equipotential surface requires highly accurate determination of the geoid. Several geophysical phenomena that urgently need to be fully understood, e.g., plate tectonics, have strong correlation with geoidal variations and therefore, require the determination of the geoid. Details of the various applications of the geoid are given in References [8] and [9]. It is further shown that determination, with high accuracy (very short wavelength through the long wavelength), of the geoid from satellite altimetry is potentially adaptable to synthesis of gravity anomalies which are needed for various purposes, including geophysical prospecting.

The role of the geoid in systems and techniques for establishing geodetic controls and surface positions has been specified. Determination of marine geodetic controls and/or surface positions is required for mapping, charting, and the establishment of territorial boundaries and test ranges for calibration of navigation systems and satellite altimetry data. Efforts for direct measurement of sea floor spreading and other activities in resources exploration, e.g., gravity/magnetic/seismic surveys, geologic surveys, pipelines/cable laying, search/rescue/salvage, and waste disposal, all require determination of positions and/or geodetic control as shown in Table 1. Table 2 is the basis for the assessment of the accuracy requirements for the various application activities as shown in Table 3.

MARINE GEODESY TOOLS AND TECHNIQUES

Marine geodesy activities fall into two major categories--the ocean surface and the ocean bottom. Geodetic satellite systems, classical physical geodesy systems, EDM, and acoustic systems are the main tools, while the techniques are modified conventional geodetic techniques adapted for use in the marine environment.

Ocean Surface Geodetic Activities

The ocean surface activities involve (a) position and (b) geoid determinations. A distinction is made between (1) position determination in marine geodesy, which requires accuracy between 10 to 100 meters in support of requirements of specific marine activities (see Table 3), and (2) position determination for general navigation purposes, which can tolerate an error of one to several kilometers, depending on geographic location. The latter is not a geodetic problem except in the area of establishing test ranges for testing and calibration of navigation systems, and so will not be discussed further.

Surface position determination in marine geodesy branches into two categories: one is for geographic or relative position location of sites or routes of activities shown in Tables 1 and 3; the other, which has the highest accuracy demand, is used as staging positions for transferring geodetic coordinates to ocean bottom markers. This latter case, the establishment of marine geodetic control, is discussed later. Because of

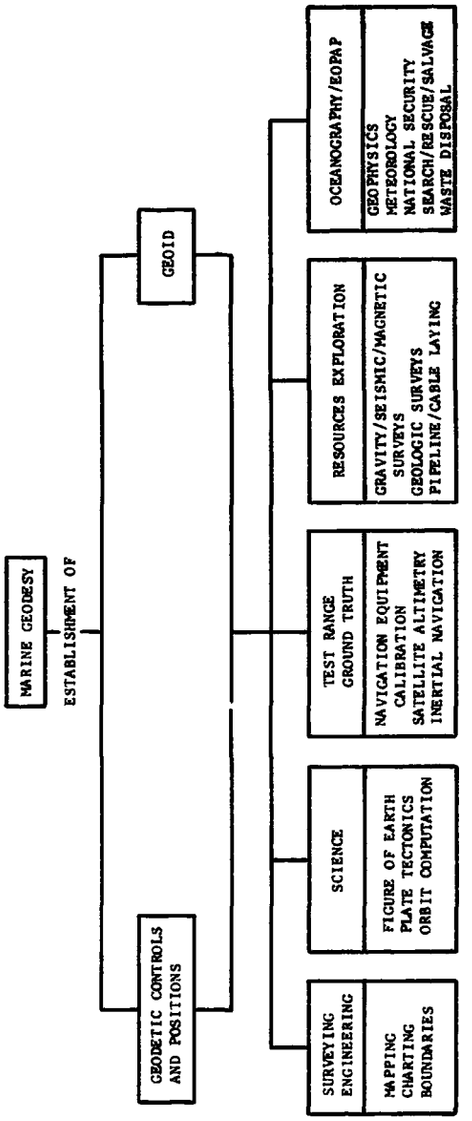

FIGURE 1. MARINE GEODESY - GOALS AND APPLICATIONS

TABLE 1. DEGREE OF RELEVANCY[a] OF MARINE GEODESY TO SOME OCEAN ACTIVITIES

	Marine Geodesy Areas			
	Control Points	Surface Positioning	M.S.L. (Geoid)	Surveying & Mapping
Practical Geodetic Applications				
Bathymetric mapping and charting	1	1	1	1
Boundaries	1	1	3	1
Ground truth/test range	1	1	1	1
Gravity measurement	1	1	1	2
Search, rescue, and salvage	1	1	-	2
Environmental Prediction & Ocean Physics				
Air-sea interaction	P	3	1	3
Tides and mean sea level	1	1	-	3
Ocean currents and transport	3	2	1	2
Waste disposal	2	1	-	1
Ice-sheets motion	P	1	-	2
Geology/Geophysics & Resources				
Gravity/seismic/magnetic	2	1	2	2
Geologic surveys	2	1	-	2
Pipelines and cable laying	3	1	-	1
Petroleum and gas	2	1	P	1
Solid minerals	1	2	P	2
Scientific and Educational Applications				
Figure of the earth	1	1	1	1
Ocean spreading	P	1	3	1
Ship/satellite tracking and orbit determination	1	1	1	1
Inertial navigation	P	1	1	-

(a) *Degree of Relevancy*

1 - Primary
2 - Secondary
3 - Tertiary
P - Potential Utility

TABLE 2. MAJOR BASIS FOR COMPILATION OF ACCURACY REQUIREMENTS

Activity/Publication	Conducted By	Sponsor	Date	No. of I,Q,P,R*	Comments
Effective Use of the Sea	President's Sci.Advis.Comm.	White House	1966	18P	States positional accuracy needs p.21
First Marine Geodesy Symposium	--	C&GS and Battelle	1966	392P	Marine Geodetic Requirements of Industry, DoD, Commerce & Scientific Communities were identified. Heavy industrial participation.
Development Potential of the U.S. Continental Shelf	Battelle	ESSA/C&GS	1966	1541	Results based on interviews with private industry, Local, State and Federal Government, research firms, universities and literature.
Satellite Applications to Marine Geodesy and Ship Positioning (CR-1253)	Battelle	NASA/OSSA	1968	271, 99R	Based on selected interviews, literature study and evaluation of technical problems and their applicability (p. 10 and Appendix A).
Precise Positioning Requirements for Special Purpose Operations	Geonautics	USCG	1969	281,140Q	Confirmed results of previous studies on position requirement.
Our Nation and the Sea	Commission on Marine Sci. Engr., & Resources	President & Congress	1969	Many	Extensive efforts and interviews throughout the U.S. covering all aspects of oceans activities.
The Terrestrial Environment: Solid Earth & Ocean Physics	Invited Experts from many Disciplines	NASA/MIT	1969	78P	Used as basis for EOPAP. Identified marine geodetic requirement.
Marine Mapping, Charting and Geodesy Workshop	NSIA	DoD	1969	160P	Invited people representing industry & Government
Second Marine Geodesy Symposium	Marine Geodesy Committee	Marine Tech. Society	1969/70	164P	Several positioning and accuracy requirement tables were presented, also confirmed earlier studies. Marine boundaries highlighted.

TABLE 2. MAJOR BASIS FOR COMPILATION OF ACCURACY REQUIREMENTS
(Continued)

Activity/Publication	Conducted By	Sponsor	Date	No. of I,Q,P,R*	Comments
An Ocean Quest	Committee	NAS/NAE	1969	119P	This report formed the basis for the International Decade of Ocean Exploration.
Mineral Resources of the Sea (United Nations Economic and Social Council)	--	UN	1969	185R	Report of the Secretary General-Extensive Coverage of Resources
Hydrographic Surveying and Bathymetric Charting	Ad Hoc Committee	UN	1970	6R, 8P	Based on expert opinions in Hydrographic Surveys & Charting. Presents marine mapping inadequacy & Requirements.
A Proposed Aid to Geodesy: The Spatial System "GEOLE" - Inter. Hydrog. Review	Husson & Thieriet	France	1970	--	Presents a table on Marine Geodetic Accuracy Requirements (P. 129 130).
Exploiting the Resource of the Seabed	Library of Congress	Congress	1971	147R	Covers resources, boundaries, legislation and implications.
Marine Geodesy - 1967,1971	Sq. Study Committee	Intern.Assoc. of Geodesy (IAG)	1971	124R, 25P	Extensive review of marine geodesy, identified problems areas, approved by IAG and passed resolution No. 4 (attached)

* I = Interviews
Q = Questionnaires
P = Participants
R = Reports

TABLE 3. POSITIONAL ACCURACY REQUIREMENTS

MARINE ACTIVITIES	Desired Relative* Accuracy (m) φ	λ	H	Desired Absolute** Accuracy (m) φ	λ	H
Geodetic Operations						
Control points	1	1	1	10	10	5
Geoid	-	-	0.1	-	-	0.5
Calibration test ranges	1	1	0.3	10	10	5
Gravity base stations	10	10	1	10	10	5
Ocean Physics and Oceanography						
Mean sea level/tides	-	-	-	50-100	50-100	0.1
Ice sheet motion	1-5	1-5	-	?	?	-
Stationary buoys location	10	10	-	10	10	-
Drifting buoys location	50-100	50-100	-	50-100	50-100	-
Ocean Tracking Stations	-	-	-	10	10	5
Search and Rescue and Salvage	1-10	1-10	-	20-100	20-100	-
Ocean Resources						
Geophysical surveys	10-100	10-100	5	?	?	?
Drilling	1-5	1-5	1-5	?	?	?
Pipelines/cable laying	1-10	1-10	-	?	?	?
Dredging	2-10	2-10	-	?	?	?

* Relative - Repeatability
** Absolute - Referenced to known geodetic system

the brevity of this review, we will merely list some of the various systems applicable to marine geodesy surface position determination. Currently, these include electronic systems such as Lorac, Loran, Shoran, Hiran, Raydist, Hydrodist, Autotape, Decca HI-FIX and LAMBDA, RANA, Toran; and satellite systems using Doppler (e.g., Geoceiver), ranging (e.g., C-band radar, laser) and VLBI principles. Sometimes, several of these systems are used simultaneously with least-squares processing or simple averaging of the different coordinates indicated by each system. Such hybrid systems integration should be approached cautiously, because each system usually is based on a different coordinate or geodetic reference system. For geodetic purposes, such an integration should never include astronomic-coordinate-based systems of the inertial navigation type, such as SINS (ship inertial navigation system). Civilian standardization of these various systems or operational performance accuracy establishment for them is lacking, because there are neither the necessary civilian test ranges nor the support for such activities.

Marine geoid determination is still mostly dependent on measured gravity data, supplemented in recent times with satellite-derived geopotential coefficients transformed into gravity anomalies or geoid heights [12, 20, 22]. Sometimes, purely satellite-derived data are used [19]. Astro-geodetic techniques have had limited use and success [23], due to the nonexistence of adequately accurate (1 to 2 arc sec rms or better) marine geodetic astronomy instruments. Satellite-derived X, Y, Z geocentric Cartesian coordinates have been transformed into geodetic latitude, longitude, and height as a means of deriving geoid heights. This is done by assuming that the geoid and the sea surface nearly coincide, so that the orthometric height, H, is zero and, hence, the geodetic height, h, equals the geoid height, N [18, 21], based on the relation that

$$N = h - H \quad . \tag{1}$$

Further details about various practical and theoretical details of the marine geoid are discussed in Reference [4].

Ocean Bottom Geodetic Control

It is not the intention here to review the concepts of ocean bottom controls and the various experiments conducted so far. These have been extensively publicized in literature, including about ten publications of the authors. References [1], [3], [5], [6], [10], [11], [15], [16] and [17] and their bibliographies may be referred to for further details. The rest of the text is restricted to results of some of the latest investigations of the authors.

A geodetic control point is a physically marked point whose three-dimensional geodetic coordinates are known in a chosen geodetic datum. In the case of the ocean bottom control, the marker has usually been an acoustic transponder or hydrophone. One of the most practical uses of geodetic control is for future relocation of position whose coordinates are known. For obvious reasons, a minimum of three and an optimum of four or more ocean bottom markers in a previously surveyed array are used at sea. Position relocation from a functioning array is easy and involves the survey principle of "resection". The exacting part of the task, especially in terms of accuracy, is the initial process of determining the geodetic coordinates of each marker of the array.

The geodetic principle adapted for marine geodetic control point establishment is based on the classical surveying technique of "intersection". Each surveying surface ship position is the "instrument station" from which the spatial range or distance between the instrument station and the bottom control marker is made. In three-dimensional space, the necessary and sufficient condition for unique position location by intersection is three spatial ranges measured from three noncolinear preknown stations to the marker being located [6, 18]. The accuracy of the new position's coordinates is dependent on the (1) coordinate accuracy of the instrument stations, (2) spatial distribution of both the instrument stations and the new point being located--the influence of geometric configuration, and (3) accuracy of the measured ranges. These sources of errors are not unique to marine geodetic control establishment. Each time the coordinates of a new point are determined from the coordinates of previously established reference points or stations, either by "intersection" or "resection", these three sources of error come into play. Sometimes, for practical expendiency, the coordinates of the reference stations are treated as if they were errorless. Examples are (1) star coordinates used in geodetic astronomy, (2) satellite ephemeris used in satellite geodesy, (3) tracking station coordinates for orbit definition, and (4) terrestrial geodetic network coordinates used in network extension and/or densification. Theoretically, this assumption of errorlessness should be avoided. In practice, the influence of errors in the reference station coordinates cannot be completely eliminated but can be statistically minimized by well-known error modeling techniques. However, this merely gives a better propagation of estimated errors of the reference coordinates and a more reliable variance-covariance estimate of the new coordinates. In an absolute sense, the accuracy of coordinates of the new station can never be superior to that of the reference points.

The results of a limited investigation of accuracy criteria in marine geodetic control establishment are given below, and Referenc [5] contains further details. Table 4 shows results concerning errors in the reference or instrument stations (surface ship positions, in this case) from a simulation computation. The ship's coordinates, the transponder (ocean bottom marker) coordinates, and the corresponding exact range from ship to transponder were simulated. Random errors of practical magnitude were added to the ship's coordinates and the simulated ranges. These modified data were then used to compute the new coordinates of the transponder and their variances. The absolute error of recovery, i.e.--the difference between the exact coordinate value and that computed from the modified data--is given for the cases in which ship position errors are "modeled" or "not modeled". The results, as to be expected, show that, by assuming errorlessness when the ship positions have errors, misleading variance estimates of the transponder coordinates are obtained. By applying error

TABLE 4. EFFECT OF EFFICIENT ERROR MODELING[a]

	Recovery of True Coordinates of Transponder in Meters			
	Ship Position Errors Not Modeled[b]		Ship Position Errors Modeled[c]	
Transponder Coordinates	Absolute Error of Recovery of Transponder Coordinates	Precision of Recovery-The Square Root of the Variance Indicated by Weight Coefficient Matrix	Absolute Error of Recovery of Transponder Coordinates	Precision of Recovery-The Square Root of the Variance Indicated by Weight Coefficient Matrix
X	-22.8	±3.6	-1.9	±20.5
Y	-3.0	±2.1	-0.2	±20.0
Z	12.6	±3.3	1.4	±20.1

(a) The simulations involved the following errors:
Ship Positions - ±20 m in each of X, Y, Z
Slant Ranges - ±3 x (a function of Slant Ranges).

(b) "Not modeled" assumes errorless ship coordinates.

(c) "Modeled" takes into account errors in ship coordinates.

modeling, the variance estimate gives a better indication of absolute accuracy. However, Columns 2 and 5 of Table 4 indicate that absolute accuracy of the new coordinates is bounded by errors in the reference station coordinates. As in all geodetic intersection or resection computations, the coordinates of the ocean bottom transponders are automatically in the same geodetic datum as the surface coordinates.

In marine geodetic control point establishment, the issue of spatial distribution of points or geometric configuration can be analyzed in terms of slant range (ship to transponder distance) versus ocean depth ratio. Figure 2 shows the results of a simulation study in terms of accuracy of position recovery as a function of the slant range/ocean depth ratio. It appears that the optimum ratio lies between 1·2 and 1·9. Problems associated with the third accuracy criteria--the measured acoustic ranges and the roles of velocity of sound, systems delays, etc., have been discussed in Reference [6]. On the issue of using an ocean bottom control array to track or relocate ships and other ocean surface or subsurface objects by "resection", three transponders give a unique relocation solution. More than three is, however, desirable for practical expediencies, such as for improved position relocation accuracy and accommodation of transponder failures [17]. As in all technical areas, necessary and sound mathematical models are available, but adequate statistical models are subjects for research.

The results of actual measurements achieved in the past are briefly summarized. In the Pacific experiment, a standard point error of ± 16 m to ± 18 was achieved in determining the horizontal geodetic coordinates of a marine geodetic control point with respect to the U.S. geodetic datum (NAD 27). The point was about 200 km from shore at depths of about 2000 m. Each line between the U.S. land control point and the ship was independently measured 16 times using aircraft LORAC line crossing technique [2, 14]. In the Bahamas experiment, standard errors of ± 6 to ± 7 m were achieved in determining the horizontal geodetic coordinates and errors of ± 2 to ± 3 m in determining the depth. Most important, however, was the achievement of

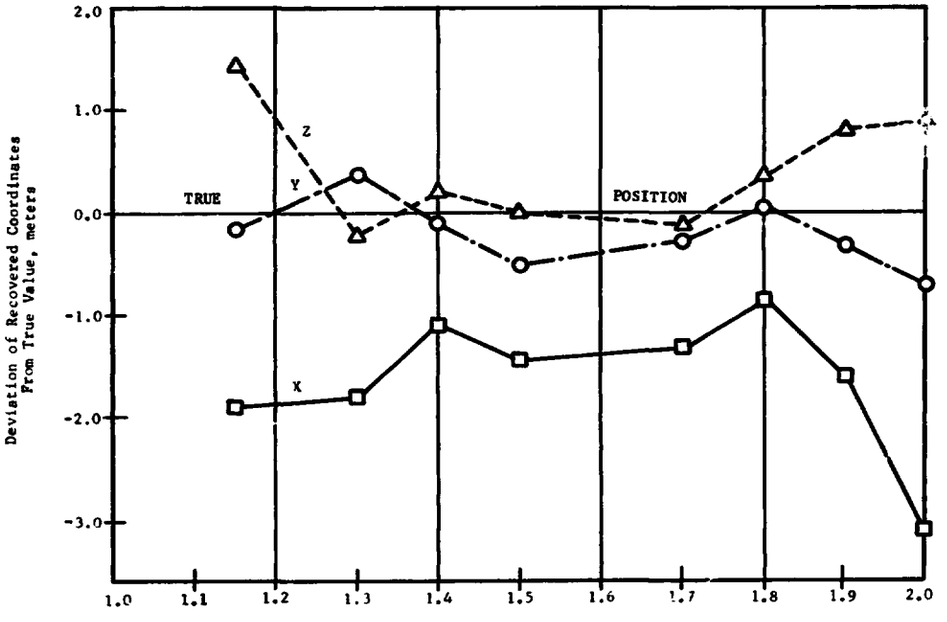

FIGURE 2. INFLUENCE OF GEOMETRIC CONFIGURATION IN 3-D LEAST SQUARES SOLUTION FOR GEODETIC LOCATION OF OCEAN BOTTOM TRANSPONDER

a ± 1·6 standard deviation in recovery of ship heights above the transponders using independent acoustic range measurement from the ship to the ocean bottom transponders (see Figure 3).

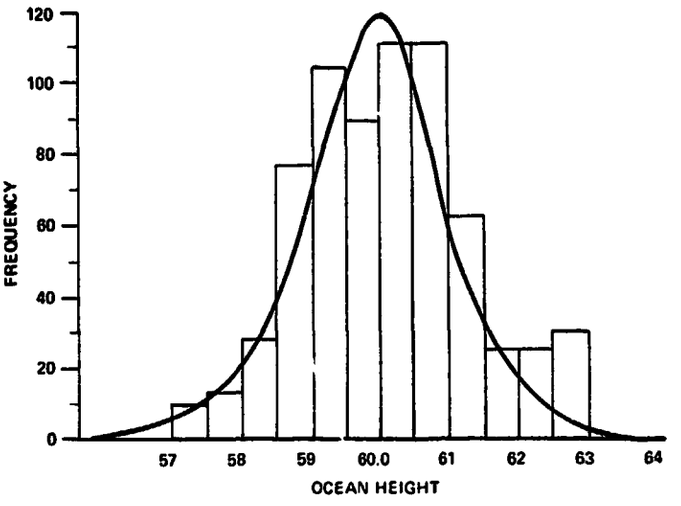

FIGURE 3. PRECISION OF SHIP HEIGHT DETERMINATION FROM OCEAN BOTTOM MARINE GEODETIC CONTROL

CONCLUSION

Marine geodesy has been shown to be highly relevant to man's various practical and scientific operations at sea, including those on the continental shelves. Being a new geodetic venture, it has many unanswered challenges that should be adequately addressed to permit full realization of its great potential. The following is an extract from Resolution No. 4 of IAG during the IUGG General Assembly in Moscow in 1971. The International Association of Geodesy recommends that (1) the following activities be encouraged: (a) establishment of "marine test sites" or "marine geodetic ranges", (b) conduct of "controlled condition" experiments to determine the best accuracy attainable...; (2) determination of the form of the geoid by satellite altimetry; (3) design and conduct of specific marine geodetic experiments, and development of improved data-analysis techniques and (4) development of astronomic instruments that are usable at sea and capable of obtaining 1 second of arc or better in position determination. This resolution is a recognition of the potential practical and scientific applications of marine geodesy, but it has largely remained an unanswered challenge.

ACKNOWLEDGEMENT

The information in this paper is based on results of research over several years, supported in parts by NASA/HQ, NASA Wallops Flight Center and Battelle's Columbus Laboratories. The authors are indebted to various NASA personnel, especially Mr. D. Rosenberg, Dr. M. Swetnick and Mr. H. Ray Stanley for various roles in research support.

REFERENCES

1. Anonymous, Proceedings of First Marine Geodesy Symposium, U. S. Government Printing Office, Washington, D. C., 1967.

2. Curlin, M. H., "LORAC System Trilateration for an Experiment in Marine Geodesy", Presented at the 2nd Marine Geodesy Symposium, New Orleans, Louisiana, November 3-5, 1969.

3. De Luchi, D. A., Error Analyses of Various Acoustic Transponders Networks, a Thesis, The Ohio State University, 1968.

4. Fubara, D.M.J., and Mourad, A. G., Requirements for a Marine Geoid Compatible with Geoid Deducible from Satellite Altimetry, Proceedings of NOAA/NASA/NAVY Conference on Sea Surface Topography from Space, NOAA TR ERL 228-AOML7, Boulder, Colorado, 1972a.

5. Fubara, D.M.J., and Mourad, A. G., Marine Geodetic Control for Geoidal Profile Mapping Across the Puerto Rican Trench, Draft Report Prepared by Battelle's Columbus Laboratories to NASA Wallops Flight Center, under Contract Number NAS6-2006, April 1972b.

6. Fubara, D.M.J., Non-Classical Determination of Spatial Coordinates of Ocean-Bottom Acoustic Transponders, Bull. Geod., 107, 43-63, 1973a.

7. Fubara, D.M.J., and Mourad, A. G., Applications of Satellite and Marine Geodesy to Operations in the Ocean Environment, Technical Report by Battelle's Columbus Laboratories to NASA Wallops, under Contract Number NAS -2006, March 1973.

8. Fubara, D.M.J., and Mourad, A. G., Impact of Satellite Altimetry on Geodetic Datum Definition, Proceedings of Int. Symposium on Redefinition of North American Geodetic Networks, University of New Brunswick, Fredericton, Canada, May 1974.

9. Fubara, D.M.J., Fischer, N. H., and Robinson, A. C., Applications of the Geoid and the Role of Satellite Altimetry, Technical Report to ECON, Inc. to NASA/HQ Office of Applications, 1974.

10. Husson, J. C., and Thieriet, D., "A Proposed Aid to Geodesy: The Spatial System (GEOLE)", International Hydrographic Review, Vol. XLVII, No. 2, July 1970

11. Knowles, T. C., and Roy, R. D., Geodetic Survey of Deep Ocean Acoustic Transponder Array and Evaluation of Recovered Ship Locations, Paper presented at the AGU Fall Meeting, San Francisco, December 4-5, 1972.

12. Moritz, H., Combination of Satellite Harmonics and Gravimetry, Report Number 146, Department of Geodetic Science, Ohio State University, Columbus, Ohio, 1970.

13. Mourad, A. G., Frazier, N. A., Holdahl, J. H., Semeraski, F. W., and Hopper, A. T., "Satellite Applications to Marine Geodesy", NASA CR-1253, January 1969.

14. Mourad, A. G., Holdahl, J. H., and Frazier, N. A., "Preliminary Results of the Establishment of a Marine Geodetic Point in the Pacific Ocean", Bulletin Geodesique, No. 96, pp 107-124, June 1970.

15. Mourad, A. G., New Techniques for Geodetic Measurements at Sea, Transaction American Geophysical Union, EOS, 51, pp 864-873, 1970.

16. Mourad, A. G., Marine Geodesy -- 1967-1971, Special Study Group (SSG1-25) Report to the International Association of Geodesy, Section 1, Moscow, August, 1971, Travaux De L'Association Internationale De Geodesie, Tome 24, pp 109-144, Paris, 1972.

17. Mourad, A. G., and Fubara, D.M.J., Hopper, A. T., and Ruck, G. T., Geodetic Location of Acoustic Ocean-Bottom Transponders from Surface Positions, EOS, Trans., AGU, 53, pp 664-649, 1972.

18. Mourad, A. G., and Fubara, D.M.J., Interaction of Marine Geodesy, Satellite Technology and Ocean Physics, Report prepared by Battelle's Columbus Laboratories for NASA Wallops Flight Center under Contract NAS6-2006, June 1972.

19. Rapp, R. H., Methods for the Computation of Geoid Undulations from Potential Coefficients, Report Number 132, Dept. of Geodetic Sci., Ohio State University, Columbus, Ohio, 1970.

20. Rapp, R. H., Numerical Results from the Combination of Gravimetric and Satellite Data Using the Principles of Least Squares Collocation, Report No. 200, Dept. of Geodetic Sci., Ohio State University, Columbus, Ohio 1973.

21. Stanley, H. R., Martin, C. F., Roy, N. A., and Brooks, R. L., Geodetic Ship Positions from Satellite Measurements by C-Band Radars Confirm Ocean Surface Profile, (Abstract) EOS, Trans., AGU, 52, p 817, 1971.

22. Vincent, S., Strange, W. E., and Marsh, J. G., A Detailed Gravimetric Geoid of North American, North Atlantic, Eurasia, and Australia, paper presented at the International Symposium on Earth Gravity Models and Related Problems, 1972.

23. von Arx, W. S., "Relationship of Marine Physical Geodesy to Physical Oceanographic Measurements", Proceedings of First Marine Geodesy Symposium, held at Battelle Memorial Institute, Columbus, Ohio, 1966, U. S. Government Printing Office, Washington, D. C., 1967.

BOUNDARY AND POSITIONING PROBLEMS IN OFFSHORE NORWAY

S. Bakkelid and J. Chr. Blankenburgh*
Geographical Survey of Norway
Geodetic Department

ABSTRACT

The discovery of natural resources in Offshore Norway has made it necessary to improve the existing navigational systems: Decca Main Chain, Decca Hi Fix and Loran C. In the near future a Navigation Committee will be given the mandate to explore and propose possible changes that will improve the systems. The Geographical Survey of Norway (NGO), who has the responsibility for the geodetic control, will be represented in this committee. This paper presents a preliminary review of the existing systems, and some proposals for new systems. In addition, the geodetic network will be discussed, and a presentation is given of some boundary delineation problems on the Norwegian continental shelf.

DEMANDS ON GEODESY IN OFFSHORE NORWAY - THE OBLIGATIONS OF NGO

The Geographical Survey of Norway (NGO) is the official cartographic institution of Norway. One of its duties according to the directives governing its work, is to provide the geodetic control of official maps and charts. The NGO has taken it for granted that these duties include an obligation to possess adequate knowledge of geodetic theory, and of methods and use of instruments, equipment - and the organization needed to undertake new official geodetic assignments. Determination of boundaries in the North Sea, search for exploitable resources on the seabed and its subsoil, and the discovery of oil and gas deposits in the North Sea, faced the NGO with new demands for its services. The NGO found it important to get to understand the nature of this new activity, and - above all - acquire some idea of what this would imply with regard to navigation and positioning aids, to accuracy of position and boundary determination, all with the aim to make the NGO able to anticipate future assignments in Offshore Norway.

The Norwegian Telecommunication Directorate also had to face very much the same problems as the NGO. On its initiative a meeting was called between representatives of interested authorities and government agencies. The outcome of this meeting was a proposal to appoint a committee - the Navigation Committee - which is to make an appraisal of what kind of services are needed, and of how these are best organized. The draft of the mandate to the Navigation Committee reads as follows:

1. Appraise the requirements and demands of the oil industry as

*On leave to NTNF, Continental Shelf Division.

to positioning and accuracy of navigation on the Norwegian continental shelf - included the requirements for a common reference system.
2. Clarify what known systems - or combinations of systems - do best meet these requirements. Primarily is to be considered the development which has already taken place in the areas of actual interest. Secondarily is to be clarified the question of implementation of new systems - if existing systems give unsatisfactory results.
3. Appraise the suitability and requirements for using permanent installations on the continental shelf as a composite part of navigation/positioning systems, and - if possible - elucidate the problems of legal rights and practical consequences.
4. Give an outline of the costs entailed by the implementation and operation of the different alternatives - including user expences.
5. The proposals from the committee should in particular clarify problems concerning
   a) Use of Norwegian goods and services in connection with extensions or reconstructions,
   b) Practical and economic value of use for users not connected with or part of the oil industry, as the Fishery Inspection, Hydrography, Sea Rescue, Shipping, Scientific Research etc.
6. The work of the committee shall in its conclusion include specification of alternative solutions arranged according to priority determined by the Committee itself.

The Committee has not yet started its work. Points of view and appraisals expressed in this paper, are therefore only those of the authors.

DELIMITATION OF THE NORWEGIAN CONTINENTAL SHELF

The NGO was acquainted with some of the problems associated with the determination of territorial boundaries at sea in 1964, when the boundary line between the UK and Norway was delineated. The Article 6 of the Geneva Convention on the Continental Shelf, and the Geneva Convention on the Territorial Sea and the Contiguous Zone, lay down the principles for determining the territorial boundaries in the continental shelf areas. The Conventions came into force on June 10, 1964. In accordance with the decisions in the Conventions, Norway has concluded agreements about the delimitation of its continental shelf with Great Britain (March 10, 1965), Denmark (December 8, 1965), and with Sweden (July 24, 1968).

In all three agreements it is stated that the delimitation should be based on the median or equidistance-line principle; i.e. that every point of the boundary should be equidistant from the nearest points of the baselines from which the breadth of the territorial sea of each state is measured. The principles for drawing the baselines are given by the Convention on the Territorial Sea and the Contiguous Zone.

The implementation of these principles is rather difficult, and has been very much debated - and will continue to be debated. Due to the increasing importance of the continental shelf areas, we might foresee that baselines will become the subject of negotiations, and/or will need bi-lateral or international (multilateral) recognition - like boundaries on land. The corner points of the baselines should be marked where possible, and geodetical positioned. And the "straight lines" between them should be defined as arcs of Great Circles.

Provided that the fundamental requirement is fulfilled, so that the corner points of the baselines of any two countries are positioned within the same geodetic frame, the median line between

the two countries can be determined mathematically. The median would be a succession of great circle arcs and segments of parabolas, which could be depicted with an adequate degree of accuracy on charts in any scale and projection.

The boundaries between UK and Norway and Denmark and Norway, were determined graphically on specified charts on a small scale (ca 1:1M), inconsistent geodetic frames - and not on shrinkproof paper. The so determined median lines were adjusted slightly to meet administrative requirements. Both boundaries are drawn as great circle arcs between eight corner points, the positions of which are defined by latitude and longitude on European Datum (1st Adjustment 1950), and given with a precision of one second-of-arc on the UK-Norwegian boundary, and with one tenth of a second on the Danish-Norwegian boundary. Before the Danish-Norwegian agreement was amended in 1974, the segments of the boundary were defined as compass lines, and the precision of the corner points was 0.1 minutes-of-arc. Computer checks of spherical distances from a few points on either boundary to points on the baselines agreed within 550 m for the UK-Norwegian boundary, and within 1070 m for the Danish-Norwegian one, which. however, is consistent with chart errors.

The boundary between Sweden and Norway in the Skagerrak, was first determined mathematically as the median line of the baselines. Latitude and longitude of the baseline cornerpoints were, however, poorly determined on the European Datum (~ 100 m). Next, the mathematical median line was approximated by two compass lines and two great circle arcs using the equal area "give and take" principle. The agreed geographical coordinates of the corner points are defined to be on European Datum 1950 and given with a precision of 0.1 second-of-arc. It is argued that this precision (±2 m) is in accordance with probable future needs as to positioning accuracy.

Negotiations between the Soviet Union and Norway about the delimitation of the continental shelf in the Barents Sea is scheduled to start this year. Preliminary talks took place two years ago.

The outer boundary of the Norwegian continental shelf in the Norwegian Sea is not determined. The principles of delimitation of continental shelf areas towards the high sea will be on the agenda of the Conference on the Law of the Sea at its meeting in Caracas, Venezuela in June this year.

POSITIONING RELATIVE TO A MARINE BOUNDARY

Marine boundaries, such as fishing limits, continental shelf delimitations, territorial water deviding lines, or consession limits, are mostly given as a great or small circle arc, a loxodromic line or even more commonly as a "straight line" between given points in terms of geographical coordinates.

A great circle arc is a good approximation to the shortest line between two points on the surface of the earth, and is increasingly used as boundary dividing line. On ordinary nautical charts on the Mercator projection, a compass line is always a straight line. A great circle arc, however, will ordinarily be depicted as a curve.

The maximum separation of the portrayed dividing line and the straight line between corner points on a chart, is dependent on the definition of the line, the azimuth, the length and the mean latitude of the curve segment, and on the projection of the chart. The segments of the boundaries of the Norwegian continental shelf so far established, are "great circle arcs" between a sequence of corner points.

To demonstrate the size of maximum separation of the boundary and the straight line between corner points, we give the values for the segments of the Danish-Norwegian and the British-Norwegian boundaries with the greatest and smallest separation on a chart on Mercator projection:

	Segment	Sph.dist (km)	Azimuth (°)	Latitude (°)	Separation (m)
Denmark-Norway	3-4	27.1	70.0	57.7	21
	6-7	93.0	61.0	56.9	228
UK-Norway	2-3	147.9	165.0	57.3	98
	7-8	44.1	164.0	61.5	22

Navigation and positioning relative to a boundary requires therefore, either tabulated coordinates of points on the boundary, lying close enough to permit interpolation with adequate accuracy, or charts with the boundary depicted. For actual needs charts on scale 1:25 000 to 1:50 000 would do.

POSITIONING REQUIREMENTS

In 1960 the Ministry of Defence and the Ministry of Fisheries jointly appointed a Committee to Investigate the Demands for Electronic Navigational Aids for the fishing fleet and other users. The Committee collected reports from the Fishing Fleet, the Fishery Inspection, the Hydrographic Office, the Polar Institute, the Oceanographic Research Institute, the Sea Rescue Service, the Navy, the Merchant Marine, and the Directorate of Aviation on their needs with regard to range and accuracy of navigational aids.

We have to assume that the requirements of these users, are the same to-day, and certainly not less, and should be satisfied also in the future, and not sacrified for the benefit of new users with different requirements.

Designation of desired accuracy as "very high", "highest degree of accuracy", "exact" and "best possible" is vague and does not mean the same from one user to the other. The different users realize they will have to make do with what is available at any time. Improvements will be helpful and even necessary and will be used, but they are limited to what is technical possible and justifiable from an economic point of view. For most users it was and is quite impossible to state either the upper limit for the accuracy that can be used to advantage, or the lower limit where the navigational aid ceases to be of any use at all.

The Committee analyzed the requirements of the different users and concluded that 5 Decca Main Chains along the west coast of Norway and three Consol stations to a large extent would cover the registered requirements. The proposed installations were established.
The Committee did not consider the requirements of the oil industry. This activity had only made a feeble start in the North Sea at that time, and only in areas outside Norwegian waters.

REQUIREMENTS OF THE OIL INDUSTRY

Systematic hydrocarbon exploration of the North Sea began in 1961. The first legislation relating to Exploration and Exploitation of Submarine Natural Resources on the Norwegian Continental Shelf was enacted in 1963.

The first reconnaissence licence and the first production licence was issued in 1963 and 1965 respectively. Since then it has been

a rapid increase in exploration and exploitation activities, so far, mainly restricted to the North Sea south 62° N.

The oil industry incorporates a variety of activities; exploration, surveying and engineering work, where relative or absolute positioning is an important facet. Such as - without pretending to be exhaustive,

1. The need to correlate sub-bottom seismic surveys with drilling holes, since these operations cannot be carried out simultaneously.
2. The necessity of returning to and recovering the unmarked well head.
3. The surveying of pipeline routes, and the subsequent laying of pipelines along the selected route.
4. The need to survey in detail on a large scale, and pinpoint rig positioning, fixed platforms, or sea bed structures, and likewise return to exactly the same point for construction work.
5. To be able to define with accuracy boundaries of concession and median lines.

The required or optimum accuracy varies of course somewhat from one application to the other. For exploration work an accuracy of 30-50 m relative to a specified reference frame, is acceptable. For other applications a higher accuracy can be used to advantage, and in some cases will be a necessity. Positions, however, are determined at the surface of the sea and a very high accuracy would be invalidated by projection of the position to the sea bed. It seems that a repeatability of 10-15 m would do well for most applications, and that with present techniques it is possible to achieve this accuracy in positioning in large parts of the North Sea. Special conditions, however, as prevailing adverse weather and sea conditions, might be detrimental to its implementation. High latitude has its advantages: Navy Navigation Satellite passes are more frequent, making Doppler positioning more applicable for updating of integrated positions.

EXISTING POSITIONING SYSTEMS

The Norwegian Decca Main Chain, composed of five single chains established 1967-1969, covers the offshore areas of the western and northwestern coast of Norway. Decca chains in the other countries around the North Sea, cover the remaining part of these waters. The Norwegian Defence Communications Administration inspects and monitors the Norwegian chain on an assignment from the Ministry of Fisheries. The British chain is operated by Decca Navigator Co Ltd. On establishing the Norwegian chain, the special Norwegian topography made it difficult to find suitable station sites, considering such things as access, ground plane conditions, groundpath length, and lightning danger.

Antenna positions were determined geodetically, partly by NGO and partly by private surveying companies. NGO assumes that the relative standard accuracy of any two stations of a Decca chain in continental Norway, is better than ±2 m. The Vestlandet chain has one of its slave stations in Shetland. Chains in UK and Norway are all referred to European Datum, but due to error propagation in the geodetic grid, the chains on each side of the North Sea will be on different local geodetic frames, which introduce ambiquity of the positions. The amount is difficult to assess, but is estimated by Decca Navigator Co to be not more than 120 m. Corrections are applied, leaving ±10 to ±30 m as a probable residual ambiguity.

The different chains have throughout its area of coverage a varying fixed error, which is the difference between pattern and Decometer position, and is caused by instrumental deficiencies and

effects of ground conductivity on propagation.
Superimposed is the varying or repeatability error caused by instrumental instability, and varying atmospheric and ionospheric conditions. Maps showing repeatability accuracy are available for the different chains. We can read from these that the attainable repeatable positioning accuracy using Decca for the two important areas Ekofisk (φ = 56,5° N, λ = 3° E) and Frigg (φ = 60° N, λ = 2° E) are 200 m and 50 m respectively.

Adverse physical performance characteristics of the Decca Navigator System is its susceptibility to skywave interference.

Loran C was established to cover military requirements in the North-Atlantic. For navigation in Offshore Norway the stations Sandur (Iceland), Bø and Jan Mayen (Norway) and Sylt (Germany) are available, with their Master station at Eide (Faeroe Islands). Advantages of the system are: Little skywave interference and extensive coverage. Disadvantages are unsatisfactory geometry for greater parts of the Norwegian shelf.
The existing Loran C chain covers only a part of the Barents Sea and with poor geometric fixing accuracy.
Loran C is used extensively in Offshore Norway by exploration companies for lane identification by concurrent application of Decca, and as a composite part of integrated systems for lane. identification and for continuous speed and heading determination alone, or as a back-up for Doppler Sonar.

Decca Main Chain, Loran C and the other electronical aids to navigation such as LORAN A and Consol that existed in the early sixties did not satisfy the requirements of the oil industry. The research and engineering work on the continental shelf that was initiated, required the development and wider use of electronic positioning systems designed specially for survey work rather than navigation.
This requirement was more perceptible in the North Sea than for most offshore areas of the world with similar activity, where the exploration and production started close to the shore, and was successively developed in areas more distant from the shore.

In the North Sea, and in particular on the Norwegian shelf, the activity started 100-200 miles offshore and is still localized to such areas. To meet the further requirements of the oil industry, Decca established Decca Hi-Fix chains on either a semi-permanent, or a "on call" basis. Permanent chains in the Norwegian part of the North Sea are: Hordaland, Rogaland, Cromarty, Forth. Mobile Hi-Fix systems, which can be established to meet a temporary need, are also available. In Offshore Norway these are used by the Hydrographic Office and the Polar Institute for hydrographic surveying.

According to statements by major companies operating in the offshore industry and from other sources, it has become clear that because of shortcomings of the existing systems, there is an urgent need for more accurate position fixing systems. This applies not only to the oil industry, but to some extent also to hydrographic surveying of fishing grounds, minelaying and minesweeping, and for the surveillance of the fishing limit, especially if a 50 or 200 mile limit is introduced.

For implementation of this, three roads are open:
1. Improvements and optimisation of the existing systems.
2. Establishement of new systems giving adequate overall coverage and accuracy for all users.
3. Establishment of new systems for particular areas or for particular engineering tasks.

IMPROVEMENTS AND OPTIMISATION OF THE EXISTING SYSTEMS

There is probably little to be done to improve the repeatability accuracy of a particular system. The fixed error relative to a specified Datum can to some extent be determined. Such determinations are currently done by the Hydrographic Office for Decca Main Chain on the Norwegian Coast, using the well established method of observing the position of the ship's receiving antenna by hydrodist, theodolite, or a combination of these, computing the geoid coordinates of this intersected or resected position, converting to hyperbolic pattern coordinates, and comparing these with the observed pattern readings. By this method the fixed error can be determined only for points relatively close to shore.

The Decca Survey Limited have also made extensive determinations of the fixed error within 15 km of the coast. The calibration data so obtained, were used to determine the fixed error for far offshore areas by extrapolation. The unusual advantage of the North Sea is that phase comparison signals can be received from opposite shores, and from widely differing directions, providing observed data with which to test these extrapolations. A network of traverses was observed in each of which simultaneous records of as much as nine or more patterns at each station and at frequent intervals

Over-land radio propagation can often not be avoided for Decca position fixing near the coast. The very low conductivity, and the rugged, mountaineous topography contribute to an extremely complex pattern of fixed errors. In fact, it is very difficult to chart these errors, but very roughly, let alone to publish corrections in a rational and meaningful way. Attempts to define the fishery borders in terms of Decca coordinates have therefore been somewhat discouraging. Nevertheless, the variable errors are generally small enough to make the chains useful for many purposes in near-shore navigation.

Mathematical formulas developed to take propagation variations into account when computing radio position lines, can only be used with advantage in cases of very simple topography. In the case of the Norwegian coast, it is virtually impossible to find a terrain model to fit the formulas.

For special purposes, such as offshore surveying etc., more accuracy could be attained when using Decca main chains in a direct ranging mode. This necessitates that the chain's frequency is controlled by an atomic frequency standard, and also that an atomic frequency standard is carried on board the survey vessel. The cost of equipment and modifications is moderate compared with many other systems proposed for such purposes. By this procedure, overland propagation paths could be avoided or minimized, and LOP pattern geometry could be improved. This would result in reducing both fixed and variable errors. However, the day-to-night ratio of variable errors would not be appreciably improved.

ESTABLISHMENT OF NEW SYSTEMS

To discard the existing systems and replace them by new systems is an economic impossibility. There are too many users and too big investment made, so it is reasonable to assume that supplementary systems will be established as the need arises. The number of systems, however, must be kept at a minimum, considering both economic aspects and that a modest use of frequencies should be persued. All relevant positioning systems, Hi-Fix, Toran, Loran etc., operate in the frequency band 1.6-3.3 MHz, which internationally is allocated to radiocommunications. There is no international provision in this band for frequencies for use of navigation. Furthermore, this band is for international use. Allo-

cations of frequencies are therefore subject to negotiations and neighbourly sharing of frequencies with neighbouring countries.

Several instrument firms have submitted plans to the Norwegian government for establishment of new systems in the 100 KHz band: Decca Survey Limited UK, and Kongsberg Våpenfabrikk (KVF), Norway, have applied for concession for Mini Loran C systems. The Decca version is named Pulse 8 and the KVF (Mega Pulse) version is named Accufix. The systems will be operated separately or more likely in cooperation by the two firms.
Offshore Navigation has also applied for concession for a Mini Loran C system (Accufix).
Kelvin Hughes has proposed the establishment of a Toran system.

It seems reasonable to choose systems that have a high repeatability accuracy, and to determine the fixed error by geodetic methods close offshore. To test the extrapolated or mathematically derived fixed errors throughout the pattern, every opportunity to establish test points should be made the most of. Such opportunities will be provided by permanent or semipermanent production platforms. In the absence of such, bottom transponder systems or surface buoys could be used as exceptional checkpoints. Buoys could also carry instruments for recording of pattern variations. Permanent constructions as the Ekofisk-tank, can provide a site for a station for positioning system.

GEODETIC FRAME AND REQUIRED IMPROVEMENTS

Determination of boundaries, establishment of these on the ground and establishment of adequate aids for navigation and positioning, require, as we have seen, a geodetic frame. Continental Norway is completely covered by geodetic horizontal control on the European Datum 1950, and so are the other land and island areas surrounding the North Sea.
The adjustment of the first-order triangulation network of continental Europe was initiated in 1945 and finished in 1951. This first adjustment was not considered to be the final one by any of the countries involved, and it was decided as early as 1956 at a meeting in Munich, that a new adjustment (RETrig) should be made. This will probably be done in the near future.

Since the first adjustment there has been a steady work to improve the networks and the data. In Norway the first order network has been extended to cover the whole country using trilateration. Two distances across Skagerrak were measured in 1972 using a slightly modified commercial microwave rangefinder. The method has been developed at the Technical University of Hannover, and is based upon superrefraction in the maritime surface layer. The method allows measuring of more than 130 km long distances when an evaporation duct is present above a surface of water. In 1963 a new connection between the British and the French triangulation was added to the former. A recomputation of the Shoran triangulation is foreseen, and will probably be incorporated in the new RETrig. Data from Geoceiver observations at two Shoran stations in UK and three Shoran stations in Norway will also probably be available and incorporated in the RETrig.

The accuracy of the present horizontal control has been satisfactory for most practical needs, so far. For points on either side of Skagerrak the estimated relative accuracy is 1:100 000. For the relative accuracy of points on either side of the North Sea, in UK and Norway, the available estimates are less reliable. Figures of ±10 to ±30 m are quoted, probably based on the results of the Shoran connection. An ambiguity of this size does probably not satisfy present requirements, and even less those of the future.

The North Sea, 200-400 miles across, is surrounded by land and

islands separated by narrow straits. The RETrig, being a product of sophisticated statistical tests and adjustment procedures, will hopefully provide a consistent geodetic network throughout this area, and throughout Scandinavia. It is reasonable to anticipate that the relative accuracy between points in UK and Norway will be better than 1:100 000, and this should be a fully adequate accuracy for all forseeable applications anywhere in the North Sea.

Going northwards we come into the Norwegian Sea. Geodetic control on the shelf in this area has to be extended from the coast of Norway by classic or Doppler satellite methods. Jan Mayen was positioned by Doppler in 1968.

In the extreme north we have the Barents Sea and the shelf surrounding the islands of the Svalbard archipelago. The Barents Sea is less confined than the North Sea. The islands there have a wider separation, which is difficult to bridge using classic geodetic methods.
New-Alesund on West-Spitsbergen and six other points in the Svalbard archipelago were determined in 1971 by Doppler translocation. An additional tie between the archipelago and continental Norway should be contemplated. The station in New-Alesund is also determined by the satellite-triangulation method.

The delimitation of the shelf between Soviet and Norway presupposes that the land and island areas of the two countries surrounding the area to be partitioned, are brought into the same geodetic frame, which one, is of no consequence for this particular purpose. This can only be accomplished at required standard by the use of geodetic Doppler positioning procedures.

Knowledge of geoidal heights is necessary for the transferring of two-dimentional Dopplercoordinates to European Datum.
Inertial navigation needs to know the deflection of the vertical. Integrated navigation should also benefit from a better knowledge of the geoid as it would reduce the standard error of geographical coordinates. Our present knowledge, nowever, of the details of the local geoid is poor. Estimated heights might be in error by more than 10 m.
Several methods can be applied for the determination of the geoid in offshore areas. They all either depend on the knowledge of the geoid in surrounding land areas, or benefit from such knowledge. Knowing the geoid on land it can be extended offshore by Doppler translocation or inertial navigation between points of known positions. Conversion of geoidal heights and deflections of the vertical determined gravimetrically or by altimetry on a different datum to European Datum, can be based on the knowledge of the geoid in adjacent areas.

We conclude that it should be to the purpose of the NGO to pursue determination of the geoid in Norwegian offshore areas more vigoriously, and that dynamic satellite positioning will be an indispensable tool for geodetic positioning offshore as for the establishment of the geodetic frame for such work.

It is the opinion of the authors that it is imperative that the NGO has the knowledge and facilities to carry out such work to geodetic standard.

REFERENCES

Tamsborg, Milan. Geodetic Hydrography as related to Maritime Boundary Problems.
(in The International Hydrographic Review. Vol.LI(1974) No 1.)

Beazly, P.B. Territorial Sea Baselines.
(in The International Hydrographic Review. Vol.XLVIII(1971) No 1)

Roberts, W.J.M. Large Scale Offshore Surveying for the Oil Industry. Decca Survey Ltd, London (1970).

Figure 1. The Norwegian Continental Shelf south of 62° N. with Territorial Boundaries and Leases December 31 1973

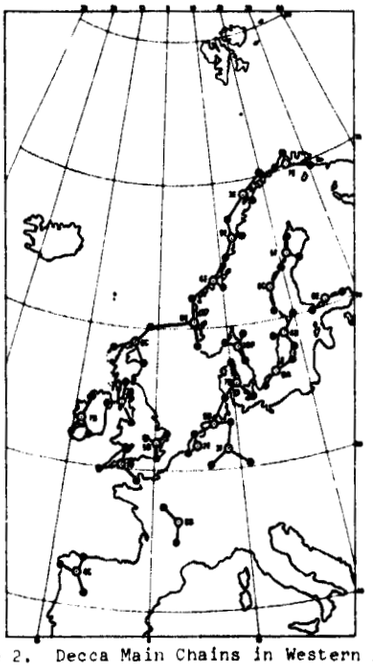

Figure 2. Decca Main Chains in Western Europe

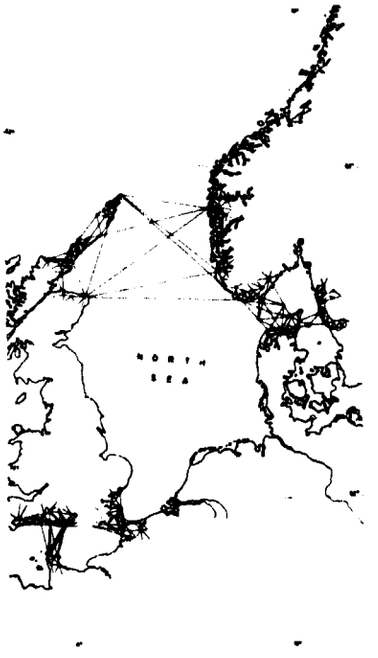

Figure 3. Geodetic Connections across the North Sea

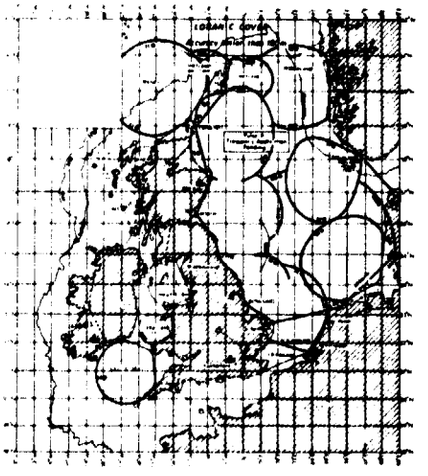

Figure 4. Decca Hi Fix Covering of the North Sea (with repeatability accuracies given by Decca Survey Ltd.)

NAVIGATION REQUIREMENTS FOR MANGANESE NODULE EXPLORATION AND MINING

William D. Siapno and George A. Zahn, Jr.
Deepsea Ventures, Inc.
Gloucester Point, Virginia 23062

ABSTRACT

The paper discusses the navigation and position fixing requirements for exploration and mining of manganese nodules. Four types of surveys are conducted preparatory to actual mining operations--prospecting, preliminary survey, evaluation survey and detail survey. Accuracy requirements for position fixing become progressively more stringent with each advance in stage of survey. The goal is to gather data suitable for shoreside analysis and decision making with regard to the ongoing program.

Exploration and mining in the deep ocean requires the ability to continuously plot the position of survey vessel or mining ship and to track an instrument package or dredge device on the sea floor. Positioning data must be recorded to generate maps of ore bodies, obstructions and claim boundaries. Accuracy of location is of paramount importance for safe operation and to assure efficiency by not reworking areas already mined. Highly accurate and reliable positioning must be achievable over a wide range of environmental and operating conditions.

INTRODUCTION

The subject of navigation and position fixing is basic to the potential ocean miner, just as it is to most other maritime activities. The degree of accuracy and the efficiency with which these functions are accomplished is, however, as varied as the types of maritime activities. The normal merchant ship, while far at sea on a transoceanic voyage, will keep track of its position on a geodetic basis, primarily by reference to celestial bodies, only recently supplemented by long range radio navigation systems. For this portion of the voyage, accuracies on the order of a few miles will suffice. As the ship approaches the coast, the limited range radio navigation aids become available. The mates will take advantage of these systems and will obtain position with accuracies of one mile or better. The final phase of the voyage will be made within the harbor of the destination port. Positions will now be determined within a matter of feet by means of visual reference to fixed objects.

This increase in accuracy, as the ship approaches and gains the land mass, is to be completely expected, as man has spent most of his history ashore. Techniques for the mapping of the land surface have been developed over centuries of practice and,

References and illustrations at end of paper.

in the recent past, precision, accuracy, and reliability have been sharply upgraded. The degrees of proficiency and the accuracy of the results of these surveys have been carefully analyzed. The surveys themselves are classified as to precision and the means to conduct surveys within clearly defined limits of accuracy have come to be everyday happenings.

The extensions of these standards to the ocean, beyond where a bottom-mounted platform can be erected or line of sight signals can be received from a shore station, is yet to be achieved for commercial programs. In mid-ocean the survey platform is, for practical purposes, continuously in motion, both horizontally and vertically, and there is no easy means to mark and identify a given site. This is the problem which is presented to the potential ocean miner.

THE PROBLEM

In a situation somewhat analogous to that of the conventional ocean transit, the ocean miner's navigational requirements change, not, however, as a function of the phase of the voyage, but rather as a function of the current phase of activity in which he is then involved.

The phases of a commercial mineral exploration program leading to full scale ocean mining have been identified variously. One such scheme groups the activities into four principal areas:

Prospecting - Seeking of nodule deposits of potential commercial interest.

Preliminary Survey - Coarse Grid surveys to define the suitability of the topography for further activity.

Evaluation Survey - Sampling surveys to delineate the extent of the deposit and confirm the deposit as an ore body.

Detail Surveys - Fine Grid surveys to develop mining plans for ore acquisition.

As with the merchant ship, the ocean miner's navigational requirements become more demanding as he approaches his goal, the end of his voyage. Unfortunately for the ocean miner this is not the familiar and hospitable land mass, but rather, the deep and unfamiliar mid-ocean regions.

One of the major aims of each of these surveys is to produce a chart or map. These are graphic presentations of features in respect to their position on earth, or relative to each other. Problems regarding the production of maps have long been with us, but only in the recent past has the need arisen to accurately map features of the ocean floor in great depths of water and at great distances from shore. Each of these factors; accuracy desired, water depth, and remoteness from shore, add to the complexity of map generation. Combined, they represent a fundamental problem for the potential ocean miner.

OBJECTIVES

The generation of a topographic map has traditionally been one of the early steps in mineral exploration and development. The extension of this requirement to manganese nodule resource evaluation is premised on the need to find areas of acceptable

relief and roughness. These conditions assure survival of the bottom traversing devices and permit their efficient operation.

The development of a bathymetric map, of the maximum accuracy feasible within the constraints of time and cost, is therefore of first order importance in the mid-ocean exploration program. The data for this map also forms the basis of the topographic map. This work will be initiated during the preliminary survey phase of the operation.

Prior to this time, reasonable means to produce a contour map of large areas (in the order of 15-20 thousand square miles) of the sea floor have not been available. The intention now is to equip ocean exploration vessels with the necessary equipment to allow a continuous plot of the vessel's position within specified limits, and record this data in conjunction with information obtained from a precise narrow beam bathymetric system.

The accuracy with which position (x,y data) must be known in order to generate a satisfactory bathymetric (z data) map depends on a wide number of variables. Included in these variables are; the purpose for which the map is to be generated, the variability of the topography, and the accuracy with which the depth can be measured.

For the ocean miner the basic purpose of the bathymetric and subsequent topographic maps has already been identified. It is to identify areas of sufficiently low relief over large enough extent so as to provide a reasonable probability that the necessary ocean floor mining equipment will not only survive, but will in fact perform its required function with an acceptable efficiency. We have previously identified the acceptable depth variation within a given local area as being in the order of ±100 feet with slopes not exceeding 10 degrees.(3)

As the program continues, it will become necessary to identify and locate obstructions of considerably smaller dimensions than ±100 feet and so it is reasonable to expect that greater positional accuracies will be required.

The variability of the topography is generally little known during the initial phases of the survey, in fact, determination of the variability is the reason the survey is being conducted. Surveys conducted using wide beam bathymetric systems tend to mask some of the variability, particularly the narrower valleys.

In the present discussion the only "Z" variable considered is water depth, however, maps must also be developed based on numerous other quantities such as nodule concentration and mineral assay. The variability of these quantities may be quite different than the variability of topography and may cause changes in the required positional accuracies. An experiential judgement will be required on the basis of the results of some of the initial survey work.

The accuracy with which depth can be measured is primarily a function of the equipment being used. Conventional wide beam acoustic systems, which insonify areas of the ocean floor in excess of five square miles when operating in water depths of 15,000 feet, can hardly justify an ultra precise navigation system, or form the basis of a detailed topographic map. For this reason narrow beam systems incorporating stabilized transducers and other advanced features must be considered. Such a system utilizing a 2-2/3 degree beam width will insonify an area of less than 1/100 square mile and can measure differences in depth of less than two fathoms.

The navigational accuracy which we feel is required for the preliminary surveys, as outlined earlier, is the ability to define the ship position continuously, during transit or wide area survey, within ±0.2 NM. The vessel operational characteristics associated with this requirement are speeds in the order of seven knots while towing a near surface submerged body in seas up to five feet. The surveying will be continuous on track lines up to 150 miles long.

EXISTING SURVEY STANDARDS

A review of the existing standards for hydrographic surveys was made in order to determine the reasonableness of the above operational requirement. Three "standards" were identified, each somewhat different in statement and requirement.

The first of these is the International Accuracy Standard for Hydrographic Surveys adopted at the 7th Cartographic Consultation of the Pan American Institute of Geography and History meeting in Mexico City in 1955.(2) The same standards were recommended by the United States for adoption by the International Hydrographic Bureau States Members at the 7th International Hydrographic Conference in Monaco in May 1957. For depth, the maximum error increases from one fathom in depths to 11 fathoms up to one percent of the depth in areas 55 fathoms and deeper. Spacing of sounding lines, interval of plotted soundings, frequency of position fixes and accuracy of fixes, are all defined in terms of measurements made on the final chart and are therefore a function of the resultant chart scale.

The second of the standards is that listed in the NOAA surveyor's "bible", Publication 20-2, The Hydrographic Manual of the Coast and Geodetic Survey of the U. S. Department of Commerce.(2) Survey line spacing, frequency of sounding, frequency of position fixing and accuracy of sounding are identified both with relation to the final chart scale as well as the general depth in the area for which the chart is being developed. There is no absolute statement of positional accuracy required, rather, specific procedures are identified for determining position which it must be presumed will yield adequate control. It must be noted, however, that most of the work covered by this manual is close to shore where visual or highly precise radio navigation systems are available.

The third standard is that of the U. S. Navy Hydrographic Office as stated in Special Publication SP-4, Technical Specifications for U. S. Naval Surveys.(1) These are stated in the same manner as the International Standards and generally agree with them, however, the line spacing is halved and fifty percent more cross lines are required. The required positional accuracy is the same. The Hydrographic Office Manual in addition recognizes a "bathymetric survey" although not providing specific data accuracy requirements. Navigation "in accordance with best standard practices" is as far as they go although they do acknowledge that "the value of the data obtained will be much greater when the ship's position is determined as frequently and precisely as practicable."

A summary of Deepsea Ventures' proposed practice for three levels of survey is presented in Table 1 and also compared with the International Standard.

From this discussion so far it can be deduced that the normal hydrographic chart is primarily concerned with the safe navigation of a vessel and not the detail character of the bottom. This is an essential difference between the ocean miner's needs and those of the normal maritime chart user.

An additional difference is that the miner's needs for information increase with distance from land and water depth rather than the opposite, which is the need for safe navigational purposes. In fact it should be noted that the ocean miner's requirement is such that he essentially demands charts of the accuracy and scale of conventional harbor charts. The difficulty arises in that these charts must be developed in areas of the deep ocean far removed from the land supported precise navigation systems.

It is expected that, in order to provide the desired accuracy figures for the survey vessel, an integrated navigation system incorporating: (a) a gyrocompass, (b) a precise log system, (c) a satellite navigation receiver, (d) a long range radio navigation interface, and (e) a central digital computer will be required. Numerous authors, among them Morgan and Stansell et.al.[5 & 6], have presented the capabilities of various systems, but so far the required accuracy does not appear to be fully available, although it does not seem to be beyond our grasp.

One of our purposes in presenting this paper is to identify our needs to the navigation community in the expectation of uncovering a satisfactory solution. Without this identification we cannot expect the industry to develop systems which will do the job.

ADDITIONAL REQUIREMENTS

A further difficulty with regard to the navigational problem develops during the evaluation surveys, when the vessel will no longer be operated in a continuous mode on long survey tracks. These surveys will involve a great deal of maneuvering and repeated stopping to launch and recover sampling devices. No longer will we be able to refine our dead reckoning over long tracks or collect data amenable to post mission manipulation to improve our estimates of position.

While it is true that we will be able to tolerate some degradation in positional accuracy at this time, the extent of this relief is not so great as to totally avoid any problems. During this phase of the operation we would expect to introduce Omega data into our integrated navigation system. Omega will provide continuous positional data while the satellite system will be used to aid in determining the appropriate corrections. It is hoped that this type of combined system will be able to supply positional data during this period of survey in the order of ±1.0 NM on a full time basis.

The final phase of the exploration program is the conduct of detail surveys to develop mining plans for ore acquisition. These surveys are also required to identify and locate obstructions which must be avoided during the actual mining operations. As with the merchant ship entering port, the ocean miner's requirement for positional accuracy has increased to its maximum. But the problem does not end there. Because of the data required at this time, a deep towed instrument platform will be used. This device will include such sensors as: real time TV for bottom observation, still cameras for high resolution bottom photography, depth and altitude sonars to obtain microbathymetry, forward scan sonars for obstacle detection, side scan sonar for increased bottom coverage and devices for collection of sediment or nodule samples. Now we must know not only the ship location, but also the location of the instrument package, and we must know these locations within limits unheard of for deep ocean navigation. Positions for this phase of exploration are

essentially the same as for the actual mining phase and we consider ±75 feet as the realistic requirement.

Again in a situation similar to the merchant ship in the harbor, our navigational requirements no longer need be referenced to geodetic position, but can be relative to local fixed markers. It is because of this change in system reference that we may be able to satisfy this requirement.

Table 2 provides a brief summary of the accuracies and ranges of a number of navigation and position fixing systems. The only systems capable of the positional accuracies in the order required are the local acoustic systems.

The use of acoustic equipment during a detailed bathymetric survey is discussed by Keibuzinski.[4] The purpose of this survey was to form the reference for the Bathymetric Navigation System (BNS) used to accurately position the tracking ships during the NASA Apollo Project. The detail survey of the deep ocean accomplished at that time probably provides the closest similarity to the survey needed by the ocean miner.

SUMMARY

It has been our intention that this short paper present to the navigation community, the requirements which we, as ocean miners, feel will be necessary for the satisfactory accomplishment of our goal. Unlike the defense oriented military systems, the ocean miner exists in an environment of firm budgetary and schedule limitations and his specific desires are often significantly affected by these factors.

We feel that the positional accuracy requirements identified herein can be satisfied within the limits of the above constraints and will be adequate for our needs. Experience may in time demonstrate that our present estimates are either too lax or too stringent.

REFERENCES

1 Hydrographic Office Technical Specifications for U. S. Naval Surveys and Supplementary Data, U. S. Navy Hydrographic Office, SP-4, 1961.

2 Jeffers, Karl B., "Hydrographic Manual," U. S. Department of Commerce, Coast and Geodetic Survey, Publication 20-2, 1960.

3 Kaufman, R. A. and Siapno, W. D., "Future Needs of Deep Ocean Mineral Exploration and Surveying," Offshore Technology Conference Preprints, OTC 1541, May 1972.

4 Keibuzinski, G. I., "Ocean Bottom Mapping and Navigation Calibration in Real Time," Second Symposium on Marine Geodesy, Marine Technology Society, November 1969.

5 Morgan, J. G., Kronberger, F. P. and Strickland, J. V., "Accuracy of an Integrated Satellite Navigation System Obtained from Geophysical Survey Data," Offshore Technology Conference Preprints, OTC 2009, May 1974.

6 Stansell, Thomas A., "Accuracy of Geophysical Offshore Navigation Systems," *Offshore Technology Conference Preprints*, OTC 1789, April 1973.

TABLE 1

COMPARISON OF INTERNATIONAL STANDARDS AND PROPOSED DEEPSEA PRACTICE FOR THREE TYPICAL CONDITIONS

TYPE OF SURVEY	PRELIMINARY		EVALUATION		DETAIL	
Distance "X"	80 n.mi.		50 n.mi.		10 n.mi.	
Distance "Y"	150 n.mi.		80 n.mi.		10 n.mi.	
Area	12,000 sq.mi.		4,000 sq.mi.		100 sq.mi.	
Scale [1]	1:200,000		1:120,000		1:25,000	
Miles/In	2.78		1.66		0.35	
Chart Length	54 inches		48		30	
Accuracy Standard	INT [2]	DVI [3]	INT	DVI	INT	DVI
Spacing of Sounding Lines	1.11 n.mi.	5.0 n.mi.	0.66 n.mi.	5.0 n.mi.	0.14 n.mi.	0.5 n.mi.
Spacing of Cross Lines	8.35 n.mi.	5.0 n.mi.	5.0 n.mi.	5.0 n.mi.	1.04 n.mi.	0.5 n.mi.
Sounding Interval (Along Lines)	0.56 n.mi.	75 feet	0.33 n.mi.	Variable	0.07 n.mi.	15 feet
Fix Spacing (Along Lines)	4.5 n.mi.	10 n.mi.	2.5 n.mi.	Variable	0.5 n.mi.	15 feet
Maximum Allowable Position Error	±0.14 n.mi.	±0.20 n.mi.	±0.08 n.mi.	±1.0 n.mi.	±105 feet	±75 feet
Allowable Depth Error	25 fm.	±2 fm.	25 fm.	±2 fm.	25 fm.	<1 fm.

(1) Scale based on vertical chart dimension limited to 30 inches.
(2) Based on International Hydrographic Conference Standards.
(3) Proposed Deepsea Ventures practice.

TABLE 2

SUMMARY OF NAVIGATION SYSTEM
RANGE AND ACCURACY

SYSTEM	RANGE	ACCURACY
Satellite System	Global	<200 ft rms (fixed location)
Hyperbolic Systems (Long Range)		
Omega	Global (when fully implemented)	1-2.0 nm
Loran-A	700 nm (day) 1400 nm (night)	2.0 nm
Loran-C	1200 nm	250-1500 ft
Hyperbolic Systems (Medium Range)		
Decca Navigator	250 nm	0.25-2.0 nm
Lorac	200 nm	15-300 ft
Decca Survey	200 nm	25-300 ft
Decca Hi-Fix	25-200 nm	3.7 ft (hyperbolic) 2.5 ft (2-range)
Rana F&G	50-76 nm	30-75 ft
Toran	400 nm	3-100 ft
Consul	700 nm	6.0 nm
Ranging Systems		
Radar (typical)	420,000 ft	±5.0 ft
LAMDA	150-400 nm	15-40 ft
Hydrodist	25 nm	5-100 ft
Shoran	12-40 nm	30-50 ft
EPI	12-400 nm	135-1500 ft
Raydist DR-S	250 nm (day) 150 nm (night)	"few meters"
Acoustic System	Approximately 6 nm in 18,000 ft depth	range within 5 ft position within 50 ft

Seabed Assessment, Resource Geology And Their Relation To Marine Geodesy

Edward M. Davin
Office For The International
Decade Of Ocean Exploration
National Science Foundation
Washington, D.C. 20550

ABSTRACT

A major goal of the International Decade of Ocean Exploration (IDOE) programs is to expand Seabed Assessment activities to permit better management of marine mineral exploration and exploitation by acquiring needed knowledge of the dynamic processes of the ocean floor and continental margins. Studies of the continental margins of South America and Africa are now underway. The processes operative at mid-oceanic ridges and deep trenches are being investigated on the Nazca Plate and the Mid-Atlantic Ridge. The mineral resources of the ocean floor, especially manganese nodules, are the subject of several studies. Satellite navigation reduced the uncertainty in surveying methods to hundreds of meters. Increase pressure for exploitation of the seafloor will require a precision location methods with undertainties of a few meters or less.

INTRODUCTION

The International Decade of Ocean Exploration's program in Seabed Assessment is designed to increase understanding of the geologic processes active along the continental margins, the mid-oceanic ridges and the deep ocean basins. Geologists are investigating these processes as part of their efforts to understand global tectonics. At the same time, these resource geologists are discovering that they generate the raw materials of industrial civilization, petroleum and heavy metals. The projects supported by IDOE are designed to be useful to resource geologists, but do not duplicate the efforts of oil and mining companies. Until the present time, we have been answering first order questions and satellite navigation has been adequate for our needs. As we undertake more precise measurements, however, the requirements for more precise locations is bound to increase. I plan to review the several areas of current investigation and will leave to the potential users of these data the need to determine the degree of geodetic precision required.

CONTINENTAL MARGIN STUDIES

Our present knowledge of the continental margins is based largely on work done by oil companies and, therefore, is greatest for the U.S. Gulf Coast, Venezuela, the North Sea, etc. Work by oceanographic research institutions has been handicapped by lack of multichannel seismic equipment which records deep penetration seismic equipment. This equipment is both costly to acquire and the data equally costly to process. Our present state of knowledge of continental margins varies from the poorly known areas

which have bathymetry only to the well known areas which have sediment and geophysical data. Those that are moderately known have either sediment or geophysical, but not both.

Major studies of the continental margins along th South Atlantic are now underway. These are known as "rifted" continental margins because they are formed by the spreading mid-oceanic ridge and its associated fracture zones. The continental margin of Peru-Chile parallels a deep trough which is the surface trace of the edge of the Nazca Plate as it moves under the continent of South America. A third type of margin is the island-arc marginal trench system of East and Southeast Asia. Studies in this area are just getting underway.

In the South Atlantic, scientists from Woods Hole Oceanographic Institution have completed a systematic study extending from Port Elizabeth, South Africa to Lisbon. Although track charts concentrate on the continental margin, a few regional lines extend out the Mid-Atlantic Ridge. A total of 50,000 kilometers of seismic reflection, gravity, and magnetics were recorded. Precision bathmetry data and seismic refraction data, using sonobuoys, were routinely recorded. Location of lines at sea was controlled by satellite navigation.

These data are now being analyzed. Preliminary reports, however, indicate two areas of potential oil accumulation: one in a thick sedimentary section off the delta of the Orange River in Southwest Africa; the other, a large diapiric salt basin extending from Angola to Nigeria. The areal extent and thickness of both deposits were outlined using geophysical methods, and their internal structure has been analyzed using seismic reflection and refraction data.

On one or more of the various legs, twenty-one scientists, technicians, and students from Argentina, Brazil, the Republic of the Congo, England, France, Portugal, the Republic of South Africa, and Spain participated. Preparatory to the cruise, about 150 African and other interested scientists received a bathymetric atlas, and preliminary reports on geomagnetics, gravity, and sediments. The profiles and charts of geophysical data from the 1972 cruise were printed and distributed in January 1973.

A similar study, being carried out simultaneously in the Southwest Atlantic, will extend from the Scotia Arc to the Caribbean. This cooperative program involves scientists from the Lamont-Doherty Geological Observatory, the Woods Hole Oceanographic Institute, Brazil, Argentina and France. A Brazilian Research vessel was equipped under the guidance of WHOI scientists. Teams of scientists from Brazil trained to study the mineral distribution along the continental shelf. Scientists from both Brazil and Argentina have received additional training aboard ship and in residence at Lamont and Woods Hole. Two-ship refraction will add greatly to our understanding of the structures of the prominent ridges which run normal to the coast line and of the great sedimentary thickness such as the Amazon cone.

We are now reaching the stage where it will be possible to match up key features on both sides of the Atlantic. Areas of great salt accumulation on the Sao Paulo Plateau appear to be the counterpart of the large salt deposits off Angola. Indeed, during the early stage of opening of the Atlantic, the Rio Grande Rise, a major feature off Brazil, and Walvis Ridge off Southwest Africa, may have served as a restricting barrier, which not only formed the large salt basins, but also the restrictive sedimentary conditions necessary to produce large scale oil accumulation. The geologic age of the oil fields on both sides of the Atlantic is approximately the same as the early opening of the Atlantic Ocean.

This project is being followed with great interest by oil company geologists for the value to several fundamental problems in oil geology.

METALLOGENESIS AND PLATE TECTONICS

The concept of plate tectonics, that has provided a unifying theory to the study of the earth, throws new light on the processes of mineral deposit formation. The suites of rocks formed in some large mining areas appear to have been formed originally under marine conditions. The Kuroko copper deposit in Japan and the well-known copper mines of Cyprus appear to have been formed by processes now recognized on the mid-oceanic ridges. The large scale copper deposits of Peruvian and Chilean Andes may be the end product of the processes now active on the Nazca Plate.

As part of its program in Seabed Assessment, the International Decade of Ocean Exploration supports basic research proposals which contribute to our understanding of the genesis of metallic ore formations under marine conditions. The IDOE interest is based on hypotheses on the origin of ores which developed out of the concept of plate tectonics. Since many metallic ore deposits were formed under marine conditions, better understanding of these conditions will provide more powerful exploration tools in the search for new deposits of strategic metals. Conversely, it is recognized that the occurrence of the metals in themselves provides evidence of the conditions under which the earth's crust is formed.

The Nazca Plate is defined on the west by the East Pacific Rise and on the east by the Peru-Chile Trench. As new crust rises to the surface along the East Pacific Rise (EPR), it carries with it heavy metals, some of which become part of the crust and others are deposited as sediments. The Bauer Basin, which parallels the EPR, is particularly rich in metalliferous sediments. Since the rate of spreading along the EPR is relatively high, the processes producing metals must be quite intense. Along the Peru-Chile Trench geophysical data suggest that the plate is moving under the South American Continent. The high pressures and temperatures at depth may transform the crust and sediment and ultimately produce the mineral deposits found in the Andes of Peru and Chile. Isotope studies in mining areas suggest that the ores were formed under marine conditions. Isotopes are being used to test this thesis by tracing key isotopes from their sources on the EPR, across the plate and across the subduction zone into the mountain front.

The Hawaiian Institute of Geophysics (HIG) and Oregon State University are conductiong a study of the plate margins using complimentary geophysical, geochemical and geological techniques. Scientists from Colombia, Ecuador, Peru, and Chile are all actively participating in the cruises and in the data analysis. In addition, a large-scale study of the subduction zone under the Andes, as it extends from Colombia south through Chile, is being done simultaneously by the Carnegie Institute. Although this study goes beyond the scope of IDOE, the data on the subduction zone has obvious implications for the Nazca Plate metallogenesis study and vice versa.

Studies along the Mid-Atlantic Ridge are being carried out in several places. A major project is jointly supported by U.S. and French Scientists in an area near the Azores. During the past three years, site surveys have aimed at identifying an area of unusual seafloor activity. The project will reach its culmination this summer when teams of U.S. and French scientists using manned submersible crafts will descend to the rift valley. Approximately fifty dives are planned: thirty by the US ALVIN

and another twenty between the French Archimede and Cyranus. These trained scientists. will make first-hand observations from the submersible, take photographs, collect samples and emplace geophysical instruments. These data will be evaluated by teams of scientists on the R/V KNORR and plans made for guiding subsequent dives to the most interesting scientific sites. The Glomar Challenger will attempt to drill its deepest hole to date in the igneous rocks of the earth's crust. This will be compared with the section measured along the rift valley. Last August, investigators from the U.S. and Canada drilled a 3,000 foot hole in the Azores. The hole encountered submarine volcanic rocks and high temperature hydrothermal solutions at shallow depth. The hole temperatures (200° C) forced termination of the drilling far short of the goal of 5,000 feet.

Results from all three projects are being coordinated and should provide valuable insights into those processes driving the ridge apart and others that are concentrating heavy metal deposits.

MANGANESE NODULES

The third major area of investigation is the origin and distribution of manganese nodules. It is estimated that approximately 25% of the ocean floor is covered with these deposits and that their total weight approaches 600 million tons. "Polymetallic" nodules is a more descriptive term, since in addition to high percentages of iron and manganese, nodules may contain a variety of minerals including copper, nickel and cobalt in economically attractive amounts. Although the existence of the nodules has been known since the days of the first Challenger expedition in 1871, they have remained largely a geological curiosity until the steady rise in the price of copper made mining feasible. The factors which control the copper and nickel content are not clearly understood, at least not to a degree where large scale mining operations can begin with the assurance that the presence of nodules with consistant high metal content can be predicted. Under the IDOE/SBA program, therefore, focus is placed on the origin and distribution of the nodules. A workshop was held at Lamont, in January 1972, which brought together all interested parties. There was widespread agreement that substantial amounts of data were available but not yet published. Phase I of the IDOE project, therefore, was to publish a series of world wide synoptic maps of the chemical composition of the nodules and the chemical and physical properties of the substrate. As a result, it appears that an area near Hawaii is particularly rich in copper and nickel. Phase II is now underway and will sample this area extensively. Twenty teams of scientists will analyze the results in order to get a better understanding of the processes which form the nodules. If a working hypothesis can be developed, then we envision Phase III as an effort to test this hypothesis in other parts of the world.

NOAA PROGRAMS AND REQUIREMENTS

James Collins
Deputy Director, National Geodetic Survey
NOAA, National Ocean Survey

Joseph D. D'Onofrio
Chief, Satellite and Marine Applications Section
NOAA, NOS, NGS
Rockville, Maryland

ABSTRACT

The National Oceanic and Atmospheric Administration's marine geodetic requirements and mission are discussed. A recent experiment involving the location of offshore structures by Doppler satellite methods is discussed, and the results of this experiment are given. A plan for the cooperative extension of the offshore National Horizontal Control Network and NOAA's policy on the reduction of Doppler satellite observations are presented.

INTRODUCTION

The Department of Commerce's National Oceanic and Atmospheric Administration has the sole responsibility for a number of integrated scientific programs in the marine area. Specifically, NOAA conducts research in the atmosphere, air-sea interface, in the ocean, and on land.

NOAA'S MARINE PROGRAMS AND REQUIREMENTS

The two marine programs within the scope of NOAA's responsibility, that are of interest to this gathering, are the marine charting program and the marine geodetic program.

A. Ocean and Coastal Charting

The principal mission of NOAA's National Ocean Survey and its predecessor, the Coast and Geodetic Survey, is, and has historically been to conduct mapping surveys of the coastal and ocean areas. Originally, the sole purpose of these surveys was to promote commerce along the coast by providing marine charts and other data to aid the navigator. However, today NOAA's marine mapping program has expanded into a multi-disciplined program.

NOS's change from a small charting agency to a multi-faceted marine organization resulted from NOS taking advantage of a data base that extended back to the early nineteenth century. The primary bathymetric, tidal, geologic, and physical water data collected by the Survey provide a long time series from which valuable scientific results can be obtained. Over the years, NOAA

has expanded its marine programs to meet the ever-increasing National need for marine data and marine products.

In addition to the well-established responsibility for providing a variety of data in the marine regions, NOAA has also been responsible for determining various marine legal boundaries. Some of these boundaries are based upon low-water base lines which are determined by NOAA, and are additionally referenced to the National Horizontal and Vertical Datums.

Today NOAA's major marine use of the National Horizontal Control Reference System, or Horizontal Datum, is in the positioning of vessels engaged in bathymetric charting surveys. Recent developments in the marine area and advanced technology dictate that accurate geodetic positions be established and permanently marked in the ocean areas. Large-scale hydrography, necessary for detailed offshore site planning, cannot adequately be accomplished without an accurate, well-spaced geodetic reference network offshore.

B. Geodetic Reference System

NOAA and its predecessors have been expanding and developing national spatial reference systems since 1816. These systems are the National Horizontal and Vertical Control Networks to which most state and national boundaries are referenced.

The extension of the horizontal and vertical control networks into the marine area logically followed the requirement for positional information offshore. Prior to offshore mineral development, NOAA's only marine geodetic requirement was the positioning of vessels engaged in survey activities. However, today many industries require a well-monumented, accurate offshore reference network.

MARINE GEODESY WITHIN NOAA

NOAA's mission in marine geodesy is a natural result of its original coastal mapping and land-based geodetic statutory responsibilities. The congressional charge to survey the coasts included the delineation of low-water lines; and the position of this low-water line has recently been used as a base from which various territorial boundaries are derived.

The determination of geodetic positions of points in the marine area is a logical extension of the horizontal survey control network on land. An example of this extension is the offshore mineral lease boundary delineation. These lease boundaries are described in terms of state plane coordinates which are, in turn, derived from geodetic coordinates referenced to the horizontal survey control network.

A. NOAA's Marine Geodetic Mission

NOAA's marine geodetic mission is identical to its National mission of providing and maintaining survey control networks. Monumented points in these networks are planned to be of sufficient density so that major boundaries and features can be located from the network monuments.

This does not mean that NOAA is responsible for individual boundary determinations. Locating offshore

lease boundaries, and insuring that drilling, mining, and other activities are confined to the proper lease area are the responsibility of the private sector. Privately-owned surveying firms are currently providing offshore developers with excellent service in this regard.

However, it is NOAA's responsibility to see that there are sufficient offshore network reference monuments so that the private sector can conveniently and adequately do its job.

B. History of Network Extension into the Marine Area

The extension of the national survey reference networks into the offshore area has logically followed technical offshore development. As lease parcels further offshore began to be developed, interest in parcel boundary location and state-federal boundaries prompted NOAA to make tidal and horizontal surveys in marine areas. In 1959 the first major low-water line delineation survey was undertaken off the coast of Louisiana. This survey has become the standard for state-federal offshore boundary determinations.

The Horizontal Control Network was first extended into the marine area in 1955 at the request of the Offshore Petroleum Industry. This survey, and a subsequent survey in 1963, used conventional triangulation procedures to extend the control network into the offshore areas.

These surveys were a logistics nightmare. Personnel and equipment had to be transported by boat from staging areas onshore to offshore rigs--at times under severe weather conditions. When adjacent platforms were widely separated, Bilby steel towers had to be erected on platform decks. The conventional triangulation procedures proved to be costly, but were the only means available at the time to provide accurate offshore positions.

C. NOAA's Present Marine Geodetic Experience

The use of Doppler satellite positioning equipment is a relatively new method that is described in detail in numerous papers on the subject. NOAA's experience with satellite systems to date includes both onshore and offshore position determinations.

NOAA is currently systematically determining the position of approximately 100 horizontal control points throughout the United States by Doppler satellite techniques. These points will be used in the redefinition of the new North American Horizontal Datum, expected to be established by 1980.

In the early part of this year, NOAA teams occupied two offshore drilling platforms to test the feasibility of using Doppler satellite positioning of offshore structures. Chevron Oil Company platform number 160A, located about 40 miles offshore, was occupied in early February, and Pennzoil platform 587A, 100 miles offshore, was occupied in late February. Both of these occupations by NOAA Geoceiver teams followed the same procedure that is used for positioning land stations; that is, 40 passes of a Navy Navigation satellite were observed with a Magnavox Geoceiver, and the point was permanently marked. Although Doppler satellite receivers have been used aboard ship for navigation for some time, NOAA had not previously used a Geoceiver to position an offshore structure.

The Chevron platform occupied had been positioned by conventional surveys in 1963. This structure provides a base or reference to which the Geoceiver position can be compared.

The second structure, 100 miles offshore, had been previously located by a private surveying firm.

The operational test conducted by the NOAA team provided a realistic appraisal of the applicability of using this method to position offshore structures. Since no major problems were encountered, the project was an operational success. It was therefore concluded that Doppler satellite positioning would be highly adaptable to offshore use.

D. NOAA's Future Marine Geodetic Programs

NOAA recognizes the fact that a continuing need for network reference monuments exists in the marine area. Research into improved techniques for providing ocean monumentation is a continuous search. Current advances in technology are being monitored by NOAA with the anticipation that new and improved instrumentation may someday solve the permanent geodetic marker problem.

Due to practical considerations, network markers now must be placed on existing offshore platforms. Since 1963 over 400 offshore platforms have been erected and located by private surveying firms. In most cases, the techniques used to locate these structures provide excellent positional information that can then be reused to locate additional platforms. However, from NOAA's point of view, positions obtained by private surveyors cannot be accepted and published by the Federal Government without verification.

NOAA's policy of publishing positions of network points, that are doubly determined, has been strengthened by the numerous court decisions based upon the near infallibility of network markers.

Geodesists within NOAA have arrived at a scheme that will satisfy both the federal requirement for positional integrity and also take advantage of the voluminous survey work performed by private contractors. It has been proposed that Doppler satellite positions be established on key offshore platforms, to which observational data determined by private firms could be referenced. For example, if the corner stations in a rectangular array were positioned by Doppler satellite techniques, other platforms in the area could be located from the satellite positioned structures. The corner stations in the array could be held fixed, and the observed distances between contiguous platforms would be used in a least squares solution to minimize the errors in the platform locations. This scheme provides sufficient verification of the survey work so that the positions of all stations in the array could be published and thus officially sanctioned.

Implementation of this scheme to publish positions of existing offshore structures will, of course, require the cooperation of both federal and private organizations. However, it is anticipated that the benefits to be derived from this cooperation will be of significant value to all concerned, and that private firms will relinquish proprietary data for the benefit of the public.

When a Geoceiver is used, the positioning of key structures by the Doppler satellite technique provides sufficient redundancy and internal checks so that it would be possible for NOAA to certify the marker location by processing Doppler data collected by non-NOAA survey teams. This means that other federal, state, or private organizations can use Doppler satellite positioning equipment, perform observations according to a specified NOAA scheme, and have NOAA process and publish the location of the surveyed point for a nominal charge.

NOAA geodesists responsible for the satellite program are willing to meet with individuals interested in establishing satellite positioned points and discuss NOAA's program in detail. To date, NOAA has only processed Geoceiver data collected by federal organizations; however, no problem will be encountered by private firms wishing to use NOAA's processing capabilities.

In this paper, the Geoceiver is specifically mentioned as the Doppler satellite positioning device--mainly because this particular instrument is the one currently used by NOAA. Other equally accurate instruments may eventually become available; however, to date no other instrument has been demonstrated to NOAA that has the Geoceiver's capability.

The following steps are involved in determining a precise geodetic Doppler satellite position:

1. Observe approximately 40 passes of a specified Navy Navigation satellite. This requires about 10 days.

2. Submit the data to NOAA for processing in mutually agreeable format.

3. NOAA will then request the post-ephemeral data from the Naval Weapons Laboratory.

4. The post-ephemeral data is matched to the observed data, and a geodetic position of the point is determined.

This entire process normally takes from six to ten weeks, depending on workload, request and receipt of post-ephemeral data, and related considerations. It is expected that government and private surveyors could receive geodetic positions of points about two months after they submit their observed data to NOAA.

Individual programs will be reviewed by NOAA, and any help that can be given to the private as well as public sector will be gladly given. Satellite positioning holds promise for the future, in that geodetic positions can be determined for remote points fairly easily and rapidly. NOAA accepts the challenge of this new method and hopes to be in the vanguard for developing new and improved programs and services for the benefit of the public.

The advantages of the Doppler satellite system are such that point positions can be established rapidly and economically in an absolute sense. This method provides only latitude and longitude; however, azimuths must be

determined by another method such as astronomic observations. Furthermore, intervisible structures can be readily located by conventional methods.

NOAA recommends that Doppler satellite positioning be used in combination with triangulation and trilateration to position offshore structures.

OCEANOGRAPHY AND THE MARINE GEOID

John R. Apel and H. Michael Byrne
Ocean Remote Sensing Laboratory
Atlantic Oceanographic and Meteorological Laboratories
National Oceanic and Atmospheric Administration
Miami, Florida 33149

ABSTRACT

Topographic features of the sea surface of interest in physical oceanography are briefly reviewed and the relationships between these features, the marine geoid, and satellite altimeter measurements are discussed. Oceanographic requirements on measurement of the marine geoid are laid out in light of forthcoming attempts to determine ocean topography from spacecraft. Sampling intervals for altimetric data in time and space are suggested, and methods of separating geoidal and oceanographic components offered.

INTRODUCTION

The suggestion that precision altimetric measurements made from spacecraft could be used to observe several interesting oceanographic phenomena[1] has led to a set of measurement requirements on the marine geoid that are very difficult to meet. A root-mean-square precision in geoidal heights of $\pm$ 10 cm, relative to the center of mass of the earth, has been specified as one ultimate requirement for determining the global ocean circulation with a precision of order $\pm$ 20 cm/s in the surface current speed. In this paper we will sketch out the oceanographic features to be addressed, briefly explain their relationships to the geoid, and offer suggestions for arriving at the measurements of interest.

TOPOGRAPHIC FEATURES ON THE OCEAN SURFACE

The explanation of the steady-state and time-varying departures of the ocean surface--termed sea surface topography--from a gravitational equipotential surface is found from the application of the hydrodynamic equations to the case of fluid flow on a rotating earth. From the momentum equation for a nonviscous fluid,

$$\frac{\partial \vec{u}}{\partial t} + \vec{u} \cdot \nabla \vec{u} + 2 \vec{\Omega} \times \vec{u} = - \frac{1}{\rho} \nabla p - \vec{g},$$

one takes the vertical (z) component to obtain the hydrostatic equation for steady, uniform flow:

$$0 = \frac{\partial \rho}{\partial t} + \rho g \ ;$$

the horizontal component yields the so-called geostrophic flow equations[2]:

$$(2\ \vec{\Omega}\times\vec{u})_h = -\frac{1}{\rho}\nabla_h p$$

This last equation states that, for steady flow at a velocity $\vec{u}$ to exist on an earth having a rotational angular velocity $\vec{\Omega}$, a horizontal pressure gradient $\nabla_h p$ must develop to offset the horizontal component of Coriolis force, $(2\ \vec{\Omega}\times\vec{u})_h$. This horizontal gradient is obtained via the fluid tilting itself with respect to the local level surface, or geoid, in such a way as to just balance the Coriolis force. For present purposes, we define the geoid to be that surface assumed by a uniform, motionless ocean on the rotating earth, in the absence of tidal forcing, wind stress, and barometric pressure variations.

The slope of any isobaric surface, relative to the geopotential surface, tan γ, can be simply related to the fluid velocity at that surface and the Coriolis parameter $f = 2\Omega\sin\Lambda$, where Λ is the latitude. In particular, for the free upper surface of the ocean, the surface speed u_o due to this geostrophic balance is given by

$$u_o = \frac{g}{f}\tan\gamma_o, \qquad (1)$$

so that surface slopes, relative to the geoid, measure surface current speeds.

Although it is not apparent from this simple derivation, the velocity, u_o, as given by Eq. (1) is a combination of baroclinic and barotropic components. The baroclinic component is due to horizontal density gradients in the ocean and gives rise to vertically varying velocities. A barotropic current system is constant throughout the veritical water column and can exist in a homogeneous ocean. A barotropic current system can be measured by measuring the surface slope. It is the combination of the two currents that is measured by altimetry at the ocean's surface.

The slopes of even rapidly moving current systems such as the Gulf Stream are very small, of order $1\text{-}2 \times 10^{-5}$ for speeds of order 200 cm/sec. Figure 1 shows a typical rise in the surface of the Gulf Stream in traversing across the current from west to east; a one-meter elevation occurs over a cross-stream

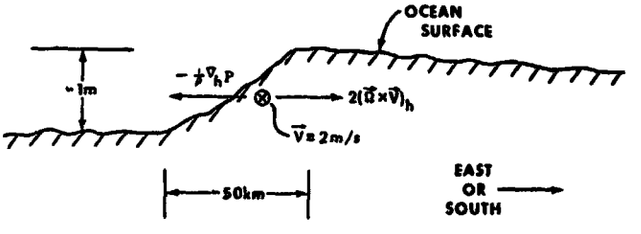

Fig. 1 - Topography of northwestern boundary of Gulf Stream sh balance between Coriolis f and horizontal pressure gra t

distance of approximately 50 km, which, according to Eq. (1), is due to a surface speed of approximately 200 cm/s at $\Lambda \approx 40^{\circ}$. Figure 2 illustrates the overall relief of the western Atlantic as calculated from long-term current averages for that area; the elevations are given in centimeters relative to the geoid[3]. It is seen that, while the slope of the northwest edge of a western boundary current is relatively steep, the general circulation away from the boundary currents results in a topography whose slope may be of order 10^{-7} in mid-latitudes. Such small values may be very difficult to determine from spacecraft.

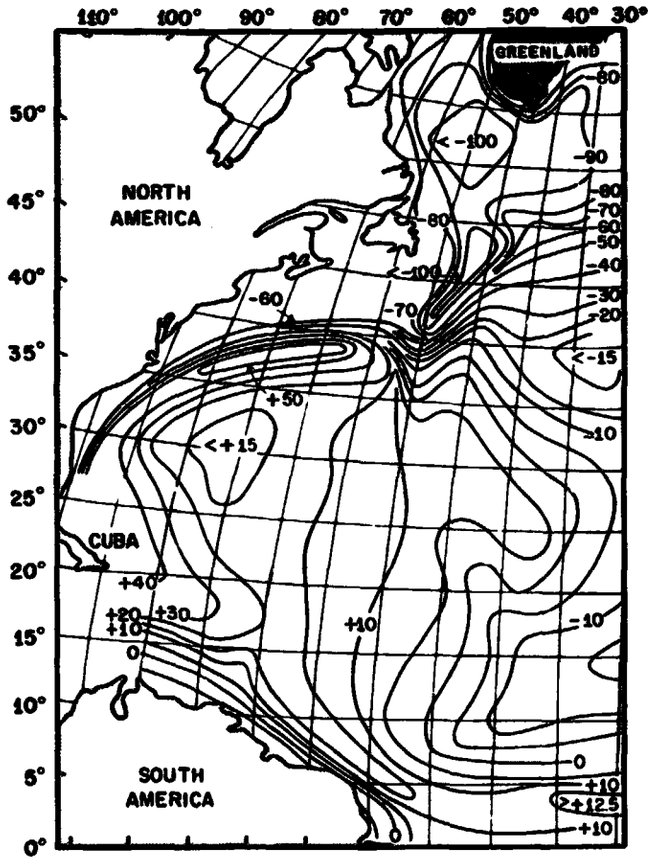

Fig. 2 - Topographic relief due to averaged currents in the western Atlantic (Defant[2])

Rather than being stationary flows, the Gulf Stream, the Kuroshio, and other major current systems undergo considerable variations in space and time, as described by the full hydrodynamic equations. An example of such meanders is shown on Figure 3, which illustrates the positions of the northwest edge of the Gulf Stream as determined by Hanson[4] during approximately 15 months of ship cruises; the spatially growing wavelike features have a period of order 40 days and a wavelength of about 300 km. In this region, the position of the stream axis may shift by amounts exceeding 300 km. Smaller, higher frequency excursions are observed elsewhere. This dynamic behavior differs dramatically from the climatologically averaged picture given in Figure 2, and measuring the variable currents requires reasonably dense sampling in space and time.

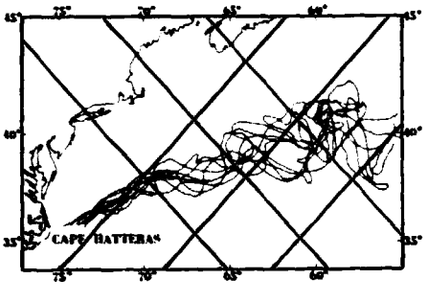

Fig. 3 - Gulf Stream meanders during September 1965 - August 1966, with GEOS-C suborbital tracks superimposed (Hanson[4])

In addition to currents and their associated dynamic topography, many other phenomena lead to departures of the ocean surface from the geoid. Astronomical tides, whose range in the open ocean may vary from essentially zero to greater than 100 cm, occur at well defined frequencies, some five of which contain 95 per cent of the tidal energy. There is considerable spatial variation in the tidal ranges, with the existence of amphidromes (nodes) in the oscillation patterns being a prominent feature predicted by existing tidal models[5]. Only a few dozen deep-sea tide measurements have ever been made, so tide models have little experimental verification.

Long-term wind stress such as trade winds blowing over the ocean will pile up water against the edge of a continent to a height of order one meter. Such a steady-state setup may be difficult to distinguish from geoidal undulations. Short-term, time-varying wind effects due to storms may lead to surges whose height can approach 10 meters over several tens of kilometers along a coast, during a hurricane; such inundations last for only a few hours, however. Atmospheric pressure loading also leads to variations in sea level of about one centimeter per millibar of barometric pressure change, over scales that correspond to the size of atmospheric pressure cells. Finally, tsunamis and ocean surface waves lead to topographic variations ranging from perhaps 50 cm for the former to over 30 m for the latter.

REQUIREMENTS FOR THE MARINE GEOID

In light of the previous discussion, it is apparent that the maximum oceanographic signal, disregarding waves and localized storm surges, is a departure from the geoid of order 1.5 meters, and the associated relative slopes are of order 10^{-5}. If a 10 per cent measurement of surface slope is to be obtained from the differencing of satellite altitude, orbit and geoid measurements[6], it is obvious that the overall noise in these combined measurements must be of order $\pm$ 15 cm over arcs of approximately 1000 km length. A measurement with this accuracy would yield surface currents with a precision of about $\pm$ 20 cm/s, which, in oceanographic terms, is quite a sizable value. (Currents considerably less than 20 cm/s are of interest; at present, there is no spacecraft method apparent for measuring these, with the exception of drifting buoys whose positions are relayed through data collection systems on satellites.)

Figure 4, taken from Fubara and Mourad[7], shows the various earth-oriented surfaces associated with satellite altimetry. For oceanographers, the desired quantity is the sea surface elevation, $GS = \eta(\Lambda,\phi,t)$, expressed as a function of latitude and longitude, Λ, ϕ, and time, t. This will be obtained by simple (but onerous) differencing of the geocentric orbit radius

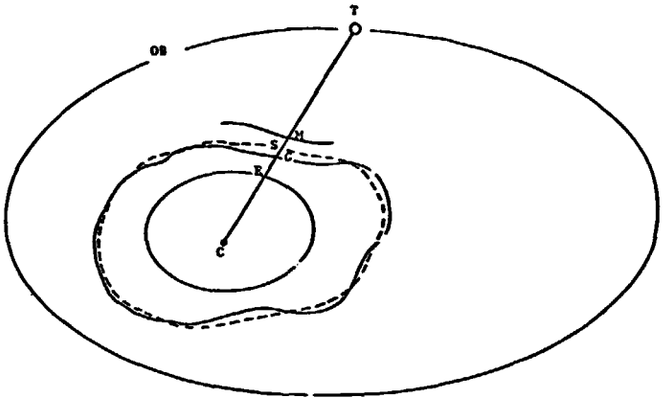

FIGURE 4. REPRESENTATION OF SURFACES ASSOCIATED WITH SATELLITE ALTIMETRY

C = Earth's Center of Gravity

E = Surface of a Geocentric Reference Ellipsoid

G = Geoid (the undisturbed Mean Sea Level)

S = Mean Instantaneous Sea Surface (MISS)

OB = Mean Satellite Orbit

T = Satellite Altimeter at an Instant

M = An Arbitrary Surface Defined by a "Hardware" Calibrated Altimeter

Fig. 4 - Surfaces associated with satellite altimetry (Fubara and Mourad[7])

CT = $r(\Lambda,\phi,t)$, the geoidal height CG = $h(\Lambda,\phi)$, and altimeter elevation ST = $\rho(\Lambda,\phi,t,T)$, via

$$\eta = r - \rho - h. \qquad (2)$$

We have explicitly noted a two-time-scale variation in ρ via t and T. Assuming an error budget of δr = 10 cm for the orbit determination, $\delta\rho$ = 7 cm for a precision altimeter (as projected for Seasat-A, say) and $\delta\eta$ = 15 cm for sea surface topography, as specified above, an rms combination of these errors yields

$$\delta h = 10 \text{ cm}$$

as the allowable geoidal precision. Larger, constant biases are of course permissible since they have little effect on slope measurements.

An up-to-date geoidal calculation[8] that uses a combination of satellite orbital geodesy and integrations of marine gravity data is shown on Figure 5. The contours here are given at one-meter intervals relative to a reference ellipsoid of flattening 1/298.255. It is impossible to accurately estimate the errors associated with this calculation, but they are unlikely to be much below 5 m rms. Early evidence from the Skylab altimeter[9] showing a 4-m undulation associated with the Blake plateau east of Florida suggests high-frequency, 5-m undulations are probably invisible in this model. Thus the oceanographic requirements for a 10-cm geoid are at present away from realization by a factor of order 50.

The question of how to resolve the small, high-frequency geoidal undulations from similar-sized oceanographic ones can be partially answered by using the two time scales, t and T, noted above in Eq. (2). Oceanic features (Gulf Stream meanders, tides, etc.) tend to have long-term variations compared with the smoothly varying satellite changes and can be separated out by appropriate filtering or averaging[10]. The remaining steady-state undulations are then either geoidal or are oceanographically constant in time. An additional clue to separating these comes from noting the strong relation between high spatial frequency geoidal undulations and the local ocean-bottom topography, at least for bathymetric features removed from the abyssal plains, as pointed out by Talwani[11].

After the temporal and spatial differences between oceanic and geodetic undulations have been taken into account, there will remain a body of unresolved topographic features in altimeter data that will be not clearly ascribable to one class or the other. These may only be removed by patient work at sea, through shipborne gravimeter, density, and current measurements, indeed if at all. Clearly this is a long-term process.

CONCLUSIONS

If satellite altimetry is to usefully measure ocean currents and tides, it will be necessary for decimeter-level precisions to be achieved in orbit determination, altimeter measurements, and geoidal undulations. The geoid should be specified with an rms precision of order 10 cm on a grid of approximately 20 km spacing over the unfrozen oceans of the world. Along-track averaging intervals for altimeter data of order 10 km are required; areas several hundred kilometers on a side must be sampled often enough to meet a time-space Nyquist sampling criterion for variations having monthly time scales and 100-km space scales. The process of separating out oceanographic from geodetic variations will require the use of

ancillary data, several iterations, and much time and energy.

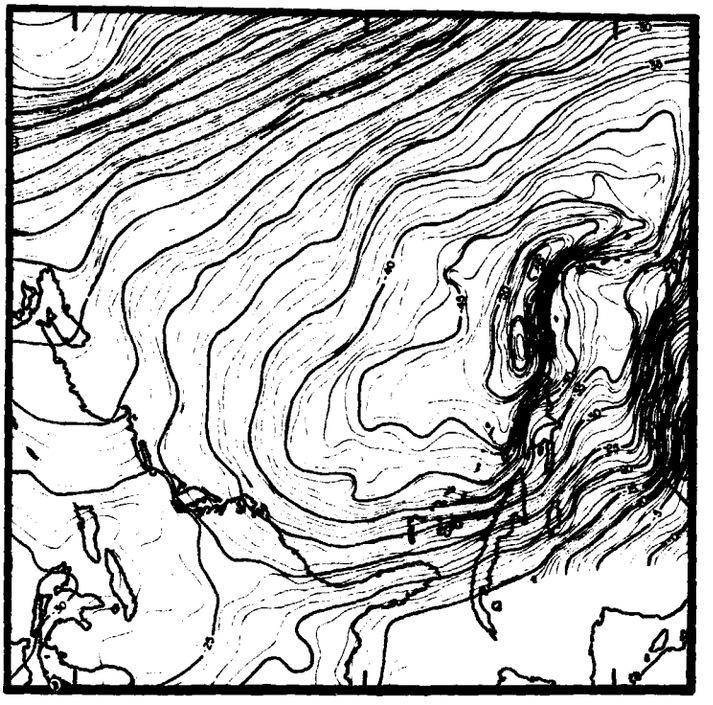

Fig. 5 - Geoid in western Atlantic as derived from satellite orbit perturbations and marine gravity measurements (Vincent, Strange, and Marsh[6])

BIBLIOGRAPHY

1. Kaula, William M., editor, "The Terrestrial Environment: Solid Earth and Ocean Physics," NASA (August 1969)

2. Defant, Albert, Physical Oceanography, V. I, pp. 301-512, Pergamon Press (1961)

3. Defant, op cit , p. 596

4. Hanson, Donald V., Deep Sea Research 17, p. 495 (1970)

5. Hendershott, Myrl, and Walter Munk, "Tides," Annual Review of Fluid Mechanics 2, p. 205 (1970)

6. Apel, John R., editor, "Sea Surface Topography from Space," V. I & II, NOAA Technical Report ERL 228 (May 1972)

7. Fubara, D.M.J., and A. G. Mourad, "Requirements for a Marine Geoid Compatible with Geoid Deducible from Satellite Altimetry," in "Sea Surface Topography from Space," V. I, p. 5-1, NOAA Technical Report ERL 228 (May 1972)

8. Vincent, Samir, William E. Strange, and James G. March, "A Detailed Gravimetric Geoid from North America to Eurasia," Goddard Space Flight Center, NASA, X-553-72-94 (March 1972)

9. McGoogan, Joseph, private communication.

10. Byrne, H. Michael, "On Measuring Ocean Phenomena from Space," M. S. thesis, Massachusetts Institute of Technology (January 1974)

11. Talwani, Manik, Herbert R. Poppe, and Philip D. Rabinowitz, "Gravimetrically Determined Geoid in the Western North Atlantic," in"Sea Surface Topography from Space," V. II, p. 23-1, NOAA Technical Report ERL 228 (May 1972)

SEASAT-A - A USER ORIENTED SYSTEMS DESIGN

S. Walter McCandless, Jr.
National Aeronautics and Space Administration

Abstract: The SEASAT-A program began with users of ocean dynamics data getting together in the spring of 1973 to discuss measurement requirements. Since that time, SEASAT-A has become a new start (FY 75) NASA program dedicated to satisfying these user desires. It was important to have a working interface between Users and System Designers during the early phases of project definition. These past dialogs and working integration meetings become even more important, and serve as the key ingredient, in the successful conversion of user requirements into a system which creates user products. This paper describes this process during development of the SEASAT program by showing how user requirements influenced instrument selection, mission planning, satellite systems design, and the end-to-end data system. These elements all form part of the systems design depicted in Figure 1.

SEASAT-A INSTRUMENTS

Each of the instruments or sensors proposed for SEASAT-A has had predecessors which have been flown successfully in both aircraft and spacecraft. The instruments carried aboard Apollo, Skylab, and the development of GEOS-C, to be flown this year, provide confidence that the specific hardware for SEASAT-A has a high degree of inheritance as shown in Figure 2. The selection of ocean-sensing instruments was made in accordance with user measurement requirements set forth during NASA-sponsored meetings in early 1973. The sensors form a set of mutually supportive devices wherein the total information derived from the integrated sensor system would be greater than the sum of mission mutually exclusive sensors. While it is impossible to meet user data requirements in their totality because of limitations of mission design and system performance, the four sensors described below constitute a large first step toward an optimum configuration.

1. Compressed Pulse Radar Altimeter. The altimeter of SEASAT-A will have two separate functions: first, to measure the altitude between the spacecraft and the ocean surface to $\pm$10 cm root-mean-square and second, to measure wave height from one to about 20 meters with an accuracy of 0.5 m or 10%.

This instrument is a newer and more accurate version of the Skylab radar altimeter, S-193, and is similar to the altimeter which will fly on GEOS-C early next year. The Skylab altimeter was the first to give a continuous direct measurement of the sea surface topography from a satellite.

Prominent surface depressions due to deep ocean trenches and corresponding elevations resulting from seamounts, plateaus, and ridges, already roughly observed from Skylab, will now be more precisely measured. Having a measurement precision of ± 10 cm will enable the SEASAT altimeter to identify and "see" such time-varying features as intense currents, tides, wind pile-up, and storm surges. It should also be capable of locating and mapping ocean surface currents ranging upwards from 30-50 cm/sec since the slope of the surface is proportional to the surface speed.

The measurements of sea state or wave height are a source of error and are required in order to reach a 10 cm precision in altitude. Additionally, sea state measurements are valuable in their own right, since combined with surface wind measurements they can be used to make world-wide sea state forecasts.

2. Coherent Synthetic Aperture Imaging Radar. Wave pattern and dynamic behavior information will be obtained by using the coherent imaging radar to obtain images of the ocean. The device will yield images of waves of lengths in the 50- to 1000-meter range and can establish a wave direction correct to within $\pm 10^{o}$ to $\pm 20^{o}$. Wave heights may be computed from the data for fully developed seas but the length/height relationships for developing seas needs the wind and wave information from other SEASAT-A sensors in order for the theory to be established. Potentially, the imaging radar can function through clouds and nominal rain to provide wave patterns near shoreline and also high resolution pictures of ice, oil spills, current patterns and other event features. The data rate from any fine resolution imaging device is necessarily high and onboard data processing for global data collection and storage is costly. For SEASAT-A, an experimental radar will allow judicious use of the device with specific mission limitations relative to global coverage. Nevertheless, it will be possible to sample wave spectra over significant areas of the ocean within line of sight of any ERTS ground stations. The images will be especially useful for the mapping of ice leads and open water and will yield synoptic ocean data near potential offshore nuclear power plant sites, deep water oil ports, harbors, breakwaters, and other coastal developments in North America.

3. Microwave Wind Scatterometer. This third active radar system is intended to measure wind speed in the range from about 4 m/sec to 26 m/sec with an accuracy of ±2 m/sec or ±10%. Inherited from the Skylab experimental scatterometer, it will determine wind direction in the range from 0 to 360 degrees with a direction correct within $\pm 20^{o}$. The scatterometer will take measurements over two 460 km-wide swaths equally displaced about the nadir by 235 km.

4. Scanning Visible/Infrared Radiometer (SR). This sensor, originally flown on ITOS, will provide images of visible and thermal infrared emission from oceans, coastal and atmospheric features in support of the other instruments, and will help identify currents and storms. From its imagery, clear weather temperatures can also be deduced.

MISSION DESCRIPTION

The SEASAT-A spacecraft is tentatively scheduled for launch in the early part of calendar year 1978 into a nearly circular orbit with an eccentricity less than 0.006 and an altitude of approximately 800 km. Figure 3 identifies the important mission parameters. The orbit will be inclined 108^{o} to the Equator with a period of 6045.0 ± .1 second (100 minutes 45 seconds), resulting in about 14 1/3 orbits per day. This orbit is non-

sun-synchronous and will precess through a day/night cycle in approximately 3.5 to 5.5 months.

Launch in the spring allows for an early sequence of instrument demonstration and calibration following acquisition, orbit establishment and trim and deployment of antennas, arrays, etc. This permits the user data products to be available during the northern winter months when the range of wind and wave conditions in the northern hemisphere is most active. While in this configuration, efforts will be made to coordinate ground truth experiments with sensor operations, data acquisition, and timely delivery to evaluators.

The major ground coverage requirement for SEASAT-A is 36 hours for about a 95% coverage of the earth's surface (assumes instrument swath width of 1000 km). Several candidate fill-in-patterns are possible to achieve a required 10-nautical-mile grid (referenced at the Equator) of the subsatellite nadir track for geodetic purposes in three to six months.

It should be noted that while spacecraft velocity is typically about 7.45 km/sec at 800 km altitude, the motion of the ground track is only 6.62 km/sec. Of the five sensors to be carried by SEASAT-A, only the compressed pulse radar altimeter will be limited to measurements along the subsatellite track. The other instruments have considerably extended ranges with the following swath coverages of the ocean:

Synthetic Aperture Imaging Radar--one 60- to 100-swath displaced from nadir by 200 km

Visible and Infrared Radiometer--full track or horizon-to-horizon

Microwave Wind Scatterometer--two 460-km swaths equally displaced about nadir by 235 km

SATELLITE SYSTEM AND SUBSYSTEMS

The satellite system has not been a major concern in SEASAT. Preliminary investigations in the feasibility phase identified a number of existing satellite buses developed for other Air Force and NASA programs, as shown in Figure 2, which already had the support capabilities needed by SEASAT. Further in-depth studies with specific contractors have only confirmed and expanded this concept. Thus, a group of sensors could be integrated on either a separate but simple sensor-module structure or on a sensor-module structure already in existence from another program. This sensor module could also contain any sensor unique data system components in terms of data storage, handling, or processing capabilities. The module could then have a clean attachment interface with an existing spacecraft bus which furnishes power, attitude control, telemetry, tracking, command, and orbit adjust. Many of these buses also have data storage and handling capability within the existing designs. The satellite systems design approach is outlined in Figure 4. These existing satellite systems and available launch vehicles (Atlas E/F or Delta) provide adequate weight margins ranging from 1.4 to 1.8 over the estimated requirement, and the satellites have space histories exceeding the one year design life of SEASAT-A. Sensor module subsystem elements are existing designs and/or hardware and exist in most cases as part of ongoing and continuing programs.

The most important SEASAT-A program objective is to place most of the program money on the project-peculiar sensors and direct sensor support subsystems. To accomplish this, the selection of an existing

low cost spacecraft bus supplying the requisites for satellite support is essential; and selection of the specific existing spacecraft to be used for SEASAT-A must necessarily be made early in the program so that sensor and sensor support subsystems design and integration planning can take advantage--low cost--of the peculiar attributes of a specific existing spacecraft.

END-TO-END DATA SYSTEM

In the SEASAT-A end-to-end data system, the concept of an integrated data system design, from the conversion of sensor response into digital data, to the output of information requested by the users, is an important part of systems design and program planning. Figure 5 illustrates the scope of the end-to-end data system. Included in such a system design are tradeoffs of which function, performed on the data as it travels through the system, should be performed both on the ground and on the satellite.

For the standard satellite-to-ground link through the STDN network, the real-time rates of all the instruments except the imaging radar can be handled on the unified S-band. The real-time rates for the imaging radar would be transmitted on separate wideband S-band links.

The SEASAT-A mission operations will be planned for a nominal one-year duration, with at least one tracking and real-time telemetry pass per orbit, and one "command" pass per day for reprogramming a possible onboard computer. The data processing requirements will be primarily for non-real-time data package production, but a real-time mode of data handling and dissemination, with a delay of three hours or less, is possible on a limited operational demonstration basis.

Beginning during the feasibility study phase of SEASAT-A, which took place in early 1973, NASA sought the involvement of the "user" community--the agencies and institutions that are the intended users of SEASAT-A data. The continuation of this involvement insures that the needs of the oceanographic organizations will be met and that the types and quantity of data to flow from the spacecraft and its associated ground-based data handling systems will be as meaningful and useful as possible.

In summary, the program objectives of SEASAT-A are to:

Demonstrate a capability for -

1. Global monitoring of wave height and spectra, surface winds, ocean temperature and current patterns.

2. Measuring precise sea surface topography; detecting currents, tides, storm surges, and tsunamis.

3. Charting ice fields and leads.

4. Mapping the global ocean geoid.

Provide data for user applications -

1. Predictions of wave heights and spectra, and wind fields for ship routing, ship design, storm-damage avoidance, coastal disaster warning, coastal protection and development, and offshore power plant siting.

2. Maps of current patterns and temperatures for ship routing, fishing, pollution dispersion, iceberg hazard avoidance.

3. Charts of ice fields and leads for navigation and weather prediction.

4. Ocean geoid fine structures.

Demonstrate the key features of an operational system -

1. Global sampling.

2. Near-real-time data processing and dissemination.

3. User feedback for operational programming.

Demonstrate economic and social benefits of user agency products.

While many of these objectives can be achieved by the receipt of quality data from SEASAT-A, it will still be necessary to have the support and commitment of interested user organizations in order to derive the full scientific and economic benefits from the information derived from this and subsequent spacecraft systems devoted to remotely sensing the ocean environment.

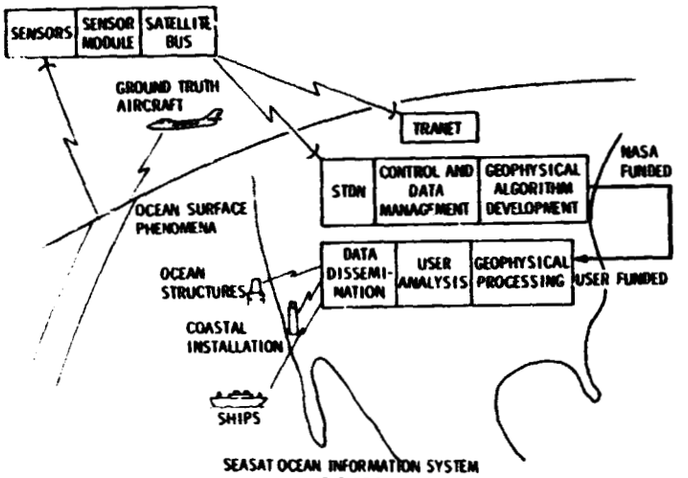

SEASAT OCEAN INFORMATION SYSTEM
FIGURE 1

MISSION/SATELLITE/SYSTEM EXPERIENCE

SYSTEM LEVEL DESIGN AND CONTROL AT JPL	RANGER ⇒ SURVEYOR ⇒ MARINER 3 yr PROJECT TYPICAL TO FIXED LAUNCH DATE

SENSOR EVOLUTIONARY EXPERIENCE

ALTIMETER (WALLOPS	AIRPLANE ⇒ SKYLAB ⇒ GEOS-C ⇒ AAFE ⇒ SEASAT-A
SCATTEROMETER (LANGLEY)	AIRPLANE ⇒ SKYLAB ⇒ SEASAT-A
EXPERIMENTAL IMAGING RADAR (JPL)	AIRPLANE ⇒ APOLLO 17 ⇒ SEASAT-A
VHR RADIOMETER (GODDARD)	ITOS SR1 ⇒ SEASAT-A

EXISTING BUS DESIGNS

AIR FORCE CANDIDATES	STP-71-2	LOCKHEED
	-72-1	BOEING
	-72-2	ROCKWELL
	DSP-M-35	TRW
	DMSS-D-5	RCA
NASA CANDIDATE	[illegible]	GE

SENSOR MODULE FOCUSED EXPERIENCE/RECORD

SHIPBOARD RADAR SYSTEMS DESIGN AND INTEGRATION - APPLIED PHYSICS LABORATORY (APL)
ONBOARD DATA HANDLING/PROCESSING - APL AND [illegible] RECOGNIZED LEADERS OVER INDUSTRY AND HAVE EXISTING APPLICABLE DESIGNS

GROUND DATA SYSTEM

COMMITTED NASA GSFC FACILITIES -
- S[illegible]OM FACILITIES
- [illegible]Y FOR DATA PREPROCESSING
- [illegible]CONTROL CENTER FOR SATELLITE COMMAND AND CONTROL
- SIGMA DATA MANAGEMENT FACILITY OR EQUIVALENT

SEASAT-A TECHNICAL INHERITANCE
FIGURE 2

MEASUREMENTS

- GLOBAL OCEAN TOPOGRAPHY - TO < 10 cm PRECISION (RELATIVE ACCURACY)
- GLOBAL AVERAGE WIND SPEED AND DIRECTION - ±2 m/s AND ±20 deg ACCURACY
- GLOBAL WIND SPEED AND DIRECTION - ±2 m/s AND ±20 deg ACCURACY
- LOCAL IMAGES (ICE, CURRENTS, COASTAL, OIL SPILL, etc.) - 25-m RESOLUTION
- WAVE LENGTH SPECTRA - LENGTH ACCURACY ±20%, DIRECTION ±10 deg

SENSORS

- RADAR ALTIMETER
- MICROWAVE SCATTEROMETER
- EXPERIMENTAL SYNTHETIC APERTURE RADAR
- VISIBLE/IR RADIOMETER

MISSION DESCRIPTION

- HIGH INCLINATION (108 deg), NEAR CIRCULAR (2,006-c), NON-SUN SYNCHRONOUS ORBIT (~800 km ALTITUDE)
- 95% GLOBAL COVERAGE IN 36 hr
- NOMINAL 18 km EQUATORIAL CROSSINGS IN LESS THAN 6 months
- INITIAL ORBIT ADJUST PRECISION - PERIOD ±0.1 sec, ALTITUDE ≃ ±80 m
- 1 yr DESIGN LIFE, 3 yr EXPENDABLES
- 1978 LAUNCH

RECOMMENDED SEASAT-A MISSION
FIGURE 3

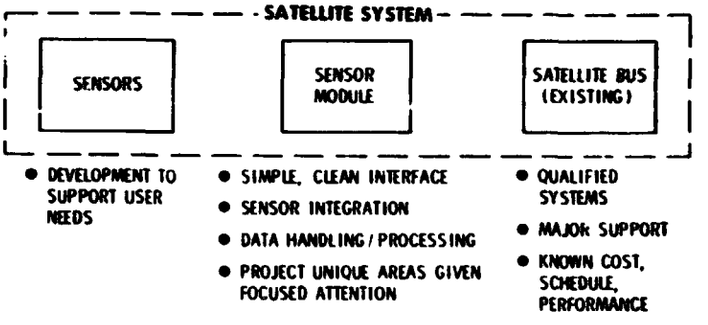

SATELLITE APPROACH
FIGURE 4

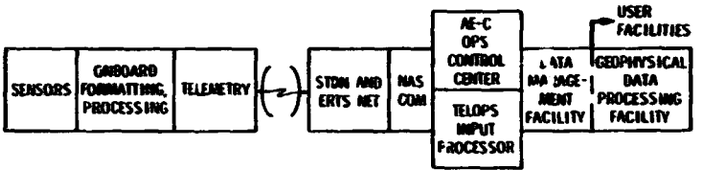

- MAXIMUM USE OF EXISTING SUBSYSTEMS
- SOME ADAPTIVE CAPABILITY
  - FORMATING
  - PROCESSING
- GLOBAL COVERAGE EXCEPT SAR
- ALL MEASUREMENTS DEMONSTRATED FOR LATER SEASATS
- MAXIMUM USE OF EXISTING NASA GROUND FACILITIES
- WELL UNDERSTOOD FLEXIBILITIES
- SEVERAL ALTERNATIVE PROCESSING MECHANIZATIONS VIABLE

END-TO-END DATA SYSTEM
FIGURE 5

DETERMINATION OF MARINE BOUNDARIES AT SEA AND THEIR GEODETIC IMPLICATION

Lieutenant James A. Wexler, NOAA
National Ocean Survey

ABSTRACT

Current world opinion indicates that a revision in the law of the sea towards extending territorial seas and providing more extensive economic zones is inevitable. At the next United Nations Conference on the Law of the Sea ratification is expected for twelve mile territorial seas. In addition, a two hundred mile economic zone is seriously being considered by participant nations.

Focus is now shifting toward the technical capabilities to accurately determine and physically delineate such limits.

A review of both surface and subsurface systems and devices for positioning at sea is presented. In addition, physical problems of delineating such positions are examined and solutions suggested. A discussion concerning the accuracy required for present and future legal determinations for both near shore and deep ocean boundary demarcation is included with additional reference to the necessary technology transfer to assure uniform world-wide participation.

Recently released official United States Territorial Sea and Contiguous Zone Boundary Documents are presented and their construction discussed.

INTRODUCTION

Studies of shore and sea boundaries indicate the number of technical questions that arise and the extent of judgment for the delimitation of sea boundaries.

It is not intended here to resolve the problem but rather to underline the importance continuing efforts are to solving the problem. Until economical geodetic positioning systems can be developed and available to all; enforcement will continue to be difficult.

PRESENT GEODETIC IMPLICATIONS

Exploration and exploitation of natural resources in the water column, on the seabed and within it, as well as other marine activities are presently possible beyond the two hundred meter isobath. This emphasizes the necessity for reliable positional accuracy and a definition of all relevant boundary lines, both near shore and distant.

The International Conference on the Law of the Sea, scheduled next month in Caracas, Venezuela visualizes an international regime for the seabed and subsoil beyond the limits of national jurisdiction based on straight distance criteria; possibly in combination with a depth criterion. Such an agreement will prompt nations to delimit their outer shelf boundaries and invite bids for exploration and exploitation of their territories. Failure to reach international agreement will not prevent nations either from extending their shelf limits or exploiting resources beyond the shelf. [7]

Among the important items on the agenda at the Law of the Sea Conference will be the nature of lines used to delimit any boundaries agreed upon. Inevitable in such a discussion is the comparison of lines drawn on charts and their accuracies, with the field capability of locating oneself at distances within the order of two hundred nautical miles.

Similar to problems of boundary demarcation on land, boundary determinations at sea must consider the engineering and cartographic problems of physical demarcation.

International law may define the boundaries, but they must be determined and then located and mapped for practical purposes.

Of prime importance, obviously, is the determination of the shoreline as it is the base from which boundaries are determined from.

The physical problem is to either define the boundary by bottom markers or to devise a method by which a buoy, ship or structure can be placed on a boundary "station".

Furthermore, precision in offshore boundary delimitation is necessary in order to resolve legal problems of jurisdiction. The boundaries must be positioned in terms of geographical coordinates.

The question then arises, what degree of positional accuracy is required. Obviously the most immediate demands come from the oil and mining industries who must know the exact limits of their ownership to prevent encroachment on adjacent property. From their point of view even a few meters could be significant, especially when a geologic structure being exploited extends across a property line. [7]

Up to the present it has not been possible to readily determine a position at great distances from shore to within an accuracy of a few meters.

MARITIME POSITIONING SYSTEMS

To locate oneself at sea, two methods may be used. Either positioning by onboard capabilities or positioning in relation to surface or sub-surface systems.

Marine positions are determined by either an extension of the shore-based triangulation net or by a variation of the three point fix or the intersection of two lines of position. The triangulation method is the most precise but the cost has demonstrated itself to be prohibitive for practical use in marine positioning. [5]

Positions in sight of shore can be determined by visual methods, where angles are measured or electronic methods, where distances are measured. A marine position within three to five nautical miles from shore can be determined within ten feet in clear weather using the resection method. Electronic positioning systems measure either distances (circular systems) or differences in distances (hyperbolic systems) between stations by measuring the electro-magnetic wave transit time. Positions within one foot apparently can be attained for very short ranges.

Projects have been conducted to determine the feasibility of establishing and recovering passive markers on the continental shelf with geodetic precision. These were successful where electronic positioning equipment was utilized and line of sight observations were possible (shallow water). An onboard accurate positioning device was necessary to recover the passive system.

Disadvantages of the circular systems are that they require a signal transmitter on board ship with an ample power supply. In addition, only one ship may use the system at a time.

The hyperbolic system, overcomes these difficulties, requiring a signal receiver on board and a transmitter on shore. Accuracy with the system, however, can be less than desired. Due to the divergence of the hyperbolic lines of position, the average lane width one hundred miles from the baseline for systems approaching geodetic precision is of the order of one thousand feet. In addition, distortion of the hyperbolic pattern by islands in the signal path, non-linearity in the electronic systems and drift in the system increase error. [5]

An inertial system depends on gyros for detecting angular motion; upon accelerometers for detecting variations in linear velocity; and upon computers to process data to provide position information. Among the major problems with these systems are drift of the gyro (variation in orientation with time not associated with the earth's rotation) and the local variation of the direction of the plumb bob from that of the model earth adopted to provide this direction. The systems are expensive and probably out of the reach for most commercial users.

For acoustic positioning, a ship transmits a signal which is picked up by and re-transmitted by three electronic transponders emplaced on the sea floor. These signals may be converted to distances when compared with time. If the position of the transponders is known, the ship may determine its locations with respect to them within twenty five feet.[5]

The question of the right, or lack thereof, to emplace equipment within the territorial sea and other areas adjacent to particular states has been analyzed before this body in the past.

The installation and maintenance of geodetic systems within the water column is a use fully protected by Article 2 of the *Convention of the High Seas* (1958) which states "....These freedoms and others which are recognized by the general principles of international law shall be exercised by all states with reasonable regard to the interests of other states in their exercise of the freedom of the high seas." No problems are anticipated when such systems are installed within a states territorial sea.[8]

Satellite methods employ elements of the doppler effect. The doppler effect occurs when a source of wave motion approaches or moves away from an observer, the frequency of the waves received by the observer increases and decreases. Radio signals from six polar orbiting satellites (600 to 750 nautical miles above the earth) produce the same phenomenon.[2]

In a test survey conducted by the National Geodetic Survey, a geodetic receiver (Geoceiver) received signals from the satellites and measured the doppler shift and precise time of the satellite signals with signals generated by the Geoceiver. With this information and precise orbital data supplied by the Naval Weapons Laboratory at Dahlgren, Virginia, the National Geodetic Survey was able to determine, within six feet, the positions of two platforms forty and one hundred miles off the coast of Louisiana.

CARTOGRAPHIC DETERMINATIONS

The dividing line in most existing treaties, related to maritime boundaries, is as a great circle arc, a loxodromic line, a small circle arc or even as a "straight" line between two geographical coordinates. The spheroidal geodesic, however, represents the shortest distance between two points on the spheroidal ellipsoid.[7]

The Law of the Sea Conference should define more specifically the scale of map to be used when delimiting sea boundaries. The scale of the chart, of course, relates directly to the purpose of the delimitation. The United States provisionally delimits its Territorial Sea and Contiguous Zone using relatively large scale charts, i.e. approximately 1:50,000 to 1:200,000.

Most developing nations, however, have no advanced cartographic or nautical survey capabilities. It would be difficult, therefore, to expect a specific large scale chart from all lesser developed countries without undue expense at this point in their development. Certain minimum scales should, however, be agreed upon. When charts are used at unrealistic scales as a means for determining boundaries at sea, the possibility of confusion is enhanced.

The geodetic or geodesic is the curve on the sphere which is drawn so that the variation on the arc length between any two of its points is zero. The spheroidal geodesic conforms directly to the mathematical spheroid which represents the shape of the earth most accurately. Differences in area can be great when comparing geodesics, great circles and loxodromes as boundary lines.

Besides the choice of a mathematical line or curve to define the boundary; accuracy of definition and of position when determining a boundary line or segment of such a line must also be questioned.

True accuracy can be defined as the degree of precision of the geographical coordinates for boundary turning points, i.e. full minutes of arc, in tenths of a minute of arc, or in seconds of arc. The coordinates should be expressed to the same degree of precision as those for the control points in the surrounding coastal area for both the case of a boundary line determined by geodetic calculations on the basis of coastal control points and for that of a line merely "negotiated".[7]

The positional accuracy can be defined as the accuracy of fixing at sea your position by navigational, hydrographic or geodetic means.

Under the submerged lands act, the boundary between state and federal submerged lands is defined with reference to the coast line. The boundary itself is to be found by measuring seaward the required distance from the controlling coastal features. This is what is known as the "arcs of circles" method of measurement; which means that the territorial sea includes everything lying within the determined distance from any point of the baseline. In the case of the United States all measurements are made from the Mean Low Water line or Mean Lower Low Water line (West Coast) as depicted on official National Ocean Survey charts; and approved by the Interagency Committee on the determination of the Territorial Sea and Contiguous Zone of the United States.

CONCLUSIONS

It is essential that a system of demarcation of boundaries at sea be recoverable. Present technology limits st[illegible] surface marker delimitation to relatively smooth, shallow regions of the seafloor. If a boundary intersects the seafloor at great depth or great distance from shore it may not be technologically possible to implant a bottom marker with the accuracy required.

Surface markers again imply initial costs combined with maintenance costs. Additionally, surface markers are subject to the continuous effects of the sea and are thus capable of breaking their moorings. Envisioning the possible number of "surface markers" to properly define an area - such systems could become hazards to navigation. Since these systems would be attached to the bottom; boundary markers in deep water would have a scope of tether that could exceed the necessary accuracy.

I submit that for the present we should concentrate efforts on developing the most economical and practical geodetic positioning equipment for field use.

If exploiters of the ocean and enforcement agencies have the same geodetic positioning capabilities encroachment would be minimized.

Initially, spot boundary determinations can be conducted and approved before operations commence; especially when they approach the limits of ownership.

I am confident advances (perhaps to be revealed during this symposium) will be made in hydrographic, geodetic and physical and chemical oceanographic methodology which will eventually enable us to actually mark the boundary line at sea from subsurface to surface without adversely affecting the environment.

The nature of line could be resolved by allowing a nation to determine its boundaries with whatever line they so define and be bound to its positional determination on the spheroid, even after their capabilities for geodetic determinations mature.

Straight baselines could reduce the number of points to be fixed (and therefore recoverable) by geodetic positioning, overcoming a monumental task to geodetically determine an "arcs of circles" boundary line.

Accuracies required will undoubtedly increase as the world races to exploit the sea and its subsurface. Technology must meet the legal challenge to adequately define ownership at both near shore and deep ocean locales.

Whatever accurate method is finally selected, it is critical that it can be reasonable enough to be utilized by all nations and that the necessary technology transfer be effected to assure international capability for compliance.

REFERENCES

1 H.R. Cravat & R.K. Brewer, "Baseline Establishment for Positioning Federal State Offshore Boundaries", Offshore Technology Conference Proceedings, May 1972.

2 J.D. D'Onofrio, after "Location of oil platforms in Gulf of Mexico", U.S. Dept. of Commerce New (NOAA 74-44), March 1974.

3 W.L. Griffin et. al., "Establishing Tidal Datum Lines for Sea Boundaries", Joint Amer. Soc. of Photogr. Amer. Cong. on Surv. & Map Proceedings, March 1967.

4 C.L. Gumm, "Surveying Involvement in Controverted Offshore Boundaries", Surveying and Mapping, June 1973.

5 H. Orlin, after "Positioning on the Continental Shelf", Proceedings from Law of the Sea Institute Conference, 1968.

6 J.O. Phillips, "Coastal Boundary Surveys", Symposium on Coastal Geodesy, Int. Union of Geodesy and Geophysics Proceedings, July 1970.

7 M. Thamsborg, after "Geodetic Hydrography as related to Maritime Boundary Problems", Int. Hydr. Rev., LI(1), 1974 pp. 157 - 173.

8 J.C. Tison, "Marine Geodesy", Int. Hydr. Rev., XLVI(1), 1969 pp . 109 - 113.

9 W.T. Burke, "The Law and Marine Geodesy", Proceedings of First Marine Geodesy Symposium, Sept. 1966.

Research Connected with Marine Geodesy at the Technical University at Hanover, Germany

Günter Seeber

Institut für Theoretische Geodäsie
Technische Universität Hannover

The Technical University of Hanover has established a research center for the study of geodetic measuring techniques in coastal and marine regions.

Some communications are given on plans for the determination of detailed astrogeodetic and gravimetric deflections in a coastal and marine test area. Main observing instrument is a transportable photographic zenith tube.

Seeber

During the last year (1973) a research center on geodetic and photogrammetric measuring techniques in coastal and marine regions was founded within the Geodetic Department at the Technical University of Hanover, sponsored by the German Research Foundation (Deutsche Forschungsgemeinschaft).

Some 40 scientists from university and from different agencies outside of the university are cooperating within this group to study different questions on measuring problems related to the coast and sea.

The main topics of investigations are:

- Remote Sensing
- Topography and Cartography
- Methods and techniques for determining and permanent marking of height reference points
- Investigations on coastal subsidence
- Determination of the geoid
- Application of satellite techniques for determining geodetic coordinates of surface positions

in coastal and marine areas.

The aim of this report is, to give some short communications on the last two topics which are related very closely to the subject of this symposium and which are treated in the Institute for Theoretical Geodesy at Hanover-University. The corresponding research work is just at the beginning, but there are some encouraging results from preliminary studies.

The scientific aim of the project "geoid determination" is to find out suitable methods for the determination of the detailed structure of the geoid in a limited coastal and marine area. It is planned to begin with an astrogeodetic approach in a test-area of some 2000 km^2 in the mouth of the river Weser and to enlarge then this test-area to some 25.000 km^2 into the "Deutsche Bucht".

The direction of the gravity vector shall be determined with a transportable photographic zenith tube. This instrument was developed in our institute as a prototype and gives reasonable results on land marks (GESSLER, PILOWSKI, 1972).

The principle of the instrument is rather simple: A photographic camera with a focal length of 80 cm is mounted in a vertical manner on a ground circle, which enables the camera to be turned into two positions. The electronic shutter is placed immediately in front of the photographic plate. The verticality of the

camera can be proved by two electronic levels. Small tilt-changes are also registered by these levels.

The main advantage of the instrument can be seen in the observing velocity. One observation, i.e. one plate exposed in two different positions of 180°, takes 3 minutes of time. The proper exposition time however is only 1 second in every position. That means: for applications on moving points the stability of the camera must be guaranteed only during this rather short time of one second.

The accuracy for the reduced point out of one plate was found to be 0".4. In general it should be sufficient to take two plates, which means less than ten minutes observing time for one point.

This fact enables us to measure astrogeodetic deflections in very dense profiles at the coast or on islands. Furtheron it is possible to observe very quickly on oil-drill-hole-platforms or in tidal flat regions.

The instrument described is a prototype with rather simple optics and without automatic data collecting equipment. A new construction with better lenses and perhaps better registration of the tube-inclination should give also better results.

For the next two years it is planned to measure "astros" with the "Hanover Zenith Camera" on fixed points along the coast, on islands, on light-houses near the coast and - so far as possible- on oil-drill-hole-platforms. The geodetic coordinates will be determined by conventional terrestrial methods, by long electromagnetic distance measurements over sea, by precise navigation methods, by satellite (DOPPLER) methods and by a combination of these methods (CAMPBELL, SEEBER, WITTE, 1973).

It is one topic of our Hanover research group at the Institute for Theoretical Geodesy, to study the questions of precise position determination at coast and sea when different observing methods are used and combined. Special emphasis is directed towards the application of satellite techniques as with transportable Doppler equipment.

Beside the astrogeodetic approach it is planned to measure gravity values (gravimeter) and their derivatives using a torsion-balance. With this observation material the next step will be to compute a detailed geoid of the marine region using astrogeodetic, gravimetric and combined methods. Hereby emphasis is layed on the study of interpolation methods.

A further step will be the astrogeodetic approach into the open sea. Attempts to observe astros on stabilized platforms led - as far as we know - to accuracies in the order of 10 arcseconds (MOURAD 1972). We hope, regarding the short observation time necessary for the "Hanover Zenith Camera" in the order of one second of time or less, to improve this accuracy, although we see a lot of difficulties in defining the direction of the vertical on a moving point.

References:

GESSLER, J., PILOWSKI, K.: Erste Ergebnisse mit einer transportablen Zenitkamera. Zeitschrift für Vermessungswesen, Stuttgart 1972.

CAMPBELL, J., SEEBER, G., WITTE, B.: Kombination von Doppler-, Laser- und photographischen Beobachtungen in Satellitennetzen. Deutsche Geodätische Kommission, Reihe A, Heft 200, München 1973.

MOURAD, A.G.: Marine Geodesy 1967-1971. IAG Special Study Group I-25. Travaux de l'Assoc.Int. de Géod., Tome 24. Paris 1972.

C 13

SATELLITE TECHNIQUES IN GEOPHYSICS AND THEIR RELATIONSHIP TO MARINE GEODESY

M. A. Khan*
Geodynamics Program Division
Goddard Space Flight Center
Greenbelt, Maryland 20771

ABSTRACT

A statistical evaluation of some of the recent satellite determined gravity models, including some with distinct data base, indicates that the geopotential coefficients of these models are individually meaningful for frequencies with wavenumbers n = 2 through 7 certainly and wavenumbers n = 8 through 10 probably. Geopotential coefficients in higher frequency ranges while apparently important for computing accurate satellite orbits seem to have little geophysical significance in an individual sense. Differences between various gravity models and those between purely satellite determined geopotential models and their associated combination models show no consistent relationship to surface gravimetric coverage. Additional classical tracking data are important in improving the existing description of the Earth's gravity field but their contribution in extending its frequency range beyond what is now available is uncertain. New tracking data types such as laser, satellite-to-satellite and altimetry data seem to have the potential of improving gravity field description but a quantitative assessment of their contribution is difficult at this stage.

INTRODUCTION

Two major areas of geophysical applications of artificial Earth satellites directly related to marine geodesy are determination of the Earth's gravity field and satellite altimetry. Contribution of the latter is in the realm of determination of the dynamic topography of sea level, perhaps as a function of time in future. Mean Sea level will then be used to construct the geoidal surface and also in a number of important oceanographic studies. Satellite altimetry, however, is still in a nascent stage. Some aspects of altimetry techniques are reviewed in this volume (see for example, Brown, this volume; Strange, this volume) and elsewhere by Khan (in prep.). As to the former, it has constituted a major part of the total geodetic effort at a number of institutions. In this paper I will deal only with the evaluations and comparisons aspect of the various versions generated by these efforts and discuss their relationship to marine geodesy.

An accurate satellite determined gravity field has multiple applications in marine geodesy. Its long wavelength components can be used as a control for systematic errors in instrumental calibration and drift. In oceanic areas where only an isolated ship gravity profile is available, accurate satellite field will provide better mean gravity anomalies than the surface data from this isolated ship gravity profile (Woollard and Khan, 1972). The long wavelength field could also be used to apply regional correction to marine gravity profiles in order to obtain localized gravity

*On leave from University of Hawaii, Honolulu, Hawaii 96822

anomalies which have important use in studies of relationships of marine gravity with bathymetry and shallow crustal structures. Such relationships are needed in the prediction of gravity over oceanic areas as well as in understanding the geophysical and geological character of the oceanic areas. Bathymetric data can also be used to predict the higher frequencies of the gravity field over ocean areas (Woollard and Khan, 1972), the lower frequencies being provided by satellite determinations of the earth's gravity field.

Last decade and a half has seen applications of artificial Earth satellite orbital perturbation techniques in their analytical and numerical form, to determination of the gravity field of the Earth. More recently existing surface gravity data, after some interpolation and extrapolation, have been combined with various forms of satellite tracking data to improve upon these gravity field representations. Since there are so many solutions that differ from each other significantly, it is important to evaluate and compare them and perhaps attempt to select the best representation. Geopotential solutions considered in this paper are Goddard Space Flight Center's GEM solutions (Lerch, et al, 74), Smithsonian Astrophysical Observatory's recent Standard Earth (SE) models (Gaposchkin, 73; Gaposchkin and Lambeck, 70) and Naval Weapons Laboratory's most recent solutions (these solutions are classified but we need only their unclassified statistical parameters for this analysis which were kindly made available by Dr. Richard Anderle of Naval Weapons Laboratory). To test these solutions, the surest standard of comparison, of course, is gravimetric representation of the Earth's gravity field but if we had such a representation, we would not need to obtain these solutions in the first place. Any other test is essentially inferential in nature.

ANALYSIS TECHNIQUES

Let

$$f_1(x) = \text{Est } f(x)$$

$$f_2(x) = \text{Est } f(x)$$

where Est indicates the estimated value, then

$$R(f_1, f_2) = \frac{\int_x f_1(x) f_2(x)\, dx}{\left[\int_x f_1^2(x)\, dx \int_x f_2^2(x)\, dx\right]^{1/2}} = 1 \tag{1}$$

$$\sigma(f_1) = (f_2) \tag{2}$$

$$\sigma(f_1 - f_2) = 0 \tag{3}$$

$$S(f_1, f_2) = 1 \tag{4}$$

$$S(f_1 - f_2, f_1) = 0 \tag{5}$$

$$S(f_1 - f_2, f_2) = 0 \tag{6}$$

where $\sigma(f)$ indicates the degree variance of $f(x)$ and $S(f_1, f_2)$ the spectral ratio function of $f_1(x)$ and $f(x)$. Inversely if $f_1(x)$ and $f_2(x)$ are independent estimates of the function $f(x)$ and, if the conditions stated in Equations (1) through (6) are satisfied,

$$f_1(x) = f(x) = f_2(x)$$

Note that Equations (1) through (6) will not be satisfied if either $f_1(x)$ or $f_2(x)$ is an incorrect estimate of the function $f(x)$.

On the other hand, the equations will be satisfied if $f_1(x)$ and $f_2(x)$ are not independent and neither is essentially a correct estimate of $f(x)$. In either of the above cases, this test should be supplemented by other analysis.

COMPARISONS

Geopotential models used in the comparisons reported here are Goddard Space Flight Center, GEM solutions GEM 1 through 6, the Smithsonian Standard Earth solutions SE II and SE III, and the Naval Weapons Laboratory's geopotential solutions 10E and WGSN 44. The Naval Weapons Laboratory's solutions are classified; therefore, only some unclassified statistical parameters could be used in this study.

The statistical parameters defined in Equations (1) through (6) are given in Tables 1 through 9. Table 1 gives the correlation functions for intercomparisons of various GEM Solutions. Table 2 lists correlation functions for GEM and SE models. Correlations between selected GEM and SE solutions and the NWL's 10E and WGSN 44 solutions are reported in Table 3. Tables 4 through 6 list spectral ratio functions for various geopotential solutions in the same order. Tables 7 through 9 report spectral ratio functions for some selected difference fields. A few representative correlation curves are shown in Figures 1 through 3 for a quick visual examination. A typical spectral ratio function of two geopotential fields and their differences is plotted in Figure 4. Figures 5 through 9 show degree variances for GEM 6, SE III, 10E, WGSN 44 and their differences.

Table 1
INTERCORRELATION FUNCTION OF GODDARD EARTH MODELS (GEMs)
A: PURELY SATELLITE DETERMINED GEOPOTENTIAL SOLUTIONS

n	GEM 5 VS. GEM 1	GEM 5 VS. GEM 3	GEM 3 VS. GEM 1
2	1.0000	1.0000	1.0000
3	1.0000	1.0000	0.9999
4	0.9996	0.9999	0.9998
5	0.9994	0.9995	0.9998
6	0.9983	0.9990	0.9967
7	0.9971	0.9966	0.9922
8	0.9941	0.9943	0.9917
9	0.9918	0.9909	0.9792
10	0.9860	0.9796	0.9616
11	0.9741	0.9653	0.9503
12	0.9463	0.9046	0.8740
13	0.9824	0.9498	0.8838
14	0.9889	0.9424	0.9029
15	0.8594	0.9419	0.7834
16	0.9231	0.9661	0.8889
17	-0.0741	0.9106	0.1780
18	0.9487	0.9509	0.8960
19	0.8671	0.7493	0.6775
20	0.1208	0.8231	0.0181
21	0.8389	0.6281	0.4016
22	0.8433	0.8001	0.5031

Table 1
INTERCORRELATION FUNCTION OF GODDARD EARTH MODELS (GEMs)
B: COMBINATION SOLUTIONS

n	GEM 6 VS. GEM 2	GEM 6 VS. GEM 4	GEM 4 VS. GEM 2
2	1.0000	1.0000	0.9999
3	0.9998	1.0000	0.9999
4	0.9996	0.9998	0.9999
5	0.9966	0.9969	0.9961
6	0.9968	0.9978	0.9958
7	0.9752	0.9918	0.9917
8	0.9803	0.9892	0.9883
9	0.8781	0.9502	0.9677
10	0.9039	0.9695	0.9723
11	0.7386	0.9188	0.9662
12	0.7420	0.8596	0.9276
13	0.4961	0.8099	0.9707
14	0.4678	0.7703	0.9637
15	0.2036	0.4998	0.9756
16	0.2970	0.3907	0.9606
17	-0.0366	0.9457	0.8695
18	0.9745	0.9617	0.8569
19	0.8739	0.7885	0.7434
20	0.3398	0.8160	-0.1730
21	0.7212	0.4879	0.3686
22	0.8814	0.7521	0.3880

Table 1
INTERCORRELATION OF GODDARD EARTH MOEDLS (GEMs)
C: PURELY SATELLITE DETERMINED VS. COMBINATION SOLUTIONS

n	GEM 6 VS. GEM 5	GEM 6 VS. GEM 3	GEM 6 VS. GEM 1	GEM 5 VS. GEM 4	GEM 4 VS. GEM 1	GEM 2 VS. GEM 1
2	1.0000	1.0000	1.0000	1.0000	0.9998	1.0000
3	0.9999	0.9999	0.9998	0.9998	0.9999	0.9997
4	0.9999	0.9997	0.9996	0.9998	0.9997	0.9996
5	0.9963	0.9948	0.9956	0.9994	0.9965	0.9950
6	0.9978	0.9961	0.9968	0.9807	0.9964	0.9970
7	0.9868	0.9879	0.9752	0.7044	0.9877	0.9863
8	0.9827	0.9724	0.9803	0.9906	0.9846	0.9840
9	0.9025	0.9067	0.8781	0.9701	0.9552	0.9091
10	0.9289	0.9304	0.9039	0.9846	0.9412	0.9426
11	0.7776	0.8308	0.7386	0.8919	0.8641	0.7995
12	0.8167	0.7761	0.7420	0.8191	0.7480	0.7278
13	0.5327	0.5509	0.4961	0.4702	0.4237	0.5162
14	0.4710	0.4531	0.4678	0.2637	0.2540	0.3171
15	0.2462	0.2538	0.2036	0.2263	0.1761	0.2627
16	0.3069	0.2944	0.2970	0.2836	0.2656	0.3457
17	0.9856	0.9543	-0.0366	0.8972	0.1978	0.2018
18	0.9905	0.9511	0.9745	0.9569	0.9061	0.9867
19	0.9963	0.7791	0.8739	0.7593	0.7003	0.9368
20	0.7968	0.7546	0.3398	0.8273	0.0819	0.7811
21	0.8065	0.4229	0.7212	0.6843	0.4625	0.9337
22	0.9454	0.7665	0.8844	0.7802	0.4842	0.9803

Table 2
CORRELATIONS OF GODDARD EARTH MODELS (GEMs) WITH STANDARD EARTH MODELS

n	GEM 6 VS. SE III	GEM 6 VS. SE II	GEM 5 VS. SE III	GEM 5 VS. SE II	GEM 4 VS. SE III	GEM 4 VS. SE II	GEM 1 VS. SE III	GEM 1 VS. SE II
2	1.0000	1.0000	0.9999	0.9999	0.9999	0.9999	1.0000	1.0000
3	0.9947	0.9999	0.9934	0.9997	0.9947	0.9999	0.9930	0.9996
4	0.9960	0.9971	0.9964	0.9964	0.9964	0.9961	0.9957	0.9964
5	0.9786	0.9907	0.9865	0.9879	0.9873	0.9857	0.9845	0.9861
6	0.3666	0.9675	0.9571	0.9679	0.9559	0.9678	0.9636	0.9656
7	0.9124	0.9561	0.9152	0.9424	0.9107	0.9582	0.9108	0.9293
8	0.6917	0.9430	0.6606	0.9483	0.6343	0.9416	0.6753	0.9413
9	0.8053	0.8189	0.7742	0.8672	0.7919	0.8811	0.7604	0.8828
10	0.5840	0.8310	0.4823	0.7542	0.5060	0.7681	0.5042	0.7365
11	0.7075	0.5204	0.5812	0.6851	0.6426	0.5531	0.5303	0.6587
12	0.5041	0.4473	0.2233	0.3520	0.4322	0.3902	0.1211	0.3060
13	0.7856	0.3628	0.5302	0.4611	0.7289	0.3323	0.4580	0.4168
14	0.8043	0.6070	0.4030	0.5866	0.6808	0.3998	0.4115	0.5836
15	0.6147	0.3628	0.1706	0.1625	0.6884	0.4569	0.0804	0.2119
16	0.5052	0.3238	0.0958	0.1341	0.6800	0.5516	0.1337	0.2061
17	0.2416	0.4276	0.2443	0.4422	0.2193	0.5639	-0.0820	0.4327
18	0.1891	0.2440	0.2172	0.2814	0.2077	0.4068	0.1784	0.2616
19	0.1309	-0.0903	0.1576	-0.0884	-0.2249	-0.2912	0.1348	0.1771
20	0.0787	-0.0142	-0.0868	-0.3619	-0.0892	-0.0205	0.8473	0.4276
21	0.2406	0.0046	0.0025	-0.1759	-0.1488	-0.0324	0.1605	0.3326
22	0.1475	0.0263	0.1260	-0.0075	-0.0629	-0.0065	0.0705	0.1016

Table 3
CORRELATIONS OF REPRESENTATIVE GODDARD EARTH MODEL AND STANDARD EARTH MODEL WITH NAVAL WEAPONS LABORATORY'S RECENT GEOPOTENTIAL SOLUTIONS

n	SSE III VS. NWL WGSN 44	SSE III VS. NWL 10E	GEM 6 VS. NWL WGSN 44	GEM 6 VS. NWL 10E
2	1.0000	1.0000	1.0000	1.0000
3	0.9946	0.9948	0.9998	0.9998
4	0.9961	0.9961	0.9995	0.9995
5	0.9664	0.9681	0.9972	0.9982
6	0.9660	0.9612	0.9977	0.9963
7	0.9192	0.9076	0.9826	0.9816
8	0.6713	0.6954	0.9693	0.9562
9	0.8129	0.8315	0.8796	0.8703
10	0.5695	0.5360	0.9159	0.8900
11	0.5367	0.5107	0.7694	0.7358
12	0.2582	0.3140	0.5556	0.5727
13	0.5782	0.4778	0.5825	0.5398
14	0.4296	0.4223	0.3642	0.3702
15	0.3981	0.2953	0.3021	0.2406
16	0.1296	0.3008	0.3467	0.7191
17	0.2542	0.4262	0.1382	0.3093
18	0.4063	0.1933	0.1854	0.4371
19	0.1728	0.2872	−0.0554	0.0905
20	0.5495	0.4512	−0.1788	−0.0974
21	0.1122	0.4478	−0.1875	0.1950
22	0.3300	−0.0339	−0.0661	0.3092

Table 4
SPECTRAL RATIO FUNCTION: GODDARD EARTH MODELS

n	GEM 5 VS. GEM 1	GEM 3 VS. GEM 5	GEM 3 VS. GEM 1	GEM 4 VS. GEM 6	GEM 2 VS. GEM 6	GEM 4 VS. GEM 2	GEM 6 VS. GEM 5	GEM 3 VS. GEM 6	GEM 6 VS. GEM 1	GEM 5 VS. GEM 4	GEM 4 VS. GEM 1	GEM 3 VS. GEM 1	GEM 2 VS. GEM 1
2	100	99	100	100	100	100	99	100	99	100	100	100	100
3	100	99	99	100	100	100	99	100	99	99	99	99	99
4	100	101	101	99	98	101	101	100	100	101	100	101	99
5	97	93	90	99	106	93	94	99	91	93	90	90	97
6	101	98	99	104	102	102	92	105	93	65	97	99	95
7	98	101	99	90	97	93	115	87	113	149	102	99	111
8	98	96	94	83	93	89	125	77	122	104	102	94	114
9	115	88	102	77	83	93	113	78	130	88	101	102	109
10	103	91	94	109	114	95	95	96	98	104	107	94	112
11	115	90	103	92	104	88	92	97	106	85	98	103	111
12	121	77	94	77	94	82	96	80	117	75	91	94	111
13	96	129	118	60	79	76	49	252	47	30	28	118	37
14	41	99	139	40	52	77	29	338	41	12	18	139	21
15	123	171	210	50	76	65	21	779	26	11	13	210	21
16	94	112	105	98	111	88	10	1131	9	10	9	105	10
17	123	31	39	32	282	11	105	30	130	34	42	39	369
18	72	69	49	75	143	52	99	69	71	75	54	49	103
19	226	265	599	239	55	433	101	262	228	241	546	599	126
20	13	23	33	28	223	13	93	24	11	26	3	33	26
21	178	82	146	91	64	143	88	92	158	81	144	146	101
22	100	61	61	59	109	54	110	56	109	64	64	61	119

Table 5
SPECTRAL RATIO FUNCTION: GODDARD EARTH MODELS AND SMITHSONIAN STANDARD EARTH MODELS

n	GEM 6 VS SE III	GEM 6 VS. SE II	GEM 5 VS. SE III	GEM 5 VS. SE II	GEM 4 VS. SE II	GEM 3 VS. SE III	GEM 3 VS. SE II	GEM 2 VS. SE III	GEM 2 VS. SE II	GEM 1 VS. SE III	GEM 1 VS. SE II
2	96	98	104	102	98	96	98	97	99	97	99
3	99	98	100	102	97	99	97	99	98	100	98
4	105	103	96	98	103	106	104	104	102	105	103
5	119	82	79	115	81	118	81	127	87	131	90
6	90	78	102	119	81	95	82	92	80	97	83
7	110	89	105	130	80	97	76	108	87	97	78
8	232	78	54	158	66	178	61	216	74	189	64
9	132	143	85	79	111	104	112	111	120	102	110
10	95	112	99	84	123	92	108	110	129	98	115
11	130	159	71	58	146	127	155	136	166	122	150
12	219	124	44	78	96	175	99	207	117	187	106
13	87	104	57	47	63	219	263	69	83	185	222
14	138	143	21	20	57	467	485	72	74	335	348
15	96	124	23	18	62	753	967	74	95	359	461
16	148	204	7	5	200	1678	2309	165	227	1597	2197
17	3081	702	3	15	226	915	208	8693	1980	2357	537
18	367	70	27	142	53	254	49	527	101	513	98
19	217	363	46	28	867	570	951	120	200	95	159
20	476	321	20	29	91	115	77	1061	715	4050	2731
21	80	150	111	59	137	74	139	51	96	51	95
22	59	22	186	499	13	33	12	64	24	54	20

Table 6
SPECTRAL FUNCTION: GEM 6, SE III AND NWL MODELS

n	NWL WGSN 44 / SAO SE III	NWL 10E / SAO SE III	NWL WGSN 44 / GEM 6	NWL 10E / GEM 6
2	105	105	102	102
3	103	102	102	101
4	95	96	101	101
5	80	81	96	97
6	108	108	97	98
7	110	101	121	110
8	57	55	132	128
9	87	105	119	143
10	84	99	80	94
11	72	62	118	101
12	51	51	112	112
13	96	101	84	88
14	77	42	106	58
15	104	23	101	22
16	93	57	137	85
17	121	25	3744	781
18	192	36	704	130
19	1216	136	2644	296
20	29	32	136	151
21	667	85	539	68
22	138		82	

Table 7
SPECTRAL RATIO FUNCTION: GODDARD EARTH MODELS DIFFERENCES

n	GEM 6– GEM 5 VS. GEM 6	GEM 6– GEM 4 VS. GEM 6	GEM 4– GEM 2 VS. GEM 4	GEM 6– GEM 3 VS. GEM 6	GEM 6– GEM 2 VS. GEM 6	GEM 6– GEM 1 VS. GEM 6	GEM 5– GEM 4 VS. GEM 5	GEM 5– GEM 3 VS. GEM 5	GEM 5– GEM 1 VS. GEM 5	GEM 4– GEM 1 VS. GEM 4	GEM 3– GEM 1 VS. GEM 3	GEM 2– GEM 1 VS. GEM 2
2	0	0	0	0	0	0	0	0	0	0	0	0
3	0	0	0	0	0	0	0	0	0	0	0	0
4	0	0	0	0	0	0	0	0	0	0	0	0
5	1	1	1	1	0	1	0	0	0	1	1	1
6	1	0	1	1	0	1	28	0	0	1	1	1
7	3	2	2	3	2	6	77	1	1	2	2	3
8	5	5	3	8	3	6	2	1	1	3	2	4
9	21	13	6	23	14	29	6	2	3	9	4	19
10	13	6	6	14	4	19	7	5	3	12	8	13
11	42	18	7	34	17	54	20	8	6	27	10	43
12	36	34	14	52	25	56	33	23	12	48	25	57
13	74	57	7	70	45	78	78	10	7	63	24	74
14	78	109	8	80	71	81	93	12	6	96	26	92
15	98	159	8	95	104	105	95	14	32	109	83	97
16	90	123	8	91	109	91	92	9	14	93	23	88
17	3	77	53	87	27	230	29	93	230	116	117	391
18	2	11	28	16	14	6	9	16	11	21	23	3
19	1	40	223	42	17	64	105	46	65	319	387	16
20	39	147	124	200	137	88	41	196	103	100	102	46
21	36	188	156	121	35	76	57	83	54	133	149	13
22	11	74	97	74	38	24	39	59	31	87	82	5

Table 8
SPECTRAL RATIO FUNCTION: REPRESENTATIVE GEM AND SE DIFFERENCE

n	GEM 6–SE III VS. GEM 6	GEM 6–SE II VS. GEM 6	GEM 5–SE III VS. GEM 5	GEM 5–SE II VS. GEM 5	GEM 1–SE III VS. GEM 1	GEM 1–SE II VS. GEM 1	GEM 2–SE III VS. GEM 2	GEM 2–SE II VS. GEM 2	GEM 4–SE II VS. GEM 4
2	0	0	0	0	0	0	0	0	0
3	1	0	1	0	1	0	1	0	0
4	1	1	1	1	1	1	1	1	1
5	6	3	7	3	10	3	8	2	3
6	7	7	8	7	7	7	6	8	7
7	18	8	17	12	18	14	19	12	9
8	121	11	57	12	104	13	128	12	13
9	47	47	42	32	48	25	34	19	25
10	81	38	103	54	98	57	84	35	52
11	68	127	73	98	105	88	75	77	112
12	176	124	114	148	254	143	163	109	128
13	49	126	77	176	160	198	39	142	110
14	49	98	84	328	284	236	45	132	97
15	75	143	106	588	428	470	49	90	90
16	125	211	182	2038	1598	2104	83	60	144
17	2913	575	94	535	2538	436	8458	98	160
18	396	129	104	128	532	146	582	149	94
19	278	497	125	492	189	214	170	141	1139
20	542	426	120	572	3072	2384	626	54	184
21	137	249	218	315	128	130	118	162	245
22	136	119	251	128	144	111	148	493	112

Table 9
SPECTRAL RATIO FUNCTION: GEM 6, SE III AND NWL MODELS.

n	SAO SE III - NWL WGSN 44 / SAO SE III	SAO III - NWL 10E / SAO III	GEM 6 - WGSN 44 / GEM 6	GEM 6 - MWL 10E / GEM 6
2	0	0	0	0
3	1	1	0	0
4	1	1	0	0
5	7	7	1	0
6	7	8	1	1
7	17	19	5	4
8	56	52	9	12
9	35	34	27	34
10	80	91	15	21
11	80	82	57	60
12	114	105	93	91
13	83	106	77	87
14	102	87	131	102
15	123	95	140	99
16	167	112	156	53
17	165	83	3687	719
18	180	112	706	130
19	1197	169	2806	367
20	71	83	2773	264
21	710	99	727	136
22	161	172	193	102

Of the Goddard Space Flight Center geopotential solutions GEM 1, 3 and 5 are purely satellite derived solutions. These solutions are complete to (12, 12) but have some selected higher degree coefficients up to (22, 14). GEM 2, 4, and 6 are combination solutions, i.e., they are based on satellite tracking data as well as surface gravimetry information; these solutions are complete to (16, 16) with a few selected higher degree coefficients up to (22, 14). Generally various combination solutions are based on their satellite determined predecessors. Smithsonian SE II and SE III models are both combination solutions. The surface gravity data base in these solutions is similar to that in GEM solutions. SE II is complete to (16, 16) with a few higher coefficients. SE III is complete to (18, 18) with a few higher coefficients.

Naval Weapons Laboratory's solution 10E is purely satellite derived solution based primarily on doppler data; hence it should provide an independent standard of comparison for GEM and SE models. The NWL solution WGSN 44 is a combination solution.

The statistical parameters reported in Tables 1 through 9 in which any of the GEM 1, 3, or 5 are involved are meaningful to n = 12 only. All other comparisons are valid to n = 16. Comparisons in the higher frequency range (n > 16) are meaningless as these are based only on a limited number of harmonic coefficients.

INTERCOMPARISON OF GODDARD EARTH MODELS

GEM solutions based purely on the satellite data (Table 1A; Figure 1) show a high degree of correlation at all frequencies up to n = 12 (the correlation function for n > 12 should be neglected as it is based only on a few selected coefficients). The spectral ratio function for these fields (Table 4), which is a more sensitive parameter, is largely in the neighborhood of 100 for frequencies up to n = 12. The spectral ratio function for their differences (Table 7) is close to zero for frequencies up to n = 8 and reasonably close to zero for frequencies up to n = 12. As indicated earlier, the correlation statistics beyond n = 12 are not significant in this case as these solutions are complete to (12, 12) only.

Of the combination GEM solutions which are complete to (16, 16), GEM 6 shows a high degree of correlation with GEM 4 and GEM 2 up to n = 10 and reasonably high correlation (>0.7) to n=12 (Table 1B, Figure 1) beyond which (n > 12) the correlation function becomes irregular. On the other hand, GEM 4 is very highly correlated with Gem 2 up to n = 16 (correlation coefficient > 0.93). These findings are supported by the spectral ratio function (Table 4, Figure 1) which show considerable departures from the reference value of 100 beyond n = 12 in case of comparisons involving GEM 6 and beyond n = 16 in case of GEM 4 versus GEM 2. The spectral ratio function of the differences shows variations of close to 100 percent for frequencies n > 12 except for GEM 4 versus GEM 2 in which case this function shows less than 15% variation for frequencies up to n = 16. This fact is interesting as these solutions are derived from highly correlated GEM 1, GEM 3 and GEM 5 but the set of mean surface gravity anomalies used in GEM 6 is somewhat different from that used in earlier GEM combination solutions.

Comparison of combination solutions with those based purely on satellite orbital data (Table 1C) shows a high degree of correlation to n = 10 and a fairly high correlation to n = 12 (>0.7). Spectral ratio function statistics in Tables 4 and 7 support this high internal consistency (to n = 12) with the notable exception of GEM 4 versus GEM 5 at n = 7 (Table 7). However, this discordance is not noticeable in other comparisons.

These intracomparisons, however, show merely internal consistency of the GEM solutions. Since these solutions are not independent of each other, the high correlations cannot be interpreted in terms of the degree of accuracy of these solutions. It is interesting to note, however, that the earliest (GEM 1) and the latest (GEM 6) solutions (from amongst the solutions analyzed here) show such a high degree of correlation in spite of vastly improved data fed into the later solutions.

GODDARD EARTH MODELS VERSUS SMITHSONIAN STANDARD EARTH MODELS

The GEM solutions and the SE models are derived principally from the same type of satellite and surface gravity data, though the amount of data used in the more recent GEM solutions is larger than that used in the SE models and the methods of analysis used in the two sets of solutions are somewhat different. Thus, although the two sets of solutions do not constitute independent standards of comparison against each other, their comparisons will yield useful insights.

The comparison statistics for GEM and SE models are listed in Tables 2, 5, and 8. Some representative curves are illustrated in Figures 1, 2, and 4. The correlation function between GEM 6 and SE III is high (>0.9) to wavenumber n = 7 beyond which it falls off showing inconsistent peaks at n = 9, 11, 13, and 14 (Table 2). The spectral ratio function (Table 5) shows less than 20 percent variation to n = 7 but shows significant departures for higher frequencies. The spectral ratio function of the differences (Table 8) corroborates this pattern in that the differences are practically zero to n = 4, less than 20 percent to n = 7 and significantly higher for n > 8. The degree variances of the differences are close to zero to n = 7 but reach about the same amplitude as those of the total fields for n = 8 and higher as illustrated in Figure 5. The comparisons of SE III with GEM 5, GEM 4, GEM 3, GEM 2, and GEM 1 follow exactly analogous patterns in all the three correlations parameters (Tables 2, 5 and 8; Figures 2 and 4).

Comparison of GEM 6 and SE II shows correlation coefficients of >0.9 to n = 8 and those >0.8 to n = 10 (Table 2). The spectral ratio function (Table 5) departs from its reference value of 100 by about 20 percent up to n = 8. The spectral ratio function of the differences departs less than 10 percent to n = 7 and 11 percent for n = 8 (Table 8). This function is again practically at its reference values up to n = 4 (Table 8). This is corroborated by the correlation function plot in Figure 1 and the spectral ratio function values given in Table 5. Comparisons of SE II with GEM 5, GEM 4, GEM 3, GEM 2, and GEM 1 show even higher consistency for frequencies up to n = 10. Note that

SE II and SE III as well as GEM 2, 4 and 6 are all combination solutions while GEM 1, 3 and 5 are purely satellites derived gravity models.

NAVAL WEAPONS LABORATORY'S (NWL) GRAVITY MODELS VERSUS GEM AND SE MODELS

The Naval Weapons Laboratory's gravity models are derived principally from doppler tracking data and are independent enough from the Goddard and Smithsonian efforts to institute a fairly reasonable standard of comparison in relation to GEM and SE solutions. Unfortunately, however, NWL's gravity fields are classified. Therefore, only those statistical parameters of the NWL gravity fields which cannot be used to derive their information content are available for this study.

The NWL gravity model 10E is a purely satellite derived gravity model based principally on doppler tracking data. The NWL gravity model WGSN 44 is a combination solution. These two models are compared against GEM 6 and SE III. The correlation coefficient (Table 3) between SE III and WGSN 44 is high to wavenumber n = 7; the spectral ratio function is close to 100 to n = 4 and shows less than 20 percent variation to n = 7; the spectral ratio function of the differences is practically zero to n = 4, varies less than 10 percent to n = 6 and less than 20 percent at n = 7.

NWL 10E shows a high correlation with SE III to n = 7; the spectral ratio function for the two fields is very close to 100 up to n = 4, varies less than 20 percent between n = 5 to 7; the spectral ratio function of the differences is practically zero to n = 4, varies less than 20 percent between n = 5 to 7. The degree variances of the difference fields as illustrated in Figures 6 and 7, are close to zero up to n = 7 and reach about the same amplitude as the total fields for higher frequencies. For frequencies $n > 7$, the correlations decay rapidly, the spectral ratio function departs significantly from its reference value and the spectral ratio function of the differences rises to large values. The correlation coefficient between GEM 6 and WGSN 44 is high ($\gtrsim 0.9$) to n = 10 (Table 3). The spectral ratio function is close to 100 up to n = 6 (Table 6); the spectral ratio function of the difference fields is practically zero to n = 6, less than 20 percent to n = 10 except for n = 9 for which it is 27 percent (Table 9). The degree variances of the differences are close to zero to n = 8, reasonably small for n = 9 and 10 and equal or exceed the amplitude of those of the parent fields for higher frequencies (Figure 8). For frequencies higher than n = 10 or 11, the correlations decay rapidly and the spectral ratio functions show large variations.

GEM 6 shows a high degree of correlation ($\gtrsim 0.9$) with 10E up to n = 10 (Table 3); the spectral ratio function between the two fields (Table 6) is practically at its reference value to n = 6; the spectral ratio function of the difference fields (Table 9) is zero to n = 6 and is in the neighborhood of 20 percent to n = 10 except for n = 9. The degree variances of differences (Figure 9) are close to zero to n = 8, reasonably small to n = 10 and acquire or exceed the amplitudes of those of the parent fields for higher frequencies. Also, for higher frequencies the correlations are small and the variations of the spectral ratio function from their reference values are large.

ANALYSIS AND INTERPRETATION

For all geopotential models compared here, the correlations are practically equal to one up to wavenumber n = 4. For the same frequency range, the spectral ratio function of the total fields is practically equal to its reference value of 100 and the spectral ratio function of the differences is approximately equal to zero. The degree variances of the differences are also zero. All this indicates that the various geopotential solutions are completely consistent in this frequency range. This is most convincingly shown in Figure 10 which shows the gravity differences in milligals between GEM 6 and SE III solutions for this frequency range. Notice that the maximum amplitudes of these differences are ±2 milligals while most of the differences are in the neighborhood of 0 milligal as indicated by the rms value of close to zero for these differences.

Between the frequency range n = 5 to n = 7 the correlation function, though slightly less than 1, is still very close to one. The spectral ratio function of the total fields is in the neighborhood of its reference value and variations shown by the spectral ratio function of the differences are less than 20 percent. This is supported by the difference degree variances. Thus the various geopotential solutions are nearly identical in this frequency range. The extent of their variations is shown in Figure 11, which illustrates differences between GEM 6 and SE III in the frequency range of n = 2 to n = 7. Notice that while the maximum amplitudes of the differences reach 6 milligals, the differences are generally far less in amplitude and the rms of the differences is only 2.3 milligals.

The comparison studies indicate that in the frequency range n = 8 to 12 the various GEM solutions are internally consistent as would be expected. GEM solutions also show good agreement with the NWL solutions to n = 10. But the differences between SE III and either GEM or NWL models become significant at n = 8. This is demonstrated in Figure 12 which shows the gravity differences in GEM 6 and SE III for frequencies n = 8 and higher. Notice that the maximum amplitudes reach 36 milligals and whereas these amplitude maxima occur in the southern hemisphere, the gravity differences have comparable amplitudes and frequencies in the northern hemisphere. These gravity anomaly differences have an rms value of 9.3 milligals.

Figure 13 shows the total gravity contribution of GEM 6 in the same frequency range. Compare it with Figure 12 and notice that the amplitudes of these gravity anomalies are comparable with those of gravity anomaly differences in Figure 12. Also that the anomalous patterns, though not identical, are intriguingly similar. The rms value of these gravity anomalies is 9 milligals — very close to the rms value of the gravity anomaly differences shown in Figure 12.

The differences in geoidal heights arising from gravity anomaly differences shown in Figure 12 are given in Figure 14. The reason that geoidal differences are milder in amplitudes as well as gradients than the corresponding gravity anomaly differences is that the process of transforming the gravity anomalies into geoidal heights is equivalent to passing the gravity anomalies through the type of filter (in a spectral form) shown in Figure 15. This process tends to accentuate the effects of long wavelength gravity anomalies and scale down the effects of the shorter wavelengths. It is for this reason that geoidal comparisons are not regarded as an ideal instrument for comparative and evaluative investigations of the various gravity solutions.

The characteristics derived from the comparison of GEM 6 with SE III are shown more or less by all other solutions though the value of n may change somewhat in each case. Table 10 shows in a summary form, the concentration of spectral energy in the different frequency ranges of representative gravity solutions. For GEM 6, the total power in the frequency range of n = 2 through 7 is 119.8 milligals^2 or 876 meters^2. For the same frequency range the total power of the GEM 6 and SE III differences is 6.3 milligals^2 or 14 meters^2. Thus, the differences constitute only 5.3 percent (or 1.6 percent for geoid) of the total spectral energy in this frequency range. For the same frequency range, total spectral power in WGSN 44 and 10E is 123 milligals^2 and 121.3 milligals^2, respectively. Their differences from GEM 6, 1.1 milligals^2 and 1 milligals^2, respectively are less than 1 percent of the total spectral power for these frequencies. Same holds for geoidal comparisons (Table 10). This, together with the comparison studies, is interpreted to mean that the coefficients in this frequency range are well-determined in all recent geopotential solutions, though GEM 6 seems to test better against the independently obtained gravity solutions of the Naval Weapons Laboratory.

However, the picture is different for higher frequencies. For n > 9 the total spectral energy in GEM 6 is 79 milligals^2, that in the differences between GEM 6 and SE III is 86 milligals^2 so that the power in differences is 109 percent of the total power of the solution itself. Since GEM 6 is complete only to (16, 16) and SE III to (18, 18) it could perhaps be argued that the different cutoff frequency ranges magnify the differences spuriously. However, truncation of the two solutions at (16, 16) does not change the

Table 10
TYPICAL SPECTRAL CONTENTS OF VARIOUS FREQUENCY RANGES OF SOME REPRESENTATIVE GRAVITY MODELS.

	GRAVITY $mgals^2$			GEOID $METERS^2$		
	$n = 0-7$	$n = 8 \rightarrow$	TOTAL	$n = 0-7$	$n = 8 \rightarrow$	TOTAL
GEM 6	119.8	79.0	198.8	876.0	32.5	908.5
GEM 6 - SAO III	6.3	86.0	92.3	14.0	30.1	44.1
$\frac{\text{GEM 6 - SAO III}}{\text{GEM 6}}$ %	5.3	109.0	46.0	1.6	93.0	4.9
NWL WGSN 44	123.0	137.0	260.0	889.4	42.3	931.7
GEM 6 - WGSN 44	1.1	130.8	131.9	1.8	25.6	27.4
$\frac{\text{GEM 6 - WGSN 44}}{\text{GEM 6}}$ %	0.9	95.5	50.7	0.2	60.5	2.9
NWL 10E	121.3	75.3	196.6	885.8	34.0	919.8
GEM 6 - NWL 10E	1.0	52.8	53.8	1.7	15.3	17.0
$\frac{\text{GEM 6 - NWL 10E}}{\text{GEM 6}}$ %	0.8	69.5	27.4	0.2	45.0	1.9

above results in any significant manner. GEM 6 seems to compare somewhat better with WGSN 44 and 10E in which case the spectral power of the differences constitutes about 96 percent and 70 percent of the total spectral powers, respectively. But the important point here is that in the higher frequency range ($n \geq 8$ or 10 depending upon the models being considered), the difference spectra are of the same order of magnitude as the spectra of the total fields. This has, of course, also been demonstrated earlier in Figures 12 and 13 which show that amplitudes of the gravity anomaly differences between GEM 6 and SE III for $n \geq 8$ are of the same order of magnitude as the gravity contribution of higher frequency coefficients ($n \geq 8$) of GEM 6 or SE III. Since NWL 10E and WGSN 44 are classified it is not possible to study their individual gravity differences with respect to GEM 6 or SE III. But the comparison statistics (Tables 3, 6 and 9), indicate that GEM 6 is consistent with the NWL gravity fields up to $n = 10$ beyond which the difference coefficients acquire the same amplitude as the coefficients of the parent fields. It is thus clear that the individual values of these higher frequency harmonic coefficients should be treated with caution.

It is interesting to see the relationship between the surface gravity data used in a typical combination solution and the gravity anomaly differences between this typical combination solution and the associated purely satellite determined solution. Figure 16 shows the gravity anomaly differences between GEM 6 and GEM 5 solutions. The basic distribution of the surface gravimetric data used in the GEM 6 combination solution is shown in Figure 17. There seems to be no consistent relationship between surface gravimetric data coverage and the gravity anomaly differences.

Let us now examine Table 11 which gives rms values of observation residuals for weekly orbital arcs based on optical data for 23 satellites, 11 daily arcs based on USB Doppler data for ERTS-1 satellite, 22 BE-C short arcs based on laser data, long term zonal perturbations on 21 satellites and rms of residuals with respect to $5° \times 5°$ surface gravity anomalies (Lerch et. al., personal communication). Note that ERTS-1 Doppler arcs and BE-C laser arcs were not used in the computation of gravity models considered here and thus deserve special weight. With the exception of GEM 4, the orbital residuals from all other GEM solutions are nearly equal and while those based n GEM 5 and GEM 6 show some improvement relative to GEM 3 and GEM 4, they seem to show no recognizable improvement over GEM 1.

Table 11
SUMMARY OF GRAVITY MODEL COMPARISONS WITH SATELLITE AND GRAVIMETRY DATA

MODELS		OPTICAL DATA ON WEEKLY ARCS FOR 23 SATELLITES (SECONDS OF ARC)	U.S.B DOPPLER* DATA ON 11 DAILY ERTS 1 ARCS (CM./SEC.)	LASER DATA* ON 22 SEC SHORT ARCS (METERS)	LONG TERM GOAL PERTURBATIONS ON 21 SATELLITES (RELATIVE MEASURE)	5° TERRESTIAL GRAVITY ANOMALIES (MGAL)
GEM	1	2.54	5.9	1.33	3.62	12.5
GEM	3	2.71	5.9	2.00	2.92	12.3
GEM	4	3.10	7.2	4.05	2.89	12.2
GEM	5	2.37	5.9	1.54	3.13	12.3
GEM	6	2.74	5.5	1.65	2.97	11.6
SAO S.E.	II	3.44	10.3	2.51	5.49	12.8
SAO S.E.	III	–	11.2	–	–	12.5

*DATA FOR THESE TWO CATEGORIES WERE INDEPENDENT OF THE SOLUTIONS FOR ALL MODELS.

The rms with respect to gravimetric data is computed from $\langle (g_T - g_s)^2 \rangle$ where g_T denotes the 5° × 5° mean gravity anomaly based on surface gravity data and g_s is the corresponding gravity value computed from the specific geopotential model. GEM 6 seems to agree with the surface gravity data somewhat better than the other models. But it is probably due to the fact that the set of mean surface gravity anomalies used in the computation of GEM 6 is the same as that used in the computation of rms residuals, whereas it is somewhat different from that used in obtaining earlier GEM and SE solutions.

CONCLUSIONS

1. The spherical harmonic coefficients of Earth's gravity field up to n = 4 seem to have been determined accurately.

2. The geopotential coefficients corresponding to wavenumbers n = 5 through 7 seem to have been determined quite accurately though they show minor differences from one solution to the other.

3. The geopotential coefficients for wavenumbers n = 8 through 10 seem to be determined fairly accurately in GEM 6 and NWL solutions.

4. For frequencies higher than n > 11, the various geopotential solutions seem to be very divergent and although a cumulative contribution of these frequencies seems to make a marked improvement in the satellite orbital residuals, the significance of their individual values and their geophysical contribution are not clear.

5. While the satellite orbital data make the predominant contribution to the geopotential coefficients up to wavenumber n = 10, the higher frequencies (particularly n > 12) seem to be primarily controlled by the surface gravimetric contribution. The full potential of this contribution, however, does not appear to be realized in combination solutions.

6. While the value of the additional classical tracking data in improving the description of the Earth's gravity field in long wavelength components cannot be overstated, their contribution in extending the range of frequency of Earth's gravity field description is uncertain. New tracking data types such as laser, satellite-to-satellite and altimtery data seem to have the potential of improving the frequency range of Earth's gravity field description but a quantitative assessment of their impact is difficult at this stage.

7. On the basis of analysis reported here, it is difficult to select a particular GEM solution over other GEM solutions. For geophysical studies, however, GEM 6 is recommended because of its more updated and extensive data base. For studies based on orbital dynamics, either GEM 1 or GEM 5 seem suitable.

   NWL 10E or WGSN 44 are not available for such studies.

A note of caution. The analysis reported here is not against an absolute standard but on a relative basis so that each field which is being tested itself forms a standard of comparison for other fields in the evaluation process.

APPLICATIONS TO MARINE GEODESY:

1. In areas where only an isolated ship gravity profile is available the satellite determined gravity field can provide a better estimate of the average gravity in the area, i. e., mean gravity anomalies (at appropriate frequency range) than the profile data.

2. The long wavelength portions of the satellite determined gravity field would provide useful controls for the drift and base calibration adjustments of the ship gravimeter.

3. The long wavelength components could be used to apply a regional correction to obtain localized marine gravity anomalies for local studies. By the same token the definition of the reference surface could be extended from an ellipsoidal model to a higher degree reference surface in order to compute the residual anomalies in the frequency range of particular interest.

ACKNOWLEDGMENTS

I am indebted to Dr. Richard Anderle of Naval Weapons Laboratory and Mr. Phil Schwimmer of Defense Mapping Agency for making statistical data on NWL gravity models available to me. I am also obliged to Mr. Frank Lerch and his associates at Goddard Space Flight Center for making the geopotential coefficents of various GEM solutions available to me for this study.

REFERENCES

1. Brown, R., Geoid Determinations from Satellite Altimetry using sample functions, this volume.

2. Gaposchkin, E. M., 1973 Smithsonian Standard Earth III Special Report 353. Smithsonian Astrophysical Obsy., Cambridge, Mass. 1973.

3. Gaposchkin, E. M. and Lambeck, K., 1969 Smithsonian Standard Earth II, Special Report 315, Smithsonian Astrophysical Obsy., Cambridge, Mass. 1970.

4. Khan, M. A., Satellite Altimetry, in prep.

5. Lerch, Frank, et. al., Personal Communication. Also see Goddard Space Flight Center Contributions to National Geodetic Satellite Program, National Geodetic Satellite Handbook, Am. Geophys, J. (in press).

6. Strange, W. E., Computation of Ocean Geoids using satellite altimetry with minimal orbital accuracy, this volume.

7. Woollard, G. P. and Khan, M. A., Prediction of Gravity in Oceanic Areas, Hawaii Inst. of Geophysics Report, No. HIG-72-11, 1972.

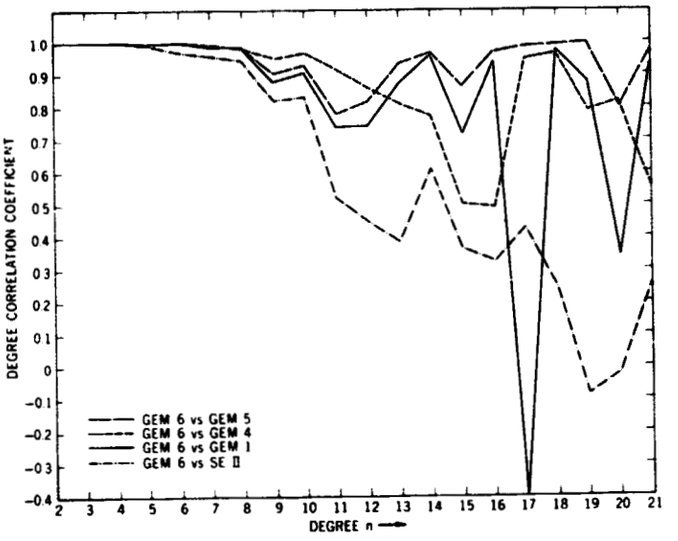

Figure 1. Degree Correlation Function

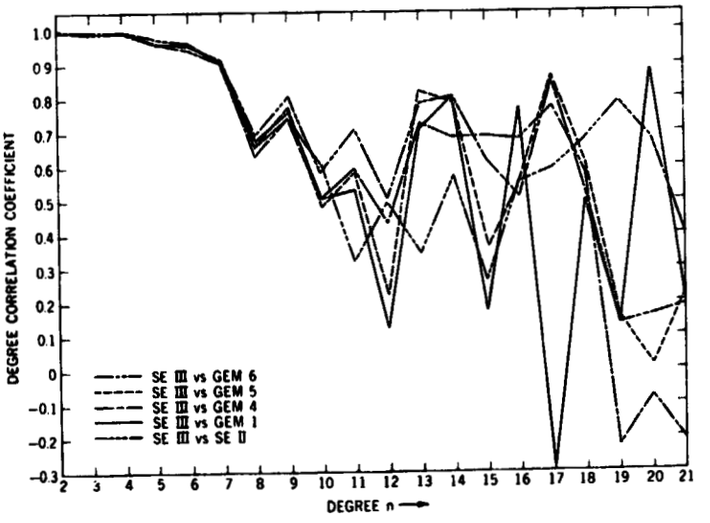

Figure 2. Degree Correlation Function

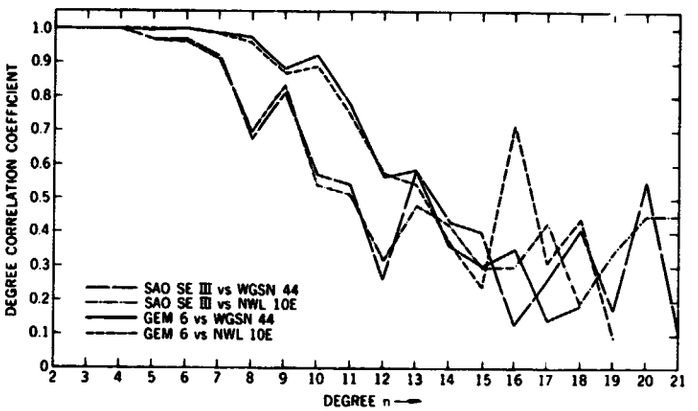

Figure 3. Degree Correlation Function

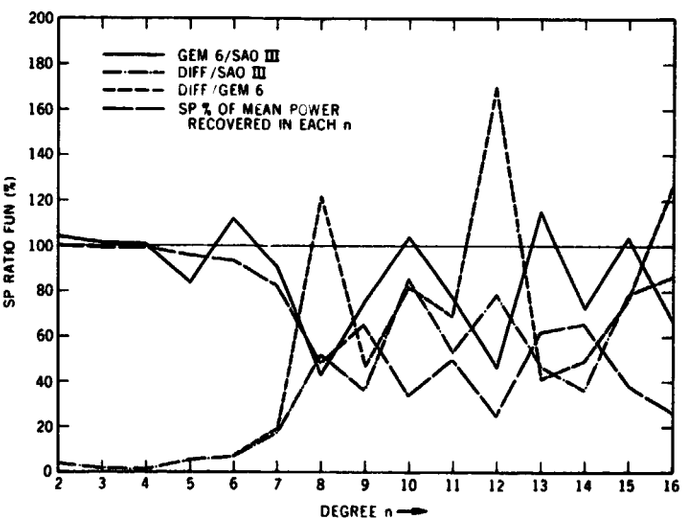

Figure 4. Spectral Ratio Function

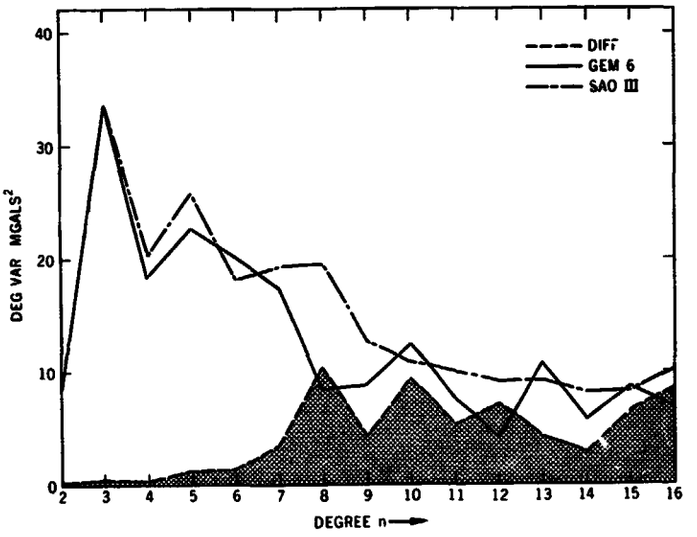

Figure 5. Degree Variances: GEM 6 and SE III

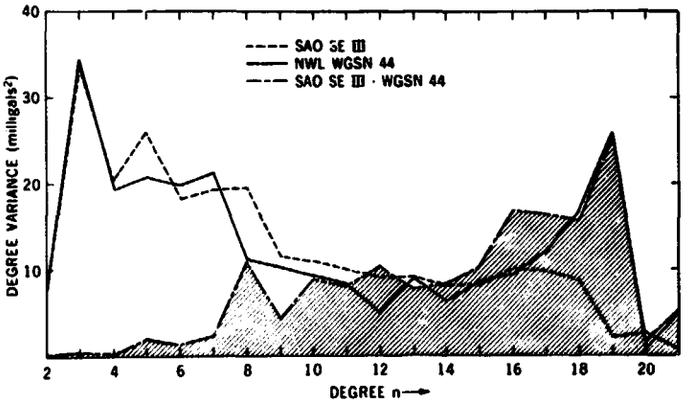

Figure 6. Degree Variances: SE III and NWL WGSN 44.

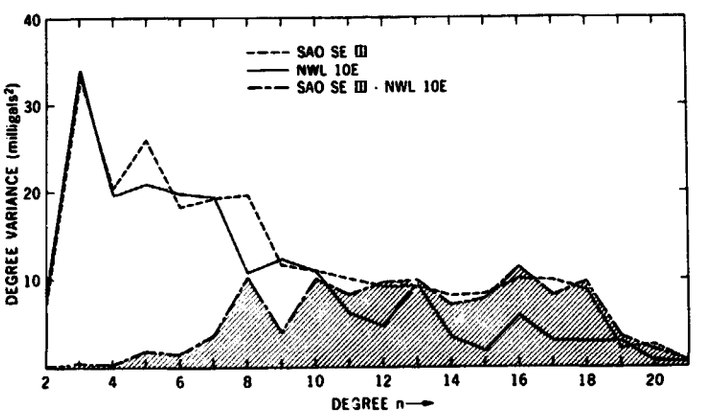

Figure 7. Degree Variances: SE III and NWL 10E

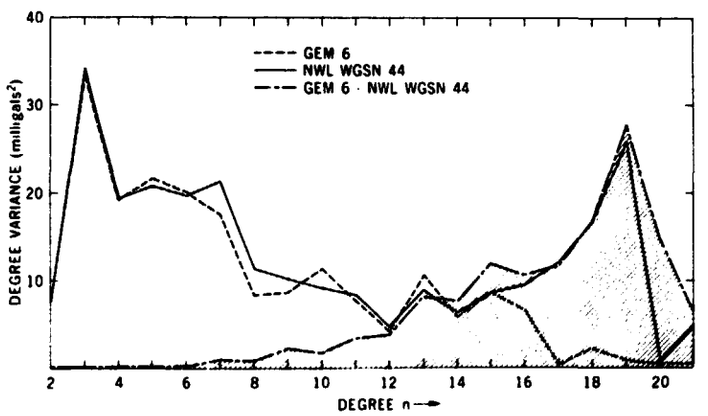

Figure 8. Degree Variances: GEM 6 and WGSN 44

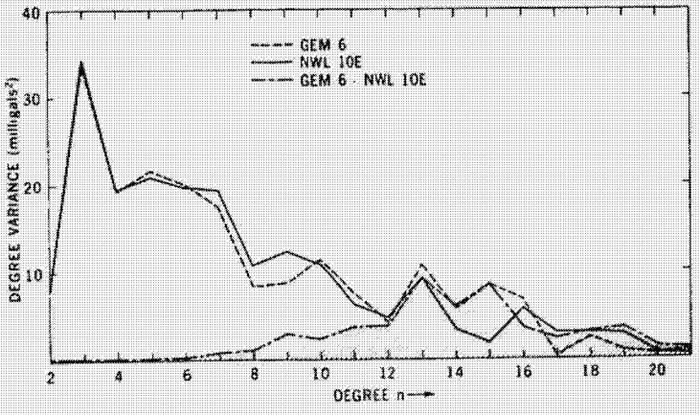

Figure 9. Degree Variances: GEM 6 and 10E

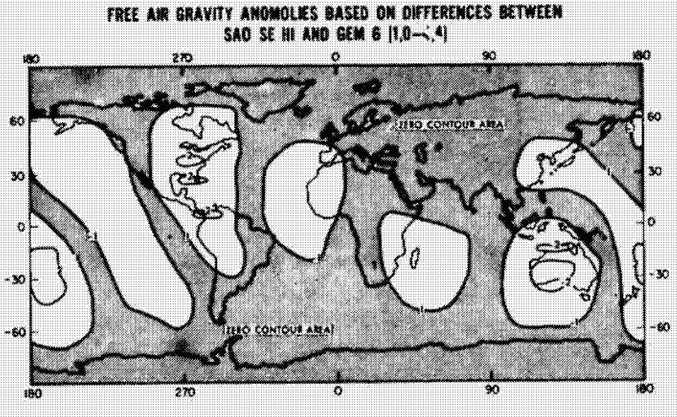

Figure 10. Free Air Gravity Anomalies based on differences between SE III and GEM 6 (2, 0 - 4, 4).

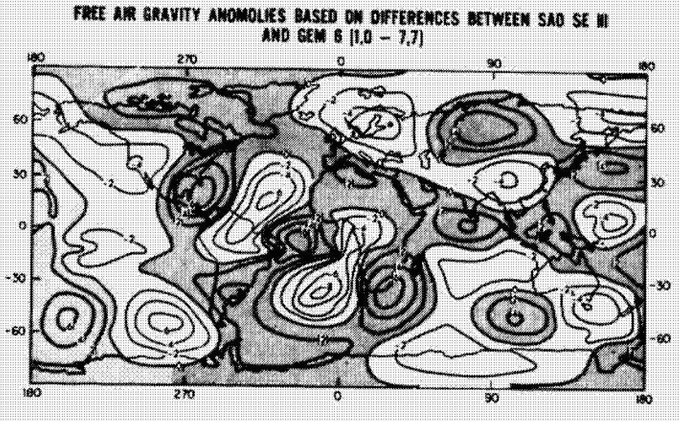

Figure 11. Free Air Gravity Anomalies based on differences betw.en SE III and GEM 6 (2, 0 - 7, 7).

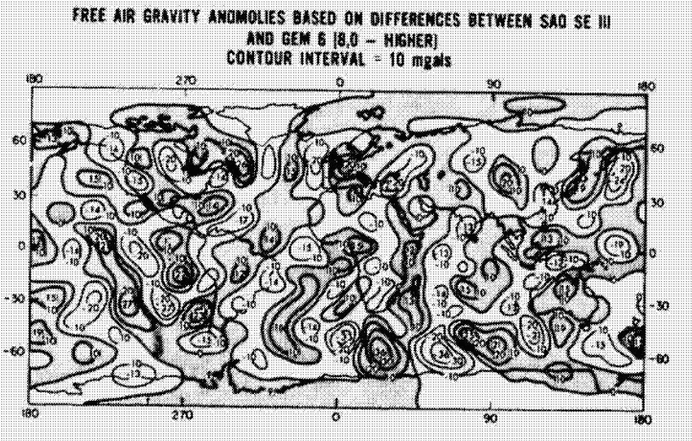

Figure 12. Free Air Gravity Anomalies based on differences between SE III and GEM 6 (8, 0 higher).

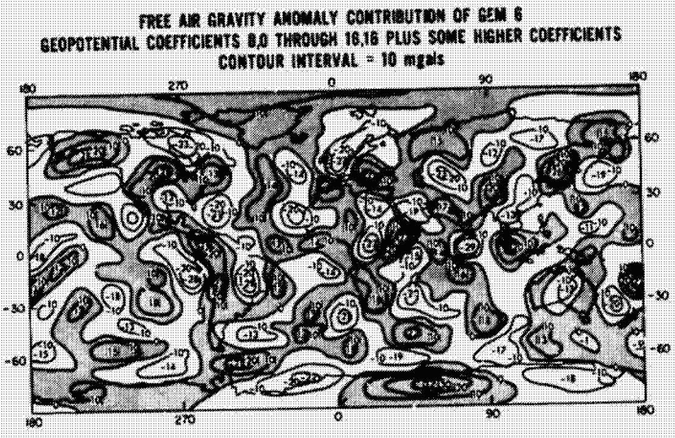

Figure 13. Free Air Gravity Anomaly contribution of GEM 6 geopotential coefficients (8, 0) through (16, 16) plus some higher coefficients.

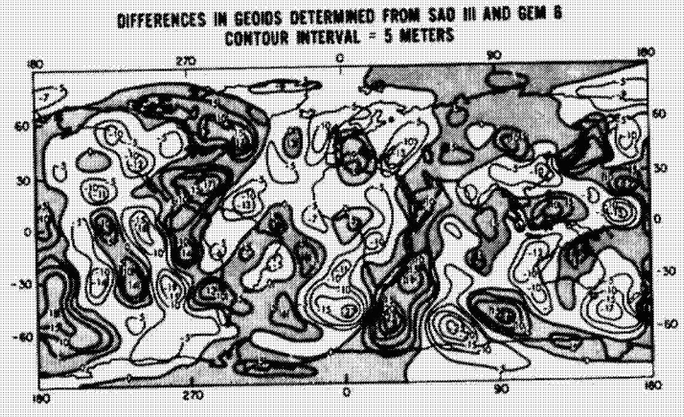

Figure 14. Differences in geoids determined from SE III and GEM 6.

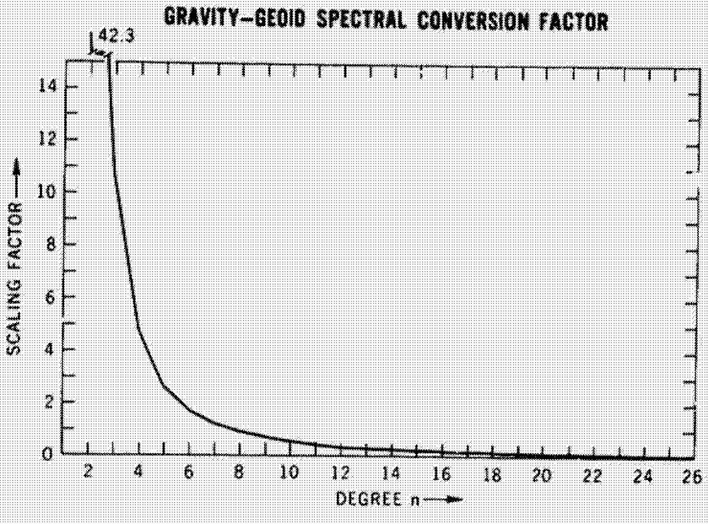

Figure 15. Spectral conversion factor from gravity anomalies to geoidal heights.

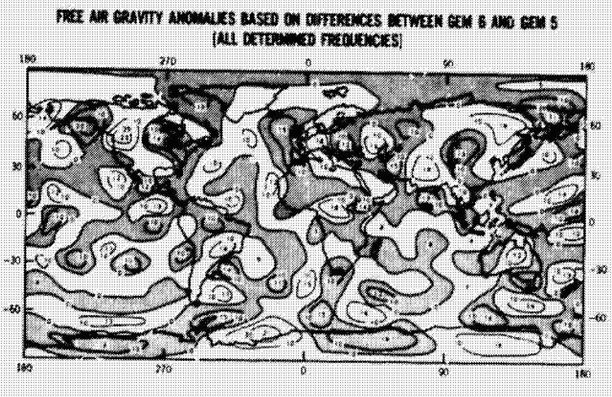

Figure 16. Free Air Gravity Anomalies based on differences between GEM 6 and GEM 5.

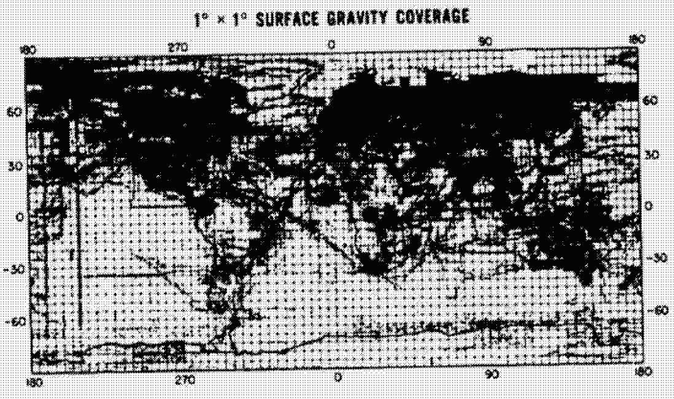

Figure 17. 1° × 1° surface gravity coverage. The number of dots in each 5° × 5° square indicates the number of 1° × 1° mean anomalies used in computing the 5° × 5° mean gravity anomaly in that square

OPEN OCEAN NAVIGATION ACCURACY CONSIDERATIONS FOR MARINE GRAVITY REQUIREMENTS

John C. Rose
Hawaii Institute of Geophysics
University of Hawaii
Honolulu, Hawaii 96822

ABSTRACT

In order to approach a ±1 mgal marine gravity accuracy, the the Eotvos correction should be as accurate as possible. Without an inertial navigation system, navigation uncertainties can produce Eotvos correction errors from 1 to 10 mgal. Shipboard navigation aids used aboard RV KANA KEOKI of the Hawaii Institute of Geophysics, coupled with a computer program for navigation adjustment can reduce the Eotvos error to ±1 mgal, resulting in a gravity reliability of ±1.4 mgal. Gyro courses and associated errors are accounted for, and circular arc turns with start and finish times known to a few seconds of time are employed. Speed and elapsed miles through the water are recorded. Satellite fix positions are corrected in the computer program for initialization errors. More than 100 recomputes of satellite fixes between 40 and 85 degrees elevation indicate that the longitude error per knot north departs significantly from the error curves published by Stansell. The longitude error in nautical miles per knot north is greater than Stansell's by 0.02 at 40°, 0.06 at 60°, and 0.08 at 70° satellite elevation. For a sequence of fixes A, B, C obtained while the ship is not doing excessive maneuvering, corrected B from AB agrees with corrected B from BC generally within a few hundredths of a mile, even though the correction of B may be 0.5 mile or so.

INTRODUCTION

Comparisons of open ocean sea gravity results obtained by different investigators in the same area shows that crossing agreement of from 10 to 20 mgal is quite common, agreement of 5 to 10 mgal is less so, and 0 to 5 mgal agreement is seldom found. Some of this discrepancy could be caused by the gravimeters. The most likely source, however, is error in the Eotvos correction which is directly linked to navigation.

The purpose of this paper is to examine navigation dead reckoning (DR) events, and procedures in order to evaluate possible errors in the Eotvos correction. Since we are most familiar with our own ship and procedures we will use examples taken from them.

The marine research activities of the Hawaii Institute of Geophysics have been carried out in the past three years on a relatively small vessel (160 feet) the R/V KANA KEOKI. Investigations are multidisciplinary, involving underway as well as

on-station work. Speed as well as course changes are quite common. The sea gravimeter on board is LaCoste and Romberg S33 with a gyro stabilized platform. There do not seem to be any serious problems with cross-coupling correction, drift, or calibration. The only limitation we have found to obtaining ±1 mgal accuracy is the error in the Eotvos correction. For this reason we take special care with the navigation procedures.

Position control almost always consists of satellite fixes from the Navy Navigation Satellite System. Other control such as Loran or VLF Omega would be welcome, but are not very useful in areas where KANA KEOKI usually operates. These areas include the Solomon Islands, the south central Pacific, and the Nazca Plate off western South America. Navigation procedures are complicated by the frequent course and speed changes sometimes required for studies other than the gravity observations. Accurate adjusted DR requires accurate information as to course, speed, and times of occurrence of navigation events such as speed change, course change and end of course change.

The aids to DR, employed on KANA KEOKI at the present time, in addition to the gyroscope and automatic-pilot, are a Sperry course recorder, a shaft rpm recorder, and a Chesapeake Instruments electromagnetic speed log with associated recorders. The course recorder chart speed drive is too slow for accurate determination of the start and end of a turn, so the ship's officers endeavor to start a turn on an even second of an even minute of time. The elapsed time from the start of the turn to the first crossing of the new heading is taken to within a few seconds. The analog knots recorder is unfiltered and is driven from precision AC, so it functions as an excellent "lie" detector for the start time of speed changes, as well as an excellent indicator of time required for a steady state new speed to be achieved. Elapsed miles to 0.01 nautical mile are printed once a minute by a printing counter.

DR SPEED ERROR

Probably the largest source of error in adjusted DR navigation, except for blunders, is the DR speed through the water. In the case where the ship has no speed log, and engine or shaft revolutions are used to estimate speed, one must account for the direct effect of wind and sea on the ship. With KANA KEOKI, a twenty knot wind directly on the bow will slow the ship down by at least one knot from the speed expected on the basis of shaft revolutions per minute. Merely because the DR speed error is of no consequence when the ship is on a long straight run between fixes (except forthe error in calculated apparent current), does not mean that the DR adjustment to the fixes will always magically remove DR speed errors. To illustrate this, consider the case of a ship at the equator receiving a good fix and subsequently travelling due east at 10.0 knots through the water for exactly two hours until it turns due south. Assume that the turn is a point turn. Now the ship proceeds due south for exactly one hour at which time another good fix is obtained. Assume that there is no wind, wave, or current action present. If there is no error in the DR speed, the DR end position is the same as that for the second fix, and the adjusted and DR tracks are identical. However, if there is an error in the DR speed through the water, the Eotvos correction can be very much in error. The errors associated with 1, 5 and 10% speed errors for the example are given in Table 1.

TABLE 1. Errors in Adjusted DR for 1, 5 and 10% Errors in DR Speed

DR SPEED ERROR %	0	1	5	10
FIX 1 TO TURN KTS	10.00	10.03	10.17	10.34
ADJUSTED CSE DEG.	090.0	089.8	089.1	088.2
EOTVOS CORR. MGAL	75.0	75.2	76.3	77.5
TURN POINT N. MI. ERROR	0.0	0.07 N,E.	0.34 N,E.	0.67 N.E.
TURN TO FIX 2 KTS	10.0	10.07	10.34	10.69
ADJUSTED CSE DEG	180.0	180.4	181.9	183.6
EOTVOS CORR MGAL	0.0	-0.5	-2.6	-5.0
APP. CURRENT SET DEG.	0	297	297	297
APP. CURRENT DRIFT KT	0.00	0.07	0.37	0.75

If the speed error is a simple percent because of either a poor calibration, or a shift in calibration, it can be evaluated from looking at the apparent current in a particular area for various courses. The wind and sea conditions must remain reasonably constant, of course. The samples should be taken within a few hours of each other and well controlled by fixes. This kind of problem has been discussed by Talwani, et al. (1966) and Talwani (1971). The ideal type of sample consists of reciprocal straight courses, each having a good pair of fixes. For such a case, the mean speed made good and mean DR speed should be the same unless the DR speed has an error. Because the effect of current has been cancelled through use of reciprocal courses, the percent error in DR speed can be evaluated directly.

SPEED CHANGES

The distance travelled through the water after the start of a speed change can either be taken from the distance indicator of the electromagnetic (or other) speed log, or it can be calculated on one of three different assumptions: Instantaneous speed change, average of initial and final speeds, or an equation taking into account viscous drag factors during the change. Ideally the best way is to use the elapsed miles from the distance indicators. Unfortunately, this is not always possible, because of excessive sparker interferance, failure of the miles printer, etc. In such cases, an equation that gives results agreeing very well with actual miles can be used.

The derivation that follows was developed in 1971 on a tentative basis by Dr. Wilton Hardy of the Hawaii Institute of Geophysics: Assume that the distance travelled after a speed change depends on a drag factor related to a viscosity parameter as well as the square of the ship's instantaneous velocity. For a velocity V, a thrust, F, of the propellors, and a viscosity parameter a, the thrust and drag cancel during a steady-state condition, and

$$F = a*v^2 \qquad (1)$$

During a speed change, an additional force $m\dot{V}$ exists so that

$$m\dot{V} = - a*v^2 \qquad (2)$$

Assuming that initial and final thrusts F_i and F_f respectively are steady state conditions, the relations are:

$$F_i = a*v_i^2$$

Rose

$$F_f = a*V_f^2$$

An increase in speed would give

$$m*\dot{V} = a*[V_f^2 - V^2]$$

$$\dot{V} = A*[V_f^2 - V^2] \; ; \; A = \frac{a}{m} \qquad (3)$$

which has the solution

$$V = V_f*(\tanh(\tanh^{-1}(V_i/V_f) + A*V_f*t/60)) \text{ knots} \qquad (4)$$

and the drag factor can be calculated from

$$A = (60/(2*V_f*t)) \ln \frac{(1+V/V_f)\ (V_f/V_i-1)}{(1-V/V_f)\ (V/V_f+1)} \qquad (5)$$

for speeds in knots and time in minutes. Letting $P = A*V_f*t/60$, integration of equation (4) yields the nautical miles travelled, which can be written as:

$$AL = (1/A)*\ln((\exp(P)*(1+V_i/V_f)+\exp(-P)(1-V_i/V_f))/2). \qquad (6)$$

A reference time interval of five minutes was adopted for R/V KANA KEOKI, as this is long enough for steady-state conditions to be achieved on either an increase or decrease in speed. Equations (5) and (6) can be shown to apply equally well to speed increases or decreases; however, V_f should be made equal to some small number rather than zero, should the case arise.

Figure 1 shows some determinations of A for R/V KANA KEOKI and Figure 2 shows comparisons between miles travelled according to the electromagnetic sword and the miles calculated from equation (6). The agreement is within a few hundredths of a mile at four minutes and so is quite satisfactory. Use of either average speed for speed changes, or instantaneous speed change assumptions leads to errors in adjusted position of about 0.1 mi and Eotvos correction errors of one mgal or more.

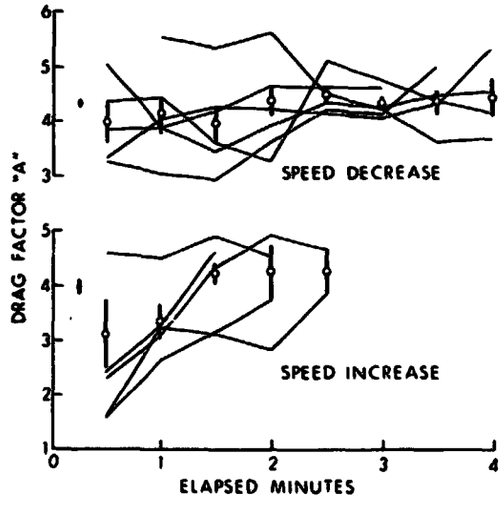

Figure 1. Determination of R/V KANA KEOKI drag-factor "A" from equations (5) for several speed changes.

Rose

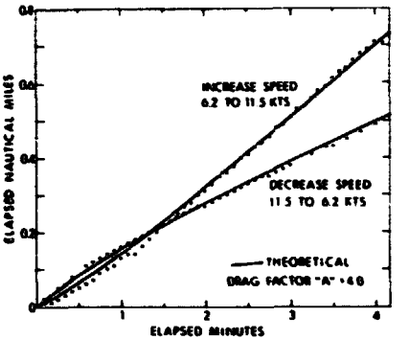

Figure 2. Comparison of distance travelled after a speed change as determined theoretically from equation (6) with that obtained experimentally from the electromagnetic speed log.

TURNS

The proper way to treat a turn for DR adjustment would be to use the advance and transfer characteristics of the ship. For a ship the size of the 160 foot KANA KEOKI, with no skegs and a flat run aft to the rudders, turns are usually made with a 3° rudder angle. So called "mud boats" of this kind can virtually turn 180° in their own length. We have adopted the assumption that the turns of KANA KEOKI can be treated as circular arcs, which is probably reasonable because in any sea state greater than moderate the ship turns are strongly affected by waves. The advance and transfer of KANA KEOKI have never been determined. However, a number of turns were monitored carefully with respect to elapsed time. Figure 3 shows three of them. The two on the left are the usual "well-behaved" S-shaped turns, and the one on the right is a "bad" turn for the circular arc assumption. For a circular arc, the radius of the turn, R, in nautical miles is given by:

$$R = \frac{\bar{V} * \Delta t_m}{\Delta\theta} * \frac{6}{2\pi} \qquad (7)$$

where $\bar{V}$ is the mean speed in knots during the turn, Δt_m is the duration of the turn in minutes, and $\Delta\theta$ is the number of degrees involved. It should be noted that the ship's speed generally drops for turns larger than 10°. For turns larger than 45° a speed loss of 20% is not unusual. After crossing the new course, the ship usually gets back up to cruising speed within 30 seconds. To get an estimate of position displacements involved, straight-line approximations to segments of two of the turns in Figure 3 were used to calculate the effective turn radius corresponding to each segment of a turn. The analog recorder associated mean speed for each segment was used. The end point was then compared with that obtained with an assumed circular arc turn whose radius was calculated from (7) using the analog speed recorder mean for the total turn. The total time interval was taken to be from the initiation of the turn to the first crossing of the new course. The results are shown in Figure 4, which shows that the displacement error in a circular arc assumption can be as small as 0.02 miles for a well behaved turn, and as large as 0.16 miles for a "bad" one. In any case, however, it is obviously better to use some kind of arc assumption rather than a point turn, which would have resulted in 0.23 and 0.14 mile errors in latitude and longitude respectively for the "bad" turn.

Rose

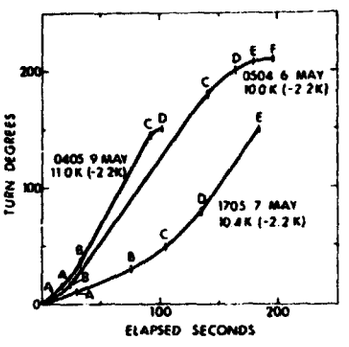

Figure 3. Several turns of R/V KANA KEOKI plotted as a function of time. The end time is the first crossing of the new heading. Straight line segments between lettered points were used for calculating the effective turn radii. Total speed-loss in knots during the turn is given in the parentheses.

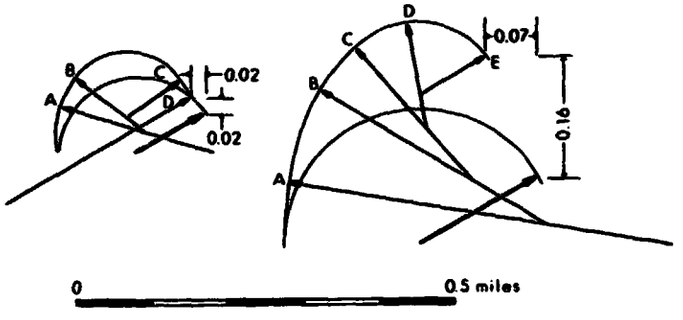

Figure 4. Comparison between the end positions of a turn by segments, and by a circular-arc and total time interval assumption. The left-hand and right-hand figures in Figure 3 were used.

It is important to distinguish between the time of first crossing the new course (XNC) and the old favorite phrase "steady on" (S/O). Use of the latter usually means that the helmsman has been fiddling with the steering for some time after XNC in trying to get the new course to approximate the new heading. A turn radius based on the time difference between "change course" (CC) and S/O would therefore be quite unreliable. On our ship the bridge officers use a stopwatch to get the CC to XNC time interval. They also activate an event marker button briefly for each event. The signal goes on to most of the science laboratory recorders.

An example of the consequences of using a point turn

assumption will be illustrated for the case of a ship with KANA KEOKI characteristics: There is no current, no wind, and the ship is at the equator. The ship proceeds from fix A at 0000:00 time on course AB deg at 10.00 kt for one hour. At 0100:00 the ship starts a course change of 90° right to course CD deg and it crosses the new course at 0102:15. Assume that it lost no speed during the turn. Its true turn radius is 0.25 nautical mile. It proceeds on course CD. At 0200 a new fix is acquired. Because there is no wind and no current, the 0200 DR position coincides with the 0200 fix position if a circular arc turn of radius 0.25 miles and 2^m15^s turn duration has been used for the DR. No adjustment is necessary. If a point turn assumption had been used, the DR position and the 0200 fix would have been different and the adjustment process would have created a fictitious 0.25 kt apparent current.

For a point turn the corner would have been incorrect in position by 0.125 mi, and the errors in the EOTVOS correction for the two segments would have been as follows:

$$\text{False } E_{AB}\text{-True } E_{AB}=7.5*[10.125*\sin(AB°+.7)-10.0*\sin(AB°)] \text{ mgal}$$

$$\text{False } E_{CD}\text{-True } E_{CD}=7.5*[9.875*\sin(CD°-.7)-\frac{9.75}{.9625}*\sin(CD°)] \text{ mgal}$$

If course AB is 045° the AB and CD errors are +2.3 and -0.7 mgal respectively, and if AB is 090° the errors are +0.9 and +0.9 mgal respectively. The conclusion is obvious: It is better to use an arcuate turn than a point turn assumption, even if one has to estimate the turn duration.

GYRO ERROR

Gyro compasses are generally set by the bridge officers to compensate for speed and damping errors approximately every three degrees of latitude. The expected gyro error, GE_E, would be the difference between the calculated error and the compensation, taking into account the latitude and speed differences from the compensation setting. The gyro error observed by the bridge officers should be normalized to the equivalent latitude and speed of the compensation setting by subtracting GE_E. For a Sperry Mk 14 gyro, the total speed and damping error in degrees for which the compensation is set, GE_C, is given by

$$GE_C = -0.0635*V_C*\cos C/\cos\varphi_C + 1.7 \tan \varphi_C \qquad (8)$$

where V_C and φ_C are the compensation knots and latitude respectively, and C is the ship's course. The expected error is then the difference, at some other speed and latitude, from GE_C, or

$$GE_E = 0.0635*\cos C*(V_c/\cos\varphi_c - V/\cos\varphi) - 1.7*(\tan\varphi_c - \tan\varphi) \qquad (9)$$

and the error observed by the bridge personnel GE_B, with respect to celestial objects and normalized to the compensation setting situation is given by

$$GE_{BC} = GE_B - GE_E. \qquad (10)$$

A fixed error in the DR course tends to be removed completely in the navigation adjustment process, because it amounts to a rotation of coordinates. Also, at normal cruising speeds, GE_E will be negligible. However, from (9) it is seen that when there is an appreciable difference between V and V_C, GE_E can be perhaps 0.3 deg. In a worst case north-south course this could be 0.4 mgal and should not be ignored.

SATELLITE FIX POSITION ERROR

The Navy Navigation Satellite System has been discussed by Stansell (1970), and its use at sea by Talwani, et al. (1966).

The particular matter to examine here is the fix position error which can be caused by incorrect course and speed initialization of the satellite receiver. This can be the result of operator error, strong local currents, etc. In particular, we were concerned about the relatively large longitude errors which result from initialization errors in the north component of the speed. We plotted the position errors from more than 180 satellite fixes in which the knots north and knots east errors were known. Twenty-six of these were taken from Talwani et al. (1966) and twenty from Matzke (1971). The rest were all done by us as recomputes. There was no apparent difference between the Stansell curves and the data we examined except for the case of longitude error per knot north. This is shown in Figure 5. The open squares with error bars are from the

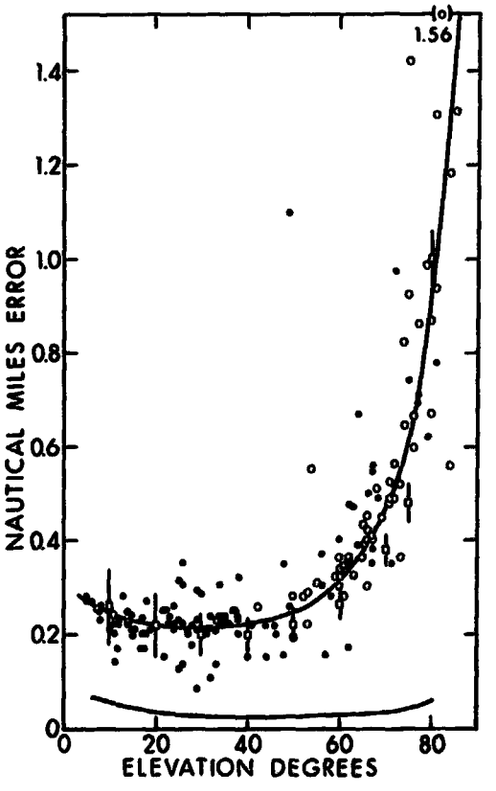

Figure 5. Nautical miles error in latitude (lower curve) and longitude (upper curve) per knot north error in initialization of the satellite navigation system. Lower curve and upper open squares are equivalent to latitude and longitude errors respectively as published by Stansell. Open circles are from recomputes specifically intended to examine the longitude error for elevations larger than 50 deg.

published Stansell curve of longitude error per knot N. The open circles show specific fixes obtained at sea in 1972 for which the elevation was usually 50 or more degrees above the horizon. They were recomputed for the three cases: Zero knots; one knot north; and one knot east. We have adopted the upper curve shown in Figure 5 for the longitude error per knot north. The differences in nautical miles error between the curve and the points taken from Stansell are 0.02, 0.04 and 0.06 at 40, 60 and 70 degrees elevation respectively.

The direction of the latitude and longitude errors depends on the geometry of the satellite pass. Our navigation program uses an iteration loop to correct the position of all satellite fixes we use. For a sequence of fixes A, B and C, the A to B adjusted B position generally agrees with the B to C adjusted B position within a few hundredths of a mile, even though the correction may be as large as 0.5 mile.

The effect of satellite position fixups on track crossing errors was checked for two site surveys done with KANA KEOKI in 1971. For "Site 3" there were 77 tracks for 35 crossing samples or 42 degrees of freedom. The site 3 seas were state 1 to 2. The standard deviation was ±1.9 mgal for the case of no fixups, and ±1.75 mgal with fixups. Assuming a one-mgal gravimeter error, the implied navigation errors are ±1.6 and ±1.4 mgal respectively, a slight improvement of 0.2 mgal. For another location, "Site 4", where sea states were 5 to 6, the before and after fixup standard deviations were ±3.1 and ±2.5 mgal respectively. For this site the gravimeter error is assumed to be ±2 mgal. Then the implied navigation errors are ±2.4 and ±1.5 mgal respectively, a significant improvement. At site 4 there were 65 tracks and 32 crossing sample locations for 33 degrees of freedom.

CONCLUSIONS

1. The largest errors in the adjusted DR track could easily be the result of DR speed errors. These could be caused by no speed log, speed log calibration error, or interferance with the speed log caused either electrically, or mechanically as with cavitation or skin effects. In the case of calibration, error smaller than 5% is difficult to detect because then the adjusted track would exhibit Eotvos correction errors of only a few mgal.

2. The most direct and accurate DR procedure for speed changes is to use elapsed miles (suitably corrected for calibration error) from the speed log to bridge the transient time interval of the speed change. The next best method appears to be the use of an equation that takes the drag of the water on the ship into account. The use of old speed and new speed average for DR through a speed change can easily result in position errors of 0.1 n.m. and Eotvos correction errors of 1 mgal.

3. The start time as well as duration of a turn are very important. In case the duration is unknown, it should be estimated. In case advance and transfer characteristics of the ship are unknown, a circular arc assumption should be used. A point turn assumption for our ship leads to Eotvos correction errors of about 1 mgal.

4. Gyro errors are usually not very serious because they are constant and are corrected as coordinate rotation

in the DR adjustment. For ship speeds quite different from that for which the compensation was set, the Eotvos correction for essentially north-south courses could be off by 0.5 mgal.

5. Satellite fixes can easily be off in longitude position by 0.1 n.m. if errors in initialized course and speed are not taken into account.

6. For a localized area survey involving turns, speed changes, etc., possible Eotvos correction errors might be as follows:

Source	Mgal Error
Speed calibration	2.0
Speed change DR assumption	1
Turn DR assumption	0.9
Turn error	0.5
Time of event error	0.3
Gyro error	0.2
Satellite fix position	0.5
Net Variance	6.44 $(\text{mgal})^2$.

Thus navigation DR adjustment alone might result in ±2.5 mgal uncertainties. If a ±2 mgal gravimeter error is assumed as well, the net error could be ±3.2 mgal. If another ship had similar errors, the crossings of the tracks of the two could easily show errors of ±4.5 mgal or so.

7. An obvious improvement would be the use of an inertial navigation system to provide E-W velocity components. This would be expensive.

ACKNOWLEDGEMENTS

Dr. Wilton Hardy of the Hawaii Institute of Geophysics was very helpful regarding speed change equations he had developed. This research was supported in part by the Office of Naval Research under Contract N00014-70-A-0016-0001, in part by the National Science Foundation under GX28674, and in part through funds from the State of Hawaii.

REFERENCES

Hatzke, D. E. An optimum six parameter estimation process for Navigation Satellite (SRN-9) data, Marine Technology Society Journal, 5 (2), 37-42, 1971.

Stansell, P. A., Jr. The Navy navigation satellite system: description and status, The International Hydrographic Review, XLVII, 51-70, 1970.

Talwani, M., J. Dorman, J. L. Worzel, and G. M. Bryan. Navigation at sea by satellite, J. Geophys. Res., 71, 5891-5902, 1966.

Talwani, M. Gravity in The Sea, Vol. 4, part 1, edited by A. Maxwell, 251-297, Interscience, N.Y., 1971.

Hawaii Institute of Geophysics Contribution No. 607.

INTEGRATED NAVIGATION BY LEAST SQUARE ADJUSTMENT, A MEANS FOR PRECISE POSITION DETERMINATION IN MARINE GEODESY

K. H. RAMSAYER
UNIVERSITY OF STUTTGART
GEODAETISCHES INSTITUT AND INSTITUT FUER FLUGNAVIGATION

ABSTRACT

For position finding at sea different navigation systems are available. Unfortunately the accuracy of these systems is in most cases insufficient for marine geodesy. This problem can be overcome partially by integrated navigation, that means a combination of different navigation systems in such a way, that the qualities of the combined system are better than the qualities of its components. A good tool for such a combination is the integrated navigation by least square adjustment which is under development by the Institute of Air Navigation of the University of Stuttgart.

The principle is the following: The basic navigational system of a vehicle (ship or aircraft) is a dead reckoning system (DRS), e. g. an inertial navigation system (INS) or a Doppler navigation system (DNS). This DRS, the accuracy of which is mainly depending on some systematic errors, is combined with other navigational aids by a computer in such a way that its most important systematic errors can be determined and taken into account by corresponding corrections.

The other navigational aids are used to get control measurements, e. g. distances, bearings, differences of distances etc., which refer to points with known position. Simultaneously just the same quantities for the indicated D. R. position are computed. The differences between the measured and the computed quantities, which are caused by the errors of D. R. and the errors of control measurements, are described by observation equations. These observation equations take into account the influence of the most important systematic error sources of the DRS and include all other errors as unknown corrections. The quantities of the systematic errors, which are described by the error model of the DRS, are then determined by a least square adjustment and are used for a corresponding correction of the DRS.

The method is demonstrated for an integrated INS/LORAN resp. INS/OMEGA system, possibly combined with the Navy Navigation Satellite System. The data can be processed in real time during cruising. A more complex but also more accurate method is the evaluation of the navigation data after the mission. In this case the data of the different navigation systems must be stored in short time intervals.

RAMSAYER

INTRODUCTION

For position finding at sea different navigation systems are available, such as OMEGA, LORAN, Satellite Navigation System, Inertial Navigation Systems, etc. For marine geodesy the accuracy of these systems is in most cases insufficient. This problem can be overcome partially by integrated navigation, that means a combination of different navigation systems in such a way, that the qualities of the combined system are better than the qualities of its components. Kalman filtering has proved to be a good tool for such a combination. A much simpler method is the integrated navigation by least square adjustment which is in development by the Institute of Air Navigation of the University of Stuttgart.

PRINCIPLE

The principle of this method is the following: The primary navigational system of the vehicle (ship or aircraft) is a dead reckoning system (DRS). This can be an inertial navigation system (INS), a Doppler navigation system (DNS) or, less accurate, a classical dead reckoning system, which determines the path from speed and current resp. wind. Error analysis of DNS has shown that the accuracy is mainly depending on some systematic error sources which are constant or only slowly changing with time [5, 6] . The same behaviour, though somewhat more complex, can be expected of INS. Hence we can expect an essential improvement of accuracy if it is possible to determine the most important systematic errors of the DRS and to take them into account by corresponding corrections.

This can be done by combining the DRS with other navigational aids by a computer in the following way: The other navigational aids are used to get control measurements, either continuously or from time to time. These measurements include according to the available ground based navigation system distances, differences of distances, bearings, etc.,which refer to points the position of which is known. Simultaneously just the same quantities for the indicated D. R. position are computed. The differences between the measured and the computed quantities, which are caused by the errors of dead reckoning and the errors of control measurements, are described by observation equations. These observation equations take into account the influence of the most important systematic error sources of the DRS and include all other errors as unknown corrections. The values of the systematic errors, which are described by the error model of the DRS, are then determined by least square adjustment. So there is no difficulty to calculate the influence of the systematic errors on D. R. and to get a corresponding correction.

ERROR MODELS OF INS

The error model of INS is usually described by a set of second order differential equations. For a least square adjustment an essentially simplified error model with linear combination of the unknowns is required. For a cruise of three hours or shorter with approximately constant speed and course, the error model can be described according to [3] with good approximation by the following equations:

$$\Delta\varphi = r \cdot \Delta B = x_1 + x_2 \cdot \sin \omega t + x_3 \cdot \cos \omega t + x_4 \cdot t \,, \qquad (1)$$

$$\Delta\eta = r \cdot \cos B \cdot \Delta L = x_5 + x_6 \cdot \sin \omega t + x_7 \cdot \cos \omega t + x_8 \cdot t \,, \qquad (2)$$

$\Delta\xi$ = northern component of position error,
$\Delta\eta$ = eastern component of position error,
r = mean radius of the earth,
B = latitude,
ΔB = error in latitude,
ΔL = error in longitude,
$x_1 \ldots x_8$ = unknown parameters of INS,
ω = Schuler circular frequency,
t = time.

If we reduce the duration to 15 minutes or shorter the error model can be simplified according to [7] to

$$\Delta B = \Delta B_m + (B' - B_m') \cdot k - (L' - L_m') \cdot \cos B_m' \cdot \Delta T, \tag{3}$$

$$\Delta L = \Delta L_m + (L' - L_m') \cdot k + (B' - B_m') \cdot \sec B_m' \cdot \Delta T + (L' - L_m') \tan B_m' \cdot \Delta B_m, \tag{4}$$

ΔB, ΔL = error of indicated latitude B' resp. longitude L',
B_m', L_m' = mean values of all indicated values B' and L' within the time interval taken into account,
ΔB_m, ΔL_m = corrections of B_m' and L_m',
$k = \Delta v / v'$ = influence of speed error Δv, v' = mean value of indicated speed,
ΔT = course error.

This model is especially suited for an airborne INS by which a flight path of 200 km or more can be covered within 15 minutes.

INTEGRATED INS/LORAN-NAVIGATION SYSTEM

As an example an integrated INS/LORAN-System is described in the following, Fig. 1. The main components are the INS, a LORAN-C receiver, an atomic clock and a computer. The integrated system is operated within the range of the LORAN chain with the transmitters S_1, S_2, S_3. By the LORAN receiver usually the hyperbolic coordinates $(R_2 - R_1)$ and $(R_3 - R_2)$ are measured. This has the disadvantage that the adjustment is complicated by the fact that the measured quantities are not independent but correlated by the range R_2. To overcome this difficulty we do not measure range differences but ranges themselves [2]. This can be done with the help of an atomic clock [9]. In this case we measure the times of arrival of the signals transmitted by the different stations with the atomic clock, and determine the unknown clock correction or the corresponding distance correction simultaneously with the other unknowns by adjustment. The range method is more accurate than the range difference method because of its better geometry and because the disturbed LORAN signal is not compared with another disturbed LORAN signal but with an undisturbed normal frequency [2, 4].

The available data are integrated in the following way: We compute in regular time intervals, for example every minute, the lengths R_1', R_2', R_3' of the geodesics from the INS-positions B', L' to the LORAN-stations S_1, S_2, S_3 and compare these ranges with the measured ranges R_1^{gem}, R_2^{gem}, R_3^{gem}. The differences between the measured and computed ranges are explained by observation equations of the following type:

$$v = \frac{1}{r} \cdot \frac{\partial f}{\partial B'} (x_1 + x_2 \cdot \sin \omega t + x_3 \cdot \cos \omega t + x_4 \cdot t) + \frac{1}{r \cdot \cos B'} \cdot \frac{\partial f}{\partial L'} (x_5 + x_6 \cdot \sin \omega t + x_7 \cdot \cos \omega t + x_8 \cdot t) - x_9 \cdot c - (R^{gem} - R'), \tag{5}$$

$$R' = f(B', L', B_s, L_s), \tag{6}$$

V	=	unknown correction,
r	=	mean radius of the earth,
$x_1, x_2 \ldots x_8$	=	unknown parameters of INS,
x_9	=	unknown correction of the clock,
C	=	speed of electromagnetic waves.

Each range measurement gives such an observation equation. If more than 9 measurements are available, the unknown quantities $x_1 \ldots x_9$ are determined by a least square adjustment. The adjustment is repeated in regular time intervals, for example every 5 minutes. That means that the accuracy of the error parameters is increasing with the number of control measurements which are processed by the adjustment. The parameters determined are used to correct continuously the output of INS. The corrected values B, L are more accurate than the values B', L' of the unaided INS. They are also better than the positions which are derived from LORAN only, because the integration method can be understood as a means to average the LORAN positions over a long time respectively a large distance.

OTHER POSSIBILITIES FOR INTEGRATED NAVIGATION

The integrated INS/LORAN-Navigation is applicable only within the area covered by LORAN. A worldwide but somewhat less accurate system could be established by the integration of INS with OMEGA and the Navy Navigation Satellite System (NNSS). The INS/OMEGA-System would average the short periodic errors of OMEGA and would be corrected for a great deal of long periodic errors about every 90 minutes by NNSS fixes. If we add an atomic clock both OMEGA and NNSS can be operated as rangesystems and the data can be processed by least square adjustment in a way which is similar to the described INS/LORAN-system. A further improvement could be obtained if Differential-OMEGA would be available. In this case the change of velocity of electromagnetic waves would be controlled by a receiver at a fix position in the neighborhood of the ship.

Other possibilities for integrated navigation of ships are the combination of DOPPLER SONAR + COMPASS with NNSS [1,8] for a water depth up to 400 m and DOPPLER SONAR + COMPASS with NNSS and LORAN-C [4] for operations in deep sea. In both cases the different components could be integrated by least square adjustment.

EVALUATION AFTER THE MISSION

The described method of integrated navigation can be understood as a calibration of the dead reckoning system by each adjustment and an extrapolation of the last state vector until the next adjustment is completed. That means that the accuracy of the integrated system is changing with time. At the beginning the accuracy will be relatively low because only a limited number of control measurements is available. Within the period of validity of the error model of the DRS the accuracy will increase from adjustment to adjustment because the DRS is updated by an increasing number of control measurements. If the period of validity of the error model is exceeded the accuracy of the integrated system will decrease because the influence of the neglected errors is increasing with time.

These disadvantages can be overcome if during the mission the data which are to be processed are stored on magnetic or punched tapes, and if the stored data are adjusted afterwards. In this case we get a higher and more uniform accuracy and can try to improve the results by variation of the error model.

REFERENCES

[1] Clavelloux, N.: Doppler-Sonargerät. Theoretische Untersuchung der Begrenzungen. Anwendung auf die Navigation von Schiffen. Kopplung Doppler-Inertialsystem. Kopplung Doppler-Ortung mit Hilfe von Satelliten. Paper presented at the International Congress of the European and American Institutes of Navigation, Hannover, 2. - 5. October 1973.

[2] Horowitz, L.: Direct-Ranging LORAN. Navigation: Journal of the Institute of Navigation (USA). 1970, pp. 200-204.

[3] Joos, D. K.: Fehlermodell eines Inertialnavigationssystems als Bestandteil eines integrierten Navigationssystems. Veröffentlichung des Instituts für Flugnavigation der Universität Stuttgart. In preparation.

[4] Kampmann, J.: Ein um die Radionavigation erweitertes Doppler-Sonar-Navigationssystem mit Satellitenfixkalibrierungsmöglichkeiten. Paper presented at the International Congress of the European and American Institutes of Navigation. Hannover, 2. - 5. October 1973.

[5] Ramsayer, K.: Untersuchungen über die Genauigkeit der Dopplernavigation. Ortung und Navigation, 1964, Heft 4.

[6] Ramsayer, K.: Integrated Navigation by Least Square Adjustment. Paper presented at the AGARD-meeting "HYBRID NAVIGATION SYSTEMS" Delft-Netherlands, 22. - 26. Sept.1969.

[7] Ramsayer, K.: Integrierte Inertial/VOR/DME-Navigation durch Ausgleichung nach der Methode der kleinsten Quadrate. Ortung und Navigation, 1972, Heft I.

[8] Rehmert, H.: Navigationsanforderungen für geophysikalische und ozeanographische Explorationen und Erfahrungen mit einem integrierten rechnergestützten Schiffssteuerungssystem. Paper presented at the International Congress of the European and American Institutes of Navigation. Hannover, 2.-5. October.1973.

[9] Sender, F.: Mit Atomfrequenznormalen gestützte Radionavigationsverfahren für weltweite Navigation. Paper presented at the International Congress of the European and American Institutes of Navigation. Hannover, 2. - 5. October 1973.

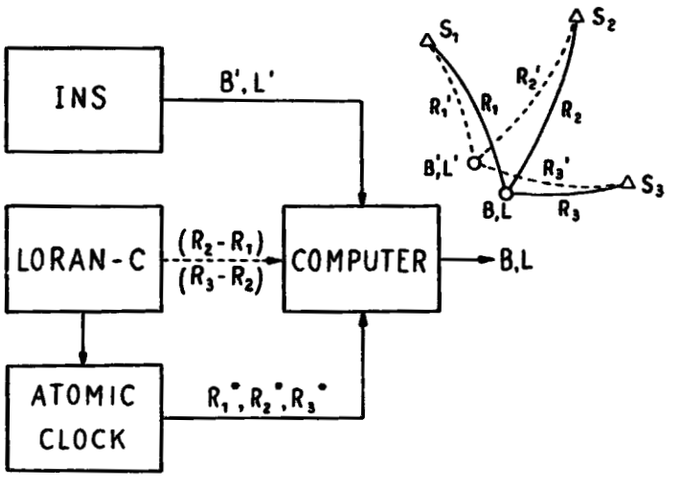

Figure 1. Integrated INS/LORAN-Navigation System.

Prof. Ramsayer: Yes.

DIFFERENTIAL LORAN-C IN INTEGRATED MARINE NAVIGATION SYSTEMS

R. R. Hatch
Manager, Navigation Systems Software
Magnavox Research Laboratories
Torrance, California

J. J. Winterhalter
Technical Director, Doppler Sonar Department
Magnavox Research Laboratories
Torrance, California

ABSTRACT

As the exploration for oil has moved to increasingly deeper water, the requirement for a highly accurate navigation system not limited by the depth constraints of the doppler sonar has become more obvious. This paper describes the Magnavox Model 200 Integrated Navigation System, which has been expanded to include Loran-C as a velocity sensor in order to meet this requirement.

First, a complete description of the principal equipment which comprises the system is provided. Particular emphasis is placed upon the equipment used to provide the Loran-C capability.

Next, a description is given of the Loran-C signal processing techniques employed by Magnavox. These techniques are shown to have wide applicability, not only to Loran-C, but also to other radio navigation aids such as LORAC, Raydist, SHORAN, and Decca.

The combined result is a system which is very flexible and uniquely suited to provide a highly accurate navigation system, even in deep waters.

INTRODUCTION

Satellite navigation in conjunction with automatic dead reckoning, using doppler sonar and gyrocompass inputs, has become the standard navigation system in use by the geophysical exploration industry. The principal reasons for this wide acceptance are the excellent accuracy, 24-hour operation, and world-wide availability. The Magnavox Model 200 (Figure 1) is an example of such a system. Position accuracy of less than 0.5% of distance traveled between satellite fixes can be maintained with this system (Reference 3).

However, the increasing interest in seismic exploration at water depths exceeding the bottom tracking capabilities of the doppler sonar has stimulated a demand for alternate navigation systems. To meet this demand, Magnavox has chosen to incorporate a Loran-C radio navigation capability into the Model 200 system. Principal reasons for this choice are its availability, particularly in areas of geophysical interest, its accuracy potential, and its relatively simple shipboard equipment.

This expanded Model 200 system has demonstrated the capability of operating in deep water with an accuracy on a par with that of a doppler sonar system in shallow water. The equipment selected and the processing techniques employed by Magnavox are described in the following pages.

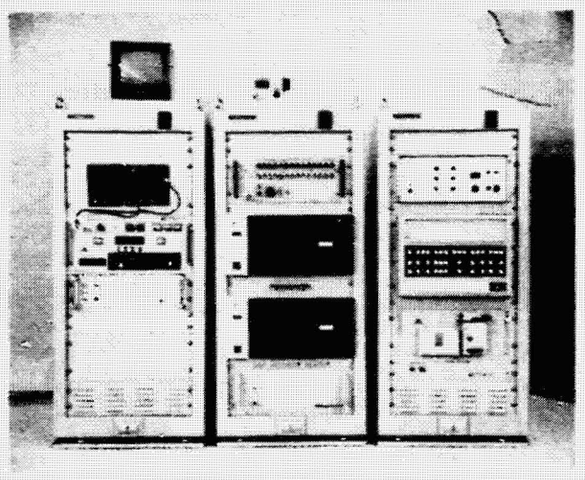

Figure 1. Model 200 System

SYSTEM ELEMENTS

The following elements comprise the basic Magnavox Model 200 Integrated Navigation System with Loran-C.

- Magnavox MX 702A two-channel Satellite Receiver
- Hewlett Packard 2100A Minicomputer with 16K memory
- Teledyne TDL 601G Loran-C Receiver
- Hewlett Packard 5065A Rubidium Frequency Standard
- Magnavox Model 200 Interface Unit
- Magnavox MX 600 Doppler Sonar
- Sperry MK 227 Gyrocompass or S. G. Brown MK 10 Gyrocompass

Figure 2 shows the major system elements in block diagram form. The computer accepts raw sensor data from both the doppler sonar and the gyrocompass through the Model 200 Interface Unit. Simultaneously data is passed directly from the MX 702A Satellite Receiver and the Teledyne 601G Loran-C Receiver to the computer. The computer then outputs the navigation results to the various displays. The succeeding paragraphs will describe the first four of these elements with the heaviest emphasis on the TDL 601G Receiver. Reference 3 gives a further description of the remaining elements.

MX 702A Satellite Receiver

The MX 702A is a dual-channel (400 and 150 mHz) satellite receiver. When ship's velocity and antenna height are known precisely, the system is capable of achieving an rms accuracy of 35 meters.

The receiver has automatic signal acquisition, built-in self test, and automatic break lock on noise.

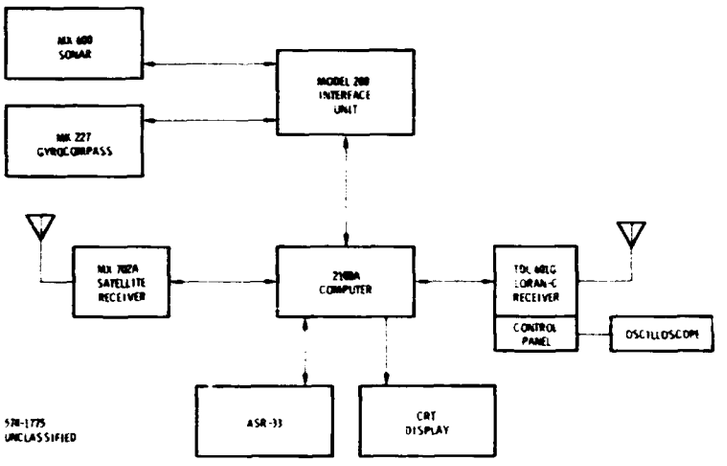

Figure 2. Integrated Loran-C Navigation System

HP 2100A Computer

Normally supplied with the system is a Hewlett-Packard 2100A Computer. This computer has the capability for 32,000 words of memory with space for sixteen input/output functions. The system with Loran-C is normally equipped with 16,000 words and at a minimum will use five input/output card slots. The computer is equipped with a front panel which allows for manual switch register control, computer status display and program loading control. Normally, computer access is required only when loading and starting the main navigation program. A significant feature of the navigation program is a diagnostic routine which allows real time display on the CRT of input/output data flow and computer memory data while the normal navigation program continues to function.

TDL 601G Loran-C Receiver

The TDL 601G Receiver developed by Teledyne is normally supplied with the system. This receiver is a slightly modified version of the one Teledyne developed for the low-cost navigation market. Modifications were made to allow for the following functions:

External Clock — The external clock capability permits a 5 mHz rubidium or cesium standard required for RHO-RHO operation to be used in place of the internal crystal oscillator.

Disable Master Signal — When Loran-C is used in the RHO-RHO mode the master is not required for operation. However, the TDL 601G logic requires a master signal before it will track any of the slaves. The 'Disable Master' function was provided to override this requirement.

Disable Slave B — Disable Slave B provides the same function as disable master except for the Slave B signal.

ΔTM — ΔTM is a pulse stream representing plus and minus 0.1 μsec changes in Master signal phase, as obtained from the tracking filter.

TDA, TDB — TDA and TDB are the accumulated time delay in Slave A and Slave B signals measured with respect to Master signal receipt. Resolution is to 0.1 μseconds.

Magnavox modifies the receiver further by adding an additional card to the receiver and a new, larger front panel. The added card buffers all signals between the receiver and computer to insure that computer noise does not cause a signal interference in the receiver. The card also contains logic and timing for an oscilloscope display. This allows the operator to monitor the Loran signal, check the skywave content and check the tracking point of the receiver. The operator can change the tracking point of the receiver by the 'HOLD' and 'STEP' controls that are part of the basic receiver. In addition, the front panel contains control and status indicators which are provided to the computer. The operator, by monitoring each Loran-C signal on the scope, can decide that Master, Slave A, and Slave B are suitable for navigation purposes. He then signifies this to the computer by 'USE M', 'USE A' and 'USE B' switches respectively. The computer then monitors the requested signals and assuming signal noise is at an acceptable level, the computer will turn on the associated 'USE M', 'USE A' and 'USE B' status lights.

Computer Interface

In conjunction with the TDL 601G, a computer interface card was developed by Magnavox. This card accepts the data which is comprised of the receiver and control panel status bits, the accumulated Slave A and Slave B time delay and the positive or negative 0.1 sec steps by which the Master signal has changed. The timing signals for the data interface are also contained on this card. The timing is adjustable from a basic period of each GRI (Group Repetition Interval) to a one second or a ten second interval. Status lines to the display panel are also contained on the card.

Frequency Standard

Since the system contains the MX 702A Receiver which gives accurate position fixes, it is possible to remove clock drift errors at each position fix. This allows the use of the lower cost Hewlett-Packard 5065 Rubidium Frequency Standard in place of the cesium standard normally used for RHO-RHO operation. This rubidium standard has the following specifications:

Stability — *Long term* $\pm 1 \times 10^{-11}$ per month

Short term 5×10^{-12} per sec

1.6×10^{-12} per ten sec.

5×10^{-13} per 100 sec.

Calibration Accuracy — $\pm 1 \times 10^{-11}$ (factory set)

A dockside calibration procedure is provided for removing large frequency errors by adjustment of the frequency standard. The standard is normally supplied with battery back-up to maintain operating stability during power interruptions.

This concludes a brief description of the major hardware elements which comprise the Integrated Loran-C Navigation System.

FUNCTIONAL DIAGRAM AND SPECIAL FEATURES

Since the Loran-C operating principles are familiar to most marine personnel and since they have been widely published, no general description of Loran-C operation will be given. The functional diagram (Figure 3) shows the general characteristics of the Magnavox Loran-C implementation. Using Figure 3 for reference some of the features which make the Magnavox system unique are given below.

Differential Mode

Conventional techniques of operating radio navigation aids in a differential mode have been to locate a second receiver at a near-by known location and then

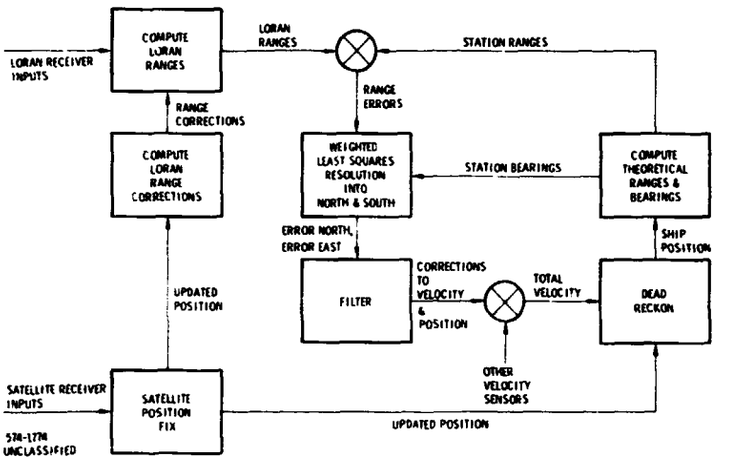

Figure 3. Functional Block Diagram

to transmit the measured errors to the operational system. Implementations of this technique have varied from continuous transmission of the measured errors to 'snapshot' corrections separated by hours in time.

In the Magnavox system, the 'snapshot' error measurements are obtained by differencing system position with a satellite position fix obtained from the Navy Navigation Satellite System. The Loran-C range measurements are then adjusted to force agreement between the two systems, effectively removing signal propagation effects.

This technique has been successfully applied both with separate Loran-C and satellite systems and with a completely integrated hardware and software package. In the integrated systems, the forced agreement is normally done using a minimum variance technique which is less sensitive to errors in the satellite position fix.

Other advantages of this implementation are that, due to the frequent 'snapshot' resets of system error, the Loran-C is less sensitive to errors in transmitter location and to offsets in the local reference oscillator.

The decreased sensitivity to transmitter location means that one generally need not worry about the datum in which station coordinates are expressed. Further, less effort is required to establish the positions of the new portable Loran-C transmitters now being offered by equipment manufacturers.

The decreased sensitivity to oscillator offset means that the lower cost rubidium standard may be substituted for the cesium standard normally used for RHO-RHO operation.

Differential Range Processing

The Magnavox system might also be referred to as a differential system for a second rather unconventional reason. The Loran-C range measurements are differenced with the theoretical range values based on ship and transmitter locations. The prime benefit obtained from this technique is that a simple linear equation can be used to convert the resultant range errors into errors in ship latitude and longitude or, as in our implementation, error North and error East. This avoids the iterative task required in the conventional implementation to convert the Loran-C ranges into latitude and longitude coordinates (Reference 1).

Another benefit obtained is that any number of stations can be accounted for by simply expanding the linear conversion to a linear least squares solution for error North and East. By measuring the variance of the range errors dynamically and using these values as weights in the least squares process, the effectiveness of the technique is further enhanced. In addition, by a simple modification of the least squares matrix elements, the solution can provide useful line of position corrections even when signals from only one station are usable.

Differential Velocity Solution

There is a third reason why the Magnavox system might be referred to as a differential system. The Loran-C system has the capability for accepting velocity inputs from other velocity sensors, (e.g., Speed Log, Doppler Sonar, and Gyrocompass). The Loran-C measurements are then used to solve for the difference between the actual and the measured (by other sensors) ship's velocity.

The prime advantage obtained by this implementation is that now each velocity sensor can perform the task which it does best. In a typical installation, a gyrocompass and doppler sonar are used to provide the first estimate of ship's velocity. If, as is increasingly the case in seismic exploration tasks, the depth of the water exceeds the sonar tracking capabilities, then the sonar velocity will be corrupted by the water velocity.

In this situation the advantage becomes obvious. The Loran-C system can provide a measure of ship's velocity which has a substantial 'high frequency' noise content but with very little 'low frequency' noise, while the doppler sonar/gyrocompass combination has minimal 'high frequency' noise and substantial 'low frequency' noise.

Let us illustrate. If one takes two samples of Loran-C position separated in time by one second and differentiates to obtain ship's velocity, the resultant estimate is very poor due to the Loran-C measurement noise. On the other hand, a one second reading from the sonar will represent the ship's velocity quite accurately. If, however, one takes two Loran-C positions separated in time by 15 minutes and differentiates, then the resultant velocity estimate will easily exceed in accuracy the measurement obtained from the sonar which is subject to 'random walk' and water velocity errors. Thus, by using the Loran-C to solve only for the differential velocity instead of total ship's velocity, it is possible to increase the level of filtering (smoothing) without adversely affecting the representation of ship's position during rapid ('high spatial frequency') maneuvers.

Filter Implementation

The filter implemented in the Magnavox system to smooth the Loran-C error North and error East outputs is best described as an 'exponential time decaying weighted least squares' filter. The rate at which old data is eliminated is controlled by a single time constant, '1/K' which can be adjusted by the operator.

The operation of this filter is best described by referring to Figure 4.

The technique used is to solve for the least squares fit of a straight line, $y = mt + b$, through the measured error, where 'y' is the least squares estimate of actual error, 't' is time 'm' is the slope or desired change in velocity and 'b' is the 'y' axis intercept or desired change in position.

Each time the weighted least squares computation is performed a new estimate of 'm' and 'b' is obtained. However, when the velocity and position are adjusted at time $t = i - 1$ by 'm_{i-1}' and 'b_{i-1}' then the next error measured, ϵ_i, will be with respect to this newly established velocity and position.

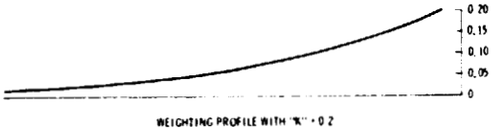

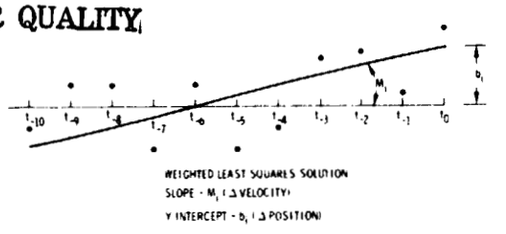

Figure 4. Filter Implementation

It can be shown that, as a result, the adjustments 'm_i' and 'b_i' are a function only of 'ϵ_i' and the exponential time constant 'k' used in deweighting past measurements.

Specifically:

$$m_i = K^2 \epsilon_i \tag{1}$$

and

$$b_i = 2K\epsilon_i - K^2 \epsilon_i \tag{2}$$

In the Magnavox implementation the above equations are modified slightly by two effects. First, the Loran-C measurements are averaged for 10 seconds to decrease the computational requirements. Thus, the measurement is 5 seconds old (one half the averaging period) before it is applied. This causes the position update to be larger by one half the velocity update. Equations (1) and (2) become:

$$m_i = K^2 \tau \epsilon_i \tag{3}$$

and

$$b_i = 2K\tau\epsilon_i - K^2\tau\epsilon_i/2 \tag{4}$$

where τ is the averaging interval.

Second, in our implementation the position update is rated in over the next averaging interval. Since it is delayed by one half the averaging interval it causes the next ϵ_i' to be larger than it would be otherwise.

Thus, a new ϵ_i' is defined such that:

$$\epsilon_i' = \epsilon_i - b_{i-1}/2 \tag{5}$$

This new value of ϵ_i' is used in place of ϵ_i in equations (3) and (4).

This filter is very simple to implement, very easy to adjust to differing external conditions, and very effective in practice.

As an example of the inherent power of this filtering technique Magnavox has provided several Raydist navigation systems with no algorithm modifications. The decay time constant '1/K' was simply decreased to provide more rapid response and to reflect the higher accuracy of the Raydist system.

RHO-RHO or Hyperbolic Operation

One other significant feature of the Magnavox implementation is the simplicity by which the algorithm can be switched from the RHO-RHO operation to hyperbolic operation.

Combined with the features already discussed above this makes the technique a virtually universal radio navigation package. Indeed, Magnavox has already delivered systems using this implementation in Loran-C, Raydist and SHORAN versions and is currently working on a system which will employ the Decca Radio Navigation System in like manner.

The conversion of the algorithms to work in the hyperbolic mode is startingly simple. In the functional block diagram of Figure 3 a new block is added in front of the 'Weighted Least Squares Resolution into North and South'.

This new block forms the value:

$$\bar{\epsilon}_i = (\epsilon_{mi} + \epsilon_{Ai} + \epsilon_{Bi})/3 \tag{6}$$

where

$\bar{\epsilon}_i$ is the average range error

ϵ_{mi} is the master station range error

ϵ_{Ai} is the A station range error

ϵ_{Bi} is the B station range error

This value is then used to modify the individual range errors to obtain:

$$\epsilon_{mi} = \epsilon_{Mi} - \bar{\epsilon}_i \tag{7}$$

$$\epsilon_{Ai} = \epsilon_{Ai} - \bar{\epsilon}_i \tag{8}$$

$$\epsilon_{Bi} = \epsilon_{Bi} - \bar{\epsilon}_i \tag{9}$$

These new values are then fed to the least squares solution for error North and East as before. Only one other adjustment is made and this purely to avoid register overflow. Specifically the range correction factors are each increased by $\bar{\epsilon}_i$ so that the average error will not grow without limit.

It is not difficult to show that the ranging solution has now been converted to a hyperbolic solution. This negates the requirement for a rubidium standard but, of course, reduces the accuracy obtained at long ranges from the stations due to geometric dilution effects.

SUMMARY

The Magnavox Loran-C system represents what we believe is a practical implementation with application to a wide variety of radio navigation systems. Its flexibility permits its use with very accurate short range systems as well as with lower accuracy long range systems.

The Loran-C configuration has demonstrated accuracies in deep water that compete with the doppler sonar implementations while in the bottom track mode.

REFERENCES

1. Friedland, B. and Hutton, M. F., New Algorithms for Converting Time Differences to Position, Navigation, Vol. 20, No. 2, Summer 1974, pp. 178-188.

2. Stansell, T., Extended Applications of the Transit Satellite Navigation System, Offshore Technology Conference, February 23, 1971.

3. Stansell, T., Accuracy of Geophysical Offshore Navigation Systems, Offshore Technology Conference, OTC 1789, April 29-May 2, 1974.

THE AN/WRN-5; A NEW TOOL FOR MARINE POSITIONING

John F. Clark, Head, Computer Systems Department

Frank W. Christensen, Head, Military Systems Department

Magnavox Research Laboratories, Torrance California

ABSTRACT:

The coherent development of a line of satellite navigation receiver equipment is illuminated. A discussion of heretofore unutilized capabilities now possible by the AN/WRN-5 Navigator offering some insights into how the system can improve the accuracy and reliability of navigation and guidance.

Test results are presented, illustrating the significance of the somewhat unconventional design approaches found throughout the unit. These data identify the accuracies presently achievable with the WRN-5 navigator.

The value of coherent development work in complex navigation systems is illustrated by the application of the AN/WRN-5 technology to the NAVSTAR Global Positioning System is presented in closing.

Ever since man began to travel out of range of familiar landmarks, he has felt the need for some form of navigation system. The evolution of a methodology based on an accumulation of knowledge on the subject from a diversity of sources probably did not begin before the appearance of the astrolabe, during the middle ages.

The astrolabe is undoubtedly the predecessor of the mariner's sextant, and was in extensive use into the 17th Century. Derivatives of this instrument were used in general land surveying, determining differences in elevation of land masses, and related activities. Most important, however, was the astrolabe's value as an auxilary computing device. It enabled the astronomer to work out the position of the sun and principal stars with respect to the meridian as well as the horizon, to find his geographical latitude and the direction of true north (even by day, when the stars were not visible). Above all, in the days before reliable clocks were commonly available, the astrolabe provided its owner a means of telling time by day or by night as long as the sun or some recognizable star marked on the instrument was visible.

Although historians are amazed at the accumulation of technology in ancient systems such as the astrolabe, in the minds of modern purveyors of advanced technical systems, it is merely a reiteration of a basic fact: The success of a project depends upon the systematic application of proven technological accomplish-

ments.

About twenty years ago the U. S. Navy identified the need for a precise navigation system for use by ships at sea. A wide variety of systems were developed in an attempt to answer this requirement. A major step in the achievement of high precision, all weather, worldwide navigation was taken when the Navy Navigation Satellite System (TRANSIT) became a reality in the mid-1960's.

Since its inception, a number of equipments have been developed to provide the user with positional information obtainable from the NNSS. The latest of these equipments, the AN/WRN-5, was built by the Magnavox Company for the U. S. Navy. It provides the mariner with a number of new and useful capabilities.

These features did not just happen, but rather were evolved from the work of many years. There is an amazing correlation between the evolution of the astrolabe through ancient times, and the development of satellite navigation equipment at Magnavox. The AN/WRN-5 reflects the development of Magnavox satellite navigation experience and technology extending back to 1961.

Magnavox, in conjunction with the Applied Physics Laboratory, initially developed the

AN/SRN-9 (XN-5)

for the U. S. Navy for use on surface ships. Using the same technology the

Geoceiver - AN/PRR-14

was developed. This device, a receiver only, was designed for geodetic survey applications. It is currently being used around the world for precise survey work and is capable of providing measurements to an accuracy of better than one meter. A photograph of the Geoceiver is shown in figure 1.

Next on the list of equipment to be developed was the

MX/702-CA

This unit, basically a two channel satellite receiver, was the first commercially available NNSS receiver. When used in conjunction with a digital computer, it was capable of providing real time position fixing from the NNSS.

Figure 2 is a photograph of the MX/702-CA along with its computer, photoreader and teleprinter in a rack. Note in particular the construction techniques which were used for the RF components (shown more clearly in figure 3). Individual RF modules, enclosed in metal cans were used to obtain the sensitivity required.

The next stage in the evolutionary development of NNSS equipment was the

AN/WRN-4 - MX/706

Shown in figure 4 (on the right) the AN/WRN-4 used the same receiver technology. This unit was developed for the Office of Naval Research and was designed specifically as a tool to aid the marine scientist. In order to make the unit small, the computer was built right into the same enclosure along with a display device and data entry equipment. Primary disadvantages of this equipment were computer limitations, forced by the size of the equipment, and the cost.

In an effort to reduce the cost of satellite receivers, alternate construction techniques were investigated. The availability of new components such as MSI

integrated circuitry, and the experience gained from the development of the previous equipments permitted a significant change in construction without sacrificing performance.

The

MX/702 A Receiver

shown in figure 5 is the latest commercial receiver which we have developed. Its construction represents a radical departure from the previous technology. In this view the five lower-most boards represent the analog receivers (two channels), while the digital circuitry is contained on the eight boards to the right of the unit. All boards are 5 by 9 inch printed circuit boards. RF shielding is obtained from five plates which form part of the card cage assembly.

All of the devices described up to now are fundamentally satellite receiver units. Position fixes are obtained by interfacing the receiver outputs to a general purpose digital computer programmed to provide a position fix each time one of the operational NNSS satellites is tracked.

The device shown in figure 6 is the

AN/WRN-5

It has been designed using the receiver technology developed over the years but with a significantly different system philosophy. Fundamentally, the AN/WRN-5 is a computer-based dead reckoning system in which ship's speed and heading information, in the form of either synchro or digital signals, are processed by the computer to obtain positional information.

This positioning data is provided to the operator by a built-in (and also by a remote) CRT display unit. The set is thus a continuous positioning device, with display updates occurring once per second.

In addition, the set contains a two channel satellite receiver (with significant differences from previous receivers) and a magnetic tape cassette (used for both program storage and loading of the computer as well as a data logging device using the record mode).

Let's look at some of the features of the AN/WRN-5 (developed for NAVELEX under Contract N00039-72-C-0125) that make it uniquely suited for marine positioning and survey application.

During the design of the AN/WRN-5, it was recognized that the computer portion of such a system forms a part of the "on-line" system and therefore contributes significantly to the overall system reliability. Once the computer's reliability has been established, the overall system reliability is enhanced by removing as many other hardware elements as possible from the rest of the system.

In the AN/WRN-5, this concept was used to remove as many 'normal" receiver functions as possible and perform these funtions in the computer. This has resulted in a substantial reduction in hardware complexity, increased the reliability and made the system less expensive than would otherwise be the case.

The following functions, normally considered as receiver functions, are performed by the computer in the AN/WRN-5

Tuning of the two receiver channels

rate aided tuning of the receivers will essentially provide the tracking performance of a third order tracking loop with the stability and simplicity of second order loop hardware.

the phase locked time recovery loop is closed through the computer to provide performance considerably better than that which has been heretofore achieved.

all doublet, bit and message synchronization functions are performed in software with all data bits transferred to the computer as two 8 level samples (the analog data is digitized through an 8 bit A-D convertor).

In addition, the computer continually senses and monitors all key power supply voltages in the set and provides to the operator (under manual request) a digital display of the value of each voltage in the set.

Furthermore, additional BITE capability, in the form of a satellite signal simulator is built in to the set. This simulator is controlled by the computer in terms of both its modulation and signal level. It provides the system with the ability to measure a number of significant performance parameters such as sensitivity, doppler count stability, bit error rate, and tuning control.

A number of other features of importance are incorporated into the set in its basic configuration. For example, the set is the first to employ a zero offset doppler counting technique. This technique, coupled with the significant reduction in time recovery jitter, reduces the most significant source of receiver measurement noise by a factor of five to ten over its value in more conventional receivers. Figure 8 indicates the improvement in doppler count accuracy by the zero offset doppler technique.

The computer forms the heart of the AN/WRN-5 and a few words should be said about its characteristics. First, it is a mini-computer whose instruction set has been tailored for navigation-like functions. These instructions include the normal add, subtract, etc., of conventional machines and, in addition, include double word add and subtract as well as hardware multiply and divide instructions which greatly assist in implementing the floating point computations used in the navigation process.

The basic computer is very fast, employing an 850 nano-second memory cycle time. A 16K core memory is provided in the basic system with plug-in expansion within the set to 24K and external expansion to 32K permitted.

The computer is a 16 bit word machine with two accumulators (used for double word operations) and three hardware index registers.

While all of these words are fine, the proof of the pudding is in the results - as of this writing, over thirty AN/WRN-5 units have been delivered to the Navy and are deployed throughout the world.

The data in Table I provides a good idea of the level of accuracy which can be obtained from the set. The data used in preparing the table was taken from the acceptance test data of 27 of the AN/WRN-5's which have been delivered. The calculated position represents the mean position obtained from a total of 501 satellite passes - all tracked automatically by the 27 units (approximately 18 passes from each unit).

The position uncertainty represents the statistical 1 sigma deviation in the mean positions obtained from receiver to receiver. It thus reflects the survey repeatability of a group of AN/WRN-5's, i.e., their measurement error is less than five meters.

The mean uncertainty is a measure of the pass-to-pass variability obtained from individual position fixes. The predominant portion of the errors is caused by noise in the transmitted satellite orbit as indicated by the 18 meter uncertainty.

Clearly, the AN/WRN-5 is a survey quality instrument. The flexibility afforded by the general purpose computer interface techniques have only been partially exploited in the baseline software developed thus far.

Further evolution of this technique is currently being supported at Magnavox. In particular, we are very actively involved in the determination of the basic operational parameters of NAVSTAR, the Global Positioning System.

Being extremely interested in the promulgation of satellite receiver technology, we have begun to capitalize upon those characteristics which have made the AN/WRN-5 system so much like the astrolabe; flexibility, power and technical durability. The AN/WRN-5 hardware provides a baseline technology from which advanced navigation techniques are evolving, such as GPS.

To be more specific, we have determined that the AN/WRN-5 can be readily converted to receive the GPS waveform by modifying approximately 30% of the system; namely, replacement of the RF preamplifier, the data decoder and appropriate software modification. The RF preamplifier designed for GPS use is somewhat smaller than the AN/WRN-5 unit, the GPS data decoder system requires a replacement of only eight AN/WRN-5 boards with a like number of GPS boards. The MAXAL computer system used in the AN/WRN-5 has more than adequate capacity.

The reader must understand that any impact to be made upon the navigation community by an operational GPS system is at least ten years away. While Magnavox will invest considerable energies in the development of the best possible GPS user equipments, it is important to realize that we are fully committed to the continuing development of NNSS technology.

Indeed, the AN/WRN-5 is the modern astrolabe.

TABLE I

STATISTICAL RESULTS

Number of Units in Sample 27	
Reference Position (Surveyed)	33° 50'.465 North Latitude
	118° 20'.265 West Longitude
Calculated Position (Via Satellite Instrument).	33° 50'.46535 North Latitude
	118° 20'.26356 West Longitude
Position Uncertainty (1 sigma deviations) Receiver-to-Receiver	
Latitude	± 4.72 meters
Longitude	3.09 meters
Mean Uncertainty from pass-to-pass for each receiver (1 sigma deviations)	
Latitude	14.03 meters
Longitude	10.82 meters
Radial	17.96 meters

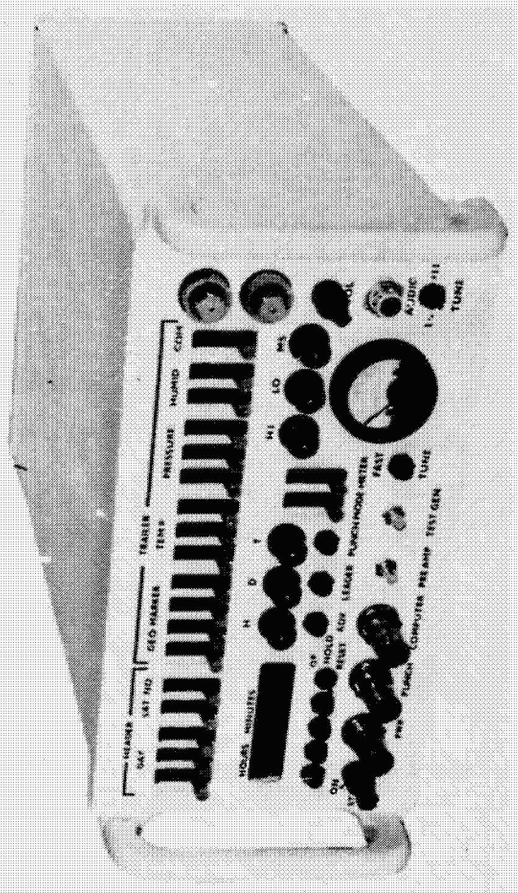

Figure 1. AN/PRR-14 Geceelver.

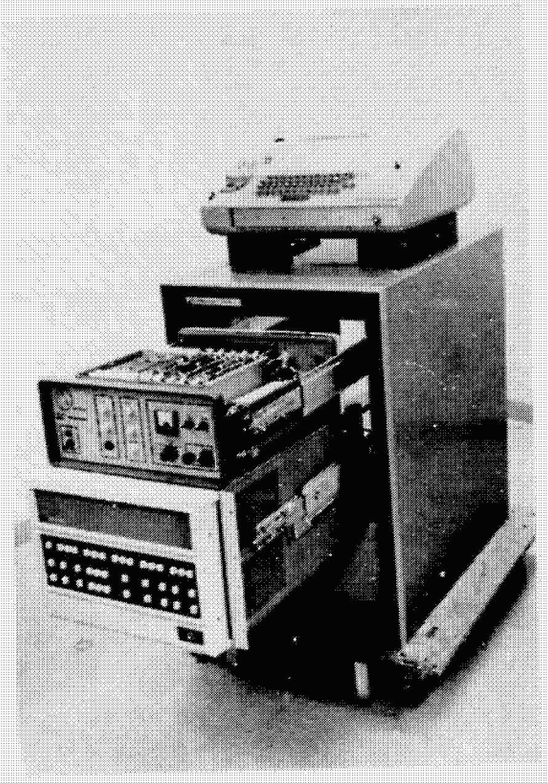

Figure 2. MX/702CA, Rack Mounted.

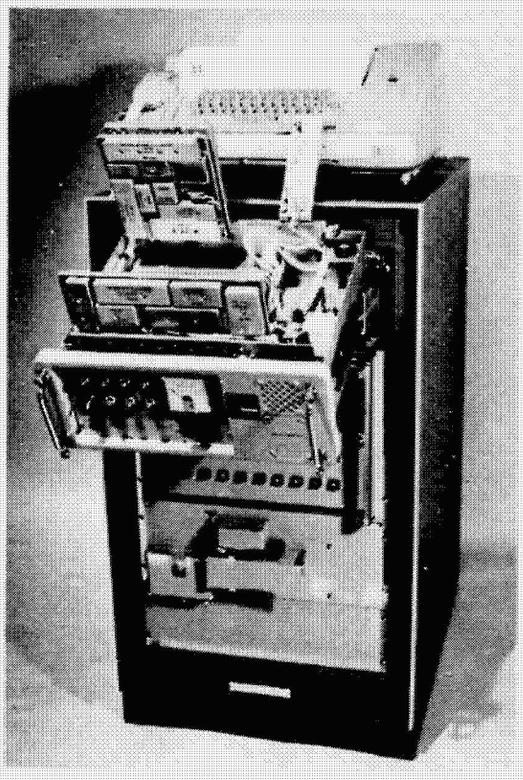

Figure 3. MX/702CA, Rack Mounted. This view shows the receiver assembly open for servicing.

Figure 4. AN/WRN-4 (MX/706).

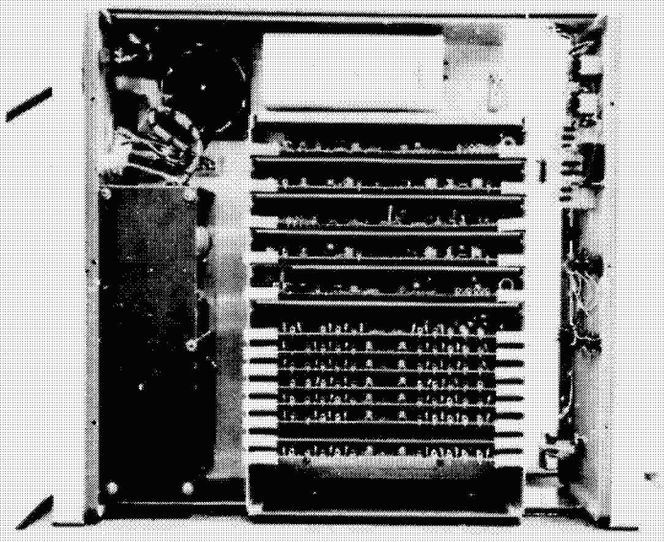

Figure 5. MX/702A Receiver, top view.

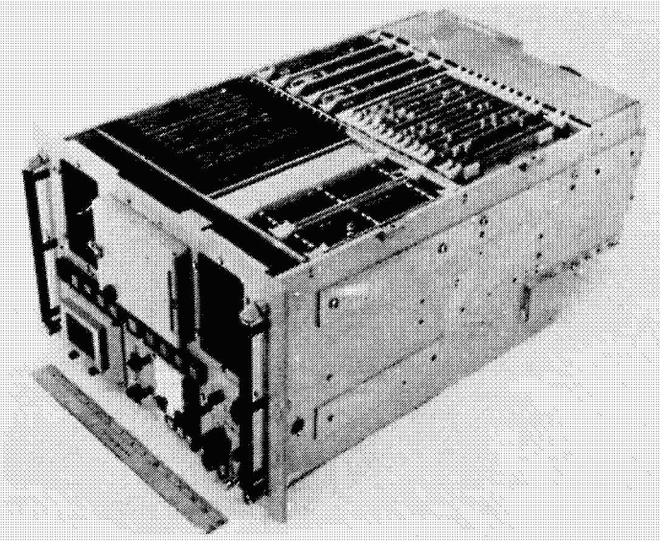

Figure 6. AN/WRN-5 Navigator System.

THE FRENCH EOLE POSITIONNING SYSTEM
APPLICATION TO DRIFTING BUOYS TRACKING

G. BRACHET - M. VINCENT
CENTRE NATIONAL D'ETUDES SPATIALES - FRANCE
Y. KAKINUMA
THE RADIO RESEARCH LABORATORIES - JAPAN

The EOLE data collection and positionning system is operationnal since early September 1971. It is essentially a satellite which tracks and collects data from meteorological balloons and ground transponders. During each pass, the satellite interrogates the transponders and stores range and range-rate observations which are later transmitted to ground telemetry stations and processed at the CNES computing center in Bretigny, near Paris.

Although originally designed for balloon tracking, the EOLE system has proved to be an ideal tool for other applications such as drifting objects positionning (icebergs, buoys). The routine operation can provide positions with accuracies of about two to three kilometers within 24 to 48 hours. However, a special data processing system was used in 1973 - 1974 for some investigators, therefore improving the positionning accuracy to better than one kilometer. This experiment is described and results are given for both fixed and drifting transponders.

DESCRIPTION OF THE EOLE SYSTEM

The EOLE system was designed originally as a data collection and positionning system for the tracking of a large number of meteorological balloons flying at constant level (200 millibars) in the southern hemisphere. The objective was a better understanding of the general atmosphere circulation and therefore did not require very accurate positionning capability (Morel, 1972).

The system is schematized in figure 1 :

1 - The interrogation program is established on the ground and fed into a special memory in the satellite.

2 - According to this program, the satellite interrogates each transponder in sequence on 460 MHz (coded 30 bits message).

3 - When a transponders recognizes its code number, it answers back on 400 MHz and transmits information from four sensors.
In this process, two-way range and range-rate are measured by the satellite and stored in its 131 Kbits core memory together with the data received from the transponder.
The same process repeats on other transponders with a time cycle of 625 msec. Three to thirty interrogations are thus made during one pass in the visibility of a transponder, according to the interrogation program.

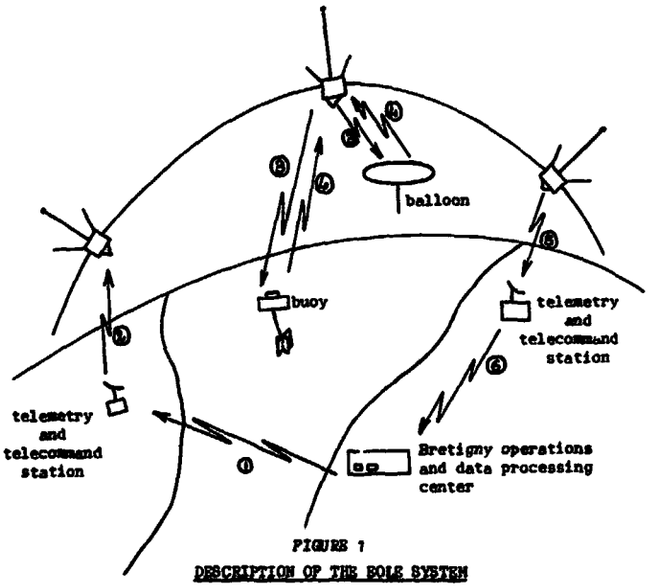

FIGURE 1

DESCRIPTION OF THE EOLE SYSTEM

1 - The interrogation program is prepared and transmitted to a telecommand station
2 - The program is fed in satellite memory
3 - Transponders interrogations
4 - Transponders answers
5 - Data collected from transponders are transmitted down to a telemetry station
6 - Data are transmitted to Bretigny and processed

4 - On command from a ground telemetry station from the CNES network, the memory is transmitted down and recorded.

5 - The information is then transmitted to the CNES Bretigny data processing center where it is processed on a Control Data Corporation 6600 computer on a 24 hours a day basis (Dargent, 1972).

Results are generally available within 24 to 36 hours after the actual satellite transponder link, although this delay has been reduced to an average of seven hours for some special experiments.

The EOLE (or Cooperative Application Satellite, CAS-A in the NASA nomenclature) is a 80 kg gravity gradient stabilized spacecraft with its 400 MHz cone-shaped antenna pointing downwards (figure 2). It was launched on August 16 1971 by a scout launcher from the NASA wallops Island station in Virginia. Its orbit is 690 km perigee, 900 km apogee, 50° inclination.

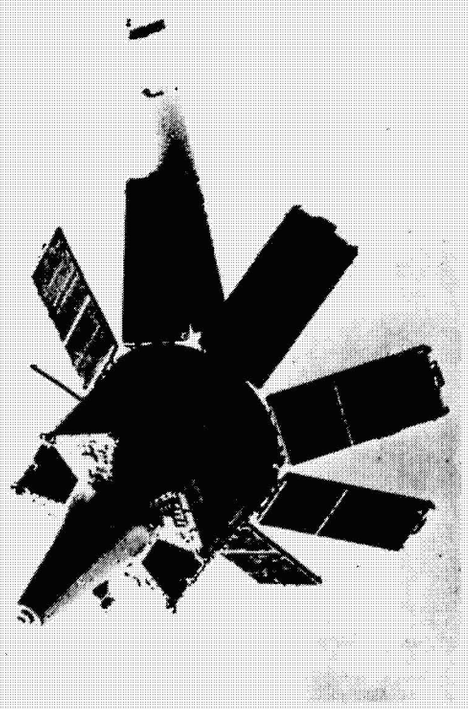

FIGURE 2

THE EOLE SATELLITE

G. BRACHET

MAIN EOLE EXPERIMENTS

The experiments which have been conducted with the Eole system are of three types :

- Isobaric balloons tracking (main experiment)
- Data collection
- Positionning of ships and drifting objects.

The main experiment was conducted from Septembre 1971 to mid-1972. It involved the tracking of 479 balloons launched between August and November 1971 from three special launching stations set up by CNES in Argentina in a cooperative program with the "Comision Nacional de Investigaciones Espaciales". These stations were located in Mendoza (33° latitude south), Neuquen (39°), Lago-Fagnano (53°), thus allowing an even latitude distribution of balloons in the southern hemisphere, the longitude distribution being obtained by the launch schedule. The average life time of successfully launched balloons was about 150 days.

It was obvious from the beginning, however that other applications of the Eole system could be experimented, such as message transmission from remotely located sites and positionning of ships or other objects for which an accuracy of 2 to 3 kilometers would be sufficient.

Thus started a completely new program, called "Eole Complementaire" which involved a large variety of experiments, oriented either towards data collection only, or positionning only, or both.

Table 1 gives a break-down of these various experiments according to organisations and main objectives. The experiments were primarily feasability demonstrations, however, since the number of available transponders was very limited. Besides, some problems were encountered with the reliability of the electronics since it had been designed for the very different environmental conditions of the 11 kilometers altitude balloons, including special specifications due to aircraft safety requirements.

Among these experiments, some were particulary spectacular, such as the tracking of sailboats, including PEN DUICK IV, the winner of the 1972 single handled transatlantic race, the first long term tracking of an iceberg along the coast of Antarctic, from February 1972 to March 1973, and even the tracking of a NASA car along the Washington D.C. Beltway !

A detailed report of the implementation and main results of these experiments is available from CNES (CNES, 1973). It demonstrates the wide range of applications of satellite systems such as EOLE and how the scientific community gradually gained interest in this new technique.

ACCURACY ANALYSIS OF THE POSITIONNING SYSTEM

The accuracy of the positionning system has been analysed in detail in (Brachet, 1972).
The transponder position is computed by a least square adjustment using all range and range-rate data collected during onepass. For fast moving objects such as the balloons of the main experiment, however, the accuracy is limited by our knowledge of the wind velocity and direction since the duration of the pass does not allow for a significant recovery of these parameters. In this case an iterative procedure has to be used : a mean wind vector is computed from positions computed on several successive passes and the process is reiterated.
Fixed and slowly moving transponders do not present this difficulty : Figure 3 gives the plot of positions computed during the routine operations for one transponder which was located in the CNES tracking and telemetry station in Pretoria (South Africa). It gives a good idea of the spread and accuracy of the positionning system (1.3 km rms). The accuracy of a given position, however, is very much a function of the pass geometry, i.e. it degrades significantly for zenithal passes (ground track distance less than two degrees). This is shown on figure 4, where relative dispersions of positions of a set of transponders located in Victoria, B.C. (Canada) is plotted against the ground track distance.

TABLE 1

EOLE EXPERIMENTS

ORGANISATION	COUNTRY	EXPERIMENTS
Laboratoire de Météorologie Dynamique (CNRS)	FRANCE	1) Balloons tracking (200mb) and data collection 2) Drifting buoys tracking and data collection
Centre National pour l'exploitation des Océans (CNEXO)	FRANCE	Drifting buoys tracking and data collection
Terres Australes et Antarctiques Françaises (TAAF)	FRANCE	1) Drifting buoys tracking and data collection 2) Ship positionning
Expéditions Polaires Françaises (EPF)	FRANCE	Iceberg positionning
Pen Duick IV (Transatlantic race 1972)	FRANCE	Sailboat positionning
Institut de physique du glob (IPG)	FRANCE	Ship positionning
Compagnie Générale de Géophysique (CGG)	FRANCE	Data collection from ships
Institut scientifique et technique des pêches maritimes (ISPM)	FRANCE	Ship positionning and data collection
Compagnie Générale Transatlantique (CGT)	FRANCE	Meteorological data collection from ships
Compagnie maritime des chargeurs réunis (CMCR)	FRANCE	Data collection from ships
Groupe de recherches de géodésie spatiale (GRGS)	FRANCE	Analysis of ultimate positionning accuracy
Office de la recherche scientifique et technique d'Outre-Mer (ORSTOM)	FRANCE	Meteorological and hydrological data collection
National Ocean and Atmosphere administration (NOAA)	U S A	Drifting buoys tracking and data collection
Virginia Institute of Marine Sciences (VIMS)	U S A	Drifting buoys tracking and data collection
Laboratoire d'étude des grandes masses (LEGM)	ITALY	Meteorological and hydrological data collection
Service météorologique de l'aéronautique militaire (SMAM)	ITALY	Meteorological data collection
Ministry of Agriculture, Fisheries and Food (MAFF)	U. K.	Drifting buoys tracking
Comision Nacional de Investigaciones Espaciales (CNIE)	ARGENTINA	Meteorolcgical data collection
Instituto Nacional de Pesquisas Espaciais (INPE)	BRAZIL	Meteorological data collection
Indian Space Research Organisation (ISRO)	INDIA	Meteorological data collection
Commonwealth Scientific and Industrial Research Organisation (CSIRO)	AUSTRALIA	Drifting buoys tracking
Commonwealth Scientific and Industrial Research (CSIR)	South AFRICA	Drifting buoys tracking
Scientific Committee for Antarctic Research (SCAR)	International	Icebergs tracking

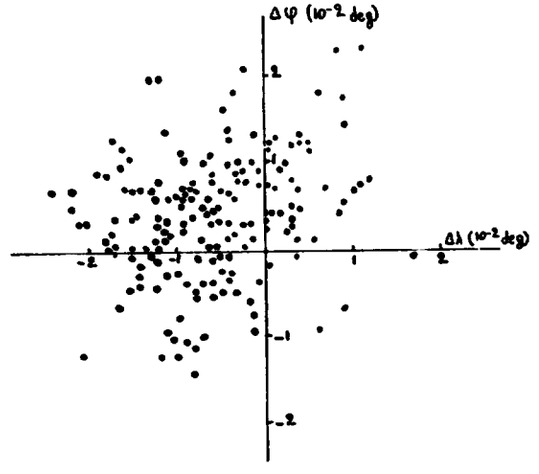

FIGURE 3

POSITIONS OF EOLE GROUND TRANSPONDER IN PRETORIA (SOUTH AFRICA)

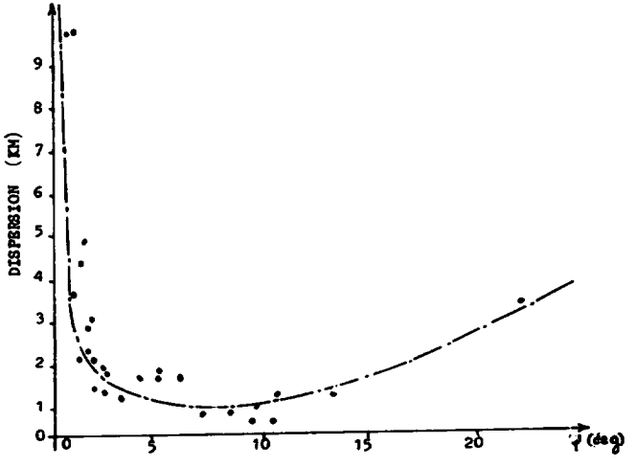

FIGURE 4

DISPERSION OF TRANSPONDERS POSITIONS
AS A FUNCTION OF GROUND TRACK DISTANCE ψ
(VICTORIA, B.C CANADA)

The main sources of errors are

satellite position errors
transponder altitude error
range measurements biases
rante-rate measurements errors
timing

Among these, experience and a series of special analyses (Brachet, 1973) have shown that the largest error contributions are found in the satellite position estimation and the range measurement biases. The operational EOLE data processing system uses a simple analytical perturbation model for the orbit computation, providing satellite position recovery accurate to 1.7 kilometer along track and 1 kilometer cross track (3 sigma).
Besides, calibration of the transponder and satellite electronics is necessary for the range measurement. Since high accuracy was not a requirement for the main objective of the mission, biases of up to 1 km have been found with respect to the standard calibration data.
Special off-line data processing, however, can minimize the effet of satellite position errors by using more sophisticated perturbation models, and observations of transponders located in well known geodetic positions can help in recovering the range bias for each transponder. Such experiments have been conducted in France in 1972 and in the U.S. in 1973. The next section presents the results of this last experiment.

VIMS BUOYS TRACKING

The Virginia Institute of Marine Sciences (VIMS) started drifting buoys experiments using the EOLE positionning system in September 1972. The main objective is the study of currents along the coast of Virginia, outside the mouth of the Chesapeake bay. The buoys are round discs carrying the radio and EOLE antennas and under which is attached a cubic case containing the electronics. A 5 to 20 meters cable links it to a cross like sail.
After a first and successfull experiment, CNES proposed to VIMS that a special processing be done for their buoys in order to obtain improved position accuracy. For this purpose, a calibration experiment was organized in October 1973, before setting the buoys at sea : four transponders were put in operation in a common location along the coast and the exact coordinates were provided by VIMS.
These transponders were intensively interrogated by EOLE from 16 to 23 October 1973, while EOLE itself was tracked by more ground stations, including some of the NASA minitrack stations.
The improvement in tracking data coverage, combined with the use of very sophisticated perturbation model for the orbit computation, allowed satellite position errors not exceeding 300 meters (150 m r.m.s), a value which is considered the lower-bound of orbit estimation accuracy with routine interferometric data. The calibration of each transponder was computed by comparing the theoretical and observed ranges for all passes and deriving a mean constant calibration for each transponder (Brachet, 1974).
The positionning accuracy improvement is very spectacular :
Figure 5 compares the positions of these four transponders derived from the routine operations and the positions after the calibration and special data processing. The dispersion around the mean position is improved from 2500 to 350 meters (r.m.s) and the mean point, previously 2000 meters to the west of the reference position, moves to within 300 meters.
These spectacular results could not, unfortunately, be applied to the buoy tracking experiment which was to follow immediately the calibration. The buoys were not set at sea before end of January 1974, so that there is no guarantee that the calibration values obtained in October 1973 are still valid. The same procedure, however, was followed : intensive tracking of EOLE, special orbit computation, detailed analysis of each pass in order to make full use of all available data.
Five buoys were set at sea on January 29 1974 by 38.8 latitude north and longitudes varying between 284.95 and 285.50 degrees. Two of them were tracked by EOLE until March 1974. After an excursion to the north, they went south along the coast, to about 36.00 degrees latitude before being caught by the Gulf-Stream about the 8 or 9 February. From then on, they dirfted quickly to the East. On March 26 for example, buoys no 24 had

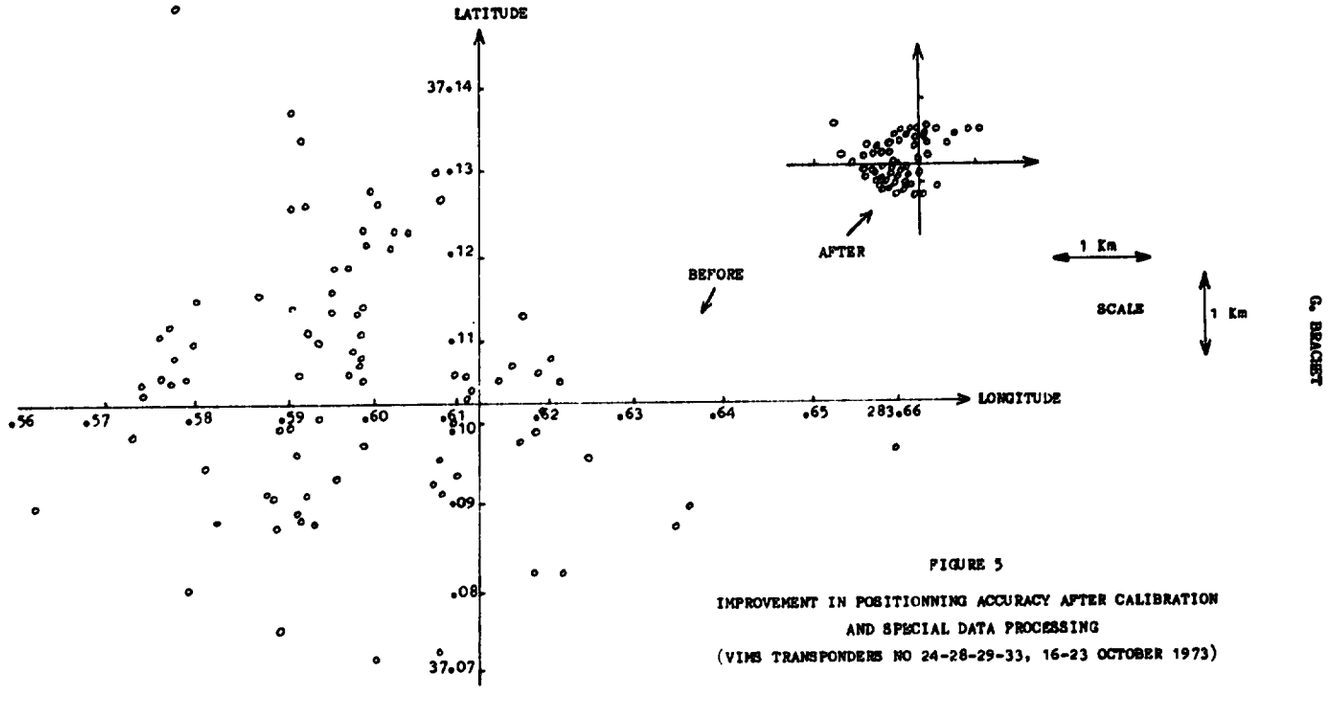

FIGURE 5

IMPROVEMENT IN POSITIONNING ACCURACY AFTER CALIBRATION
AND SPECIAL DATA PROCESSING
(VIMS TRANSPONDERS NO 24-28-29-33, 16-23 OCTOBER 1973)

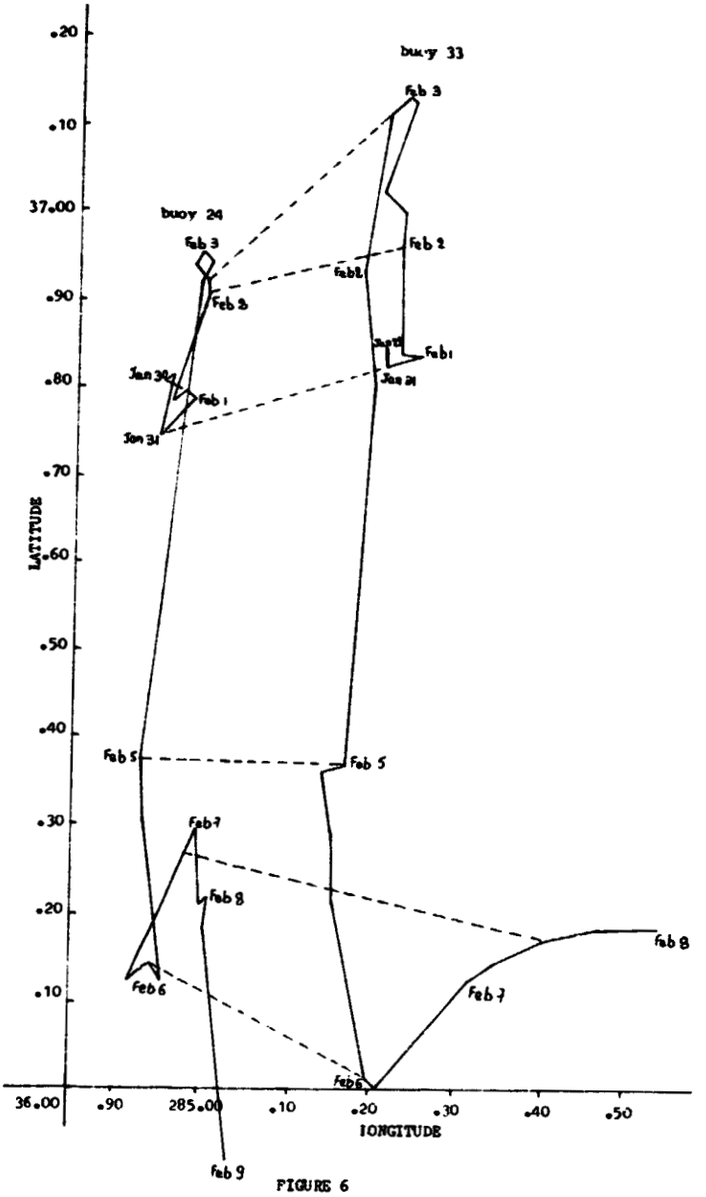

FIGURE 6

DRIFT OF VIMS BUOYS 24 AND 33 FROM JAN 29 TO FEB 8 1974

reached the longitude 308° East, having traveled more than a thousand nautical miles.

Figure 6 represents the drift of buoys no 24 and 33 along the coast during the first ten days of the experiment, the most significant for the study of coastal currents.

CONCLUSION

The EOLE positionning system has demonstrated the great potential of satellite techniques for the tracking of drifting objects such as balloons, buoys, icebergs. Being operationnal for more than two and a half years, it has also provided valuable scientific data to investigators all over the world. It has opened the way to new satellite systems, providing improved possibilities, which are being developped now : The U.S. TIROS-M program for the National Ocean and Atmosphere Administration (NOAA), and the french DIALOGUE and GEOLE programs which are being presented at this symposium (PIEPIU, 1974).

REFERENCES

BRACHET, G. : 1972, 'Results and evaluation of the EOLE operationnal location system', Astronautical Research 1972, 259-272, L.G. Napolitano et al (eds).

BRACHET, G. and PIEPIU, J.L. : 1973, 'EOLE, performances ultimes du systeme de localisation de balises fixes, synthèse des résultats', CNES report 73.364/CB/MT/OB.

BRACHET, G. and VINCENT, M. : 1974, 'EOLE, buoys tracking experiment, calibration of VIMS transponders', CNES report 74.170/CB/MT/ML.

CNES : 1973, 'Le programme EOLE, synthèse d'ensemble, tome VI, volume 1 and 2'.

DARGENT, A. : 1972, 'Data processing for the EOLE project, International Telemetry Conference, Los Angeles.

MOREL, P. : 1972, 'Latest results in space meteorology : Experiments in satellite platform location and data relay techniques', COSPAR XVth General Assembly, Madrid.

PIEPIU, J.L. : 1974, 'Results of the GEOLE system simulations', International symposium on applications of marine geodesy, Columbus.

GEOLE

Ph. GUERIT
Ingénieur
CENTRE NATIONAL D'ETUDES SPATIALES
Direction des Programmes et de la Politique Industrielle

ABSTRACT

Since 1967 the Centre National de Recherches Spatiales has been studying a high-accuracy location system employing a near-earth satellite and designed to find the coordinates of isolated fixed or slightly mobile points. Efforts are being concentrated on achieving an extremely accurate performance with a relatively short delay in making the results available - of the order of a few hours with an accuracy of one to two metres, and down to a few minutes, with an accuracy of the order of 10 to 20 metres.

This system has been dubbed GEOLE, a combination of EOLE (the name of an earlier CNES project) and the word Geodesy.

It is still in the project stage, and the ways and means of setting up and using the system (as well as its main technical features) remain to be decided.

The first operational satellites could be available by 1981, and the system will then be put into use.

1. INTRODUCTION

Towards the end of 1967 the study of the EOLE satellite system undertaken at the Centre National d'Etudes Spatiales (France) reached a degree of definition sufficient to allow a start to be made on the development phase of this project. The EOLE programme involved a satellite on a low circular orbit inclined at 60° to the equator, operated in conjunction with several hundred fixed or slow-moving terrestrial platforms (balloons, buoys, etc) The satellite, by interrogating the platforms via a radio link when passing in view, picked up the data needed to pinpoint their location by measurements of angle (Doppler effect) and satellite-to-platform distance. The transmissions from the platforms also included a variety of data generated by sensors, etc. (EOLE, launched in 1971, is still operational after 30 months).

The degree of pinpointing accuracy looked for with EOLE was of the order of 1 km under good conditions, assuming an excellent knowledge of the satellite's orbit. While this was more than sufficient for meteorological and oceanographic purposes, the relative coarseness of measurement ruled out a number of possible applications of the system, since location missions call for measuring to within a few metres.

For this reason a proposal keeping the same measuring principle as EOLE but aiming at measurements accurate to within one metre

began to be studied by CNES from November 1967 onwards, under the name of the "GEOLE Programme".

Although this satellite system, because of the level of performance it promised, very soon prompted thoughts of fascinating scientific experiments, the basic concept and the design studies have always been centred on the provision of an operational applications system serving users of different nationalities working in a wide variety of fields. Between 1968 and 1971, therefore, work was done in three main areas in order to gain a clearer picture of the difficulties involved in a project of this kind :

(a) Identification of possible applications, by surveys of potential users. Study of level of demand, competing systems, etc ;

(b) Technical studies of the measurement system, its sources of error, methods of correction, data processing methods, orbit-plottin , etc .

(c) Production of models and mock-ups to check, in certain critical areas, that practical results would match theoretical data.

In November 1971 this work culminated in a technical review that led to the following main conclusions :

(i) The GEOLE programme could reasonably be regarded as feasible even with the most ambitious specifications, although it called for advanced engineering skills and a step-by-step approach to solving the problems ;

(ii) The programme evoked definite interest among the potential users who had been consulted.

These conclusions led CNES to decide to press ahead with its efforts in the three areas mentioned, and in addition to undertake a study on a preliminary project for a satellite designed to pave the way for GEOLE by proving the soudness of the measuring principle and finalising the main components to be employed in the future operational system.

This preliminary project, code-named DIALOGUE, was completed in 1973 and development and production began towards the end of that year. Concurrently, in order to ensure that the lessons learned from DIALOGUE yield maximum profit for the GEOLE programme, the main choices of basic characteristics for the project will be made in mid-1974 or thereabouts, and a preliminary project study of GEOLE will then be begun.

2. THE GEOLE PROGRAMME

2.1. General

All the work done up to the beginning of 1974 has been directed towards the "location pinpointing experiment" wich forms the heart of the whole system and is the most difficult to try out experimentally. All the other definition options for the space system are, to a very large extent, still open : they include, for example, the major subsystems and ancillary equipment of the satellite, the number of beacons and their optimisation and the method of running the operational system.

2.2. Objectives

The objective aimed at by the GEOLE project is to satisfy virtually all the needs expressed by users. There are expected to be certain exceptions, in particular in cases

where overcoming a constraint would be excessively costly seen against the level of demand.

If the demand is to be satisfied, there are several goals that need to be reached, such as :

- Worldwide location, absolute or relative, of isolated fixed points within 10 to 30 metres in a single pass and within 1 metre over a whole day, and of slightly-mobile points ;
- Worldwide location, absolute or relative, of isolated points within 20 metres and very rapid availability of results (15 to 20 minutes) through the use of an on-board computer.

These two targets can be reached only by setting up a worldwide first-order network of triangulation points comprising 30 to 40 apices, whose positions are known to within 2 metres ; this will provide the terrestrial reference system within which the satellite (and hence the isolated point) will be pinpointed.

The process of setting up and operating the GEOLE system can be summarised as follows :

Phase 1 : During the first few months of the satellite's life the first-order network is plotted, using measurements carried out by the satellite. This plotting is purely geometrical and does not involve celestial mechanics - i.e. it is a terrestrial potential model.

Phase 2 : After Phase 1 is complete it becomes possible to use the system to locate isolated points. The beacons sited at the apices of the first-order network now have known positions, and can be used to plot the satellite's track permanently and continuously.

All that is necessary to find the coordinates of an isolated point is to position a beacon and then wait for - depending on the degree of accuracy required - one or more passes of the satellite. The measurements of range and radial velocity between the satellite and the beacon place the latter at the intersection of spheres and cones.

3. MAIN CHARACTERISTICS OF THE GEOLE SYSTEM

3.1. General

The system is made up of automatic, self-contained beacons, to be located, and one or more satellites which interrogate the responder beacons, measure their range and radial velocity and store this information in order to retransmit it, over a conventional telemetry link, to a central EDP station.

3.2. Requirements on the system

The principal requirements on the system are :

(a) the highest possible accuracy, of the order of one metre ;

(b) completely automatic operation of the ground beacons ;

(c) location-data transfer via the satellite ;

(d) data-processing at a single point (described below as "operations centre").

The satellite has a twofold role - locating the beacons and transferring data.

The transfer of data between the various beacons scattered round the world and the operations centre is made possible by having a memory carried on board the satellite. There is therefore a certain time-lag between the time when a measurement is made and the moment when it reaches the operations centre ; it can be up toseveral hours. The satellite memory is also used to store the telecommand orders for the beacons to be interrogated.

The operating principale of Geole is shown in Fig. 1 The sequence of events is as follows :

1. The work programme for the satellite covering a given period (from 2 1/2 hours to several days) is drawn up at the operations centre.

   This programme accommodates requests from users, who have to state :

   (a) the date on which the beacon will be in position ready to be interrogated ;

   (b) the beacon's approximate position (within a few hundred kilometres) ;

   (c) the accuracy of location-pinpointing needed, and the messages to be passed to the beacon.

2. This programme is transmitted to stations in the telecommand network (e.g. by teleprinter).

3. Orders are transmitted to the satellite by telecommand so that it can carry out the work programme.

4. The satellite stores the orders it has received. These orders comprise the addresses of the beacons to be interrogated, the times at which they are to be interrogated and the messages to be passed to the beacons (calculated positions, signal to terminate operations, etc.).

5. The orders are carried out at the times indicated, and the beacons specified are interrogated. At each interrogation the beacon (assuming it is in view and its receiver has locked onto the carrier) will on decoding its own address retransmit this together with location-fixing signals and the date generated by the beacon's sensors.

   At each interrogation, the satellite stores in its memory :

   (a) the address of the beacon being interrogated ;

   (b) the time (using the satellite clock) ;

   (c) the location measurement data (2 range measurements and 2 Doppler measurements) ;

   (d) the data from the beacon sensors (temperature, pressure and humidity for correction of tropospheric errors) and messages to be transmitted via the satellite.

6. The satellite passes over a telemetry station, and the contents of the satellite data store are transmitted to the ground.

7. These data are passed to the operations centre (e.g. by teleprinter).

8. The data are computer-processed, calculating the positions of the beacons and pre-processing the messages received.

9. The beacon positions and messages are passed on to the users.

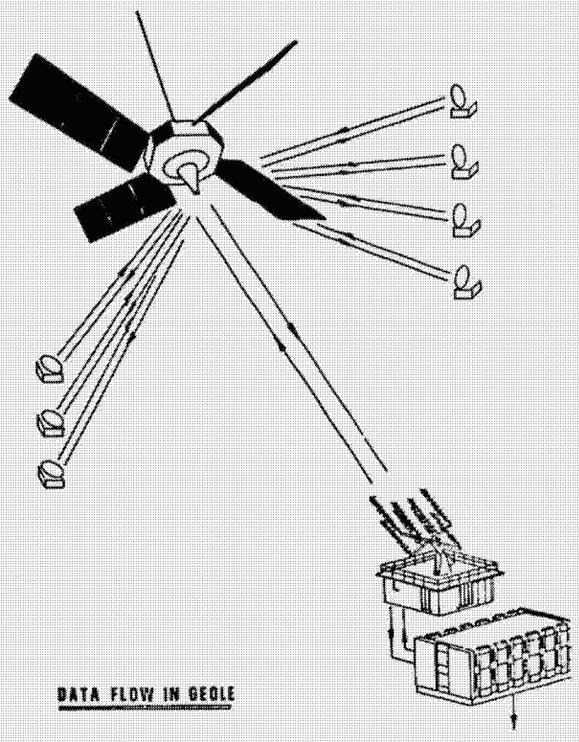

FIGURE 1

The system operates in a sequential mode, so that there is no simultaneous interrogation of a number of beacons. During one satellite pass above a beacon, the latter will be interrogated a number of times, in order to allow interpolations.

The following instance, illustrated in Fig. 2 will serve as an example :

- A user wants to know the position of Beacon No. 40 (= the beacon address). In the same area as this beacon there are three beacons of known position, with the addresses 22, 31 and 34. These latter beacons will be used for plotting the satellite's track.

  The work programme drawn up by the computer centre might then be :

time H_o	interrogation of Beacon 22
time H_o + 5 s	interrogation of Beacon 31
time H_o + 10 s	interrogation of Beacon 34
time H_o + 15 s	interrogation of Beacon 40

followed by interrogation of the other beacons of unknown position, with the same sequence at H_o + 60 s and H_o + 120 s.

The interpolations make it possible to construct three groups of simultaneous pseudo-measurements at the four beacons. The pseudo-measurements at Beacons 22, 31 ans 34 fix the three positions of the satellite, while the pseudo-measurements at Beacon 40 allow the latter to be pinpointed.

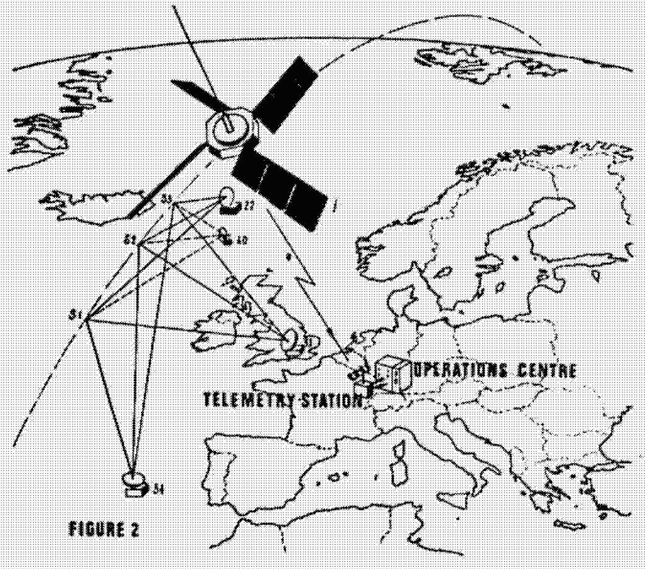

FIGURE 2

4. UTILISATION OF THE SYSTEM

4.1. A basic datum : the standard lattice network

As already stated, the satellite's trajectory will be calculated by means of measurements made from the apices of the polyhedral lattice network set up in the first phase of the mission. This means, in particular, that points to be located will be referred to this network.

4.1.1. Choice of a terrestrial datum

The datum system chosen for Geole does not involve the vertical, which is surely revolutionary for the surveyor. The choice is a natural one, namely a trihedron determined by four given fixed points has no need to be trirectangular it will always be possible to define a trirectangular trihedron.

In practice, a single trihedron would scarcely be practical for obtaining coordinates of points, and it is planned to construct a polyhedral lattice network encompassing the Earth and passing through the four fixed points mentioned above. For reasons of homgeneity, the mathematical treatment of the network (including the four fixed points) will be carried out in one single operation.

4.1.2. Determination of the lattice network

In the system, whether one is concerned with determining the apices or locating isolated points, the law governing the satellite's movement plays no part, except to obtain the best possible interpolation between measurements. The advantage of this procedure is that it does not introduce systematic errors due, for example, to an imperfect knowledge of the Earth's GM (gravitational constant multiplied by the mass of Earth) or to certain harmonics of the earth's potential with which the satellite might resonate.

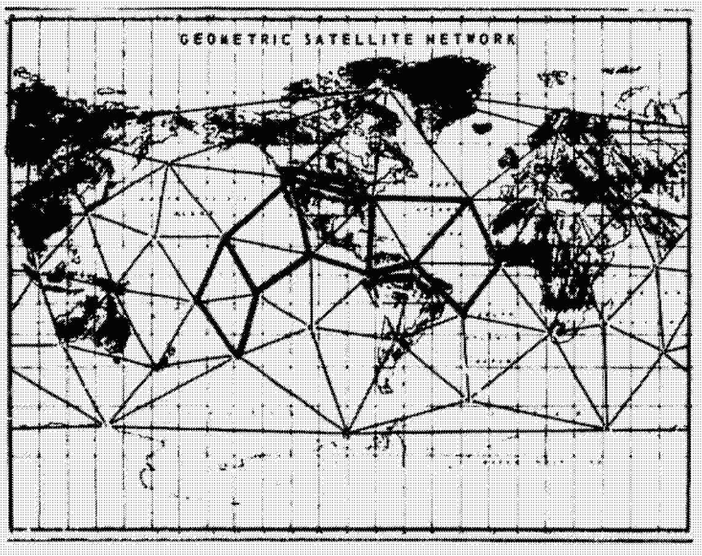

The reference lattice network can be determined by means of distance measurements between the satellite and the apices, or, better still, by measuring distances and radial velocities between these same points.

4.1.2.1. Number of unknowns governing a polyhedral lattice network

To fix the position of the lattice network with reference to the Earth, it is necessary and sufficient to determine six unknowns, viz : 1 point (3 unknowns) and 3 Euler angles (3 unknowns). Since each apex of the lattice network is determined by 3 coordinates, the number of unknowns to be determined for a network having n apices is therefore 3 n - 6.

4.2. Normal method of use

An unknown point can be determined by introducing one new apex of the datum lattice network. We have seen (see para. 4.1.2.) that to solve the problem it is necessary to have simultaneous visibility of four apices (the unknown point and three points of the basic network) and at least :

6 different satellite positions when distance measurements alone are used,

14 different satellite positions when distance and Doppler measurements are used.

In practice, the number of measurements should exceed these minimum values ; furthermore, the ultimate accuracy can only be achieved by observations at several passes giving sufficient geomatrical diversity to get rid of possible bias in the measurements. In addition, during a single pass, the measurement positions should be equally distributed over the arc of the orbit visible from the beacon concerned.

4.3. Insertion of measurements made by Geole in local geodesic systems

The lattice network determined during the first phase of the mission will enable us to define an axis system related to the Earth and fixed once for all. The axis system best suited to user requirements will be chosen. Its characteristics would be :

Trirectangular axes, o, x, y and z ;

Origin close to the Earth's centre of mass ;

Z axis very near to the geographical pole ;

Plane o x z lying virtually along the Greenwich meridian.

The assuracy of the system and the possibility of treating the orbit by means of a semi-dynamic method makes it possible to assert that :

. The origin will be few metres from the centre of mass ;
. The o z axis will be aligned on the geographical pole with an accuracy better than 0.1" ;
. The plane o x z will differ from the Greenwich meridian by an amount not greater than 0.1".

When the axis system has been set up, certain users may have to establish a relationship with regional geodesic systems (e.g. Europe 50, North American Datum, etc.) or local systems (e.g. the system of a given country).

To a first approximation, the transition from the axis system to local systems will be achieved by means of one translation movement (of about 100 metres at most), a rotation and a scale conversion by determining three known points in the geodesic system with Geole, the transformation parameters will be obtained. It is clear that the distribution of points in the initial lattice network will enable transformation formulae to be obtained for the major regional systems. Special operations might be necessary for local systems.

4.4. Utilisation : conclusion

The system will be set up in two stages :

- The first will consist of placing a satellite in orbit associated with about 100 beacons.

- The second will consist of adding to the system one or more satellites so as to give permanent cover all over the globe. One might envisage putting a satellite in orbit once every year or 18 months.

Such a system can only be set up if it is economically attractive. The customers will probably pay on the basis of the time for which the use it. The cost will depend to a large extent on the number of contract customers actually using the system. A rapid calculation shows that if the system was used continuously by 100 beacons :

- The cost of pinpointing a single triangulation point with high accuracy (1 metre) would be of the order of 5000 to 6000 francs.

- The cost of pinpointing an isolated triangulation point with average accuracy (10 metres) would be of the order of 1000 to 2000 francs.

At the beginning of the coming decaden the system could thus become the ideal tool for surveyors, hydrographers, prospectors and topographers.

5. CURRENT THINKING ON THE PROJECT

5.1. Measurement system

For each beacon interrogated, two types of measurement are made by the satellite : radial velocity and distance between the beacon and the satellite.

Radial velocity is measured by means of the Doppler effect : on board the satellite, a comparison is made between the frequency of a carrier as transmitted by the satellite (1500 MHz) to the beacon and is re-transmitted by the beacon. Because the passage through the ionosphere and troposphere alters the signal's propagation velocity and falsifies the measurement, the beacon retransmits on two separate frequencies (2000 MHz and 400 MHz) and a linear combination of these two velocity measurements enables a correction to be made for the effect of the ionosphere. Assuming the satellite's position on its orbit to be known, the corrected value of the radial velocity makes it possible to define the geometrical locus of the beacon, which is a cone whose apex angle is a function of the velocity. Several measurements at different points on the orbit make it possible to define several cones intersecting at the beacon's location.

The distance from satellite to beacon is determined by measuring on board the satellite the propagation time of a low-frequency signal (sub-carrier) sent out by the satellite towards the

beacon to be located and re-transmitted in phase by the beacon towards the satellite. Here again, the passage through the ionosphere and troposphere falsifies the measurement ; to correct the error, the measuring signal is re-transmitted by the beacon on two carriers (2000 MHz and 400 MHz) ; two distance measurements are then carried out and combined linearly. Because of the accuracy required, the sub-carrier frequency is relatively high (1 MHz). Since the distance measurement is in fact a measurement of phase-shift between the signal transmitted by the satellite and that re-transmitted by the beacon, there is a measurement ambiguity corresponding to a 360° phase-shift of the sub-carrier. Since a measurement ambiguity exceeding 30 km is desired, the signal is in fact made up of 9 sub-carriers transmitted sequentially whose successive frequencies are in the ratio of 1 to 2, the lowest sub-carrier being about 4 kHz. Since the satellite position is assumed to be known, the corrected distance measurement makes it possible to establish the geometrical locus of the beacon to be located, which is a sphere with the satellite as its centre. Several measurements at various points on the orbit make it possible to define several spheres that intersect at the beacon location.

5.2. Errors

The accuracy required in locating the beacons in the most exacting circumstances will call for high-quality performance by the measuring system. Its main causes of error are :

- Ionospheric and tropospheric errors, which can be corrected by using two frequencies on the up-link, provided that the beacon look angle is greater than about 20° when the measurement is made, and by measuring the atmospheric parameters (temperature, pressure and humidity).
- Errors associated with antennas and due either to the displacement of the phase centre of the satellite or beacon antennas, or to obstacles in their vicinity (reflection or diffraction effects). These errors can be quite easily overcome by good satellite stability and by taking measurements at fairly high beacon look angles ($\geqslant 20°$).
- Errors due to measuring equipment - frequencymeter for velocity and phasemeter for distance. These pose no special problems.
- Errors due to thermal noise on the links : with reasonable link budget assumptions, these errors can be reduced to 2 m in distance and 2 mm/s in velocity.
- Errors associated with transit time stability in beacon and satellite circuits. This is the most difficult problem. The transit time must be stabilised to within 2 ns.A likely solution is negative feed-back in the beacon modulation circuits and self-calibration on board the satellite.
- Errors associated with time-logging of measurements : this is not critical.

General technical characteristics of the measurement system thus comprises : on board of the satellite :

(a) A 1.5 GHz transmitter (with a power of 10 to 20 W) modulated by the address and distance measurement signals and the data to be sent to the beacon.

(b) A 2.1 GHz receiver,

(c) A 0.4 GHz receiver,

(d) An ultra-stable oscillator (stability 10-11 s),

(e) Two frequencymeters for velocity measurement,

(f) Antennas for use at 400 MHz and 1.5 - 2 GHz,

(g) Laser reflectors for calibration measurements.

On each beacon :

(a) Antennas for use at 400 MHz and 1.5 - 2 GHz,

(b) A 1.5 GHz receiver,

(c) Two transmitters operating at 400 MHz and 2 GHz respectively,

(d) Circuits for extracting the address signal, the distance signal and the data,

(e) Data transmission circuits (for tropospheric correction).

5.3. Choice of orbit

The satellite altitude is chosen so that at any moment 4 beacons of the datum lattice network are simultaneously visible from it. This enables the network to be defined by a purely geometrical method. Since these beacons can only be situated on dry land, the orbit altitude is related to intercontinental distances and will lie between 3500 and 4000 km.

The inclination of orbit is such that a beacon situated at the pole can be correctly located, i.e. the beacon look angle will be around the optimum value of some 30°. The inclination will therefore be some 60°.

Orbit eccentricity is not a critical parameter. Reducing it to a small figure of the order of 1 % confers certain advantages in the dimensioning of the system : reduction of the dynamic of radio signals, an improved mathematical model of the orbit and easier satellite stabilisation.

5.4. Satellite characteristics

The factors governing the satellite's dimensions are :

- The size of the solar generator determined by the transmitted power at 1.5 GHz and by the fact that at an altitude of 3500 km the satellite is subjected to high doses of radiation,
- The mass of the experiment, which is relatively complex,
- Redundancy necessary to ensure a lifetime of at least three years,
- The size of the memory required to store all the information in transit in the satellite between beacons and the processing centre.

Currently, the planned satellite has a mass of some 250 kg and can be launched by a Thor-Delta 2310 without apogee motor. It is geocentrically stabilised to within about 10°, which makes it possible to have fixed antennas pointed towards the Earth. The solar generator is fixed and omnidirectional because operation is continuous.

With regard to electronic facilities, the satellite is equipped with a 136 MHz telemetry system and a 146 MHz telecommand system working to the stations of the European network. Data are stored on a 250 000-bit core memory.

5.4. Beacon characteristics

At least two types of beacon are envisaged, depending on the level of performance required :

- Beacons with directional self-pointing antennas required to attain the system's ultimate accuracy and which will be used in particular to set up the datum lattice network,
- Beacons with omnidirectional antennas, less costly and more simple in use, whose accuracy will be about three times less good.

In addition to the coherent responders already mentioned, the beacons comprise :

- Sensors for physical measurements to carry out tropospheric corrections (measurement of temperature, pressure and humidity),
- A display system for presenting data to the user (e.g. point co-ordinates),
- A power source capable of providing 50 W peaks during transmissions.

6. DIALOGUE

6.1. Objectives of Dialogue

6.1.1. Test of location sub-system

The DIALOGUE project is intended to allow testing of the GEOLE measuring sub-system, and to prepare potential users for this new method of location-pinpointing.

The location and data transmission sub-system, which is shared by the two projects, comprises :

- In the satellite : antennas, pilot oscillator, transmitter, receiver, range and Doppler measuring instruments, data collection and transmission.
- In the beacon : antennas, responder unit, data transmission equipment.

6.1.2. Test of measuring principles and methods to be employed in GEOLE

6.1.3. Maintaining or arousing interest among potential users

DIALOGUE represents an essential stage in developing the GEOLE programme. If it is completely to achieve its aim, not only must experiments with the location sub-system and the associated data-processing prove that the degree of accuracy sought is being obtained, but potential clients must be made aware of the usefulness and advantages of such a system. To ensure this, it has been decided to offer these potential users a place in the DIALOGUE project.

They might participate in two ways :

(a) They could be invited in the CNES experiment, or kept very fully informed of the progress of development and, later, of the results obtained ; or

(b) They could be offered the opportunity of using DIALOGUE as soon as the location sub-system and associated processing are yielding the expected accuracy.

While this objective comes only in the final stage of the DIALOGUE project, it must not be thought of as secondary, for the future of GEOLE lies not only with being able to build a location sub-system that will give the necessary performances, but also with having a large number of likely users who become firm customers when this experimental stage is over.

6.2. Main technical characteristics

Launcher :

The launcher will be a DIAMANT B with a P4 2nd stage.

Orbit :

The orbit has been selected as function of :

. constraints due to the data handling
. the overall objectives to be obtained
. the launcher performance

The orbital characteristics are :

. apogee : 650 km
. perigee : 650 km
. inclination : 60°

Satellite :

The DIALOGUE satellite will be built from the second flight model of the "EOLE" programm, the first satellite having been launched in 1971. The equipment of the EOLE experiment will be replaced by the position finding sub-system to be tested.

The main satellite sur-systems are the following :

a) the position finding sub-system with :

- a 1530 MHz transmitted with a radiated power of 5 W modulated by the ranging and data signals.

  The ranging signal is a binary code with a basic rate of 1 MHz and 200 µs recursion (distance without ambiguity of 30 km).

  The frequency band occupied is ± 2 MHz

- a receiver centred on 2098 MHz demodulating the ranging signal

- a 402 MHz receiver

- an ultra stable oscillator controlling the transmitter and the clocks

- a frequency measurements system (Doppler) on the 2 links

- a ranging system on the 2 links

- an antenna pointed towards earth

- laser reflectors for the calibration measurements.

b) The EOLE sub-systems :

- 136 MHz telemetry transmitter

- 148 MHz telecommand receiver and decoder

- gravity gradient stabilisation.

The total satellite mass is estimated t · be 84 kg.

Beacons :

The beacons are coherent repeaters comprising essentially :

- an antenna
- transmission and reception equipment
- data handling equipment (address recognition, measurements enabling tropospheric errors to be corrected, i.e. pressure, temperature and relative humidity)
- a power supply.

Two types of beacon will be used :

- type II with directional antenna pointed automatically to the satellite
- type I which are identical to type II except that they have an omnidirectional antenna.

Only type II beacons enable position determination to within 1 metre ; however, type I beacons with an omnidirectional pattern are easier to use and can be installed in certain vehicles.

6.3. Planning

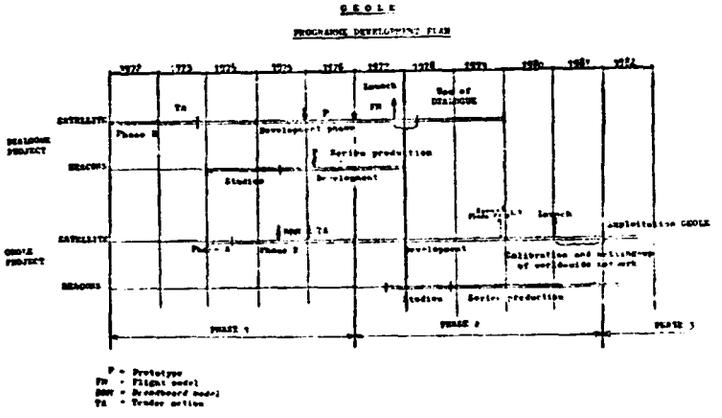

RESULTS OF GEOLE SYSTEM SIMULATIONS

Jean-Louis PIEPLU

Groupe de Recherches de Géodésie Spatiale
CENTRE NATIONAL D'ETUDES SPATIALES

(FRANCE)

ABSTRACT

Simulations on the précise and opérationnal positionning system GEOLE are presented. The position of user's transponders will be computed, in a world wide reference coordinates system, from range and range rate measurements. This datum consists in the set of coordinates of a net of stations, well distributed all around the earth. The respective positions of these points will be determined with GEOLE itself during a preliminary step.

A significant simulation of the real system, particularly concerning errors on measurements, had been carried out. In a geometrical approach, which leads to a satellite altitude of 3500 to 4000 km, it is showed that the reference station net can be known with an accuracy better than one meter in less than 20 days of observations. On a more local scale, each summit of this polyhedron will be linked to the nearest others, something like 3 or 4000 km apart, with an accuracy of about 50 centimeters.

A long arc technique leads to results 2 or 3 times not so accurate, on the hypothesis of present uncertainties on knowledge of earth gravity field. These capabilities are able to be brought down to those of the geometrical method, with, in addition, fifting of some lump coefficients to absorb the more important orbital perturbations.

Simulations showed also that in the operationnal phase, users can get their position with accuracy better than 10 meters on one pass and better than 1 meter, whatever the latitude of transponders, after one day observations.

- Introduction -

During the second part of the sixty years, the Centre National d'Etudes Spatiales (CNES), took interest in one category of application satellite intended to position operational fixed or mobile users. It's in this way that was conceived, then carried out the EOLE satellite, launched during 1971. The purpose of this project was to get position of balloons in high atmosphere. The spacecraft do, with transpondeurs set on board of balloons, range and range rate measurements. This prime objective was followed by complementary applications, as positionning of fixed transpondeurs, buoys, icebergs. After, soon, three years of good running, the satellite works yet.

J.L.- PIEPLU

On 1967, during the realization phase of EOLE, was born the idea of a more ambitions project, having objectives of geodetic accuracy. The main features of this operationnal system remind those of EOLE and the new project was named GEOLE 1 where "G" is a kind of geodetic quality flag added to EOLE system.

- Objectives of GEOLE -

GEOLE is an operationnal positionning system that gives the position of transponders in a worldwide coordinates system. The accuracy scope needed answers two different classes of requests of the potential users :

- Relatively short delay between observations and delivery of the fix to the users. Datas of only one pass will be used. Accuracy will be on the order of 10 meters,

- short delays are not a so great constraint, but a better accuracy is needed. Observations of a whole day are used. Accuracy is about 1 meter.

These figures are for fixed transponders or if velocity was known. For mobile transponders, accuracy is limited by factors external to the system which are the bad knowledge of all the platform movements. Nevertheless, the conception of the GEOLE system can extend to an integrated system which gives informations on these movements.

The realization of these applications objectives and particularly the definition of the world wide coordinate system, implies to settle on the earth surface a polyhedron of reference stations. The respectives positions of these fundamental points must be determined, by the GEOLE system itself, in a preliminary step, with an accuracy of about 1 meter. This intermediate objective, has an actual scientific interest, the more recent publications on stations net coordinates showing discrepancies from 10 to 20 meters.

Objectives of the simulations -

The analysis of results obtained by different centers, like SAO [2] GSFC [3] or NWL, using space techniques for geodesy purposes, gives the order of magnitude necessary in the accuracy of elementary measurements to perform the GEOLE objectives. It leads to aim accuracy of about 1 meter for range measurements and 1 millimeter per second for range rate measurements.

Some experience had been gained also in France after the launching of geodetic satellites as DIC (670111) and DID (670141), equipped with laser retroreflectors and very stable oscillators which give range and range rate measurements. Processing of the data, made by the Groupe de Recherches des Géodésie Spatiale (GRGS) according to geometrical and long arc techniques , had led to the linking of stations more than one thousand kilometers apart, with accuracy of some meters [4] . The GEOLE system with an far better quality for range rate data will lead to a determination better than one meter on such distances. In the same way, results get with EOLE system, two orders of magnitude less accurate than GEOLE, show that current accuracy is about 1000 meters but a refined processing gives 2 or 300 meters. Furthermore, GEOLE has the advantages, with regard to the above experiment, except EOLE, of unicity of measurements system and unicity of synchronization with the satellite borne clock.

The above considerations give confidence in the hypothesis chosen for GEOLE, but they give only an idea of the global capa-

bilities of the system.

In opposition with this general approach of the problem, a specific simulation tool of the GEOLE system had been carried out. In a first part, it generates measurements as significant as possible of those of the operationnal system, and in a second part these data are processed with statistical evaluation algorithms significant of techniques that will be used in the operation phase. This instrument tool allows to study more in details tails the influence on the final objectives of elements of the system or subsystems, such as orbital characteristics or number and location of reference stations or type of errors on measurements. The results presented further on concern the two phases of the experiment, the preliminary one in which the reference polyhedron is settled, and the operationnal one, in which users get this position in this reference system.

- Hypothesis of the simulations -

- The geometrical approach we intend to use in the preliminary step implies a regular distribution of the reference stations. The approximate length of the chords is fixed by the geographical possibilities to put transponders on islands or coasts around the Pacific Ocean. This length is of about 3500km which gives a total number of 30 to 40 stations for the reference polyhedron. In the simulations, we had taken 36 stations and their location is showed on figure 1.

- - The visibility of the satellite by a station is limited by the maximum zenithal angle of the station to satellite direction, The limit value results from compromise between technical constraints (acquisition of frequencies, troposphere errors ...) and coverage considerations. In the simulations we took two values : 70° and 75°,

- The geometrical approach implies too, that the satellite would be able to see simultaneously 4 stations of the reference net. This constraint associate with the limit visibility one, fixes the minimum of the orbit altitude . To get sufficient coverage we have chosen the following values :

Zenithal maximum angle	orbit altitude
70°	4000 km
75°	3500 km

The other characteristics of orbit in the simulation are :

Excentricity : 0.01
Inclination : 60°

This inclinaison permits to see transponders near the poles.

The positions of the satellite had been generate, from these orbital elements, by numerical inegration of the movement equations. Forces taken into account are those due to earth gravity field (the model used is Standard Earth II, SAO [5]), Luni-Solar effect, radiation pressure.

- The calling mode of the transponders in GEOLE system is a sequential one. The calling sequence will be elaborate in the computing center and load in the memory of satellite. But the geometrical method needs simultaneous data. So, it will be necessary to interpolate in the range measurement and the range rate one of each pass to get fictive simultaneous data. To keep accuracy of measures in this fitting, a sufficient number of observations points is necessary (order of 20). For that purpose, the calling recurrence with each reference station was taken to

1 minute.

- Detailed study had been made on the errors of the measurement system(electronics, propagation, geometry ...). The simulation program can generate a particular type of error by adding a specialized routine. We have selected only the main type of errors which are given in the following table :

	TYPE	MAGNITUDE
RANGE UNITS : meters	1. Thermal noise	0.8
	2. Time delay in transponders	0.0 to 1.0
	3. Time delay in satellite	0.8
	4. Propagation (troposphère)	$k_1/\sin h$, $0. < k_1 < 0.1$
RANGE RATE UNITS : millimt./Sec.	5. Thermal noise	1.75
	6. Propagation (troposphère)	$k_2/\sin h$, $0. < k_2 < 0.2$
	7. geometrical effect	$k_3/\sin h$, $-0.4 < k_3 < 0.4$

Errors N°1 and 5 are gaussian with R.M.S. indicated,
Error N° 3 is a constant biais,
Error N° 2 is constant for one pass with a transponder, but this constant is regularly distributed between the two bounds indicated for all the passes. It take into account the sensibility of transponders to meteorological variations.

Errors N° 4, 6 and 7 have a profile bound to the angular elevation of station to satellite direction above horizon of the station. The K_i values, constant on one pass are regularly distributed for all passes. The propagation errors are residuals after corrections computed from models [6] , [7] where ground meteorological parameters are introduced. These parameters (temperature, pressure and humidity) are measured in the transponders and collected by the satellite .

- Methods of Resolution and Results -

Processing consists of statistical evaluation of parameters of which measures depend. By its ground end the measure is dependent of the coordinates of the station and by its space one, it is dependent of the coordinates of the satellite. If observations are simulatenous, no more parameters are concerned. If they are not, relative motion between satellite and stations must be introduced during the interval separating measures. Orbital parameters and forces acting on the satellite are involved and also the global earth movements in an inertial reference.

These 2 approaches were studied for the polyhedron determination phase. In the geometrical method, by interpolation on very small time intervals, we get simultaneous observations from groups of 4 stations. From each simultaneous set, we can eliminate the satellite position and it remains one (range only) or two (range and range rate) conditions equations, between station

coordinates only. After some days of observations, the whole system of equations becomes well made up and can be resolve. Before resolution it's necessary to fix barycenter of the polyhedron and its "mean" orientation by constraints because the geometrical method cannot determine them. We had taken this constraints as follow :

$$\sum \overrightarrow{\Delta P} = 0 \qquad \text{and} \qquad \sum \overrightarrow{OP} \wedge \overrightarrow{\Delta P} = 0$$

where P is the initial position of a station and $\overrightarrow{\Delta P}$ the proposed solution for this station.

The two cases of altitude orbit mentioned above were studied. Thirty days of data were generate in each case. Resolution of the condition equation system was made with data of 2.5 days, 5 days, 7.5 days ... 30 days to study the convergence of solution. Initial position of each station had an offset of about 300 meters (randomly distributed over the whole polyhedron) from the true cvalue which serve to generate data. Direct comparison on station coordinates between each solution and true reference value is not easily readable because of global translation and rotation of polyhedron - So, we made these comparisons on the chords that link each summit of the polyhedron.

Statistical distribution of errors on all the chords (630) is showed figure 2, for a 2.5 days, 12.5 days and 25 days observation period. First, sensible difference can be noted between the 3500 km orbit altitude case and the 4000 km one. But we must remember that in the first case, the minimum elevation angle above station horizon is 15° and 20° in the other case. It gives, in the 3500 km and 15° hypothesis, a better geometry for the elementary tetrahedrons which are less sensitive to data errors. We note also that in the two cases the chord errors are not equally distributed each side from zero. This biais is about of 1 meter. Its origin is in the biais on measurements and essentially those on range data : the constant time delay in satellite electronics and the time delay in transponders equally distributed between 0 and 1 meter. The effect is to expand the whole geometrical figure. It would be of great interest to reduce the first error, by frequent calibration, and to center the transponders errors. It must be outlined that despite biais, all the chords are computed after 25 days with an accurarcy better than 2 meters. This fulfils the objectives of GEOLE for the first phase.

Convergence of the solution is sensible on the three check points of figure 2, but it is more visible on the figure 3 were the percentage of chords computed with an accuracy better than 2 meters is plotted against the number of days of data. It clearly shows that convergence is reached in about 20 days.

Global representation as above is note quite satisfactory because distribution of chord length is not uniform (the longer ones are more numerous) and it does not give idea of local accuracy. On figure 4 are shown discrepancies on chords that link one particular station, in this case an equatorial one, to all the 35 others. The biais effect is also visible and its dependance to chord length is clear. For the nearest stations (< 5000 km) error on the chord is on the order of 50 centimeters. Relative accuracy dr / r is about 10^{-7}. Results are the same when we take a high latitude station. Dispersion of points is even smaller.

The determination of the polyhedron was also tried with a long arc technique where orbital parameters and the coordinates of the stations are fitted. Numerical integration was used to des-

cribe the satellite movement. In addition to the above data errors discrepancies in the earth gravity field were introduced. For the generation of data SE II was used, the GEM 4 model for processing Differences between the two models reach 20 meters on the geoid height, principaly in Southern Hemisphere. Computations made on one day to five days observation interval, with statistical gathering of solutions show that :

- results are globally 2 or 3 times not so accurate as in the geometrical method,
- results are worst in southern hemisphere,
- errors on stations are sensibly stable with time (on one month interval),

This indicat high correlations between station position and potential coefficients as often outlined by geodesist who determine earth gravity models.

Nevertheless, hypothesis taken for uncertainties on knowledge of earth potential is very severe. It was probably true on 1970 but for 1980 which is the expected launching date for GEOLE an improvment by a factor 3 or 5 would not be a surprise.

It is the reason that led to study the application phase with the orbital method. In this technique, orbital parameters are computed first, with data from a sub-set of the reference polyhedron stations, the position of which had been determined at 1 meter with geometrical method. Then the orbit serves as reference to compute the position of user'transponders. With this practice, the final accuracy is sensitive also to earth gravity field model errors. If globally, on 1980, the models will have sufficient accuracy, it is possible that some resonnant perturbations raise to a significant level. These effects can be smoothed by adjustment of lump coefficients, for example on the same data that had served to compute geometrically the reference polyhedron. Simulations based on the first order perturbations formalism given by KAULA [8] show that 80 to 90% of the resonnant effect was absorbed, bringing down the residual to the mean level of other perturbations spectrum.

The effect of data errors on fixed user positionning is shown on figure 5 and 6.

Figure 5 gives errors for a one pass determination. As very often said, the main direction of error is cross-track. It increases rapidly when the transponder is very near the satellite track. Cross track error is lower than 10 meters for geocentric track distance greater than 5° and lower than 20 meters at more than 2°. Along track error is lower than 1 meter and height error lower than 5 meters. It is important to note that because of the two kinds of data (range and range rate) GEOLE has the possibilities to compute on a single pass, the 3 components of a fixed user.

Figure 6 shows errors on the fixed user position with one day observations. Results are dependant of relative values of the user latitude and the orbital inclination. Three inclinations are studied : 0°, 30° and 60°. For the last one, whatever the user latitude, even near poles, error is on the order of 1 meter.

- CONCLUSION -

Simulations representative of the GEOLE operationnal system show that :

- by a geometrical method, the polyhedron of station which will serve as reference coordinate system for

positionning users, is able to be determine with an accuracy of 1 meter in a time interval of about 20 days. Relative accuracy reaches 10^{-7},

- Fitting of lump potential coefficients to resorb resonnant perturbations allow the use of orbital method during the user's phase,

- errors on users position will be of about 10 meters on one pass and 1 meter with one day observations. In both case, the three components of the users are determined.

- REFERENCES -

[1] - HUSSON J.C., THIRIET D.- "A proposed aid to geodesy : the spatial system GEOLE" - International Hydrographic Review - Vol XLVII N° 2 - July 1970 -

[2] - GAPOSCHKIN E.M., "Smithsonian Institution Standard Earth III", Presented at the American Geophysical Union Meeting, April 1973 -

[3] - MARSH J.G., DOUGLAS B.C., KLOSKO S.M., "A global station coordinate solution based upon camera and laser data" Paper presented at the First International Symposium on the use of Artificial Satellites for Geodesy and Geodynamics, Athens - Greece, May 1973.

[4] - CAZENAVE A, DARGNIES, O, BALMINO G., LEFEBVRE M., "Geometrical Adjustement with simultaneous Laser and Photographic Observations on the European Datum", American Geophysical Union Monograph 15, 1972.

[5] - GAPOSCHKIN E.M., LAMBECK K.,"1969 Smithsonian Standard Earth II", SAO Special Report, N° 315, Smithsonian Astro-Physical Observatory, Cambridge, Mass. May 1970.

[6] - HOPFIELD H.S., "Tropospheric Range error parameters : further studies". APL/JHU CP 015, June 1972.

[7] - YIONOULIS, S.M., "Algorithm to compute tropospheric refraction effect on range measurements", APL/JHU TG 1125, July 1970.

[8] - KAULA, W.M. "Theory of Satellite Geodesy" - Blaisdell Publishing Company - 1966.

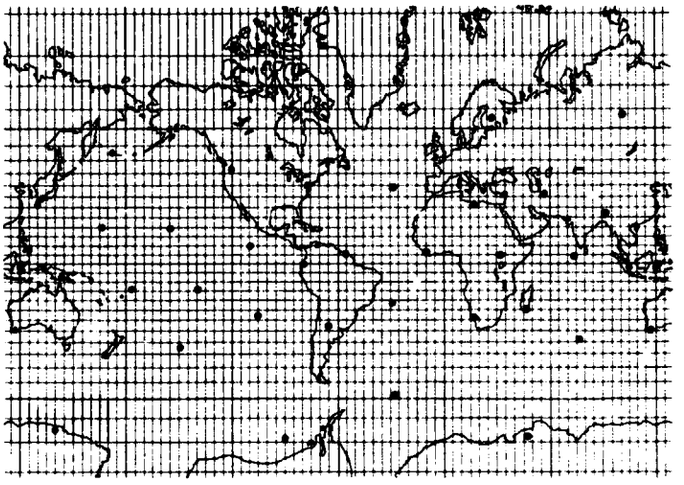

FIGURE 1 - REFERENCE POLYHEDRON -

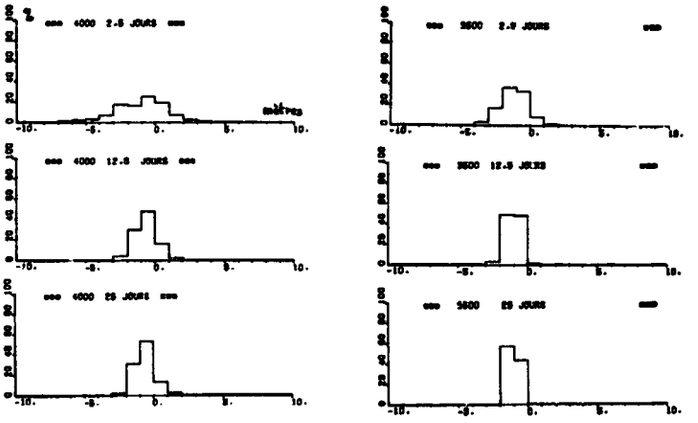

FIGURE 2 - STATISTICAL DISTRIBUTION OF ERRORS ON COMPUTED CHORDS - On the left, orbital altitude is 4000 km and minimum elevation angle for each station is 20°. On the right, orbital altitude is 3500 km and limit elevation angle is 15°. Statistics are made with 2,5 days, 12,5 days and 25 days of observations.

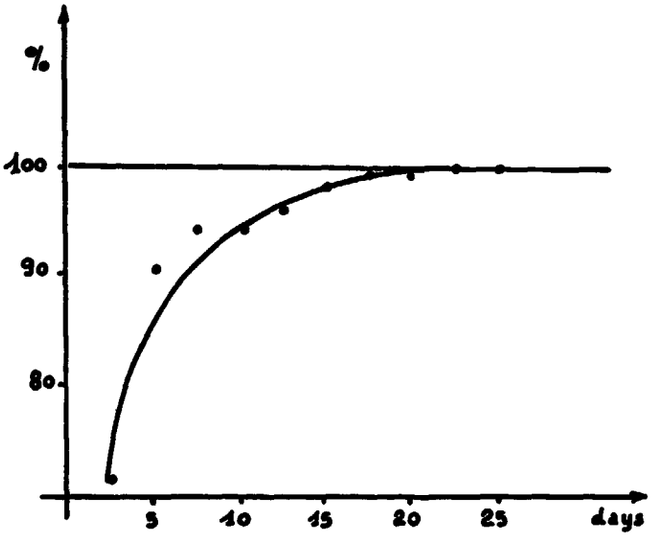

FIGURE 3 - CONVERGENCE IN POLYHEDRON PHASE -
The percentage of chords which are determined with an accuracy better than 2 meters is given with respect to the time interval of observations

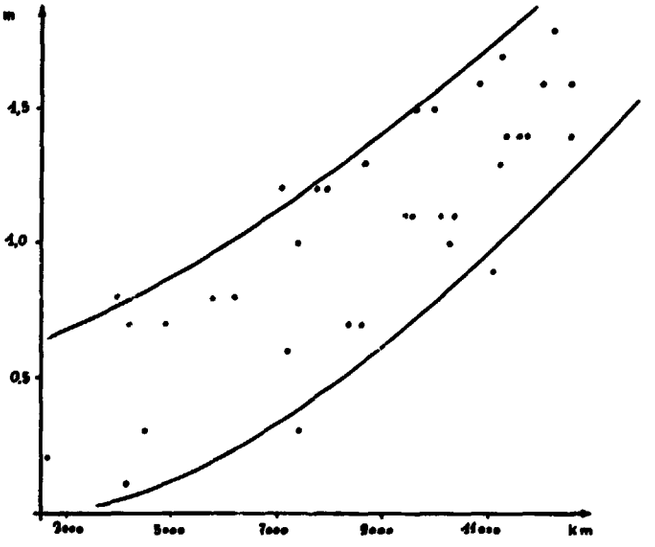

FIGURE 4 - RELATIVE ACCURACY IN POLYHEDRON DETERMINATION -
Errors on computed chords with respect to the length of chords. Relative accuracy dr/r is nearly 10^{-7}.

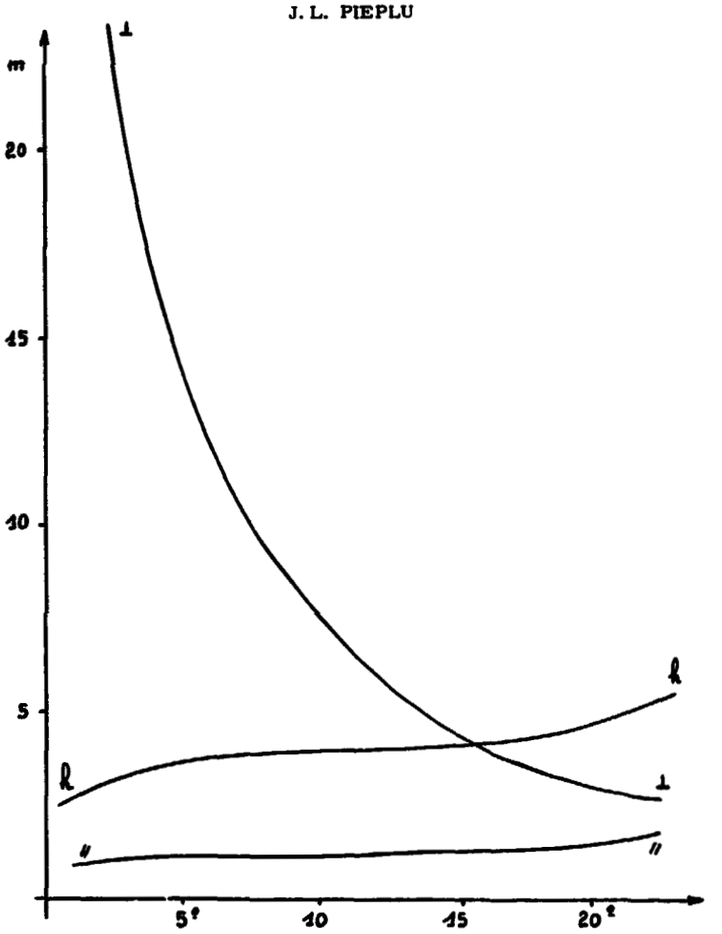

FIGURE 5 - POSITIONNING ON ONE PASS -
Errors cross track (⊥), along track (//) and on the altitude are given with respect to the geocentric distance between the transponder and the satellite track.

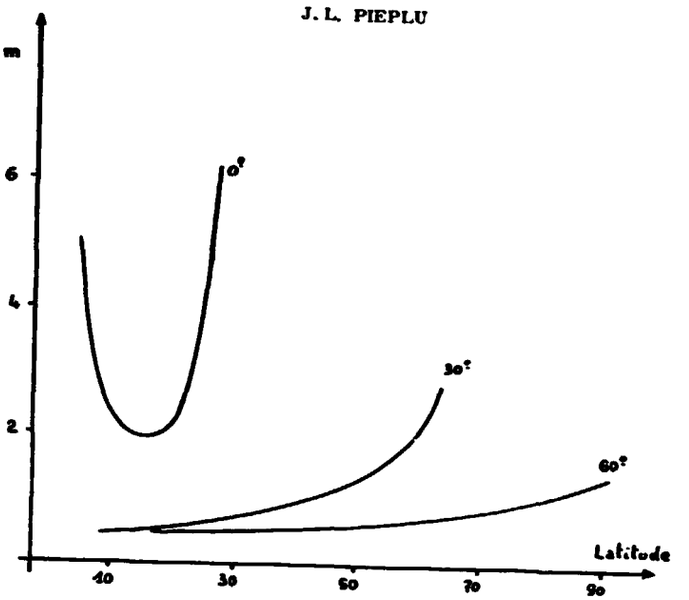

FIGURE 6 - POSITIONNING ON ONE DAY -
Total error of positionning is given with respect to the transponder latitude, for 3 values of the orbit inclination.

C-3

SURVEY OF ACOUSTIC NAVIGATION TECHNIQUES

Don B. Heckman

Sea-Link Systems
AMF Electrical Products Development Division
of AMF, INCORPORATED
Alexandria, Virginia

ABSTRACT

Acoustic navigation techniques, utilizing bottom moored acoustic references, (e.g. transponders or beacons) can provide very precise (1-10m) relative positioning of both surface and subsurface objects. This precision relative positioning can be extended to the geodetic coordinates by integrating the acoustic system into a geodetically referenced navigation system such as NAVSAT. This paper is a tutorial treatment in which the subject is partitioned into two major topics. First is a discussion of the measurement of the geometric parameters required to determine position relative to an array of bottom moored references. This describes the basic terminology and principles employed in various techniques such as Range-Range, Range-Bearing, Doppler, Pulse-Doppler, etc. The relative merits and limitations of these techniques are also presented. The second major topic treated is that of solution techniques. That is, given that the appropriate geometric parameters can be measured to within a reasonably known accuracy, how is an acceptable mathematical solution effected given the raw geometric data. This problem can be conveniently subdivided into two parts: (a) calibration of the bottom moored acoustic references; and (b) navigation operations. Due to the impracticality of precisely implanting these reference devices, the first step in utilizing an acoustic array for navigation is to accurately determine the relative positions of the references. Described is the classical (that of baseline crossing and cloverleaf maneuvers) and more advanced techniques such as those described by Vanderkulk, Lowenstein, Short and Travis, and Heckman and Abbott. Generally, the survey technique can be easily constrained to yield a powerful technique for the determination of the position (navigation operations) of the vehicle given the positions of the bottom moored references. A bibliography is included.

INTRODUCTION

Navigation with reference to an array of bottom-moored acoustic references provides the highest position resolution and accuracy of any technique available at present for surface ships and submerged vehicles beyond sight of land. It is the only practical method of accurately determining the position of a submerged vehicle.

This discussion will be restricted primarily to those techniques that provide for a useful operating horizontal range of several times the water depth as opposed to schemes used to maintain a fixed position nearly over an acoustic reference on the bottom. For those interested, such techniques are described in references 3, 5 and 9. Also, this will be limited to so called portable reference arrays, i.e., the bottom references are such that they can be freely deployed and are not connected by wire to land or to a ship.

Following the text is a bibliography.

BASIC DEFINITIONS

Baseline - The line or separation between hydrophones, transponders, or beacons comprising an array of acoustic devices used to determine the position of vehicle.

Continuous Wave (CW) Beacon - An underwater device which continuously emits an acoustic signal with precisely known frequency and phase characteristics (usually a single frequency sinusoid).

Pinger - An underwater device that repeatedly transmits acoustic pulses at a non-precise rate (approximately periodic).

Pulsed Beacon - An underwater device which repeatedly (usually periodically) emits an acoustic pulsed signal at precisely known times.

Responder - An underwater device that emits an acoustic pulsed signal upon receipt of an electrical trigger pulse via a wire connection.

Transponder - An underwater acoustic device which after receiving a proper acoustic pulsed interrogation signal, transmits generally a different acoustic pulsed signal delayed a precise and fixed period of time after receipt of the interrogation pulse.

In order to uniquely distinguish between many transponders, the reply signals are usually different (for example different reply frequencies) while all the transponders in an array are interrogated by the same signal. This is called reply diversity.

RANGE-RANGE/LONG BASELINE

Long baseline systems determine position of a vehicle by measuring the slant range from the vehicle to a number (two or more) of bottom moored transponders or beacons. The bottom references are configured in a nonlinear array and are separated by about 0.25 to 0.5 of the transponder's maximum range (Ref. 23). Maximum range of transponders available for deep ocean applications is generally 5 to 10 nautical miles. The geometry is depicted in Figure 1 for a surface ship. To determine slant range, an interrogation pulse is transmitted from the vehicle (ship or submersible) and by measuring the time between this and the time of arrival of the transponder reply the range to each transponder is determined. For deep ocean transponder arrays the position accuracy achievable is about 5 - 20m with a resolution of approximately 1 meter (Ref. 14).

Obviously the number of interrogating ships (or subs) is limited for such a transponder array. Using pulsed beacons

instead of transponders will allow for positioning of an unlimited number of vehicles within the acoustic range of the array. Here, the interval between the known time of beacon pulse transmission and the time of arrival of the acoustic pulse at the vehicle's hydrophone is measured to provide slant range data (Ref. 27). It is pointed out that there is a cumulative error associated with the beacon array due to relative drift of the time references in the beacons and the ship where as the transponder array does not have such a cumulative error. Also transponders lend themselves to longer term applications than beacons since much more power is required to operate a beacon due to the precision time reference and constant transmission of output pulses. With either transponders or beacons the data rate is low; approximately 1 cycle/10 seconds to 1 cycle/60 seconds.

Figure 2 shows a scheme for determining the positions of a surface ship and a submerged vehicle relative to a 3 transponder array. Initially, ship position (U,V,0) is determined by measuring slant ranges r_1, r_2, and r_3. To determine the position of the submerged vehicle, a transponder mounted on it is interrogated to measure $r_{4,s}$. It's reply is such that it will interrogate the bottom moored transponders. When this signal is received by each bottom transponder, it replies with a signal which is received at the ship to give a measure of the quantity $(r_{4,s} + r_{i,s} + r_i)$, where i represents each transponder, i=1,2,3. Since $r_{4,s}$ and each r_i are known, $r_{i,s}$ can be determined by subtraction (Ref. 15). For noisy submerged objects it is better to use a beacon or responder on it due to the problem of the transponder "hearing" the interrogation signal in a local high noise level.

The solution for the position of the surface ship or the submerged vehicle is the intersection of a number of spheres equal in quantity to the number of slant ranges available. Due to measurement errors, these spheres do not generally intersect at a single point but rather the solution is contained within a volume of uncertainty (a nearly simultaneous solution). Simple algebraic techniques have been used which usually choose the point of intersection of two of the spheres and other slant range data is used to resolve ambiguities. The solution is thus on the outside surface of the volume of uncertainty and is very unlikely to be the best estimate of the actual location.

More powerful techniques have been developed which generally use a least-mean-squared-error fit of all data available to provide a better estimate of the most likely position of the object within this volume of uncertainty (Ref. 22, 15, and 26).

Due to the impracticality of precisely implanting the bottom references, their relative positions must be determined as accurately as possible generally before the array can be used for positioning. This array calibration has traditionally been performed using cloverleaf and baseline crossing techniques (classical array calibration, Ref. 8 and 11). The cloverleaf maneuver is used to determine the depth of the references by positioning a ship on a series of four or more successive lines, such that each line passes through the closest-point-of-approach (CPA) of the previous line. See figure 3. The shortest CPA is assumed to be depth coordinate of the transponder. The baseline lengths between transponders are determined classically by a surface ship running additional lines through the reference array (figure 4) crossing each baseline at least twice, and summing the horizontal range components of each position determined along the line. The minimum sum of the horizontal components is the baseline length.

This calibration scheme requires large amounts of ship time and critical ship maneuvers.

A calibration method, made practical by high speed digital computation, that places minimal restrictions on the precision of ship operation and greatly reduces ship time is described in Reference 15, 22, 25, 26 and 10. In this method slant range data from a minimum number (six for a surface ship in a three transponder array) of diverse ship positions allows the solution of a sufficient number of equations to determine the coordinates of the bottom references. In practice, additional ship position data provides for an overdeterministic solution of coordinates allowing a least-mean-squared-error best estimate. This is desired due to measurement uncertainties as discussed previously.

RANGE-RANGE/SHORT BASELINE

This scheme is depicted in figure 5. Three hydrophones, arranged in a triangle that lies in a horizontal plane are attached below the hull of a surface ship. A pulsed beacon, transponder, or responder is attached to a submerged vehicle the position of which is to be determined with respect to the surface ship. The acoustic pulses from the submerged vehicle are received by the hydrophones and the three slant ranges R_1, R_2 and R_3 are determined which provide sufficient information to calculate the x, y, and z coordinates of the vehicle. Due to the fact that the surface ship is not a stable platform, roll, pitch and yaw motions must be measured and included in the calculations to compensate for the relative motion of the short baseline hydrophones. This scheme can be referenced to a bottom datum by implanting a bottom moored transponder that is tracked by the surface ship (Ref. 1). Equations are shown in Reference 17.

Since the pulses from the submerged object or transponer all arrive at the three hydrophones very close in time to one another and since hydrophones most likely are each located in essentially uncorrelated noise fields, this technique is very prone to large errors. Van Ness et al (Ref. 17) states that for timing errors of 0.2mS the errors in x, y, and z are on the order of tens of feet to almost 1000 feet depending on the relative location of the submerged vehicle to the surface ship.

TIME DIFFERENCE/SHORT BASELINE

This method is primarily suited to station keeping applications but since it is so closely related to the Range-Range/Short Baseline scheme it seems worth mentioning. This system consists of a ship mounted hydrophone array, roll, pitch and yaw sensors and processing electronics just as in the above technique. However, the difference in the time of arrival of the acoustic pulses from a bottom moored acoustic pinger allows determination of the ships x and y coordinates on the surface. Figure 6 shows the geometry for one of the two planes (x-z), the (y-z) plane being similar. The acoustic signal can be a series of pulses from a pinger in which a pulse time of arrival measurement is made, or it can be a modulated Continuous Wave (CW) carrier on which a phase difference measurement is made or a hybrid of these. In this latter case, the pulse is used for a course measurement and the phase is used to provide for high resolution (Ref. 3 and 9). This technique is limited to x and y offsets of approximately less than 30 percent of the water depth.

RANGE-BEARING

A scheme that uses an extremely short baseline (approximately λ/3 in spacing) pulsed phase comparison technique to determine the relative bearing and a pulse time of arrival technique to determine range from a transponder or beacon is described in Reference 28 and 29, and is shown in figure 7. This scheme was designed for the transponder or beacon to be essentially in the same plane as the hydrophone array (e.g. relocation of buoys and etc.). It is possible to extend the technique to the measurement of depression angle as well as bearing angle by the addition of a fourth hydrophone in the plane of hydrophones 1 and 2 and "a" units directly below hydrophone 2 as shown in figure 7. The range accuracy here is the same as for the Range-Range/Long Baseline being 5 to 20M with a resolution of about 1M. The bearing accuracy is approximately ±5° for relative bearings of less than about ±45°; beyond 45° the resolution falls towards zero at 90° as implied by the equation in the figure.

Davies in Reference 12 refers to a range-bearing navigation system where a bearing accuracy of approximately ±0.5 degrees is achievable and based on this estimate concludes that a Range-Bearing System has the most desired error distribution of several techniques considered. To the present author's knowledge, however, it is quite difficult to achieve bearing accuracies in order of ±0.5 degrees with pulsed reference devices for ranges on the order of 10NM.

BEARING-BEARING

Obviously if a satisfactory bearing can be taken on an acoustic reference device then bearings to two references at known locations will produce a position fix. This technique is mentioned in Reference 12 but has not been generally used in practice due to the difficulty in accurately determining bearing in a simple manner.

RANGE-RANGE HYPERBOLIC

This technique as described in previous literature known to the author has been limited to the case of position determination in a single plane (Ref. 6 and 12). The basic hyperbolic system described is an acoustic version of LORAN where if two (or pairs of) moored beacons transmit signals simultaneously, the locus of equal time delays between receipt of the two signals is a hyperbola. Such a scheme is shown in figure 8. Obviously, two intersecting hyperbolae obtained from two pairs of beacons are required to determine a position. This requires at least three beacons. The time drift and high power consumption problems associated with precision beacons are encountered here of course, but such a system can support an unlimited number of vehicles and they do not need to be synchronized to a master time base. Also ambiguities can be reduced by knowing which beacon signal was received first.

This technique could be extended to three dimensional space by measuring at least three independent time delays (from 3 independent pairs of beacons) and solving for the intersection of the three hyperboloids. An overdeterministic solution as was described in the Range-Range/Long Baseline section could be used in such a case.

DOPPLER SYSTEM

Basically two types of doppler techniques have been described previously, first that in which a bottom moored CW beacon with a precisely known frequency transmits to an object which receives the signal; and, secondly that in which a pulsed simusoidal signal is transmitted and reflected back to the same acoustic transducer and is used for dead reckoning.

The first type of system is described in Reference 7 and 31. This reference array consists of three bottom-moored CW beacons, each separated in frequency. The receiving vehicle derives its displacement information by integrating velocity that is obtained from the beacon signal doppler shift. Doppler frequency shift is given by

$$f = f_B - f_D = -f_B(V/C)$$

where f_D is the doppler - shifted beacon frequency due to a vehicle velocity V (positive for increasing range rate), f_B is the beacon frequency, and C is the speed of sound in the water. By determining the velocity and displacement components to each beacon, the positions of which are known, sufficient information is available to position an object in three dimensions. This tracking system was designed for displacement resolution of approximately 10 cm and data rates of 6Hz. The price paid for such high resolution is of course short life acoustic beacons due to continuous transmission (on the order 1 to 10 days presently), complex receiving and detection equipment, and difficulty in initially determining the location of the beacons (array calibration). Also such a system does not provide an initial location at which one can start accumulating doppler shift information.

The second scheme, active doppler, is described in References 13 and 16 and is shown in figure 9. Here a special acoustic transducer transmits pulsed sinusoidal signals of known frequency at a depression angle of α fore, aft and in both directions athwart ships. Such an arrangement cancels out vertical velocity and provides two dimensional velocity and displacement information. In most cases the transmitted acoustic energy is reflected or scattered off the bottom, but can be scattered from volume inhomogeneities for deep water applications.

PULSE-DOPPLER NAVIGATION

Marquet, Porter and Spindel have proposed a scheme that combines the advantages of Range-Range/Long Baseline and the passive doppler techniques (Ref. 14). It is estimated that an accuracy of 1-2 meters with a resolution of 10cm could be achieved over a local area of about 50 square NM in the open ocean. This system would employ three or more bottom moored acoustic reference beacons which would operate in both a continuous wave and pulsed mode. The array calibration and the initial vehicle position information (updated at the pulse rate) would be determined from pulse arrival times and between these, the position would be determined from doppler shifts of the continuous tone signals sampled at a high rate.

The accuracy of pulse measurements is dependent on the pulse bandwidth and the signal-to-noise ratio in the receiver bandwidth which generally is considerably larger than the pulse bandwidth. Since the doppler system measures the frequency change of a continuous tone signal due to relative vehicle motion, the receiver bandwidth can be extremely narrow, thus greatly enhancing the signal-to-noise ratio. In fact, it is possible and desirable to use a tracking phase lock loop for

such an application so that relatively large doppler frequency shifts can be accomodated in a very narrow bandwidth.

REFERENCES AND BIBLIOGRAPHY

1. Holmes, R. T., "Navigation of Deep Submersibles", IREE Elect. Engineers in Ocean Technology Confer. Swansea S.A. September 1970.
2. Cambell, D. E., "Precise Acoustic Navigation and Position Keeping", Proceedings of the Institute of Navigation, November 1969.
3. Van Calcar, H., "Acoustic Position Reference Methods for Offshore Drilling Operations", Offshore Technology Conference 1969, OTC 1141.
4. Dorr, J. A., and I. B. Gereben, "Effects of Acoustic Ray Bending on Navigation of Manned Submersibles", Undersea Technology, June 1966.
5. "Vessel Positioning Control Systems", Undersea Technology, April 1967.
6. Cobb, A. D., "Acoustic Navigation....The Untapped Resource" IEEE International Conference on Engineering in the Ocean Environment, 1973.
7. Porter, R. P., R. C. Spindel, and R. J. Jaffee, "A CW Beacon System for Hydrophone Motion Determination", Contribution No. 2995 of the Woods Hole Oceanographic Institution.
8. Haehnle, R. J., "Survey Operations with Acoustic Ship Positioning System", U.S. Naval Oceanographic Office, Informal Report - IR67-69, September 1967.
9. Randsep, I. G., "Acoustic Position Reference System", U.S. Patent 3,559,161.
10. Vanderkulk, W., "Remarks on a Hydrophone Location Method", U.S. Navy Journal of Underwater Acoustics, April 1961.
11. Hart, W. E., "Calibration of an Ocean Bottom Acoustic Transponder Net", U.S. Naval Oceanographic Office, Informal Report - IR 67-24, 1967.
12. Davies, N. R., "A Theoretical Comparison of Acoustic Systems for Near-Bottom Navigation", IEEE International Conference on Engineering in the Ocean Environment, 1972.
13. Kritz, J., "Doppler Sonar Navigation for Work Submersibles" Offshore Technology Conference 1970, OTC 1266.
14. Marquet, W. M., R. P. Porter, and R. C. Spindel, " A High Resolution Pulse - Doppler Navigation System", Private Communications.
15. Heckman, D. B., and R. C. Abbott, "An Acoustic Navigation Technique", IEEE International Conference on Engineering in the Ocean Environment, 1973.
16. Turner, E. E., O. H. Jackson and B. J. Thompson, "The Raytheon Acoustic Doppler Navigation", The Institute of Navigation, Proceedings National Marine Navigational Meeting, 1966.
17. Van Ness, H. N., R. L. Mills and K. R. Stewart, "An Acoustic Ray Ship Positioning and Tracking System" The Institute of Navigation, Proceed. National Marine Marine Navigation Meeting, 1966.
18. Martin, R. L., S. F. Neidzwecki and R. J. Neilsen, "Acoustic Navigation Studies Utilizing the Snap-7E Beacon", The Institute of Navigation, Proceedings National Marine Navigation Meeting, 1966.
19. Cline, J. B., "Acoustic Navigation Surface and Subsurface" The Institute of Navigation, Proceedings National Marine Navigational Meeting, 1966.
20. Peugh, J. A., "Method for Undersea Navigation and Orientation Determination Using a Phase Compensated Line Hydrophone Array", The Institute of Navigation, Proceeding National Marine Navigational Meeting, 1966.

21. Pearlman, M. D., "An Acoustic Navigation System and Operating Techniques", The Institute of Navigation, Proceedings National Marine Navigational Meeting, 1966.
22. Lowenstein, C. D., "Computations for Transponder Navigation", The Institute of Navigation, Proceedings National Marine Navigational Meeting, 1966.
23. Lowenstein, C. D., and J. D. Mudie, "On the Optimization of Transponder Spacing for Range-Range Navigation", The Institute of Navigation, Proceedings National Marine Navigational Meeting, 1966.
24. Short, J. R., and S. P. Travis, "A Real Time Transponder Location Method", IEEE International Conference on Engineering in the Ocean Environment, 1973.
25. Young, M. C., "Improved Technique for Calibration of Transponder Arrays Used in Positioning Applications", IEEE International Conference on Engineering in the Ocean Environment, 1973.
26. McKeown, D. L., "Survey Techniques for Acoustic Positioning Arrays", Bedford Institute for Oceanography, Private Communications.
27. Marquet, W. M., D. C. Webb, and K. D. Fairhurst, "A Recoverable Deep Ocean Navigational Beacon", Marine Sciences Instrumentation, Volume 4, pp. 325-346.
28. Heckman, D. B., "Transponder/Pinger Relocation Receiver", IEEE International Conference on Engineering in the Ocean Environment, 1971.
29. Heckman, D. B., "Shipboard Acoustic Receiver", U.S. Patent No. 3,701,090.
30. Lowenstein, C. D., and J. D. Mudie, "On the Optimization of Transponder Spacing for Range-Range Navigation", Journal of Ocean Technology, Volume 1, No. 2, 1967.
31. Porter, R. P., R. C. Spindel, and R. J. Jaffee, "CW Beacon System For Hydrophone Motion Determination", JASA, Volume 53, No. 6, 1973.
32. Fang, B. T., "An Acoustic Ranging and Doppler Navigation System for Deep Submergence Vehicles", Institute of Navigation, Proceedings Marine Navigational Meeting - Second Symposium on Manned Deep Submersible Vehicles, 1969.

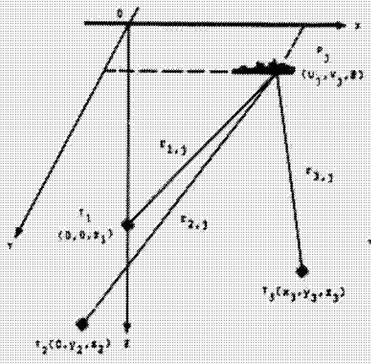

FIGURE 1. SHIP AND TRANSPONDERS

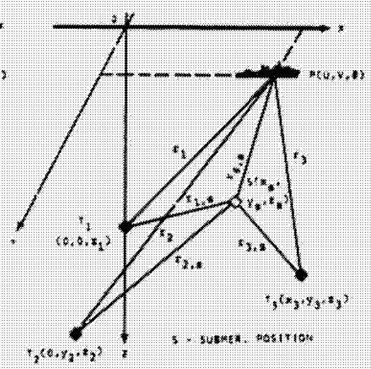

FIGURE 2. SHIP AND SUBMERGED VEHICLE

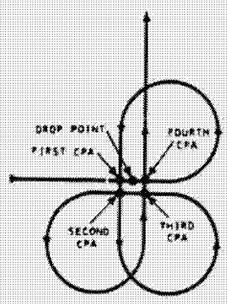

FIGURE 3. CLOVERLEAF MANEUVER

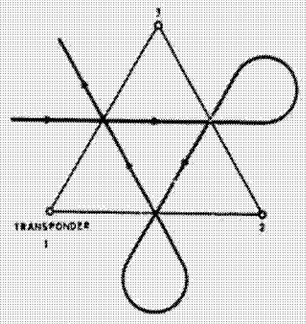

FIGURE 4. BASELINE CROSSING

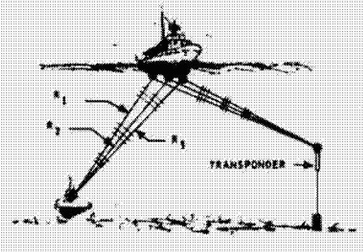

FIGURE 5. RANGE-RANGE SHORT BASE LINE

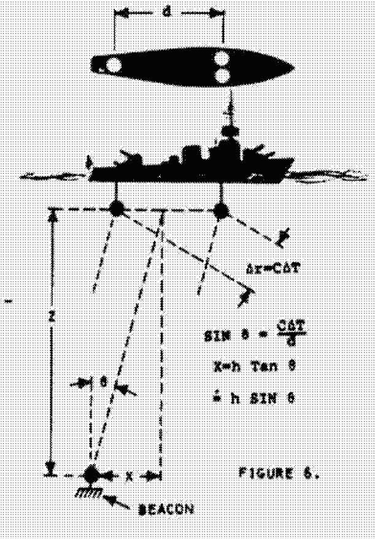

$$\text{SIN } \theta = \frac{C\Delta T}{d}$$

$$X = h \text{ Tan } \theta$$

$$\doteq h \text{ SIN } \theta$$

FIGURE 6.

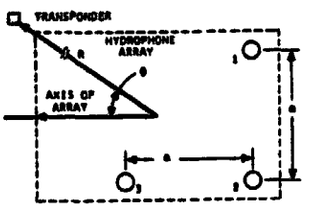

$\theta = \frac{2\pi a}{\lambda} \sin\theta$

WHERE θ IS ELECTRICAL PHASE SHIFT BETWEEN HYDROPHONE 1 AND 2.

FIGURE 7.

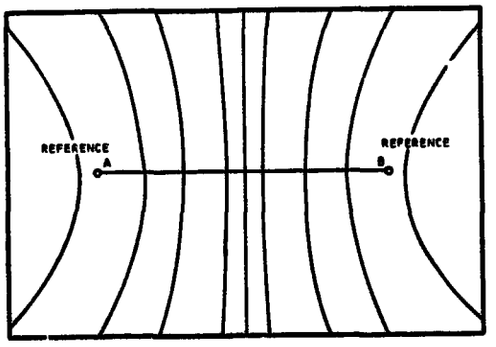

FIGURE 8. TIME CONTOURS FOR RANGE-RANGE HYPERBOLIC.

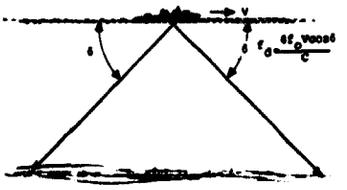

FIGURE 9. DOPPLER

AN EXPERIMENT TO DETERMINE THE REPEATABILITY OF AN ACOUSTIC RANGE-RANGE POSITIONING SYSTEM

D.L. McKeown and R.M. Eaton

Atlantic Oceanographic Laboratory
Bedford Institute of Oceanography
Dartmouth, Canada

ABSTRACT

An experiment was conducted to establish the repeatability of a long-baseline range-range acoustic positioning system. Precise-ranging radar transponders were located at geodetic stations on two islands and six acoustic transponders were moored 12 to 20 km offshore at depths of 356 to 2461 m. Sound speed profiles were measured and harmonic mean sound speeds with straight line ray path were used to convert measured acoustic travel times to slant distances from ship to acoustic transponders. The acoustic transponder array coordinates were determined by an iterative least squares fitting process, and checked by Cloverleef depth and Baseline Crossing maneuvers. Approximately 2900 simultaneous acoustic and radar fixes of ship's position were obtained. The acoustic array was translated and rotated until selected acoustic fixes of ship's position corresponded to radar fixes obtained simultaneously. Differences between acoustic and radar ship's position were computed for 2900 fixes uniformly distributed over the acoustic transponder array including fixes on or near baselines. Circular Error Probable (CEP) radii, a measure of repeatability, were 11.2, 8.5, and 7.2 m for 2, 3, and 4 acoustic transponder buoy (ATB) fixes respectively. For all fixes, irrespective of the number of ATBs interrogated, the CEP was 9.0 m.

INTRODUCTION

In situations where a high degree of accuracy and repeatability of surface ship positions is required, acoustic positioning systems utilizing ocean floor acoustic markers are commonly used. These may take the form of a short baseline system with a single acoustic source on the bottom and a hydrophone array on the ship, or a long baseline system utilizing several bottom markers and a single hydrophone on the ship being positioned. The latter accomplishes the positioning task by measuring the ranges from ship to acoustic sources, hence, it is a range-range type system. From theoretical considerations, this configuration has been shown to be the most accurate for area type surveys while the short baseline systems are more suitable for locating the vessel over a reference point (Fain, 1969).

In order to effectively utilize an array of acoustic bottom markers to position a surface vessel, it is necessary to know system repeatability. Positioning errors are the result of a number of factors: sound velocity or refraction effects, bottom marker survey errors, instrumental errors, ambient acoustic noise, and fix geometry. While several attempts have been made to assess the errors theoretically (Fain, 1969; Campbell, 1970; Davies, 1972), only Korbel (1972) has included the effects of all these error sources. Mourad et al. (1972) have utilized LORAC, an accurate surface positioning system, to determine transponder array survey errors. They conclude that,

using appropriate algorithms, acoustic bottom marker horizontal positions can be found with an error of ±7 m and depth to within ±3 m.

The purpose of the experiment described herein was to determine the repeatability of surface positions found with respect to an acoustic array on the ocean floor. Included in the overall error are the effects of all the above noted sources. The specifications for repeatability derived indicate how well a surface vessel can be positioned throughout the coverage area provided by an acoustic transponder array when survey methods and ship position algorithms described are used in conjunction with the particular hardware employed in this experiment.

RADAR TRANSPONDER POSITIONING SYSTEM

A Motorola Range Positioning System (RPS) X-band transponder was mounted on each of two geodetic stations on small islands off Cannouan Island at the north end of the Grenadines (Figure 1). These stations were 63 m and 41 m above mean sea level with a baseline length of 19 627.5 m. The radar scanner on the ship was 14 m above mean sea level. The assumption that the slant ranges corresponded to horizontal ranges in the following computations causes a maximum range error of 0.1 m. Slant ranges from ship to radar transponders varied from 12 700 m to 22 300 m over the working area. The RPS was calibrated against a Tellurometer over a distance of 19 518 m prior to the experiment. Aboard ship, RPS ranges were checked against Hydrodist during the course of the experiment.

The radar transponders were interrogated via a rotating antenna and ranges digitized by the Range Console of the Motorola Range Positioning System for recording in binary coded decimal (BCD) format. The plot of ship's movement from radar ranges was used to monitor the quality of the RPS data.

ACOUSTIC TRANSPONDER POSITIONING SYSTEM

Six Acoustic Transponder Buoys (ATBs) incorporating American Machine and Foundry (AMF) Model 322 acoustic transponders were moored at depths ranging from 356 m to 2461 m in the configuration illustrated in Figure 1. Acoustic slant ranges were measured and digitized aboard ship utilizing a hull-mounted transducer, an AMF power amplifier and coder, and an AMF four-channel Model 205 Navigation Receiver (Figure 2). The acoustic transponders were interrogated on a common frequency of 11 kHz and replied at unique frequencies of 9 to 13 kHz to permit identification. Four different reply frequencies were used and transponders with common reply frequencies were placed on opposite sides of the array. In this way the receiving system could be made to record a maximum of four acoustic slant ranges available on each interrogation. For each fix, time, acoustic slant ranges, and radar slant ranges were recorded on punched paper tape for computer analysis. Ship's head was recorded as a function of time on an analogue chart recorder and ship's speed was noted periodically. The four digital slant ranges were converted to equivalent analogue voltages and displayed on chart recorders to monitor the quality of the acoustic data.

REFRACTION EFFECTS

Sound speed as a function of depth was measured at two locations within the acoustic transponder array using an NUS Model 1000-005 velocimeter. For travel times out to the equivalent of 8000 m, true slant range computed by Snell's law was compared with that determined by assuming that rays travel in a straight line between acoustic transponder and ship at a speed equal to the harmonic mean sound speed (Maul, 1970) which is accurate only for vertical paths. The greatest discrepancy between the two for this experimental situation was 6.3 metres at a slant range of 3500 m for ATB-3. In all cases the value of computed harmonic mean sound speed was higher than the optimum value required to minimize refraction effects. In most acoustic

positioning work done at the Bedford Institute, a small on-line computer is used, making exact refraction corrections impractical. Therefore, it was decided that system repeatability would be determined assuming rays travel in straight lines at the harmonic mean sound speed.

ACOUSTIC TRANSPONDER ARRAY COORDINATES

The coordinates of each acoustic transponder position were found by a least squares fitting technique described in detail elsewhere (McKeown, 1974). Briefly, the method was as follows:

1. Slant ranges to all possible ATBs were measured simultaneously from several different surface positions;

2. ATB depths and baselines were adjusted by an iterative least squares process to minimize differences between measured and calculated slant range from each ship position to each transponder to produce the 'acoustic' array coordinates;

3. Independently, 'radar' coordinates of each ATB were found by measuring the slant range to it from several different locations whose positions were defined by the radar positioning system and adjusting transponder northing, easting and depth to minimize the calculated slant range error to each known interrogation position;

4. Finally, the 'acoustic' array coordinates were rotated and translated to best fit the 'radar' coordinates of each ATB.

In this particular experiment slant ranges to only four of the six ATBs could be measured simultaneously. To establish 'acoustic' coordinates of the six transponder acoustic array, all possible combinations of three and four ATB arrays were interrogated and baseline lengths, that is, horizontal separation between acoustic transponder pairs, and depths determined by the iterative method. Approximately 30 ship positions were used for each group of three or four ATBs. The maximum root mean square slant range error was less than 3 m for any set of three or four ATBs. The arithmetic mean of each baseline length and depth was then found to establish the 'acoustic' array coordinates. As an independent check on this technique, Peterson (1973) adjusted the raw data using a method developed to adjust Aerodist geodetic trilateration observations and produced virtually identical array coordinates. He estimates the errors in baseline lengths to be one part in 2000 and errors in the northing, easting and depth of each ATB to be less than ±3 m. Final ATB coordinates used in the computations are given in Table 1. The coordinate system origin was chosen to ensure that all ship positions were contained in the first quadrant.

Table 1

RADAR AND ACOUSTIC TRANSPONDER STATION COORDINATES

Station	Northing (m)	Easting (m)	Depth (m)
RPS-1	2028	9843	0
RPS-2	16573	23023	0
ATB-1	19170	6832	1664
ATB-2	22067	4935	2461
ATB-3	22905	8124	2293
ATB-5	17132	10396	356
ATB-6	16595	4632	1704
ATB-7	20315	9638	1345

Only ATB-3 showed a marked difference between true slant range and that determined by the harmonic mean sound speed approximation to Snell's Law. To investigate the error this introduces, the harmonic mean sound speed used for ATB-3 was reduced by 2 m/s and acoustic transponder positions recalculated. This did not alter any of the coordinates associated with ATB-3.

Between transmission and reception of acoustic signals from the transponders, the ship moved a significant distance. Although all computations were carried out after correcting measured acoustic travel times from ship to ATB for movement of the ship during the interrogation, one three-transponder array coordinate set was recomputed without correction for ship movement. There was no difference in baseline lengths and transponder depths between the two at ship speeds up to 6 knots.

All ATP depths were checked by the Cloverleaf method (McKeown, 1974). The maximum difference between mean depth by least squares analysis and by Cloverleaf was 14 m in 1345 m for ATB-7. Baseline lengths were measured using the Baseline Crossing method (McKeown, 1974). The maximum difference between the mean length by least squares analysis and by Baseline Crossing was 24 m in 3030 m for baseline ATB 1-7. An error in measuring depth by Cloverleaf will cause an error in determining baseline length by the Baseline Crossing method. Ship positions found relative to ATB-7 (using coordinates determined by iterative method) did not show any anomalous errors. When baseline crossing data was re-computed using depths by the least squares method, the discrepancy in baseline length ATB1-7 was reduced to 5 m. Therefore, it appears that ATB-7 depth by Cloverleaf is in error.

COMPARISON OF ACOUSTIC AND RPS SHIP POSITIONS

The ship was maneuvered in the vicinity of the acoustic transponder array out to the limits of a two-transponder fix on any pair of ATBs at speeds of 4 to 6 knots. A total of 9500 simultaneous acoustic and radar fixes were obtained at an interrogation period of 10 seconds. Of these fixes, 7200 or 76% were considered 'good', that is, the ship's position could be determined by both techniques. A significant portion of these fixes occurred on or near an acoustic transponder baseline where the fix error is expected to be high (Korbel, 1972) but were included in the analysis as they are representative of conditions one would meet in a practical positioning problem. A preliminary analysis of all 7200 'good' fixes was conducted but the results described below concern only the analysis of a representative 2900 'good' fixes. This is still a far larger set than was used to adjust the 'acoustic' coordinates to 'radar' coordinates as described in step 4 of the Acoustic Transponder Array Coordinates section.

All acoustic fixes were corrected for ship's movement during the interrogation using a ship's speed and course estimated from a one-minute average (6 fixes) of the radar fixes, although similar information could have been obtained by digitizing the ship's head and speed records. For a small sample of data, the actual ship's gyro heading and log were digitized by hand and used to correct the acoustic slant ranges for ship movement during a fix. No appreciable difference was noted between the two correction methods. Significantly poorer positioning repeatability occurred when correction for ship's movement was omitted. All fixes were corrected for offset between the shipboard acoustic transducer and radar scanner.

Repeatability of the acoustic positioning system was evaluated in terms of Circular Error Probable (MacTaggart, 1972) defined as follows.

Let x_i = (easting of acoustic) - (easting of radar ship position i) after transducer offset correction

y_i = (northing of acoustic) - (northing of radar ship position i) after transducer offset correction

Then mean bias errors are

$$\bar{x} = \frac{1}{N} \sum_{i}^{N} x_i \tag{1}$$

$$\bar{y} = \frac{1}{N} \sum_{i}^{N} y_i \tag{2}$$

where N = number of fixes in the set.

All future derivations will be about this mean bias, the residual errors being defined as follows:

$$x_i' = x_i - \bar{x} \tag{3}$$

$$y_i' = y_i - \bar{y} \tag{4}$$

Defining the scalar product

$$\langle a_i, b_i \rangle = \sum_{i}^{N} a_i \cdot b_i \tag{5}$$

and the covariance matrix Q'

$$Q' = \begin{pmatrix} (\sigma_x')^2 & \sigma_{xy}' \\ \sigma_{yx}' & (\sigma_y')^2 \end{pmatrix}$$

$$= \frac{1}{N} \begin{pmatrix} \langle x_i, x_i \rangle & \langle x_i, y_i \rangle \\ \langle y_i, x_i \rangle & \langle y_i, y_i \rangle \end{pmatrix} \tag{6}$$

then the eigenvalues of Q' are the semi-major and semi-minor axis of the one-sigma probability contour or standard error ellipse. The data is correlated about these axes with a correlation factor

$$\rho = \frac{\sigma_{xy}'}{\sigma_x' \cdot \sigma_y'} \tag{7}$$

To find these eignevalues, Q' is diagonalized to obtain

$$Q' = \begin{pmatrix} (\sigma_x)^2 & 0 \\ 0 & (\sigma_y)^2 \end{pmatrix} \tag{8}$$

which is accomplished by setting

$$(\sigma_x)^2 = (\sigma_x')^2 \cos^2\theta + (\sigma_y')^2 \sin^2\theta - \sigma_{xy}' \sin\theta \cos\theta \quad (9)$$

$$(\sigma_y)^2 = (\sigma_x')^2 \sin^2\theta + (\sigma_y')^2 \cos^2\theta + \sigma_{xy}' \sin\theta \cos\theta \quad (10)$$

where θ is the angle measured clockwise from north required to rotate the northing-easting coordinate system into the system whose axes, σ_x and σ_y, are the semi-axes of the one-sigma probability contour ellipse. This angle θ is given by

$$\tfrac{1}{2} \tan 2\theta = - \frac{\sigma_{xy}'}{(\sigma_x')^2 - (\sigma_y')^2} \quad (11)$$

The Circular Error Probable (CEP), a circle about the mean enclosing 50% of the measurements, has a radius:

$$\text{CEP radius} = 0.59 (\sigma_x + \sigma_y) \quad (12)$$

These computations were performed separately for acoustic fixes relative to 2, 3 and 4 acoustic transponders, these sets being completely exclusive and not subsets, and for all fixes irrespective of the number of ATBs interrogated. The results are summarized in Table 2 and one-sigma error ellipses and CEP circles plotted in Figure 3. Histograms of $\sqrt{(x_1')^2 + (y_1')^2}$ in one-metre increments are illustrated in Figure 4. These histograms were subject to minor rounding errors during the computational process. The results include fixes on or near ATB baselines.

Table 2

SHIP'S POSITION ERROR ANALYSIS SUMMARY

Type of Fix	2 ATBs	3 ATBs	4 ATBs	All Fixes
No. of fixes	759	1153	1002	2914
Mean northing (m)	2.9	1.1	1.9	1.8
Mean easting (m)	-0.8	0.4	2.4	0.8
Correlation ρ	0.112	-0.066	0.084	0.036
Error Ellipse Major Axis (m)	21.1	17.1	15.2	17.4
Error Ellipse Minor Axis (m)	18.9	14.1	12.0	15.4
CEP radius (m)	11.8	9.2	8.0	9.7

There was some scatter in the radar range readings. Furthermore, the radar system interrogated each radar transponder at the instant the scanner was directed toward it. Since this interrogation was uncorrelated with the time of the acoustic fix, there is a further random error contribution. The overall RPS repeatability under these circumstances was about 3.6 m (50% probability). Therefore, the CEP radii for 2, 3, 4, and all ATB

fixes after elimination of radar fix scatter became 11.2 m, 8.5 m, 7.2 m, and 9.0 m respectively.

The improvement in repeatability achieved by increasing the number of ATBs successfully interrogated is readily apparent. Computations indicated that there was no correlation between the acoustic transponders interrogated and the magnitude of the discrepancy between acoustic and radar positions of the ship.

In the above computations, it was assumed that acoustic rays travelled in straight lines at an appropriate constant speed. To test the validity of this assumption the integrated ship's tracks over a period of 11 hours as determined acoustically and by radar were compared for 2, 3, and 4 acoustic transponder fixes. The ratios of acoustic to radar distances were 1.0095, 1.0032 and 1.0008 respectively. The acoustic fixes exhibited a poorer repeatability than the radar fixes. By integrating ship's track between successive fixes, it was to be expected that the scatter in acoustic ship's position would lead to a greater distance travelled than that determined by radar fixes. As more acoustic transponders were successfully interrogated scatter was decreased. As shown above, the integrated ship's track for four ATB fixes was virtually the same as the equivalent ship's track from radar fixes. This indicates that there is no scale effect introduced by applying the approximations to a true refraction correction of acoustic slant ranges.

CONCLUSION

If the following acoustic positioning procedure is adopted, repeatability CEP radii of 2, 3, and 4 ATB fixes will be 11.2, 8.5, and 7.2 m respectively, and for any successful acoustic fix irrespective of the number of acoustic transponders interrogated CEP will be 9.0 m:

1. Convert measured travel times to slant range by assuming an appropriate harmonic mean sound speed computed from a measured sound speed profile and straight line ray path between ship and acoustic transponder;

2. Establish transponder depths and baseline lengths by an iterative least squares fitting process;

3. Correct measured slant ranges for ship movement during the interrogation.

This repeatability applies to the entire coverage area irrespective of proximity to ATBs or ATB baselines for acoustic transponders moored at depths from 356 to 2461 m.

REFERENCES

Campbell, D., "Precise acoustic navigation and position keeping", Navigation, J. of Inst. of Navigation, 17, 2, pp. 124 (1970).

Davies, N.R., "A theoretical comparison of acoustic systems for near-bottom navigation", IEEE 1972 Conference Proceedings, Engineering in the Ocean Environment, Newport, Rhode Island, Sept. 13-15, 1972, pp. 468.

Fain, G., "Error analysis of several bottom referenced navigation systems for small submersibles", Proc. 5th Annual Marine Technology Society Conference, Washington, D.C., June 15-18, 1969.

Korbel, H., "Transponder-field optimization: error in vessel position estimates based on distance measurements", Institute of Navigation Conference, October 1972, pp. 113

Naul, G.A., "Precise echo sounding in deep water", Int. Hyd. Rev., 47, 2, p. 93 (1970).

MacTaggart, D., "Design and performance of CMA-719 computerized airborne Omega receiver", Navigation, J. of Inst. of Navigation, 19, 2, p. 159 (1972).

McKeown, D.L., "Survey Techniques for acoustic positioning arrays", submitted to Navigation, J. of Inst. of Navigation, 1974.

Mourad, A.G., D.M. Fubara, A.T. Hopper, and G.T. Ruck, "Geodetic location of acoustic ocean-bottom transponders from surface positions", Trans. AGU, 53, 6, p. 644 (1972).

Peterson, A., Geodetic Survey of Canada, private communication (1973).

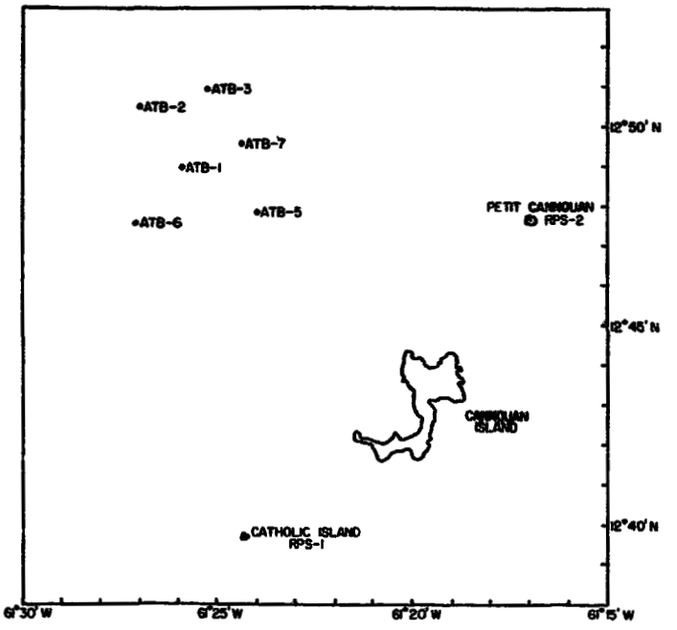

Figure 1: Radar transponder stations (RPS) and acoustic transponder buoy (ATB) locations off Cannouan Island, West Indies.

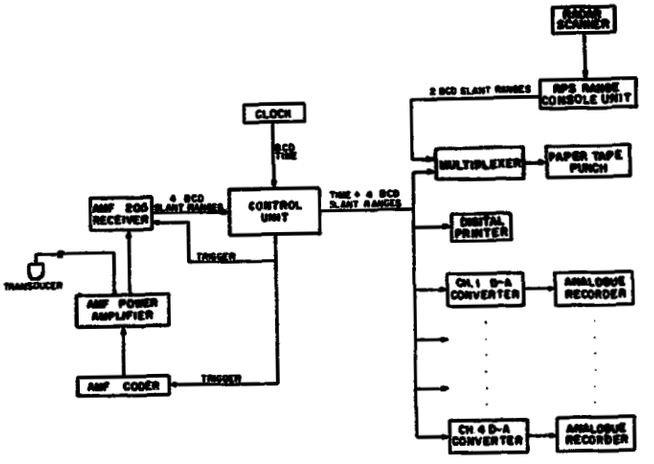

Figure 2: Block diagram of shipboard acoustic and radar data acquisition system.

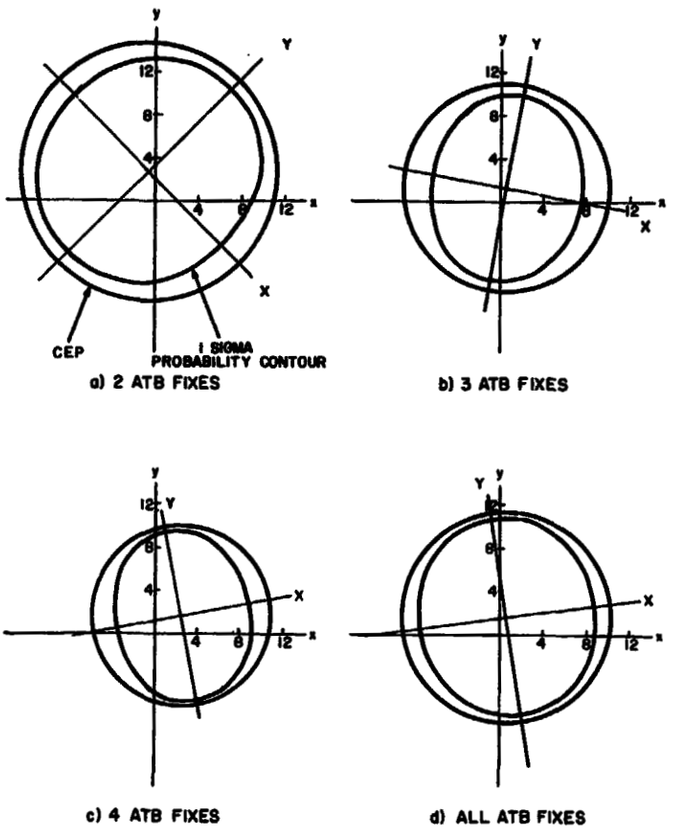

Figure 3: Circular Error Probable (CEP) and One Sigma Probability Contours for two, three, four ATB 'good' fixes and all 2900 'good' ship's positions.

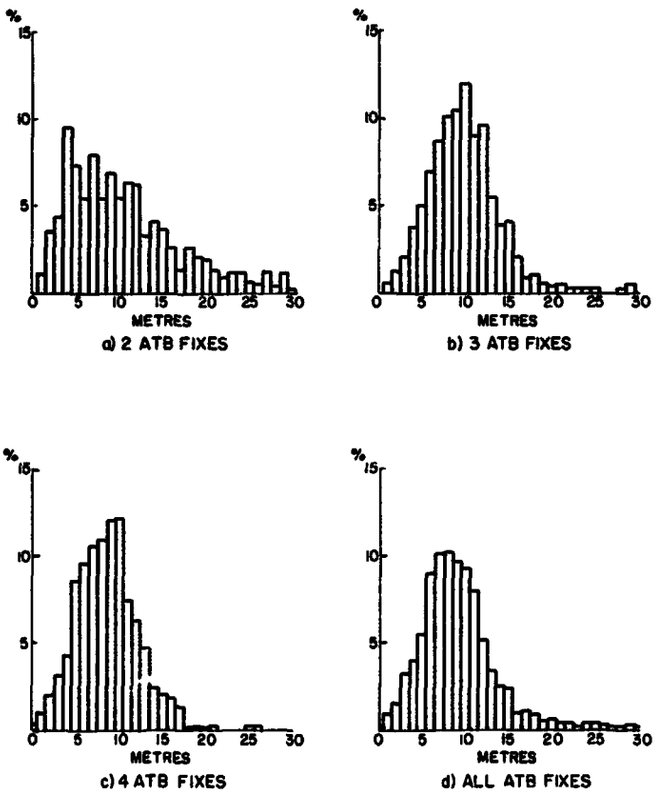

Figure 4: Histograms of $\sqrt{(x_i')^2 + (y_i')^2}$ in one-metre increments as percent of total fixes in each category for two, three, four ATB 'good' fixes and all 2900 'good' ship positions.

MARINE AND COASTAL GEODESY AND SEA LEVEL RESEARCHES

Eugenie Lisitsin
Helsinki, Finland

Abstract: During the First Marine Geodesy Symposium in 1967 a paper was presented by the author on a world-wide mean sea level and its relationship to marine geodesy. This paper gave some numerical information about the mean sea level in separate oceans. As a rule, these data coincided well with the results for geodetic precise levelling in all cases where these results were available. There are, however, also cases where the conformity between the results achieved by the two different methods are rather inconsistent.

The first of these cases refers to the Atlantic coast of the United States. According to precise levelling the mean sea level along this coast increases continuously from south to north. This increase in mean sea level is in disagreement with the requirement of the observed flow of the Gulf Stream. Also along the Pacific coast of the United States there is a lack of conformity between the geodetic and the oceanographic results concerning the coastal slope of the water surface.

A further instance of non-conformity between data for precise levelling and results based on sea level records concerns the rate of the vertical movements of the earth's crust in coastal areas in Denmark.

COLLABORATION BETWEEN MARINE GEODESY AND SEA LEVEL STUDIES.

The close relationship between geodetic measurements and some aspects of oceanographic and sea level researches was noted years ago. The two branches of geo-sciences effectively assist one another in numerous cases where, left alone, they might be more or less handicapped. Especially in connection with problems where geodetic precise levelling confirms the results achieved by sea level studies and vice versa the coincidence may be significant for the development of the two sciences. It is always a pleasure and an encouragement for a sea level student to note the cases where the results are at least in approximate conformity with the data achieved by geodetic measurements. In this connection it may be appropriate to mention an interesting example illustrating what has been said above. According to so-called dynamic computations based on a considerable number of oceanographic data the Pacific Ocean, as a whole, stands 72 cm higher than the Atlantic Ocean. The results of a first order levelling performed in the United States by Braaten and McCombs show that the difference in mean sea level heights is between Neah Bay (Washington) and Portland

(Maine) 71 cm, between San Francisco (California) and Atlantic City (New Jersey) 60 cm, and, finally, between San Diego (California) and Fernandina (Florida) 65 cm, thus resulting in an average value of 65 cm. The deviation of 7 cm between the oceanographic and the geodetic results is easily accounted for, if we take into consideration the fact that the average sea level is generally higher in the western parts of the oceans than in their eastern parts, and the geodetic data for the Atlantic coast thus give values which are somewhat too high, for the Pacific coast, on the other hand, the values are too low, when compared with the mean conditions in the two oceans.

In this connection it may be of interest to refer shortly to a detail which may become significant for the continued development of the problem of determining the mean sea level in the oceans. Braaten and McCombs have chosen Portland as the point of comparison for the mean sea level along the entire coasts of the United States. Fully unaware of this way of proceeding the author of this paper has suggested that Portland could be chosen as starting point for all determinations of mean sea level in the oceans and seas, since the average sea level at this locality seems to correspond fairly well to the mean sea level in the whole water covered area. Nevertheless, it must be pointed out in this connection that the above suggestion is a preliminary one, since all the determinations of mean sea level are so far only approximate, and may change in the future when more accurate data are available.

It has already been mentioned above that the correspondence between geodetic and oceanographic results is always highly encouraging. However, the concerned scientists are also frequenly confronted with cases, where the conformity between the results achieved on the basis of geodetic measurements, on the one hand, and those reached with the help of oceanographic and sea level data, on the other hand, is rather inconsistent.

THE ATLANTIC COAST OF THE UNITED STATES.

The first of these embarrassing cases concerns the Atlantic coat of the United States. According to precise levelling performed by Braaten and McCombs and already referred to above the mean sea level along this coast increases continuously from the south to the north. The total rise from Key West (Florida) to Portland has been determined at 58 cm. In this connection it may be emphasized that the increase in mean sea level has by some oceanographers been ascribed to the withdrawal of the Gulf Stream from the immediate vicinity of the coast and the occurrence of a counter-current between the Gulf Stream and the coast. This counter-current is more powerful in the north and thus the effect of Coriolis parameter is also more pronounced, resulting in higher values of mean sea level. On the other hand, interesting results on mean sea level and the slope of the water surface have been given by Sturges, who in his study paid special attention to the topography of the sea surface in the Gulf Stream area between Bermuda and the east coast of the United States. The problem has been approached by Sturges in two different ways. In one case, ship's drift observations were utilized for the determination, considering the effect of the wind. The difference in sea level was found to be 110 cm. In the other case, the difference in sea level heights across the Gulf Stream was computed by Sturges from oceanographic data and estimates of deep water flow. After application of some corrections this method gave 100 cm relative to the 2000 decibar surface. The agreement between the two results is fairly satisfactory. Starting from these data Sturges has discussed the slope of the water surface along the Atlantic coast of the United States and has been able to establish that the increase in sea level from south to north achieved by precise levelling is in disagreement with the

requirements of the observed flow of the Gulf Stream. Thus the problem has not been solved so far and requires additional studies.

THE PACIFIC COAST OF THE UNITED STATES.

Concerning the Pacific coast of the United States the problem of the character of the slope of the water surface is still unsolved, too. Precise levelling results in an increase of mean sea level from south to north, amounting from San Diego to Neah Bay to 46 cm. For the tide gauge stations which are situated to the north of San Francisco this increase is very pronounced. However, Sverdrup has already pointed out that the result "is based on records of sea level at the south of the Columbia river (Fort Stewens) where the outflow of fresh water may account for the higher sea level, and further to the north, on records of sea level at great distances from the open coast. The rise towards the north is therefore not well established". In addition, significant results on mean sea level and the slope of the water surface in the area off the Pacific coast of the United States have been given by Sturges. Sturges' computations, which are based on oceanographic data relative to the 1000 decibar surface, have suggested that the marked increase in mean sea level from San Diego to Neah Bay is non-existent. To the contrary, mean sea level has been found by Sturges to be at Neah Bay 9 cm lower than at San Diego. Sturges has, moreover, emphasized that according to a careful examination the 1000 decibar surface is sufficiently level as reference surface along the coast. It may also be pointed out that the departure of 9 cm in mean sea level height determined on the basis of dynamic computations is consistent with the effect of the changes in latitude as the Californian current flows southward. The decrease in mean sea level determined by Sturges is also in better agreement with the general picture of the distribution of mean sea level heights in the eastern parts of the Pacific Ocean.

The discrepancy between the geodetic och the oceanographic results must probably be mainly sought in the deviating approaches to the problem of the determination of the slope of the water surface along the coasts. Geodesists are principally landbound. They compare their results with bench marks on land and the mean sea level at a specific locality is of decisive significance. For oceanographers the water covered area is, self-evidently, the most important. They approach the coast from this direction. Being keen to reach more general results, they are less interested in the conditions characteristic of special places which may be effected by markedly local meteorological or hydrographic factors. Nevertheless, the question of the causes for the deviations should never be disregarded and every effort should be made to explain the occurrence of these deviations.

VERTICAL MOUVEMENTS OF THE EARTH'S CRUST.

A problem in the solving of which geodesists and sea level researcn workers have already been collaborating for a prolonged time is the vertical movement of the earth's crust along the coasts. Owing to the character of the phenomenon this is a problem which more closely concerns the geodesists, but it cannot be denied that the most adequate way in approaching and solving this problem is by means of sea level data. There are numerous coastal areas for which the correspondence between the geodetically determined rates for land uplift and the results based on sea level records agree satisfactorily and within the limits of the mean deviations determined for the particular

rates. One of these regions is the Finnish coastal area. Unfortunately, within the aquatory of the Baltic Sea and its approaches to the North Sea, the Danish Straits, there is also an area where the agreement between the data achieved in two different ways is not consistent. To be sure, for the Danish stations Hornbaek and Korsör the coincidence between the rates determined by means of precise levelling and those computed with the help of sea level records by Rossiter was fairly satisfactory. On the other hand, the results of Rossiter for Gedser and Copenhagen did not agree with the geodetic values, at least not as well as might be expected from the estimate of accuracy. According to Rossiter there was at Gedser a land subsidence amounting to 1.04 cm per year, while the geodetic levelling resulted in a land subsidence of 0.23 cm per year only. For Copenhagen the rates were a subsidence of 0.23 cm per year according to Rossiter and a land uplift of 0.44 cm per year according to precise levelling. Since the rates are numerically rather weak, the discrepancy may not seem to be particularly significant, but it must be borne in mind that on the long run the deviations tend to become pronounced. Since the effect of the meteorological contribution has been eliminated by Rossiter, the discrepancy should be sought in oceanographic factors, mainly in the disturbing influence of currents. Therefore, Borre has made an attempt to investigate the records of the tide gauges more closely in order to get an idea of the reliability of these data for the purpose in question. Since a strong correlation seems to exist between the surface current at the lightship Drogden and the differences of mean sea level at the two stations, this factor was utilized for the determination of the sea level at these stations in cases where there was no surface current at Drogden. Moreover, a correction was applied in order to eliminate the effect of the principal meterological factors, and the data thus corrected were used for the determination of the vertical movement of the earth's crust. Unfortunately, this way of proceeding could not provide a final answer to the question. In this connection it must always be kept in mind that the configuration of the Danish Straits is rather complex, and it is therefore difficult to construct a model which would correspond to the natural conditions. In addition, the effect of salinity should be considered before drawing more general conclusions. Since the problem of the water transport through the transition area around Denmark is at the present time highly significant, mainly in connection with the studies of the water renewal in the Baltic Sea basin, it may be anticipated that these researches will also contribute to the solving of the question of the disagreement of the rates characteristic of the vertical movements of the earth's crust determined by two different methods. Preliminary studies have already indicated that a close relationship exists between the configuration of the water surface in the transition area around Denmark and the variations of the mean sea level in the Baltic Sea during periods covering a month.

With these few instances above I have tried to give a conception of the present situation arising from the collaboration between geodesists and oceanographers.

REFERENCES

Borre, K., 1970. The influence of current and meteorological forces on the mean sea level in the Danish Straits. Geod. Inst. Medd. Kbh., 47. 63 pp.

Braaten, H.P. and McCombs, C.E., 1963. Mean Sea Level Variations as Indicated by a 1963 Adjustment of First-Order Leveling in the United States. Coast and Geodetic Survey, Washington, D.C. 22 pp.

Lisitzin, Eugenie, 1965. The mean sea level of the world ocean. Comment. Phys.-Math. Helsingf., 30. 35 pp.

Lisitzin, Eugenie, 1967. A World Mean Sea Level and Marine Geodesy. Proc. First Marine Geodesy Symposium. Washington, D.C. 71-73.

Rossiter, J.R., 1967. An analysis of annual sea level variations in European waters. Geophys. J. R. Astr. Soc., 12. 259-299.

Sturges, W., 1967. Slope of sea levels along the Pacific coast of the United States. J. Geophys. Res., 72. 3627-3637.

Sturges, W., 1968. Sea surface topography near the Gulf Stream. Deep-Sea Res., 15. 149-156.

Sverdrup, H.U., Johnson, M.W. and Fleming, R.H., 1942. The Oceans, their Physics, Chemistry and General Biology. Prentice Hall, New York. 400-575.

PLATE TECTONICS, SEA FLOOR SPREADING AND CONTINENTAL DRIFT

Robert S. Dietz
National Oceanic and Atmospheric Administration
Atlantic Oceanographic and Meteorological Laboratories
Miami, Florida 33149

ABSTRACT

Plate tectonics, based upon sea floor spreading, transform faulting and lithosphere subduction, provides a revolutionary new model for geotectonics. Although the mechanism of plate motion remains obscure, the general concept seems now firmly established. It is of prime importance to marine geodesy, especially as the plate boundaries virtually all are located beneath the deep ocean. It also opens a new approach to understanding the geoid. We can anticipate that future precise triangulation in the future will quantify relative plate motions.

Modern rates of sea floor spreading suggest that an area equivalent to the modern ocean floors can be generated in 150×10^6 years, or since mid-Jurassic. Thus the ocean floor is young, and ocean basins expand and collapse, while the continents remain as the earth's old features.

This paper reviews plate tectonics, especially as applie. to continental drift,and traces the displacement of the continental platforms over the past 200 million years. Some emphasis is placed on "hot spots" as these mantle plumes may well provide a key to the absolute drift of continents with respect to the earth spin axis. Attention is also given to the reconstruction of Pangaea based upon the jigsaw fit of modern continents around the Atlantic and Pacific oceans.

Some aspects of plate tectonics which are of specific interest to marine geodesy are the following. (1) Are the plates truly rigid caps on the globe or are they somewhat plastic? Roper has recently suggested that the plates are sufficiently plastic to permit a closing of the Atlantic Ocean in which South America is congruent with the Gulf of Mexico while Africa fits against eastern North America. Such a fit is prohibited under rigid plate tectonics followed in the reconstruction by Bullard. (2) Are the low-harmonic undulations in the geoid due to convection cells (Runcorn) or to mantle plumes (Morgan)? (3) Is the asthenosphere irregular so that many aspects of vertical tectonics are the consequence of the lithosphere riding ove: a bumpy asthenosphere (Menard)? (4) Are the mantle plumes fixed, approximately so, or drifting? If drifting, is this due to the drift of the deep mantle? Is the deep mantle or any other realm of the earth fixed relative to the earth's spin axis? (5) What makes the plates go? Are they being pushed, pulled down, gravitationally sliding, carried by classical convection cells, some special type of convection pattern, or by asthenosphere flows

associated with plumes. (6) A recent claim by Bird et al. suggests that josephenite xenoliths in ultrabasic rocks in Oregon may be from the core-mantle interface, having been carried to the surface by plumes. Is this possible? Is there a relationship between velocity of sea floor spreading, volume of the ocean basin and sea level (Rona)? These are but a sampling of the many questions which remain to be resolved.

MAPPING PLATE BOUNDARIES WITH REFERENCE TO MEAN GRAVITY ANOMALIES

LUMAN E. WILCOX
RONALD S. BLOUSE
Defense Mapping Agency Aerospace Center
Research Department
DOD Gravity Services Division
Gravity Correlations Branch

ABSTRACT

A global chart showing plate boundaries as defined by the $1^{\circ} \times 1^{\circ}$ mean free air gravity anomaly holdings of the DOD Gravity Library has been compiled. The chart confirms and, in some cases, redefines the plate boundaries as now delineated from seismic and magnetic evidence. The gravity anomaly values have patterns suggesting that there are fossil or inactive subduction zones bounding the south side of the Caribbean plate, and that there are major discontinuities in the subduction zones of the Western Pacific. In this paper, a fairly detailed surface gravity anomaly field is used for the first time on a global scale as evidence for the theory of global tectonics.

INTRODUCTION

The well established theory of global tectonics depicts a dynamic earth in which a number of lithospheric plates are being transported over the earth's surface. The plate motion may or may not be systematic; however, the general magnitude and direction of motions are known. The mobile lithospheric plates and their boundaries probably are passive surficial expressions of an active viscous flow system in the aesthenosphere.

Plate boundaries are formed by zones of accretion, subduction, and faulting which correspond, respectively, to the rift system, trenches, and transform/transcurrent fault zones. These boundaries have been identified and mapped as linear zones of intense seismic activity (for example, Isacos and Oliver, 1968). Magnetic lineations also have been used to identify and delineate zones of accretion (for example, Vine, 1968, Pitman et al., 1968, and LePichon et al., 1968). The

The views expressed herein are those of the authors and do not necessarily reflect the views of the Department of Defense.

plate boundaries as determined by seismic and magnetic data are shown on Plate I.

A worldwide analysis of 1^{o} x 1^{o} mean free air gravity anomalies is used in this paper to define and delineate active and, in some cases, fossil plate boundaries. This work is intended to complement the seismic and magnetic approaches to plate boundary mapping.

DATA AND METHODS

Gravity input to this study includes the $1^{o}x1^{o}$ mean free air gravity anomalies published by the Defense Mapping Agency Aerospace Center (DMAAC, 1973). The mean anomaly values were predicted using conventional, statistical, and gravity correlation methods together with the extensive gravity data holdings of the DOD Gravity Library.

The 1^{o} x 1^{o} mean anomaly values were plotted and isoanomaly contours were drawn by automatic equipment. The contoured mean anomaly field was analyzed to identify the positive and negative gravity anomaly patterns indicative of plate boundaries. The trace of these patterns was plotted by automatic equipment on a base map of the world, Plate II, and delineates the gravimetrically defined plate boundaries.

In all, approximately 53,000 miles of plate boundaries have been so identified.

GRAVIMETRIC DEFINITION OF PLATE BOUNDARIES

1. Trenches (Subduction Zones): A narrow belt of intensely negative gravity anomalies follows and marks the location of the active trenches as shown on Plate II. The negative belt typically is flanked on both sides by belts of positive gravity anomalies. The stronger of the positive belts, located on the landward side of the trench, is generated by the relatively dense oceanic lithospheric slab being downthrusted under a less dense continental lithospheric plate (Kaula, 1972b). The negative gravity anomaly belt is associated with the low velocity (low density) region just above the down thrusted plate (Jacoby, 1972). The cause for the weaker seaward belt of positive gravity anomalies is less clear. The two belts of positive anomalies which parallel the negative expression dominate the regional gravity anomaly pattern and, hence, most global gravity representations show broad gravity highs in the vicinity of the active subduction zones (Talwani and Watts, 1972).

The narrow negative gravity anomaly belts are used in this study to delineate the subduction zone plate boundaries. The degree of intensity of the negative belts is subdivided into intensely negative, moderately negative and slightly negative to give a gravimetric measure of the level of activity in the subduction zone.

A currently active subduction zone must be characterized by both seismic activity and a negative gravity belt. A fossil (or, at least, dormant) subduction zone should be characterized by a negative gravity anomaly belt with little or no seismic activity. Activity in such zones ceased not more than 3×10^{3} to 10^{4} years ago--this time span is the decay time of the earth to Pleistocene glaciation. Major features in the gravitational field do not persist for longer periods unless they are dynamically supported (Kaula, 1972a). A belt of seismic

activity not having a corresponding gravity low suggests a very recent initiation of subduction activity.

2. Zones of Accretion (rift system): The 1° x 1° mean free air anomalies in the eastern Pacific Ocean define a regional decrease from ±5 to ±10 milligals on the rise crest down to about -15 milligals for a crustal age of about 25 million years (Woollard and Daugherty, 1973: Woollard, 1973). A similar regional positive has been noted over the mid-ocean ridge in the North Atlantic Ocean by the authors. Since large positive anomaly areas are located over most of the active ocean rises on global gravity representations (Kaula, 1972b), it is likely that all active zones of accretion are marked by a positive regional expression in the 1° x 1° mean gravity field. In some cases, such as the Red Sea rift, large local variations in the gravity field mask the regional field such that the normal regional positive expression is not identifiable. The regional positive which marks the ridges is due to a combination of isostatic effects and regional changes in crust and upper mantle structure (Woollard and Daugherty, 1973; Woollard, 1973). The regionally positive gravity anomaly belts are used in this study to delineate the accretion plate boundaries in areas where sufficient gravity data is available to support the analyses.

3. Transform/Transcurrent Faults: The gravitational expression of transform faults is complex. Abrupt changes in the regional gravity level sometimes occur when such faults are crossed. Local effects due to topographic and structural changes are superimposed on and sometimes mask the regional changes. Although no fault boundaries are gravimetrically identified in this study, there is a good possibility that at least some transform fault boundaries can be delineated using gravimetric analysis.

DISCUSSION OF GRAVITY DEFINED PLATE BOUNDARIES

The subduction zones are the most easily recognized type of gravity-defined plate boundary. The greatest concentration of such zones is found in the Pacific Ocean; these are discussed in counter-clockwise order beginning with the Peru-Chile trench, Plate II.

The southernmost portion of the Peru-Chile trench, extending about 5° northward from its junction with the Chile rise, is marked by a linear belt of slightly negative 1° x 1° mean free air anomalies (MFAA). The central portion of this trench is characterized by an intensely negative anomaly belt. Between 38°S and 5°N, the mean anomalies fluctuate in value between slightly and intensely negative along the trench. The northern terminus of the negative anomaly belt is the small Panama plate, 5°N, 78°W.

A slightly negative gravity anomaly belt, such as that which occurs at the southern end of the Peru-Chile trench, typically is found at the extremeties of most of the subduction zones in the Pacific Ocean. These belts of slightly negative MFAA values may signify a recent lengthening or shortening of the subduction zones. The existence of some seismic events in the region suggests that the Peru-Chile trench may be lengthening toward the south.

The intensely negative gravity anomaly belt along the central portion of the Peru-Chile trench corresponds to a belt of intense seismic activity and indicates a region of maximum plate subduction.

The lack of a negative gravity belt between Buenaventura, Colombia, and the Costa Rica-Nicaragua Border corresponds to a similar break in seismic activity and shows that the Mid America and Peru-Chile trench systems are not continuous.

Due to the proximity of the North American land mass, the MFAA do not define the Pacific plate boundary north of the Mid America trench.

The Aleutian trench is marked with the characteristic gravity anomaly patterns. An intensely negative (-161 milligal maximum) MFAA belt follows the central portion of the trench while the MFAA belts at either end of the trench are only slightly negative. Whereas the trace of seismic activity places the eastern end of the trench under the Alaskan land mass near Anchorage, the trace of the gravity lows continues 10° further to the east terminating under the Gulf of Alaska near 58°N, 145°W.

Although often referred to as a series of individual trenches, the Kuril, Izu-Bonin, and Mariana trenches are defined gravimetrically to be one continuous system which is here called, collectively, the West Pacific subduction zone. The MFAA expression of this subduction zone begins on the north with a slightly negative anomaly belt near Kamchatka at 55°N and 164°E and becomes intensely negative at 45°N, 155°E. This gravimetric expression continues to 12°N, 141°E where the belt abruptly ends. The maximum negative MFAA values in the West Pacific subduction zone occur in the Izu-Bonin and Mariana portions of the subduction system with values of -200 milligals and -225 milligals at 35°N, 142°E and 12°N, 142°E respectively.

The Philippines plate generally is considered to be surrounded by trenches with the Izu-Bonin, Mariana, Yap, and Palau trenches on the east and the Ryukyu and Mindanao trenches in the west (Isaacs and Oliver, 1968). However, only three of these trenches have a distinct gravity anomaly expression. The Izu-Bonin-Mariana and Mindanao trenches are marked by belts of intensely negative MFAA--up to -255 milligals in magnitude. The negative belt over the Mindanao trench connects with the negative belt over the Java trench forming one continuous feature here called the Philippine-Java subduction system. The Ryukyu trench is marked by a belt of slightly to moderately negative MFAA--the maximum value being -57 milligals. The Ryukyu trench is not connected gravimetrically either to the Mariana trench on the north or the Mindanao trench on the south. Although a short slightly negative belt of MFAA occurs over the Yap and Palau trenches, these features are considered to be currently inactive.

The authors' interpretation of the peculiar Philippine Sea area relations is that a northwesterly moving Pacific plate is being subducted in the trench regions marked by intensely negative MFAA. A line joining the southern terminus of the West Pacific subduction zone with the northern terminus of the Philippine-Java subduction zone has the bearing 286° (N74°W). This bearing is interpreted to indicate the direction of movement of the Pacific plate adjacent to the southern Mariana trench and also of the Philippine plate adjacent to the Mindanao trench.

Tectonic movement marginal to Luzon includes underthrusting along the west coast of the island. A mean azimuth of underthrusting of 283° has been inferred from analyses of focal mechanisms in the West Mindanao trench (Allen, 1962). Thus, the direction of plate motion in the area is confirmed by both seismic and gravitational evidence.

With the sole exception of the Ryukyu-Mindanao trench complex, the typical arcuate expression of trench systems is always convex toward the plate being subducted. The exceptional and, probably, unstable situation along the western boundary of the Philippine plate has been corrected partially by an oceanward migration of the subduction zone and by the creation of the convex Izu-Bonin-Mariana trench system (Mitchell and Bell, 1973). The Izu-Bonin trench is considered to be in a nascent stage of development (Fitch, 1972).

Cessation of subduction in Ryukyu trench is suspected because of the lack of an intensely negative gravity anomaly belt over the system and the deposition of a thick sedimentary sequence (Mitchell and Bell, 1973). The numerous epicenters in the region which suggest that the trench is still active may be caused by the formerly subducted plate seeking isostatic equilibrium.

It can be hypothesized that subduction activity gradually will become more intense along the Palau and Yap trenches thus creating a continuous convex subduction zone along the entire western Pacific plate.

The entire spectrum of MFAA values occurs along the plate boundaries from New Guinea to New Zealand. A series of discontinuous but intensely negative belts of MFAA extend through New Guinea and into the Bismark Archipelago. The existence of a slight isostatic imbalance around the Fiji plate is evident but the discontinuous slightly negative MFAA only provide a location for segments of the plate boundary. The Tonga-Kermadec trench is readily distinguishable by the characteristic pattern of intensely negative anomalies from Samoa to North Island, New Zealand.

The uninterrupted continuation of the intensely negative Philippine-Java subduction zone from the Philippines to the Java trench begins near the junction of the Asian, India, and Philippine-Pacific plates, at approximately 3°N, 128°E. However because of the uncertain location of the Philippine-Pacific plate boundary in this region, a juncture of the plates could also be placed north of Halmahero Island at approximately 3°S, 129°E.

If the juncture is chosen at 3°N, 128°E, the plate boundary between the Asia and Australia would pass through the eastern Molucca Sea to near the north shore of Buru Island. From Buru Island the boundary turns eastward and passes north of Ceram Island and around the Banda Sea.

The MFAA in the area fluctuate around -100 milligals with a maximum negative of -150 milligals occuring over the Weber Deep at 5°S, 132°E. The intensely negative MFAA arc over the Weber Deep is a four degree wide band, but narrows to one or two degrees as the Java trench is encountered. The intensity decreases from -147 milligals to an average of -75 milligals southwest of Sumba Island, Indonesia and, except for three intensely negative areas at 8°S, 111°E (-114 milligals), 9°S, 108°E (-121 miligals), and 6°S, 103°E (-133 milligals), a gradual decrease in MFAA values occurs into the western trench terminus in the Andaman Basin.

Except for the trace of slightly negative MFAA midway into the Andaman Basin and the location of the area of subduction around the Banda and the Malucca seas the MFAA complement the seismic and bathymetric plate boundary location along the entire length of the Java trench.

Continental zones of compression suggesting recent collision of plates is indicated by the belt of intensely negative MFAA along the India-China border and the belts of slightly to moderately negative MFAA through southern Iran and across the southern boundary of USSR from Afghanistan to the Black Sea.

Another zone of compression in the eastern Mediterranean Sea is confirmed by the negative gravimetric expression.

The mid-ocean ridge in the North Atlantic is marked by regionally positive 1° x 1° mean free air anomaly. This slightly positive MFAA expression is best seen using mean anomaly profiles across the strike of the ridge. There is not sufficient gravity data to define the zones of expansion in other areas.

The negative expression of the Caribbean plate's northwest boundary begins over the Caymen trough. Although individual free air anomalies to -230 milligals (Bowin, 1968) were recorded over the Orient Deep, the largest MFAA over the same area is -124 milligals, 20°N, 57°W. The western end of the trough becomes rapidly less negative with one MFAA being an unexplainable +25 milligals. The MFAA in the eastern end of the Caymen trough also becomes less negative as the bathymetric high between Cuba and Hispanola is approached but remains moderately negative. This moderately negative MFAA of -48 milligals between the Caymen and Puerto Rico trench supports the contention of Bowin (1968) that the Caymen trough structure is not a westward continuation of the structure producing the Puerto Rico trench negative free air anomaly belt.

A negative MFAA (-119 milligals) at 27°N, 77°W, marks the start of a continuous series of intensely negative mean free air anomalies that pass seaward of the north Hispanola coast, through the Puerto Rico trough and into the Lesser Antilles trough where the intensity decreases from -168 milligals to -40 milligals at 14°N, 60°W. The maximum MFAA over this northern boundary of the Caribbean plate is -268 milligals in the Puerto Rico trench, but averages -180 milligals over the length of the boundary.

Moderately to intensely negative MFAA pass between the Tobago and Barbados troughs (-90) milligals and then through Trinidad and the Paria Peninsula, Venezuela. The negative MFAA expression continues along the 4000 metric isobath of Venezuela, Colombia, and Panama. A gradation from intensely negative (-157 milligals) just north of Caracas, to only slightly negative (-10 milligals) at the western terminus of the negative trend, 83°W, 10°N, with only one major reversal in gradient at 12°N, 74°W (-146 milligals) occurs.

Insufficient gravity data is available to define the plate boundaries in the vicinity of the Scotia Arc and South Sandwich trench.

CONCLUSION

The feasibility of using 1° x 1° mean free-air anomalies to define and delineate plate boundaries has been established. This method is presently limited to zones of accretion and subduction; however, study of MFAA over fault boundaries is in progress. In most areas the MFAA complement existing seismic and magnetic data, but, as stated, variations in boundary location and interpretation do occur.

With the continuing collection of gravity data by the Defense Mapping Agency Aerospace Center, the gravimetric delineation and interpretation of plate boundaries on a worldwide basis will be continued.

REFERENCES

1. Allen, C. R., "Circum-Pacific Faulting in the Philippines-Taiwan Region," Journal of Geophysical Research, Vol. 67, pp. 4795-4812, 1962.

2. Bowin, C. O., "Geophysical Study of the Caymen Trough," Journal of Geophysical Research, Vol. 73, No. 16, pp. 5159-5173, 1968.

3. Defense Mapping Agency Aerospace Center (DMAAC), "1° x 1° Mean Free Air Gravity Anomalies," DMAAC Reference Publication 73-0002, 1973.

4. Dickson, G. O., W. C. Pitman, III, and J. R. Heirtzler, "Magnetic Anomalies in the South Atlantic and Ocean Floor Spreading," Journal of Geophysical Research, Vol. 73, No. 6, 1968.

5. Fitch, Thomas J., "Plate Convergence, Trans-Current Faults, and Internal Deformation Adjacent to Southeast Asia and the Western Pacific," Journal of Geophysical Research, Vol. 77, pp. 4432-4460, 1972.

6. Isacks, Bryan, and Jack Oliver, "Seismology and the New Global Tectonics," Journal of Geophysical Research, Vol. 73, No. 18, 1968.

7. Jacoby, W. R., "Models of the Upper Mantle, Based on Gravity and Seismic Data, and Tectonic Implications," paper presented to the International Symposium on Earth Gravity Models and Related Problems, St. Louis, Missouri, August 16-18, 1972.

8. Kaula, W. M., "Attempts to Utilize the Gravity Field for Convective Models," paper presented to the International Symposium on Earth Gravity Models and Related Problems, St. Louis, Missouri, August 16-18, 1972a.

9. Kaula, W. M., "Global Gravity and Tectonics," in The Nature of the Solid Earth, edited by E. C. Robertson; McGraw Hill, New York, pp. 383-405, 1972b.

10. Le Pichon, Xavier, and J. R. Heirtzler, "Magnetic Anomalies," in the "Indian Ocean and Sea Floor Spreading," Journal of Geophysical Research, Vol. 73, No. 6, 1968.

11. Meyerhoff, A. A. and H. A. Meyerhoff, "Continental Drift, IV; The Caribbean Plate," Journal of Geology, Vol. 80, pp. 34-60, 1972.

12. Mitchell, A. H., and J. D. Bell, "Island Arc Evaluation and Related Mineral Deposits," The Journal of Geology, Vol. 8, pp. 381-405, 1973.

13. Pitman, W. C., III, E. M. Herron, and J. R. Heirtzler, "Magnetic Anomalies in the Pacific and Sea Floor Spreading," Journal of Geophysical Research, Vol. 73, No. 6, 1968.

14. Talwani, M., and A. B. Watts, "Gravity Studies Over Stable and Unstable Continental Margins," abstract of paper

presented to the International Symposium on Earth Gravity Models and Related Problems, St. Louis, Missouri, August 16-18, 1972.

15. Vine, F. J., "Magnetic Anomalies Associated with Mid-Ocean Ridges," in The History of the Earth's Crust, R. A. Phinney, editor, Princeton University Press, 1968.

16. Woollard, G. P., The Interrelationships of Crustal and Upper Mantle Parameter Values in the Pacific, Hawaii Institute of Geophysics, University of Hawaii, 1973.

17. Woollard, G. P., and K. I. Daugherty, Investigations on the Prediction of Gravity in Oceanic Areas, Hawaii Institute of Geophysics, University of Hawaii, 1973.

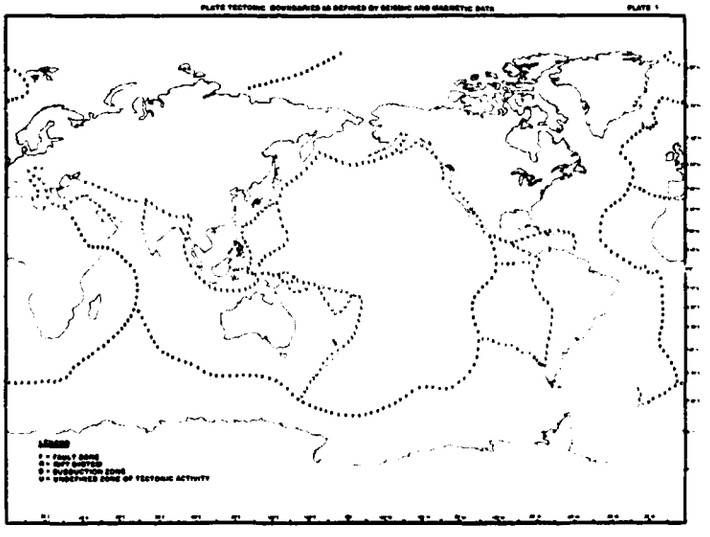

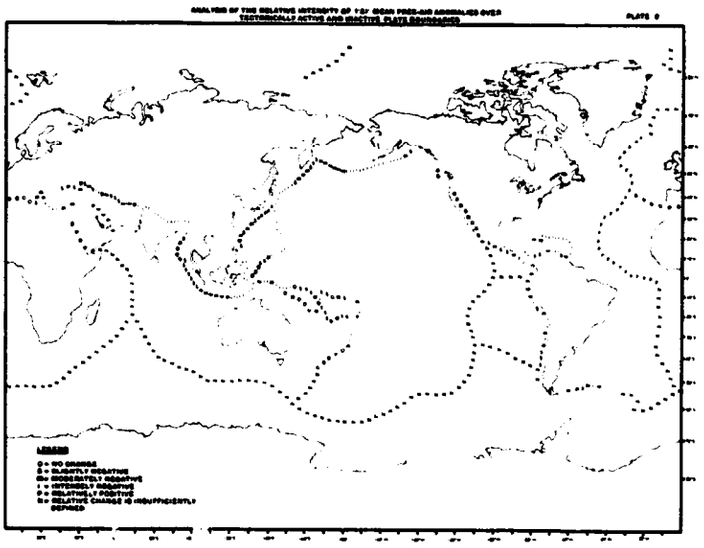

THE THIRD-ORDER CLAIRAUT EQUATION FOR A ROTATING BODY OF ARBITRARY DENSITY AND ITS APPLICATION TO MARINE GEODESY

Zdeněk Kopal* and Paolo Lanzano
U.S. Naval Research Laboratory
Washington, D. C. 20375

ABSTRACT

This paper derives the Clairaut equations, which govern the deformation of the equipotential surfaces within a rotating mass in hydrostatic equilibrium, as ordinary differential equations containing up to third-order terms in a small parameter. This has been achieved by (1) eliminating the two integral terms which appeared in the original formulation, and (2) by expanding the equipotential surfaces into a power series of a small parameter, which is essentially the ratio between the rotational and potential energy of the body.

It is expected that the numerical integration of these newly obtained equations, which requires the knowledge of the density profile within the rotating body, will contribute toward a solution of the following problems: (1) the determination of the geoid to a precision of one meter, (2) correction to the travel-time of seismic waves, and (3) the determination of the exterior shape of the rapidly rotating planets Jupiter and Saturn.

The need for the third-order and higher order theories is dictated by our interest in ascertaining the planetary deformations to a higher degree of accuracy than heretofore available. In the case of Earth and Moon, the accuracy requirement is of the order of one meter. Such stringent requirement is related to laser ranging and will provide more precise information on tectonic plates movements and on other questions of interest in marine geodesy.

INTRODUCTION

The fundamental problem of geodesy is the determination of an accurate shape of the geoid with respect to a chosen reference surface. For this purpose, geodetic activity in the last few decades has been primarily concerned with obtaining accurate gravity anomaly measurements in various locations on the Earth. By introducing these measurements into Stokes integral formula, one can evaluate the deviations of the geoid from the standard reference surface. This formula however requires contributions from all over the Earth. To gravimetrically map extensive areas is an expensive and time-consuming proposition, which sometimes is unattainable because of the inaccessibility of certain areas of the globe. The theoretical refinements due to Molodenskii (1960), although responsible for having brought a slight increase in accuracy, are predicated to the same limitations and pitfalls, (see, e.g., Rapp, 1973).

To alleviate this situation, recourse has been made, from time to time, to theoretical considerations to provide alternate and/or more suitable methods. Recent research has been dealing with the representation of the geopotential by a series of functions different from spherical harmonics.

---

* Normally at the Astronomy Department, University of Manchester, England.

Th... for example, Hotine (1969) and Walter (1970) have considered ellipsoidal harmonics; Giacaglia and Lundquist (1972) have introduced certain matrix transforms of harmonic functions which they have labelled sampling functions. Statistical models have also been introduced (e.g. by Jordan, 1972) to systematize the numerous data pertaining to gravity anomalies and deflections of the vertical. Elegant as they might be, these mathematical devices do not seem ultimately to help in the final numerical evaluation.

Satellite geodesy has, in the past, been quite successful in ascertaining the harmonics up to the tenth order and degree (Gaposhkin and Lambeck, 1971), representing wavelengths longer than 4,000 km. Claims have been made of having obtained undulations of only few meters. However, the determination of higher order harmonics (say, up to the sixteenth order and degree) by the same method has not met with great success and one has to fall back to surface gravity measurements for reliable data.

Recently, sea-gravity measurements performed in the western North Atlantic ocean by Talwani (1972) have revealed undulations of the geoid with wavelength of few hundred kilometers having amplitudes of few tens of meters.

Thus, one has the situation whereby undulations of long wavelengths (few thousand kilometers) have amplitudes of few meters, whereas undulations of few hundred kilometers have amplitudes one order of magnitude higher.

This lack of convergence and the existing discrepancy between data obtained by sea or land measurements versus satellite data contribute to a situation which is far from being optimal and which calls for the introduction of new ideas and/or working procedures if one wants to make use of all available gravity measurements for a more precise determination of the geoid.

It is our contention that there is a physical reason for the observed discrepancy and that any knowledge on the density distribution within our planet is fundamental for obtaining a more refined figure of equilibrium that should be used as the "spheroid" of reference. The inadequacy of the present reference surface (oblate ellipsoid of revolution) to represent a good global fit of the geoid is responsible, in our opinion, for the fact that one cannot accomodate at present all the available data. Both from a mathematical and physical point of view, it is evident that if initially one does not start with a good fit to the physical surface, a loss of accuracy will ensue.

The theory for the equilibrium configuration of a rotating mass with arbitrary density distribution under hydrostatic equilibrium (the so-called theory of Clairaut), appears to be the most logical physical way to provide a good approximation to the geoid. This theory, relating the shape and gravitational potential of a heterogeneous Earth deformed by diurnal rotation was developed by A. C. Clairaut to first-order terms in the centrifugal force to surface gravity ratio. It was capable of describing the shape of the Earth within the errors of the order of ±100 meters. To increase the accuracy necessitated retention of second-order terms in the same parameter. The first steps in this direction were taken by G. H. Darwin (1900) and the second-order theory was finally brought to a successful conclusion by W. DeSitter (1924). Perhaps the most general results are those obtained by one of us (Kopal, 1960) and published in a monograph which has since received extensive use. Applications of this second-order theory to geophysics (Bullard, 1948, and James and Kopal, 1963) have disclosed that a retention of second-order terms will approximate the surface of the Earth by quantities of the order of a few tens of meters. Should, however, the current operational requirements call for an improvement of the precision to quantities of the order of ±1 meter or less, a retention of third-order terms in the underlying theory becomes indispensable. The first steps toward developing such a theory were taken by Lanzano (1962), and more recently both authors while at NRL have developed the Clairaut theory up to and including third-order terms in the small parameter. We are virtually certain that no similar work has been undertaken anywhere else. The numerical solution of the ensuing Clairaut equation should provide the sought spheroid of reference to a higher degree of approximation than heretofore available. The essential features of the method are described in what follows.

CLAIRAUT EQUATIONS

Consider any deformable nonviscous body and denote by ρ the density at any internal point, by p the pressure, and by ψ the sum of the self-gravitational and disturbing potential. Assuming hydrostatic equilibrium, we have

$$\text{grad } p = \rho \text{ grad } \psi. \tag{1}$$

The compatibility conditions for this equation reveal that ψ must be a function of ρ alone; from equation (1), it follows that p is then also a function of ρ alone: the so-called equation of state. One can then deduce that the surfaces ψ = constant constitute equilibrium configurations.

Let us suppose that the mass in consideration rotates about an axis which remains fixed with respect to its surface. Because of this rotation, both the outermost surface and the other equipotential surfaces, which were originally spherical in shape, will be distorted into spheroidal configurations. These spheroids depend continuously on a parameter a, which represents the mean radius of the spheroid, and are such that through each point within the mass there passes one and only one spheroid.

Let us introduce a system of spherical polar coordinates $(O; r, \theta, \phi)$ with the origin O coinciding with the centroid of the rotating mass, where the colatitude θ is measured from the rotational axis, and the longitude ϕ is measured in the equatorial plane from an arbitrary axis. If we assume both axial symmetry and symmetry with respect to the equatorial plane, the equipotential surfaces can be represented as

$$r/a = 1 + \sum_{j=0}^{\infty} f_{2j}(a/a_1)P_{2j}(\cos\theta), \tag{2}$$

where the P's are Legendre polynomials, and a_1 denotes the mean radius of the outermost surface.

The distortion coefficients f can be determined from the total potential ψ expanded in terms of spherical harmonics of ascending order. For this purpose, replace in this potential expansion the radius-vector r by equation (2); and, after having performed all the necessary operations, rearrange this expression into a new expansion of ψ in spherical harmonics. Since ψ must reduce to a constant, we equate the coefficients of $P_j (j = 1, 2, 3, \ldots)$ to zero and the coefficient of P_o to a constant.

These steps give rise to Clairaut's integral equations for the f's which entail not only the density $\rho(a)$ within the mass but also its mean density

$$\bar{\rho}(a) = (3/a^3)\int_0^a \rho a^2 \, da. \tag{3}$$

Thus, one would be compelled to ascertain the density distribution within the mass by making use of the Poisson equation associated with the given potential. For the Earth, this last step is not essential since an accurate model for its internal density can be deduced from seismological considerations.

To establish a recurrent approximation procedure, we introduce the rotational parameter

$$q = \omega^2 a_1^3/3Gm_1, \tag{4}$$

where G is the gravitational constant, m_1 is the total mass, ω is the rate of axial rotation, and we express the distortion coefficients f_j as power series in q:

$$f_{2j}(a,q) = \sum_{k=1}^{\infty} q^k f_{2j,k}(a). \tag{5}$$

Notice that q is essentially the ratio between the rotational and the potential energy of the mass, for the Earth we know that $q = 0.00115$. Preliminary computations, meant to establish order of magnitude relations in q, reveal that f_2 is of the first order, both f_o and f_4 are of the second order, f_6 is of the third order, and f_8 is already of the fourth order in q. Thus, up to third-order terms, the equations of the equipotential surfaces can be written as

$$r/a = 1 + \sum_{j=0}^{3} \sum_{k=1}^{3} q^k f_{2j,k}(a/a_1)P_{2j}(\cos\theta) \tag{6}$$

with

$$f_{01} = f_{41} = f_{61} = f_{62} = 0. \tag{7}$$

The first-order theory provides the function f_{21}; the second-order theory consists of determining f_{02}, f_{22} and f_{42} in terms of the lower order results. All these functions have to be used in order to ascertain f_{03}, f_{23}, f_{43}, f_{63} which constitute the third-order theory.

Let us consider the expression for the total potential. The only disturbing potential is the rotational potential and this can be written as

$$W = \tfrac{1}{2}\omega^2 r^2 \sin^2\theta = q\,\frac{Gm_1}{a_1^3}\,r^2\left[1 - P_2(\cos\theta)\right]. \tag{8}$$

The self-gravitational potential at an interior point P located onto an equipotential surface of mean radius a consists of two terms

$$V = \sum_{j=0}^{\infty} r^{-(1+j)} V_j(\theta,\vartheta),$$

due to the attraction on P by the mass located within said equipotential surface, and

$$U = \sum_{j=0}^{\infty} r^j U_j(\theta,\vartheta),$$

due to the attraction of the mass lying outside such surface and extending as far as the external boundary of the body. U_j and V_j are well-known triple integrals with respect to the mean radius and two angular variables (see, e.g. Kopal, 1960); their integrands consist of products of powers of r and Legendre polynomials. U_2 contains a logarithmic term in r/a.

To carry out the first two steps of the above-described procedure upon $\psi = U + V + W$, we have to:

(1) Use the orthogonality condition for spherical harmonics in its integral form; and

(2) Reduce the product of two or three Legendre polynomials to a linear expression of the same polynomials according to the Neumann-Adams formula

$$P_j P_k P_r = \sum_h A^h_{jkr} P_h$$

for $h = j + k + r,\ j + k + r - 2,\ \ldots$, (see, e.g. Bailey, 1935).

Thus, the n-th power of an equipotential surface has been expressed as

$$\frac{(r/a)^n - 1}{n} = \sum_{j=0}^{3}\left\{q f_{2j,1} + q^2\left(f_{2j,2} + \frac{n-1}{2} A^{2j}_{22} f^2_{21}\right) + q^3\left[f_{2j,3} + (n-1)B_{2j} + \frac{(n-1)(n-2)}{6} A^{2j}_{222} f^3_{21}\right]\right\} P_{2j}, \tag{9}$$

where

$$B_{2j} = \sum_{k=0}^{2} A^{2j}_{2k,2}\, f_{21}\, f_{2k,2}, \tag{10}$$

and a comma is used to separate the sets of lower indices when they appear in literal form. Notice that $\ln(r/a)$, required within U_2, can be evaluated by taking the limit of equation (9) when n tends to zero.

Using these results, we have obtained the expansion of ψ into spherical harmonics of the form

$$\psi = \sum_{j=0}^{3}\sum_{k=1}^{3} q^k\, \psi_{2j,k}(a) P_{2j}(\cos\theta),$$

where the coefficients of the various harmonics are polynomials in q. The ψ's for $j = 0$ and $k = 1, 2, 3$ need not be written explicitly since they must be equated to arbitrary constants. The nonvanishing coefficients of the expansion are reproduced below (primes denoting derivatives with respect to the mean radius a):

$$\psi_{21}(a) = -\left(Gm_1/a_1\right)\left(a/a_1\right)^2 +$$

$$(kmG/a)\left[-f_{21}\int_0^a \rho a^2\,da + \left(a^{-2}/5\right)\int_0^a \rho\left(a^5 f_{21}\right)'\,da + \left(a^3/5\right)\int_a^{a_1} \rho f_{21}'\,da\right], \tag{11}$$

$$\psi_{2j,2} = 2\left(Gm_1/a_1\right)\left(a/a_1\right)^2\left(A_{20}^{2j} - A_{22}^{2j}\right)f_{21} +$$

$$(kmG/a)\left\{\left(a^{-2j}/1+kj\right)\int_0^a \rho\left(a^{3+2j} F_{2j,2}\right)'\,da + \left(a^{1+2j}/1+kj\right)\int_a^{a_1} \rho\left(a^{2-2j} E_{2j,2}\right)'\,da + \right. \tag{12}$$

$$(1/5)A_{22}^{2j}\left[2a^3\int_a^{a_1} \rho f_{21}'\,da - 3a^{-2}\int_0^a \rho\left(a^5 f_{21}\right)'\,da\right]f_{21} -$$

$$\left.\left(f_{2j,2} - A_{22}^{2j} f_{21}^2\right)\int_0^a \rho a^2\,da\right\},$$

for $j = 1, 2$ with

$$E_{2j,2} = f_{2j,2} + \tfrac{1}{2}(1-2j)A_{22}^{2j} f_{21}^2$$

$$F_{2j,2} = f_{2j,2} + (1+j)A_{22}^{2j} f_{21}^2, \tag{13}$$

and

$$\psi_{2j,3} = \left(Gm_1/a_1\right)\left(a/a_1\right)^2\left[2f_{2j,2} + A_{22}^{2j} f_{21}^2 - \sum_{k=0}^{2} A_{2k,2}^{2j}\left(2f_{2k,2} + A_{22}^{2k} f_{21}^2\right)\right] +$$

$$(kmG/a)\left\{\left(a^{-2j}/1+kj\right)\int_0^a \rho\left(a^{3+2j} F_{2j,3}\right)'\,da + \left(a^{1+2j}/1+kj\right)\int_a^{a_1} \rho\left(a^{2-2j} E_{2j,3}\right)'\,da + \right. \tag{14}$$

$$(1/5)A_{22}^{2j}\left[2a^3\int_a^{a_1} \rho E_{22}'\,da - 3a^{-2}\int_0^a \rho\left(a^5 F_{22}\right)'\,da\right]f_{21} +$$

$$(1/9)A_{42}^{2j}\left[4a^5\int_a^{a_1} \rho\left(a^{-2} E_{42}\right)'\,da - 5a^{-4}\int_0^a \rho\left(a^7 F_{42}\right)'\,da\right]f_{21} -$$

$$(3/5)a^{-2}\sum_{k=0}^{2} A_{2k,2}^{2j}\left(f_{2k,2} - 2A_{22}^{2k} f_{21}^2\right)\int_0^a \rho\left(a^5 f_{21}\right)'\,da +$$

$$\left(a^3/5\right)\sum_{k=0}^{2} A_{2k,2}^{2j}\left(2f_{2k,2} + A_{22}^{2k} f_{21}^2\right)\int_a^{a_1} \rho f_{21}'\,da -$$

$$\left(f_{2j,3} - 2B_{2j} + A_{222}^{2j} f_{21}^{3}\right) \int_{0}^{a} \rho a^{2}\, da, \tag{14}$$

for $j = 1, 2, 3$, where

$$\begin{aligned} E_{2j,3} &= f_{2j,3} + (1 - 2j)B_{2j} - \tfrac{1}{3}j(1 - 2j)A_{222}^{2j} f_{21}^{3} \\ F_{2j,3} &= f_{2j,3} + 2(1 + j)B_{2j} + \tfrac{1}{3}(1 + j)(1 + 2j)A_{222}^{2j} f_{21}^{3} \end{aligned} \tag{15}$$

and the B's are defined by equation (10). It is also clear that

$$\psi_{41} = \psi_{61} = \psi_{62} = 0.$$

By equating ψ_{21} to zero we obtain an integral equation in which the unknown function $f_{21}(a)$ appears twice under the integral sign: one integral vanishing at the center of mass ($a = o$), the second vanishing at the external boundary ($a = a_1$). If, in turn, we isolate each integral and differentiate with respect to the variable a, we get an integral equation expressing the remaining integral of the unknown function in terms of the density and the deformation coefficients. These two expressions are needed for higher order approximations. Next, consider that expression which contains the integral vanishing at the boundary, and evaluate it at $a = a_1$; we find the boundary condition, valid at $a = a_1$:

$$2f_{21} + af'_{21} + 5 = 0. \tag{16}$$

A third differentiation upon the previous results is required to reach an ordinary differential equation

$$a^{2} f''_{21} + 6D\left(f_{21} + af'_{21}\right) - 6f_{21} = 0, \tag{17}$$

where $D = \rho/\bar{\rho}$ and $\bar{\rho}$, the mean density, is given by equation (3). By introducing the logarithmic derivative

$$\eta = af'/f, \tag{18}$$

the Clairaut equation will be taken into the Radau equation

$$a\eta'_{21} + 6D\left(1 + \eta_{21}\right) - \left(1 - \eta_{21}\right)\eta_{21} - 6 = 0, \tag{19}$$

which is of the first order but nonlinear.

The conservation of total mass within the distorted configuration allows one to evaluate the function $f_o(a)$ in its various approximations. In fact, we can write

$$\begin{aligned} m_1 = {} & 4\pi \int_{0}^{a_1} \rho a^{2}\, da + 4\pi q^{2} \int_{0}^{a_1} \rho(a)\left[a^{3}\left(f_{02} + \tfrac{1}{5}f_{21}^{2}\right)\right]' da \\ & + 4\pi q^{3} \int_{0}^{a_1} \rho(a)\left[a^{3}\left(f_{03} + \tfrac{2}{5}f_{21}\, f_{22} + \tfrac{2}{105}\, f_{21}^{3}\right)\right]' da, \end{aligned}$$

where primes, as usual, denote derivatives with respect to a. Since $\rho(a)$ is the density of the undistorted configuration and no change in total mass can occur because of the rotational motion, the first term alone appearing in the right-hand side shall represent the total mass. The other two integrands must vanish, thus yielding

$$\begin{aligned} f_{02} &= -(1/5)f_{21}^{2}, \\ f_{03} &= -(2/5)f_{21}\, f_{22} - (2/105)f_{21}^{3}. \end{aligned} \tag{20}$$

By equating to zero $\psi_{2j,2}$ $(j = 1, 2)$, as given by equation (12), and eliminating the two integrals of f_{21}, we get integral equations in which each unknown function $f_{2j,2}$ appears twice under an integral sign. Two differentiations are required to represent each one of these integrals in finite terms: these expressions are required for the next higher order approximation. One of these expressions provides the boundary conditions at $a = a_1$:

$$2f_{22} + af'_{22} = \frac{2}{7}\left(6 + 3\eta_{21} + \eta_{21}^2\right)f_{21}^2 + 2\left(5 + \eta_{21}\right)f_{21},$$

$$4f_{42} + af'_{42} = \frac{18}{35}\left(6 + 5\eta_{21} + \eta_{21}^2\right)f_{21}^2. \tag{21}$$

A third differentiation yields the second-order Clairaut equation

$$a^2 f''_{2j,2} + 6D\left(f_{2j,2} + af'_{2j,2}\right) - 2j(2j+1)f_{2j,2} = R_{2j,2}$$

valid for $j = 1, 2$ and where

$$R_{22} = \frac{2}{7}\left[\left(2 - 9D\right)\eta_{21} + 18\left(1 - D\right)\right]\eta_{21} f_{21}^2 + 12H(1-D)\left(1 + \eta_{21}\right)f_{21},$$

$$R_{42} = \frac{18}{35}\left[(2-9D)\eta_{21}\left(2 + \eta_{21}\right) - 21D\right]f_{21}^2, \tag{22}$$

and

$$H(a) = \bar{\rho}(a_1)/\bar{\rho}(a).$$

The corresponding Radau equation is easily obtainable.

To obtain third-order terms, we equate $\psi_{2j,3}$, $(j = 1, 2, 3)$, to zero and follow basically the same steps as in the previous case making use of the first and second-order results. One differentiation is required to get the boundary conditions and a second one to obtain the third-order Clairaut equations. The operations of substitution and simplification entail the handling of approximately two hundred literal terms. This work was done by hand and checked independently by both authors. A computer program is being envisaged in the near future to pursue expansions to higher powers of the parameter.

The third-order results can be summarized as follows:

(1) Boundary conditions at $a = a_1$

$$\begin{aligned} 2f_{23} + af'_{23} = {} & 2\left(5 + \eta_{22}\right)f_{22} - \\ & \frac{2}{7}\left(15+6\eta_{21}+2\eta_{21}^2\right)f_{21}^2 + \frac{2}{7}\left(12+3\eta_{21}+3\eta_{22}+2\eta_{21}\,\eta_{22}\right)f_{21}\,f_{22} + \\ & \frac{2}{7}\left(26 + 3\eta_{21} + 3\eta_{42} + 2\eta_{21}\,\eta_{42}\right)f_{21}\,f_{42} - \\ & \frac{4}{35}\left(38 + 30\eta_{21} + 15\eta_{21}^2 + 2\eta_{21}^3\right)f_{21}^3; \end{aligned} \tag{23}$$

$$\begin{aligned} 4f_{43} + af'_{43} = {} & 2\left(7 + \eta_{42}\right)f_{42} - \\ & \frac{18}{35}\left(21+10\eta_{21}+2\eta_{21}^2\right)f_{21}^2 + \frac{18}{35}\left(12+5\eta_{21}+5\eta_{22}+2\eta_{21}\,\eta_{22}\right)f_{21}\,f_{22} + \\ & \frac{20}{77}\left(26 + 5\eta_{21} + 5\eta_{42} + 2\eta_{21}\,\eta_{42}\right)f_{21}f_{42} - \\ & \frac{36}{385}\left(54 + 44\eta_{21} + 18\eta_{21}^2 + 3\eta_{21}^3\right)f_{21}^3; \end{aligned} \tag{24}$$

$$6f_{63} + af'_{23} = \frac{5}{11}\left(26 + 7\eta_{21} + 7\eta_{42} + 2\eta_{21}\,\eta_{42}\right)f_{21}\,f_{42} - \frac{18}{77}\left(2 + \eta_{21}\right)\left(12 + 6\eta_{21} + \eta_{21}^2\right)f_{21}^3; \tag{25}$$

(2) Clairaut equations

$$a^2 f''_{2j,3} + 6D\left(f_{2j,3} + af'_{2j,3}\right) - 2j(1 + 2j)f_{2j,3} = R_{2j,3}, \quad (j = 1, 2, 3)$$

where

$$\begin{aligned} R_{23} = {} & \frac{4}{7}\left[(2 - 9D)\eta_{21}\,\eta_{22} + 9(1 - D)\left(\eta_{21} + \eta_{22}\right)\right]f_{21}\,f_{22} + \\ & \frac{4}{7}\left[(2-9D)\eta_{21}\,\eta_{42} + 3(10-3D)\eta_{21} + (16-9D)\eta_{42} + 21D\right]f_{21}\,f_{42} - \\ & \frac{4}{35}\left[(7+6D)\eta_{21}^3 + 3(11-15D)\eta_{21}^2 + 9(20-9D)\eta_{21} + 3(22+5D)\right]f_{21}^3 + \\ & 12H(1-D)\left(1+\eta_{22}\right)f_{22} + \frac{36}{7}H(1-D)\left(2+\eta_{21}\right)\eta_{21}\,f_{21}^2 + \\ & 24H^2(1-D)\left(1 + \eta_{21}\right)f_{21}; \end{aligned} \tag{26}$$

$$\begin{aligned} R_{43} = {} & \frac{36}{35}\left[(2-9D)\left(\eta_{21}\,\eta_{22} + \eta_{21} + \eta_{22}\right) - 21D\right]f_{21}\,f_{22} + \\ & \frac{40}{77}\left[(2-9D)\eta_{21}\,\eta_{42} + (23-9D)\eta_{21} + 9(1-D)\eta_{42}\right]f_{21}\,f_{42} - \\ & \frac{36}{385}\left[9D\eta_{21}^3 - (10-27D)\eta_{21}^2 + 4(8+9D)\eta_{21} - 6(1-2D)\right]f_{21}^3 + \\ & 12H(1-D)\left(1+\eta_{42}\right)f_{42} + \frac{108}{35}H\left(3\eta_{21}^2 + 6\eta_{21} + 7\right)(1-D)f_{21}^2; \end{aligned} \tag{27}$$

$$\begin{aligned} R_{63} = {} & \frac{10}{11}\left[(2-9D)\eta_{21}\,\eta_{42} + 3(4-3D)\eta_{21} - (2+9D)\eta_{42} - 33D\right]f_{21}\,f_{42} - \\ & \frac{18}{77}\left[3D\eta_{21}^3 + (4+7D)\eta_{21}^2 - (4-45D)\eta_{21} - 24 + 15D\right]f_{21}^3. \end{aligned} \tag{28}$$

For a deeper insight into the mathematical details, see Lanzano (1962 and 1974), and Kopal (1973).

APPLICATIONS

Our principal result is the third-order approximation of the Clairaut equations. Two analytical developments of our results are the evaluation of the exterior potential and the various moments of inertia for the distorted configuration up to third-order terms in the parameter. We plan in the future to numerically integrate the Clairaut equations subject to the boundary conditions at the free surface expressed by eqts. (23) to (25), and to the boundary conditions at the center of the configuration given by

$$f_{2j,3}(o) = f'_{2j,3}(o) \qquad \text{for } j = 1, 2, 3.$$

The numerical solution of this boundary value problem provides values for the deformation for every equipotential surface within the rotating body. This naturally requires the knowledge of the lower order approximations.

The numerical integration of the Clairaut equation necessitates a knowledge of the density distribution within the rotating body. In the case of the Earth, a very plausible model which we are advocating is the HB$_1$ model of Haddon and Bullen (1969) or a modification thereof. This model, which is characterized by its parametric simplicity, represents in our opinion, one of the most advanced steps in our present knowledge of the Earth's density distribution. In fact, not only is it compatible with seismic wave travel-time data and the revised value of the Earth's moment of inertia but it also incorporates the free Earth spheroidal and torsional oscillation data.

James and Kopal's 1963 numerical work is based upon the 1940-42 Bullen model and is limited to the second-order approximation.

For a rapidly rotating planet, like Jupiter or Saturn, third-order effects might not be sufficient to determine the shape of these planets. If this be the case, we are in a position to analytically extend our theory to the fourth or higher order by means of a computer program which allows one to perform all the algebraic and differential manipulations through the computer. For the fourth-order case this has already been done, but the results, while available, are too complicated for us to include them in this paper.

In the terrestrial case, it is expected that by solving the third-order Clairaut equations, a precision of ±1 meter for the geoid will be achieved and will represent the best "surface of interpolation" for isolating other factors not attributable to hydrostatic equilibrium.

Another reason for wanting to know the equipotential surfaces within the Earth to a higher precision is to be able to calculate corrections to seismic wave travel-time, as mentioned recently by Bullen (1973).

A more accurate determination of the geoid should also help to understand the rotational motion of the tectonic plates.

Future measurements via radar altimeters like the ones planned in the GEOS-C satellite will be very fruitful, however, in order to calibrate the altimeter, it is imperative to know the geoid undulations by independent means.

In conclusion, we feel confident that our analytical procedure, which stems from a deep-rooted physical condition, if backed by valid density data, will provide a better approximation to the geoid and a better usage of the available or future gravity measurements.

REFERENCES

Bailey, W. N.: (1935), Generalized Hypergeometric Series, Cambridge University Press.

Bullard, E. C.: (1948), Monthly Notices Roy. Astron. Soc. (Geophys. Suppl.) 5, 186.

Bullen, K. E., and Haddon, R. A. W.: (1973), Phys. Earth Planet. Interiors 7, 199.

Darwin, G. H.: (1900), Monthly Notices Roy. Astron. Soc. 60, 82.

DeSitter, W.: (1924), Bull. Astron. Inst. Neth. 2, 97.

Gaposhkin, E. M., and Lambeck, K.: (1971), J. Geophys. Res. 76, 20, 4855.

Haddon, R. A. W., and Bullen, K. E.: (1969), Phys. Earth Planet. Interiors 2, 35.

Hotine, M.: (1969), Mathematical Geodesy, U. S. Gov. Printing Office.

James, R., and Kopal, Z.: (1963), Icarus 1, 442.

Jordan, S. K.: (1972), J. Geophys. Res. 77, 20, 3660.

Kopal, Z.: (1960), Figures of Equilibrium of Celestial Bodies, University of Wisconsin Press, Madison.

Kopal, Z.: (1973), Astrophys. Space Sci. 24, 145.

Lanzano, P.: (1962), Icarus 1, 121.

Lanzano, P.: (1974) to appear in Astrophys. Space Sci.

Lundquist, C. A., Giacaglia, G. E. O., and Gay R. H.: (1972) Application of Sampling Functions to Earth Gravity Models, International Symposium on Earth Gravity, St. Louis, Mo.

Molodenskii, M. S., Eremeev, V. F., and Yurkina, M. I.: (1960), Methods for Study of the External Gravitational Field and Figure of the Earth, OTS61-31207, translated from the Russian, Israel Program for Scientific Translations, Jerusalem.

Rapp, R. H.: (1973), The Geoid: Definition and Determination, Fourth GEOP Res. Conf. on Geoid and Ocean Surface, Boulder, Colo.

Talwani, M., Poppe, H. R., and Rabinowitz, P. D.: (1972), Gravimetrically Determined Geoid in the Western North Atlantic, in Sea Surface Topography from Space 2, NOAA Tech. Rep. ERL-228-AOML 7-2.

Walter, H. G. (1970), The Use of Ellipsoidal Harmonics for the Representation of the Potential, in Dynamics of Satellite, B. Morando, ed.

BISTATIC SEA STATE RADAR MONITORING SYSTEM AND APPLICATIONS TO MARINE GEODESY

GEORGE T. RUCK
Battelle Columbus Laboratories

ABSTRACT

Battelle's Columbus Laboratories have developed for NASA-Wallops a bistatic radar system capable of sea state sensing from an orbital or aircraft platform. This system employs a simple low power transmitter in conjunction with a separate receiving unit. Operating in the HF region (3-30 MHz), a vertically polarized pulse or FMCW waveform is transmitted. The transmitted energy is scattered from the sea surface and received at a given time delay after reception of the direct signal from the transmitter. By sweeping or stepping the pulse carrier frequency or FMCW center frequency through the HF band, the heights of the larger ocean waves whose length are equal to the radar wavelength are sampled. Spectral processing of the received signal permits the directional component of the ocean-wave spectrum in the sea scattering region to be determined. This system can be configured using the transmitter on the surface or in an orbital or airborne platform. Using the transmitter in a satellite and the receiver on the surface will allow directional wave-height spectrum measurements of an area around the receiver to be made without the requirement for data processing in the satellite or direct data transfer from the satellite. If the receiver is placed in the satellite, directional ocean wave-height spectra can be obtained from large ocean areas.

An aircraft test of the system has been recently conducted using a transmitter mounted on the Chesapeake Light Tower and a receiver mounted in a NASA-Wallops aircraft. Applications of this instrumentation include precise measurement of the ocean wave-height spectrum in conjunction with satellite altimetry for geodetic determinations. Directional wave height spectra measurements in conjunction with wind speed and directional information will allow various wind-sea interaction-theories and models to be evaluated. In addition, detailed directional wave-height spectrum measurements are required in order to design deep sea drilling platforms and modern ship hulls to insure their safety and physical integrity during severe wave-height conditions.

INTRODUCTION

The bistatic scattering of high frequency radio waves can be used to observe directional ocean-wave spectra and consequently measure RMS wave heights. The potential exists for carrying out such measurements using either satellite or aircraft platforms allowing large areas of the oceans to be monitored. Synoptic data on wave heights, directions, slope statistics, etc., are required if satellite altimetry is to provide the hoped-for accuracies of Geoid definition as well as for a variety of oceanographic and marine applications.

Bistatic sea state measurements are possible because at long and medium wavelengths, the sea surface scatters in a Bragg scatter mode which allows the ocean-wave spectrum to be sampled by changing the incident radio frequency. A measurement system can take two configurations. One in which a transmitter is located on or near the surface such as on a ship, bouy, tower, or small island and a receiver is located in an orbital or airborne platform. This allows one receiver to operate in conjunction with many transmitters and gather data from a wide area. Another operational mode would be to place the transmitter in an orbital or airborne platform and one or more receivers on the surface. This would avoid the requirement for any data processing or telemetry functions in the satellite or aircraft, although each receiver would provide data only on wave conditions in its vicinity.

This paper will describe an experimental aircraft system operating in the 3-30 MHz region which has been developed for NASA-Wallops Flight Center, and the current and expected results from the system. A brief description of the Bragg scattering process will also be given along with the requirements for a satellite system.

HIGH FREQUENCY SCATTERING FROM THE OCEAN SURFACE

The ocean surface can be described by a model in which the random variable $h(\bar{r}, t)$ defines the surface heights at some position $\bar{r}$ and time t relative to a reference surface (Phillips, 1966 and Longuet-Higgins, 1957). The power spectrum of the surface height is the generalized Fourier transform of the surface covariance function and is a function of the vector spatial wave number, frequency, position, and time. If the sea is stationary or homogeneous, or both, then one or more of these variables can be suppressed. For a stationary, homogeneous sea, the surface can be fully described in terms of its three dimensional height spectrum $\phi(\bar{k}, f)$. For small amplitude gravity waves, which are a good approximation for the sea, then the dispersion relation

$$v^2 = (g/k) \tanh (kh) \tag{1}$$

is valid, and for deep water ($kh \gg 1$) $v^2 \approx g/k$ where v is the phase velocity of a wave with wave number k and g is the acceleration due to gravity (Kinsman, 1965). For small amplitude gravity waves, the surface height spectrum for a stationary, homogeneous sea becomes a function only of the vector wave number $\bar{k}$. The total potential energy of the surface is given in this case by

$$E = (1/2)\rho g \int_{\bar{k}} w(\bar{k})d\bar{k} \tag{2}$$

where

$$\int_{\bar{k}} w(\bar{k})d\bar{k} = \int_{-\infty}^{\infty}\int_{-\infty}^{\infty} w(k_x, k_y)\, dk_x\, dk_y = \overline{\zeta^2} \tag{3}$$

the mean square surface height.

For an electromagnetic wave propagating over a rough surface such as the ocean at angles near grazing incidence, the boundary perturbation theory of Rice can be used to determine the incoherent energy scattered from the surface (Rice, 1957 and Barrick and Peake, 1968). For a plane wave incident at a polar angle θ_i with radian frequency ω_o and wave number k_o, the scattering cross section per unit surface area is

$$\sigma_{ij}(\theta_s, \phi_s, \theta_i) = 4\pi k_o^4 \cos^2\theta_i \cos^2\theta_s\, |a_{ij}|^2 \left\{ w^- \delta(\omega - \omega_o + \omega_g) + w^+ \delta(\omega - \omega_o - \omega_g) \right\} \tag{4}$$

with

$$w^- = w[k_o(\sin\theta_s \cos\varphi_s - \sin\theta_i),\ k_o(\sin\theta_s \sin\varphi_s)] \qquad (5)$$

$$w^+ = w[-k_o(\sin\theta_s \cos\varphi_s - \sin\theta_i),\ -k_o(\sin\theta_s \sin\varphi_s)]$$

$$\omega_g = \sqrt{gk_o}\,[(\sin\theta_s \cos\varphi_s - \sin\theta_i)^2 + (\sin\theta_s \sin\varphi_s)^2]^{1/4}$$

The parameters α_{ij} are complex scattering matrix elements which depend upon the polarization states and propagation angles of the incident and scattered fields and the dielectric properties of the ocean surface.

For incident radio wavelengths longer than approximately 10 meters at grazing angles ($\theta_i \approx \pi/2$), the condition for application of Rice's slightly rough surface theory is valid and the conductivity of sea water is sufficient that the polarization parameter α_{ij} reduces to only two of importance. These are for vertically polarized incidence and vertically and horizontally polarized scattering. The resulting cross sections become

$$\sigma_{vv}(\theta_s, \varphi_s) \approx 2\pi k_o^4 (\sin\theta_s - \cos\varphi_s)^2 \left\{w^- \delta^- + w^+ \delta^+\right\} \qquad (6)$$

and

$$\sigma_{hv}(\theta_s, \varphi_s) \approx 2\pi k_o^4 \cos^2\theta_s \sin^2\varphi_s \left\{w^- \delta^- + w^+ \delta^+\right\} \qquad (7)$$

with

$$w^- = w[k_o(\sin\theta_s \cos\varphi_s - 1),\ k_o \sin\theta_s \sin\varphi_s]$$

$$w^+ = w[-k_o(\sin\theta_s \cos\varphi_s - 1),\ -k_o \sin\theta_s \sin\varphi_s] \qquad (8)$$

$$\delta^- = \delta(\omega - \omega_o + \omega_g),\ \delta^+ = \delta(\omega - \omega_o - \omega_g)$$

The nature of the scattering phenomena is illustrated more clearly if a polar coordinate representation of the surface height spectrum is used. This is defined by

$$\overline{\zeta^2} = \int_{-\infty}^{\infty}\int_{-\infty}^{\infty} w(k_x, k_y)\, dk_x\, dk_y = \int_0^{2\pi}\int_0^{\infty} w(k, \psi)\, k\, dk\, d\psi \qquad (9)$$

If this polar representation is used in Equations 6 and 7 above for the cross sections, then

$$w^{+} = w(k, \psi), \quad w^{-} = w(k, -\psi)$$
$$k = k_o \sqrt{1 + \sin^2\theta_s - 2\sin\theta_s \cos\phi_s} \tag{10}$$

and

$$\psi = \tan^{-1}\left(\frac{\sin\theta_s \sin\phi_s}{\sin\theta_s \cos\phi_s - 1}\right) \tag{11}$$

If the scattering direction is also near grazing, with $\theta_s \approx \pi/2$, then the expressions for k and ψ reduce to

$$k = k_o \sqrt{2 - 2\cos\phi_s}, \quad \text{and} \quad \psi = \tan^{-1}\left(\frac{\sin\phi_s}{\cos\phi_s - 1}\right)$$

Only those components of the surface which satisfy these conditions contribute to the scattered fields. For forward scatter where $\phi_s = 0$, then $k = 0$ and $\psi = 0, 180^{o}$. Thus, the scattering is zero since only those surface components of wave number zero contribute and these are of zero amplitude. For the 90^{o} bistatic case where $\phi_s = \pm \pi/2$, than $k = \sqrt{2}k_o$ and $\psi = \pm \pi/4$. Thus, those surface components of wavenumber $\sqrt{2}k_o$ traveling along the bisector of the scattering angle contribute. For backscatter, only components with wavenumber $2k_o$ traveling parallel to the scattering direction contribute. To the extent that the above models are valid, the scattering phenomena is Bragg scatter with the ocean surface acting like a diffraction grating of electrical spacing k.

Experimental confirmation of this performance has been obtained by a number of researchers. Figure 1 presents the backscatter, frequency versus amplitude spectrum of a region of the ocean surface located approximately 45 km off Barbados Island and measured at a frequency of 2.9 MHz (Crombie, 1970). According to Equation 5, the scattered energy should appear at frequencies offset $\pm \sqrt{2gk_o}$ from the carrier or ±.174 Hz. This is precisely where the measured scattered energy occurs. At the time of this measurement, the surface spectrum was highly directional with the dominant waves moving towards the radar in accordance with the westward trade winds in the area.

SURFACE SPECTRUM MEASUREMENTS

As indicated above, the average power scattered from an incremental area of the ocean surface for grazing illumination or observation is proportional to the surface height spectrum at a particular wavenumber k. If the surface is illuminated at a number of wavelengths in the HF region, this is equivalent to sampling the magnitude of the surface spectrum at a number of wavelengths. The RMS surface height is the integral of the surface spectrum over all wavenumbers. Since sampling at all wavenumbers cannot be accomplished, the portion of the spectrum not being sampled must contribute negligibly to the total potential energy of the surface. Both experimental

measurements and theory indicate that for wavenumbers smaller than some cut-off value, the surface spectrum for a fully developed wind sea contains negligible energy (Longuet-Higgins, 1969 and Chase, et.al., 1957). For larger wave numbers, the spectrum has approximately a k^{-4} dependence. One of several models for the spectrum of a fully developed wind sea predicts that

$$\int_0^{2\pi} w(k,\psi)d\psi = S(k) = .01k^{-4} \exp(-2g/v^2) \qquad (12)$$

where v is the surface wind velocity. If this is used in Equation 4 for a geometry in which $\theta_i = \pi/2$ or grazing incidence, and $\theta_s = 0$, or scattering vertically upward then the cross section σ_{vv} becomes

$$\sigma_{vv} \approx 4\pi k_o^{-4} \cos^2\varphi_s \left\{S(k_o)\right\} \qquad (13)$$

for an isotropic spectrum. This function is plotted in Figures 2a, b, and c for incident frequencies from 1-30 MHz and wind velocities of 5, 10, and 20 knots. At the higher frequencies corresponding to higher surface wave numbers, the spectrum saturates at a value of -17 dbm. This value has been verified by experimental measurements of the type illustrated in Figure 1 (Munk and Niesenberg, 1969).

Examining Figure 2a for 5 knot winds, it is apparent that at a frequency of 30 MHz, the saturation value of k has not been reached and the received power will vary greatly between radiated frequencies of 3 MHz and 30 MHz. For the assumed spectrum, this amounts to a 120 db change. Similarly, for a 10 knot wind, the difference is about 30 db, while for 20 knot winds, it is about 8 db. For wind velocities such that the spectrum is saturated to 3 MHz or above, no significant change would occur. This would be the case for 30 knot winds or above.

The RMS surface height is given by the integral over all wavenumbers of the surface height spectrum. For wavenumbers above the saturation point, the contribution to the integral comes from the k^{-4} dependence. For wavenumbers well below the cutoff point, the contribution is negligible. Thus, the region in the vicinity of the spectral peak is the major unknown contributor to the wave height and is the region in which measurements should be made. For an operating frequency range of 3 to 30 MHz, this corresponds to a surface with wind speeds of 10 to 30 knots. For either greater or smaller wind speeds, the 3 to 30 MHz region is not optimum for wave height measurements.

The curves given in Figures 2a, b, and c represent the magnitude of the surface spectrum with no directional effects exhibited. To obtain directional information, a bistatic geometry is used with the receiver carried on a moving platform, i.e., a satellite or aircraft, and the differential Doppler shift imposed on the signal from different parts of the surface is used to obtain the directional information.

The geometry appropriate to such a configuration is one in which the positive x-axis of the coordinate system is assumed to lie along the mean wind direction, and the receiver is moving with a velocity $\bar{V}_o$ in a direction α degrees from the mean wind direction. The instantaneous position of the receiver relative to the transmitter is given by the polar coordinate θ, ϖ', while the location of the surface region contributing to the scatter is given by the cylindrical coordinate ρ, ϖ.

If the radiated waveform used is such that the received signal can be processed so as to resolve range and Doppler, the location of the various scattering regions on the surface can be determined. For example, Figure 3 illustrates constant time delay and Doppler contours on the surface for the situation where the receiver is located at CPA and moving with a velocity of

8 km/sec at an angle of 40° with respect to the mean wind direction shown as 0° in this Figure. This corresponds to a satellite at an altitude of 400 km whose zenith point is 70 km from the transmitter.

The constant delay contours are shown for 20, 30, and 50 μsec delays and Doppler contours for -2.2, 0, and +2.2 Hz Dopplers. It is apparent that for a specific time delay, a specific Doppler frequency can be associated with each azimuthal location on the surface. There is, however, a 180° Doppler ambiguity; for example at a delay of 30 μsec, a Doppler shift of +2.2 Hz is associated with 107° and 336° azimuths. This can be resolved by using the redundant data gathered from several range cells.

Based on the associated Doppler, the magnitude of the field scattered from all azimuths around the transmitter can be determined. With the appropriate geometric effects included, the contribution to the directional surface spectrum from each azimuthal direction can thus be determined. The received Doppler resolved signal scattered with a constant time delay is illustrated in Figure 4 for the cases where the surface spectrum has the Phillips form and is directionally isotropic or cosine squared along the wind direction respectively. This Figure illustrates the vertically polarized field received at a satellite with a 10 MHz transmitted frequency. The satellite, located at a 400 km height, is moving 8 km/sec along a path oriented 40° relative to the surface wind direction at the transmitter and the subsatellite point is 70 km from the transmitter. The received signal is from those surface regions which have a range delay of 60 μsec relative to the direct signal path. The differences in the spectra are obvious with only those portions of the surface where waves are traveling down wind contributing to the cosine squared case.

AN AIRCRAFT EXPERIMENT

To determine the capabilities of the technique as a function of the system parameters and surface conditions as well as to validate a hardware and data processing approach, an experimental aircraft system has been assembled and a preliminary test conducted.

For a satellite-borne HF bistatic sea state sensor, the orbital motion of the satellite and the resultant Doppler shift imposed on the scattered signal can result in Doppler spreads of as much as 40 to 50 Hz, and Doppler processing to provide a 1-Hz resolution would allow the surface spectrum directionality to be obtained with about a 10° resolution under these conditions.

For a typical aircraft-borne receiver, however, the Doppler spread would be of the order of a few hertz. Thus, to achieve the same surface resolution would require Doppler processing to a resolution of the order of 0.04 to 0.05 Hz. This requires more complex hardware for an aircraft system than for the satellite case, and an FMCW waveform was chosen as the only approach capable of meeting the requirements which could be assembled using largely off-the-shelf hardware.

The FMCW hardware configuration used in the experiment consists of two digitally controlled HF frequency synthesizers. One is used to drive an amplifier providing a power output of the order of 5 W and constitutes the transmitting equipment. The other is used as the local oscillator for the receiving equipment. An off-the-shelf HF communications receiver is used with this configuration. The two synthesizers constitute the most critical and expensive items, with the rest of the required components, such as the transmitter power amplifier, receiver, etc., available either as off-the-shelf equipment or assembled at BCL. The digital sweep controllers necessary to control and program the synthesizer switching so as to provide the required frequency sweeps were designed, constructed, and tested at BCL.

The basic FMCW system is relatively simple, in that the transmitter radiates a coherent waveform which is swept over intervals of 50 kHz at a

basic sweep rate of 500 kHz thus providing 10 sweeps per second. The frequency versus time waveform is essentially a sawtooth in shape. At the receiver, the local oscillator is synchronously swept over the same frequency interval at the same rate, except that the sweep starting points are delayed in frequency by an amount corresponding to the range delay between the transmitter and receiver. The receiver local oscillator is also offset by an additional fixed amount corresponding to a desired IF frequency. This is in the HF band, and a conventional communications receiver is used as the IF amplifier. The scattered signal, after mixing with the receiver local oscillator then has a spectral spread which corresponds to different ranges. At the receiver output, the signal for each sweep is recorded on analog tape. The number of sweeps recorded is determined by the desired Doppler resolution. For example, if 256 sweeps are recorded at a rate of 10 sweeps per second, a Doppler resolution of 0.04 Hz results. Typically, a 50 kHz bandwidth is swept 10 times per second for 25.6 s. If 128 received signal samples per sweep are obtained in an A/D converter, then sufficient data exists to generate 64 range cells with a 6-km resolution per cell and 256 Doppler cells with a resolution of 0.04 Hz per cell. These are generated digitally by the application of a Fourier transform row by row and then column by column to the 128 X 256 matrix of data consisting of the 128 samples per sweep and the 256 sweeps. Actually, to save processing time, only the desired range cells are processed. Thus, only a few of the columns resulting from the first row-by-row transform are transformed.

In terms of hardware requirements, the stability and spectral purity required of the transmitter and receiver local oscillator for the FMCW case are the same as for a pulse-Doppler system. For the FMCW waveform, however, no peak power problems exist and the IF bandwidth required in the receiver is comparable to that normally encountered in HF communications receivers. For example, with the waveform parameters quoted above, an IF bandwidth of 1.28 kHz is required.

The FMCW approach does require good time synchronization between the transmitter and receiver, however. For example, a 1-μs timing error in the sweep start time corresponds to a 0.3-km range error.

The transmitting antenna system consists of a broadband vertical radiator and associated matching networks which are capable of operating satisfactorily over the range from 3 to 30 MHz.

The receiving equipment consists of one of the synthesizers and its associated sweep controller, an antenna preamplifier, an automatically band switchable RF preselector-mixer and a conventional communications receiver. The output of the receiver is coherently reduced to a baseband frequency and is recorded on an analog tape recorder for subsequent A/D conversion.

The experimental system was set up to transmit sequentially on 10 frequencies spaced from 3 MHz to 25 MHz. The transmitting equipment was installed on the Coast Guard operated Chesapeake Bay Light Tower located at 75° 42.8' West longitude and 36° 54.02' North latitude. The tower deck where the transmitting antenna was installed is located 90' above mean sea level and is 60' square. The average water depth in the tower area is 50'.

On April 26, an initial series of flight paths were flown and data recorded. In-so-far as can be ascertained, the bistatic equipment appeared to be functioning properly. The flight paths flown consisted of three calibration circles around the transmitting site at an altitude of approximately 500' at a radius of $\approx$ 1 mile. During these flights, the transmitter was not sweeping and was transmitting pure CW at 3.15 MHz, 8.53 MHz, and 25.15 MHz in succession. Following this, three along-wind flights were made over the tower at an altitude of approximately 5000'. Each path was flown for approximately a 10-minute period. A similar series of paths was flown in the cross-wind direction. The system was sweeping properly during these flights.

During this period, the surface winds were from the SW at an average speed of 8 knots. The wave heights in the area of the tower were visually estimated to be 1 to 2' with 3' of swell running north. As a result of the low waveheights, no useful laser profilometer data was obtained, thus the measured data could not be validated.

The low sea state existing at the time of the flight resulted in the signal-to-noise ratio of the scattered signal being quite low. For an 8 knot wind, the cutoff point for the surface spectrum is approximately 27 MHz. At 3 MHz, the k_o^{-4} dependence of the scattering cross section combined with the rapid decrease in surface energy below the cutoff point resulted in little scattered energy. Although the data obtained is of no value for wave height determination, it did allow the identification of several easily rectified minor hardware and operational problems and the exercising of the data reduction algorithms. Subsequent flights during periods of higher sea state should result in meaningful data.

CONCLUSION

An experimental bistatic radar aircraft sea state measurement system has been constructed and an initial flight test conducted. It is anticipated that the present experimental system can, with minor modifications, be used routinely for directional surface spectrum measurements when significant wave heights range from 3 to 15 feet. The present system utilizes a surface transmitter and an airborne receiver. Either this configuration or a surface receiver and an orbital transmitter can be used for a satellite system. Because of the greater Doppler shift of the scattered signal for a satellite system, the hardware requirements are simpler. Table 1 lists the system specifications for a pulse Doppler satellite system.

TABLE 1. SATELLITE SYSTEM SPECIFICATIONS

Transmitter
Power Output - 10 watts average
Frequency - 3 to 30 MHz, switched in 1 to 2 MHz steps
Stability - 1 part in 10^9
Spectral width - < 0.5 Hz
Pulse width - 10 to 20 μs
Antenna - vertical polarization, azimuthally omnidirectional
Receiver
Frequency - 3 to 30 MHz, switched in 1 MHz steps
Noise figure - not critical
Local oscillator stability - 1 part in 10^9
Time synchronization - not critical
IF bandwidth - 50 to 100 kHz
System bandwidth - 25 to 50 Hz
Coherent integration time - 1 s
Range gates - 3 or more
Antenna - horizontally polarized

The bistatic system discussed here is presently the only all-weather system capable of measuring the full directional surface spectrum in essentially real time. Knowledge of the directional spectrum allows all of the surface moments to be calculated and determination of the statistical properties of the surface such as RMS heights, mean surface slopes, etc. These are necessary for interpretation of satellite altimeter and scatterometer data.

ACKNOWLEDGEMENTS

The results of the research reported in this paper were supported by NASA Wallops Flight Center under Contract No. NAS6-2006. The Battelle program manager is A. G. Mourad and the NASA technical monitor is R. H. Stanley.

REFERENCES

(1) Barrick, D. E. and Peake, W. H., "A Review of Scattering from Surfaces with Different Roughness Scales", Radio Science, 3, p 865, 1968.

(2) Chase, J., Cote, L. J., Marks, W., Mehr, E., Pierson, W. J., Jr., Rouse, F. G., Stephenson, G., Better, R. C., and Walden, R. C., "The Directional Spectrum of a Wind Generated Sea as Determined from Data Obtained by the Stereo Wave Observation Project", N.Y.U., College of Engineering, 1957.

(3) Crombie, D. D., Watts, J. M., and Berry, W. M., "Spectral Characteristics of HF Ground Wave Signals Backscattered from the Sea", in AGARD Conference Proceedings, No. 77, Electromagnetics of the Sea, AGARD-CP-77-70, p 16-1, 1970.

(4) Kinsman, B., Wind Waves, Prentice-Hall, Inc., Englewood Cliffs, New Jersey, 1965.

(5) Longuet-Higgins, M. S., "On Wave Breaking and the Equilibrium Spectrum of Wind-Generated Waves", Proceedings of the Royal Society, Series A, Volume 310, p 151, 1969.

(6) Longuet-Higgins, M. S., "The Statistical Analysis of a Random Moving Surface", Trans. of the Royal Society, Series A, Volume 249, pp 321-387, 1957.

(7) Munk, W. H. and Wiesenberg, W. A., "High Frequency Radar Sea Return and the Phillips Saturation Constant", Nature, 224, p 1215, December 27, 1969.

(8) Phillips, O. M., Dynamics of the Upper Ocean, Cambridge University Press, 1966.

(9) Rice, S. O., "Reflection of Electromagnetic Waves from Slightly Rough Surfaces", in Theory of Electromagnetic Waves, M. Kline, Editor, p 351, Interscience, New York, 1957.

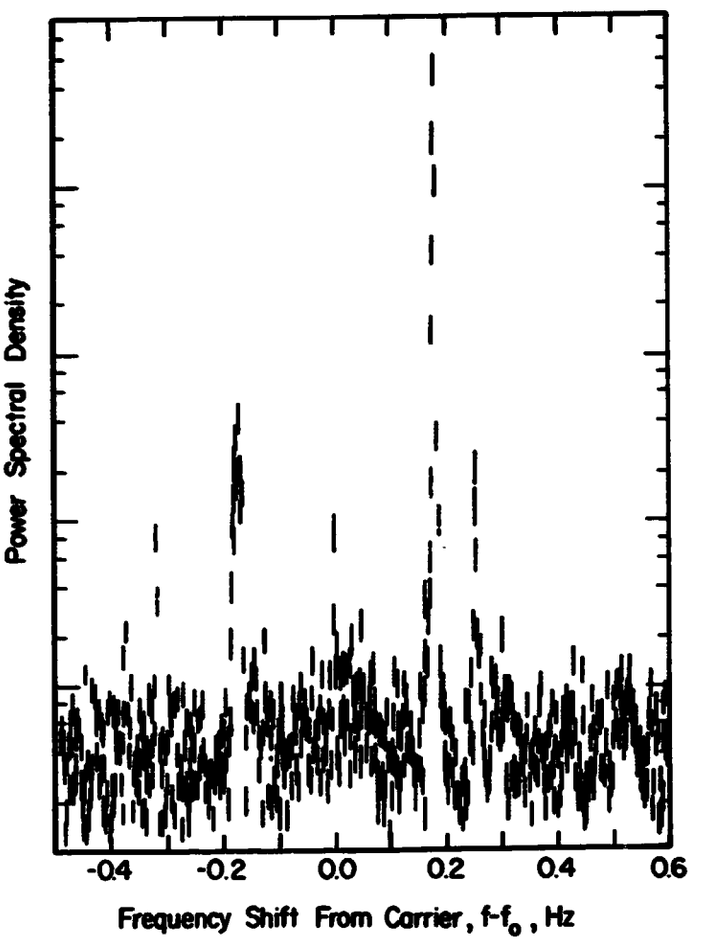

Figure 1. Experimental Backscatter Doppler Spectrum from the Ocean Surface at 2.9 MHz

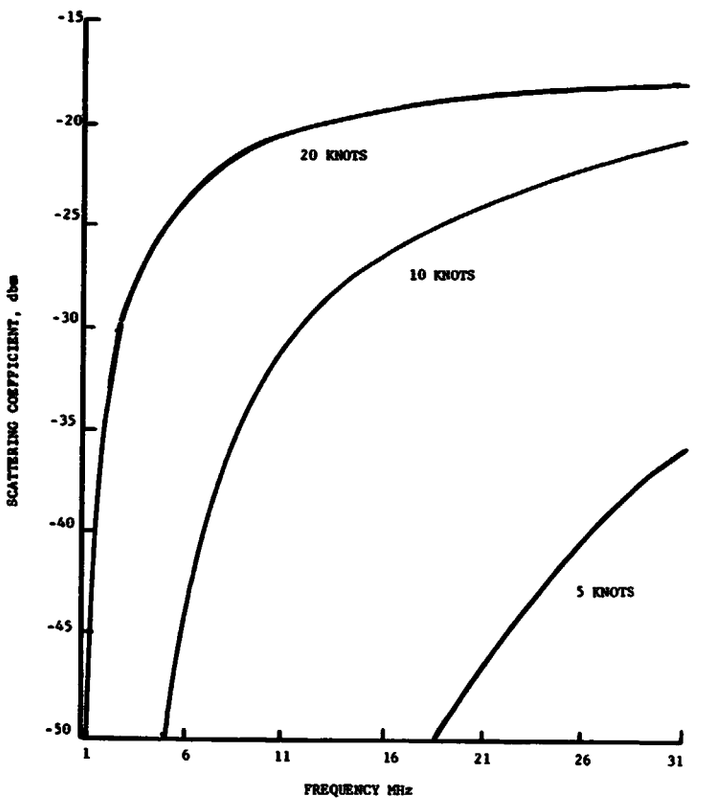

Figure 2. Normalized Received Power Versus Frequency in MHz, Neumann-Pierson Spectrum

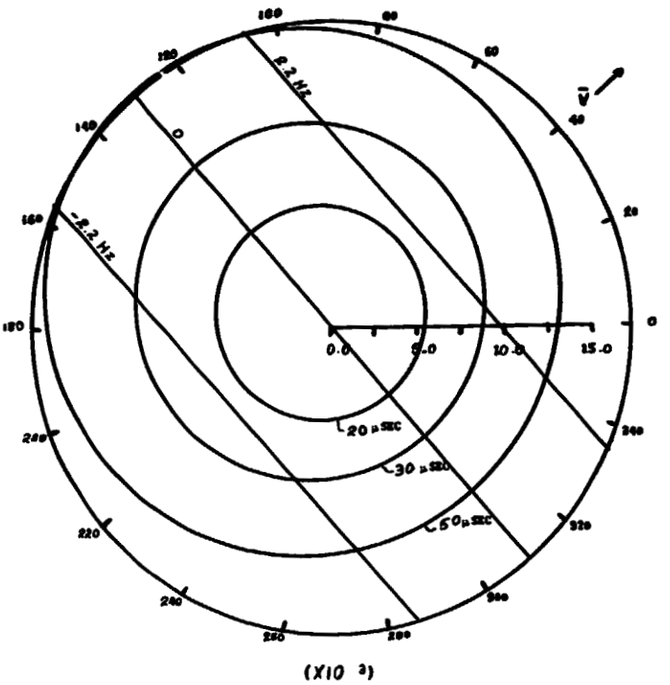

Figure 3. Constant Delay and Doppler Contours on the Surface for a Satellite Receiver

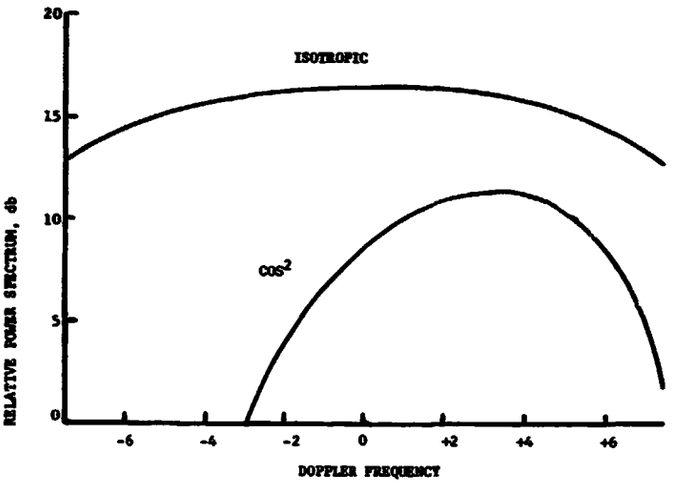

Figure 4. Received Doppler Spectrum for Isotropic and Cosine Squared Directionality

NEW STRATEGIES FOR ADVANCING MARINE GEODESY

Milton G. Johnson

Chief, Special Studies Staff
Office of NOAA Corps
National Oceanic and Atmospheric Administration
U. S. Department of Commerce

ABSTRACT

Although many changes are taking place in the various fields of marine geodesy, what consideration should be given to changes in related fields? How will the marine geodesist react to the increasing confrontations with complex economic, political and environmental changes occurring with respect to offshore areas? The energy crisis alone raises serious questions which are of vital concern to the disciplines of marine geodesy. In the international debates over "Who Owns the Ocean", the varied expertise of marine geodesists should be ready to offer assistance which will help in the answering of legal, political and economic questions. New demands for maintaining and improving the quality of the ocean environment may place new and perplexing demands upon the science and technology of marine geodesy. The exploitation of resources raises numerous questions. In the economic considerations, marine geodetic efforts should proceed in harmony with governmental research programs as well as burgeoning marine industrial development. This paper reviews some of the obstacles to exploitation by private enterprise and raises the challenge of marine geodesy for a widening concern in solutions to these questions.

INTRODUCTION

I want to discuss some of the related challenges that face marine geodesists today and in the days ahead. Although the excellent presentations of this symposium illustrate many changes in advancing marine geodesy, it should be recognized that we are also in the midst of complex economic, political, and environmental changes taking place in the coastal and offshore areas. The marine geodesist should be continually updating his knowledge and understanding of these changes in such a way that he is not deterred from his scientific and technological efforts. At the same time he should be aware of the presence of these related developments and proceed in harmony with their vicissitudes.

The energy crisis alone has raised serious questions as to the growing shortage of fuels which threatens to decrease our nation's output of goods and services. The search for solutions will extend more and more to the offshore areas which are of vital concern to marine geodesy. Our Secretary of State, Henry Kissinger, in his first speech before the United Nations several months ago, stated that we are members of a society drawn by modern science, technology and new forms of communication into a closeness for which we are politically unprepared. With each passing day, technology outstrips the ability of our institutions to cope with its fruits. Our political imagination must catch up with our scientific vision.(1)

In viewing the controversies raging over the question of "who owns the oceans", in other words, what is happening with respect to "Law of the Sea" questions, we must keep in mind that this summer there are crucial questions to be debated at the United Nations sessions in Caracas, Venezuela. At best, modest progress will be made; already the continuation of these meetings is being arranged for Vienna, Austria in 1975. Out of these international discussions there will come an increasing need for the expertise of marine geodesy, for the legal and political questions cannot be properly developed without taking into consideration the inputs of your science and technology.

The possible environmental changes tax the imagination. When we talk of such advances as offshore oil ports, nuclear power plants, oil drilling platforms, and related water transportation, we again see the importance of the knowledge that is gained through marine geodetic efforts. What man does to the ocean may become as important to the marine geodesist as what nature does. This means new dimensions of measurement, new and sophisticated equipment, new methods of data analysis and interpretation. The physicist, the chemist, the biologist and the engineer -- even the economist and political scientist -- must join forces with marine geodesists, across disciplinary lines, across organizational lines, across geographical boundaries -- united around the world -- to better understand the oceans.(2)

COMPLEX DEMANDS, GROWTH AND PLANNING

The contention here is that for marine geodesy to make proper progress there must be an appreciation of the tremendous complexity and significance of the area in which we are bringing our expertise to bear. Ed Wenk has said that the principal issue permeating the coastal and offshore zones is to provide for many diverse and conflicting demands and still obtain the greatest long-term social and economic benefits.(3) How do we work toward the solution of this principal issue? Several approaches have been evolving: On the one hand, the slow down or "stop" philosophy contends that industrial progress should be curtailed or stopped. This may be all right in certain situations but generally, growth must be promoted rather than hampered. The approach gaining rapid acceptance is that of coordinated planning for future development in the zone of marine geodetic actions. But the details of who does the planning may be troublesome. Should it be Federal or State government? Where does the United Nations organization fit in, particularly with respect to international waters where "Law of the Sea" problems are arising?

ECOLOGICAL AND SOCIO-ECONOMIC CONSIDERATIONS

Whether we look at the problems of planning and development off the coast of New England or California, or in innumerable other regions of the world, we are confronted with the reality that (1) control of ecological and physical disturbances and (2) design of the environment are key elements of economic development and planning work. Most scientists, by the very nature of their concentration of efforts, have failed to effect a systematic, coordinated presentation of their diverse findings within the highly interrelated ecosystem. Therefore, a pertinent objective is to encourage planners and environmental analysts to become more aware of the intricate interrelationships between the economy and the ecosystem, and between economic development and environmental management.(4)

President Nixon made a very valid point about the oceans when he was dedicating the Ocean Science Center of the Atlantic at Skidway Island near Savannah, Georgia in October, 1970. He pointed out that on the one side we will develop resources of the waters around us for the future benefit and progress of mankind, but on the other side, we will see to it that as we use the oceans we do not abuse the oceans. However, it is not necessary to make an either/or choice between nature and progress. The two are not mutually exclusive. Each individual is a part of the ecological system. What must change is our attitude toward nature. On the part of some individuals or companies there has been a cavalier or "public be damned" attitude. But these attitudes can no longer be accepted.

We must appreciate the fact that our offshore environment is a natural resource in and of itself and that it is a scarce commodity with a large demand. In the words of Dr. T. D. Barrow, top official of Exxon Petroleum Company: "We must plan for its use. As Herculean as it will be, we must make

an inventory and an assessment of the activities and resources of our offshore areas. Only by an objective socio-economic analysis can we ever hope that technical considerations will be the bases for our future decisions." (5)

FORMULATION OF USE PRIORITIES

Following the making of an inventory of resources, a flexible framework of use priority must be created to obtain the greatest long-term social and economic benefits. The framework needs to be flexible in order to analyze the circumstances of each individual case. Probably the best approach to determining use priorities is through the institution of performance standards. This means that according to local area circumstances and requirements, we might develop guidelines that could degrade, protect, or improve our environment to any degree we wish or can afford. Activities within this area would have to meet these requirements. No use would be prejudicially excluded or included using this approach. Each individual case would stand or fall on its own merits. It may be contended that this approach would incorporate new technology and science more readily than any other method. It would balance our economic considerations with our concern for the ecology, environment, or aesthetics. Only with an open mind, accurate information, and plenty of common sense can we hope to make the proper decisions. (5)

INTERDEPENDENCE OF ECONOMIC/ECOLOGIC FACTORS

Of high concern is the extremely complex interdependence of economic and ecologic factors. For example, a decision to stop offshore oil development on the continental shelf of the East Coast is not merely a matter of issue between Eastern residents and the oil companies. Any oil not produced from this area over the next three decades will have to be replaced by oil brought in by tankers probably from foreign sources. Thus, the risks of ecological damage in this offshore area from development must be equated to what are probably greater risks from tanker accidents in the New York, Philadelphia, or Baltimore areas. Furthermore, any gas not produced to fuel electrical generation equipment may have to be replaced by increased nuclear generation capacity to satisfy the increasing demands for electrical power.

MARINE GEODESY AND THE ENCOURAGEMENT OF PRIVATE INVESTMENT ENTERPRISE (6)

Although exploitation of the wealth of the oceans may be more firmly in our grasp through the efforts of marine geodesy, there are still many questions that need to be addressed, for example: (1) How fast can private enterprise go and what are the obstacles being encountered? (2) Should the public interest require that public programs support some private undertakings? (3) What kinds of public programs would be most effective?

The field of marine geodesy provides some answers to the scientific and technical aspects of coastal offshore, continental shelf and deep ocean resource development. In support of these physical developments, socio-economic studies such as the following need to be made: (1) The development and growth of coastal lands and marine-oriented industries. (2) Studies dealing with the efficient use of ocean resources. (3) Studies of the efficient allocation of scarce public funds for marine programs and projects.

OBSTACLES TO EXPLOITATION BY PRIVATE ENTERPRISE (6)

Although marine research is experiencing modest growth, the immediate outlook has been enhanced by the energy crisis. Despite the efforts going forward, all of this is still on a very small scale in contrast with the immense task, and compared with other programs, which, in the long run may be less promising. One might well question why industry has not made greater investments in oceanic exploitation, and why those who have made some research expenditures have not developed them into commercially successful processes. What then are these obstacles which prevent rapid development of marine resources?

1. Although it is well agreed that ocean resources are becoming increasingly valuable, there is considerable uncertainty as to when this will actually happen for various products.

2. Some hesitancy results because of the possibility that one firm may develop better technology before the original innovation is put to actual use.

3. Much of the necessary marine research is such that the whole industry may benefit from the research being carried out by a single company.

4. One of the greater deterrents to seabed exploration is the question of international jurisdiction in areas beyond our territorial limits. As mentioned above,great importance is attached to the United Nations Law of the Sea Conference being held this summer at Caracas, Venezuela.

5. There is hesitation by the financial community to make loans available for marine resource development even where early pay-off seems possible. However, this is more true with smaller companies than large corporations which are more able to reinvest profits derived from other activities such as in petroleum development, or electronics fields.

6. The outlook of the national program of ocean science and technology is uncertain.

7. There is always the possibility that alternative land resources will be developed in such a way that this would deter marine developments.

ENCOURAGEMENT OF OCEANIC EXPLOITATION THROUGH GOVERNMENT MEASURES (6)

Exploitation of the oceans, as exploration of space, requires innovations in managerial methods and government-business relations and in international cooperation. One of the objectives of a Federal marine science program, according to the Marine Resources and Engineering Development Act of 1966, is to contribute to the "encouragement of private investment enterprise in exploration, technological development, marine commerce and economic utilization of the resources of the marine environment." Although this implies a preference for private activities, nevertheless, there are functions that can best be performed by direct Government operations. These activities are summarized here:

1. There are basic needs such as mapping the ocean floors, studying characteristics of the oceans, and surveying the potential resources of the oceans, which are a prerequisite for a step-up of private activities in this field. Such activities are now carried out by Government and private (mostly nonprofit) research organizations on a small scale. Research into the potentially undesirable effects of oceanic exploitation and other activities on the oceans is a matter of some urgency. Included are such concerns as thermal pollution from nuclear or fossil fuel power plants, the concentrated bitterns of desalination plants, and numerous other forms of solid and liquid industrial and urban wastepollution.

2. There is a need for training of scientists and engineers in marine geodesy, oceanography, and oceanic engineering.

3. There is the need for developing the infra-structure for a more rapid development in oceanics, including an advanced weather service. (Here, cooperation is taking place between space research and oceanographic research.)

These three functions are of an "overhead" character for the general benefit of all oceanic exploitation to be undertaken or at least financed mainly by the Government. Some of these research activities would be desirable even if there were only a limited need for resource exploitation.

4. There is need to assist private enterprise in the development and testing of technologies suitable for oceanic exploitation. The need for Government support is based on the fact that major development investments by private industry are not likely to be adequate because of the uncertainty about the time when these investments are likely to pay off, as well as other special risks involved.

5. There is need to support research and promote international cooperation on the possible use of the products of the ocean. This is particularly the case for unconventional food, the use of which has to overcome serious obstacles.

THE CHALLENGE OF SERVING THE PUBLIC INTEREST

We are here today because each of us has some appreciation of the tremendous complexity and significance of the potentials and challenges which are before us in the offshore areas. Our aim has been to bring into clearer focus a discussion of the very important long-term task for Government and private enterprise because it deeply involves the public interest of the United States and the international community. But perhaps our friend, Dr. Barrow of Exxon whom we have referred to above, has summed up the problem of balancing interests best of all in this statement:

> What is needed today from government, from business, from science and technology, and from the private citizen is leadership which is realistic rather than dogmatic; leadership which can identify not only its own best interests but the true public interest in a given situation, and reconcile the two; and, perhaps most of all, leadership which greets change with an open mind.

FOOTNOTES: REFERENCES

(1) Speech before United Nations, September 24, 1973, See also Science, May 17, 1974, p. 780; "Kissinger on Science: Making the Linkage with Diplomacy".

(2) Adapted from talk by Dr. Lee A. Du Bridge, Science Advisor to the President, speaking before a NOAA group, February, 1970.

(3) Edward Wenk, The Politics of the Ocean (Seattle, University of Washington Press, 1972).

(4) Walter Isard and co-authors, Ecologic-Economic Analysis for Regional Development (The Free Press, New York, 1972).

(5) Thomas D. Barrow; from writings and speeches, particularly "Developing Our Coastal Zones: Economics and the Environment," Conference on Recreation and Conservation, Long Beach, Calif.,1971.

(6) Adapted from "An Overview" by Gerhard Colm in A Preliminary Review of Alternative Federal Measures of Encouraging Private Investment Enterprise in Marine Resource Development. Miller B. Spangler and co-authors, National Planning Association, 1968, Washington, D.C. (Clearing House for Federal Scientific and Technical Information, U. S. Dept of Commerce, No. PB 178 2 3).

MARINE GEODESY - PROBLEM AREAS AND SOLUTION CONCEPTS

Narendra Saxena
Department of Geodetic Science
The Ohio State University
Columbus, Ohio

ABSTRACT

This paper deals with a conceptional geodetic approach to solve various oceanic problems, such as submersible navigation under iced seas, demarcation/determination of boundaries in open ocean, resolving sea-level slope discrepancy, improving tsunami warning system, ecology, etc., etc. The required instrumentation is not described here. The achieved as well as desired positional accuracy estimates in open ocean for various tasks are also given.

1. INTRODUCTION

Since over a decade scientists have been involved with precise location of stations in the oceans for obtaining gravimetric, geophysical and oceanographic data. The first published paper, proposing a method for the establishment of such station, is the result of the research done at Lamont Geological Observatory [Ewing, et al. 1959, pp. 7-21]. Ewing called such stations as "Geodetic bench marks at sea", which were established by using the SOFAR sound transmission, by which the high geodetic accuracy could not be achieved. George Mourad [1965, p. 5-10] proposed a geodetic method for establishing the ocean-bottom bench marks, by using satellites, EDM- and sonar instrumentation. As sonar instrumentation is the only way for underwater measurements, Mourad introduced a new term "marine geodesy" to differentiate it from the classical geodesy. We will see later in sections 3 and 4 that to solve most of the problems, precisely located stations on the ocean-bottom are needed, which could be considered partial or local geodetic nets, thus the term "marine geodesy" appears to be very appropriate. We would define marine geodesy as the science which defines and establishes control-points in and/or on ocean, and the shape of the ocean, including its floor.

This paper describes a study of the published research, the drawbacks of the classical marine geodetic techniques, a conceptional approach of an ocean-bottom control-net and the problems such a conceptional approach can solve.

2. PROBLEM AREAS AND ACCURACY ESTIMATES

The problem (application) areas could be classified either according to the physical aspects of the ocean (on the oceanic surface or within oceanic water) or according to the scientific and practical needs. The following scientific problem areas have been partially mentioned in many publications [Anon, 1972b; Kaula, 1969; Loomis, 1972; Mourad and Pubara, 1972]:

a. Topography and Mapping
b. Positioning and Navigation
c. Boundary Demarcation and Determination
d. Sea-level Slope Determination
e. Tsunami Warning System
f. Recovery of Underwater Objects and Equipment
g. Ecology
h. Gravity Measurements at Ocean floor
i. Ground Truth and System Calibration.

It is worth mentioning here that our effort will be concentrated on the subsurface (underwater) problems.

a. Topography and Mapping. As the resources of the ocean bottom become more developed, the need for an extensive survey of its topography increases. Projections indicate that by 1980 a third of the oil production - four times the present output of 6.5 millions barrels a day - will come from the oceans [Anon, 1969, p. 85]. Further for laying cables and oil pipelines, for emplacing geophysical and geodetic station at the ocean floor, for determining the dump-sites and new land acquisition (similar to Hawaii Experiment to acquire land from the ocean for airport expansion), and for bathymetric navigation a reasonably good knowledge of ocean-bottom topography is necessary. How far are the oceans mapped can be realized from the following statement [Cohen, 1970, p. ix]: "When a student recently requested a government agency to send him "a map of the uncharted areas of the Pacific," he received exactly that--a graphic based on extremely sparse and dated information. It is deplorable and dangerous fact that this situation still exists in vast areas of ocean. For much of the Pacific, the most recent source of information is the United States Exploring Expedition which Lieutenant Charles Wilkes led in 1838."

b. Positioning and Navigation. Positioning and navigation can be subdivided into the following three categories:

(i) General Navigation (long range). This includes ships and other vehicles on the ocean surface. Its accuracy requirements are most probably met with the existing Navy Navigational Satellite, and in future with the stationary satellites using doppler systems. However, navigational accuracy requirements for certain fishing "boats" is ±45 m; these boats are used up to 300 miles off coast in up to 250 fathom depths [Anon, 1972b]. To achieve such accuracies better navigational systems are required.

(ii) Submersible Navigation (short range). The short range submersibles are used for underwater research, for multipurpose exploitations on the continental shelf and deep oceans. These small vehicles are usually battery operated, and are brought to the work-area from where they initiate their operation. Their navigation system is limited within 5 mile range with capability of pinpointing their position to ±1 foot in each of the three dimentions of movements; this ±1 foot accuracy is with respect to local control.

To achieve this accuracy three basic types of devices are used: sonar doppler system to obtain speed and distance, sector display system for passive target location and general collision warning, and sonar buoys for position fixing. The last system using sonar buoys is of interest to us. The conventional position determination underwater is done by emplacing three transponders on the ocean-bottom, whose known positions along with sonar range data are used to determine the unknown position of the submersible. Details of this system and its drawbacks will be dealt with in section 3.

(iii) Submersible Navigation (long-range). To this group belongs the submarines (Polaris i.e., missile and non-missile) and the submarine cargo tankers. The systems used for submarine navigation include 3 SINS (ship's inertial navigation system), Doppler and Loran-C. Due to the lack of precise information regarding submarine navigation, which is a classified area, let us evaluate the accuracies of the above mentioned systems.

Although SINS is a self-contained system, which needs no external reference, its accuracy is low, caused by an inertial drift of 108 m/hr which is accumulative with respect to time. To update SINS, doppler observations are regularly made by "popping up" the doppler pole antenna over the ocean surface after a few days, and also continuous positioning is done using Loran-C floating antenna, which always remains on the ocean surface. The positional accuracies obtained by doppler (Navy Navigation Satellite) is ± 0.22 n.m, and by Loran-C ± 0.5 miles up to 1000 miles and ± 5-15 miles beyond 1000 miles off coast [Beck, 197[illegible]. p. 48-50]. As such the total accuracy of submarine navigation can not be better than ± 0.5 miles (± 800 meter) up to 1000 miles and ± 5-15 miles beyond 1000 miles off the coast.

These accuracy estimates might be satisfactory for long-range submarine navigational requirements so far as they can obtain measurements from Loran-C and doppler. But the problem remains for the following two submarine navigational needs:

1. Submarine navigation under ice-capped oceans, where one has to depend only upon the SIN-systems, which have a drift rate of 2.6 km/day. To update SINS under iced seas, the only possible way is sonar navigation by providing ocean-bottom transponders along the desired route. Such a technique could open an easy and fast way of transporting oil from the North Slope of Alaska.

2. Short [illegible]ge submersible navigation beyond 1000 miles off coast. As the short range [illegible]mersible is brought to the work-area due to its limited 5 mile range navigation system, their "carriers" - the long-range submersibles - should have their positional accuracy within ± 5 miles when they are beyond 1000 miles. This is however not the case. Thus we require better navigational system at least for those long-range submersibles which cooperate with short-range submersibles.

c. Boundary Demarcation and Determination. The boundary demarcation could be either for national, international or commercial purposes. International boundary limits, which include national limits, for territorial seas and fishing jurisdiction are mostly within 12 n.m from the coastal line, seldom up to 200 n.m [Anon, 1972a, pp. 118-121]. Boundary determination and demarcation up to 12 n.m from the coast can be done by using EDM-Instrumentation. The demarcation in free ocean, such as 200 n.m limits, remains an unsolved problem.

Further continental shelves/slopes and free oceans are being searched for mineral resources and fuel (gas and oil). As the existing port facilities are inadequate for huge oil tankers, plans are to construct super-ports in the ocean far away from the crowded not-deep enough coastal area. Recommended are construction of large nuclear power plants in the ocean for the ocean will serve as the logical coolant [Shoupp, 1973]. A nuclear power plant is under consideration for the Pacific Ocean - off the California Coast [Hwang, February 7, 1974 - Personal Communication]. All these developments make the ocean very valuable. To accomodate all these groups interested in getting their share of ocean, it should be divided in cells and leases granted to the interested group. Leasing of cells involves legal definition of underwater boundaries and their practical demarcation becomes necessary specially when the lease bid from the oil industry went as high as $27,400 per acre [Anon., 1970a, p. 215]. According to Jones and Smith [Anon, 1970a, p. 219] an accuracy of ± 25 feet is satisfactory for practically all work performed in the development of an offshore oil field. In deep-ocean after 100 miles from the coast this accuracy is not yet available, though perhaps technologically feasible.

Thus the situation remains the same whether the boundary determination is for oil exploration, for superport site or for nuclear power plant site. Due to the high leasing costs the boundaries in the oceans have to be determined accurately up to ± 10 m.

d. Sea-Level Slope Determination. The oceanographic results, on both the Pacific and Atlantic Coasts of the U.S., indicate a slope downward to the north, with the large magnitude on the Atlantic Coast. Whereas U.S. Levelling net adjustment of 1963 indicate a rise in sea-level from south to north, with a slope of 2.8×10^{-7} on both sides [Sturges, 1974, p. 90]. A discrepancy of about 1 m exists between geodetic and oceanic levelling in north-south direction.

If a $\pm$ 10 cm accuracy could be achieved in determining the ocean depth at a particular point, i.e., between the ocean surface and the ocean-bottom transponder, the discrepancy between the geodetic and oceanic levelling could be resolved.

Once the three-dimensional position of the ocean-bottom transponders is known, change of water column height with an accuracy of $\pm$ 1 mm could be measured by the water-pressure sensor [Loomis, 1972, p. C-15]. Thus the average sea-levels for certain stations on the Pacific and the Atlantic coasts could be determined, from which the comparison of geodetic and oceanic levelling results can be made.

e. Tsunami Warning System. Tsunamis are long sea waves, which are generated by a sudden vertical faulting (shift) of the sea-floor associated either by an earthquake with its hypocenter (focus) beneath the sea bed or by a submarine landslide caused by an earthquake with its epicenter possibly on land.

The abrupt vertical displacement of sea floor is transmitted to the sea surface as a crest or a trough. The wave then propagates in all directions across the entire ocean basins with a speed, which is a function of water depth, given by $\sqrt{g.h}$, where h = water depth. In the open ocean 1000 meter deep, a tsunami wave will have the speed of 100 m/sec and the wave height is limited to a few meters, normally a few tenths of a meter according to [Bullen, 1963, p. 319-20; Loomis, 1972, p. C-9 to C-10]; and about 30 cm [Zetler, 1972, p. 26-22], but the principal wave-length may be of the order of some hundreds of kilometer, and the principal wave-period of the order of some tens of minutes [Bullen, 1963, p. 319].

As these waves approach the coastal slopes, the wave-length decreases and the amplitude increases, building up to destructive heights. In U- and V- shaped inlets the tsunami wave can reach a height of the order of 20-30 meters with an on-rush speed of above 10m/sec (36 km/hr).

Destructive tsunami waves have been almost entirely restricted to the Pacific Ocean where 90-95% have occurred [Loomis, 1972, p. C-10]. They have tended to be generated in approximately 15 specific seismic areas in the approximately 36,000 mile earthquake and volcanic belt circumscribing the Pacific; only about half of these are currently active. However, the active areas are limited to approximately 15,000 miles.

The existing tsunami warning system with headquarters at the NOAA Honolulu Observatory uses an array of 21 seismograph and 41 tide stations around the Pacific. The initial warning of a potential tsunami is the recording at the Honolulu and Tokyo Centers, of an earthquake of 7.0 magnitude or larger within the Pacific area. The location of an epicenter for such an ear. quake is usually computed in less than an hour. The tide stations near the epicenter are then asked to report their data and to confirm if a tsunami wave has actually been generated.

After reviewing the seismic and tide-guage data, and the past histories of the known tsunami origin points and their destruction areas, a decision to issue a tsunami warning is made. For localities near the epicenter warnings may be issued on seismological data only [Zetler, 1972, p. 26-27]. Two-thirds or more of all tsunamis warnings are false alarms [Loomis, 1972, p. C-11].

Thus we face three problems:

(i) Our present ability to predict tsunamis is practically unsatisfactory;
(ii) Even after a tsunami has been generated, its energy density and its velocity of propagation in open sea is impossible to predict; and
(iii) The most serious problem is the fact that the propagation velocity of tsunami in shallow areas is strongly affected by the ocean bottom topography and shore line contours, and as a result a substantial portion of energy in a particular tsunami can be focussed on a relatively small segment of the ocean shoreline, where the most destructive effects are experienced.

f. Recovery of Underwater Objects and Equipments. Scientists working with submerged instrumentation face a basic uncertainty about the recovery of the instrumentation from the ocean. Oceanographers and geophysicists have often mentioned their failure to recover most of their submerged equipment. The fact that the ocean bottom transponder net with 3 transponders-array-configuration is used in the test areas, it appears that either this 3 transpooder configuration is not functional, or the geodetic technique is not clear to the users. Whatever may be the reason, the problem to recover the valuable scientific equipment from the ocean remains to be solved.

g. Ecology. For ecological reasons trend is to dispose of the garbage in the oceans at pre-selected sites. Experiments are being conducted here in America and in Japan for finding a suitable way for ocean waste disposal. The by-products of this ecology experiment are: (i) cities have no more dump site problems, and (ii) acquisition of "new land" from the oceans; such ideas exist to obtain "new land" from the ocean for airport expansion in Hawaii.

The garbage undergoes chemical tests and treatment; before compacting the garbage in rectangular bundles, it should have a well-defined chemical composition and density. These garbage rectangular packages can then be dumped at pre-selected sites, for which a good knowledge of ocean bottom topography and a good positional accuracy of the dump vehicle (ship/boat) are necessary. Both of these requirements are lacking.

h. Gravity Measurements at Ocean Floor. Gravity work and other geophysical surveys in the oceans could neither be interconnected nor connected to a datum. According to Hendershott [Loomis, 1972, p. C-16] for meaningful results these surveys should be connected to some ocean-bottom control net, which does not yet exist.

i. Ground-truth and System Calibration. It is surprising that the existing instrumentation for measuring water depth in free ocean can not be tested for its claimed accuracy due to non-existing civilian facilities for calibration [Thompson, 1973]. However, there exist 5 naval calibration sites [Anon, 1970b, p. 118].

In Table 1 are shown the accuracy requirements for various tasks as estimated by various studies. In the last column are given our estimated accuracies.

3. SOLUTION OF PROBLEMS AND CONCEPTUAL APPROACHES

The above-mentioned problem areas can be solved by means of (A) a Global Marine Geodetic Control-Net (GMGCN) on the ocean-floor, (B) Advanced Satellite Instrumentation (ASI), and (C) Underwater Sonar Instrumentation (USI).

Table 1

Positional Accuracies Requirements [in meters]

TASKS	Chart Acc. [Cohen, 1970]	Battelle Study						Achieved	OSU Estimated Desired Accuracy+
		Desired Absolute			Desired Relative				
		ϕ	λ	h	ψ	λ	h		
Navigation:									
General Navigation (L.R.)[1]	± 3000								± 45-500
Submersible* (S.R.)[1]	± 300								± 1 m
Submersible* (L.R.)[1]	± 2000								± 500
Ocean Resources									
Geophysical Surveys (oil expl.)	± 200				± 10-100	± 10-100	± 5		± 15
Drilling	± 25				± 1-5	± 1-5	± 1-5		± 10
Pipelines					± 1-10	± 1-10	--		± 3
Cable laying	± 100				± 1-10	± 1-10	--		± 3 - ± 10
Dredging/Mining	± 25				± 2-10	± 2-10	--		± 2
Geodesy & Ocean Physics									
Control Stations	± 10	± 10	± 10	± 5	± 1	± 1	± 1		± 10
Geoid		--	--	± 0.5	--	--	± 0.1		± 0.1
Calibration Standards		± 10	± 10	± 5	± 1	± 1	± 0.3		± 1
Mean Sea Level					± 50-100	± 50-100	± 0.1		± 0.1
Stationary Buoys Loc.		± 10	± 10	--	± 10	± 10	--		± 0.1
Boundary Demarcation								± 50-300	± 10
- National									± 10
-International									± 10
-Ocean Cadastral									± 10
Ecology	± 250								± 10-50
Search & Rescue	± 25	± 20-100	± 20-100	--	± 1-10	± 1-10	--	± 12-200	± 10-20
Tsunamis									± 0.1

*Excluding Submarines - No Estimate Available
+[Jones and Sheriff, 1969; Putzke, 1969; and Anon., 1972b; Beck, 1971].
[1]L.R. = Long Range; S.R. = Short Range

a. Global Marine Geodetic Control-net (GMGCN)

The idea of a global marine geodetic control net (GMGCN) was first mentioned by Ewing and his associates [1959], and later modified by Mourad [1965]. Ewing proposed SOFAR sound transmission to measure distances between two bench-marks where a bench mark was defined as the point on or below the water surface from which the round-trip travel time to all the three ocean-bottom acoustic transpondars, placed at the corners of an equilateral triangle, would be equal. Mourad proposed geodetic (electronic distance measuring instruments), acoustic (sonar instrument) and space (satellite instrumentation) techniques.

The deficiencies of the above-mentioned systems are:

(1) The accuracies given by them are not "realistic", as these ocean-bottom arrays were neither connected to any geodetic coordinate system nor any provision was made for such a connection, which is one of the main objectives of EOPAP.

(2) Although a ship is used to determine the positions of the ocean-bottom transponders, i (ship's) coordinates are considered errorless, which are either obtai. by Navy Navigation Satellite or by airborne techniques (Lorac) to an accuracy of a few dekameters or more (30-100m) [Loomis, 1972, p. IV-6]. Thus the accuracies of transpondes positions are derived from in-error ship positions.

(3) Transponder depths are used in the computations. These are not the measured quantities, but are computed from slant ranges between the ship and the transponders. To be mathematically rigorous, the depth should be measured quantities and due weights should be applied to them.

(4) The mathematical derivations are rigorous in the beginning, but are approximated later, thus introducing modelling error.

The above mentioned deficiencies can be overcome in the following way:

(1) An ocean-bottom transponder array should consist of 4 transponders instead he conventional 3 in each array; this will avoid the singularity of the em, and also will be useable if one transponder ceases functioning. However, a study is imperative to find how many transponders are necessary in one ocean-bottom transponder array. We have also to think how these transpander arrays are placed: before emplacement of these transponders a reasonably large area (25-40 miles squares) of the ocean bottom is mapped using Depth Sounders. Then a smaller flat area proportional to its water depth is selected for transponder arrays. This water depth-flat area ratio limits the array configuration, and hence the number of transponders in each array. For practical reasons the term bench-mark should be defined physically as a particular transpander of a particular array and not as a fictitious point as defined by Ewing, et al. [1959] and Mourad [1965].

(2) The number of transponders in each array could be decreased to 3 if somehow the directions between the ocean-bottom transponders and the ocean-surface transducer could be determined. These directions would provide necessary constraint to the control-net, thus avoiding the singularity and providing a unique solution. A system to measure the directions between two sound sources can be designed with the existing technical knowledge similar to that of Electronic Angles Measurement Systems.

(3) The depths of the transponders should be actually measured, and then compared with the computed depths. The only problem in this is that there are no exactly known depths in the free ocean, which can be used as ground-truth to verify the accuracy of these modern sonar instruments [Thompson, 1973]. The instrument (Innerspace Autotrack Model 404) can measure depths up to 10,000 meters with an accuracy of $\pm$ 4.36 m. This optimistic accuracy estimate takes into account three sources of error (assuming a constant velocity of sound 4800 ft/sec.): (i) timing accuracy of the oscillator ($\pm$0.00 25%) (ii) resolution of the display ($\pm$0.3 m) (iii) reply integrator time constant (.1 to 10 ms).

However, the above accuracies are quite small compared to the effect caused by the difference between the actual and assumed velocity of sound. A 10 ft/sec velocity difference will contribute to an error of 2.04%, which is one magnitude larger than the accuracy of the system (0.04%). Thus to obtain geodetic accuracies, it would be necessary to determine a profile of the sound velocity vs. depth and then to calculate the average velocity at the location of interest.

(4) The transponder arrays should be connected to some geodetic datum, which can be achieved by using an Active Laser Satellite similar to Geole system of DIALOGUE Project [Thieriet, 1972], "floating buoy reflectors" on the ocean surface and ground-based reflectors at known stations. Thus a truly unified global network can be achieved even in the remotest ocean areas.

(5) A rigorous mathematical model is necessary, and the use of the gravity information should be made.

(6) To make the transponder arrays more versatile to be used also as a geophysical station for Tsunami warning, it should consist of a water-pressure sensor and a vertical seismometer, both of these would be on the ocean floor [Loomis, p. C-15]. A study of the essential instrumentation at the ocean-bottom transponder site to enable it a multi-purpose station is necessary, for which discussion with oceanographers, geophysicists and other users are needed.

b. Advanced Satellite Instrumentation

An active laser satellite like Geole system of Dialogue Project could be very useful. The Geole system should obtain accurate positioning of slowly moving points (like buoys) to $\pm$ 1m over one-day measurements, and to $\pm$ 10-20m every two hours from one single measurement [Thieriet, 1972]. The satellite will be at 3500 km height and will make the measurements.

c. Underwater Sonar Instruments

As the only form of radiation, which propagates effectively underwater, is sound, it is most important for underwater measurement. The sonar instruments operate on a fixed theoretical sound velocity (4800 ft/sec), although velocity of sound depends upon the conditions of the water layers (salinity, pressure, temperature) and depth of water. How to calculate the correct velocity at required depth or the average velocity during many water layers has been achieved by determining a profile of the sound velocity vs. depth, and then to calculate the average velocity.

What has not been done and should be done is to verify the accuracies of these instruments, which indirectly will involve verification of the calculated average velocity. There is no calibration range for civil scientific purposes, although five test ranges exist for naval use [Anon., 1970, p. 118].

A comparatively easy development of an acoustic instrument to determine directions between two sound sources is necessary to lessen the number of transponders in each array.

The conceptional approaches mentioned in this section can be summarized as follows:

(1) An active laser satellite around 3500 km high in circular orbit is necessary. Thus the position of floating buoys/ships could be determined within $\pm$ 1 to 10 meters, which will further improve the ocean-bottom transponder position. It will also connect the ocean-bottom transponder net to a unified global datum, and demarcate and determine the boundaries (national, international, leasing) in the open ocean to a high accuracy.

(2) Underwater sonar instruments require calibration for which a Civilian Test Range is needed. A new development to determine the direction between the sound sources is necessary so as to lessen the number of transponders in each array.

Just t illustrate how our conceptional approach can be used to solve the problems mentioned in Section 2, it will be applied to improve the Tsunami Warning System.

Conceptual Approach for an Improvement in Tsunami Warning System. As mentioned earlier that two-thirds or more of all tsunami warnings are false alarms, the existing Tsunami Warning System needs improvement.

Van Dorn [Loomis, 1972, p. C-12] suggested that stations should be located on the ocean floor (and not on the continental shelves) off the seismically active belt. He suggested a 6 station critical net as follows:

1 station off Japan
2 stations off the Aleutians
2 stations off South America
1 station off the South-western Pacific Island.

Zetler [1972, p. 26-27] mentions that if a tsunami could be detected on the open ocean, it would be very valuable to the warning system. According to Zetler, it does not seem likely that space craft/satellite measurements could be helpful for tsunami detection in open ocean.

It is quite evident that tsunami data from the open ocean is very valuable to improve the existing tsunami warning system; this could be achieved by combining laser and ocean-floor station data.

A system could be designed using the existing technology: At "suitable" locations on the Pacific ocean-floor acoustical transponder arrays could be placed. Each transponder should be equipped with water pressure sensor, vertical seismometer and other essential instrumentation to make it a multi-purpose station. On the ocean surface are placed stabilized platforms (floating buoys) whose bottom is mounted with acoustical transmitter/transponder and upper surface with a laser reflector. The active laser satellite of DIALOGUE type could position these reflectors (slowly moving objects) to $\pm$ 10 m for one measurement, and $\pm$ 1 m from one day data; the range accuracy is $\pm$ 2 m and radial accuracy $\pm$ 2 mm/sec [Thieriet, 1972].

The sonar data from the ocean-bottom transponder unit will provide the relative position of the "floating buoy" in all the three dimensions.

Note that the sonar data will be always available on command; but laser and satellite data will be available only when the satellite is in that region.

Operational Procedure: After the recording of an earthquake of 6.3 magnitude [Iida, 1970, p. 3] and consequently locating its epicenter, the ocean-bottom transponders, the surface buoys and the laser satellite will be asked to report their "height difference" data at one minute interval. Thus a complete record of the wave-height and its speed can be computed. This "sonar" height data is measured automatically and with the speed of sound, which is approximately equal to the velocity of P-waves (1.5 km/sec) [Bullen, 1963, p. 321]. Whereas the tsunami speed in open ocean of 1000 m depth is only 100 m/sec. Thus the tsunami warning - after reviewing the sonar, laser and seismic data - could be issued more reliably within minutes after the earthquake occurence.

Due to the fact that a harmless tsunami wave of the open ocean may become destructive reaching the shore depends upon the topography of the continental slope and of the continental shelf, a few transponders/floating buoys have to be located in this region.

4. CONCLUSIONS AND RECOMMENDATIONS

Although it has been shown that a multi-purpose ocean-bottom control-net can solve various problem areas, a thorough research in the following areas is urgently needed:

(a) Accuracies Available and Required. The instrumentation accuracies as given by the manufacturer have to be evaluated. This will require study of investigations done by various users using the instrument under evaluation. After this evaluation it could be decided which instruments should be used for obtaining the specific accuracies.

Also needed is a scientific survey of users' accuracy requirement. This is a very difficult task as most users do not want to discuss their desired accuracies.

(b) Simulated Network Design. A basic simulated network design by using the modern instrumentation is necessary as this is the "back-bone" of the entire operation. For such design one has to consider primarily, the users' requirements, the configuration criteria, and how best a hybrid system can be used.

The important advantage of ocean-bottom transponder net over satellites is that satellites can track for a limited time when they are above a particular station, while ocean-bottom transponders can either track continuously or can be activated on command. This is very important for tsunami warning system.

The network design can be conducted in three stages: (1) Unit Array: Configuration and number of transponders necessary in one array; the type of observations needed; type of instrumentation in each array and/or at each transponder to make it a multi-purpose station; (2) Regional Net: Configuration of transponder arrays in areas of scientific interest and in practical problem areas, like boundary determination; (3) Global Net: Eventually to plan and design a global net based upon scientific regional nets mentioned in (2) above.

The network design in each of the three stages should be connected to a geodetic datum.

(c) Ocean Surface Determination. The existing discrepancy between geodetic and oceanic levelling should be clarified. This could be done by using a regional net in the areas of discrepancies.

(d) General Navigation. Inertial navigation systems, which usually have large drift rates, can be updated with geodetic information. A study in this area, probably supplementing inertial navigation systems with gradiometers, could provide a solution to other specific navigational problems.

(e) Master Plan for Ocean-bottom Network. Looking at certain publications, it becomes clear that some users and scientists have their "own" transponder net on the ocean bottom. It will be worthwhile at least to plan a global network, using the existing scattered transponder nets, if possible.

A master plan should be prepared which should provide information about the transponder types, their locations and working frequencies, obtained data and type of data.

5. ACKNOWLEDGEMENT

I wish to thank Dr. Ivan I. Mueller for his constructive criticism and moral support for this study. I also thank Dr. Mike Fubara and Mr. George Mourad for their cooperation and discussions. Discussions regarding the practical feasibility of this conceptual approach with Drs. Bernard D. Zetler and Li-San Hwang are gratefully acknowledged. This study was supported by NASA Grant No. NGR 36-008-093.

6. REFERENCES

Anonymous (1969). The Ocean - A Scientific American Book, W. H. Freeman and Co., San Francisco, California.

Anonymous (1970a). Marine Geodesy - A Practical View, A Second Symposium on Marine Geodesy, held November 3-5, 1969, New Orleans, Marine Technology Society, Washington, D. C.

Anonymous (1970b). Present and Future Civil Uses of Underwater Sound. National Academy of Science, Washington, D. C.

Anonymous (1972a). The Federal Ocean Program. US Govt. Printing. Office, Washington, D. C., April.

Anonymous (1972b). Earth and Ocean Physics Applications Program. Vol. II - Rationale and Program Plans. National Aeronautics and Space Administration, Washington, D. C., September.

Anonymous (1972c). GEOS-II C-Band Radar System Project - Final Report: Marine Studies Using C-Band Radars. Studies performed for NASA/Wallops Sta. by Wolf Research and Development Corp. and RCA Corporation, October.

Anonymous (1972d). Radio Aids to Navigation for the U.S. Coastal Confluence Region, Interim Report No. 1 - User Requirements. Prepared by Polhemus Navigation Sciences, Inc., Vermont 05401, March.

Beck, G. E. (Ed.) (1971). Navigation Systems - A Survey of Modern Electronic Aids. Van Nostrand Reinhold London/New York.

Bullen, K. E. (1963). An Introduction to the Theory of Seismology, Third Edition, Cambridge University Press, Cambridge, U.K.

Cohen, Philip M. (1970). Bathymetric Navigation and Charting. United States Naval Institute, Annapolis, Maryland.

Ewing, M., et al. (1959). "Some Aspects of Physical Geodesy", in AGU Geophysical Monograph No. 4: Contemporary Geodesy - Proceedings of a Conference held at the Harvard College Observatory - Smithsonian Astrophysical Observatory, Cambridge, Mass., De. 1-2, 1958 edited by C.A. Whitten and K. N. Drummond.

Howell, Benjamin F., Jr. (1959). Introduction to Geophysics, McGraw-Hill Book Co., Inc., New York.

Iida, Kumizi (1970). "The Generation of Tsunamis and the Focal Mechanism of Earthquakes", in Tsunamis in the Pacific Ocean, ed. by William M. Adams, East West Center Press, Honolulu, P. 3-18.

Kaula, W. M. (Ed.)(1969). The Terrestrial Environment - Solid-Earth and Ocean Physics - Application of Space and Astronomic Techniques. Report of a Study at Williamstown, Mass. to the National Aero. and Space Adm., August.

Knowles, T. C. and R. E. Roy, Jr. (1972). "Geodetic Survey of Deep Ocean Acoustic Transponder Arrays and Evaluation of Recovered Ship Locations", Paper presented at the AGU-Fall Meeting, San Francisco, Dec. 4-7.

Loomis, A. A. (1972). Earth and Ocean Physics Applications Planning Study. Jet Propulsion Laboratory, Pasadena, California, May 17.

Mourad, A. G. (1965). "Marine Geodesy", in Battelle Technical Review, Battelle Memorial Institute, Columbus, Ohio, February.

Mourad, A. G. and Fubara, D. M. (1972). Technical Report on Interaction of Marine Geodesy, Satellite Technology and Ocean Physics, Battelle Columbus Laboratories, Columbus, Ohio, June.

Shoupp, William E. (1973). The Second Annual Sea-Grant Lecture, MIT Sea Grant Program, Massachusetts Institute of Technology, Boston, October 18.

Sturges, W. (1974). "Sea-Level Slope along Continental Boundaries", Journal of Geophysical Research, 79, 6, p. 85-90.

Thieriet, D. (1972). "The DIALOGUE Project", Centre National D'Etudes Spatiales Report No. CNES/PR/AM-DA-72-T-109, Bretigmy, May.

Thompson, Phillip R. (1973). Private Communication, July 24.

Zetler, Bernard D. (1972). "Tides and Tsunamis", in Sea-Surface Topography From Space, Vol II, Ed. by John R. Apel, NOAA Technical Report ERL 228-AOML 7-2, May.

ANALYSIS OF REAL TIME MAPPING OF HORIZONTAL AND VERTICAL GRAVITY ANOMALIES ABOARD A MOVING VEHICLE SUCH AS AN AIRCRAFT

ERNEST H. METZGER
ALBERT JIRCITANO
BELL AEROSPACE DIVISION OF TEXTRON
BUFFALO, NEW YORK

ABSTRACT

The horizontal gravity anomalies are known at the lower harmonic degrees of the earth from satellite data. However, little gravity anomaly data exists at the higher harmonic degrees which are of primary concern for high performance inertial navigation systems. Present day inertial navigators have reached a performance level where the horizontal gravity anomalies are the predominant error source.

The paper consists of two parts:

1. Definition of problem.

2. Theoretical solution of measuring gravity anomalies on a real time basis using gravity gradiometer, statistical model of gravity field, with Kalman integration of inertial navigation system. The accuracy of gravity anomaly measurements to be expected under various conditions such as vehicle speeds, altitude and gradiometer errors are discussed.

I. INTRODUCTION

This paper discusses the analysis of an airborne or shipboard gravity field mapping system for real time determination of the gravity gradient, gravity and undulation anomalies. The study was originally prompted to determine the errors induced by horizontal gravity anomalies on high performance inertial navigation systems and to explore possible approaches for correcting them. One promising method is the real time measurement of the horizontal gravity gradients and deriving the gravity anomalies from them. The main purpose of the analysis was to establish how to integrate the gravity gradient measurements with the inertial navigation system and what gravity gradiometer performance levels were required to be useful. A Kalman filter integration of the gravity gradiometer, the inertial navigation system using a statistical model of the earth gravity field was formulated and a computer analysis conducted for various vehicle velocity, altitude and instrumentation errors.

A slight variation of this system was subsequently investigated to explore how accurately the various anomalies of the gravity field could be measured using the additional information available, such as periodic position update of the inertial navigation system from external references, deterministic anomaly data of the gravity field known from surveys or satellite information and a gravity meter. This approach to moving base gradiometry is attractive in that it does not involve the development of a new instrument nor electronic or electromechanical requirements beyond the present state of the art. The rotating accelerometer gravity gradiometer rather depends on systems technique to accomplish the very difficult problem of moving base gradiometry.

The conclusion drawn by this analysis is very encouraging. A gravity field measuring system consisting of available inertial navigator and gravity meter, Kalman integrated with a gravity gradiometer could map the anomalies of the gravity field to a high degree of accuracy. The mapping could be achieved on a real time basis and hence large areas could be covered in a short time. Gravity anomaly data at the higher harmonic degrees of the Geoid would become available where at this time little information exists.

Bell is presently developing a moving base gravity gradiometer for the Technology Directorate of SAMSO USAF using a slightly modified version of the proven Model VII accelerometer mounted on a rotating fixture and hence our interest in this subject. This gradiometer is not the subject of this paper.

II. EFFECT OF HORIZONTAL GRAVITY ANOMALIES ON INERTIAL NAVIGATION SYSTEM

Horizontal gravity anomalies affect an inertial navigator in the same manner as accelerometer noise. Gravity anomalies at or near the Schuler frequency drive the Schuler Loop and cause velocity, position and attitude oscillations which generally increase as a function of the square root of time. This is schematically shown by block diagram Figure 1. Since acceleration errors predominantly propagate in the Schuler Loop and since the orthogonal horizontal gravity anomalies are not highly correlated, this simplification of an error model of the inertial system is permissible.

The latest generation of high performance inertial systems have attained a performance level where the horizontal gravity anomalies are in fact the major error source and hence the present interest in moving base gravity gradiometry. The estimated navigation velocity error of an aircraft flying at 30,000 ft and at 540 knots is illustrated in Figure 2. A gravity anomaly with a one sigma value of 40 milligals and correlation distance of 200,000 ft has been assumed. With an undamped Schuler Loop and in the absence of other errors the estimated velocity error will exceed 2 ft/sec after 4 hours of flight.

III. STRAIGHTFORWARD INTEGRATION OF GRADIOMETER WITH INERTIAL NAVIGATION SYSTEM

Multiplying the appropriate horizontal gravity gradients with vehicle velocity and subsequent time integration yields the change in the horizontal anomaly from a reference point. The instantaneous horizontal anomaly can be expressed as follows:

$$g_x = \int_o^t W_{xx} V_x \, dt + \int_o^t W_{xy} V_y \, dt + \int_o^t W_{xz} V_z \, dt + g_{xo}$$

where

g is the horizontal gravity anomaly along the x coordinate axis,

W_{xx}, W_{xy}, and W_{xz} are gradients of gravity,

V_x, V_y, and V_z are the components of the vehicle along the navigation coordinate,

g_{xo} is the reference horizontal anomaly along the x coordinate in port,

g_x is the instantaneous horizontal anomaly.

A similar expression can be written for the orthogonal horizontal anomaly g_y and the vertical anomaly g_z.

If the gradiometer had no errors, the simple process of multiplication an integration would result in perfect compensation of the horizontal gravity anomalies. However, a realistic error model must be assumed, including bias W_{bias}, white noise W_{wn} and possibly some correlated noise W_{cn}. These gradiometer errors will also be multiplied by vehicle velocity and time integrated to yield the following horizontal anomaly error.

$$g_{he} = \int_0^t (W_{Bias} + W_{wn} + W_t)\, V\, dt + g_{oe}$$

where

g_{oe} is the anomaly error at the reference point,
g_{he} is the computed anomaly error,
other terms have been defined previously.

The error block diagram for straightforward integration of a gradiometer is illustrated in Figure 3. The gradiometer error model is shown on the lefthand side exciting the Schuler Loop described previously.

Even a small bias will eventually integrate to an acceleration error larger than the gravity anomalies to be corrected. Moving base gravity gradiometry is an extremely difficult instrumentation problem, one EU producing a difference of acceleration of only 10^{-11} g at two points 10 cm apart. A gravity gradiometer bias must therefore be expected and a system devised which will tolerate this.

IV. KALMAN INTEGRATION OF GRADIOMETER AND INERTIAL NAVIGATION SYSTEM

The conventional integration of the gradiometer with an inertial system discussed in the last section cannot achieve the ultimate performance capability of the combined systems because the implied characterization of the gravity field is inaccurate. In particular, by assuming the output of the gradiometer is the gradient, the white noise and bias errors of the instrument imply a similar characterization of the physical gravity field itself. Such a view results in both the gradient and gravity anomalies having unbounded power spectra. Much is known about the statistical nature of these fields. The Kalman integration discussed in this section utilizes a more accurate characterization of the gravity field along with a modeling of the gradiometer instrument itself to arrive at an optimal integration of the gradiometer and navigation system.

The statistical characterization of the gravity gradient, gravity and height undulation anomalies which has been assumed for the Kalman filter is illustrated on Figure 4. Power spectra as a function of earth harmonic degree used with one sigma content of 24 EU, 43 milligals and 27 meters respectively. The correlation distances are 200,000 ft and 15,000 at sea level.

This characterization of the Geoid gravity anomaly field can be modelled in the frequency domain as shown by the block diagram on the right. The break points corresponding to the correlation distances are generated by feedback functions $V(1/D_1 + 1/D_2)$ and $V(1/D_1 D_2)$ respectively.

Representations of the anomaly field in this manner usually raises a number of questions since power spectra from deterministic data may not be exactly like this. A few words of how this model of the earth gravity gradient field is used is therefore in order. The white noise of the gravity gradiometer is represented in Figure 4 by a dotted line. Gradiometer bias would be represented by an infinite spike at zero frequency. The purpose of the modelled gravity gradient anomaly power spectra is to decide for which portion of the frequency domain the gravity gradiometer signal is used and for which portion the experienced horizontal gravity anomalies are allowed to disturb the navigator. At the very low frequency end (low harmonic degrees) it would be unnecessary to accept gradiometer null bias and low frequency noise when the actual gravity gradient field has little power. The same is true about the high frequency end. The gradiometer signal is only wanted where the gravity gradient anomaly field has a higher power spectral density than gradiometer noise. If errors are made in the characterization of either spectra, suboptimal filtering will occur with little change in the results, as long as the assumption is not out by orders of magnitude.

Gravity gradients diminish rapidly with altitude because of averaging effects. An extra break point has been added to the power spectra which varies inversely with altitude (V/h) and results in a reduction in the one sigma gravity gradient anomaly value to 17 EU to 20,000 ft but with representing the effect of altitude on the gravity power spectrum is an assumption at this time to show a trend.

Block diagram Figure 5 illustrates the Kalman filter integration of the gravity mapping system. The inertial navigation system is shown on the lower right hand corner. It is being disturbed by the experienced horizontal gravity anomalies and corrected by the modelled ones. The gravity field model at the lower lefthand corner is the same as discussed previously. The gradient anomaly output from the model is compared to the measured gravity gradient anomalies by the gradiometer and the difference fed to the Kalman filter. Should gradient information of the model and the gradiometer be perfect no error signal to the Kalman filter would exist or be required. However, the gravity gradiometer output will contain random noise and bias, and the gradient signal from the model will initially be zero. Hence, a correction signal to the Kalman filter will develop. The Kalman filter output corrects the gravity anomaly field model as well as the gradiometer error model.

Additional inputs for the gravity mapping field system can be obtained from deterministic undulation anomaly information from satellite observations. This would yield improved gravity anomaly mapping accuracies at the low harmonic degrees of the earth, as there is little gravity gradient information at the low frequencies. It will also be useful in reducing the settling out time in response to gravity gradiometer bias. The undulation data in this case would be stored in a computer. The output of the gravity anomaly model and the stored undulation data are compared and the difference fed to the Kalman filter similar to the gravity gradient anomaly error signal.

Position updating at the navigator is permissible for the mapping mission where secure operation is not an issue. It reduces the navigation system errors and provides additional correction signals for deriving the gravity anomaly field data. This is also shown on Figure 5.

For the vertical gravity anomaly channel, a gravity meter is substituted for the undulation anomaly map as an additional mapping aid. Precision gravity meters such as the BGM-2 (Bell Gravity Meter) are excellent for measuring vertical gravity anomalies in the low frequency domain, but require fairly long time constant filters to remove higher frequency noise and vehicle accelerations. The vertical gravity anomaly output of the model on the other hand yield good data at higher frequency. Figure 6 is a block diagram of the vertical axis Kalman filter integration of the gravity anomaly mapping system.

V. RESULTS OF COMPUTER ANALYSIS OF GRAVITY ANOMALY MAPPING SYSTEM

An error model of the gravity anomaly mapping system outlined in the previous section was analyzed with a computer to program the accuracies to which gravity gradients, gravity and undulation anomalies could be measured. Two principle cases were selected, at sea level travelling at 20 knots and at 30,000 ft flying at 300 knots.

The computer program is flexible and amenable to characterizing of each subsystem performance with bias, white and colored noise. Gyro drift, accelerometer bias, undulation map accuracy, gravity meter performance and updating were characterized as described below on Table I. The gradiometer noise, being the object of this analysis, was varied from 1 to 5 EU as measured over a 10 second period for the airborne case, and 5 to 20 EU for the shipboard case. No biases were introduced for this because the mapping system compensates for bias after an initial settling-out period. The analysis so far has been carried on limited in-house funds and we have not been able to investigate even a small fraction of the conditions the system is capable of evaluating.

A. DISCUSSION OF RESULTS

The computer derived horizontal and vertical gravity anomalies as a function of gravity gradiometer noise is shown on Figures 7 and 8. Gravity gradiometer noise is defined by the one-sigma randomness as measured over a 10-second period. The gradiometer noise spectrum has been assumed to be white for this analysis. The role of the gravity gradiometer for deriving the horizontal gravity anomalies and the vertical ones are different and separate discussions for the two cases are given.

1. Horizontal Gravity Anomalies

Figure 7 shows that at sea level and low speed a 10 EU gravity gradiometer will result in accurate mapping of the horizontal gravity anomalies to better than 4 milligals. For the

high-speed airborne case on the other hand a 1 EU gravity gradiometer is required. There are two reasons for this.

a. At lower speed the Kalman integration provides longer time constant filtering for the gradiometer noise because the gravity anomaly power spectrum is translated from the spatial to the frequency domain by vehicle velocity.

b. There is less power in the gravity anomaly field at higher altitudes because of averaging effects, and hence less accurate mapping of the higher harmonics of the gravity anomalies is possible.

Not explicit in this data is the fact that the horizontal gravity anomalies are very accurately mapped at the higher harmonic degrees of the geoid where little information is available at the present. The region of accurate mapping is defined by the intercepts of the gravity gradiometer white noise and the gravity gradient anomaly power spectra shown on Figure 4. The remaining mapping error of the horizontal gravity anomalies as shown on Figure 7 lie in the intermediate region of harmonic degrees where the undulation map has little information and the gravity gradients are small. A better undulation anomaly map than assumed for this analysis in combination with a 1 EU gravity gradiometer could result in near perfect mapping of the horizontal gravity anomalies.

A few additional observations can be made. Position update of the inertial navigator, which for this analysis bounded the navigation error to a one-sigma value of 220 ft. does not significantly help in the gravity anomaly determination for the airborne case. For the sea-level case the position update measures the raw gravity anomalies of 42 milligals to about 28.9 milligals without using a gravity gradiometer.

The primary purpose of the undulation anomaly map for this analysis was to assist in the settling out of initial conditions. Near steady-state values were achieved in 12 hours at slow speed and 1.5 hours in the aircraft travelling at 300 knots.

2. Vertical Gravity Anomalies

The relationship between the mapping accuracy of the vertical gravity anomalies and gravity gradiometer noise is illustrated on Figure 8. The primary roll of the gravity gradiometer in this case is to furnish gravity anomaly data at the higher frequencies where the vertical acceleration of the vehicle prevents accurate gravity determination with a gravity meter alone. A rather severe vertical acceleration input of 0.1 g one sigma with a correlation time of 15 seconds has been assumed.

For the shipboard case the determination of vertical gravity anomalies deteriorates to 3.73 milligals without a gradiometer. Since it is unlikely that mapping mission would take place under the vertical accelerations assumed (50 ft. waves at sea for example) there is little need for a gravity gradiometer. This is born out by the survey data obtained by the U.S. Navy for the BGM-2 (Bell Gravity Meter).

A good gravity gradiometer with a noise of 1 EU would make accurate airborne gravimetry possible. The reason for the deterioration of vertical gravity anomaly data with a gravity meter alone is similar to the one given for the horizontal anomalies. Less smoothing of the vertical vehicle acceleration is permissible at higher speed.

Good knowledge of the altitude of the mapping vehicle has been assumed.

B. CONCLUSION

A moving base gravity gradiometer would make accurate real-time mapping of the geoid gravity anomaly field possible using available gravity meters and inertial navigation systems. A gravity gradiometer with a performance of 1 EU as measured over a 10-second period will be required for high-speed airborne gravity mapping vehicle while a 10 EU gravity gradiometer will suffice for the sea-level low-speed case.

With Kalman integration of the subsystems and using the best statistical and deterministic data of the geoid the horizontal gravity anomalies should be measurable to less than 4 milligals and the vertical gravity anomalies to 1 milligal.

Deterministic data of the undulation and gravity gradient anomalies would become available in addition to the gravity anomalies at the higher harmonic degrees of the geoid where little information is available at this time.

TABLE I

	SHIPBOARD - SEA LEVEL		AIRBORNE
	20 KT - SEA LEVEL		300 KT - 20,000 FT
		MAGNITUDE	CORRELATION TIME
GYRO DRIFT	1σ	0.001°/HR	1/2 HR
ACCELEROMETER NOISE	1σ	10^{-5} g	1/2 HR
UNDULATION MAP ERROR	P_D	(0.5 FT)²/HARMONIC DEGREE	
GRAVITY METER	P_D	$(10^{-6}$ g)²/RAD/SEC	
POSITION UPDATE	P_D	(5200 FT)²/RAD SEC	
EQUIVALENT	1σ	220 FT	
GRADIOMETER NOISE		P_D	1/10 SEC
		(3.1 EU)²/RAD/SEC	1 EU
		(15 EU)²/RAD/SEC	5 EU
		(63.2 EU)²/RAD/SEC	20 EU

P_D = POWER SPECTRA DENSITY

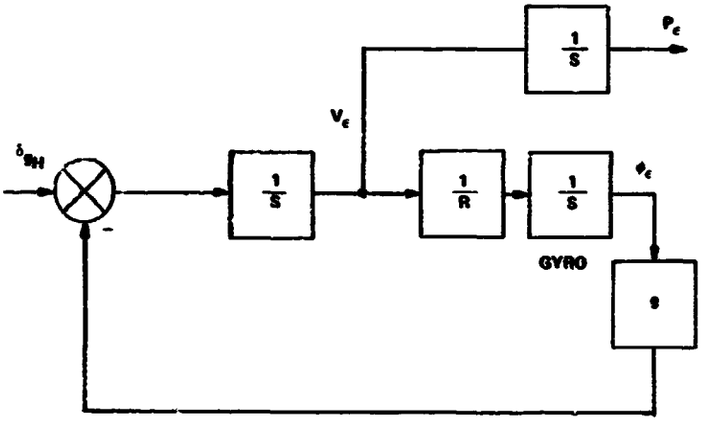

Figure 1 Horizontal anomalies driving Schuler Loop.

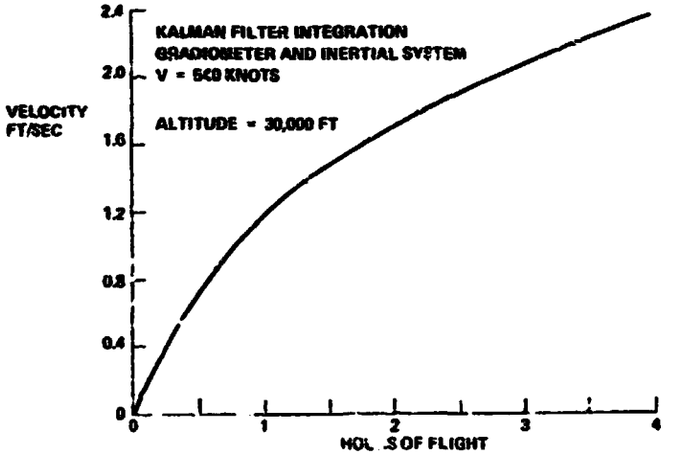

Figure 2. Velocity caused by horizontal gravity anomalies as a function of time.

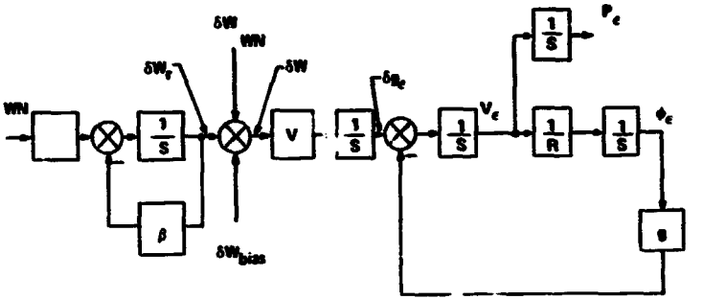

Figure 3. Straightforward integration of gradiometer and inertial system.

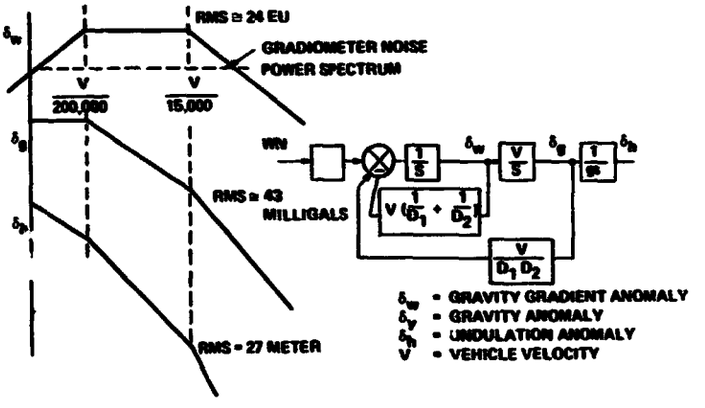

Figure 4. Characterization of gradient, gravity and altitude anomalies of Geoid.

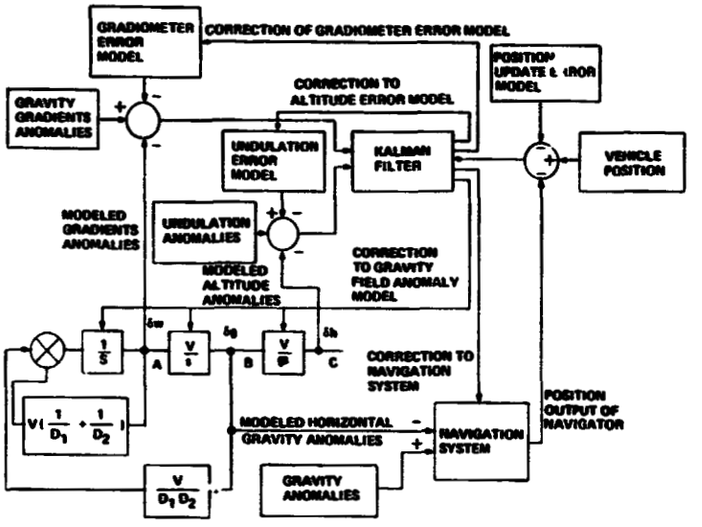

Figure 5. Block Diagram - Horizontal Gravity Anomaly Mapping System

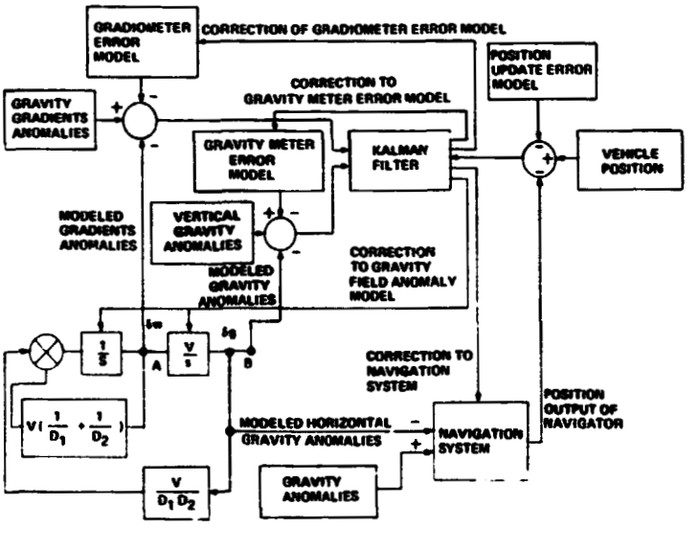

Figure 6. Block Diagram - Vertical Gravity Anomaly Mapping System

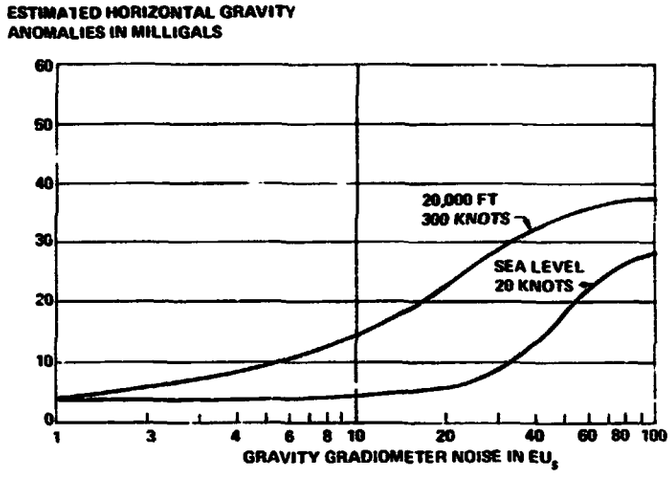

Figure 7. Estimation of horizontal gravity anomalies as function of gravity gradiometer noise.

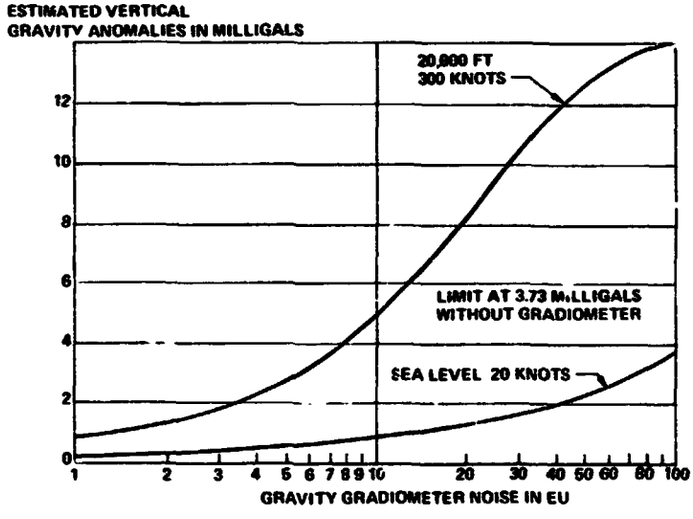

Figure 8. Estimation of vertical gravity anomalies as function of gravity gradiometer noise.

GEOID DEFINITIONS FOR THE STUDY OF SEA SURFACE TOPOGRAPHY FROM SATELLITE ALTIMETRY

R. S. Mather
The University of New South Wales
Sydney, Australia

ABSTRACT

The satellite altimeters proposed for the GEOS-C and SEASAT missions have the potential to provide valuable information which could lead to the eventual definition of sea surface topography. In the first instance, this paper concentrates on the development of techniques for obtaining geoid definitions from mixed data sets consisting of oceanic "geoid heights" deduced from the altimetry, and gravity anomalies largely in continental areas, from solutions of the geodetic boundary value problem. It discusses how data subject to significant systematic errors with substantial wavelengths can be successfully used in the quadratures evaluation of such solutions.

Arguments are outlined for the incorporation of gravity field models with errors at the 5% level in the disturbing potential, in the system of geodetic reference. The adoption of such a procedure would permit a common model to be used both in the solution of the boundary value problem, as well as in orbit determination, on reinforcement with the appropriate resonant terms. The adoption of such a procedure would be an important first step in minimizing the influence of systematic errors in the gravity model on determinations of sea surface topography. The advantage of quadratures methods in high precision determinations lies in the elimination of prohibitive matrix inversion problems, provided conditions for convergence can be established by appropriate modification of the data acquisition procedures.

1. INTRODUCTION

The successful operation of the altimeters on the GEOS-C and SEASAT missions (NASA 1972) could well open up a new era in which high precision techniques in geodesy may provide opportunities for the eventual achievement of some financial return on the high instrumentation capital outlay for obtaining the observational data. Important tasks are the determination of sea surface topography (APEL 1972) and a systematic assessment of its variation with time. The term sea surface topography is used to define the departure of the sea surface from an equipotential surface of the Earth's gravity field. The existence of such phenomena on a quasi-stationary basis has been implied from meteorological and other oceanographic data (e.g., STURGES 1972) in open oceans, and apparent stationary values deduced along coastlines from the comparison of the results of geodetic levelling and tide gauges (e.g., HAMON & GREIG 1972). It should be stated that the sea surface topography deduced in the latter instances is the subject of controversy in that it is not consistent in several cases with the magnitudes estimated from oceanographic considerations (GODFREY 1973; STURGES 1973).

The geostrophic effects associated with significant ocean currents give rise to sea surface topography at the 1-2 m level, which could be detected and monitored by satellite altimetry if:

(a) the instantaneous geocentric position of the sea surface were known at the 10 cm level; and

(b) the ocean geoid were defined with respect to the geocentre to ±10 cm for obvious reasons (e.g., see MATHER 1973b, figure 1 for an illustration). Such monitoring could have potential cost benefit, especially in navigation if, for example, an accurate knowledge of ocean circulation could save even 1% of fuel consumption. Such economies, when assessed in terms of projected growth in world trade over the next 80 years, even on 1972 fuel costs, could well amount to hundreds or millions of dollars per year (source of figures - NAE 1972).

At the present time, the global network of tracking stations is available to permit the determination of the geocentric position of a spacecraft to ±10 cm. Relative orbit determinations over restricted areas are, however, possible where the radial component of the orbital position can be determined with a precision equivalent to those of the tracking systems, even though the along track component is more weakly determined by about an order of magnitude (AGREEN & SMITH 1973). The principle error source in this case is the uncertainty in the definition of the gravity field used to model the spacecraft's perturbations.

The altimeter on GEOS-C is expected to have a resolution of ±50 cm in the short pulse mode. It is the expectation that the use of 10 cm laser tracking systems to observe the spacecraft during altimetry should define the changes in the radial component of the satellite's position at the resolution level of the altimeter. Such data could be used to study sea surface topography in limited areas of interest, where the phenomenon is significantly larger than the noise level of the altimeter, provided a geoid profile with suitably small relative error between the terminals could be defined.

Areas of interest in these terms are the north-east coast of Australia (ROELSE ET AL 1971) and the Gulf Stream (STURGES 1972). While the existence of the latter has been deduced from oceanographic considerations, the former is the subject of controversy and an independent evaluation could provide fresh insights into the nature of the coastal phenomenon. While altimetry does not provide an exact verification of coastal comparisons, it could be a source of independent information on whether or not the discrepancies are purely coastal in nature, and whether they are in any way correlated with aspects of the inter-relations between the coastline and the shelf sea-bed. Successful resolution of this phenomenon, even on a local basis, would provide pointers on how best to initiate experimentation in this area using the SEASAT mission altimeter which are expected to have a resolution about 5 times in excess of the instrument on GEOS-C (NASA 1972).

The difficulties encountered in sea surface topography determinations at the present time using the above methods are the following:

1. A model for the variations in the disturbing potential at the surface of the Earth is still unknown at the 1% level.
2. The geocentric position of the spacecraft cannot be defined as yet at the decimetre level.

One of the major goals of the GEOS-C mission is the improvement of the definition of the gravity field (CHOVITZ 1972). Broadly speaking, the altimeter data h is fitted to a set of orbital parameters a_i and a set of gravitational field parameters g_i using observation equations of the form

$$v = h_c - h + dr + \left(\frac{\partial \vec{r}_s}{\partial a_i} c_{ai} + \frac{\partial \vec{r}_s}{\partial g_i} c_{gi} - \frac{\partial \vec{r}}{\partial g_i} c_i \right) \cdot \vec{u}_n \qquad (1),$$

where $\vec{u}_n$ is the unit vector normal to the ocean surface, $\vec{r}_s$ and $\vec{r}$ are the geocentric vectors to the satellite and sub-satellite point on the ocean surface, dr is a radial offset term due to orbit determination error, and c_{gi}, c_{ai} being the corrections to the adopted parameters.

Another set of equations similar in form could be constructed around the laser ranges ℓ from the tracking station to the spacecraft. The altimetry could therefore be used conceptually in this manner to determine the corrections c_{gi} to the representation afforded by the adopted coefficients g_i and thereby improve the definition of the gravity field. This type of approach could be used either with spherical harmonic models or a variety of other representations such as surface density models (e.g., KOCH 1970), sampling functions (LUNDQUIST

& GIACAGLIA 1972), etc.

It is obvious that *this* stage, where it is hoped to improve the gravity field model largely by using satellite altimetry data in the sparsely surveyed ocean regions, must *precede* the geoid determination which is needed for the definition of sea surface topography. The precision eventually sought is ±10 cm, though only at wavelengths equivalent to the satellite altimetry (say, 100 km footprints). An representation of the gravity field which can provide a geoid definition with this degree of resolution requires about 10^4 - 10^5 parameters for adequate modeling (MATHER 1973a,p.75). It would appear that significant problems have to be overcome in the practical use of modeling techniques involving so many parameters in the context of the computer technology available at present.

Alternatively, it would be more practicable to compute the required result from solutions of the geodetic boundary value problem using data representing 10^5 - 10^6 surface elements provided the data were not subject to systematic errors of long wavelength (IBID,p.67-8). Solutions proposed for this problem at the 10 cm level have acknowledged the possibility of only a single type of data, i.e., gravity anomalies. On present indications, the types of data available for solutions of the geodetic boundary value problem will be:

(a) gravity anomalies, mainly in continental areas; and

(b) "geoid heights" derived from altimeter ranges.

The inter-relations between evaluations from these two types of data within the framework of a solution of the geodetic boundary value problem capable of defining the geoid in oceanic areas to ±10 cm, are discussed in section 3.

A discussion on the acceptable limits of accidental errors and systematic effects in the data type (a) above is available (IBID,pp.63-9). Section 4 deals with the specific problems likely to be encountered when evaluating the result using quadratures procedures for geoid heights in oceanic areas.

Section 5 looks at the problems encountered in sea surface topography determinations from satellite altimetry and the available gravity data with a view to obtaining the best possible geoid definitions for this purpose.

2. GUIDE TO NOTATION

A_n = set of surface harmonics of degree n in the representation of T
$d\sigma$ = element of solid angle
$f(\psi)$ = Stokes' function
G_n = set of surface harmonics of degree n in the representation of Δg_c
$M\{X\}$ = global mean value of X
$M(\psi)$ = $-(1 + 3 \cos \psi)$
N = ocean geoid height (= ζ in oceanic regions)
N_1 = Stokesian contribution to ζ
N^s = indirect effect
R^c = geocentric distance; subscript $_p$ refers to point of computation
$\bar{R}$ = radius of Brillouin sphere
$\bar{r}$ = $2\bar{R} \sin \frac{1}{2}\psi$
T = disturbing potential of solid Earth and oceans
$\bar{T}$ = T on Brillouin sphere
$\bar{T}_n$ = set of surface harmonics of degree n in the representation of $\bar{T}$
U^n = potential on surface of rotating equipotential reference ellipsoid
V^c = potential of atmosphere
W_o = potential of the geoid
α_o = azimuth
γ = normal gravity at Earth's surface
Δg = gravity anomaly at the surface of the Earth

Δg_c = $\Delta g + 2(V/R) + \partial V/\partial h + (\bar{R} - R)(\partial \Delta g/\partial h) + o(f \Delta g)$

$\overline{\Delta g}'$ = $\Delta g_c - 2(W_o - U_o)/R$

ζ = height anomaly (equal to geoid height in oceanic regions)
ψ = angular distance at geocentre between computation point and $d\sigma$

2. SOLUTIONS OF THE GEODETIC BOUNDARY VALUE PROBLEM FROM ALTIMETRY DATA

A solution has been proposed for the geodetic boundary value problem which is capable of defining the oceanic geoid to ±10 cm, provided sufficient gravity data were available (MATHER 1973a). This solution has been developed so that:

(a) the location of the reference ellipsoid used in defining the gravity anomalies is known in relation to the geocentre (Earth's centre of mass);
(b) spherical harmonic representations are used in the *intermediate* modeling of parameters *only* under conditions where Laplace's equation is satisfied;
(c) orthogonal properties of surface harmonic representations are used *only* under circumstances where such relations hold without approximation;
(d) the ellipsoidal reference figure is recognized; and
(e) the relevant topographic effects are allowed for.

For consistency, this requires that the potential of the atmosphere V and its gravitational effects be separated from those of the solid Earth and oceans before computing the disturbing potential T and using it in the basic equations relating the gravity anomaly Δg to the height anomaly ζ and the gradient of the disturbing potential. It is also necessary that the topography (i.e., elevations) can be considered to constitute a continuous field in a two dimensional sense, at the surface of the Earth, which is also assumed to be non-singular. A similar condition is also considered to apply to the *disturbing potential* at the surface of the Earth.

It would not be unreasonable to adopt these assumptions in the case of ocean geoid determinations as most of the problems arise when disturbed regions, where these conditions may not be fulfilled on a scale equivalent to that of the element of surface area used in the quadratures evaluation, are close to the point of computation.

The resulting solution can be expressed conceptually in the form

$$N = N_s + N_c \qquad (2),$$

where N_s is the Stokesian term, given by

$$N_s = \frac{W_o - U_o}{\gamma} - \bar{R}\frac{M(\Delta g_c)}{\gamma} + \frac{\bar{R}}{4\pi\gamma}\iint f(\psi)\,\Delta g_c\,d\sigma \qquad (3),$$

all terms being defined in section 2. The form of N_c is given in (IBID,p.45).

It is conservatively estimated that over 90% of the power in the solution is contained in what is commonly called the free air geoid, given by equation 3 with Δg_c replaced by the gravity anomaly Δg. The use of a "higher" system of reference which models the Earth's gravitational field more closely than the gravitating equipotential ellipsoid of revolution, is also possible as discussed further in section 5 (MATHER 1974). $\bar{R}$ in equation 3 is the radius of the Brillouin sphere which is concentric with the reference ellipsoid and includes all the Earth's topography. The solution outlined in equation 2 is oriented towards defining the ocean geoid to ±10 cm concomitant with the requirements of sea surface topography determinations, but from a global coverage of gravity anomalies with an uncorrelated error of representation of ±3 mGal, equivalent to a 10 km grid in non-mountainous areas.

Complete oceanic coverage of gravity anomalies still appears to be a long range goal which will probably not be realised in time for the SEASAT missions at the end of the decade (NASA 1972). An alternative type of data which should be available for the representation of the gravity field in oceanic areas are the "geoid heights" inferred from satellite altimetry to the ocean surface. The quotation marks are used because the heights deduced refer to those of the ocean *surface* above the reference figure. The former cannot be assumed to coincide with the ocean geoid. These differences, which may be characterized by amplitudes of 1-2 m and wavelengths which could be as large as 80°, require careful consideration when attempting the definition of the geoid

with a resolution which is possibly *an order of magnitude smaller*.

In the first instance, consider the relevance of the definition of the boundary value problem which is the inverse of that due to Stokes (i.e., gravity anomalies from geoid heights in the case of a spherical Earth with no matter exterior to the bounding equipotential), generally attributed to Molodensky (MOLODENSKII ET AL 1962,p.50). The main deficiency in using this approach for sea surface topography definition is that the gravity anomalies so computed (in what is presumably an intermediate stage in the use of a solution of the type described by equations 2 and 3) do not contain an estimated 20% of the signal - largely contributions of short wavelength - which are damped out as a consequence of the nature of input altimetry which represent finite area footprints. Further, the use of this kind of information in a subsequent direct solution of the geodetic boundary value problem is a rather exhaustive computational process. In addition, as integration is implied over the surface of the Earth and distant zone effects, having long wavelength characteristics, are not negligible, the continental areas require representation and have to be dealt with in a manner similar to that described in section 4.

Useful information can be obtained by formulating a solution of the boundary value problem where the dominant contribution provided by the Stokes term, with over 90% of the power of the solution, can be obtained by quadratures evaluation based on "geoid heights" from satellite altimetry data, rather than gravity anomalies; the former is a data type which should hopefully provide global oceanic coverage of adequate precision (see section 4), at least in the next decade.

To achieve the objective of a replacement for equation 3 which represents the dominant effect, by one which can handle "geoid heights" from satellite altimetry, subject to the limitations outlined above, it is necessary to go back to the basic equation from which it is derived(MATHER 1973a,p.37)

$$T_s = \frac{1}{2\pi}\iint \frac{\bar{R}^2}{\bar{r}} \sum_{n=0}^{\infty} \frac{2n+1}{2} \frac{A_n}{\bar{R}^{n+2}}\, d\sigma, \quad n\neq 1 \qquad (4),$$

where A_n are the set of surface harmonics in the spherical harmonic representation of the disturbing potential T of the solid Earth and oceans *exterior* to and *on* the surface of measurement, which is the surface of the Earth to the order of accuracy required for geoid determinations (±10 cm), given by

$$T = \sum_{n=0}^{\infty} \frac{A_n}{R^{n+1}}, \quad n\neq 1 \qquad (5).$$

Other symbols are explained in section 2. On defining $\Delta g'$ as

$$\Delta g' = \sum_{n=0}^{\infty} (n-1)\frac{A_n}{R^{n+2}}, \quad n\neq 1 \qquad (6),$$

which takes the values $\overline{\Delta g'}$ on the Brillouin sphere, given by

$$\overline{\Delta g'} = \sum_{n=0}^{\infty} (n-1)\frac{A_n}{\bar{R}^{n+2}} = \sum_{n=0}^{\infty} G_n, \quad n\neq 1 \qquad (7),$$

where G_n is a set of surface harmonics, it can be recognized that

$$\sum_{n=0}^{\infty} \frac{2n+1}{2}\cdot\frac{A_n}{\bar{R}^{n+2}}, \quad n\neq 1 = \overline{\Delta g'} + 3\bar{T}/2\bar{R} \qquad (8).$$

In the generalized Stokesian treatment which has equation 3 as its end-product, the procedure adopted is to use equation 7 to transform equation 4 into the form

$$T_s = \frac{1}{2\pi}\iint \frac{\bar{R}^2}{\bar{r}} \sum_{n=0}^{\infty} \frac{2n+1}{2(n-1)} G_n \, d\sigma, \quad n \neq 1,$$

whose solution is (IBID,p.41)

$$T_s = 2(W_o - U_o) - \bar{R}\, M(\Delta g_c) + \frac{\bar{R}}{4\pi}\iint f(\psi)\, \Delta g_c \, d\sigma \qquad (9),$$

the relation between Δg_c and $\overline{\Delta g}'$ being given in section 2.

It can be seen that the adoption of a surface harmonic representation for Δg_c (i.e. effect) gave a solution which is in terms of a kernel containing Δg_c and Stokes' function $f(\psi)$. It would be equally valid to adopt a surface harmonic representation

$$\bar{T} = \sum_{n=0}^{\infty} \frac{A_n}{\bar{R}^{n+1}} = \sum_{n=0}^{\infty} \bar{T}_n, \quad n \neq 1 \qquad (10)$$

for T on the surface of the Brillouin sphere and obtain a solution of equation 4 in terms of a kernel containing T (and hence N in oceanic areas to which it is related by the generalized Bruns equation (IBID,p.25)

$$N = \frac{1}{\gamma}\left(T - (W_o - U_o)\right) + V + o(10^{-3}m) \qquad (11)),$$

and some function of ψ, say $M(\psi)$, such that

$$\frac{\bar{R}^2}{\bar{r}}\left(\overline{\Delta g}' + \frac{3\bar{T}}{2\bar{R}}\right) - \bar{R}\, f(\psi)\, \Delta g_c = M(\psi)\bar{T} \qquad (12)$$

on surface integration, as both Δg_c and T are harmonic on the Brillouin sphere. The form of $M(\psi)$ can be obtained as follows. On adopting the zonal harmonic expansion

$$\frac{1}{\bar{r}} = \frac{1}{\bar{R}} \sum_{n=0}^{\infty} \left(\frac{R_p}{\bar{R}}\right)^n P_{no}(\cos\psi) \qquad (13)$$

for r^{-1}, separating the term of zero degree from the other terms, and on using the orthogonal properties of surface harmonics on the Brillouin sphere, the inclusion of equation 10 in equation 4 gives

$$T_s = \frac{\bar{T}_o}{4\pi}\iint \frac{\bar{R}^2}{\bar{r}} d\sigma + \frac{1}{2\pi}\iint \sum_{n=2}^{\infty} \frac{2n+1}{2}\left(\frac{R_p}{\bar{R}}\right)^n P_{no}(\cos\psi)\, \bar{T}\, d\sigma \qquad (14),$$

which can be written as

$$T_s = M(\bar{T}) + \frac{1}{4\pi}\iint M(\psi)\, \bar{T}\, d\sigma \qquad (15).$$

The use of the relation at 13 gives

$$M(\psi) = 2\bar{R}\left\{\frac{1}{\bar{R}} \sum_{n=2}^{\infty} [n+1 - \tfrac{1}{2}]\left(\frac{R_p}{\bar{R}}\right)^n P_{no}(\cos\psi)\right\}$$

$$= 2\bar{R}\left\{-\bar{R}\,\frac{\partial}{\partial \bar{R}}\left(\frac{1}{\bar{r}} - \frac{1}{\bar{R}} - \frac{R_p\cos\psi}{\bar{R}^2}\right) - \frac{1}{2}\left(\frac{1}{\bar{r}} - \frac{1}{\bar{R}} - \frac{R_p\cos\psi}{\bar{R}^2}\right)\right\}.$$

Differentiation and evaluation as $R_p \to \bar{R}$, when $(\bar{R} - R_p\cos\psi) \to 2\bar{R}\sin^2\tfrac{1}{2}\psi$, and $\bar{r} \to 2\bar{R}\sin\tfrac{1}{2}\psi$, gives

$$M(\psi) = -(1 + 3\cos\psi) \qquad (16).$$

Thus the adoption of the expression

$$N_s = \left\{ \begin{matrix} \frac{W_o - U_o}{\gamma} \\ M(\overline{T}) \end{matrix} \quad - \overline{R}\,\frac{M(\Delta g_c)}{\gamma} \right\} + \frac{1}{4\pi\gamma} \left\{ \begin{matrix} \iint \overline{R}\, f(\psi)\, \Delta g_c \, d\sigma \\ \iint M(\psi)\, \overline{T}\, d\sigma \end{matrix} \right. \qquad (17),$$

where

$$\overline{T} = \gamma N + \frac{\partial T}{\partial h}(\overline{R} - R) - V + o\{(\partial^2 T/\partial h^2)(\overline{R}-R)^2\} \qquad (18),$$

all quantities being described in section 2, define alternative methods of computing the Stokesian contribution, providing over 90% of the signal, in solutions of the boundary value problem using *either* gravity anomalies *or* "geoid heights" from satellite altimetry.

If the kernels in the two integrals were interchangeable a simple answer would be provided to the complex problem of quadratures evaluation of the boundary value problem when data of different types is available for the representation of different areas on the surface (e.g., gravity anomalies in continental areas and "geoid heights" over oceans). Such interchange is unfortunately invalid because the existence of surface distributions of $\overline{T}$ and Δg_c is implicit in the derivations of these expressions when utilizing the properties of surface harmonics in integrations on the surface of the Brillouin sphere. The lower alternative in equation 17 is nevertheless of value in studying the role sateilite altimetry can play in geoid determinations for the evaluation of sea surface topography.

3. QUADRATURES EVALUATIONS OF THE GEODETIC BOUNDARY VALUE PROBLEM FROM LARGELY ALTIMETRIC DATA

Either alternative in equation 17, when used in the proper context in equations 2 and 3, is capable of providing oceanic geoid determinations to ±10 cm *provided the data is good enough for the purpose*. For example, in determinations from gravity anomalies, a goal of ±30 cm precision in N would require that the errors in the values adopted for the representation of one degree squares to be held to below ±3 mGal (MATHER 1973a,table 2) with no correlation between the errors in the representation of contiguous squares, calling for an even sampling of the gravity field in the square with 15-20 readings. Similarly, the magnitude of correlated errors in gravity anomalies which have nodal points about 500 km apart should on the average be less than 0.5 mGal.

For gravity observations which, at the present time, tend to represent continents and their immediate environs only, the principal sources of such errors are due to:

- elevation datums not lying on the same equipotential surface (geoid);
- *gravity standardization network errors; while these are estimated* at present to only be about 0.2 mGal (MORELLI ET AL 1971), they are likely to cause errors with long wavelength due to the large spacing between stations in the network; and
- the use of regional geodetic co-ordinates instead geocentric values to compute normal gravity; this effect is at noise level for 10 cm determinations.

In the case of evaluations from "geoid heights" deduced from altimetry data, the extent of systematic error will depend on the nature of

(a) the errors in orbit determination;
(b) the error sources effecting the altimetry itself; and
(c) the departures of the sea surface from the geoid.

From the dominant contribution to the second alternative in equation 17, it can be shown that the effect of an error $e_s^{(m)}$ in the "geoid height" which behaves as a systematic error over an $n^\circ \times m^\circ$ area, but exhibits accidental error characteristics over larger areas, will affect the final computed value of the Stokesian term N_s by $e_N^{(cm)}$, given by

$$e_N^{(cm)} \doteq 1\tfrac{1}{2}\, e_s^{(m)} \times (n^\circ \times m^\circ)^{\frac{1}{2}} \qquad (19).$$

Variations of the effect with amplitude and wavelength of the error are summarized in table 1 for ease of reference.

TABLE 1
Influence of Systematic Effects on Quadratures Computations of Stokesian Contribution from "Geoid Heights" (Relation 19)

e_a (m)	$(n^\circ \times m^\circ)^{\frac{1}{2}}$ (deg)	e_N (cm) 1	5	10	50
0.1		1/10	½	1	6
0.2		1/5	1	2½	12
0.5		½	3	6	31
1		1	6	12	62
2		2½	12	25	125
3		3½	18	40	185
5		6	30	60	320
10		12	60	120	620

While recognizing that orbit determination is the result of batch processing using numerical integration procedures, it could be broadly stated that there are two conceptual possibilities when attempting to assess the effect of orbital errors on e_N:

- the spacecraft is tracked during the altimetry such that the orbital position is determined with a precision equivalent to that of the tracking system; or
- no direct tracking of spacecraft is available during the period of the altimetry; the orbital position in this case being deduced from the best available models for the force fields influencing the orbit.

In the second case, it is generally held that the main weakness in modeling the relevant force fields is from the gravity field (AGREEN & SMITH 1973). For example, it has been estimated at 2-5 m in the case of GEOS-C (WEIFFENBACH 1972), the dominant effects being due to wavelengths greater than 50°. A favourable solution for the geoid at a ±1 m level is the best that can be expected in such a case, provided the larger error estimates occur with shorter wavelengths. Such a result would hardly be of use in the resolution of sea surface topography in global terms.

At the other extreme, a planned global network of *at least* 25 tracking stations with all weather capability and 10 cm resolution may hopefully reduce the orbital uncertainty to an equivalent magnitude. The use of altimetry data obtained under circumstances of continuous tracking, should reduce the uncertainty in the ocean geoid to an acceptable limit in terms of the reckoner embodied in table 1, provided

a) oceanographic effects of long wavelength and amplitudes in excess of 50 cm have been allowed for; and
b) any altimeter bias as large as 1 m has wavelengths of less than 20°.

There are two types of oceanographic effects which cause concern when using altimetric "geoid heights" in quadratures evaluations:

- the likelihood of climatic effects being correlated with latitude, thereby exhibiting characteristics of even degree zonal harmonics if magnitudes were of order ±50 cm (e.g., see STURGES 1972,fig. 1); pronounced features with significant wavelengths like the Gulf Stream (NASA 1972,fig. 4.3); and
- oceanic tidal models.

It appears possible to iterate the evaluations of the second alternative in equation 17 to convergence in an acceptable manner using data satisfying the above conditions, provided the errors in the computed geoid introduced in the "geoid heights" by the existence of sea surface topography could be held to amplitudes of not more than ±1 m and wavelengths of upto 100°. This would enable sea surface topography to be determined to ±50-60 cm for the second iteration, giving favourable conditions for a geoid determination to ±30 cm. It can be concluded that between three and four iterations of equation 17 should enable a geoid to be determined to ±10 cm from altimetry of adequate accuracy, measured from spacecraft tracked continuously by 1 cm systems, provided all sea surface topography with amplitudes in excess of 1 m and wavelengths greater than 80° have been modeled. In the case of the minimal 25

station configuration discussed earlier, the conditions for convergence in the iteration of equation 17 will depend on the resolution of the best gravity model available. In this case, any substantial weakness in the gravity model will have to be improved in the iterative process to improve the "geoid heights" obtained from areas where no direct tracking is possible.

The discussion so far has assumed that altimetry is available on a global basis. This is not the case. If, as discussed in section 5, a "higher" reference model than that afforded by an equipotential ellipsoid of revolution were used, $\bar{T} = o(5\ kGal\ m)$, though possibly correlated through positive values. This correlation could be reduced significantly by using spherical cap calculations out to say, 20° using the surface gravity anomaly representation available over land, when

$$T_s = \frac{R}{4\pi} \int_0^{2\pi} \int_0^{\psi_o} f(\psi)\ \Delta g_c \sin\psi\ d\psi\ d\alpha \qquad (20),$$

as the contribution of the harmonic representation of the gravity field through the Molodensky truncation functions (MOLODENSKII ET AL 1962,p.148) is substantially zero when the "higher" reference model is used. The gravity field representation required for 10 cm solutions is a 10 km grid in non-mountainous areas (MATHER 1973a,p.78).

The weakness in the values of $\bar{T}$ so computed in continental areas arises from the assumption that the "higher" reference model has completely absorbed distant zone effects. This is no problem if conditions are favourable for convergence of solutions. As geoid definitions will be preceded by gravity field definitions from GEOS-C data, we can hopefully talk in terms of these errors having a 1-2 m magnitude resulting in a quadratures error of ½ - 3/4 m. Convergence is therefore likely to occur.

5. THE DETERMINATION OF SEA SURFACE TOPOGRAPHY FROM SATELLITE ALTIMETRY

The recovery of sea surface topography from satellite altimetry with confidence is one of the most exacting tasks facing not only specialists in orbit determination but also those defining oceanic geoids. The phenomenon on the basis of both oceanographic considerations (e.g., STURGES 1972; HAMON & GREIG 1972; STURGES 1973) as well as coastal evidence (see MATHER 1973b for a summary) appears to have magnitudes of 1-2 m, but with rather long wavelengths, including effects which may be expected to have the characteristics of even degree zonal harmonics.

In the absence of an ideal situation where the spacecraft is continuously tracked by 10 cm systems, a weakness will arise in the orbit determination if the gravity field representation is not adequate. As mentioned previously, long wave gravity field improvements and orbit determination has to precede sea surface topography evaluation until such time as a gravity field representation adequate for 10 cm geoid determinations (i.e., value adopted for the representation of a 100 km square has an uncorrelated error of around ± ½ mGal) becomes available. In the interim, it is desirable to adopt every possible procedure which would play some role in minimizing the effect of systematic errors in both orbit and geoid determinations so that the effect on the sea surface topography determinations are minimized, at least, on a relative basis.

A procedure mentioned in section 4 and worth serious consideration, is the adoption of a system of reference in physical geodesy which is of a higher order than that afforded by a rotating equipotential ellipsoid of revolution. Desirable criteria for such a "higher" reference model are the following:

- It should be equivalent to the gravity model commonly used in orbital analysis at satellite altitudes.
- It should have a clearly defined geometry in Earth space for solutions of the geodetic boundary value problem at the surface of the Earth.
- The effects of the common gravity model adopted for both the orbital analysis as well as the ocean geoid computations should be clearly separated from the consideration of individual gravity values so that

no unintentional ambiguity is possible on use in solutions of the geodetic boundary value problem.

Such a *procedure* would be worthwhile if the "higher" reference system were to provide an accurate representation of the long wave features of the gravity field in the light of the arguments advanced in section 4. Present day solutions may well provide a definition of such features with errors at the 5% level. It would be no surprise if the uncertainty in the terms of long wavelength were, at least in part, a function of distance from sites in the tracking station network. For example, geoid solutions based on Goddard Earth Model 6 (GEM 6) have an average discrepancy of around 0.2 m when compared with values derived from geometrical satellite geodesy at 158 tracking stations (MUELLER 1973,p.202). On the basis of these considerations, it is not unreasonable to assume that the adoption of the concept of a "higher" reference model would reduce the magnitude of T by a factor of 20. The geometry of such a system in Earth space has been defined for solutions of the geodetic boundary value problem (MATHER 1974,section 2).

The following points which are relevant to the present development, are summarized from the above reference:

- If the "higher" reference model is restricted to long wave phenomena, say 500 coefficients for global representation (similar to present-day gravity field representations), the magnitude of the gravity anomaly on this "higher" reference system is not substantially smaller, even though changes in T with position at the Earth's surface over limited areas are at the 5% level. For example, see (MATHER ET AL 1971) for determinations in Australia on a 50 km grid using gravity data on a 10 km grid. The advantages of a "higher" reference model are thus only of marginal significance in such circumstances for other aspects of quadratures evaluations.
- The effect of a given error in the gravity field definition has different consequences through geoid and orbit determinations respectively, on the computed *differential* sea surface topography along the altimetered profile. The former is affected largely through higher frequency term errors while the latter is influenced more by errors in resonant terms, while low frequency errors affect both determinations but not to the same extent. The effect of gravity field errors on the definition of sea surface topography through geoid determinations is a function of the inter-relation between these errors and the ground track of the satellite; the effect through orbit determination is due to orbit distortion in the absence of direct tracking, due to the *rate of change* of the radial error as evaluated through the equations of orbital motion.

It can be concluded that in instances where the gravity field definition is not adequate for determinations of the global geoid to ±10 *cm*, it is preferable that any local determinations of specific features of sea surface topography be based on:

(a) *a common model* for the long wave components of the Earth's gravity field; and
(b) an adequate representation of the *regional surface* gravity field.

Such determinations cannot be carried out satisfactorily *on a relative basis* unless the local gravity field is adequate for the purpose (i.e., a 10 km grid in the region is most desirable).

6. REFERENCES

AGREEN, R.W. & SMITH, D.E. 1973. A Simulation of the San Andreas Fault Experiment. *Doc. X*-592-73-216,Goddard Space Flight Center,Greenbelt Md.

APEL, J. (ed.) 1972. Sea Surface Topography from Space. *Tech.Rep.* ERL 228-AOML 7,National Oceanic & Atmospheric Administration,Boulder Colo.

CHOVITZ, B.H. 1972. Refinement of the Geoid from GEOS-C Data. *Op.cit.supra.* 2-1 - 2-8.

GODFREY, J.S. 1973. Mean Sea Level: The Oceanographer's Point of View. *Proc. AAS/IAG Symposium on Earth's Gravitational Field & Secular Variations in Position*,Univ. of New South Wales,Sydney,560-564.

HAMON, B.V. & GREIG, M.A. 1972. Sea Level in Relation to Geodetic Land Leveling Around Australia. *J.geophys.Res.* 77(36),7157-7162.

KOCH, K.R. 1970. Gravity Values for Continental Shelf Areas from Satellite Altimetry. In SIGL, R.(ed.) *Report on the Symposium on Coastal Geodesy.* Technical Univ.,Munich,567-572.

LUNDQUIST, C.A. & GIACAGLIA, G.E.O. 1972. Geopotential Representation with Sampling Functions. In "The ' se of Artificial Satellites for Geodesy". *Monograph* 15,American Geophysical Union,Washington DC.

MATHER, R.S. 1973a. A Solution of the Geodetic Boundary Value Problem to Order e^3. *Doc.X*-592-73-11,Goddard Space Flight Center,Greenbelt Md,128 pp.

MATHER, R.S. 1973b. The Influence of Sea Surface Topography on Geodetic Considerations. *Proc. AAS/IAG Symposium on Earth's Gravitational Field etc.*,Univ. of New South Wales,Sydney,585-599.

MATHER, R.S. 1974. On the Solution of the Geodetic Boundary Value Problem for the Definition of Sea Surface Topography. (To be published).

MATHER, R.S., BARLOW, B.C. & FRYER, J.G. 1971. A Study of the Earth's Gravitational Field in the Australian Region. XV General Assembly, IAG, Moscow 1971. In *UNISURV Rep.* 22,Univ. of New South Wales,Sydney,1-41.

MOLODENSKII, M.S., EREMEEV, V.F. & YURKINA, M.I. 1962. *Methods for Study of the External Gravitational Field & Figure of the Earth.* Israel Program for Scientific Translations,Jerusalem,248 pp.

MORELLI, C. ET AL 1971. *The International Gravity Standardization Network 1971.* XV General Assembly, IAG, Moscow 1971.

MUELLER, I.I. 1973. In "Discussion on Session C". *Proc.AAS/IAG Symposium on Earth's Gravitational Field etc.*,Univ. of New South Wales,Sydney,202.

NAE 1972. *Towards Fulfilment of a National Ocean Commitment.* Marine Board, National Academy of Sciences,Washington DC.

NASA 1972. *Earth & Ocean Physics Applications Program,* Vols 1 & 2, National Aeronautics & Space Administration,Washington DC.

ROELSE, A., GRANGER, H.W. & GRAHAM, J.W. 1971. The Australian Levelling Survey, 1970-1971. *Tech.Rep.* 12,Division of National Mapping,Canberra,81 pp.

STURGES, W. 1972. Comments on Ocean Circulation with Regard to Satellite Altimetry. In "Sea Surface Topography from Space". *Tech.Rep.* ERL 228-AOML 7-2, National Oceanic & Atmospheric Administration,Boulder Colo., 24-1 - 24-17.

STURGES, W. 1973. Discrepancy Between Geodetic and Oceanographic Levelling Along Continental Boundaries. *Proc.AAS/IAG Symposium on Earth's Gravitational Field etc.*,Univ. of New South Wales,Sydney,565-572.

WEIFFENBACH, G.C. 1972. An Observational Philosophy for GEOS-C Satellite Altimetry. In "Sea Surface Topography from Space". *Tech.Rep.* ERL 228-AOML 7,National Oceanic & Atmospheric Administration, Boulder Colo., 1-1 - 1-9.

SKYLAB S-193 ALTIMETER EXPERIMENT PERFORMANCE, RESULTS AND APPLICATIONS

J.T. McGoogan and C.D. Leitao
NASA Wallops Flight Center

L.S. Miller
Applied Science Assoc. Inc.

W.T. Wells
Wolf Research and Development Corp.

ABSTRACT

A description of the SKYLAB Altimeter instrument system along with the appropriate system error model is presented. The data processing flow, orbit computation, and topographic recovery techniques are discussed. Some data analysis results are presented which indicate excellent correlation with underwater topographic features. In addition, results are shown which indicate that the instrument performance was as expected.

INTRODUCTION

The S-193 satellite altimeter experiment was conducted in 1973 and 1974 during the SL2, SL3, and SL4 missions for which the primary objectives of the altimeter were to obtain data needed for design of future altimeters and to demonstrate that the instrumentation did have a capability for surface topography mapping. These topographic measurements have significant applications to marine geodesy.

Both the scientific value and the application were emphasized in the Terrestrial Environment, Solid Earth and Ocean Physics study held during August 1969 [2]. Presently the NASA Earth and Ocean Physics Applications Program (EOPAP) has adopted a long range physical ocean sensing program with objectives that rely heavily on satellite altimetry.

In all of these activities to date the role of altimetry has been visualized to include detection of dynamic ocean features (tides, waves, currents, etc.) or mapping permanent topography (geoid). However, even though it was realized that the subsurface topography has a contribution to the geoid, results obtained with the SKYLAB altimeter have shown that this correlation might well be stronger than anyone realized. In fact these correlations could well lead to new applications of altimetry for positioning and density determination of underwater topographic features.

INSTRUMENT SYSTEM

The instrument system geometrically consists of a space platform (the SKYLAB satellite) and a radar altimeter oriented to make vertical (nadir) measurements of the distance to the ocean surface. While the SKYLAB orbit (440 km height, eccentricity .001 and inclination 50°) was not an ideal reference system for long arc geodetic measurements, it did represent an excellent test bed for altimeter sensor development and short arc topography measurements. The low

orbit, payload weight and size capacity made it possible to build a radar system with good signal-to-noise and instrument versatility and flexibility. Therefore the S-193 altimeter system was optimized to provide a variety of measurements under various operating parameters. Within the hardware [8], five basic modes were developed to perform various pre-set data taking and calibration operations to gather data needed to design improved altimeters for future space missions. Basically the five experimental modes can be summarized as follows:

TABLE 1. SKYLAB ALTIMETER MODES

Mode	Unique Features	Prime Data Generated
1. Pulse Shape	.5° Step in Antenna Position Wide Receiver Bandwidth	Sample and Hold Altitude AGC
2. σ_0 (Radar–Cross–Section)	12 db Step (AGC Calibration) Antenna Position 0°, 1/2°, 15.6°, 8°, 3°, 1.5°, 0°	Sample and Hold AGC
3. Time Correlation	Two Pulsewidths Double Pulse Operation Spacings 1, 19.2, 17.8, 153.8, 409.6, 819.1 (Micro Seconds)	Sample and Hold Altitude
5. Pulse Compression	Three Pulsewidths 10 ns 10 ns (compressed) 100 ns	Sample and Hold AGC Altitude
6. Nadir Alignment	Slow Spiral Drive	AGC

The most important measurements provided by the altimeter consist of altitude, waveforms and Automatic Gain Control voltage (AGC). The altitude measurements are made approximately 8 times per second with a 2 Hz bandwidth tracking system. The spatial footprint (spot size) is about a 3 KM radius for the narrow pulse operation which represents a two dimensional filter for topography mapping missions.

The waveforms are sampled by eight moveable sample-and-hold gates placed at regular intervals on the return signals. These gates can sample the return waveform 100 times per second and can be utilized for wave height and antenna pointing angle estimation.

The AGC is available approximately 4 times per second and is useful to calibrate the above waveforms, to detect clouds, rain and other anomalies which affect signal strength.

For mapping the ocean topography [5] a typical system error model has been produced. (See Table 2.) Both the uncorrected magnitude and the residual, of the best known corrections are that applied to the data are shown so that one can appreciate the importance of the various error sources.

It is readily apparent that pointing and bias are the two factors most critical to mapping topography. Since short arcs are being used and feature mapping can be accomplished in the presence of bias the pointing errors are considered the most critical. The pointing is continually changing and without correction would yield errors that cannot be easily separated from the short wavelength topography. Therefore methods have been developed to extract pointing information from the altimeter waveforms and to apply corrections to the altitude data based on this information.

TABLE 2. TYPICAL SYSTEM ERROR MODEL & RESIDUALS

	UNCORRECTED MAGNITUDE	ERROR SOURCE	CORRECTED DATA RESIDUALS
1. INSTRUMENT ERRORS Systematic	Up to 50 meters	Zero set error, discriminator drift, servo unbalance, operating parameter changes	< 10 m (Correcting for operating parameters only)
	≃1 cm	Timing Errors	≃1 cm (No correction suggested)
	≃30 cm	Transit Time Error	<1 cm
	Up to 40 cm	Dynamic Lag Error K_a = Servo Acceleration Constant K_v = Servo Velocity Constant	< 10 cm (Using waveform analysis during high dynamic conditions)
	≃1 cm	Scaling Factor h_{os} = Oscillator Frequency Error h_1 = Velocity of Light Error	≃1 cm (No correction suggested)
Random	Up to 70 cm	σh_t = Height Thermal Noise $\sigma h_t = \frac{T\sqrt{7/8 + \frac{6}{s/n} + \frac{8}{(s/n)^2}}}{\sqrt{\frac{prf}{\pi b}}}$	≃30 cm (Where features permit more averaging can be applied)
	1 to 5 cm	σh_q = quantizing error = $\frac{\text{Bit weight}}{\sqrt{12}}$	
2. POINTING	Up to 30 meters	Off Nadir Pointing	< 1 m (If trailing edge is used to generate off nadir position)
3. OCEAN SURFACE	Up to .75 m	Electromagnetic MSL vs MSL	< 10 cm (If waveheight is known to 25%)
4. ATMOSPHERE	Up to 2 meters	Atmospheric refraction path delay	< 10 cm (If temp., pressure and humidity are known)

DATA PROCESSING

The PCM analog tape is converted by NASA JSC to a digital format and both editing and decommutation is performed. In addition, the airlock module time (AMT) of each frame of data is converted to GMT. The raw altimeter two-way range bit data (20 bits) is converted to measured altitude bit data (21 bits) by making the 21st high order bit a one if the 20th high order bit is a zero. Finally, the following algorithm is used to convert bits to kilometers [1]:

$$A_m = [(21 \text{ bits}) \times BW + ID] \times (C/2)$$

Where: BW = bit weight, 2.5×10^{-9} sec/bit,

ID = estimate of the internal delay
40×10^{-9} sec for SL-2,3
-195×10^{-9} sec for SL-4, and

C = speed of light, 299792.5 km/sec.

A processed digital tape with frame GMT, measured altitude and other altimeter measurements, statuses and housekeeping data is sent to approved Principal Investigators.

The tape received from JSC is converted to a format compatible with Wallops' Honeywell 625 Computer. Then, the following algorithm is used to preprocess the altitude data:

$$A_c = A_m - (ID \times \frac{C}{2}) + (PC\text{-}M) + MC - R$$

Where: A_c = corrected altitude,

A_m = measured altitude provided by JSC,

ID X C/2 = correction to remove internal delay correction made by JSC,

PC = premission calibration of delay line,

M = inflight measurement of the delay line,

MC = error caused by switching pulsewidths, bandwidths and pointing within certain modes and submodes, and

R = tropospheric refraction correction.

The magnitude of the different corrections vary. For example, the inflight calibration correction used is 35.97 m with an uncertainty of less than 20 cm detected in inflight measurements of the calibration delay line. The pulsewidth/bandwidth correction varies from 0 to 103 ns depending on the mode and submode used, and the pointing angle correction being used in Mode 1 is 13 ns. The refraction model[3]

$$R = \frac{2.7'(N)}{328.5\ (.026 + \sin E)}\ ,$$

assumes a constant surface refractivity of 340 N units, and E is 90 degrees when looking at nadir. This results in a correction of 2.79 m.

Unified S-Band (USB) data and in some cases C-Band data are used to estimate orbital parameters. The orbital elements are used as initial conditions to integrate an orbit from which altimeter measurement residuals are calculated. The residuals are the differences between the altimeter measurements to the sea surface and the calculated altitude from the spacecraft to the ellipsoid. Finally, the altitude residuals, and both the Marsh Vincent Geoid and ocean bottom topography along the subsatellite track are plotted for further analysis. Both qualitative and quantitative correlations are evaluated and reported to the scientific community. Figure 1 illustrates the data flow.

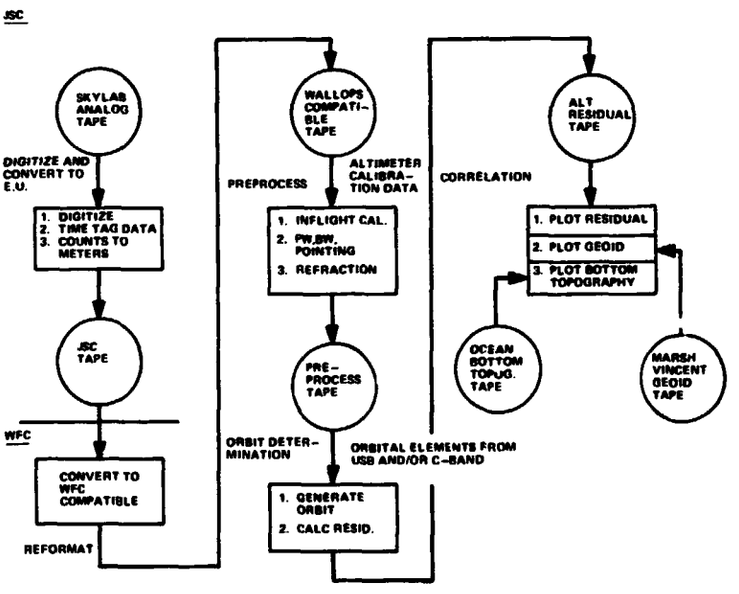

Figure 1. Skylab Altitude Data Flow

DEFINITIVE ORBIT DETERMINATION FOR SKYLAB ALTIMETER DATA ANALYSIS

Analysis and evaluation of the SKYLAB altimeter data, can best be accomplished by reducing the measurements to quantities which can be compared with independently derived data. Since the ocean surface, except for tidal and wind effects follows an equipotential surface, it is convenient to derive an estimate of the geoid height from the altimeter altitude measurements. These can then be compared with independent determination of the geoid height. The relationship between geoid height and satellite altitude measurements is given by:

$$h_g = h_s - h_a - \Delta_h$$

Where h_s = satellite height above a reference spheroid obtained from the satellite orbit determined from tracking data,

h_a = satellite altitude measured by the altimeter,

and Δh = dynamic ocean effects of tides, winds and currents.

The relationship of these quantities is shown in Figure 2.

It is obvious from this relationship that any radial orbit errors will propagate directly into errors in geoid heights determined from the data. Therefore, for analysis and evaluation of the SKYLAB altimeter data it was necessary to obtain the most accurate orbit possible from the available tracking data.

Several factors make the determination of accurate SKYLAB orbits a difficult task. The altitude of the SKYLAB orbit is approximately 440 KM and its effective area is 293 square meters with a mass of 87,441 Kg. These factors mean that atmospheric drag has a large effect on the satellite orbit. In addition, thrusting is used for spacecraft maneuvers both before and after the altimeter data is acquired. The tracking data is provided by the Goddard Space Flight Center, unified S-Band System (USB) with some C-Band support. The USB system is a worldwide system but due to workload and scheduling every station did not track at every opportunity and hence the density of tracking data is sometimes sparse in the vicinity of an altimeter data take.

Error analyses have shown[4] that in order to minimize systematic error effects due to drag, thrusting and geopotential errors, the length of arc fitted should be kept as short as possible. The arc length necessary to be able to determine an orbit with reasonably low error depends on the available tracking coverage. Experience has shown that this can vary from 2 hours (SL-2 Pass 6) to 25 hours (SL-2 Pass 4). The difference in the effects of systematic errors on these two orbits is estimated to be less than a meter due to drag on the 2 hour orbit and 50 meters on the 25 hour orbit.

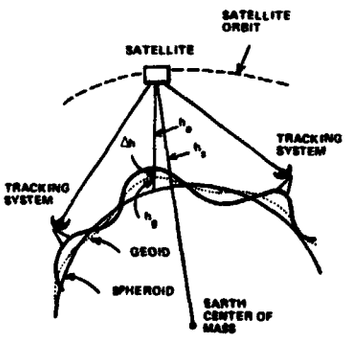

Figure 2. Relationship Between Altimeter Measurements and Geoid.

RESULTS

The following pages present some selected samples of the results which have been obtained from an analysis of the altimeter data. Some additional results can be found in [6].

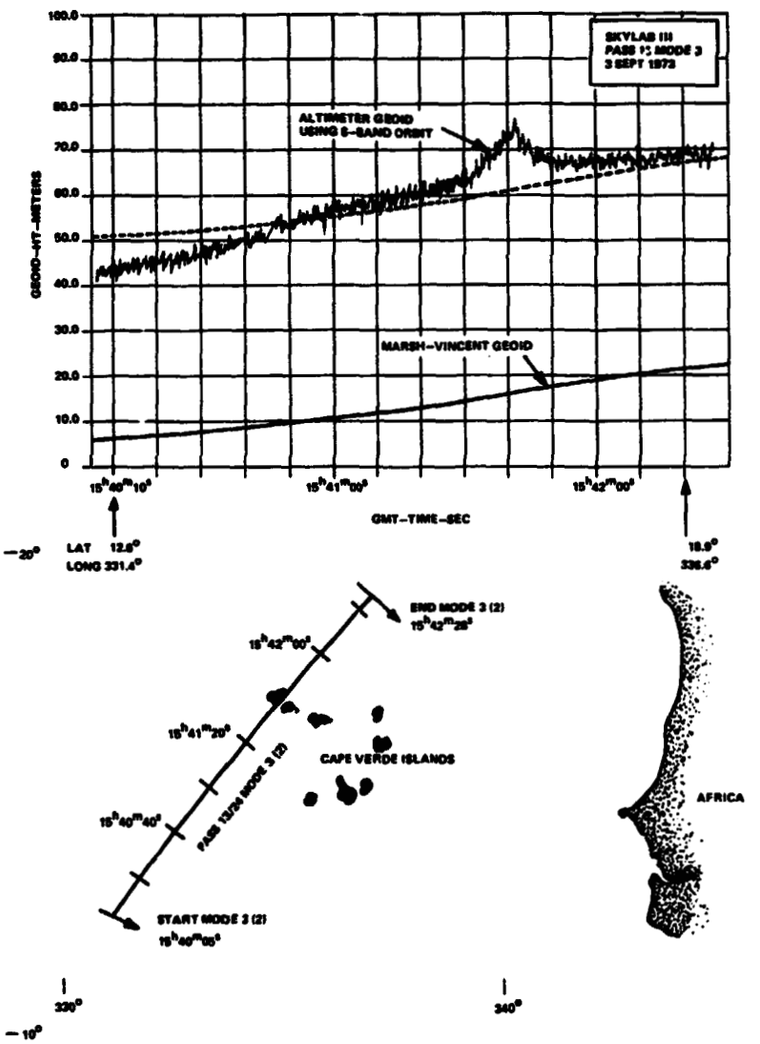

Figure 3. Skylab Altimeter Pass Over the Cape Verde Islands

Figure 3 shows a pass of data over the Cape Verde Islands obtained on 3 September 1973. For comparison the Marsh Vincent Geoid [10] is shown on the graph. The absolute difference between the altimeter geoid and the Marsh Vincent geoid of approximately 45 meters is well within the estimated orbit uncertainty. The dotted line on the graph is the Marsh Vincent geoid shifted for shape comparison. It is seen that the overall comparison is good except for the 12 meter undulation in the vicinity of the islands. A detailed analysis of the altimeter footprint, noise characteristics, and ground track indicate that the altimeter was not over land during any part of the pass. It is estimated that dynamic sea surface effects could explain only a few meters of the undulation observed and hence we surmise that the geoid undulation observed is a real feature in the geoid.

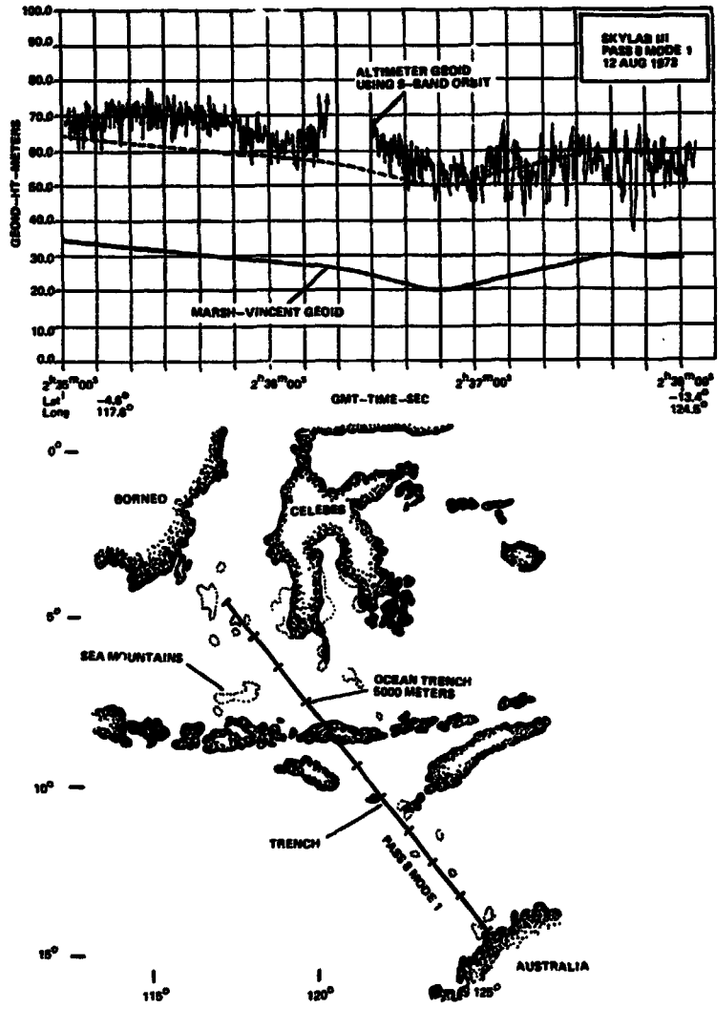

Figure 4. Skylab Altimeter Pass Off the Coast of Borneo.

Figure 4 presents the results of a pass of altimeter data taken on the SL-III mission on 12 August 1973 off the coast of Borneo. The noise level is somewhat higher than usual but again there is overall good general shape agreement with the Marsh-Vincent geoid. Matching the ground track with the altimeter geoid it is seen that geoid undulations correlate very well with the sea mountains and ocean trenches. It is to be expected that these short wavelength features would not be seen in the Marsh-Vincent geoid. The loss of data around 2h 36m 20s is due to a loss of lock as the altimeter passed over the island of Flores.

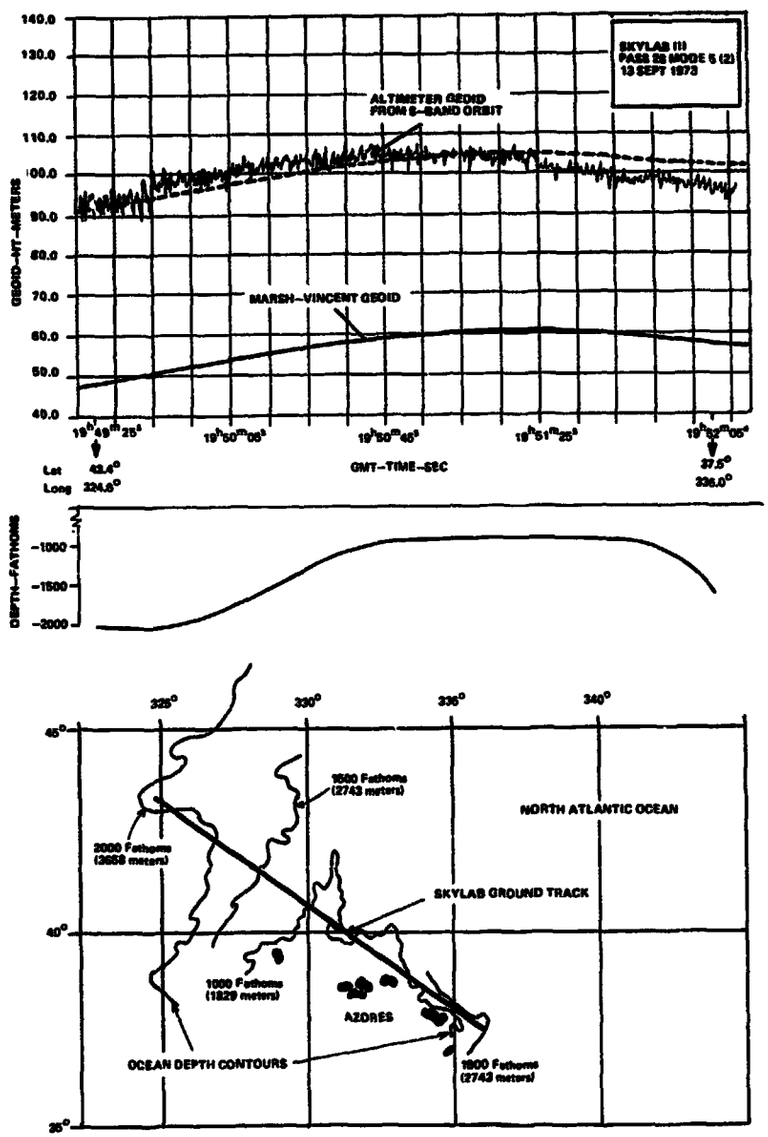

Figure 5. Skylab Altimeter Pass Over the Mid-Atlantic Ridge in the North Atlantic

Figure 5 illustrates the altimeter derived geoid for a pass of data taken on the SL-III mission on 13 September 1973. This data was taken as the altimeter passed over the Mid-Atlantic Ridge in the North Atlantic. Again there is excellent agreement with the general shape of the geoid and the offset is well within the expected orbit accuracy. A comparison of the altimeter geoid with the bottom topography in the area again shows excellent correlation. The ocean depth contours shown were obtained from [9].

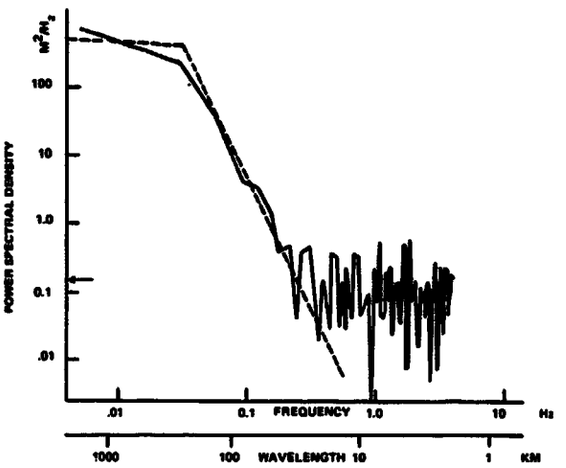

Figure 6. Power Spectral Density (PSD) of the Puerto Rican Trench

Figure 6 displays a power spectral density (PSD) of the Puerto Rican Trench region which was computed using Fourier Transform methods and a Hanning type convolution window. The data base comprised SL-2, Pass 4, Mode 5 with 100 and 130 nanosecond pulse widths (pulse compression was not functioning during SL-2). The Puerto Rican Trench data was used since we desired to obtain PSD results for an anomalous region, which should contain more energy in short-wavelength components than anomaly free regions. The PSD so obtained, and data processing results derived therefrom should represent the best opportunity for the altimeter to obtain information relating to short wavelength undulations.

Referring to Figure 6, the arrow corresponds to the density level for which a 3.3 Hz. rectangular bandwidth, white noise spectrum would yield an rms level equal to one meter. Since the S-193 tracker has an approximate 3.3 Hz. equivalent noise bandwidth, this level is consistent with observed rms noise levels in the raw data of 1 to 2 meters, and a cross-check on the computed spectral magnitude. The level is seen to be close to the noise level implied by the calculated spectrum. We also note that the spatial filter function [6] arising from the finite zone illuminated by the altimeter, corresponds to considerably shorter wavelengths (less than 10 km) and that the calculated PSD should not be contaminated by the altimeter footprint.

The PSD data given may be used to derive altimeter data-processing guidelines. Under the assumption of Gaussian statistics, or if a minimum-mean-square linear estimate is desired; the Wiener-Hopf formulation for additive noise measurements shows that the optimum filter $H_o(f)$ transfer function is

$$H_o(f) = \frac{S(f)}{S(f) + N(f)}$$

where S(f) is the geoidal spectrum and N(f) is the additive noise spectrum. Figure 6 shows an approximation to S(f) as a break-point plot using

$$S(f) = \frac{5.24 \times 10^{-4}}{f^4 + 1.75 \times 10^{-3}}$$

solving for the half-power value of $H_o(f)$ we find it to be 0.164 Hz.

Using the satellite ground track velocity, this may be expressed as a 45 km wavelength. Therefore, we conclude that this analysis shows for geoidal regions which contain pronounced short wavelength components, that (1) the Skylab altimeter is limited by measurement noise in profiling wavelengths much below 45 km and (2) data smoothing time constants of several seconds are required to adequately reduce the random error in geoid undulation measurements. This analysis can readily be extended to yield two-sided weighting functions [7], which are applicable to smoothing solutions using both past and future observations--as is appropriate for digital computations.

SUMMARY

The SKYLAB altimeter data analysis results presented here are representative of a large amount of data which has been studied. It is concluded that the instrument performance was excellent and that geoid shape information derived correlates well with the Marsh-Vincent global geoid. It is further concluded that there appears to be a strong correlation between the derived geoid and underwater topographic features.

REFERENCES

[1] "Earth Resources Production Processing Requirements for EREP Electronic Sensors," prepared by Philco-Ford Corp., Houston Operation for NASA Lyndon B. Johnson Space Center, Houston, Texas.

[2] Kaula, W.M. (Chairman), "The Terrestial Environment: Solid Earth and Ocean Physics," Report of a study at Williamstown, Mass., NASA CR-1579, August 1969.

[3] Martin, C.F. and Carroll, C.L., Jr., "Tropospheric Refraction Corrections and their Residual Errors," AFMTR-TDR-64-3, February 1965.

[4] Martin, C.F., "Optimum Use of Ground Stations for GEOS-C Orbit Determination," Sea Surface Topography from Space, Vol. 1, 9-1 to 9-15, NOAA TR ERL-AOML 7, 1972.

[5] McGoogan, J.T., "Precision Satellite Altimetry, 1974 IEEE Intercom Technical Papers, Earth and Ocean Physics Application Program, March 26-29, 1974.

[6] McGoogan, J.T., Miller, L.S., Brown, G.S., and Hayne, G.S., "The s-193 Radar Altimeter Experiment" to be published in IEEE Transactions, June 1974.

[7] Merriam, C.W., Optimization Theory and the Design of Feedback Control Systems, McGraw-Hill Book Co., New York, 1964.

[8] Miller, L.S. and Hammond, D.L., "Objectives and Capabilities of the Skylab S-193 Altimeter Experiment," IEEE Trans. on Geosc. Elect., GE-10, NO1, pp. 73-79, January 1972.

[9] Oceanographic Atlas of the North Atlantic Ocean, Section V, Marine Geology, U.S. Naval Oceanographic Office Pub. No. 700.

[10] Vincent, S., and Marsh, J.G., "Global Detailed Gravimetric Geoid," paper presented at the First International Symposium, The Use of Artificial Satellites for Geodesy and Geodynamics, Athens, Greece, GSFC Document X-592-73-266, 1973.

RESULTS OF GEODETIC PROCESSING AND ANALYSIS OF SKYLAB ALTIMETRY DATA

D. M. J. Fubara and A. G. Mourad
Battelle-Columbus Laboratories

ABSTRACT

The processing was based on a time series intrinsic relationship be between the satellite ephemeris, altimeter measured ranges, and the corresponding a priori values of subsatellite geoidal heights. Using least squares processing with parameter weighting, the objective was to recover (1) the absolute geoidal heights of the subsatellite points, and (2) the associated altimeter calibration constants(s). Preliminary results from Skylab mission SL-2 are given, using various combinations from two sets of orbit ephemeris and altimeter ranges. The influences of orbit accuracy, and a priori geoidal ground truth are described on the basis of various combination solutions. It is shown that correctly scaled geoidal heights cannot be deduced by merely subtracting the altimeter range from the geodetic height of the satellite unless the satellite ephemeris and the altimeter have no unknown significant systematic errors or biases and drifts. In particula , the results of such direct subtraction can be very misleading if the orbit used is mputed from data including altimeter data used as height constraints. In view of the current state of our knowledge of (1) satellite altimeter biases and (2) radial errors in orbit computation relative to geocenter, and because satellite altimetry is a "geodetic geometric leveling from space", the use of geodetic ground truth samples as control "benchmarks" appears indispensable for the recovery of absolute geoidal heights with correct scale. Such geodetic ground truth in the oceans has to be determined from marine geodetic techniques involving astrogravimetry and satellite geodesy.

It should be emphasized that the primary objective of the Skylab altimeter is to determine the instrument feasibility. Any additional applications of the data such as for geodesy, geophysics, and oceanography are desirable. Although accurate orbit is required for such applications, it is not a prerequisite for determining the instrument feasibility. This investigation, nevertheless, considered the influence of orbit accuracy and the effect of other parameters to assess the geodetic requirements for future satellite altimetry missions such as GEOS-C and SEASAT.

INTRODUCTION

The "Williamstown Study" [Kaula, 1970] recommended the use of spacecraft altimeters for geodetic, g physical, and oceanographic studies of the oceans and the earth's gravity field. An effort of this type was implemented for the first time in history under Skylab's experiment S-193, Stanley and McGoogan [1972]. The primary objective of the S-193 is to determine the engineering feasibility of the altimeter. The S-193 altimeter experiment is one of a number classified under "Earth Resources Experiments

Package" (EREP) whose end objectives are to solve various problems on earth, that directly affect even the man in the street.

Three manned Skylab missions--SL/2, SL/3, and SL/4--are to provide data from the S-193 system. Geodetic analysis of Skylab S-193 altimeter preliminary data from mission SL/2 and EREP pass 9 is the subject of this paper. The overall objective of our investigation was to demonstrate the feasibility of and necessary conditions in using the altimeter data for determination of the Marine Geoid (i.e., the geoid in ocean areas). The geoid is the equipotential surface that would coincide with "undisturbed" mean sea level of the earth's gravity field. "Undisturbed" is the condition that would exist if the oceans were acted on by the earth's force of gravity only, and no other forces such as ocean currents, winds, tides, etc. Thus, determination of the geoid (mean sea level) is basic to understanding the oceans and their dynamic phenomena such as currents, tides, circulation patterns and hence air-sea interactions. Improved numerical weather predictions require accurate knowledge of these ocean-dynamics phenomena. Navigation, waste disposal, and pollution control also benefit from an accurate knowledge of ocean dynamics. More accurate determination of the geoid will lead to a better definition of the earth's gravity model. Computation of the global geoid by conventional methos is so expensive and time consuming and is beset with so many problems as discussed in Fubara and Mourad [1972a] that these conventional techniques cannot be depended on for completion of the job in the foreseeable future. These factors justify the need for new systems and techniques. Current indications from the Skylab altimeter are that satellite altimetry may be the answer.

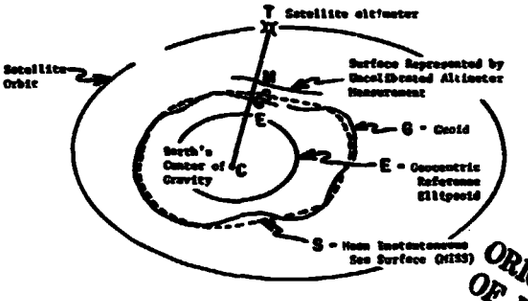

FIGURE 1. GEOCENTRIC RELATIONS OF SURFACES INVOLVED IN SATELLITE ALTIMETRY

Figure 1 shows schematic geocentric relations of the various surfaces associated with satellite altimetry. TM is the raw altimeter range which has to be corrected for laboratory instrumental calibration, electromagnetic effects, sea state, and periodic sea surface influences to give TS. S represents the nonperiodic "sea level". CT and CE the geocentric radii of the altimeter and E (its subsatellite point on the reference ellipsoid) are computed from satellite tracking information. EG is the absolute geoidal undulation to be computed from this investigation, while SG is the quasi stationary departure of the mean instantaneous sea surface from the geoid--the "undisturbed" mean sea level.

ANALYTICAL DATA HANDLING FORMULATIONS

Each measured altimeter range R_i^o with an associated measurement residual v_i is intrinsically related to (1) X_s, Y_s, and Z_s (the satellite coordinates at the instant of measurement), (2) the absolute geoidal undulation N_i^a (of the subsatellite point) based on a reference ellipsoid of parameters a, and e, and (3) the biases in all measurement systems involved. The condition equation for this intrinsic relationship can be stated as:

$$v_i + R_i^o(1 + \Delta c) - h_i + N_i^o + \Delta N_i = 0 \quad , \tag{1}$$

where

$\Delta c = f_1$ (systematic errors in X_s, Y_s, Z_s, the altimeter bias and sea state correction bias) is the total geodetic calibration constant to be determined. The exact functional mathematical expression for Δc is unknown and is treated later;

$N_i^a = N_i^o + \Delta N_i$ (N_i^o is an approximate value for N_i^a) $= f_2(a, e)$; and h_i is the geodetic satellite height above the reference ellipsoid, or

$$h_i = f_2 (X_s, Y_s, Z_s, \bar{a}, \bar{e}) \quad ,$$

where $\bar{a}$ and $\bar{e}$ are parameters of the reference ellipsoid for the geodetic datum of the tracking stations whose coordinates are used in computing the satellite coordinates X_s, Y_s, and Z_s. Equation (1) presumes that $a = \bar{a}$ and $e = \bar{e}$, and, also, that the two reference ellipsoids are concentric and geocentric.

In current geodetic practice, because of multiplicity of geodetic datums and the nonexistence of an universally accepted datum, the $a = \bar{a}$, etc. requirements are hardly ever met. A geodetic datum is uniquely determined by seven parameters. One such set of parameters is a, e, Δx, Δy, Δz, $\Delta\xi$ and $\Delta\eta$. a and e define the size and shape of the reference ellipsoid; Δx, Δy, and Δz relate the center of the reference ellipsoid to the geocenter and are purely translatory; while $\Delta\xi$ and $\Delta\eta$ are angular values to ensure paralellism between the minor and major axes of the reference ellipsoid and the mean rotational axis and mean terrestrial equator of the earth, respectively. For each geodetic datum, every effort is made to ensure that $\Delta\xi = \Delta\eta = 0$. However, as shown in Fubara and Mourad [1972a], while this condition has never been exactly realized, its effect can be neglected.

The change Δh_i in h_i due to the changes Δa and Δf in the dimensions of the reference ellipsoid and Δx_o, Δy_o, and Δz_o in its position relative to geocenter is given by Heiskanen and Moritz [1967] as

$$\Delta h_i = -\mathrm{Cos}\varphi\mathrm{Cos}\lambda\Delta x_o - \mathrm{Cos}\varphi\mathrm{Sin}\lambda\Delta y_o - \mathrm{Sin}\varphi\Delta z_o - \Delta a + a\,\mathrm{Sin}^2\varphi\Delta f \quad , \tag{2}$$

where

f = flattening of reference ellipsoid [$f = 1 - (1-e^2)^{1/2}$]

φ and λ = geodetic latitude and longitude corresponding to X_s, Y_s, and Z_s .

For the current investigation, which involves three different geodetic datums, it is further assumed that $\Delta x_o = \Delta y_o = \Delta z_o = 0$ because these values have not been reliably determined and all three datums are supposed to be geocentered. Therefore, instead of Equation (2), Equation (3) will be employed

$$\Delta h_i = -\Delta a + a\sin^2\varphi\Delta f \tag{3}$$

as the correction parameter to Equation (1) which should be rewritten as

$$v_i + R_i(1 + \Delta c) - (h_i + \Delta h_i) + N_i^o + \Delta N_i = 0 \tag{4}$$

or

$$v_i + R_i + \Delta C - (h_i + \Delta h_i) + N_i^o + \Delta N_i = 0 \tag{5}$$

to reflect changes in reference ellipsoidal parameters whenever necessary. Equation (4) or (5) was used to process the data by generalized least-squares adjustment model as developed in Fubara [1973].

ANALYSIS AND EVALUATION OF DATA

The analytical data-handling formulations for this investigation call for the following basic inputs: (1) the altimeter ranges, and exact time (usually GMT) of each measurement to correlate it with (2) the associated orbit ephemeris, and (3) geoidal information used as geodetic control or benchmark along the subsatellite track to help define the geodetic scale of the outputs. The main outputs are: (1) the residual bias of the altimeter or calibration constant required to give a correct absolute geoidal scale, and (2) the geoidal profile, both deduced from the computer processing of the inputs using least-squares processing with parameter weighting according to the aforementioned formulations.

Two sets of input data from Skylab mission SL/2, EREP pass 9, are used in this paper. Set A altimeter ranges have been corrected for all known sources of systematic errors including internal calibration constants, refraction, and pulsewidth/bandwidth biases. Set B altimeter ranges were not corrected for these specific systematic errors. Figure 2 shows a sample of both sets of ranges. The objectives for processing these two sets are to investigate

(1) how well the modelling for systematic errors in the analytical data-processing procedure can accommodate, recover, and prevent such systematic errors from degrading the final results

(2) the conditions required to optimally achieve the above objective.

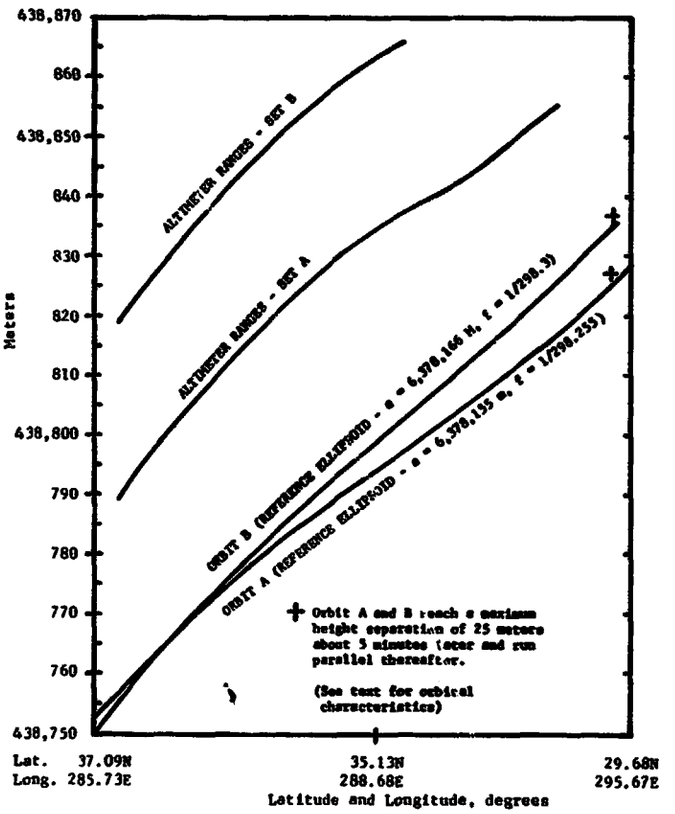

FIGURE 2. ALTIMETER RANGES (MODE 5) AND GEODETIC HEIGHT OF SKYLAB (SL-2 EREP PASS 9) GMT 13:01:50 to 13:04:50

Orbit A data are based on (a) reference ellipsoidal parameters $a = 6,378,155$ m and $f = 1/298{\cdot}255$, (b) SAO 1969 Standard Earth model with geopotential coefficients through degree 22 and order 16, (c) c-band and USB (Unified-S-Band) radar tracking data, and (d) $GM = 3.986013 \times 10^{14}$ m^3/sec^2. Orbit B data are based on (a) $a = 6,378,166$ m and $f = 1/298{\cdot}3$, (b) earth gravity model of 3 sectorial and tesseral terms, and 4 zonal terms, (c) C-band and USB radar tracking data, and (d) $GM = 3.986032 \times 10^{14}$ m^3/sec^2. Both orbits were corrected for other perturbation forces such as lunar gravitation, solar gravitation, earth tide, drag, and solar radiation pressure. The geodetic datum for the tracking stations used in each orbit computation was assumed to be geocentric which implies that $\Delta x_o = \Delta y_o = \Delta z_o = 0$ as described in the rationale for using Equation (3) instead of (2).

A segment of each of these two orbits is shown in Figure 2. In theory, the two orbits should be nearly parallel and radially separated by no more than 11 meters (i.e., the maximum value of Δh of Equation 3). Near to the U.S. east coast, (Figure 2), the two orbits are radially close but not parallel. Further away from the U.S. continent and tracking stations, the orbits diverge to a radial separation of about 25 meters and begin to run parallel. One or a combination of factors including the following may account for these deviations from theoretical expectancy

(i) One or both of the two geodetic datums of the tracking stations may not be truly geocentric and free of rotational errors as assumed, or there may be undetected systematic errors in individual tracking station geocentric coordinates.

(ii) The different gravity models influence the computed satellite ephemeris differently. However, the parallelism of the orbit segments away from continental tracking stations is either an accidental coincidence or a reflection that the geometrical constraints of the radar tracking data had ceased to be an influential factor.

(iii) Differences in orbit computational techniques.

However, it is necessary to point out that by its configuration Skylab is not and was not designed to be a geodetic satellite with highest order tracking systems. It's mass is about 87,440 kg. while the "effective" cross-sectional area employed in the orbit computations is 293.3m^2. In an absolute sense, the computed orbit may not be of geodetic quality. However, it is valid to assume that during short time intervals such as the 3 minutes involved in the data sampling being analyzed, any systematic errors in the orbit will be constant in magnitude and sign. The analytical data-processing procedure is designed to effectively accommodate this type of assumption. Therefore, the precision of the altimeter data and the satellite ephemeris are consistent enough beyond expectations to warrant geodetic analysis.

The a priori geoid input was taken from Vincent and Marsh [1973] geoid. That geoid is not purely gravimetric as the name implies and therefore, in addition to a flattening of f = 1/298·255, a = 6,378,142 m is also specified for its reference ellipsoid. To ensure compatibility of geodetic reference datums in Equation (1), Equation (3) was applied as necessary. The two sets of altimeter ranges and orbit ephemeris present four different data combinations that were processed. These various combination solutions were used in the analyses of (1) the efficiency of the data-handling formulations, (2) the influences of orbit errors, and (3) the role of the choice of a priori geoidal ground truth. Some schools of thought believe that geoidal heights could be obtained by merely subtracting the altimeter ranges from the corresponding geodetic heights of the satellite. Although we computed and evaluated results from such a method, we consider it invalid because it requires complete absence of systematic errors in the orbit and the altimeter which also must not drift, in order to ensure reliable results.

The Skylab altimeter data being analyzed are from mission SL-2, EREP pass 9 during which data were obtained in Modes 3 and 5 of the instrument operation. For this pass, there appears to be some instrument malfunction during Mode 3. Therefore, only the Mode 5 data are being analyzed.

RESULTS AND ANALYSIS

From the given satellite orbit and measured altimeter ranges, the overall objective of the investigation is to simultaneously (a) determine a geodetic calibration constant(s) that (b) corrects or adjusts the altimeter ranges for (c) determination of absolute geoidal heights with correct scale. Tables 1 and 2 and Figure 2 show the geodetic heights of

the orbits and the altimeter ranges designated as Set A and Set B as previously described. All the results being analysed have been modified to be based on a reference ellipsoid of a = 6,378,142 m and f = 1/298·255.

TABLE 1. ANALYTICALLY ADJUSTED RANGES
EREP PASS 9 OF SL-2
(values in meters)

GMT 13:01:57·981 to 13:02:52·062

Measured Altimeter Ranges		Based on Orbit A Adjusted Altimeter Ranges		Based on Orbit B Adjusted Altimeter Ranges	
SET A	SET B	SET A	SET B	SET A	SET B
438789·1	438818·6	438811·9	438811·9	438824·6	438824·7
438788·7	438819·3	438811·5	438812·6	438824·2	438825·3
438791·0	438819·8	438813·8	438813·2	438826·5	438825·9
438790·6	438821·8	438813·4	438815·2	438826·1	438827·9
438796·2	438823·4	438819·0	438816·7	438831·7	438829·4
438797·0	438825·9	438819·8	438819·3	438832·5	438832·0
438797·7	438827·7	438820·5	438821·0	438833·2	438833·8
438799·6	438829·2	438822·4	438822·5	438835·1	438835·2
438801·1	438831·4	438823·9	438824·8	438836·6	438837·5
438803·3	438832·7	438826·1	438826·0	438838·8	438838·7
438806·3	438835·1	438829·1	438828·5	438841·8	438841·3
438806·3	438835·6	438829·1	438829·0	438841·8	438841·7
438806·3	438836·2	438829·1	438829·6	438841·8	438842·3
438808·2	438837·8	438831·0	438831·1	438843·7	438843·9
438809·3	438838·8	438832·1	438832·2	438844·8	438844·9
438810·8	438840·4	438833·6	438833·8	438846·3	438846·5
438811·2	438840·8	438834·0	438834·2	438846·7	438846·9
438813·1	438841·6	438835·9	438834·9	438848·6	438847·6
438813·5	438842·0	438836·3	438835·4	438849·0	438848·1
438814·2	438844·4	438837·0	438837·7	438849·7	438850·4
438815·7	438845·6	438838·5	438838·9	438851·2	438851·6
438817·2	438846·4	438840·0	438838·8	438852·7	438852·5
438818·7	438848·5	438841·5	438841·8	438854·1	438854·6
438820·2	438849·1	438843·0	438842·5	438855·7	438855·2
438820·6	438849·4	438843·4	438842·8	438856·1	438855·5

Geodetic Calibration Constant

22·8 -6·6 35·5 6·1

TABLE 2. ANALYTICALLY ADJUSTED RANGES
EREP PASS 9 OF SL-2
(values in meters)

GMT 13:02:38·542 to 13:03:33·661

Measured Altimeter Ranges		Based on Orbit A Adjusted Altimeter Ranges		Based on Orbit B Adjusted Altimeter Ranges	
SET A	SET B	SET A	SET B	SET A	SET B
438813·5	438842·0	438836·7	438835·9	438852·3	438851·5
438814·2	438844·4	438837·4	438838·3	438853·0	438853·8
438815·7	438845·6	438838·9	438849·4	438854·5	438855·0
438817·2	438846·4	438840·4	438840·3	438856·0	438855·9
438818·7	438848·5	438841·9	438842·4	438857·5	438857·9
438820·2	438849·1	438843·4	438843·0	438859·0	438858·5
438820·6	438849·4	438843·8	438843·3	438859·4	438858·9
438821·0	438851·3	438844·2	438845·2	438859·8	438860·7
438822·8	438851·8	438846·0	438845·7	438861·6	438861·3
438824·0	438853·2	438847·2	438847·1	438862·8	438862·6
438824·3	438854·3	438847·5	438848·2	438863·1	438863·8
438825·5	438855·1	438848·7	438848·9	438864·3	438864·5
438825·5	438854·6	438848·7	438848·4	438864·3	438864·0
438826·2	438855·7	438849·4	438849·5	438865·0	438865·1
438827·3	438856·8	438850·5	438850·7	438866·1	438866·3
438828·1	438857·9	438851·3	438851·8	438866·9	438867·3
438829·2	438859·7	438852·4	438853·6	438868·0	438869·2
438831·5	438859·9	438854·7	438853·8	438870·3	438869·4
438831·8	438860·3	438855·0	438854·2	438870·6	438869·8
438833·7	438861·9	438856·9	438855·8	438872·5	438871·3
438832·6	438862·7	438855·8	438856·6	438871·4	438872·2
438835·6	438864·4	438858·8	438858·3	438874·4	438873·9
438835·2	438864·6	438858·4	438858·5	438874·0	438874·0
438834·5	438864·1	438857·7	438858·0	438873·3	438873·6
438837·1	438865·7	438860·3	438859·6	438875·9	438875·2

Geodetic Calibration Constant

23·2 -6·1 38·8 9·4

Calibration Constants and Adjusted Altimeter Ranges

As developed earlier, the altimeter bias, radial errors in orbit determination, and errors from inadequate or total lack of correction for significant sea-state variations are all algebraically additive. These errors are inseparable unless two of them are absolutely known. In this investigation, the total sum of all three is the geodetic calibration constant to be determined.

Unfortunately, unless the radial orbit error is zero, some known absolute geoidal height must be used as geodetic control or benchmark in order to determine the required geodetic calibration constant. In this case, the calibration constant so determined is scalewise-dependent on the geodetic datum of the a priori geoidal input or the geodetic control used. This is demonstrated in Figure 3 in which GG-73 is the subsatellite geoid profile taken from Vincent and Marsh [1973] geoid. AA is the resultant satellite altimetry geoid profile based on GG-73 as a priori input. This a priori input and its output are used as a yardstick or control of the experiment to investigate the effects of errors in a priori geoid height inputs and scale dependency of the computed geodetic calibration constant and satellite altimetry geoid heights on geodetic control (ground truth). Errors were introduced into GG-73 to produce A-I. The resultant satellite altimetry geoid segment from using A-I as a priori input is A-O. Similarly, B-O results from the use of B-I as a priori input.

It is obvious that the shape of AA (the control experiment) is identical to that of A-O and B-O. In all cases, even though the resultant point-to-point geoidal height differences were exactly identical, the deduced calibration constants and hence the values of the computed geoid heights depended on the a priori geoidal height inputs. Figure 3 definitely shows that such a priori inputs and the errors in them affect only the linear scale of the calibration constant and not the shape of the deduced geoid from the type of analytical processing used herein. In other words, the main effect of the a priori geoid input is reflected in the position of the computed geoid relative to geocenter. To determine the geoid with correct shape and scale and centered at geocenter (i.e., an absolute geoid) is the ultimate objective of all geoid computations, and the criteria for the geoid to contribute to solutions of problems in oceanography, geophysics, geodesy, and the earth's gravity field model.

In the current Skylab data, the altimeter bias appears to vary with the modes and the submodes described in Kern and Katucki [1973]. This was another factor taken into account. For the current data processing, the additional assumption is that (for a "short time interval") the systematic radial orbital errors are of constant magnitude and sign. These two factors constrain the current "short time interval" for this set of data to be no more than 3 minutes. From the calibration constants shown in Tables 1 and 2 the assumption of constant radial orbital errors is better satisfied by Orbit A than Orbit B. For Orbit A, the rate of change in radial errors during this period (close to tracking station) is about 0·5 m per 2 minutes, for Orbit B it is about 3 m per 2 minutes of time. Some avoidable errors are in the computation of Orbit B as shown in Wollenhaupt and Schiesser [1973]. In particular, the gravity model can be improved. This result supports a well-known fact that earth gravity model required for accurate orbit computation is a very important factor.

A key indicator of the reliability of the analytically computed geodetic calibration constant is the consistency of the adjusted ranges. The mathematical model developed for this analysis anticipated imperfections in the knowledge of (1) the orbit and (2) the delay constants (biases) for transforming the radar altimeter returns into ranges in engineering units for geodesy. These problems algebraically add up to be a linear radial error relative to the earth's geocenter. Through the use of the discussed appropriately weighted a priori geoidal heights; (a) no matter what the errors in the different sets of ranges used, the derived adjusted ranges should be identical if the same orbit is used; (b) alternatively, if a unique set of ranges is used with different orbit data, the adjusted set of ranges should differ by only the radial differences between the orbits.

The expectations (a) and (b) are established to within the noise level of the data by the results of Tables 1 and 2. Conversely, the deduced geodetic calibration constants should also satisfy condition (b). Thus from Table 1, the constants 22·8 minus 35·5 should equal -6·6 minus 6·1, and from Table 2, 23·2 minus 38·8 should equal -6·1 minus 9·4, meters.

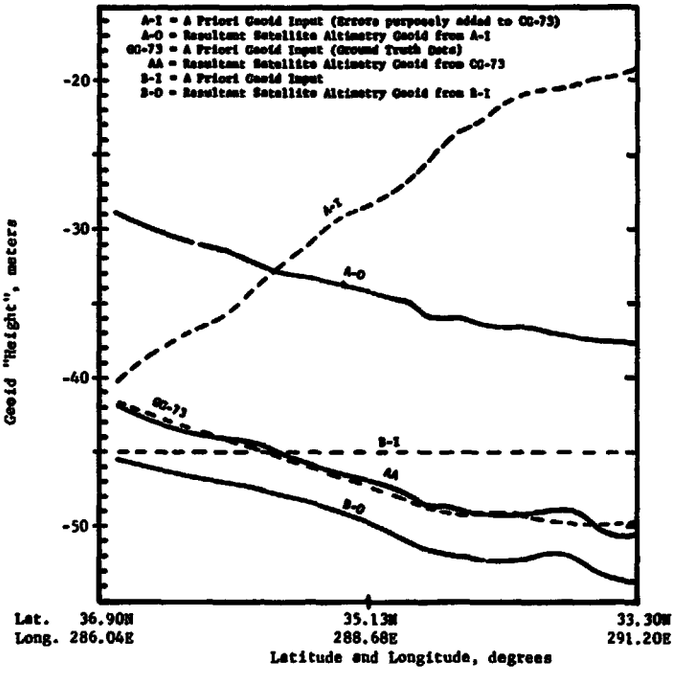

FIGURE 3. EFFECT OF ERRORS IN A PRIORI GEOID HEIGHT INPUTS AND SCALE DEPENDENCY OF CALIBRATION CONSTANT AND GEOIDAL HEIGHT ON GEODETIC CONTROL (GROUND TRUTH)

Geoidal Heights Analytically Deduced from Satellite Altimetry

Figure 4 shows the deduced geoidal heights from the analytical processing of the four data combinations already described. Figure 4 also shows three other profiles for the same segment of the geoid as given by Vincent, et al [1972 and 1973] using different conventional techniques. As usual, (see Fubara and Mourad [1972a] and Fischer, et al [1968])these other conventional geoid profiles disagree with each other significantly. In Figure 4, GG-72 and GG-73 are conventional geoid profiles primarily based on global gravity data which are too sparse and often very inaccurate in ocean areas (70 percent of the globe); therefore, satellite-derived geopotential coefficients were used to augment the measured gravity data. The present-day accuracy and extent of coverage of global gravity data and the geoid are discussed in Decker [1972] and Fubara and Mourad [1973].

In using Orbit A, the remarkable agreement achieved (Figure 4) between the analytically computed satellite altimetry geoid segments AA and AB, and GG-73, the Vincent and Marsh [1973] geoid is beyond all expectations. It implies that in the area of the investigation either the GG-73 geoid and Skylab altimeter are extremely accurate or that certain factors have cancelled out to produce such a submeter agreement. This remarkable match between the analytically computed geoid profiles from EREP pass 9, based on Orbit A and the corresponding conventional geoid profile of Vincent and Marsh [1973], should be accepted with caution. Precision estimate of this conventional geoid is about $\pm$ 5 to $\pm$ 15 meters in ocean areas, according to its authors. Furthermore, the profile of the conventional geoid plotted, was scaled off a very small scale world map. This latter process would normally introduce errors into the plotted profile. This condition easily introduces systematic displacement errors which are not conducive to reliable comparison between the two types of geoid segments. Furthermore, Orbit A and the GG-73 geoid profile are based on an identical earth gravity model. Therefore, profiles AA, AB, and GG-73 are not independent.

In spite of all these possible sources of discrepancy, and the data errors and uncertainties previously outlined, the comparison of features between the altimetry geoid and this particular conventional geoid (no two conventional geoids are alike, often differing by tens of meters and relative tilts) is very encouraging. The current preliminary results have not been corrected for the influences of sea state, possible nadir-alignment errors and departures of the sensor field of view from the nadir. Some of the high-frequency features of the satellite altimetry geoid which may be a reflection of these uncorrected influences have been smoothed out. The altimeter ranges refer to some mean sea surface topography of the instant of measurement called MISS in Figure 1. The quasistationary departures of MISS from the geoid is significant in the area of this investigation according to Figures 1 and 2 of Sturges [1972]. If the altimeter is as precise as these results indicate, the expected trend in average sea surface topography of the area could have been sensed. This is being studied further and computations from EREP pass 4 of mission SL-2 and data expected from mission SL-4 should confirm or negate this expected correlation with sea surface topography.

The results from using Orbit B shown as profiles BB and BA of Figure 4, show a systematic tilt relative to GG-73 and the results based on Orbit A. The main differences between Orbit A and B have been discussed earlier. The conclusion is that the geodetic outcome of satellite altimetry is extremely sensitive to the computed orbit. The agreement between profiles AA and AB based on the same orbit but different sets of ranges, one of which set has known systematic errors, shows that our analytical basis is valid and workable for recovery and elimination of the influences of such systematic errors. The same matching applies to BB and BA.

By merely subtracting the measured altimeter ranges from the corresponding satellite geodetic heights, the resultant profiles for the four data combinations are shown in Figure 5. Compared to the results in Figure 4, the simple subtraction results of Figure 5 show, for the Orbit A, remarkable contrast between the "geoid" AA (-19 m to 27.5 m) and AB (-49 m to -56 m); for Orbit B and the same two sets of altimeter ranges, "geoid" BB (-38 m to -40 m to -39 m) differ from BA (-8 m to -11 m to -10 m). Thus this simple-subtraction approach is sensitive not only to the orbit but also to the systematic errors in altimeter ranges unlike the analytical approach.

CONCLUSIONS

The preliminary conclusions from these quick-look data investigations and previous simulation studies include:

(1) The analytical data-handling formulations developed for this investigation appear to be very satisfactory. The main outputs required, the geodetic calibration constant, the geoid height, and the corrected altimeter ranges were reliably determined.

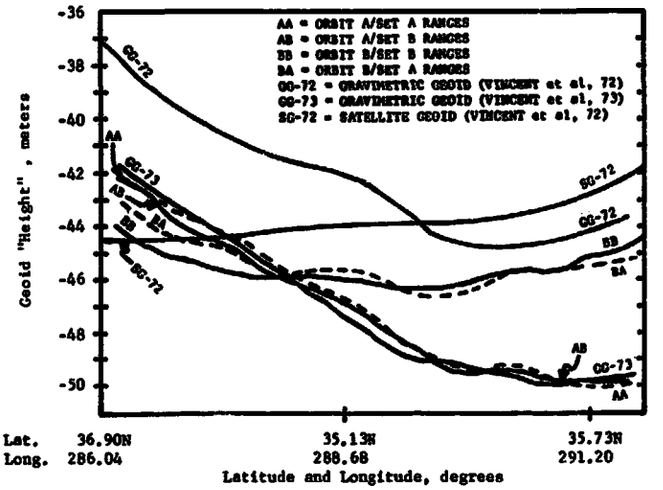

FIGURE 4. CONVENTIONAL GEOID AND SATELLITE ALTIMETRY GEOID PROFILES (SKYLAB SL-2 EREP PASS 9 DATA)

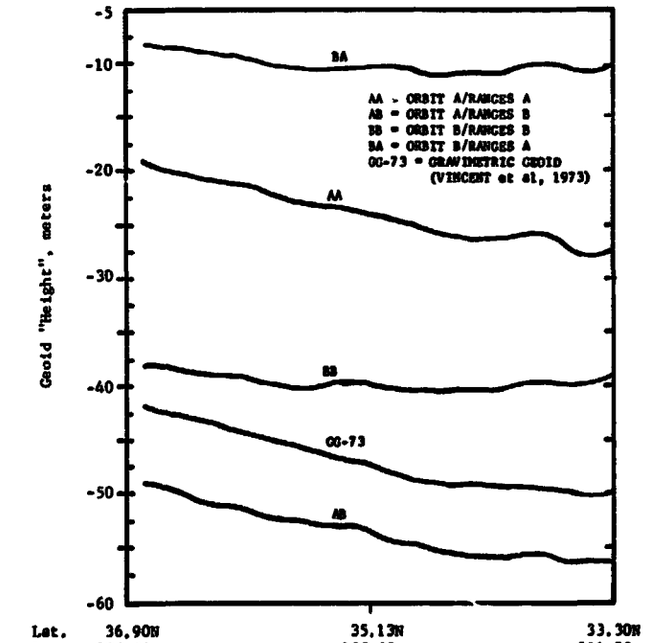

FIGURE 5. SATELLITE HEIGHT MINUS ALTIMETER RANGES AND A CONVENTIONAL GEOID PROFILE (SKYLAB SL-2 EREP PASS 9, MODE 5 DATA)

(2) To ensure that the deduced calibration constant and geodetic heights are absolute, the use of geodetic control or a benchmark whose absolute geoidal height is known is indispensable. The establishment of such controls from a combination of astrogravimetry and satellite data is discussed in Mourad and Fubara [1972], and in Fubara and Mourad [1972a] and the practical implementation is partially demonstrated in Fubara and Mourad [1972b]. There is an implicit correlation between this conclusion and the conclusion based on a different type of investigation in Rapp [1971] that: "In carrying out simulation studies with non-global data it was concluded that altimetry data could not be used alone for potential coefficient determination.... Consequently, the altimetry data was combined with geoid undulation information in non-ocean blocks and with existing terrestrial gravity data."

(3) On the assumptions that the altimeter system is stable and that systematic orbit radial errors for short time periods are constant, the altimeter geoid shows very high frequency details which have been smoothed out in the plotted geoid or more accurately the sea surface topography. Such high frequency details may also reflect the inexact fulfillment of various implied assumptions or the uncorrected influence of sea state.

(4) Subject to additional data-processing corrections which the current state of the SL-2 data precludes, these preliminary results indicate that satellite altimetry will be a valid and useful tool for computing quasistationary departures of sea surface topography from the geoid. This practical application is important to oceanographic work related to ocean dynamic phenomena such as circulation patterns, mass water transport, ocean tides, and ocean-current influences. These in turn relate to air-sea interaction and the knowledge for global numerical weather prediction. Such oceanographic factors also affect our knowledge of pollution dispersion by the oceans, an important guiding factor in waste disposal, and prediction of dispersal and control of oil-spill hazards. Further developments on these issues are in Fubara and Mourad [1973].

(5) Orbit computation in which inadequately calibrated altimeter ranges are employed as constraints is not desirable and presents no advantage for processing altimeter data to compute the geoid. First, the unmodelled range biases introduce large systematic errors that are not admissible in least-squares orbit computation. Such systematic errors cannot be accurately eliminated through modelling unless some valid geodetic controls are used as constraints. Second, the use of orbits computed in this way to deduce a geoid from the same altimeter data with purely differencing or graphical techniques would be misleading. For example, the geoid so deduced would closely match the original geoid used in applying the altimeter ranges as a constraint in the orbit computation.

(6) Deduction of a correctly scaled geoid from satellite altimetry cannot be achieved by merely subtracting altimeter ranges from the corresponding geodetic heights of the satellite unless (a) the satellite orbit is errorless, (b) the altimeter does not drift, and (c) the altimeter system biases are either nonexistent or are absolutely known. Therefore, in current practice, satellite altimetry ranges cannot be regarded as representing direct determination of absolute geoid heights as one would like to assume. At this time marine geodesy, involving the use of astrogravimetric and satellite geodesy techniques, appears indispensable for the provision of geodetic controls required for the full achievement of satellite altimetry objectives of GEOS-C, and SEASAT series of the NASA-proposed "Earth and Ocean Physics Applications Program".

ACKNOWLEDGEMENT

The research reported in this paper is sponsored by the National Aeronautics and Space Administration through NASA/Johnson Space Center. The NASA/JSC Technical Monitors are Mr. Z. H. Byrns and Dr. Dean Norris. The authors are indebted to Mr. J. T. McGoogan for some of the altimetry and some of Skylab ephemeris data used, and for several helpful discussions on the systems characteristics of the Skylab S-193 altimeter.

REFERENCES

1. Decker, B. L., "Present Day Accuracy of the Earth's Gravitational Field", presented at the International Symposium on Earth Gravity Models and Related Problems, Defense Mapping Agency Aerospace Center, St. Louis Air Force Station, Missouri, August, 1972.

2. Fischer, I., et al, "New Pieces in the Picture Puzzle of an Astrogeodetic Geoid Map of the World", Bulletin Geodesique, No. 88, p.199, 1968.

3. Fubara, D. M. J., "Geodetic Numerical and Statistical Analysis of Data", Bulletin Geodesique, No. 108, June, 1973.

4. Fubara, D. M. J. and Mourad, A. G., "Requirements for a Marine Geoid Compatible with Geoid Deducible from Satellite Altimetry", Proceedings of NOAA/NASA/NAVY Conference on Sea Surface Topography from Space, Edited by J. Apel, NOAA TR ERL 228-AOML7, 1972a.

5. Fubara, D. M. J. and Mourad, A. G., "Marine Geodetic Control for Geoidal Profile Mapping Across the Puerto Rican Trench", Draft Report Prepared by Battelle's Columbus Laboratories to NASA Wallops Station, under Contract Number NAS6-2006, April, 1972b.

6. Fubara, D. M. J. and Mourad, A. G., "Applications of Satellite and Marine Geodesy to Operations in the Ocean Environment", Draft Report Prepared by Battelle's Columbus Laboratories to NASA Wallops Station, under Contract Number NAS6-2006, March, 1973.

7. Heiskanen, W. A. and Moritz, H., Physical Geodesy, W. H. Freeman & Co. San Francisco, California, 1967.

8. Kaula, W. M. (Chairman), "The Terrestrial Environment: Solid Earth and Ocean Physics", Report of a Study at Williamstown, Massachusetts, to NASA, Report NASA CR-1579, April, 1970.

9. Kern, R. J. and Katucki, R. J., "S-193 Microwave Radiometer/Scatterometer Altimeter, Calibration Data Report, Flight Hardware", Volume 1B, Rev. D, from General Electric for NASA, March, 1973.

10. Mourad, A. G. and Fubara, D. M. J., "Interaction of Marine Geodesy, Satellite Technology and Ocean Physics", Report prepared by Battelle's Columbus Laboratories for NASA Wallops Station under Contract NAS6-2006, June, 1972.

11. Rapp, R. H., "Accuracy of Potential Coefficients Determinations from Satellite Altimetry and Terrestrial Gravity", Department of Geodetic Science Report No. 166, The Ohio State University, 1971.

12. Stanley, H. R. and McGoogan, J. T., "The Skylab Radar Altimeter", Proceedings of NOAA/NASA/NAVY Conference on Sea Surface Topography from Space, Edited by J. Apel, NOAA TR ERL 228-AOML7, 1972.

13. Sturges, W., "Comments on Ocean Circulation with Regard to Satellite Altimetry", Proceedings of NOAA/NASA/NAVY Conference on Sea Surface Topography from Space, Edited by J. Apel, NOAA TR ERL 228-AOML7, 1972.

14. Vincent, S., Strange, W. E., and Marsh, J. G., "A Detailed Gravimetric Geoid of North American, North Atlantic, Eurasia, and Asutralia", Paper presented at the International Symposium on Earth Gravity Models and Related Problems, 1972.

15. Vincent, S and Marsh, J. G., "Global Detailed Gravimetric Geoid", Computer Sciences Corporation and NASA/GSFC, 1973.

16. Wollenhaupt, W. R. and Schiesser, E. R., "Status of Skylab SL-2 EREP Skylab Tapes", FM85 (73-241), Mathematical Physics Branch, NASA/JSC, Houston, Texas, October, 1973.

GEOID DETERMINATION FROM SATELLITE ALTIMETRY USING SAMPLE FUNCTIONS

R. D. BROWN
Computer Sciences Corporation

ABSTRACT

While recent altimeter experiments have proven the ability of altimeter data by itself to define the marine geoid, in general a mathematical geoid or geopotential model must be used to interpolate and define the geoid in regions where altimeter data is sparse. Lundquist and Giacaglia (1969) have proposed using a geopotential model comprising spherical harmonic sample functions for this problem; the conventional spherical harmonic model having been found unsuitable because of the global nature of the harmonic functions. Two algorithms were proposed by Lundquist and Giacaglia for application of the sample function model to the altimeter problem. The first involves diagonalization of the normal matrix and the second, aggregation of data and interpolation between sample points. These two algorithms are evaluated in numerical simulations of the geoid definition problem in order to choose the most promising algorithm for actual data processing. Algorithm 1 is found to be fairly accurate but time consuming and difficult to implement for high degree models. Algorithm 2 is inherently less accurate but much faster and can readily model geoid details as small as 1° by 1° squares.

1. INTRODUCTION

Recent experiments with the Skylab radar altimeter have demonstrated that the fine detail of the marine geoid can be defined very well by altimeter data (McGoogan et.al. (1974)). But sufficient altimeter data for defining the global marine geoid to 1° by 1° detail may be many years in the future due to the limited number of planned altimeter satellites and their operating constraints. Also this direct method of geoid definition does not provide geoid heights in areas where there is no altimeter data such as between altimeter data points. For these areas, a less direct method such as interpolation from a mathematical model of the geoid or geopotential must be used.

As Lundquist and Giacaglia (1969) have pointed out, some geopotential models are more appropriate to the altimeter problem than others. The altimeter problem is here defined as the differential correction (DC) of model parameters to minimize the variance of altimeter measurement residuals, and the subsequent calculation of geoid heights from the corrected model. Due to the global nature of the spherical harmonics, the standard spherical harmonic expansion model is impractical for recovering 1° by 1° geoid detail from the dense but non-uniformly distributed and non-global altimeter data. Application of such a model to this problem would require inversion of a normal matrix of rank 32,761 to perform a DC on the harmonic coefficients. This operation would pose severe if not insurmountable data storage problems for even the largest computers. A possible solution is the utilization of a geopotential model comprising

local functions as opposed to the global harmonics. This would reduce the rank of the normal matrix to a manageable size.

Such a model has been proposed by Lundquist and Giacaglia (1969) using a sample function which is obtained from the spherical harmonics by linear transformation. These sample functions $\phi_k(\theta, \lambda)$ are defined on a global grid of sample points (θ_j, λ_j) by the relations

$$\phi_k(\theta_j, \lambda_j) = \delta_{kj}, \qquad \begin{matrix} k = 1, 2, \ldots, L \\ j = 1, 2, \ldots, L \end{matrix} \tag{1}$$

and

$$\vec{\phi}_k(\theta, \lambda) = [C]^{-1}\begin{pmatrix} \vec{X}(\theta, \lambda) \\ \vec{Y}(\theta, \lambda) \end{pmatrix} \tag{2}$$

where δ_{kj} is the Kronecker delta,

$\begin{pmatrix} \vec{X}(\theta, \lambda) \\ \vec{Y}(\theta, \lambda) \end{pmatrix}$ is the vector of spherical harmonics

given by

$$\begin{Bmatrix} X_{nm}(\theta, \lambda) \\ Y_{nm}(\theta, \lambda) \end{Bmatrix} = P_{nm}(\sin\theta) \begin{Bmatrix} \cos m\lambda \\ \sin m\lambda \end{Bmatrix} \tag{3}$$

$[C]$ is the matrix of transformation coefficients,

$$[C] = \begin{bmatrix} \vec{X}(\theta_1, \lambda_1), \vec{X}(\theta_2, \lambda_2), \ldots, \vec{X}(\theta_L, \lambda_L) \\ \vec{Y}(\theta_1, \lambda_1), \vec{Y}(\theta_2, \lambda_2), \ldots, \vec{Y}(\theta_L, \lambda_L) \end{bmatrix} \tag{4}$$

$L = (N + 1)^2$ is the maximum number of terms in the spherical harmonic expansion of degree N, and (θ, λ) are geocentric latitude and longitude respectively. The sample functions are local functions, i.e., they achieve a significant non-zero value only in a small neighborhood of their respective sample points. Each sample function, by virtue of this property, more or less describes the geoid in the neighborhood of its own sample point. This permits a great reduction in the rank of the normal matrix and permits calculation of geoid heights in a particular geographic area without evaluation of all terms of the geopotential model.

For implementation of the sample function geopotential model, Lundquist and Giacaglia (1969) proposed an algorithm, herein called algorithm 1, involving the assumption of a diagonal normal matrix. For example, consider the problem of fitting geoid height data in one dimension along a parallel of constant latitude. In this case the spherical harmonics reduce to trigonometric polynomials in longitude and the related sample functions are the trigonometric sample functions described in Lundquist and Giacaglia (1969). Figures 1a, b, and c show, respectively, a typical geoid data profile, the trigonometric polynomial functions of degree 2, and the related trigonometric sample functions for degree $N = 2$. In one dimension, this results in a 5 term model. We shall attempt to approximate the geoid data, represented by data points h_i, $i = 1, 2, \ldots, 18$, by a linear expansion of trigonometric polynomials of degree 2 and a linear expansion of trigonometric sample functions $\phi_j(\lambda)$ of degree 2. That is, we seek the coefficients a_k, b_k, and c_j, for which approximations

$$h_T(\lambda) = a_0 + a_1 \cos\lambda + b_1 \sin\lambda + a_2 \cos 2\lambda + b_2 \sin 2\lambda \tag{5}$$

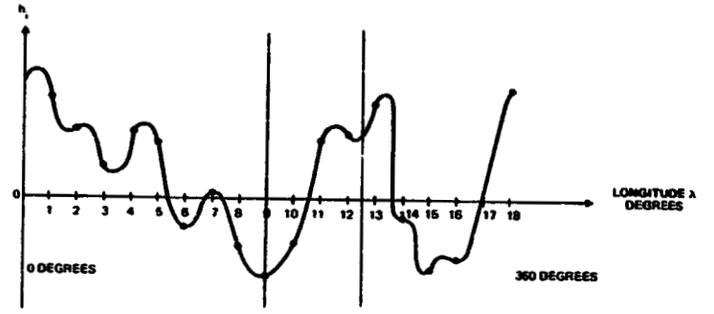

Figure 1a: Geoid Height Data at Selected Points

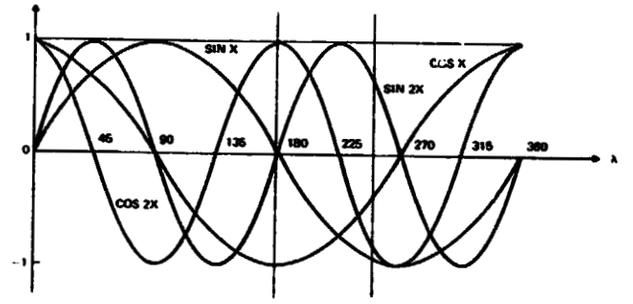

Figure 1b: Trigonometric Polynomials of Degree 2

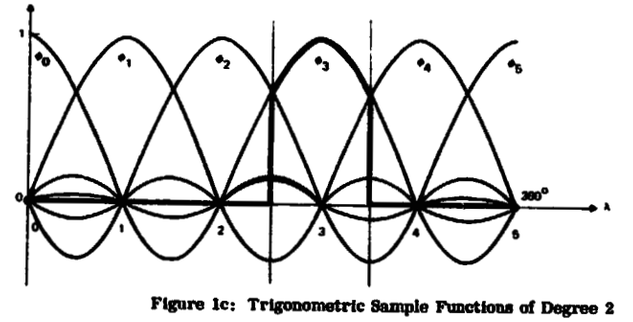

Figure 1c: Trigonometric Sample Functions of Degree 2

Figure 1. Sample Function Application Example

and

$$h_S(\lambda) = c_0\phi_0(\lambda) + c_1\phi_1(\lambda) + c_2\phi_2(\lambda) + c_3\phi_3(\lambda) + c_4\phi_4(\lambda) \qquad (6)$$

are the best fit, in the least squares sense, to the data h_i. Differential correction of coefficients a_k, b_k, and c_j, requires the formation of condition equations for each of the 18 data points. For example, for the 9th data point, we form for the trigonometric model

$$\Delta h_{T9} = \Delta a_0 + \Delta a_1 \cos\lambda_9 + \Delta a_2 \cos 2\lambda_9 + \Delta b_1 \sin\lambda_9 + \Delta b_2 \sin 2\lambda_9 + \epsilon_T \qquad (7)$$

and for the sample function model,

$$\Delta h_{S9} = \Delta c_0\phi_0(\lambda) + \Delta c_1\phi_1(\lambda_9) + \Delta c_2\phi_2(\lambda_9) + \Delta c_3\phi_3(\lambda_9) + \Delta c_4\phi_4(\lambda_9) + \epsilon_S \qquad (8)$$

where ϵ_T and ϵ_S are the random errors due to unmodeled effects.

These condition equations, one for each data point, result in general in a matrix normal equation of rank 5 which is solved by inversion for the vector of coefficient adjustments.

However, if we examine the terms of the sample function condition equations we find that they are all small except the term whose sample function region of definition contains the data point. This region is bounded by the two vertical bars in Figure 1c for function $\phi_3(\lambda)$. If we keep only the partial derivatives for data within the sample function region of definition and neglect all other partial derivatives, then the complete set of condition equations for the sample functions reduces to equations of one term. For example, for data points i = 9, 10, 11, and 12 we have

$$\Delta h_{Si} = \Delta c_3\phi_3(\lambda_i) \qquad i = 9,\ 10,\ 11,\ 12 \qquad (9)$$

The related normal equation for all data points becomes diagonal (of rank 1) and may be solved term by term. For example, the correction to C_3 is given simply as

$$\Delta C_3 = \sum_{i=9}^{12} \phi_3(\lambda_i)\,\Delta h_{Si} \Big/ \sum_{i=9}^{12} \left[\phi_3(\lambda_i)\right]^2 \qquad (10)$$

and no matrix inversion is necessary. This is the basis of algorithm 1. Of course some error is committed in assuming a diagonal matrix. This is the error due to neglect of the off-diagonal terms of the normal matrix, i.e., the terms whose sample function partial derivatives are evaluated at data points outside their regions of definition; $\phi_3(\lambda_{13})$ and $\phi_3(\lambda_8)$ for example. In effect, we assume the sample functions have null value outside their region of definition. The sample function $\phi_3(\lambda)$ is in effect assumed to have the shape shown in Figure 1c by the heavy lines. The effect of this assumption is evaluated by computer simulation described in Section 3. Computation of geoid heights from algorithm 1 involves evaluation of all of the sample functions at the desired point. No simplification is afforded by algorithm 1 for this computation, which can be rather time consuming.

For this reason, and perhaps to avoid the necessity for computing the transformation matrix $[C]^{-1}$ of Equation (2), Giacaglia and Lundquist (1972) proposed a simpler algorithm, herein called algorithm 2. In this algorithm all altimeter data within the sample region is aggregated or averaged and the average value is assigned to the sample point centroid of the sample region. Thus the sample function coefficient DC process is simply a process of data sorting and averaging. To calculate geoid heights at data points intermediate to sample points Giacaglia suggests using an elementary interpolation function technique.

Section 2 details the procedure to be used in numerical simulations of these two algorithms as applied to the altimeter problem.

Section 3 presents a discussion of the sample function geopotential and the methods of construction of the sample functions which is important to understanding algorithm 1. An exposition of the error incurred in diagonalization of the normal matrix in algorithm 1 is also presented.

Section 4 presents the development of an interpolation technique for use with algorithm 2.

Results of numerical simulation tests using both algorithms are discussed and compared in Section 5.

2. APPROACH

In this paper both algorithms are utilized in computer simulations of the altimeter problem and their performance is compared with a view toward processing operational altimeter data. The most meaningful criterion for comparing these sample function geopotential model algorithms is based on the geoid surface. This is the surface that is measured (in the mean over the ocean) by the altimeter and it is readily obtained from geopotential model parameters. The candidate formulations are written in terms of the disturbing potential T. Through Brun's formula, (Heiskanen and Moritz (1967)), the geopotential models generate a corresponding model of geoid heights. To compare the model algorithms, it is proposed to: (1) generate simulated altimeter data over a predetermined standard geoid. This standard geoid will be defined so as to represent actual altimeter data distributed over a real local geoid; (2) use this simulated altimeter data to differentially correct the coefficients of the sample function geopotential model via both algorithms and construct corresponding geoid surfaces; and (3) compare the geoid heights of the standard geoid with those calculated by the model algorithms. The resulting root sum square difference in the geoid heights between the standard geoid and the calculated geoids is a measure of the efficiency of the algorithm formulation in recovering geopotential information from altimeter data. We have defined the altimeter residual as

$$\Delta h \triangleq H - H^c \tag{11}$$

where H is the observed altitude and H^c is the altitude calculated using satellite position and a priori geoid information.

From Brown, (1972) the vector relation between altitude and geoid undulation is

$$\vec{H} \cong \vec{r}_e - \vec{r}_{se} - \vec{N} \tag{12}$$

where $\vec{r}_e$ is the geocentric vector to the satellite

$\vec{r}_{se}$ is the geocentric vector to the normal to the ellipsoid through the satellite

Therefore we may replace the altitude residual by an undulation residual

$$\Delta h = |\vec{H} - \vec{H}^c| = -|\vec{N} - \vec{N}^c| \triangleq -\Delta N \tag{13}$$

assuming that $\vec{H}$ and $\vec{H}^c$ are colinear. This enables us to replace Δh by $-\Delta N$ in condition equations, making unnecessary the simulation of the satellite position for geopotential model testing.

Geoid undulation or geoid height residuals ΔN_i are constructed by subtracting a calculated geoid height from simulated observed geoid height at a particular point. A standard geoid specified by a table of geoid heights will be used as the simulated observed geoid heights. Calculated geoid heights will be zero initially.

The chosen standard geoid is derived from astrogeodetic measurements compiled by the National Geodetic Survey.[1] This geoid is specified by a table of geoid heights at certain locations (latitude and longitude) on the reference ellipsoid.

The standard geoid serves as a standard for comparison of fit of the geopotential models and also as a basis for simulating the observed altitudes (geoid undulations). The simulated observations are generated by adopting the standard geoid values without modification.

The condition equations formation thus enabled, normal equations are formed and solved and a new geoid is calculated from the adjusted geopotential coefficients at the standard geoid point locations. The RMS value of the geoid height differences at these points, after adjusted coefficient values have converged,[2] shall be the primary criteria of the comparison. Both candidate sample function algorithms shall be fit to the standard geoid by the above procedure. Considerations of the computer central processor unit (CPU) time and input/output (I/O) time required shall be important factors in the comparison, however.

The performance of the algorithms will be compared at various levels of detail, i.e., for various degrees of model expansions. The minimum level of detail tested will correspond to 25.7° by 25.7° square elements on the surface of the globe and the maximum level of detail will correspond to 1.4° by 1.4° square elements.

3. SAMPLE FUNCTION GEOPOTENTIAL MODELS - ALGORITHM 1

To construct the sample functions in terms of spherical harmonics, one must evaluate the matrix of transformation coefficients $[C]^{-1}$ of Equation (2). This may be done in several ways. We may simply numerically evaluate and invert the $[C]$ matrix, Equation (3), provided that the chosen sample points (θ_i, λ_i) do not render this matrix singular. While straightforward, this method is difficult to implement as N increases. For $N = 180$, corresponding to an expansion capable of modeling 1° by 1° geoid detail, the matrix $[C]$ is of rank 32,761 and is invertable only by laborious partitioning methods.

Another way to implement the transformation Equation (2) is to transform the spherical harmonics to a set of functions which are orthonormal in summation over the sample points. Then the new transformation matrix $[D]$ becomes orthogonal and

$$[D]^{-1} = [D]^{T} \tag{14}$$

Lundquist and Giacaglia (1969) suggest implementing this transformation by Gram-Schmidt orthogonalization over the chosen set of sample points. This method, which involves a good deal of computer time for higher N values, is the method currently used in sample function-spherical harmonic transformations.

Of course, if the set of sample points can be found for which the spherical harmonics are orthonormal in summation, then we may write for the transformation equation

$$\vec{\sigma}(\theta, \lambda) = [C]^{T}\begin{pmatrix}\vec{X}\\ \vec{Y}\end{pmatrix} \tag{15}$$

where $[C]$ is given by Equation (4).

At the present time the sample points for which the spherical harmonics are orthogonal are unknown for degree N larger than 1. For higher degree models, spherical harmonic-like sample functions are constructed by the Gram-Schmidt method on a set of sample points distributed uniformly over the globe according to Lundquist and Giacaglia's 1-3-5 distribution rule.

The Earth's disturbing potential is expressed in terms of sample functions by transforming the spherical harmonics by Equation (2). The disturbing potential is given in terms of spherical harmonics as

$$T(r,\theta,\lambda) = \frac{\mu}{r} \sum_{n=0}^{N} \sum_{m=0}^{n} \left(\frac{a}{r}\right)^n \left\{ \delta C_{no} X_{no}(\theta,\lambda) + C_{nm} X_{nm}(\theta,\lambda) + S_{nm} Y_{nm}(\theta,\lambda) \right\} \quad (16)$$

where μ is the Earth's gravitational constant

r is the geocentric radius vector

a is the equatorial radius of the reference ellipsoid

δC_{no} are the differences between the zonal coefficients of the gravity field model and the reference field model

C_{nm}, S_{nm} are the geopotential model coefficients

By the Gram-Schmidt technique we may construct a relation between the spherical harmonics and the sample functions as

$$\vec{\phi}(\theta, \lambda) = [D]^T [E] \begin{pmatrix} \vec{X}(\theta, \lambda) \\ \vec{Y}(\theta, \lambda) \end{pmatrix} \quad (17)$$

where $[D]$ is the orthogonal matrix of vectors $[E]\left(\vec{X}(\theta, \lambda), \vec{Y}(\theta, \lambda)\right)^T$ evaluated at the sample points and $[E]$ is the matrix obtained from Gram-Schmidt orthogonalization of the spherical harmonics. Rewriting Equation (16) in vector form and substituting the inverse of Equation (17), we have for the disturbing potential in sample functions

$$T(r, \theta, \lambda) = \frac{\mu}{r} \vec{\zeta}^T \cdot \vec{\phi}(\theta, \lambda) \quad (18)$$

where $\vec{\zeta}$, the vector of sample function coefficients, is given by

$$\vec{\zeta} = \left(\frac{a}{r}\right)^n [D] \; [E]^{-1^T} \begin{pmatrix} \delta\vec{C}_{no} \\ \vec{C}_{nm} \\ \vec{S}_{nm} \end{pmatrix} \quad (19)$$

Following the development in Brown (1972) and by analogy with Equations (9) and (10), we obtain a diagonal normal matrix which may be solved for adjustments to the sample function geopotential coefficients as

$$\Delta\zeta_j = - \frac{\sum_{i=1}^{m} r_i \phi_j(\theta_i, \lambda_i) \Delta h_i}{\sum_{i=1}^{m} \left[\phi_j(\theta_i, \lambda_i)\right]^2 r_i^2} \quad (20)$$

where all measurements $i = 1, 2, \ldots, m$ fall within the region of definition of the j^{th} sample function.

This assumption of a diagonal normal matrix (single term condition equation) will cause an error in the recovered geopotential coefficient adjustment due to the neglect of the effect of adjacent correlated sample functions. The effect of adjacent sample functions on the differential correction of a sample function in whose region the data point falls is expected to be of second order due to the localized nature of the sample functions (see Figure 1c). However, the cumulative effect of all adjacent sample functions may be significant.

The actual error incurred in diagonalizing the normal matrix for the differential correction of spherical harmonic sample functions coefficients may be evaluated by computer simulation. The differential correction of geopotential coefficients is calculated from simulated altimeter data by two methods: (1) the full normal matrix, including partial derivatives of all terms of the expansion for all data, is inverted; and (2) the diagonalized normal matrix is solved term by term. The difference in the corrections to the coefficients in these two cases is one measure of the error caused by diagonalization. Another is the root-mean-square (RMS) difference between calculated and simulated altimeter data. The case simulated is shown in Figure 2 as a map of the sample function boundaries. The degree of expansion is seven, i.e., N = 7, resulting in 64 sample functions. Geoid height data, used for simulation of altitude residuals (Brown, 1973), is distributed over 34 of these function regions in a fashion which permits 5 data points per sample region. The data point positions are depicted in Figure 2. These geoid height values, obtained from the 1^{o} by 1^{o} detailed geoid maps of Vincent, et al, (1972) are differenced with geoid heights calculated from the SAO-69 geopotential model (Gaposchkin (1970)) and normal equations are formed for adjustment of the sample function coefficients. Solution of the full normal matrix of rank 34 yields the coefficient adjustments which are regarded as the standard of comparison. These are the adjustments which minimize the square of the residuals when the sensitivity of all sample functions to all the data is considered.

The results of this differential correction are shown in Table 1. The coefficients calculated from the a priori field model are presented in terms of geoid height at the centroid of the sample function area. The differential correction to several coefficients is shown for the solution of the full normal matrix (converged in one iteration) and for several iterations of the solution of the diagonal normal matrix (converged in 11 iterations). The correct adjustments, i.e., those from the solution of the full normal matrix have an average of -2.86m with a standard deviation of 30.60m.

From theoretical consideration of these statistics, (Brown (1974)), a worst case coefficient error of 41.28m is predicted when the normal matrix is diagonalized. The RMS deviation of the diagonal normal matrix adjustments from the correct adjustments was 16.33m RMS in the first iteration, dropping to 12.79m in the final iteration. This is significant but well within the predicted maximum error. The adjustments from the full normal matrix solution (the correct adjustments) were used to calculate geoid heights at the data points and the difference between these values and the observed data is 4.35m RMS. The corresponding residual statistic from the converged value of the diagonal matrix solution is 9.55m RMS. Thus diagonalization of the normal matrix resulted in an increase of RMS error of fit of about 103 percent.

Table 1. Sample Function Coefficients

Sample Function No.	A Priori Value	Adjustment Using Full Normal Matrix	Iteration No. 1	Iteration No. 5	Iteration No. 11
5	-33.35	47.15	73.06	43.88	44.47
6	-68.89	41.62	50.66	42.18	41.87
7	9.03	38.01	49.05	42.21	41.70
8	-27.42	42.32	45.08	37.70	37.87
9	-59.09	32.90	36.41	29.93	30.14

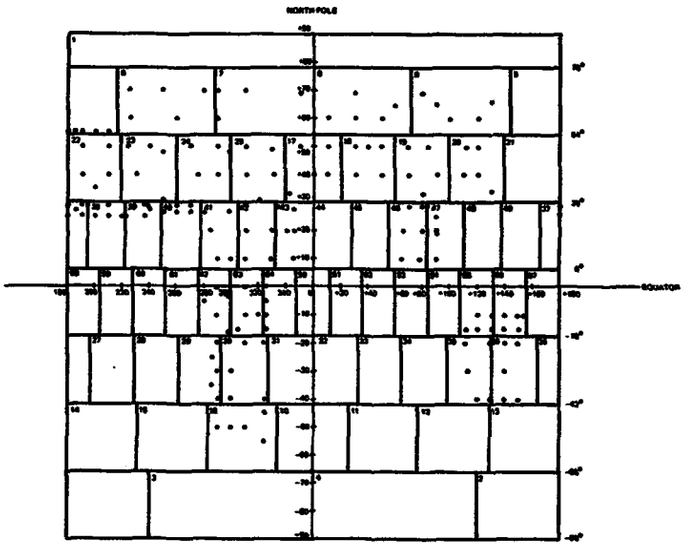

Figure 2. Sample Function Regions and Data Distribution

Table 1. Sample Function Coefficients (Cont'd)

Sample Function No.	A Priori Value	Adjustment Using Full Normal Matrix	Iteration No. 1	Iteration No. 5	Iteration No. 11
16	-16.97	25.54	24.94	19.99	19.99
17	38.68	7.69	13.36	8.16	8.11
18	0.80	9.91	20.42	8.20	8.17

4. SAMPLE FUNCTION GEOPOTENTIAL MODELS - ALGORITHM 2

Algorithm 2 represents a substantial simplification of the sample function DC process. Estimation of model coefficients (assuming zero a priori value) is merely a process of forming the average value of the geoid heights encompassed by the sample region. That is, by analogy with Equation (20),

$$\Delta\zeta_j = -\frac{a}{m}\sum_{i=1}^{m}\Delta h_i \qquad (21)$$

where the geocentric radius to the data points has been set to the constant value a, the equatorial radius of the reference surface. This value $\Delta\zeta_j$ is ascribed to the centroid of the sample region, i.e., the sample point. As Giacaglia and Lundquist (1972) point out, these coefficient values may be transformed by the matrix [C] (Equation (4)) to obtain estimates of the equivalent set of spherical harmonic coefficients.

Considerable simplification also occurs in the calculation of geoid heights at points intermediate to the sample points. Giacaglia and Lundquist (1972) suggest the use of the spherical sample function as an interpolation function between sample points. These functions have unit value at a particular sample point and null value at all immediately adjacent sample points. Numerical simulations have revealed the existence of more suitable interpolation functions but the application principle is the same. We desire the intermediate height values to lie on a smooth surface through the sample points which is continuous and preferably differentiable at all points in the modeled region. This is the classical interpolation problem in two dimensions. However, as mentioned by Jancaitis and Junkins (1973), the standard interpolation techniques result in unwieldy functions or numerical difficulties when applied to a large two dimensional array of values such as are formed by algorithm 2. To avoid these difficulties, Junkins and Jancaitis have developed a sequential surface averaging method based on locally valid polynomials which yields mth order continuity at the boundaries of the regions of validity. They have found that this interpolation method approximates local data in a weighted least square sense; permits efficient calculation and direct access of its determining parameters; is easily utilized for arbitrarily large data sets; and allows significant compaction of storage of the interpolation polynomial parameters.

In Figure 3, the profile of a sequence of algorithm 2 sample function coefficients in one dimension is presented. To obtain a smooth functional representation of this sequence, an interpolation function $\phi(x)$ is constructed as a weighted average of two adjacent sample function coefficients.

The weighting functions are shown in Figures 3b through 3d. The domain of a given local polynomial function spans the domain of the associated sample function $F_j(x)$ and extends to cover half the domain of the adjacent sample functions. Note that the weighting functions have unit value at the associated sample point and diminish to zero at the adjacent sample points. The interpolation curve profile is shown in

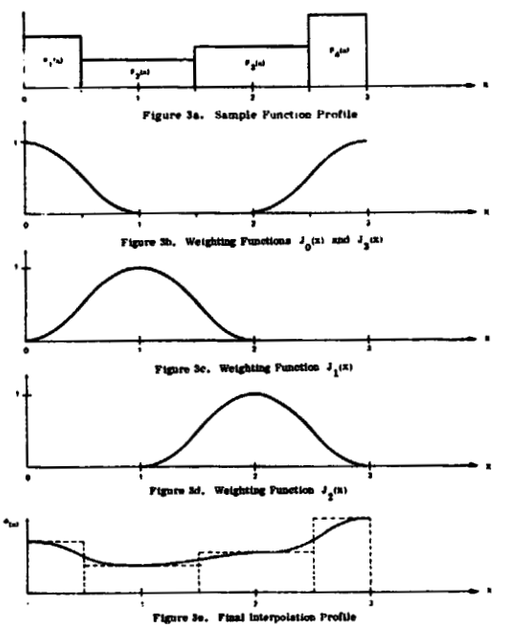

Figure 3a. Sample Function Profile

Figure 3b. Weighting Functions $J_0(x)$ and $J_3(x)$

Figure 3c. Weighting Function $J_1(x)$

Figure 3d. Weighting Function $J_2(x)$

Figure 3e. Final Interpolation Profile

Figure 3. Local Weighting Function Approach to Interpolation in One Dimension.

Figure 3e. The resulting curve is smooth, achieving the value of the sample functions at the sample point and having zero derivative at the sample point.

Generalization to two dimensions is obtained by forming the product of the weighting functions in each of two orthogonal directions.

5. COMPARISON OF SAMPLE FUNCTION ALGORITHMS

In this section the results of numerical simulations of the altimeter problem are presented and compared for the two sample function model algorithms.

5.1 Sample Function Model Test - Algorithm 1

Computer simulations of the ability of the spherical harmonic sample function model to recover the standard geoid were conducted for degrees 7, 9, 12, and 15 using algorithm 1, diagonalization of the normal matrix. The simulation results are shown in Table 2. The RMS error of fit to the standard geoid heights varies between 1.79m and 7.59m and seems to bear no relationship to the degree of the expansion. Since the standard geoid area is only 20^0 by 20^0 in size, these relatively low order models do not represent the fine details of the standard geoid. The mean spherical arc distance between adjacent sample points in the test region is 27.22 degree for $N = 7$ and 15.35^0 for $N = 15$. Because of this, small shifts in the location of the sample regions relative to the standard geoid data can cause large changes in the quality of the model fit. This may explain the absence of a pattern of decreasing RMS error as N increases. At $N = 15$ we see also the effect of numerical instability due to the Gram-Schmidt process.

Table 2. Algorithm 1 Test Results

Degree of Expansion	Mean Sample Point Spacing (deg)	RMS Error of Fit (m)	Computer Time[3] Used Per Iteration (sec)	Number of Iterations
7	27.22	5.24	41	8
9	24.77	1.79	104	4
12	19.10	1.99	(275)	5
15	15.35	7.59	554	4
36			(17,400)	
180			(10,310,000)	

Extension of these simulation tests to higher degree is not practical at this time due to the prohibitive amounts of computer time required. As the degree of the model N increases, the computer time (CPU plus I/O) needed to converge to a solution increases dramatically. The computer times in Table 2 are observed to increase proportional to $(N + 1)^4$. This is expected since the number of model terms is $(N + 1)^2$ and the number of terms in the normal matrix is $(N + 1)^4$. The observed proportionality has been extended in Table 2 to obtain running time estimates for cases $N = 36$ and $N = 180$.

5.2 Sample Function Model Test - Algorithm 2

The sample function algorithm 2 was employed to fit the two-dimensional standard geoid using a square grid of sample regions, ranging in size between 21.8 and 1.4 arc

degrees. The sample function coefficients are evaluated as per Equation (21) in Section 4. An interpolation is also calculated between sample points as described in Section 4 in order to obtain a smooth model surface. The results of these simulated geoid recovery runs are summarized in Table 3. The small amount of computer resources required for computation of these model coefficients compared to the spherical harmonic sample function coefficients allows modeling of the standard geoid to much higher detail. The maximum detail (minimum area) represented is about 1.4° by 1.4° arc degrees corresponding approximately to degree $N = 126$. The fit of the interpolated model surface to the standard geoid is 74 cm. RMS in this case (see Figure 4). The fit worsens as the degree decreases going from 0.74m to 5.74 RMS as N decreases from 125 to .

Table 3. Algorithm 2 Test Results

Degree of Expansion	Mean Sample Point Spacing (arc deg)	RMS Error of Fit (m)	Computer Time Used Per Iteration (sec)	Number of Iterations
8	21.78	5.74	6.5	6
15	11.75	4.29	7.2	5
30	5.89	1.92	6.8	4
60	2.96	1.16	7.7	3
125	1.44	.74	14.4	3

In the cases $N = 60$ and $N = 125$, the quantization of the standard geoid area into sample regions resulted in several sample regions which contained no data. To remedy this problem, a simple technique for estimating or extrapolating a value for the coefficient of the empty regions was used. If these regions were left unadjusted, the fit worsens to .88m for the case $N = 125$.

Interpolation also has a salutory effect on the RMS error of fit using algorithm 2. For example, without interpolation, the fit degrades to 1.13m for $N = 125$.

5.3 Comparison of Results

Comparison of the two spherical harmonic sample function algorithms in terms of accuracy of fit of the standard geoid is difficult. Construction of the spherical harmonic sample function model using algorithm 1 for degree sample region size smaller than 15 by 15 arc degree is impractical due to the large amount of computer time consumed. For larger sample region areas, the results are ambiguous due to data distribution-sample region location effects which occur when the sample cell size approaches that of the size of the data region (about 20 by 20 arc degrees). The best fit with algorithm 1 is 1.79m RMS for degree $N = 9$ and a mean sample point spacing of about 24.77 arc degrees. This compares roughly to the case $N = 8$ in algorithm 2 with a mean sample point spacing of 21.75° and an RMS error of fit of 5.74m RMS. Thus one might conclude that the algorithm 1 sample function model is superior to algorithm 2. But for one tenth the computer time, one may obtain a solution in algorithm 2 which fits smaller details of the standard geoid and with an RMS error of 74 cm. In practice, by increasing model degree N, this algorithm can surpass the results of algorithm 1 in accuracy with little or no increase in cost to compute. Furthermore it has been proven feasible and practical to construct a highly detailed (1.4° by 1.4°) local geoid and geopotential model by processing altimeter data using algorithm 2. At present this is not practical using algorithm 1. Thus for the forseeable future algorithm 2 is recommended for recovering geopotential and geoid information from satellite altimeter data. Extension of this modeling technique to a global geoid is elementary. Since the sample functions are orthogonal, several local geoid

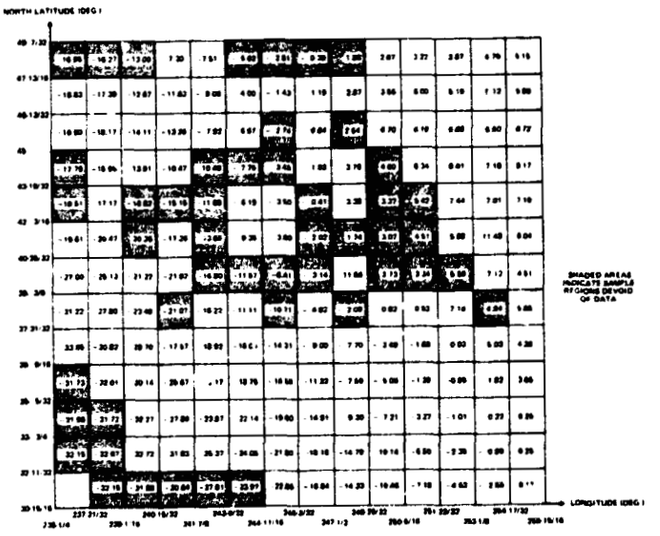

Figure 4. Solution Map for Algorithm 2 (N = 125).

models may be adjoined at their common boundaries to form larger, perhaps global, geoid models.

REFERENCES

Brown, R. D., "Note on the Diagonalization Error of the Sample Function Normal Matrix," to be published, 1974

Brown, R. D., "Test Plan for Geoid Model Comparison," Computer Sciences Corporation Technical Note 3000-08100-01TN, Prepared for NASA-GSFC under Contract No. NAS 5-11999, August 1973

Brown, R. D., and R. J. Fury, "Determination of the Geoid from Satellite Altimeter Data," National Aeronautics and Space Agency, Goddard Space Flight Center, X-550-72-268, September 1972

Gaposchkin, E. M., and K. Lambeck, "1969 Smithsonian Standard Earth (II)," Smithsonian Astrophysical Observatory (SAO) Special Report SAO SR 315, 1970

Giacaglia, G. E. O., and C. A. Lundquist, "Sampling Functions for Geophysics," SAO Special Report No. 344, July 1972

Heiskanen, W. A., and H. Moritz, Physical Geodesy, W. H. Freeman and Co., 1967

Jancaitis, J. R., and J. L. Junkins, "Modeling N-Dimensional Surfaces Using a Weighting Function Approach," paper presented at the 54th Annual AGU Meeting, April 16-20, 1973, Washington, D. C.

Lundquist, C. A., and G. E. O. Giacaglia, "Possible Geopotential Improvement from Satellite Altimetry," Smithsonian Astrophysical Observatory (SAO) Special Report No. 294, February 10, 1969

McGoogan, J. T., C. D. Leitao, W. T. Wells, and N. A. Roy, "Satellite Altimeter Results from the SKYLAB SL-3 Mission," paper presented at the 1974 Annual Spring AGU Meeting, April 8-12, 1974, Washington, D. C.

Vincent, S., W. E. Strange, and J. G. March, "A Detailed Gravimetric Geoid from North America to Eurasia," NASA-GSFC X-5 3-72-94, March 1972

FOOTNOTES

[1]Obtained from Dennis Carrol of the National Geodetic Survey, Rockville, Maryland.

[2]Even though the geopotential formulations are linear in the geopotential coefficients, convergence may require more than one iteration due to the neglect of the correlation of adjacent spherical harmonic sample functions in the spherical harmonic sample function model.

[3]Using the GSFC IBM 360/95 computer in the high speed core mode.

A TWO SATELLITE TECHNIQUE FOR MEASURING THE DEFLECTION OF THE VERTICAL (THE DOVIMETER)†

Steve M. Yionoulis
Harold D. Black
The Johns Hopkins University
Applied Physics Laboratory
Silver Spring, Maryland

ABSTRACT

A system is proposed to measure the deflection of the vertical (DOV) at sea. Two earth satellites are used, separated by about 200 km in the same, near-polar orbit. Each carries a radar altimeter. A 3 ghz satellite-to-satellite doppler link connects the two satellites. By subtracting consecutive readings of the altimeter in one satellite, the DOV component along the satellite's ground track is determined. Due to the earth's rotation, the satellite ground tracks are separated by about 14 km; thus by subtracting the altimeter readings in one satellite from those in the other, the DOV component across the ground tracks is found. Since all altimeter readings are differenced, only precision, not absolute accuracy of altitude measurement is required. Satellite orbits integrate high frequency geodetic effects; these are highly correlated between and along the satellite orbits, and introduce little error. The satellite-to-satellite link provides the necessary information to remove biases. Detailed study of the effects of geodesy, tracking, and other errors indicate that it is feasible to cover the world oceans in 3 to 6 months; measuring the DOV to an accuracy of 2 to 4 arc sec at points on a 10 to 15 km grid. A satellite altimeter capable of 10 cm precision is required and is documented in a report by MacArthur (1973).

INTRODUCTION

The Applied Physics Laboratory, sponsored by the Navy Space Projects Office (PM-16) has studied the use of satellite-borne altimeters in measuring the small scale structure of the geoid. In particular, to determine their feasibility in documenting the deflection of the vertical (DOV) in broad ocean areas. This paper is a synthesis of the detailed report (APL, 1973)

There are several factors which have motivated interest in the use of satellite-borne radar altimeters.

First, all evidence indicates that mean sea level (MSL) is a very close approximation to the geoid; a surface of constant potential in the combined gravity and centrifugal fields of the earth. The largest departures of MSL from the geoid are due to the major ocean currents. The Gulf Stream, one of the strongest currents, produces a 1 m height change over a 100 km distance, a slope of 2 arc sec (Sturges, 1972). Wind waves, tsunamis, tides etc., cause even smaller deviations. Therefore, detailed

† This work was supported by the Navy Space Projects Office/Naval Electronics Systems Command, Department of the Navy under Navy Contract N00017-72-C-4401.

information on the shape of the sea surface will greatly enhance knowledge of the earth's gravity field.

A second factor is the current status of satellite geodesy. Dynamic satellite geodesy has been a highly successful technique. When the first satellites were launched, errors in determining the position of the satellite were of the order of a kilometer. With models of the gravity field that are now available, the errors are (on the order of) 10 meters. Since, however, a satellite's motion is very insensitive to the small scale features of the earth's gravity field, the existing gravity models reflect features with a scale of 1000 kilometers or larger. To augment the current models and reflect in them the small (10 km) scale structure, new measurement techniques are required.

Since satellite-borne altimeters are capable of resolving features on the order of tens-of-kilometers over the broad ocean areas, they promise to yield significant improvement in our knowledge of the earth's gravity field. A major challenge has been the design of a radar altimeter that could provide the necessary precision. Surprisingly, within the current state-of-the-art in hardware development, this now seems feasible. MacArthur (1973) and Goldfinger (1973) present and analyze the design of a 10-cm precision altimeter.

THE DEFLECTION OF THE VERTICAL

The most precise way of using the altimeter data is in computing the deflection of the vertical. Many of the error sources are strongly correlated between consecutive measurements; thus their net effect is considerably reduced in computing the surface slope.

The DOV is defined as the angle subtended by a) the normal to the geoid and b) the normal to a reference ellipsoid at the point of intersection on the geoid surface. This angle, at any point, can be represented by two independent components; usually taken as the deflections in the north-south and in the east-west directions. However, we can start by finding the deflections in any two independent directions and subsequently resolving them into the north-south and east-west components. In studying the use of satellite altimetry, it is convenient to take the two directions as the "along-track" and "cross-track" directions, respectively. The along-track component is measured along the direction in which the sub-satellite point is moving on the surface of the earth, and the cross-track component is measured in the perpendicular direction.

The orbital motion of the satellite supplies the horizontal displacement needed for finding the along-track component, but some independent w · must be found for finding the cross-track component.

In the GEOS Program (NASA, 1973) this will be accomplished by placing the satellite into an orbit with an inclination of 115°. Thus, the intersections of north-westerly transits with south-westerly transits will provide the two necessary independent measurements needed to define the DOV.

This method is straightforward, but it requires that the altimeter continue to work in orbit for a long period of time. More seriously, complete reliance on the results obtained by a single satellite is required. The limited redundancy in the technique leaves much to be desired.

THE DOVIMETER

A method (Black, 1972) that overcomes these disadvantages is based upon the use of two identical satellites that are placed into the same orbit (Figure 1). Each of the two satellites would contain the following instrumentation:

1. A radar altimeter,
2. Data storage with telemetry readout over selected sites,
3. Doppler beacons to permit tracking by means of the TRANET tracking system,
4. A satellite-to-satellite link to permit each satellite to measure the Doppler shift of the radiation from the other satellite,
5. Low-level thrusting instrumentation to make minor adjustments in the along-orbit position.

We call this two-satellite instrument "the Dovimeter" since it is quite literally a deflection of the vertical "meter". The common orbit would have an inclination of about 70^{o}. This permits covering all open-water areas of the oceans. In the event that one satellite fails before mapping of the entire earth is complete, this inclination allows the single-satellite method of operation. An orbital altitude of 1000 km does not impose severe power requirements on the altimeter design and is high enough such that drag effects on the satellite are not a problem.

Both satellites would be launched on the same vehicle, as nearly as possible into the same orbit, except that they would be separated along orbit by 200 kilometers (30 seconds in time). This separation distance is not critical and needs only rough control to keep it within acceptable bounds. Whatever the spacing, it will be carefully monitored using the tracking data. This satellite configuration is shown in Figure 2 as viewed by an observer on the earth.

As satellite 1, the lead satellite, moves around the earth, its sub-satellite point traces out the line CD on the surface of a reference ellipsoid that approximates the earth. Satellite 2, the trailing satellite, is in the same orbit as seen from space. However, by the time it reaches the point analogous to C, the earth has rotated by a small amount. Thus, the sub-satellite track of satellite 2 is displaced westward from CD, to AB, the line BC is a cross-track line between the satellites. With an in-plane separation distance of 200 kilometers, the maximum east-west distance between the two satellite subtracks will be 14 kilometers at the equator.

The deflection angles would be computed in two different ways.

First, a polynomial fit to each one-second span of altitude data from each satellite would be performed. This computation could be done on the satellite and only the fitted parameters saved for transmission at some later time. This would greatly reduce the storage requirements needed by each satellite and simplify the logistics of transmitting the data back to earth.

The along-track slope determined by this fit will not be affected by any constant bias in the radar altimeter. The two major error sources are the differential satellite altitude errors over the data span and the altimeter measurement noise. Because of the relative geometry, satellite along-track and cross-track errors do not have a significant effect on the slope determination. In computer simulations that we have performed,

satellite ephemerides were generated which contained RMS errors of 40 meters. The differential altitude errors over 1 second time intervals in the ephemeris of each satellite had an RMS amplitude of 1.5 cm. This would cause an error in the DOV of less than 0.5 arc sec (see Appendix for details).

To compute the cross-track component of the DOV we use those height measurements between satellites when both occupy (approximately) the same argument of latitude on the same orbital revolution.

The success of this slope determination depends on several factors:

The uncorrelated geodesy error between the two satellite ephemerides computed for the same arguments of latitude. This error depends on the magnitude of the geodesy errors in each ephemeris and on the in-plane separation distance between the two satellites. It is also important, when determining the orbits of both satellites, that a "compatible" set of initial conditions be found. For example, if the ground-based Doppler data obtained from one of the satellites contained errors that are uncorrelated with those obtained from the other satellite; this could introduce uncorrelated orbital frequency errors in the two ephemerides. To minimize this effect, the satellite-to-satellite Doppler data would be processed together with the ground-based tracking data in a simultaneous determination of both satellite orbits. This technique will highly correlate the errors in two ephemerides.

A comparison of the two generated orbits containing 40 meter RMS errors, showed that the differential errors had an RMS amplitude of 16 cm. This was further reduced to 10 cm by applying short-arc tracking techniques to the differential altimeter measurements. This is equivalent to a 1.4 arc-sec error in computing the cross-track component of the DOV. The simulations also showed that differences of 100-150 meters in the mean orbital planes of the two satellites did not have a significant effect on the size of these errors.

We emphasize that those results are based on RMS orbital errors of 40 meters, a highly conservative number. It is reasonable to assume that, if necessary, using data from these satellites, current gravity models could be improved to provide 10-20 meter tracking capability. This implies that we could expect a factor of two reduction in the size of the satellite errors.

Finally, in utilizing the height measurements between satellites, we must be able to eliminate any relative bias or drift between the two altimeters. This can be accomplished via a linear least-squares fit to the differential altitude data over several orbital revolutions. If there is no bias then the average value should reflect the difference in the mean semi-major axes of both satellites. All other contributing effects should have a zero mean. An accurate confirmation of this is provided by the satellite-to-satellite data: Over a comparable time interval this data provides an accurate measure of the difference in the mean periods of the satellites. The period difference can be used to infer an independent determination of the difference in the mean semi-major axes.

Thus, the Dovimeter gives both components of the deflection for any part of the ocean that the satellite pair passes over. In addition, since the orbits are not polar, if the altimeters continue to operate, each satellite ultimately gives both components, as in the GEOS approach. However, in the time that a single satellite needs to achieve a particular amount of coverage, the satellite pair will give three independent measurements of each component. It will also provide more data and cross checks

than will two satellites operating independently. Finally, the two different methods that are involved in finding the components are "somewhat" independent; thus we may infer the accuracy of the results with considerable confidence.

REFERENCES

APL Report (1973), "Radar Altimetry Satellite Program," SDO-3476, May 7, 1973.

Black, H. D., APL Patent Office File No. 4401-51, "Method and Apparatus for Obtaining the Fine Scale Structure of the Gravity Field," September 14,1972.

Gaposchkin, E. M., and Lambeck, K., "Earth's Gravity Field to the Sixteenth Degree and Station Coordinates from Satellite and Terrestrial Data, J. Geophys. Res., 76, 4855-4883, 1971.

Goldfinger, A. D., JHU/APL Report TG-1228, "Distortion Effects in Phase-Coded Radars with Digital Signal Processing," November 1973.

MacArthur, J. L., JHU/APL Report TG-1226, "A Radar Altimeter for Satellite Applications," October 1973.

National Aeronautics and Space Administration, "GEOS-C Mission," Wallops Station, Wallops Island, Virginia, December 1973.

Sturges, W., "Comments on Ocean Circulation with Regard to Satellite Altimetry," in Sea Surface Topography from Space, Vol. II, edited by John R. Apel, NOAA Technical Report ERL 228-AOML 7-2, 1972.

Yionoulis, S. M., Heuring, F. T., and Guier, W. H., "A Geopotential Model (APL 5.0-1967) Determined from Satellite Doppler Data at Seven Inclinations," J. Geophys. Res., 77, No. 20, 3671-3677, July 10, 1972.

APPENDIX

ERROR ANALYSIS OF DOV MEASUREMENT

Notation

r_s, Φ_s, λ_s - inertial radius, latitude, and longitude, respectively, of the satellite

H_s, L_s, C_s - satellite ephemeris errors in altitude, along-track, and cross-track, respectively

r_e, Φ_c, λ_c - geocentric radius, latitude, and longitude of a point on the reference ellipsoid

a_e, f_e - semi-major axis, and flattening of the reference ellipsoid

r_g, Φ_g - geocentric radius, and latitude of a point on the geoid

Φ_G - geodetic latitude of r_e

h - altitude of satellite above geoid

ξ - North-South component of the deflection of the vertical

κ - East-West component of the deflection of the vertical

h_R - height of satellite above reference ellipsoid

H_g - geoidal height relative to reference surface

R - distance along reference ellipsoid over which deflection angle is computed

f_s - satellite true anomaly

ERROR ANALYSIS

The deflection of the vertical can be computed using the following formula (see Figure A-1).

$$\delta = \frac{(h_{R_1}-h_1^{(o)})-(h_{R_2}-h_2^{(o)})}{R} = \frac{(h_{R_1}-h_{R_2})-(h_1^{(o)}-h_2^{(o)})}{R} \qquad (1)$$

The altitude measurements obtained from the radar altimeters are given by h_1, h_2 and as shown in the figure will not in general be measured along the perpendicular to the reference surface. However, we can write that

$$h_1-h_2 = (h_1^{o}-h_2^{o}) \cos\delta \approx (h_1^{o}-h_2^{o})\left(1-\frac{\delta^2}{2}\right)$$

or (2)

$$(h_1^{o}-h_2^{o}) = (h_1-h_2) + (h_1-h_2)\frac{\delta^2}{2} + 0(\delta^4)$$

Since the maximum value that the DOV attains is about 150 arc sec then

$$\delta_{max} \approx 7.5 \times 10^{-4} \text{ rad}$$

and in the worse case

$$h_1-h_2 \leq 10^5 \text{ cm} = 1 \text{ km}.$$

Therefore

$$(h_1-h_2)\frac{\delta^2_{max}}{2} \leq 3 \times 10^{-2} \text{ cm},$$

and the approximation

$$h_1^{o}-h_2^{o} = h_1-h_2$$

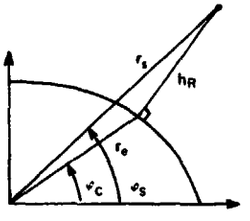

results in a negligible error. This approximation is used in Equation (1).

The parameter h_R is the perpendicular distance from the satellite to the reference surface. Given the satellite's position, h_R is computed as (see sketch above)

$$h_R^2 = r_s^2 + r_e^2 - 2 r_s r_e \cos(\varphi_s-\varphi_c)$$

or (3)

$$h_R = \left[(r_s-r_e)^2 + 2 r_s r_e (1-\cos[\varphi_s-\varphi_c])\right]^{1/2}$$

$$\varphi_c = \varphi_s + \alpha f_e \sin 2\varphi_s \left\{ 1 + f_e \left[\frac{1}{2} + 2 \left(a + \frac{1}{2} \right) \cos 2\varphi_s \right] \right\} + 0 \left(f_e^3 \right) \tag{4a}$$

$$\alpha = \frac{r_e}{r_s} - 1 \tag{4b}$$

$$r_e = a_e \left[1 + f_e \frac{(2-f_e)}{(1-f_e)^2} \sin^2 \varphi_s \right]^{-1/2} \tag{4c}$$

The subtrack distance, R , between measurements is computed from

$$R = \left[(r_{e_1} - r_{e_2})^2 + 2\, r_{e_1} r_{e_2} (1 - \cos \gamma) \right]^{1/2} \tag{5}$$

where

$$\cos \gamma = \sin \varphi_{c_1} \sin \varphi_{c_2} + \cos \varphi_{c_1} \cos \varphi_{c_2} \cos(\lambda_{c_1} - \lambda_{c_2})$$

Performing an error expansion of Equation (1) we obtain

$$\Delta\delta = \frac{\Delta(h_{R_1} - h_{R_2})}{R} - \frac{\Delta(h_1 - h_2)}{R} - \frac{\Delta R}{R}\, \delta \tag{6}$$

The first and third terms on the right-hand side of Equation (6) are the result of satellite ephemeris errors. The middle term includes the errors associated with the altimeter measurements.

GEODESY ERRORS

From Equation (3) we can obtain, with sufficient accuracy

$$\Delta(h_{R_1} - h_{R_2}) = H_{s_1} - H_{s_2} - \Delta(r_{e_1} - r_{e_2}) \tag{7}$$

utilizing $\Delta r_s \equiv H_s$.

Also, from Equation (4c) we have

$$\Delta(r_{e_1} - r_{e_2}) \approx - a_e f_e \sin 2\varphi_{c_1} \left[\Delta\varphi_{s_1} - \Delta\varphi_{s_2} \right] \tag{8}$$

As an upper bound we can write that

$$\Delta\varphi_{s_1} - \Delta\varphi_{s_2} \leq \frac{1}{r_s} \left[(L_{s_1} - L_{s_2})^2 + (C_{s_1} - C_{s_2})^2 \right]^{1/2} \tag{9}$$

Also

$$\Delta R \leq \left[(L_{s_1} - L_{s_2})^2 + (C_{s_1} - C_{s_2})^2 \right]^{1/2} \tag{10}$$

Using the above results, the satellite ephemeris errors contributing to the DOV computation can be written as

$$\Delta\delta_{sat} = \frac{H_{s_1} - H_{s_2}}{R} + \frac{\left[(L_{s_1} - L_{s_2})^2 + (C_{s_1} - C_{s_2})^2 \right]^{1/2}}{R} \left[\frac{a_e f_e \sin 2\varphi_c}{r_s} - \delta \right] \tag{11}$$

In Equation (11) note that

$$\frac{a_e f_e \sin 2\varphi_c}{r_s} - \delta \approx 0 \left(10^{-3} \right) \tag{12}$$

therefore the satellite along-track and cross-track errors will have an insignificant effect on the computed DOV. As is

intuitively obvious, the satellite altitude errors will have the most direct effect on the DOV errors. The results given in (11) are applicable for both the single satellite as well as the inter-satellite determinations of the DOV.

To minimize ephemeris errors when using the data from a single satellite, to compute deflection angles, only consecutive measurements are used. Thus the determinations are subjected only to the time rate-of-change of the errors between measurements which are at a once-per-second data rate. Similarly, minimum differential errors, between satellite ephemerides, are achieved when those ephemerides are compared for the same argument of latitude (on the same orbital revolution). However, it is also necessary that compatible sets of initial conditions be determined for both satellites. Uncorrelated errors in the doppler data used to determine the satellite orbits introduces these latter errors.

To study the magnitude and character of the expected satellite ephemeris errors, two different models of the earth's gravity field were used in performing computer simulations. Several existing models of the gravity field yield comparable tracking accuracies. For these simulations the SAO 1969 model (Gaposchkin and Lambeck, 1971) and the APL 5.0 model (Yionoulis, Heuring and Guier, 1972) were selected since different satellite constellations and data types were used in the determination of the model coefficients. The SAO 1969 model is complete through the 16th degree and order of the potential expansion, with higher order resonant coefficients determined through degree 22. The APL 5.0 model has values for the coefficients complete through [11, 11] with additional terms through the 17th degree.

In the simulations we assumed that the SAO model represented the "real" gravity field of the earth. Two 1 1/2 day ephemerides were generated with this model to represent the "true" orbits of each of the two satellites. Initially, both satellites were placed in the same mean orbital plane with an in-plane separation distance of 210 km. The true ephemerides were in turn used to generate doppler data for the TRANET system of tracking stations over the 1 1/2 day span. This doppler data for each satellite was then processed by our Orbit Determination Computer Programs (ODP) to obtain "tracked" ephemerides using the APL 5.0 gravity model. The data spans contained 68 transits at 13 different stations. The total RMS error after fitting to the data was 38 meters. The "true" ephemerides were then compared with the tracked ephemerides, based on the APL 5.0 model, for both satellites and the differences in position and velocity in the $H_s L_s C_s$-space were computed. The unit vectors associated with this space are defined as

$$\hat{H}_s = \frac{\bar{r}_s}{|\bar{r}_s|}$$

$$\hat{L}_s = \frac{\bar{r}_s \times \left(\frac{d\bar{r}_s}{d\theta} \times \bar{r}_s \right)}{\left| \bar{r}_s \times \left(\frac{d\bar{r}_s}{d\theta} \times \bar{r}_s \right) \right|}$$

$$\hat{C}_s = \frac{\frac{d\bar{r}_s}{d\theta} \times \bar{r}_s}{\left| \frac{d\bar{r}_s}{d\theta} \times \bar{r}_s \right|}$$

As stated earlier, for the single satellite determinations of the DOV the satellite error equation, (11) can be written as

$$\delta\Delta_{sat_1} = \frac{\dot{H}_s \Delta t}{R} + \left[\dot{L}_s^2 + \dot{C}_s^2\right]^{1/2} \frac{\Delta t}{R}\left[\frac{a_e f_e \sin 2\varphi_c}{r_s} - \delta\right] \qquad (13)$$

where Δt = 1 sec. The ephemeris comparisons yielded a maximum altitude velocity error, $\dot{H}_s$, of 4 cm/sec with an RMS value of 1.5 cm/sec. Thus for $R \approx 6.4 \times 10^5$ cm the resultant maximum and RMS error in the DOV is 1.25 and .47 arc sec, respectively.

To determine the extent to which the errors will be correlated between satellites, the position errors generated above for each satellite were then compared at the same argument of latitude. The effects of along-track and cross-track errors were again negligible. However, the altitude differences had an RMS of 16 cm which resulted in an RMS DOV error of 2.4 arc sec.

These results were obtained with both satellites in the same mean orbital plane. To test the sensitivity of the errors to this assumption, the above computer runs were repeated with differences in the mean kepler elements of both satellites of 100-150 meters, with the exception of $\bar{a}$, the mean semi-major axis. (Since $\bar{a}$ directly affects the satellite period and thus the relative in-plane phase of the two satellites, it will be desirable to keep this difference small. Because of the relationship between the $\bar{a}$ and the period, maintaining small differences in these elements should be easily accomplished.) As was expected, these changes did not have an appreciable effect on the final answers.

Not included in the above results are the contributions from uncorrelated errors in the initial conditions of the two satellites. There are several ways in which these errors can be eliminated. Satellite-to-satellite doppler measurements can be processed together with the ground tracking data to solve simultaneously for the initial conditions of both satellites. This data will serve as a very strong constraint between the two satellite orbits.

To further minimize the uncorrelated satellite orbit errors, the altimeter measurements would be used in a least-square fitting procedure. This would also serve to edit the measurements and detect bad data points. Computer simulations were performed to determine the effectiveness of using the altimeter measurements in this manner.

The altitude of the satellite above the geoid can be computed from

$$h = \left[(r_s - r_g)^2 + 2\, r_s r_g\,(1 - \cos\left[\varphi_s - \varphi_g\right])\right]^{1/2} \qquad (14)$$

where

$$\varphi_g = \varphi_c - (r_e/r_g - 1)\sin 2\varphi_c f_e\left[1 + f_e(1/2 + \cos 2\varphi_c)\right] + O(f_e^3)$$

$$r_g = \left[(r_e + H_g)^2 - 2\, r_e H_g\,(1 - \cos\left[\varphi_G - \varphi_C\right])\right]^{1/2}$$

$$\varphi_G = \tan^{-1}\left[\frac{1}{(1-f_e)^2}\tan\varphi_C\right] \qquad (15)$$

and r_e and φ_c are computed from Equation (4). Again the SAO model was used to simulate the "real" altitude data for each satellite, including the computation of the geoidal height, H_g. One sigma noise of 10 cm was added to this data to simulate the expected altimeter instrumentation errors. Residuals in h were computed for each satellite using the ephemerides generated with

the APL model which included the integrated effects of initial condition errors. A data selection was made to retain only those residuals occurring while the satellites were over the broad ocean areas. Then the residuals from both satellites were differenced for the same argument of latitude of the satellites. These residuals were then used in a least-squares fit to solve for relative initial condition errors between the satellite ephemerides.

From a first order error analysis, the residuals that are fitted can be written as

$$\Delta h_1 - \Delta h_2 = H_{s_1} - H_{s_2} - (\Delta H_{g_1} - \Delta H_{g_2}) - \Delta(r_{e_1} - r_{e_2}) + N_1 - N_2 \quad (16)$$

where the integer subscripts are used to distinguish between the residuals obtained from each of the two satellites. N_1-N_2 represents the noise added to the data. As was shown earlier, the only significant satellite errors are those in the altitude component. From perturbation theory we get that initial condition errors in altitude will propagate as

$$H_s = A_0 + A_1 \sin f_s + A_2 \cos f_s \quad (17)$$

where f_s is the satellite true anomaly and the A_i's are functions of the initial condition errors. The differential errors in altitude between satellites can also be parameterized as in Equation (17).

In performing the least-squares fit to the residuals over the 1 1/2 day span, we were able to recover the relative initial condition errors to better than 1 cm.

The final RMS altitude error in the residuals was 15.2 cm, after the removal of the initial condition errors. By partitioning the data and fitting over shorter time intervals (each consisting of approximately four orbital revolutions of data) this RMS was reduced to 10.5 cm.

There is an added advantage in fitting to the differences in the altimeter measurements. If there are relative biases in the altimeter data they could be absorbed into the A_0 parameter. These biases will cancel in computing the deflections in the satellite along-track direction and therefore do not contaminate the results. A further advantage is that the magnitude of these residuals will be considerably smaller than for that of each satellite's taken separately. This is due to the correlated satellite errors being cancelled in differencing the two satellites' residuals.

SUMMARY AND CONCLUSIONS

It is conservative to expect that the use of modern (1972) gravity models will result in (no greater than) 30-40 meter ephemeris errors in tracking these new orbits. The studies indicate that with ephemeris errors of this magnitude, the uncorrelated errors between the two satellites' orbits will be 15.2 cm RMS. This is for an in-plane separation distance of 210 km between satellites. There are two ways in which this error can be easily reduced.

1. By short-arc tracking techniques using the altimeter measurements, some of the geodesy errors can be absorbed by the orbit parameters. In the simulations, the data were partitioned into groups each consisting of roughly 4 satellite revolutions of data. Fitting over these intervals resulted in a reduction from 15.2 cm to 10.5 cm RMS in the effect of the uncorrelated geodesy errors. The use of a more sophisticated error model should result in a further reduction.

2. We believe that the recent (since 1972) improvements in gravity models have more than halved the geodesy errors. Consequently, the uncorrelated altitude error is most likely in the 5-10 cm range. Interestingly enough, data from this experiment itself is adequate to confirm or deny our belief. In the (unlikely) event that it is not true, the data should be adequate to supply the improvement.

In computing the deflection angles in the satellite along-track direction, the computations are sensitive only to the differential errors in each ephemeris over one-second intervals, the elapsed time between altimeter measurements. In the simulated case, these errors were less than 2 cm RMS in the presence of 38 meter RMS tracking residuals.

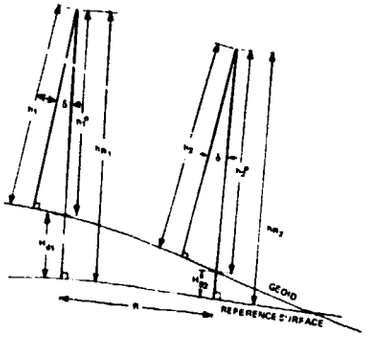

$$\delta = \frac{(h_{R_1} - h_{R_2}) - (h_1^o - h_2^o)}{R}$$

$$h_1^o - h_2^o = h_1 - h_2 + O\left[(h_1 - h_2)\frac{\delta^2}{2}\right]$$

$$\Delta\delta = \frac{H_{S_1} - H_{S_2} - \Delta(h_1 - h_2)}{R}$$

Figure A-1. Geometry Associated with the DOV Computation

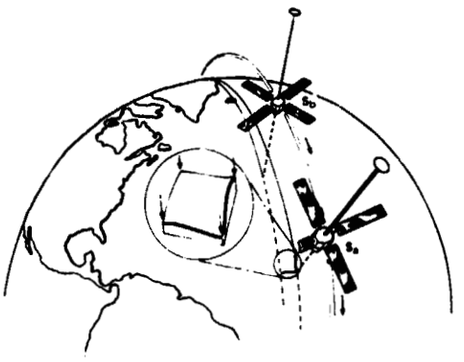

Figure 1. DOVIMETER

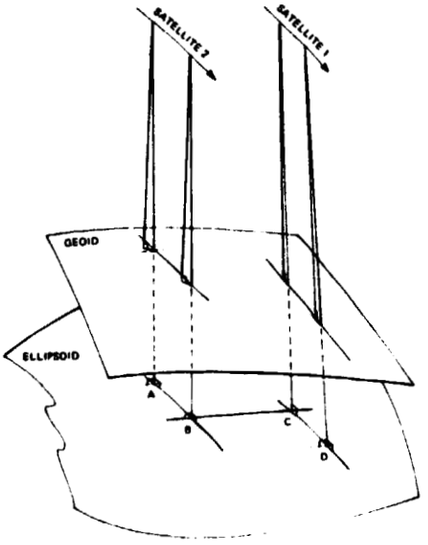

Figure 2. Geometry of the Two-Satellite Approach

THE APPLICATION OF GEOS-C DATA TO MARINE GEODESY BY MEANS OF THE SIMPLE-DENSITY LAYER CONCEPT

Foster Morrison
Geodetic Research & Development Laboratory
National Ocean Survey, N.O.A.A.
Rockville, MD 20852 U.S.A.

ABSTRACT

The availability of GEOS-C altimeter data will provide a crucial test of the mettle of the simple density layer concept. Altimetry will supply data about the geopotential in the frequency range between that of satellite orbital perturbations and the very fine structure obtained by dense gravimetry for geophysical exploration.

Required for analyzing altimeter data are formulae for point gravity anomalies (or means over small areas, 1° square or less) and for high frequency components of the geoid height. The effect of local density anomalies must be computed accurately and those of remote density anomalies rapidly and efficiently.

Geopotential representations may be thought of as interpolations, even though the parameters used are not discrete values of potential or gravity. As such, they may be evaluated in terms of accuracy and efficiency. For an enormous amount of information as is contained in the fine structure of the earth's gravity field, the questions of efficient storage and recovery are crucial.

Attempts have been made to evaluate the effectiveness of the density layer concept by computer simulations. New algorithms have been devised in the process.

Another question, important for satellite geodesy and orbit determination, is the structure of the errors in computing the gravity. Satellite orbits are highly sensitive to this structure, since large perturbations may be caused by small forces if resonance or secular accumulation effects are present. Both computer simulations and analytic models are being used to isolate and eliminate such problems.

1. INTRODUCTION

The surface density distribution already has been applied with considerable success to determining the long wave part of the geopotential [*Kooh, 1974*]. This and several other methods have been suggested for coping with the problems engendered by the slow decay of spherical harmonic coefficients. *Krarup [1969]* has given a proof that the gravity field of a planet can

be approximated arbitrarily well by *some* spherical harmonic representation. The theory of geopotential representation including the so-called gravity prediction theory [*von Luetzow, 1973*] still has some unanswered questions. For some recent results see *Koch and Pope* [*1972*]. Even the exact status of the theory is not well known due to the lack of communication between geophysicists and mathematicians.

For the purposes at hand, let us review the practical implementation of surface coating geopotential models and the heuristic reasoning that motivated what has been done. *Vinti* [*1971*] and *Giacaglia and Lundquist* [*1972*] considered surface coatings on an enclosing sphere. Their suggestions amount to nothing more than changing names, however. In these approaches the formulas and algorithms for gravity and potential would be no different from those using the usual spherical harmonic series; the density layer is just an auxiliary concept. By contrast, *Koch and Morrison* [*1970*] used a density layer located on the surface, or rather on a surface generated by adding mean topographic heights to a satellite generated geoid. No spherical harmonic coefficients were used, rather the numerical quadrature algorithm was identical to point masses fixed in location but not in magnitude [*Morrison, 1971*]. In a similar vein is the work of *Balmino* [*1972*] and some others who have sought optimal point mass distributions and solved some of the problems of singularities at the surface by burying the points at a safe depth.

Morrison [*1972b*] observed that the basic integral for potential as a function of density

$$U = G\iint \frac{\chi d\sigma}{r} , \qquad (1)$$

is a relatively tractable improper double integral and suggested that *judicious combinations of approximate analytic and numerical* quadratures would solve most of the practical problems of geopotential modeling [*Morrison, 1972a, 1973*]. The initial tests of the algorithms for (1) were made on large 15° × 15° blocks. Even though spherical harmonics may well be best for potential undulations of such wave lengths, the severe curvature of the earth's surface facilitated the analysis of numerical results. The use of the important small angle approximations needed in this approach was critically tested by arguments of 7½°; and having only 288 density blocks kept computer experiments inexpensive.

The anticipated availability of GEOS-C altimetry has removed the discussion of modeling the fine structure of the gravity field from the academic to the practical arena. Inevitably, mathematical and heuristic arguments will have to yield to the relentless discipline of the data. To prepare for this eventuality, we shall examine in a mathematical and heuristic way the capabilities of the surface coating methods and algorithms to cope with the GEOS-C data. Success of this analysis will be measured by how little numerical experimentation we shall have to do to make our computer programs operational.

2. PREDICTION PROBLEMS AND TRUNCATION ERRORS

Generalized prediction techniques were introduced into geodesy by *Kaula* [*1959*] and extended and refined by *Krarup* [*1969*] and *Moritz* [*1972*]. Geodesy has been plagued by high precision data with a very poor distribution, a problem shared by other disciplines in geophysics.

Every numerical process, including geopotential modeling, has truncation and rounding errors. For simple problems it is easiest and most economical just to use computers with long word lengths or double precision. There is such a vast amount of information in the earth's gravity field, however, that we are strongly motivated to tolerate as much truncation error as possible so that storage problems do not arise and also so that round-off errors may be kept in check by the simple expediency of having less computations. The importance of the spatial distribution of truncation errors, or their "statistical properties" if you wish, was noted by *Morrison* [*1972a*]. Satellite orbits in particular sample the gravity field in such a way that small truncation errors could become significant if they had the proper distribution to cause secular, long period, or resonant "perturbations." Estimations of stationary quantities such as point or mean gravity anomalies or deflections of the vertical are much less demanding.

A principal tool for studying the statistical properties of a geophysical parameter such as gravity is the autocorrelation function (ACF). It is defined as

$$\phi_{ff}(x,y) = E\,[f(X,Y)\, f(X+x,\, Y+y)] \qquad (2)$$

where E is the "ensemble expectation operator," which is just an average over a sufficiently large portion of the domain of f. For the theory to be viable ϕ_{ff} should not change significantly

for alterations in the area of the averaging or its precise location; it is said that ϕ_{ff} is "stationary." Usually, ϕ_{ff} is even assumed "isotropic," i.e.,

$$\phi_{ff}(x,y) = q\,(x^2 + y^2). \tag{3}$$

Where q is a function of one variable, choosing and using the ACF is as much an art as a science. What we want are some candidates for the ACF for a surface density layer. The problem of deriving internally consistant ACF's etc., for geopotential quantities has been discussed in detail by [*Jordan, 1972*].

Experimenting with Jordan's techniques has suggested the following sequence of definitions and transformations leads most easily to the desired results. Consider, first of all, Brun's formula [*Heiskanen and Moritz, 1967*]

$$N = \frac{T}{\gamma} \tag{4}$$

The derivation of (4) indicates that it does, in fact, involve a linearization; for most purposes and particularly for statistical analysis the formula is sufficiently accurate. For the disturbing potential T we substitute the integral over the surface coating to obtain

$$N = \frac{G}{\gamma}\iint\frac{\chi d\sigma}{r} \tag{5}$$

In the terminology of *linear systems* [*Papoulis, 1965*], our surface density χ is an *input process* and the geoid height N is an *output process*. The *impulse response* is

$$h\,(x,y) = \frac{G}{\gamma r} \tag{6}$$

$$= \frac{G}{\gamma}\,(x^2 + y^2)^{-\frac{1}{2}}$$

By definition, the *system function* is the Fourier transform of $h\,(x,y)$.

$$H\,(\omega_1, \omega_2) = \int_{-\infty}^{+\infty}\int_{-\infty}^{+\infty} h(x,y)\,\exp(-i\omega_1 x - i\omega_2 y)\,dxdy. \tag{7}$$

Obviously, we are retaining the "flat-earth" approximations used by *Jordan* [*1972*]. The *power spectral density* (PSD) of a process is the Fourier transform of its ACF

$$\Phi_{ff} = \iint_{-\infty}^{+\infty}\phi_{ff}\,\exp(-i\omega_1 x - i\omega_2 y)\,dxdy. \tag{8}$$

The Fundamental Theorem of linear systems relates the PSD's of the input and output of a linear system by means of the system function:

$$\Phi_{HH} = \Phi_{XX} |H|^2 . \qquad (9)$$

Where H_H is the system function for the linear system $X \rightarrow H$.

Fourier transforms of functions with circular symmetry can be "simplified" to Hankel transforms

$$\bar{f}(\Omega) = \int_0^\infty r f(r) J_0(\Omega r)\, dr ; \qquad (10)$$

$$\Omega^2 = \omega_1^2 + \omega_2^2$$

$\bar{f}(\Omega)$ is the Hankel transform of $f(r)$ and J_0 is the Bessel function of the first kind of order zero. Equation (10) is obtained by expressing the two-variable Fourier transform $F(\omega_1,\omega_2)$ in polar coordinates; a factor of 2π arises

$$F(\omega_1,\omega_2) = 2\pi \bar{f}(\Omega) \qquad (11)$$

The impulse response for our linearized surface density to geoid height transformation is evidently of the form $1/r$, whose Hankel transform is well known [*Papoulis, 1968*]. Then the system function is

$$H_H = 2\pi \frac{G}{\gamma\Omega} \qquad (12)$$

As an approximation, γ is being treated as a constant. Substituting (12) into (9) and rearranging, we obtain

$$\Phi_{XX} = \frac{\gamma^2\Omega^2}{4\pi^2 G^2} \Phi_{HH} \qquad (13)$$

To obtain the surface density ACF we need only compute the inverse of the Hankel transform of (13). Finding ϕ_{XX} from Φ_{XX} in the most general case would involve tedious calculations using the convolution theorem or direct integrations. For this particular problem we can use a special identity [*Papoulis, 1968*]

$$\frac{d^2 f(r)}{dr^2} + \frac{1}{r}\frac{df(r)}{dr} \overset{h}{\longleftrightarrow} -\Omega^2 \bar{f}(\Omega), \qquad (14)$$

where the symbol $\overset{h}{\longleftrightarrow}$ indicates the application of the Hankel transform. Identify $f(r)$ with ϕ_{HH} and obtain

$$\phi_{XX} = -\frac{4\pi^2 G^2}{\gamma^2}\left[\frac{d^2}{dr^2} + \frac{1}{r}\frac{d}{dr}\right]\phi_{HH} \qquad (15)$$

Several observations should be made at this point. One is that ϕ_{gg} and ϕ_{XX} differ only by a constant factor, where g is anomalous gravity. The relationship is

$$\phi_{XX} = \frac{4\pi^2 G^2}{\gamma^2 g_0^2} \phi_{gg} \tag{16}$$

Flat-earth Stokes' and Vening Meinesz' formulas are given by *Heiskanen and Moritz [1967, p. 121]* as formulas (2-231 and (2.232) (derived there for use in inner zone computations).

For a spherical approximation, things are not as simple as in (16). Spherical harmonic expansions for a surface density [*Pinti, 1971*] and gravity [*Heiskanen and Moritz, 1967*] are not quite the same for a given external potential, even with the proper linearizations [*Meissl, 1971*]. For the surface densities the geopotentials are multiplied by $n + \frac{1}{2}$ and for the gravity anomalies by $n + 1$, where n is the degree. The global ACF for density would be a bit different from that for gravity, which is now well known [*Kaula, 1959*]

$$\phi_{gg} = \sum_n \sigma_n^2 P_n (\cos \phi) \tag{17}$$

The σ_n^2 is the sum of the squares of the fully normalized geopotential coefficients of degree n. The coefficients for a comparable formula for ϕ_{XX} would be slightly more complicated. Numerical comparisons should be made.

3. ESTIMATING THE DENSITY BLOCK SIZE

In *Morrison [1972b]* it was assumed that a suitable approximation to the surface density could be written

$$\chi = a_0 + a_1 x + a_2 y + a_3 x^2 + a_4 xy + a_5 y^2 + \ldots, \tag{18}$$

where x and y are again, local coordinates. Let us use (18) to estimate ϕ_{XX} for very small values of r, the separation. By definition

$$\phi_{XX} = E [\chi (X,Y) \chi (X + x, Y + y)] \tag{19}$$

This becomes

$$\phi_{XX} = E [a_0 (a_0 + a_1 x + a_2 y + \ldots)] \tag{20}$$

If we substitute

$$r \sin \alpha = x$$
$$r \cos \alpha = y \tag{21}$$

where α is the azimuth, we can average over α and obtain

$$\phi_{\chi\chi} = E[a_0^2] + r^2 E[\tfrac{1}{2} a_0 (a_3 + a_5)] + 0(r^4) \quad (22)$$

The first term is just the mean square of the density and the second term *must* be negative. It makes sense for a_0 and $(a_3 + a_5)$ to be of opposite signs on the average. When $a_0 > 0$, the function should be concave downward and when $a_0 < 0$, the function should be concave upward, again, on the average. Formula (22) shows some of the advantages of using an approximation like (18) for χ instead of the step function implicitely assumed by direct numerical quadrature. Estimates of $\phi_{\chi\chi}$ could be made analytically from the coefficients $a_0, a_1, a_2, \ldots$ for small separation. A fourth degree model for χ looks very promising in this regard.

To make a preliminary estimate of density block size for GEOS-C data reduction, we can use (22) two ways. First let us assume that (22) gives a good estimate of $\phi_{\chi\chi}$, say to within 1%; this could be a lower limit or block size. The upper limit would be the size of the correlation distance r_σ for which $\phi_{\chi\chi}(r_\sigma) = \phi_{\chi\chi}(0)/e$, where e is the base of the natural logarithms. This is a very reasonable upper limit when $\phi_{\chi\chi}$ is to be approximated by a parabola.

Although functional forms for ACF's and other statistical functions of geodetic quantities abound, there exist very few determinations of the parameters in these functions. One exception is the Ohio anomaly model, derived by *Hirvonen [1962]* from surface gravity data.

$$\phi_{gg} = \frac{\sigma_g^2}{1 + (r/D)^2} \quad (23)$$

$$\sigma_g^2 = 337.0 \text{ mgal}^2$$

$$D = 40 \text{ km}$$

$$r < 100 \text{ km}$$

We do not have to convert (23) to an expression for $\phi_{\chi\chi}$, since this would change its magnitude and units, but not the ratios of values for given separations. We can just say

$$\phi_{\chi\chi} = \frac{\sigma_\chi^2}{1 + (r/D)^2} \quad (24)$$

and require for our present purposes the value of σ_χ^2. The "maximum" block size comes for

$$1 + (r_{max}/D)^2 = e. \tag{25}$$

This is easy to solve:

$$r_{max} = \sqrt{e - 1}\, D \tag{26a}$$

$$= 52.43 \text{ km} \tag{26b}$$

To find the "minimum" block size we can expand the denominator of (24) in a geometric series, assuming $r < D$ and have

$$\phi_{XX} = \sigma_X^2 \left[1 - \left(\frac{r}{D}\right)^2 + \left(\frac{r}{D}\right)^4 - \left(\frac{r}{D}\right)^6 + \ldots\right]. \tag{27}$$

Truncating (27) at the second order and observing that the series alternates with decreasing terms, we can compute

$$(r_{min}/D)^4 = 0.01 \tag{28a}$$

$$r_{min} = \sqrt[4]{0.01}\, D$$

$$= 0.316\, D$$

$$= 12.65 \text{ km} \tag{28b}$$

A block size twice that of r_{min} or r_{max} is to be used, $B_{max} = 2r_{max}$, $B_{min} = 2r_{min}$. These can be expressed in angular measure:

$$\begin{aligned} B^\circ_{max} &= 56.'0 \\ B^\circ_{min} &= 13.'6 \end{aligned} \tag{29}$$

Realistically, one may as well say

$$\begin{aligned} B^\circ_{max} &= 1^\circ \\ B^\circ_{min} &= 0.^\circ 20 = 12'. \end{aligned} \tag{30}$$

All reports have indicated surprisingly little difference between the statistical properties of gravity at sea and land measurements, so the use of (23) is perfectly justified for order of magnitude estimates.

This simple analysis does not take into account the density of the sampling of the geoid height. Along the subsatellite track the samples will be at rates of 10 to 100 per second. For purposes of geoid determination, these readings might be smoothed to an average of one per second. The area coverage will

probably be no denser than a 1° square grid at any place, however. [*GEOS-C Mission Plan, 1973*] Another modifying factor is that the geoid height is rather smooth, whereas the gravity anomalies or surface density coatings have more "power" in their PSD'S at higher frequencies [*Meissl, 1971*]. All these considerations indicate a smaller block size is not needed, at least for the GEOS-C project.

4. CONCLUSIONS

A surface density layer modeled locally by (18) will be a suitable method of parameterizing the results of the GEOS-C. Blocks 1° × 1° should be small enough to model the data and none smaller than 12' × 12' should be needed anywhere.

In most ways, gravity anomalies and surface coatings have similar behavior [see also: *Meissl, 1971*]. One advantage of surface coatings is that the potential or gravity components are obtained *exactly* from density through a linear system. The impulse response is isotropic only to zero order or for a spherical coating. This impulse response is still fairly simple. Fewer linearizations are needed in practice and those that are needed can be extended to higher order easily.

The ACF and PSD of density and of geoid height will be useful in analyzing the data. Sea state information should have its own distinctive statistical properties. It should be possible to filter the data in a fairly objective way.

Truncation errors should be included in the statistical analysis of geopotential models with high resolution. Ideas of *Hardy [1971]* and *Junkins, et al, [1973]* should be useful in improving the algorithms for geopotential from a surface coating model. Modeling of the surface density function and the impulse response both can be improved and truncation error reduced.

REFERENCES

Balmino, G., Representation of the earth potential by buried masses, *AGU Monograph 15: The Use of Artificial Satellites for Geodesy*, pp. 121-124, Washington, D. C., 1972.

GEOS-C Mission Plan, NASA, Wallops Island, Va., Dec., 1973.

Giacaglia, G. E. O., and C. A. Lundquist, Sampling functions for geophysics, *SAO Special Report No. 344*, 93 pp., Cambridge, MA., 1972.

Hardy, R. L., Multiquadric equations of topography and other irregular surfaces, *JGR, 76,* 8, pp. 1905-1915, 1971.

Heiskanen, W. A. and H. Moritz, *Physical Geodesy,* 364 pp., W. H. Freeman and Co., San Francisco, 1967.

Hirvonen, R. A., On the statistical analysis of gravity anomalies. Helsinki, *Publ. Isostat. Inst. I.A.G.,* No. 37, 1962.

Jordan, S. K., Self-consistant statistical models for the gravity anomaly, vertical deflections, and undulations of the geoid, *JGR, 77,* 20, pp. 3660-70, 1972.

Junkins, J. L., et al, A weighting function approach to modeling of irregular surfaces, *JGR, 78,* 11, pp. 1794-1803, 1973.

Kaula, W. M., Statistical and harmonic analysis of gravity, *JGR, 64,* 12, pp. 2401-21, 1959.

Koch, K. R., Earth's gravity field and station coordinates from Doppler data, satellite triangulation, and gravity anomalies, *NOAA Technical Report NOS 62,* 29 pp., Rockville, MD., 1974.

Koch, K. R. and A. J. Pope, Uniqueness and existence for the geodetic boundary value problem using the known surface of the earth, *Bulletin Géodésique, No. 106,* pp. 467-476, Dec., 1972.

Koch, K. R. and F. Morrison, A simple layer model of the geopotential from a combination of satellite and gravity data, *JGR, 75,* 8, pp. 1483-92, 1970.

Krarup, T., *A Contribution to the Mathematical Foundations of Physical Geodesy,* Publ. 80 pp., No. 44, Danish Geodetic Institute, Copenhagen, 1969.

Meissl, P., A study of covariance functions related to the earth's disturbing potential, *Reports of the Dept. of Geodetic Science, No. 151,* 88 pp., The Ohio State University, Columbus, Ohio, April, 1971.

Moritz, H., Advanced least squares methods, *Reports of the Dept. of Geodetic Science, No. 175,* 129 pp., The Ohio State University, Columbus, Ohio, 1972.

Morrison, F., Density layer models for the geopotential, *Bulletin Géodésique, No. 101,* pp. 319-328, 1971.

Morrison, F., Propagation of errors in orbits computed from density layer models, *AGU Monograph 15: The Use of Artificial Satellites for Geodesy,* pp. 111-119, Washington, D. C., 1972a.

Morrison, F., Improved representations of density layer models for the geopotential, International Symposium on Earth Gravity Models and Related Problems, AGU microfilm, 1972b (Abstract in *EOS, Trans. AGU, 53,* 10, p. 890, Oct., 1972).

Morrison, F., A rational approximation algorithm for computing geopotential and gravity from a simple layer density model, abstract in *EOS, Trans. AGU, 53,* 11, pp. 966-7, Nov, 1972c.

Morrison, F., Truncation errors of algorithms for density layer models of the geopotential, abstract in *EOS, Trans. AGU, 54*, 4, p. 230, April, 1973.

Morrison, F., The potential of a simple density layer at zero and other low altitudes, abstract in *EOS, Trans. AGU, 55*, 5, p. 547, May, 1974.

Papoulis, A., *Probability, Random Variables, and Stochastic Processes*, 583 pp., McGraw Hill, New York, 1965.

Papoulis, A., *Systems and Transforms with Applications in Optics*, 474 pp., McGraw Hill, New York, 1968.

Vinti, J. P., Representation of the earth's gravitational potential, *Celestial Mechanics, 4*, pp. 348-367, 1971.

Von Luetzow, H. B., A review of collocation methods in physical geodesy and meteorology, abstract in *EOS, Trans. AGU, 54*, 11, p. 1067, 1973.

COMBINATION SOLUTIONS IN GEOID COMPUTATIONS

Erwin Groten
Technical University
Darmstadt, Germany

A b s t r a c t

Potentialities of direct prediction of geoid heights in connection with altimetry etc. are discussed in detail; pecularities in comparison to Δg-prediction on sea and to geoid height on land are pointed out. The practical application of Molodensky's formula for computing Δg from N, i.e. the inverse of Stokes's formula, is investigated. Problems inherent in the Molodensky formula related to prediction of Δg similar to astrogravimetric levelling are studied. Corresponding potentialities of "combined solutions" are stressed. Different aspects of high-precision computations of detailed and regional geoids by Stokes's and Molodensky's formulas are presented. Consequences for computation of oceanic geoid sections are discussed.

1. INTRODUCTION

Until recently the precise evaluation of the geoid in the oceans was hampered by the lack of data. Satellite orbit analysis yields only the low order part of geoid undulations, astrogeodetic information is seldom available and gravity data are affected by several deficiencies. Meanwhile, altimetry data became available so an essential improvement is feasible and new types of combination solutions in evaluating geoid undulations, N, are of interest. In this connection the direct prediction of N has been stressed in a previous paper (Groten, 1973) and specific differences between autocovariances of N on land and at sea were shown. The use of the results of such predictions have previously been outlined in Groten (1970).

The main advantage in geoid computations at sea lies in the fact that the problems related to gravity reductions do not arise as gravity is directly measured on the geoid itself. Even if gravity reductions are applied in order to get smoother functions in the numerical integration corresponding deformations of level surfaces can be exactly taken into account. Actual deviations from mean sea level and the correction for the error of flattening in the spherical approximation (according to Stokes's and similar formulas) are not crucial at this time.

2. PRACTICAL ASPECTS OF COMPUTING Δg FROM N

The application of Molodensky's well known formula which solves the "inverse problem", i.e.

$$-\Delta g_o = \gamma \frac{N_o}{R} + \frac{1}{2\pi} \iint_\sigma \frac{(N-N_o)}{\ell^3} \, d\sigma \qquad (1)$$

where R = mean radius of the earth,
Δg_o = Δg at P_o, i.e. gravity anomaly at P_o,
N_o = N at P_o, i.e. geoid height at P_o,
σ = earth's surface, dσ is its surface element,
ℓ = chord distance $\overline{P_o d\sigma}$,
γ = normal gravity,

in combination solution was proposed in 1969 by Groten, (1970) and also by Koch (1970), Young (1970) etc.. It is well known that equ.(1) holds exactly on sea where topography does not exist so the terms representing the deviations from the level surface in Molodensky's general formula, i.e.

$$\Delta g_o = 2\pi\chi\cos^2\alpha_o - \frac{3}{2R} \iint \frac{\chi}{\ell} \, d\sigma - \iint \frac{H-H_o}{\ell^3} \chi \, d\sigma \qquad (2)$$

where α = tilt of surface normal, χ = coating function and H corresponds to N in (1),

are all equal to zero. On the other hand, in numerical evaluations of N from Δg according the inverse formula of equ.(2) using $1^o \times 1^o$ blocks or even larger compartments these corrections do not play any significant role even on land as shown for a geoid section in Central Europe by Groten et al (1974).

Koch (1970), Isner (1972) and others were mainly interested in global combination solutions. But on comparing $1/\ell^3$ in (1) with the Stokes function $S(\psi)$ (where ψ = spherical distance on σ) the overwhelming influence of the neighborhood zone in (1) is seen in comparison to the corresponding influence of the neighborhood zone in case of Stokes's formula; Fig. 1 shows both functions

multiplied by $\sin(\psi/2)$ as $d\sigma = \sin\psi d\psi d\bar{\alpha}$. The graph reveals how carefully this influence has to be considered. We know a similar problem in geophysics when the vertical gravity gradient

$$\frac{d(\Delta g)}{dh} = \frac{4\Delta g}{R} + \frac{6\gamma N_o}{R^2} - \frac{1}{2\pi}\iint_\sigma (\Delta g - \Delta g_o)\ell^{-3}d\sigma \qquad (3)$$

is evaluated from surface gravity. Consequently, the main part of the information is drawn from $(N-N_o)$ in the small zone around P_o and if smoothed values of N are used a lot of information is lost. Meißl (1973) has discussed the corresponding difficulties mostly in terms of spherical harmonics.

However, the practical application of equ.(1) is somewhat less intricate than the use of (3) because N is smoother than Δg. Therefore, the global application of (1) is indeed useful. But the principles applied in the present study are different from the previous attempts in that the local and regional differences of Δg are directly computed from $(N-N_o)$ and not Δg itself.

Instead of equ.(1) we could, of course, consider the direct numerical solution of the integral equation

$$N = \frac{1}{2\pi\gamma}\iint_\sigma \Delta g\, S(\psi)d\sigma \qquad (4)$$

where N is supposed to be known and Δg is unknown; however, the solution in form of (1) seems to be optimal. When the effect E of the outer zone, i.e. $\psi > \psi_o$, is considered we arrive, on introducing some simplifying assumptions, at

$$E(\psi_o) = C\int_{\psi=\psi_o}^{\pi}\left(\frac{1}{\ell^3}\right)^2 \sin\psi\, d\psi \qquad (5)$$

where C is a constant.

Using $\ell = 2\sin(\psi/2)$ we get finally the decrease of $E(\psi_o)$ for increasing ψ_o as shown in Fig. 2. On inspecting the curve in this figure it is realized that the influence of the zones $\psi_o > 30^o$ is almost negligible. When $S(\psi)$ is introduced instead of ℓ^{-3} in equ.(5) a completely different behavior of the integral is realized.

$E(\psi_o)$ shows the error of truncation in equ.(1) whenever an ideal evaluation of the integral for $\psi \le \psi_o$ is feasible.

Further, when $(N-N_o)$ is replaced by block averages for compartments of finite size the corresponding error covariances might in addition be taken into account in C so the corresponding

effect can be evaluated. But, at present time, only the low order part of N is mostly known with sufficient accuracy so any estimate might be misleading as long as the sufficient results of altimetry are not yet available. For $\psi_o << 30^o$ var (N) and cov (N), i.e. variances and autocovariances of N, need to be known for very high degree n as both depend on n.

For $\psi_o \to 0$ the error corresponding to the global use of block averages $(\overline{N-N_o})$ instead of $(N-N_o)$ is obtained from equ.(5). But as ℓ^{-3} tends strongly to infinity as $\ell \to 0$ numerical evaluation of $E(\psi_o=0)$ is indeed intricate. On assuming that $\Delta N=(N-N_o)$ follows a quadratic law $\Delta N(\psi^2)$ in the neighborhood of P_o and that $(N-N_o) \doteq 0$ for $\ell \leq 10$ km quite plausible results are obtained which show that averages $(\overline{N-N_o})$ for blocks of 10 km by 10 km for $\psi_o \leq 1^o$ yield useful accuracy of Δg_o. Using blocks sizes of about 30 km by 30 km within $\psi \leq$ a few degrees around P_o reasonable results in a test area have been found by proceeding similarly as described for gravity anomalies in (Groten et al. 1964). If N follows the above mentioned law the error-produced by replacing $\Delta N = (N-N_o)$ by $\overline{\Delta N} = (\overline{N-N_o})$ can be evaluated in analytical form for the central cap $\psi \leq \psi_o$. By combining this error with the corresponding error which is due to the outer zone we get $E(\psi_o=0)$.

Using polar coordinates $(r,\bar{\alpha})$ we get in plane approximation the computational formula

$$\Delta g_o = \frac{-\gamma N_o}{R} - \frac{\gamma}{2\pi} \sum_k (N_k-N_o)\Delta\bar{\alpha}\,(r_1^{-1} - r_2^{-1}) \qquad (6)$$

for the contribution of the k-the compartment where $\Delta\bar{\alpha}$ is the azimut difference and $r_i (i=1,2)$ are the radii of the compartment. When the global average of N is assumed to be zero equ.(1) reads simply (Molodensky et al. 1962)

$$\Delta g_o = \frac{-\gamma}{2\pi} \iint_\sigma (N-N_o)(\ell^{-3} - \frac{1}{2R^3})\, d\sigma \qquad (7)$$

And the corresponding integral formula for practical application becomes

$$\Delta g_o = \frac{-\gamma}{2\pi} \sum_k (N_k-N_o)\Delta\bar{\alpha}[(r_1^{-1}-r_2^{-1}) - \frac{1}{4R^3}(r_2^2-r_1^2)] \qquad (8)$$

It should be noticed that the spherical approximation formulas are found by simply replacing r_i and ℓ_i in the plane approximation formulas.

When the error $m(\Delta g_o)$ is considered then reliable information on the error covariances of the input data, i.e. altimetry results

etc., is necessary. Even though such information is not yet sufficiently available it can be anticipated that when long range error-autocorrelation and aliasing effects are corrected for we end up with a formula $m(\Delta g_o)$ which corresponds to the above formula in computing E, i.e. C then becomes a corresponding "error constant".

Moreover, it is necessary to have a dense net of N-values in solving equ.(1) numerically. This can only be achieved by interpolating N within limited areas using autoregression procedures. The corresponding autocovariance function have been discussed previously and specific problems related to this question will be dealt with below.

Besides this fact cov(N) is an efficient tool in predicting mean values of N and ΔN even though N is much smoother than Δg, i.e. the amplitude of high harmonics decrease much faster with increasing n than in case of Δg, and, consequently, prediction is essentially easier with N than with Δg and feasible even over greater distances.

Until now altimetry data were mainly considered in relation to global combination solutions of geoid and gravity field determination; in connection with evaluation of spherical harmonics coefficients aliasing effects etc. (Rapp, 1971) were found to be of main concern. In this case the application of surface coatings using Helmerts spherical approximation in combination solutions as proposed by Groten (1970) and by Molodensky's methods as proposed by Koch (1970) are of principal interest because a unified approach becomes feasible.

To some extent, autoregression prediction of N might be considered as a supplementation to the sampling function method (Giacaglia et al, 1972) and similar procedures or even as an alternative method in global solutions.

3. PREDICTION OF GRAVITY DIFFERENCES FROM ΔN

In local and regional application a procedure is useful which, in principal, is quite similar to astrogravimetric leveling. Let Δg or corresponding mean values $\overline{\Delta g}$ be known at a few stations (and blocks, respectively) within a spherical cap of $\psi \leq \psi_o$. If absolute or relative geoid heights N are available at and around these stations, too, we can predict Δg at any other point P_i where only N is known as follows.

From the truncated equ.(6), i.e.

$$\tilde{\Delta g}_i = \frac{-\gamma}{2\pi} \int_{\alpha=0}^{2\pi} \int_{\psi=0}^{\psi_o} (N-N_o) \cdot \left(\frac{1}{\ell^3} - \frac{1}{2R^3}\right) d\sigma \qquad (9)$$

we get the main part of Δg at the point P_i, i.e.

$$\Delta g_i = \tilde{\Delta g}_i + \delta(\Delta g)_i \qquad (10)$$

If the separation of points P_i is small then $\delta(\Delta g)$ is nearly constant; in any other case $\delta(\Delta g)_i$ will be a small quantity which can be interpolated linearly so that Δg can be evaluated at any point P_i where N is known but Δg is not known. In our applications ψ_o was of the order of 2^o, the separations s_i of stations P_i were somewhat greater. Of course, the smaller ψ_o/s_i the greater are the variations of $\delta(\Delta g)_i$.

When

$$\psi_o/s_i > 1 \qquad (11)$$

for any i we can predict gravity differences between the points P_i if $\delta(\Delta g)_i$ can be considered as constant. In this case we only need N to be known. From equ.(10) follows then that differences between Δg_i are equal to the differences between $\tilde{\Delta g}_i$ where the latter are evaluated from equ.(9).

In our test computations we used astrogeodetic geoid heights in Germany the absolute orientation of which has previously beer determined (Groten, 1974) because detailed (gravimetric) geoids on oceans were not available to us. s_i was of the order of $\geq$ 100 km. On taking into account the potentialities of altimetry (Kaula, 1969; Chovitz, 1972 etc.) the application of global as well as regional procedures in computing Δg from N should be useful.

4. EVALUATION OF PRECISE N FROM Δg

When continental geoid sections computed from 1^o by 1^o mean free air gravity values are compared with corresponding oceanic sections it is realized that there is no basic difference in the statistical behavior of N; this holds for degree $n \leq 180$. Nevertheless, some specific differences of autocovariances have been pointed out by Groten (1973). However, the accuracy of N obtained from mean values of 1^o by 1^o block values at sea is not basicly different from those at seas if the number of gravity measurements within the block is not much different.

Besides some coastal areas where relatively dense Δg-distribution exists the best presently available gravity material at sea

is in form of 0.5° by 0.5° blocks; at least in Europe. The corresponding accuracy of N might be of the order of one meter or somewhat less. In continental geoid sections the absolute accuracy can be investigated by comparison with astrogeodetic geoid sections as far as reliable information is available. From 0.1° block averages of free air anomalies we have obtained a geoid of Germany which by comparison with the astrogeodetic section was found to have a relative accuracy of $\pm$ 0.4 m and better (Groten el al. 1974). Because of the uncertainties in GM (gravitational constant) the absolute accuracy is, of course, different from that value. The above value of about $\pm$ 1 m for N as obtained from 1° by 1° block averages is in agreement with continental geoid sections compared with astrogeodetic geoid computations in Europe.

5. PREDICTION OF N

Linear autoregression prediction as proposed by Moritz (Heiskanen et al, 1967) can be applied to geoid undulations as far as N in the specific area can be considered as a isotropic stationary process. Problems arising when anisotropy, nonstationarity etc. prevails and corresponding effects have been discussed, f.i. in (Groten, 1973a); similar problems arised when oceanic geoid heights (Vincent et al. 1973, 1973a) and continental geoid sections (Groten et al. 1973) were analyzed statistically. The oceanic results will be discussed in detail and, in order to point out discrepancies, continental data are discussed for comparison.

For the direct prediction of N we used the well known matrix formula

$$N_p = C_{pi} C_{ik}^{-1} N_k \qquad (12)$$

where N_k = known geoid height at station P_k
N_p = predicted geoid height at point P
C_{pi} = cov(N) related to $\overline{P\,P_i}$
C_{ik} = cov(N) related to $\overline{P_i P_k}$.

One-dimensional prediction along profiles is essential in dealing with altimetry data. Two-dimensional prediction is necessary to get a densification as necessary in evaluating Δg; but in the isotropic case where C_{ik} depends only on the separation $\overline{P_i P_k}$ the twodimensional case is, in principal, also one-dimensional.

The direct evaluation of cov(N) seems to be superior to the transformation of cov(Δg) into cov(N) by well known formulas

(Meißl, 1971; Lauritzen, 1973) because of the smoothness of N. The anisotropy of cov(N) which is, of course, also inherent in cov(Δg) was clearly realized in the evaluation of cov(N). For instance, in the German geoid of 0.1° block size cov(N) becomes zero for $\psi = 2^\circ$ along meridians, and already for $\psi = 1.3^\circ$ along latitude circles ϕ = const. Similar behavior is found for the 1°-block geoid by Vincent and Marsh, where cov(N) becomes zero at sea for $\psi \doteq 18^\circ$ along meridians and only for $\psi \doteq 40^\circ$ along latitude circles ϕ = const. Fig. 3 shows the normalized mean cov(N) along meridians for the western part, i.e. $160^\circ(W) \leq \lambda \leq 50^\circ(E)$, of the northern hemisphere where the most reliable information is presently available. Typical at sea is the relatively great negative autocorrelation for remote data.

The results of onedimensional linear autoregression prediction of N can be summarized as follows: (1) On land, i.e. for the above mentioned geoid in Germany, we found: (a) prediction was made from 10 to 25 profile points of equidistant separation 0.2°; the results were not much different for any number ob points $10 \leq n \leq 25$; (b) prediction was made for points at separation 10 km $\leq$ d $\leq$ 80 km; depending on the trend functions of orders 0 to 4 the predicted values of N varied almost linearly with d where the maximum error of about N/2 was found for d = 80 km along meridians; along latitude circles the situation was better; errors of about N/5 $\doteq$ 2 meters were found at d = 80 km; (c) the choice of specific trend functions had great influence whereas the regional variations of cov(N) were not of great impact; (d) when off-shore values of N were predicted from continental N-values the prediction error was smaller than on land. (2) At sea we found for the Vincent-Harch-Geoid: In twodimensional prediction the trend elimination is still more critical than in the one-dimensional case. When N-values at stations are available which are separated from the point (or area) of prediction by 50 km or less the accuracy of prediction is much improved in comparison to one-dimensional prediction. Twodimensional prediction of mean N-values of 1°-blocks at sea is feasible over great distances because of strong negative autocorrelation of N-values at $\psi = 30^\circ$ etc.. After problems related to the appropriate analytical dtermination of covariance function and to corresponding trend elimination have been solved two-dimensional prediction was applied in the below mentioned area of Pacific and Atlantic and was found to be adapted to N-prediction.

Using trend functions of first and second order onedimensional <u>extrapolation</u> in the Pacific and <u>interpolation</u> in the Atlantic ($57^\circ \leq \phi \leq 51^\circ$, $30^\circ \leq \lambda \leq 50^\circ$) was applied to N. In both cases

equidistant point values having separation of 3° were used. In the Pacific east-west profiles of known N-values contained 20 to 45 points; points to be predicted were situated along $\phi = 51^{\circ}$, 54°, 57 and at $170^{\circ}(E) \leq \lambda \leq 200^{\circ}(E)$; the number of known points from which prediction was made was again found to be not of great importance; but the results of prediction depended on the order of trend polynomial, i.e. prediction within $s = 3^{\circ}$ separation differed by $\pm$ 1 meter or so, for $s \geq 9^{\circ}$ the predicted values differed by about $\pm$ 3 m; for $s = 30^{\circ}$ even $\pm$ 5 m differences were found. When interpolation instead of extrapolation is used slightly better results were obtained.

6. CONCLUSIONS

On concluding that, in general, a basic difference in statistical behavior does not exist between continental geoid section and the geoid at sea a nearly linear relation of cov(N) = 0 (i.e. the ψ-value of the first crossing of cov(N) with the abszissa) to the side length, s, of corresponding block compartments might be inferred for $0.1^{\circ} \leq s \leq 1^{\circ}$. The extrapolation of N using linear autoregression procedures seems to be appropriate for distances $\leq$ 50 km even if accuracy as necessary in converting altimetry data into Δg is desired. For n = 180, i.e. for 1°-blocks, the mean N-values show negative autocorrelation for $\psi > 15^{\circ}$ which might be a pecularity of geoid heights at sea; consequently, autoregression prediction over greater distances might be feasible then on land even for 0.1° blocks and combination solution in terms of Δg and of N becomes feasible. However, if mean N values for 1°-blocks or similar smoothed data are used some part of the information is lost. Local application of the $N \rightarrow \Delta g$ transformation is not affected by long-range deviations of the sea surface from the geoid. On the other hand, the precise application of the transformation can yieldshort-period deviations by comparison with sea gravimetry results.

Acknowledgement: The computational work was mainly done by J. Brennecke

7. REFERENCES

Chovitz, B.: Refinement of the geoid from Geos-C data, NOAA Tech. Rep. ERL 288-AOML 7, US Dept.Comm., J.R.Apel, ed., Vol. I, 2-1, Boulder, Col. 1972

Giacaglia, G.E.O. and C.A. Lundquist: Sampling functions for geophysics, SAO Spec.Rep. 244, 1972

Groten, E.: Outline of alternative combination solutions in satellite orbit analysis, Boll.Geof.teor.appl. 47, 13, 250-255, 1970

Groten, E.: Efficiency of methods for improving the presently available information on the earth's gravity field, paper presented at Symposium on Earth's gravitational field and secular variations in position, Sydney, November 1973

Groten, E.: Problems related to absolute orientation of geodetic systems, paper to be presented at Symp. on Redefinition of N.A.Datum, Fredericton, 1974

Groten, E.: Some numerical aspects of linear regression prediction, Comm.Geodet.Ital., VI Symp. Math. Geodesy Oct. 1972, 201-227, Firenze 1973a

Groten, E. and H. Moritz: On the accuracy of geoid heights and deflections of the vertical, Inst.geod.Phot.Cartogr. Report No. 38, The Ohio State Univ. Columbus 1964

Groten, E. and R. Rummel: Variationen zum Geoid in Europa (in press), 1974

Groten, E. and R. Rummel: Improved Gravimetric Geoid for $7^{\circ} \leq \lambda \leq 12^{\circ}$(E) and $47^{\circ} \leq \phi \leq 54^{\circ}$(N), Allg. Vermessungsnachr. (in press) 1973

Heiskanen, W.A. and H. Moritz: Physical Geodesy, Freeman & Co., San Francisco 1967

Isner, J.F.: Determination of surface densities from a combination gravimetry and satellite altimetry, Ohio State Univ., Dept. of Geodetic Sci., Rep. No. 186, Columbus 1972

Kaula, W.M.: The terrestrial environment, Solid Earth and Ocean Physics, Application of space and astronomic techniques (Williamstown-Report) Cambridge, Mass. 1969

Koch, K.R.: Gravity anomalies for ocean areas from satellite altimetry, Proc.Second Marine Geodesy Symp., Marine Technology Soc. Washington, D.C. 1970

Laur[illegible], S.L.: The probabilistic background of some statistical methods in physical geodesy, Geodaet. Inst. Med. 48, Kopenhagen 1973

Meißl, P.: A Study of covariance functions related to the earth's disturbing potential, Ohio State Univ., Dept. of Geodetic Sci. Rep. No. 151, Columbus 1971

Molodensky, M.S., V.F. Eremoev and M.I. Yurkina: Methods for study of the external gravitational field and figure of the earth, (transl. from Russian) Israel Progr. for Scientific Transl. Jerusalem 1962

Rapp, R.H.: Accuracy of potential coefficients determinations from satellite altimetry and terrestrial gravimetry, Ohio State Univ. Dept. of Geodetic Sci. Rep. No. 166, Columbus 1971

Vincent, S. and J.G. Marsh: Global detailed gravimetric geoid, Intern. Symp. "Use of artificial satellites for geodesy and geodynamics", Athens 1973

Vincent, S. and J.G. Marsh: Global detailed geoid computation and model analysis, Intern. Symp. "Earth gravity field and secular variations in position", Sydney 1973a

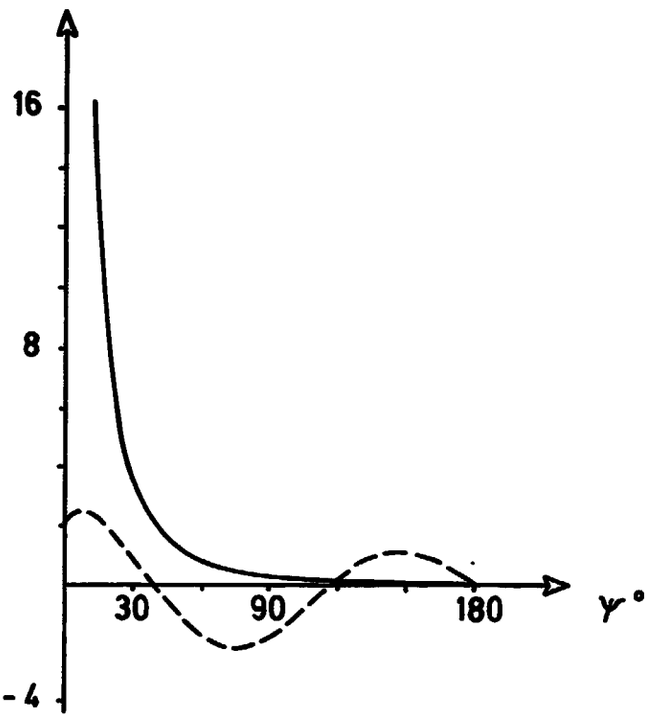

Fig. 1 Stokes's function $S(\psi)\sin\psi$ (broken line) and $\ell^{-3}\sin\psi$ for comparison.

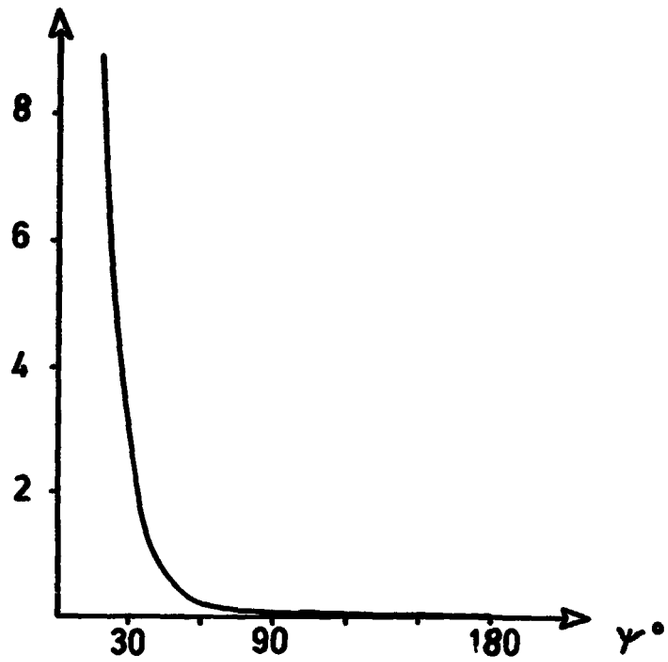

Fig. 2 The truncation function $f = 1/64\ (\sin^{-4} \psi/2)-1)$.

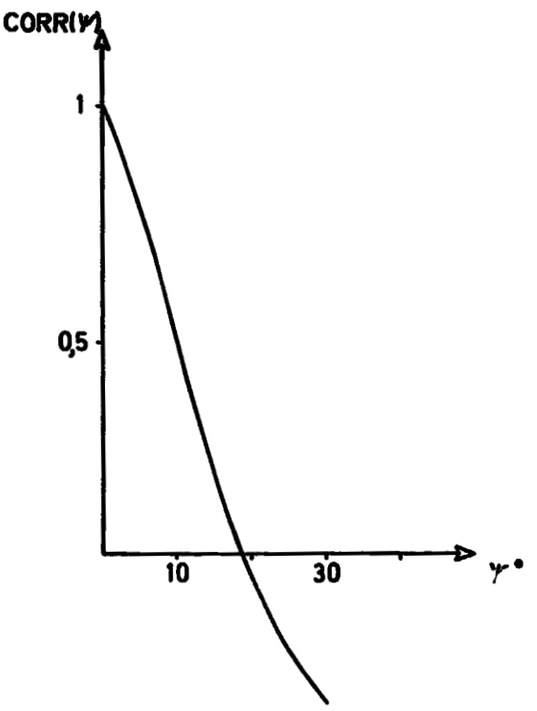

Fig. 3 Autocorrelation function of N for the western part 160° (W) $\leq \lambda \leq 50^{\circ}$(E) of the northern hemisphere

DETAILED GRAVIMETRIC GEOID FOR THE GEOS-C ALTIMETER CALIBRATION AREA

J.G. Marsh
Goddard Space Flight Center
Greenbelt, Maryland

S. Vincent
Computer Sciences Corporation
Silver Spring, Maryland

ABSTRACT

The GEOS-C spacecraft scheduled for launch in late 1974 will carry a radar altimeter for the purpose of measuring sea surface topography. In order to calibrate and evaluate the performance of the altimeter system, ground truth data are required. In this respect a detailed gravimetric geoid has been computed for the GEOS-C altimeter calibration area in the Atlantic Ocean off the East Coast of the U.S. That is, the area bounded by Wallops Island, Bermuda, Grand Turk and Merritt Island. This geoid is based upon a combination of mean free air surface gravity anomalies and the Goddard Space Flight Center GEM-6 satellite derived spherical harmonic coefficients. Surface gravity anomalies consisting of 1° x 1° and 10' x 10' mean values have been used to provide information on the short wave length undulations of the geoid while the satellite derived coefficients have provided information on the long wave length components (> 1500 km). As part of these analyses, GSFC, SAO and OSU satellite derived gravity models were used in the computations. Although geoid heights based upon the various satellite models differed by as much as 30 meters in the Southern Hemisphere, the differences in this Atlantic Ocean area were less than 4 meters.

1. INTRODUCTION

A new detailed gravimetric geoid has been computed for the GEOS-C altimeter calibration area in the Atlantic Ocean. This detailed geoid is based upon a combination of the GSFC GEM-6 Earth Model (Lerch, et al. 1974) and a set of 1° x 1° surface mean free-air gravity anomalies. This geoid incorporates a new set of 1° x 1° surface data consisting of values in the North Atlantic obtained from NOAA in addition to the previously available 1° x 1° data (Vincent and Marsh, 1973). This new set of data replaced some of the older observed data and filled in areas previously predicted.

In order to assess the effects of long wave-length errors in the satellite-derived gravity model, comparisons were made with detailed geoids computed using the Rapp 73 (Rapp, 1973) and SAO-3 (Gaposchkin, 1973) Earth Models. Comparisons were also made along a SKYLAB-Altimeter Pass in the vicinity of the Puerto Rican Trench.

2. PRINCIPLES OF COMPUTATION

The geoidal undulations at any point P on the Earth can be computed using the well known Stokes' formula:

$$N(\phi,\lambda) = \frac{R}{4\pi\bar{\gamma}} \int_{\lambda'=0}^{2\pi} \int_{\phi'=-\pi/2}^{\pi/2} \Delta g_T(\phi',\lambda') S(\Psi) \cos\phi' \, d\phi' \, d\lambda' \quad (1)$$

where

ϕ,λ = the geocentric latitude and longitude, respectively of the computation point.

ϕ',λ' = the geocentric latitude and longitude, respectively of the variable integration point.

$N(\phi,\lambda)$ = geoid undulation at ϕ,λ.

R = mean radius of the Earth.

$\bar{\gamma}$ = mean value of gravity over the Earth.

$\Delta g_T(\phi',\lambda')$ = free air gravity anomaly at the variable point ϕ',λ'.

$$S(\Psi) = \frac{1}{\sin(\Psi/2)} - 6\sin(\Psi/2) + 1 + 5\cos\Psi - 3\cos\Psi \ln(\sin(\Psi/2) + \sin^2(\Psi/2)) \quad (2)$$

where

$$\Psi = \cos^{-1}[\sin\phi \sin\phi' + \cos\phi \cos\phi' \cos(\lambda-\lambda')] \quad (3)$$

In order to provide a more accurate representation of the geoid undulations, particularly with respect to the wavelengths shorter than those resolvable with satellite observations, we have combined the satellite derived gravity data with surface 1° x 1° mean free air gravity anomaly observations. This was accomplished by dividing the Earth into two areas, a local area (A_1) surrounding the point P, and the remainder of the Earth (A_2). The anomalous gravity was partitioned into two parts represented by the symbols Δg_S and Δg_2. The Δg_S values are defined as that part of the anomalous gravity field which can be represented by the coefficients in a satellite derived spherical expansion of the gravitational potential. The Δg_2 values are defined as the remainder of the anomalous gravity field. Using the division of the Earth's surface into two areas and of the anomalous gravity into two components one can write Equation 1 in the form:

where $$N(\phi,\lambda) = N_1 + N_2 + N_3 \quad (4)$$

$$N_1 = \frac{R}{4\pi\bar{\gamma}} \int_0^{2\pi} \int_{-\pi/2}^{\pi/2} \Delta g_S(\phi',\lambda') \, S(\Psi) \cos\phi' \, d\phi' \, d\lambda'$$

$$N_2 = \frac{R}{4\pi\bar{\gamma}} \iint_{A_1} \Delta g_2(\phi',\lambda') \, S(\Psi) \cos\phi' \, d\phi' \, d\lambda' \quad (5)$$

$$N_3 = \frac{R}{4\pi\bar{\gamma}} \iint_{A_2} \Delta g_2(\phi',\lambda') \, S(\Psi) \cos\phi' \, d\phi' \, d\lambda'$$

For the computations described in this paper, the area A_1 for a point at which the geoid was being computed, was defined to consist of a twenty degree-by-twenty degree area centered on the computation point. Also in the calculations described here, the term N_3 in equation 5 was set equal to zero. This is equivalent to assuming that the satellite derived approximation to the gravity field is adequate for the area A_2 at a distance of greater than 10° from the computation point.

3. ANALYSIS

3.1 The GEM-6 Detailed Gravimetric Geoid

Figure 1 presents a contour map of the geoidal undulations for the Atlantic Ocean area (from 10° to 50° N. latitude and 280° to 320° E. longitude). Figure 2 presents the same geoid in the form of a three-dimensional plot. These geoidal undulations were computed using the GSFC GEM-6 Earth Gravity Model and a set of 1° x 1° mean surface free-air gravity anomalies. The GEM-6 gravity model is a set of spherical harmonic coefficients complete to degree and order 16 with additional terms to degree 22. This model was derived from a combination of (1) a satellite solution based on optical, electronic and laser observations of 27 satellites and (2) a global set of 5° x 5° equal area mean gravity anomalies developed by Rapp.

The parameters used in these computations were:

$\bar{W}_o$ = the potential of the geoid ($62636875\ m^2/s^3$)

$\bar{\gamma}$ = the mean value of gravity ($9.789\ m/s^2$)

a_e = the semi-major axis of the reference ellipsoid (6378142 m)

1/f = the flattening coefficient for the reference ellipsoid (298.255)

GM = the product of the universal gravitational constant and the mass of the earth ($3.986009 \times 10^{14}\ m^3/s^2$)

3.2 Inter-Model Comparisons

Previously, we have computed global detailed geoids using several satellite-derived gravity models with the same set of surface data (Marsh and Vincent, 1974). Comparisons of the geoids indicated that the precision of the geoid is highly correlated with the availability of satellite observations and surface gravity data. For example, differences as large as 30 meters were noted in the southern hemisphere. These large differences are illustrated in Figure 3 which presents detailed geoid profiles at 50°S. latitude. These geoids were computed using several recently published gravity models. In the northern hemisphere where satellite observations and surface data are more abundant, the differences in the detailed gravimetric geoids are generally less than 10 meters. Figures 4 and 5 present contour maps of the geoidal height differences when the Rapp-73 and SAO 73 models are compared with the GEM-6 model in the Atlantic Ocean area. The differences between the GEM-6 and Rapp-73 geoids are in the range of 0 to 2 meters while with the SAO-3 model, the differences were as large as 4 meters. However, these differences are relative to GEM-6 and are not necessarily an indication of the absolute long wave-length error.

3.3 Comparisons with SKYLAB Altimeter Data

As is well known, the value of Stokes' function increases rapidly as the computation point is approached. This is illustrated in Figure 5 where the value of the Stokes' function is plotted as a function of the distance from the computation point. As can be seen in Figure 6, the steepest variation is in the area of 0' to 30' from the computation point. With 1° x 1° mean values of the surface data, the shorter wavelength features cannot be detected. Therefore, with the availability of point anomalies from NOAA, a set of 10' x 10' mean anomalies were formed and incorporated into a modified program for a preliminary computation of the geoid in the vicinity of the Puerto Rican Trench. In this computation, 10' x 10' data were used for the first 3° of the computation area and 1° x 1° data were used from 3° to 10°. However, there were a large number of unobserved 10' x 10' blocks in the area of the computation. Figure 7 presents a comparison of the SKYLAB SL-2 pass 4 altimeter data (McGoogan, 1974) with the 1° x 1° detailed geoid presented in Figure 1 as well as with the preliminary 10' x 10' geoid for the Puerto Rican Trench area. As is noted in Figure 7 the relative agreement between the 10' x 10' geoid and the altimeter data is very good however, because of the large number of unobserved 10' x 10' blocks, the 1° x 1° geoid is more representative in terms of absolute scale.

4. CONCLUSIONS

An improved detailed gravimetric geoid has been computed for the Atlantic Ocean area. This geoid incorporates a new set of 1° x 1° surface data obtained from NOAA in addition to the data previously available. The precision of this geoid is on the order of 3 meters. The primary sources of error are: 1) errors in the long wave-length representation of the undulations by the satellite-derived gravity models and 2) the accuracy and density of the surface gravity data. To partially alleviate the long wave-length errors it may be necessary to increase the area of integration. The preliminary incorporation of 10' x 10' data into the geoid computations provided a better relative agreement with the satellite altimeter data as anticipated.

REFERENCES

Gaposchkin, E.M., 1973, "Smithsonian Standa ' Earth III," presented at the American Geophysical Union Meeting, Washington, D.C.; also included in the National Geodetic Satellite Program Final Report (in press).

Lerch, F., et al., 1974, "Gravitational Field Models GEM-5 and GEM-6," Goddard Space Flight Center Contribution to the National Geodetic Satellite Program Final Report (in press).

Marsh, J.G., Vincent, S., 1974, "Global Detailed Geoid Computation and Model Analysis," GSFC X-921-74-131.

McGoogan, J.T., 1974, NASA, Wallops Station, personal communication.

Rapp, R.H., 1974, "The Earth's Gravitational Field from a Combination of Satellite and Terrestrial Data," paper presented at the symposium on Earth's Gravitational Field and Secular Variations in Position, Sydney, Australia, November 1973 (in press).

Vincent, S., and Marsh, J.G., 1973, "Global Detailed Gravimetric Geoid," paper presented at the First International Symposium, The Use of Artificial Satellites for Geodesy and Geodynamics, Athens, Greece; also GSFC Document X-592-73-266.

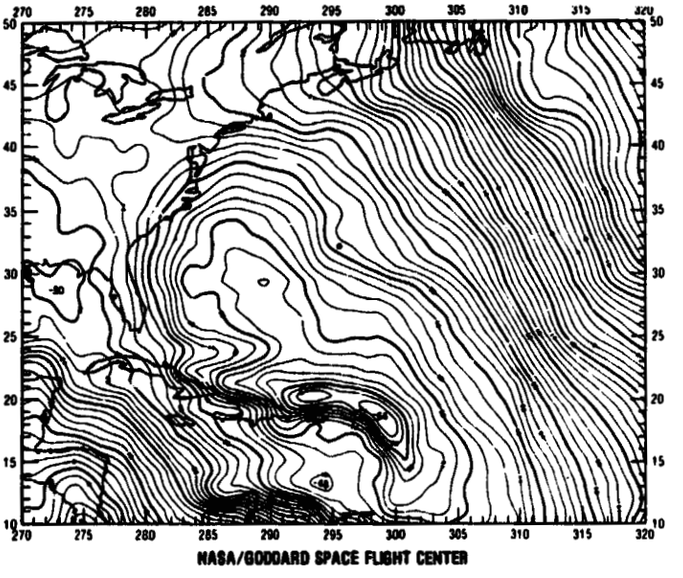

Figure 1. Detailed Gravimetric Geoid Based Upon a Combination of the GSFC GEM-6 Earth Model and 1° x 1° Surface Gravity Data. Contour Interval 2 Meters, Earth Radius=6378.142 km, 1/f = 298.255, GM = 398600.9 km^3/sec^2.

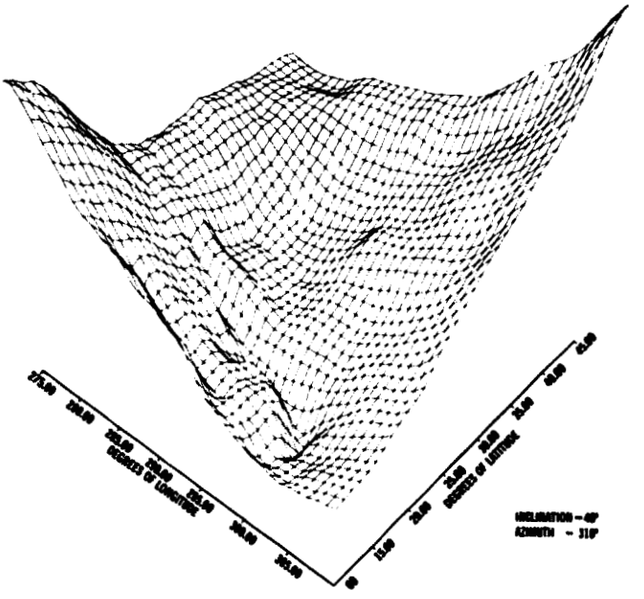

Figure 2. Detailed Gravimetric Geoid for the Caribbean

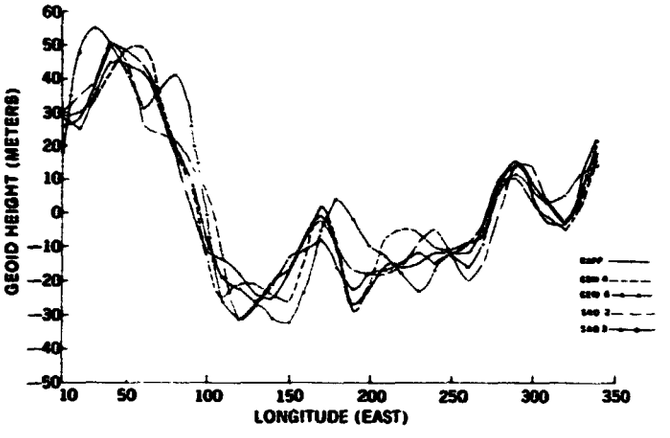

Figure 3. Comparison of Detailed Gravimetric Geoids at 50° S. Latitude

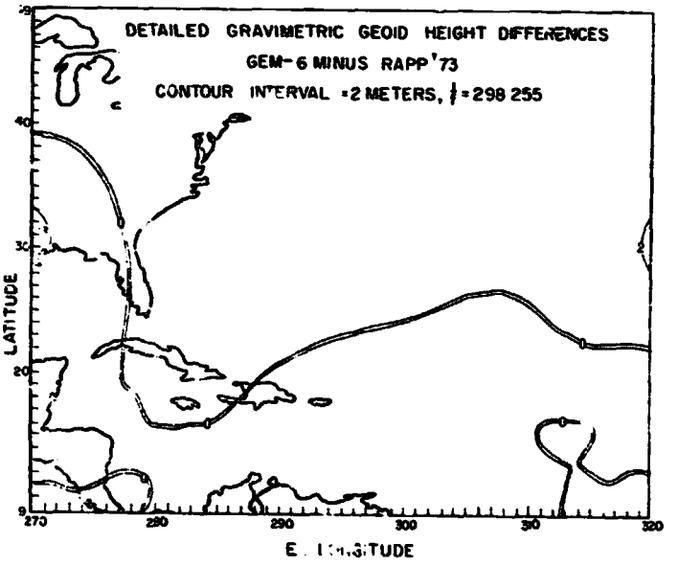

Figure 4. Detailed Gravimetric Geoid Height Differences GEM-6 Minus RAPP'73

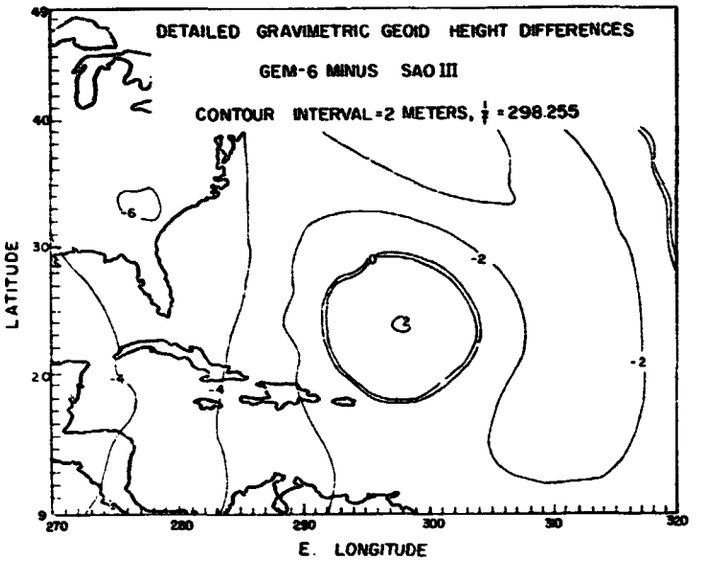

Figure 5. Detailed Gravimetric Geoid Height Differences GEM-6 Minus SAO III

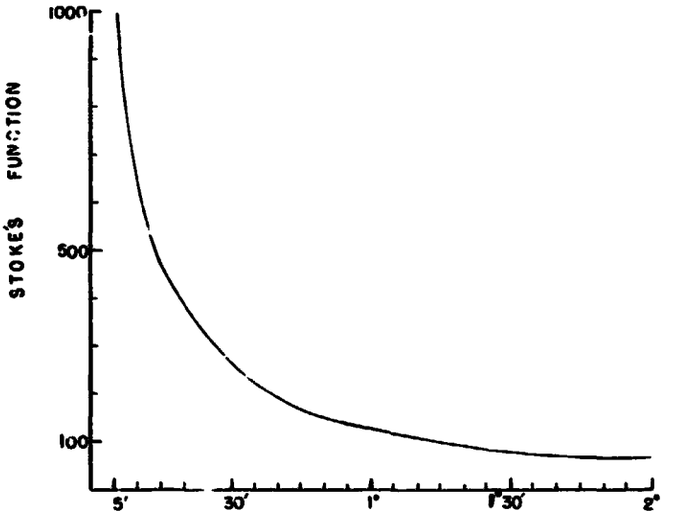

Figure . Plot of Stoke's Function versus Distance from the Computation Point

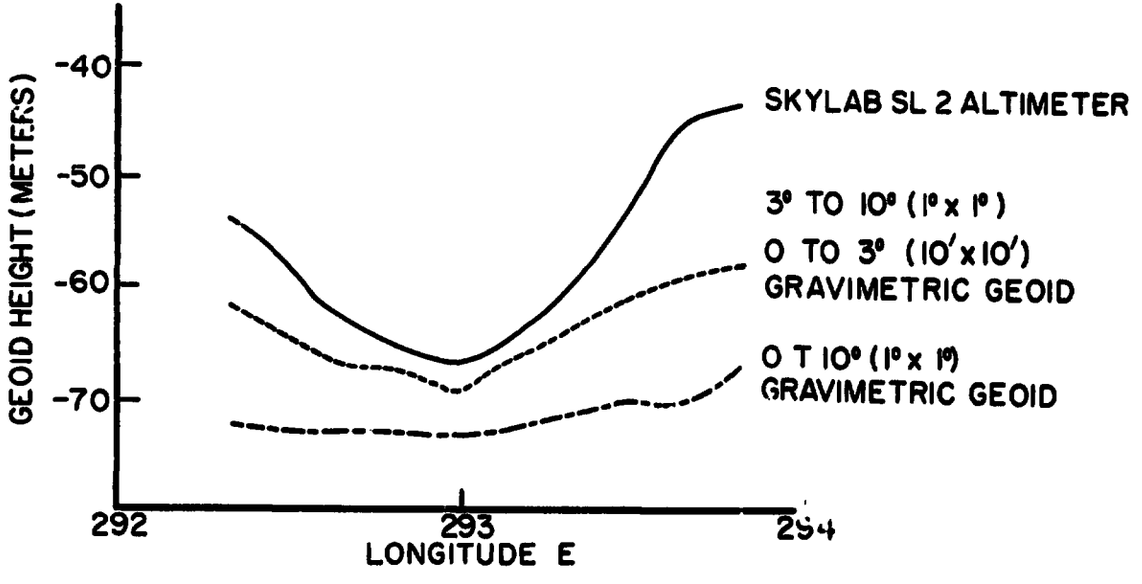

Figure 7. Comparison of Gravimetric Geoid with Skylab Altimeter Data

THE EFFECT OF SEAMOUNTS AND OTHER BOTTOM TOPOGRAPHY ON MARINE GRAVITY ANOMALIES

John C. Rose
Hawaii Institute of Geophysics
University of Hawaii
Honolulu, Hawaii 96822

Bruce R. Bowman
Hawaii Institute of Geophysics
University of Hawaii
Honolulu, Hawaii 96822

ABSTRACT

Localized bathymetric features produce large amplitude perturbations in the marine free-air gravity anomalies. In order to study long wavelength anomalies, which are of particular interest in marine geodesy, it is desirable to remove the topography "noise level". However, to do this in a truly three-dimensional fashion along a marine gravity track is not practical because of the formidable amount of data preparation required. It is also undesirable to use conventional Bouguer anomalies because these can easily be in error by 60% because of the one-dimensional nature of the correction. We have developed a computer program which calculates the sea-surface three-dimensional gravity effect of a conical seamount from a point above the apex to any distance off-axis. The results of this program are compared with those of a Talwani two-dimensional equivalent of a ship track across the off-axis hyperbolic slice of the cone. A study of more than 100 seamounts in the Pacific Ocean showed that their slope angles range from 4.5° to 17°. For this reason, model cases with slope angles of 5, 10 and 15 in water depths of 1 to 6 km were considered. For a seamount with its apex at 2 km depth and base at 5 km depth a 10° slope angle, the two-dimensional method over-corrects by 18% over the apex, but gives the same result as the three-dimensional method at an off-axis distance of 60% of the base radius. Farther out than 60% of the base radius, the two-dimensional method under-corrects. We have developed a second computer program which uses a two-dimensional method to correct the free-air anomaly for topography along the ship's track. Curves from the cone program as well as two-dimensional topography corrected free-air anomaly tracks are presented.

INTRODUCTION

Gravity anomaly data, particularly in the form of 1°x1° means, are needed in order to determine undulations of the gravimetric geoid, determine components of the deflection of the vertical, and to derive an earth gravity model, i.e., a spherical harmonic expression of gravity variations on a global basis.

In continental areas, good approximations of mean 1°x1° can be made in most areas. Part of the reason for this is that land gravity measurements can be made at relatively low cost for quite

a large number of stations. Any station location is well know, and the gravimeter is stationary during the observation. Many areas of large extent have observations on a grid-like pattern, and there are enough point anomalies available so that simple averaging can be done and a reliable mean is obtained. Good topographic maps are available so that terrain corrections can be made.

The situation is not so good as regards marine gravity result. One factor is the high cost of the sea gravimeter itself, at least 15 times the cost of land meter. Another is the very high cost of ship operation. A ship suitable for sea-gravity observations costs thousands of dollars a day to operate. These two factors alone indicate not only why there are great gaps in the sea gravity data, but also why the areal coverage usually consists of a long single track through a region rather than a grid pattern of observations. Then it becomes much more difficult with the sea data to determine mean 1°x1° anomalies than it has been for the land data. To make matters worse, the ocean bottom very often has relatively high relief which usually consists of seamounts. Because of navigation uncertainties, the exact location as well as configuration of bottom topography is not well know. In addition, slope corrections to the echo sounder depths have probably not been made, so that in bottom topography configurations where there is a high slope angle, the charted depths may be incorrect. In this regard see Krause (1962).

For land gravity observations, a several km high topographic feature only a few kilometers away has virtually no terrain effect on the vertical component of gravity. At sea, however, the observation point, instead of being at almost a right angle to the feature, is usually above the level of the top of the feature. Therefore the angle from the observation point to the center of mass of the topographic feature will be considerably different from nearly horizontal, and the gravity effect much larger.

It is well known that marine gravity results are only as good as the cross-coupling corrections, horizontal acceleration corrections, and Eotvos corrections. These matters will not be discussed in this paper. The problem which we want to examine here is that of effectively removing the "noise-level" or perturbations in the free-air anomaly, caused by the bottom topography, to obtain a residual gravity field which incorporates only the effect of the deeper mass distributions. The situation is the inverse of the one encountered by the paleomagnetic investigators where they remove the regional so that they can look at the local effects. The most difficult topography effect to remove is one that is truly three-dimensional; one of the most common features in marine bottom topography is the submerged seamount. We thought that it would be profitable to study the difference between the three-dimensional (3D), two-dimensional (2D) and one-dimensional (1D) gravity effect of conical seamounts.

THE GRAVITY EFFECT OF A CONIC SEAMOUNT

We felt that it was reasonable to assume that the form of a submerged seamount could be approximated as a perfect cone, although we realized that no such seamount probably exists. Our chief purpose in addition to producing a table of gravity effects was to compare one and two-dimensional approximations with the three-dimensionally derived gravity effects. We examined the bathymetry character of more than 100 "reasonable" seamounts in the central Pacific Ocean. The slope angles were calculated from the height divided by base radius, and were found to range from 4.5 to 17 degrees with 10 degrees as a reasonable mean. Appendix A gives a summary of the developments leading to a group of equations used for calculating the off axis vertical gravity

effect of a horizontal circular disk. The seamount was then approximated from stacking up to 100 varying sized disks. We used a density of 2.3 g/cc*, or a differential density of (2.3-1.027) g/cc.

Tables 1, 2 and 3 give the vertical gravitional attraction of conical seamounts of density 2.3 g/cc and having slopes of 5, 10 and 15 degrees respectively. The tables give the radial distance in km from the axis corresponding to an even 10 mgal unit. For cases where the on-axis mgal effect is not an even 10 mgal unit, the mgal effect is given in parentheses in place of the zero-km number. The purpose in presenting the tables in this form is to permit other investigators to construct graphs of their own to any scale. Drawn as plan view circles at the appropriate radii, they would permit the gravity effect profile of an off-axis ship track to be determined. If some other density ρ besides 2.3 is desired, multiply the mgal effect by (ρ - 1.027)/(2.3-1.027).

The 3-dimensional results were compared not only with Talwani, et. al. (1959) 2D equivalents of ship tracks across off-axis slices of the cone, but also with 1D corresponding approximations along each track. The ship track distance increments were 5 km, because this is about the distance a ship will travel in 15 minutes at 10.5 knots, and our ship gravity results are given for even quarter hour times. Table 4 presents the comparisons for the on-axis ship track cases. In order to discuss off-axis cases, it seemed best to pick a few examples of reasonable situations encountered at sea. Figure 1 shows a half-profile of the vertical gravity effect of 10° as well as 15° conical seamounts where the base depth is 5 km and the depth to the top is one km. Figure 2 shows the mgal error in using a 1D

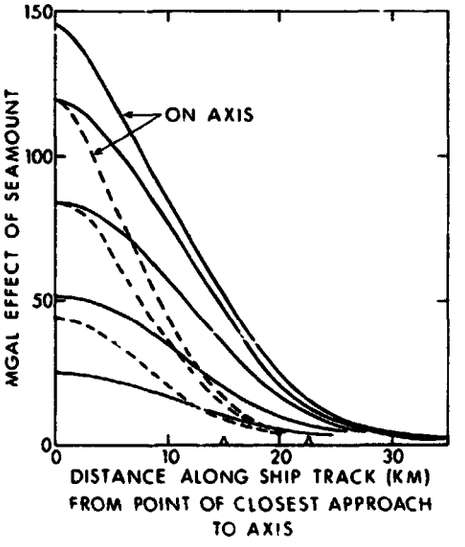

Figure 1. Vertical gravity effect at sea-level of two conical seamounts. Both have a base depth of 5 km and a top depth of 1 km. Solid lines are for one with a 10° slope from the horizontal, and dashed lines are for one with a 15° slope. Corresponding base radii are indicated by the open triangles. Effects are shown along ship tracks crossing on-axis, as well as flank crossings at 5 km successive offsets from the axis.

TABLE 1. Sea level mgal effect and corresponding distance from axis in kilometers for seamounts with a slope of 5 degrees and density 2.3 g/cc.

DEPTH OF BASE (KM)		6					5					4				3			2		1	
DEPTH OF TOP (KM)	0	1	2	3	4	5	0	1	2	3	4	0	1	2	3	0	1	2	0	1	0	
	ON AXIS MGALS IN PARENTHESES (0 KM)																					
300	(292)																					
	0.5																					
	2.7																					
	4.9																					
	7.1																					
250	9.2						(244)															
	11.5						0.7															
	13.7	(223)					3.0															
	15.9	1.6					5.1															
	18.2	4.7					7.3															
200	20.4	7.3					9.6					(195)										
	22.7	9.8					11.8					1.1										
	24.9	12.2					14.0	(175)				3.2										
	27.2	14.7	(161)				16.3	2.4				5.4										
	29.5	17.1	1.3				18.5	5.3				7.6										
150	31.9	19.5	5.4				20.8	7.9				9.9										
	34.2	21.9	8.4				23.1	10.4				12.1										
	36.6	24.3	11.2				25.4	13.1				14.4	(127)									
	38.9	26.8	13.9				27.7	15.8	(115)			16.6	3.3									
	41.3	29.2	16.5	(105)			30.1	17.8	3.3			18.9	6.0									
100	43.8	31.7	19.1	3.9			32.5	20.2	6.7			21.2	8.6									
	46.2	34.2	21.8	7.7			34.9	22.7	9.6			23.6	11.1									
	48.7	36.8	24.4	10.9			37.3	25.2	12.4			26.0	13.6									
	51.3	39.4	27.1	14.0			39.8	27.8	15.1	(62)		28.4	16.2	0								
	53.9	42.0	29.8	17.0	0		42.3	30.3	17.9	2.2		30.8	18.7	5.1								
50	56.6	44.7	32.6	20.0	4.6		44.9	33.0	20.7	6.8		33.3	21.3	8.3								
	59.5	47.6	35.5	23.0	9.0		47.7	35.8	23.5	10.3		36.0	24.0	11.3								
	62.6	50.7	38.7	26.3	12.9		50.6	38.7	26.6	13.7		38.7	26.8	14.3	(22)	27.0						
	66.2	54.3	42.3	29.9	16.9	0	53.9	42.0	29.9	17.2	(18)	41.7	29.8	17.5	2.6	29.7						
10	72.2	59.9	47.6	34.9	21.8	6.4	58.8	46.6	34.3	21.6	7.3	45.8	33.7	21.4	7.9	33.1						
5	80.0	67.0	53.7	40.1	26.0	10.7	64.8	51.9	38.8	25.4	10.9	50.1	37.5	24.6	10.9	36.1						
1	109.9	97.0	78.5	59.4	39.8	19.3	91.4	74.1	56.3	37.8	18.5	69.1	52.7	35.5	17.6	48.4						

MGALS

KILOMETERS FROM AXIS

TABLE 2. Sea level mgal effect and corresponding distance from axis in kilometers for seamounts with a slope of 10 degrees and density 2.3 g/cc.

DEPTH OF BASE (KM)		6						5					4				3			2		1
DEPTH OF TOP (KM)		0	1	2	3	4	5	0	1	2	3	4	0	1	2	3	0	1	2	0	1	0
	270	(265)																				
		0.5																				
	250	1.7						ON AXIS MGALS IN PARENTHESES (0 KM)														
		2.8																				
		3.9						(221)														
		5.1						0.1														
		6.2						1.2														
	200	7.3						2.3														
		8.5	(187)					3.4														
		9.8	2.0					4.6					(176)									
		11.0	3.7					5.8					0.7									
		12.2	5.2					7.0					1.8									
	150	13.5	6.6					8.2	(145)				3.0									
		14.7	8.0					9.4	1.6				4.2				(132)					
		16.0	9.4	(125)				10.6	3.4				5.3				0.3					
		17.3	10.7	2.3				11.9	4.9				6.5				1.4					
		18.6	12.1	4.5				13.1	6.3				7.7	(103)			2.5					
	100	20.0	13.7	6.3				14.4	7.8				9.0	1.2			3.7					
		21.4	15.0	8.0				15.8	9.2	(86)			10.2	3.1			4.9			(88)		
		22.8	16.5	9.6	(73)			17.1	10.7	2.6			11.5	4.7			6.1			0.9		
		24.1	18.0	11.3	2.3			18.5	12.2	4.8			12.9	6.2			7.4	(63)		2.1		
		25.9	19.6	13.0	5.2			20.0	13.7	6.6			14.3	7.8			8.7	1.1		3.3		
	50	27.5	21.3	14.8	7.4			21.6	15.3	8.5			15.7	9.3	(49)		10.0	3.1		4.5		(44)
		29.3	23.2	16.7	9.6	(32)		23.2	17.0	10.3	(39)		17.3	10.9	3.4		11.4	4.8		5.8		0.5
		31.5	25.2	18.8	11.9	2.4		25.1	18.9	12.3	4.5		8.9	12.7	5.7		12.9	6.5		7.2	(24)	1.6
		34.1	27.9	21.4	14.5	6.5		27.5	21.2	14.7	7.4		21.0	14.7	7.9	(11)	14.7	8.4	(16)	8.6	1.7	2.9
	10	39.0	32.4	25.5	18.4	10.6	(6)	31.4	24.8	18.0	10.8	(8)	24.0	17.6	10.8	1.8	17.1	10.7	3.3	10.5	4.0	4.3
	5	45.3	37.9	30.3	22.4	14.0	3.2	36.2	29.0	21.6	13.8	4.3	27.6	20.6	13.3	4.9	19.5	12.8	5.3	12.0	5.4	5.3
	1	69.0	58.3	47.2	35.7	23.7	10.8	54.6	44.3	33.6	22.5	10.5	41.0	31.3	21.1	10.1	28.5	19.3	9.5	17.1	8.7	7.3

MGALS KILOMETERS FROM AXIS

Table 3. Sea level mgal effect and corresponding distance from axis in kilometers for seamounts with a slope of 15 degrees and density 2.3 g/cc.

DEPTH OF BASE (KM)		6						5					4				3			2		1
DEPTH OF TOP (KM)		0	1	2	3	4	5	0	1	2	3	4	0	1	2	3	0	1	2	0	1	0
MEAN SEA LEVEL	240	(237)						ON AXIS MGALS IN PARENTHESES (0 KM)														
		0.6																				
		1.4																				
		2.2																				
	200	3.0						(198)														
		3.8						0.6														
		4.6						1.4														
		5.5						2.2														
		6.3	(156)					3.0					(158)									
	150	7.2	1.5					3.9					0.6									
		8.1	2.9					4.7					1.4									
		9.0	4.0					5.6					2.3									
		10.0	5.1					6.5	(119)				3.1				(119)					
		11.0	6.2					7.4	2.0				3.9				0.7					
	100	11.9	7.3	(98)				8.3	3.3				4.8				1.5					
		13.0	8.4	2.5				9.3	4.5				5.7	(83)			2.3					
		14.1	9.6	4.2				10.3	5.6				6.6	1.1			3.2			(79)		
		15.2	10.7	5.6				11.4	6.8	(65)			7.6	2.6			4.1			0.7		
		16.4	12.0	7.1	(52)			12.5	8.0	2.0			8.7	3.9			5.0			1.6		
	50	17.7	13.3	8.6	1.6			13.7	9.2	3.9			9.7	5.1			6.0	(49)		2.4		
		19.1	14.8	10.1	4.4			15.0	10.6	5.6			10.9	5.4	(35)		7.0	2.1		3.3		0
		20.9	16.5	11.9	6.6			16.5	12.1	7.3	(26)		12.3	7.8	2.1		8.2	3.5		4.3		0.8
		23.2	18.8	14.1	9.0	0		18.5	14.1	9.3	3.3		13.9	9.5	4.4		9.6	5.1		5.5	(17)	1.7
	10	27.4	22.6	17.7	12.4	6.2		21.9	17.1	12.3	6.7		16.6	12.0	7.0	(6)	11.6	7.1	0	7.0	2.2	2.8
	5	32.6	27.2	21.6	15.8	9.4	(3)	25.9	20.7	15.3	9.4	(4)	19.6	14.6	9.2	2.1	13.7	8.9	3.1	8.3	3.5	3.6
	1	51.4	43.4	35.1	26.5	17.3	7.0	40.5	32.8	25.0	16.5	7.3	30.3	23.1	15.4	7.1	20.9	14.0	6.8	12.5	6.3	5.3

flat-slab assumption (upper graph) in correcting to the 5 km base level, as well as the mgal error using a 2D Talwani method along the track. It is apparent that, on the axis, the 1D error is enormous, being 48% too large, while the 2D is much more reasonable at 16% too large. On axis, the 1D as well as 2D methods are blind to the deficiency of mass laterally. For the 10° seamount and 1D assumption, a conventional marine Bouguer anomaly, in which the sea water is replaced by rock, would over-correct the 145 mgal free-air anomaly by 69 mgal and appear as a large negative spike of almost half the amplitude of the original anomaly. Clearly, then, the 2D assumption is much better because in the worst case (on-axis), the 145 mgal free-air anomaly would be reduced to only -23 mgal, and at 10 km off-axis, to -8 mgal. The 2D-3D graphs for cases other than that shown in Figure 2 are quite similar in shape, and all exhibit the equality of 2D with 3D methods when the off-axis trackline distance is about 60 to 70 percent of the base radius. This percentage is given in the % RAD 2D = 3D column in Table 4. Of course, the 2D assumption under-corrects for topography when the off-axis distance is too great.

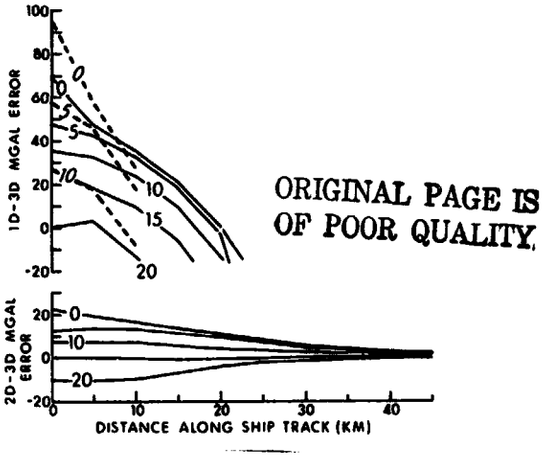

Figure 2. Mgal errors of 1D (upper) and 2D (lower) assumptions relative to the curves shown in Fig. 1. Only the 10° case is shown in the 2D-3D graph. Insert numbers give km offsets from the axis.

EFFECT OF FEATURES OFF THE TRACKLINE

It is important to know th magnitude of the gravity effect of features off to the side of the trackline and not seen directly by the echo-sounding device on the ship. The half-angle of a conventional echo-sounder cone of energy is 30° relative to the vertical. This means that the echo-sounder's lateral effectiveness ranges from 3.5 km in 6 km of water to 1.7 km in 3 km of water. From the base radii given in Table 4 it is seen that for all cases given in Tables 1, 2 and 3, the worst error encountered in ignoring seamounts off to the side of the track is 13 mgal for a 15° slope at zero km to the top and 6 km base depth. Almost all other cases are 10 mgal or less. The validity of ignoring lateral topography would not be true, however, if there were a large 2D bathymetric feature parallel to the trackline but just out of range the echo-sounder. Thus

TABLE 4. The vertical gravitational attraction, at sea level and on the axis, of a seamount, and the comparison with one as well as two-dimensional approximations. Density is 2.3 g/cc.

		5° SLOPE					10° SLOPE					15° SLOPE				
KM TO TOP	KM TO BASE	BASE KM RADIUS	3D MGAL	1D-3D MGAL	2D-3D MGAL	% RAD. 2D=3D	BASE KM RADIUS	3D MGAL	1D-3D MGAL	2D-3D MGAL	% RAD. 2D=3D	BASE KM RADIUS	3D MGAL	1D-3D MGAL	2D-3D MGAL	% RAD. 2D=3D
0	6	68.6	292	28	10	74	34.0	265	55	20	71	22.4	237	83	30	68
1	6	57.2	223	44	15	71	28.4	187	80	27	67	18.7	156	111	36	64
2	6	45.7	161	53	17	68	22.7	125	89	27	66	14.9	98	116	33	63
3	6	34.3	105	55	17	65	17.0	73	87	25	63	11.2	52	108	29	62
4	6	22.9	55	52	14	63	11.3	32	75	19	62	7.5	20	87	21	63
5	6	11.4	15	36	10	63	5.7	6	47	10	66	3.7	3	50	10	--
0	5	57.2	244	23	9	73	28.4	221	47	17	71	18.7	198	69	25	65
1	5	45.7	175	39	13	70	22.7	145	69	23	66	14.9	119	95	30	63
2	5	34.3	115	45	14	67	17.0	86	74	22	63	11.2	65	95	27	60
3	5	22.9	62	45	13	63	11.3	39	68	18	59	7.5	26	81	21	60
4	5	11.4	18	35	9	70	5.7	8	45	10	70	3.7	4	49	12	--
0	4	45.7	195	19	7	73	22.7	176	38	13	69	14.9	158	56	20	65
1	4	34.3	127	33	11	68	17.0	103	57	18	64	11.2	83	77	24	60
2	4	22.9	70	37	11	65	11.3	49	58	17	58	7.5	35	72	20	58
3	4	11.4	22	31	5	59	5.7	11	42	10	65	3.7	6	47	14	--
0	3	34.3	146	14	5	65	17.0	132	28	10	65	11.2	119	41	15	58
1	3	22.9	81	26	8	66	11.3	63	44	14	56	7.5	49	58	18	57
2	3	11.4	27	26	8	56	5.7	16	37	10	65	3.7	10	43	14	--
0	2	22.9	97	10	4	76	11.3	88	19	7	56	7.5	79	28	11	54
1	2	11.4	35	18	6	52	5.7	24	29	9	65	3.7	17	136	14	--
0	1	11.4	49	4	2	51	5.7	44	9	4	58	3.7	40	13	7	--

scraps, trenches, ridges, island chains and continental slopes, for example could not be ignored. However, such situations would be treated as special cases.

MOVING WINDOW TOPOGRAPHY CORRECTION

We have developed a computer program which we call TCFAA (Topography Corrected Free Air Anomaly). Its purpose is to be a relatively inexpensive method of correcting the marine observed free-air anomalies for the effect of bottom topography along the track. A "boxcar window" is centered on the observation point. The mean water depth, maximum water depth, and mean free-air anomaly are calculated for only the sequence of track data within the window. The Talwani 2D effect of the topography relative to the mean depth is calculated and subtracted from the free-air anomaly. Except for discrepancies between the 2D assumption and 3D configurations, the result approximates a "complete" free air anomaly relative to the mean depth for the window. The window is advanced along the track along with each new observation point.

The results of a test of the program are shown in Figure 3. The track was taken from Leg 8 of KANA KEOKI in 1973 and goes from 5.5°S 168°W (left) to 3°S 175.5°W (right). All bathymetric "bumps" are crossings of essentially conical seamounts. The center of the track is about 120 km south of Canton Island and the bathymetric depression past 800 km is a western extension of the Nova Canton Trough and is therefore two-dimensional. Figure 3a shows original data. Figure 3b shows the results of using a window width of 110 km corresponding to 1°, and Figure 3c shows the results of using a window width of 330 km corresponding to 3° geographically.

DISCUSSION OF RESULTS

Figure 3b shows a very close correspondence between the mean free-air anomaly and TCFAA. This would be expected because TCFAA is done relative to the mean water depth. Over 1° or 110 km the area should be only 50 percent isostatically compensated, as has been pointed out by Woollard (1962). Because the lateral effect of seamounts not seen by the echo-sounder can be effectively ignored, we feel that the mean topography and free-air anomalies obtained with a 110 km window and a single ship track should provide powerful information for determining a local area basic predictor. This in turn, can be used to determine the local 1°x1° mean anomaly. The TCFAA profile for a 110 km window probably cannot be used profitably for geological structure interpretation. This is because the mean water depth does not truly represent the most commonly occurring water depth for the whole region in general. The most common depth would be given by the "mode," which might not be possible to find in cases of a monocline or sawtooth topography, for example. There is a way out of this problem, however. Woollard (1962) maintained that topographic features must be about 3°x3° or larger in order to be compensated more than 80%. This is the reason we also show results obtained with a 330 km window.

Figure 3c shows that the TCFAA from a 330 km window should be very useful for local crustal structure interpretations. In particular, the departures of TCFAA from the 330 km mean free-area anomaly indicate areas of probably structural or tectonic interest. The mean free-air anomaly as well as mean topography change very slowly and would be quite useful for a regional basic predictor.

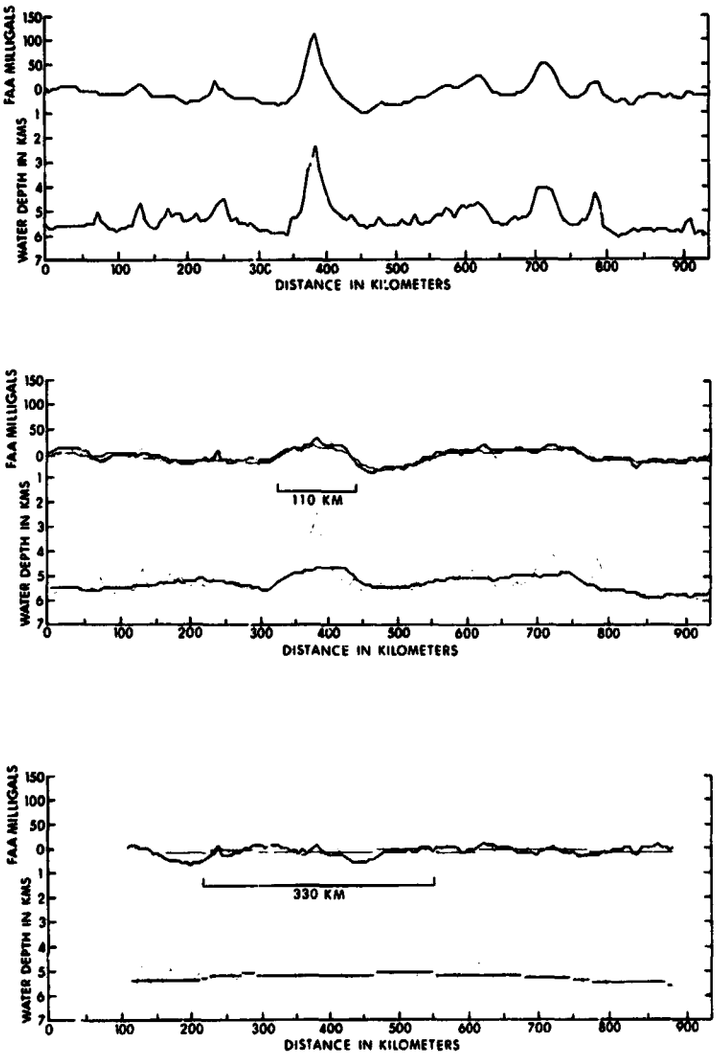

Figure 3. Profiles of the free-air anomaly and bottom topography used for a test of TCFAA. Original data are shown in (a). TCFAA (bold line) mean FAA (fine line), and mean bottom topography for a 110 km window are shown in (b). The same quantities as in (b) are shown in (c) for the case of a 330 km window.

CONCLUSIONS

1. Even in the worst case where a ship track crosses the axis of a submerged seamount, the 2D approximation for removal of bottom topography gravity effects is considerably better than use of a 1D flat-slab approximation.

2. Seamounts off to the side of the ship trackline and not seen by the echo-sounder can be effectively ignored as regards the correction of the free-air anomaly for their topographic effect.

3. The moving window TCFAA computer program with a 110 km window can be used very effectively for long ship tracks to give good 1°x1° free air anomaly approximations. In addition, the program is very useful for studying crustal structure problems when used with a 330 km window because the mean topography and mean free-air anomalies represent regional or "steady state" conditions while the TCFAA results represent local deeper structural gravity effects which are not contaminated or screened by the local topographic "noise-level."

4. The 330 km means should be very useful for setting up regional basic predictors.

5. The TCFAA program uses only what it can see, and suffers only from use of a 2D assumption. Therefore, it is in reasonable harmony with the principles of minimum astonishment.

APPENDIX A

THE VERTICAL GRAVITATIONAL ATTRACTION OF A HORIZONTAL CIRCULAR DISK

The vertical gravitational attraction of a very thin horizontal circular disk can be computed from the solid angle subtended by the disk. There are several different methods of calculating the solid angle, and the computational efficiency of each method varys with the horizontal as well as vertical distances from the disk.

The vertical gravitational attraction, g_z, of a horizontal disk is given by the volume integral

$$g_z = \int_V \frac{\gamma\delta\cos\theta}{r^2}\, dV \tag{1}$$

where γ is the gravitational constant, δ is the density, r is the distance of the field point from the source point on the disk, and θ is the angle between r and the normal to the disk. This is shown in Figure A1.

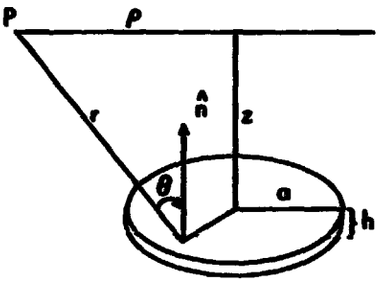

FIG. A1. Diagram of vertical gravitional effect of a horizontal disk.

For $h \ll r$, (1) reduces to

$$g_z \approx \gamma\delta h \int_A \frac{\cos\theta}{r^2}\, dA \tag{2}$$

where A represents the area of the disk. The solid angle at field point P subtended by the disk is

$$\Omega = \int_A \frac{\hat{n}\cdot\vec{dA}}{r^2} \tag{3}$$

where $\hat{n}$ is the unit vector normal to the surface of the disk and $\vec{dA}$ is the element of area (dA) vector directed along the line of length r. Now (3) reduces to

$$\Omega = \int_A \frac{\cos\theta}{r^2}\, dA \tag{4}$$

2.5

which is the same integral as the one in (2). Then (1) for a thin disk can be expressed as

$$g_z = \gamma\sigma h\Omega \ . \tag{5}$$

The value of Ω on the axis ($\rho=o$) reduces to

$$\Omega_o = 2\pi\ (1-z/\sqrt{z^2+a^2}). \tag{6}$$

The evaluation of the integral for a point off the axis is much more complicated. Some methods have used power series expansions, and others have determined closed form solutions in terms of Elliptic integrals of the first, second and third kinds.

Jaffey (1954) lists results of Zumwalt obtained by expanding the integrand in a binomial series and then integrating term by term. Since the integrand of (4), $\cos\theta/r^2$, is a solution of Laplace's equation, the solid angle can also be expressed in terms of a Legendre polynomial series of the form

$$\Omega = \sum_{n=o}^{\infty} A_n \left(\frac{a}{r}\right)^{n+1} P_n\ (\cos\theta),\ r>a \tag{7a}$$

$$\Omega = \sum_{n=o}^{\infty} A_n \left(\frac{r}{a}\right)^{n} P_n\ (\cos\theta),\ r<a \tag{7b}$$

where $\cos\theta = z/\sqrt{z^2+\rho^2}$.
The coefficients A_n can be solved for by comparison with the terms of the Zumwalt expansion for the on-axis case.

Refer to Jeans (1958), p. 431, for an example of this procedure. The particular result most suitable for our purposes is

$$\Omega = -2\pi \sum_{n=1}^{\infty} P_{2n}\ (0)\ P_{2n-1}\ (\cos\theta)\ \left(\frac{a}{r}\right)^{2n},\ r>a \tag{8}$$
$$\text{(J-7b)}$$

which converges rapidly for $r >> a$. Other types of series expansion results are also given by Jaffey. We denote (8) as our Equation (J-7b) where prefix J refers to Jaffey.

Other approaches to the problem have provided exact solutions in terms of the complete and incomplete Elliptic integrals. One such solution is derived by Paxton (1959). Starting from (4) he obtains

$$\Omega = 2\int_{o}^{\beta_{max}} \int_{o}^{\varphi_o} \sin\varphi\ d\varphi\ d\beta \ . \tag{9}$$

Refer to Figure A2. The line integral over φ is obtained first.

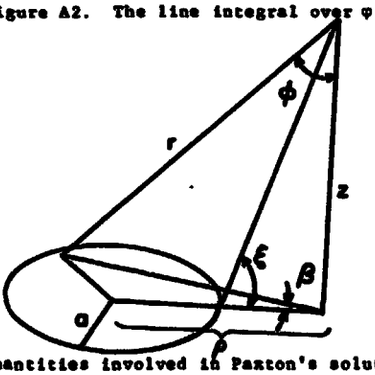

FIG. A2. Quantities involved in Paxton's solution.

After expressing φ_s and β in terms of ξ and other parameters the resulting integrals become the complete elliptic integrals of the first and third kinds. To simplify the expression, the Elliptic integral of the third kind is expressed in terms of Heuman's lambda function, Λ_0. The following results were obtained by Paxton:

$$\Omega = 2\pi - \frac{2z}{\sqrt{z^2 + (\rho+a)^2}} K(k) - \pi\Lambda_0(\xi,k), \quad \rho<a \qquad (10a)$$

$$\Omega = \pi - \frac{2z}{\sqrt{z^2 + (\rho+a)^2}} K(k), \quad \rho=a \qquad (10b)$$

$$\Omega = \frac{-2z}{\sqrt{z^2 + (\rho+a)^2}} K(k) + \pi\Lambda_0(\xi,k), \quad \rho>a \qquad (10c)$$

where

$$k^2 = \frac{4\rho a}{z^2 + (\rho+a)^2}\ ;\ \xi = \sin^{-1}\left[\frac{1-k^2/\alpha^2}{1-k^2}\right]^{1/2}\ ;\ \alpha^2 = \frac{4\rho a}{(\rho+a)^2}$$

and $K(k)$ is the complete Elliptic integral of the first kind. The Heuman lambda function can be expressed in a series containing $K(k)$, $E(k)$ (the complete Elliptic integral of the second kind), ξ, and k. To evaluate Paxton's results, refer to Nagy (1965) as well as Abramowitz and Stegun (1970), chapter 17.

Another exact solution for Ω in terms of Elliptic integrals was obtained by Tallqvist and referred to by Garrett (1954). Tallqvist approximated the exact solution as

$$\Omega = 2\pi - 2\pi\sin\theta\left[1-\tfrac{1}{4}k^2-\tfrac{1}{64}k^4(3-4\tan^2\theta)\ldots\right] \qquad (11)$$

in this case $k^2 = (\rho^2+z^2+a^2-S)/(\rho^2+z^2+a^2+S)$, $S = [(\rho^2+z^2-a^2)^2 + 4a^2z^2]^{1/2}$, $\sin^2\theta = (\rho^2+z^2-a^2+S)/2S$ and $\tan\theta = 2az/(S+a^2-\rho^2-z^2)$.

The solutions given here, as well as some others, were examined to determine the best series to use in different regions to achieve a given accuracy with a minimum number of computations involved. The accuracy of Ω was arbitrarily set at 0.0001 radian for the test case. For each solution, Ω was computed term by term until the term was less than the desired accuracy. The resulting sum for each series was then compared with tabularized solid angle values (Hasket, 1957, 1962) to confirm that the series had in fact converged. For computer applications, the regions adopted are shown in Figure A3 and indicate the particular equation used and the associated numbers of terms required to achieve an accuracy of 0.0001 radian. The scales for ρ and z are not linear as the only purpose is to show the general regions.

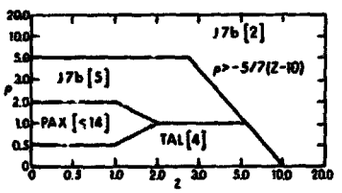

FIG. A3. Regions of ρ and z adopted for 0.0001 radian accuracy. Equation used and numbers of terms required are given, except that for the Paxton solution, 14 refers to the number of terms used in Heuman's lambda function.

ACKNOWLEDGEMENTS

The seamount studies, which had many details not reported here, as well as the Ω equation and associated computer program development, are the work of Bruce Bowman. The modifications to get pairs of (x, z) values along an off-axis flank crossing of a conical seamount, as well as the 2D-3D investigations and TCFAA are the work of J. C. Rose. The investigations were supported in part by Office of Naval Research contract N00014-70-A-0016-0001 and in part by National Science Foundation grant GX 28674 (IDOE Nazca Plate).

BIBLIOGRAPHY

Abramowitz, M., and I. Stegun. Handbook of Mathematical Functions with Formulas, Graphs, and Mathematical Tables, U.S.-Government Printing Office, Washington, D. C., 1970. (Chap. 17).

Byrd, P. F. and M. C. Friedman. Handbook of Elliptic Integrals for Engineers and Physicists, Springer-Verlag, Berlin, 1954.

Furumoto, A. S., J. P. Campbell and D. M. Hussong. Seismic refraction surveys along the Hawaiian Ridge, Kauai to Midway Island, Bulletin of the Seismological Society of America, 61, 147-166, 1971.

Garrett, M. W. Solid angle subtended by a circular aperture, Review of Scientific Instruments, 25 (12), 1954. (p. 1208).

Grosjean, C. C. Series expansions for the solid angle subtended by a circular disk at a point directly above the periphery, Rev. Sci. Instr., 38 (8), 1967. (p. 1042).

Jaffey, A. H. Solid angle subtended by a circular aperture at point and spread sources: Formulas and some tables, Rev. Sci. Instr., 25 (4), 1954. (p. 349).

Jeans, J. H. The Mathematical Theory of Electricity and Magnetism, Cambridge University Press, 1958. (p. 431).

Krause, D. C. Interpretation of echo sounding profiles, International Hydrographic Review, 39 (1), 5-123, 1962.

Ludwig, W. J., J. E. Nafe, and C. L. Drake. Seismic refraction, in the Sea, Vol. 4, part 1, edited by A. Maxwell, pp. 53-84, Interscience, N. Y., 1970.

Masket, A. V. Solid angle contour integrals, series, and tables, Rev. Sci. Instr., 28 (3), 1957. (p. 191).

Masket, A. V., and W. C. Rodgers. Tables of solid angles, U.S.A.E.C. Technical Report TID-14975 Physics, 1962.

Nagy, D. The evaluation of Heuman's Lambda Function and its application to calculate the gravitational effect of a right circular cylinder, Pure and Applied Geophysics, 62, (26)1955.

Nettleton, L. L. Gravity and magnetic calculations, Geophysics, 7, 1942.(p. 293).

Parasnis, D. S. Exact expressions for the gravitational attraction of a circular lamina at all points of space and of a right circular vertical cylinder at points external to it, Geophysical Prospecting, 9 (3), 1961. (p. 382).

Paxton, F. Solid angle calculation for a circular disk, Rev. Sci. Instr., 30 (4), 1959, (p. 254).

Rapp, R. H. The geoid: Definition and determination, EOS, 55 (3), 118-126, 1974.

Reilly, W. Gravitational and magnetic effects of a right circular cylinder, New Zealand Journal of Geology and Geophysics, 12, 1969. (p. 497).

Strange, W. E., G. P. Woollard and J. C. Rose. An analysis of the gravity field over the Hawaiian Islands in terms of crustal structure, Pacific Science, 19, 381-389, 1965.

Talwani, M., J. L. Worzel and M. Landisman. Rapid gravity computations for two dimensional bodies with application to the Mendocino submarine fracture zone, Jour. Geophys. Res., 64, 49-59, 1959.

Woollard, G. P. A gravity reconnaissance of the island of Oahu, Trans. Am. Geophys. Union, 32, 358-368, 1951.

Woollard, G. P. The relation of gravity anomalies to surface elevation, crustal structure, and geology, Research Report 62-9, AF23(601)-3455, University of Wisconsin, 1962.

Woollard, G. P. Collection, processing, and geophysical analysis of gravity and magnetic data, Final Report to AF Contract F23(601)-67-C-0168, Hawaii Institute of Geophysics, 1968.

*In 1971, R/V KANA KEOKI with LaCoste and Romberg gravimeter S33 crossed the Necker Ridge. Furumoto, et. al. (1971) had established a reversed refraction seismic line located 100 km east of the axis of the ridge and 100 km northeast of the gravity profile. The km thickness and km/sec seismic velocity values of the upper three layers of the sea floor (0.1, 2.3; 0.3, 2.9; 1.8, 3.6) along with the Ludwig, Nafe and Drake (1970) corresponding densities of 2.06, 2.21 and 2.33 g/cc yield a mean density of 2.30 g/cc. A Talwani (1959) 2D density profile was used, and 2.30 was confirmed as the best density to use. This agrees with conclusions of Woollard (1951) and to some extent with those of Strange, et al. (1965).

Hawaii Institute of Geophysics Contribution No. 608.

DEFLECTIONS OF THE VERTICAL FROM BATHYMETRIC DATA

Irene Fischer
Defense Mapping Agency Topographic Center
Washington, D.C. 20315

Philip Wyatt III
Defense Mapping Agency Topographic Center
Washington, D.C. 20315

ABSTRACT

A Pacific atoll where several astrogeodetic deflections of the vertical have been observed, served as a test area to determine whether bathymetric data could be utilized to predict deflection values. The extent of the data coverage and the type of assumptions required for the construction of a density model are explored. Guided by the evidence of some of the given deflections, a model was constructed from which the other deflection values were predicted with an r.m.s. error of less than 1".5.

INTRODUCTION

The capability of mapping the ocean floor with increasing detail will provide a new source of data for geophysical and geodetic purposes. Bathymetric survey techniques have advanced in this century from the primitive "lead and line" technique to echo-sounding while the ship is moving, and further to covering a wide swathe on either side of the ship's tracks. Based on multibeam systems of side-scan sonars (Stubbs et al., 1974), ocean depths can be measured simultaneously in a swathe of 2.5 miles on either side of the ship. The great saving in ship time and the inner consistency of the great number of continuous and simultaneous depth measurements offer the prospect of a block of data from oceanic regions, less expensive and more abundant than could have been acquired up to now. If that data could be utilized for the determination of deflections at sea, it would provide an alternative or complementary method to gravimetric determinations which require very expensive dense gravity surveys in the ocean areas. The possibility of such utilization, on principle, is explored in the following sections. Instead of the anticipated near perfect data of the future, however, we had to make do with currently existing not quite so perfect bathymetric charts. Yet, the results seem to be encouraging.

THE DATA

The Kwajalein atoll in the Marshall Islands is uniquely suited for our investigation, since several astrogeodetic deflections of the vertical have been observed there in connection with a local, first-order control network. These deflections, with an estimated accuracy of 0".2 in each component with respect to the local datum, constitute hard facts of life, against which to test the degree of success in reproducing deflection values from bathymetric data. The roughness of this test area is reflected in the wide range of deflection values over a region of less than ¼° in diameter: from −24".49 to +29".20 in the meridian and from −20".94 to +24".96 in the prime vertical.

The bathymetric data were read from Hydrographic Office charts at various scales (1:1 Mill., 1:100,000, 1:12,000, 1:10,000) and from 1:25,000 Army Map Service maps. For application of the

"rectangular method" (Fischer, 1966), a data set was collected for area units of 0'.5 x 0'.5 covering the pertinent part of the atoll, and area units of 2'.5 x 2'.5 and 5' x 5' further out. Units containing both, water and land, were adjusted proportionally. For densification in the vicinity of the astrogeodetic deflection stations, the basic 0'.5 x 0'.5 unit containing the station was subdivided into 5" x 5" parts and the surrounding eight units into 10" x 10" parts. Due to the scarcity of data in some regions, compromises had to be made in the delineation between the area categories; there was some difficulty in reconciling the given coordinates with the map grid. Such troubles should not appear with future, hopefully complete and internally consistent data sets.

The extent of the data area and the categories (Fig. 1) are the result of preliminary explorations with data sets 1 to 4. The adopted Set 5 comprises 14,000 readings in an area of 5° in latitude and 4° in longitude, where each deflection station (within the shaded area) is at least 1°.5 from the boundary. Although this seemed to be sufficient for producing the major part of the deflection values, another enlargement to Set 6 was made, in order to evaluate the gain versus the expenditure of effort and machine time. Set 6 comprises 20,000 readings in an area of 7°05' in latitude and 6°45' in longitude, where each station is at least 3° from the boundary. Both sets were used in the following analyses.

TOPOGRAPHIC DEFLECTIONS

The deflections of the vertical observed on the islands surrounding the lagoon reflect very clearly the land-water distribution, as seen from their vector representation in Figure 2. A typical depth profile across the atoll (Figure 3) shows its steep slope towards great ocean depths and makes the magnitudes of the deflections and their directions understandable. This picture of a well delineated mass, superimposed on the more or less flat ocean floor at about 5 km depth, invites the attempt to compute deflection values due to this mass distribution and to see how close they would come to the observed values.

Since the given astrogeodetic deflections are referred to a local datum which is not necessarily compatible with the computed topographic values, a datum transformation should be considered. Luckily, a transformation to a world datum, a regionally well-fitting datum, or any other datum for such a small area is equivalent to a blanket correction and can thus be applied to the results if needed for interpretation.

The depth readings together with a density value of 1.027 g/cm^3 for ocean water and an adopted constant density value for the rock down to a uniform depth of 5 km constitute a description of the "visible" topography. Earlier investigations (Fischer, 1974) have suggested 2.4 as a good density number for this area.

The topographic deflection at a station A is computed as the sum of the horizontal components of attraction of all rectangular columns belonging to the area units described above. These 5 km-columns (Fig. 4) are either fully water or rock or subdivided. For simplification the mass is treated as a point mass in the center of the water or rock column respectively.

Computations were made for 16 stations where observed astrogeodetic deflection values provided a comparison. Both data sets were used to determine the effect of the enlargement. Table 1 lists the observed values and the residuals (Observed minus computed). The difference in the data sets is evaluated here in terms of smaller absolute residuals: the larger Set 6 reduces the residuals for ξ in 10 out of 16 cases with an average of 1".2, and for η in 9 out of 16 cases with an average of 2".1. For the remainder, however, the residuals are worse, so that on balance the gain from the enlargement is questionable.

How much of these residuals is due to using the same rectangular data area for all stations instead of radially symmetric individual areas for each station? Table 2 shows the residuals computed from the largest circular area within Set 6 around each station, and the number and amount of improvements compared with Table 1. Again, the gain is questionable. If isostatic compensation is applied, however, there is practically no difference. For a specific station, Figure 5a shows the accrual of the deflection values with increasing radius. The vertical line indicates the largest radius

Table 1. "Visible" Topography, $\sigma = 2.4$
Residuals Based on Two Data Sets

Sta	Observed Deflection ξ''	η''	Set 5 v_ξ''	v_η''	Set 6 v_ξ''	v_η''	Improvement $\lvert v_5\rvert'' - \lvert v_6\rvert''$	
1	−22.73	+10.82	−1.62	+0.18	−0.94	+3.48	+0.68	−3.30
3	−24.49	+ 4.48	−3.10	−2.16	−2.37	+1.26	+0.73	+0.90
6	−21.42	−19.12	+3.44	−4.39	+4.19	−1.64	−0.75	+2.75
7	− 8.52	+20.20	+3.06	−0.89	+3.85	+2.67	−0.79	−1.78
8	−11.71	−20.94	+1.11	−3.15	+2.08	−0.71	−0.97	+2.44
9	− 0.56	+20.46	−1.08	−3.25	−0.02	+0.15	+1.06	+3.10
11	− 0.29	+17.28	−0.94	−4.06	+0.15	−0.74	+0.79	+3.32
12	−13.39	− 9.32	−2.54	−0.21	−1.37	+2.14	+1.17	−1.93
13	−20.05	−11.66	−4.79	−1.11	−3.54	+0.88	+1.25	+0.23
14	+11.69	+21.83	−0.17	−5.38	+1.10	−1.98	−0.93	+3.40
15	−20.04	−12.01	−3.21	−2.47	−1.84	−1.08	+1.37	+1.39
16	+21.34	+18.47	+0.60	+1.28	+2.25	+3.31	−1.65	−2.11
17	+21.20	− 6.94	−0.39	+2.64	+1.28	+3.46	−0.89	−0.82
18	+25.52	+13.22	−3.92	+4.55	−2.06	+6.36	+1.86	−1.81
20	+27.20	+ 7.58	−4.36	+2.80	−2.47	+4.59	+1.89	−1.79
23	−19.78	−11.92	−3.78	−1.85	−2.48	−0.08	+1.30	+1.77
$\Sigma\lvert v\rvert/16$			2.4	2.5	2.0	2.2		
r.m.s.			2.8	2.9	2.3	2.7		
better, average/number of cases							+1.2/10	+2.1/9
worse, average/number of cases							−1.0/6	−1.9/7

Table 2. Individual Largest Circles Versus Fixed Data Area
Comparison of Residuals (Set 6)

Sta	Largest Radius km	Visible Topography Circular v_ξ''	v_η''	Improvement $\Delta\lvert v_\xi\rvert''$	$\Delta\lvert v_\eta\rvert''$	With Isostatic Compensation, 113.7 km Circular v_ξ''	v_η''	Improvement $\Delta\lvert v_\xi\rvert''$	$\Delta\lvert v_\eta\rvert''$
1	350	−3.37	+4.52	−2.43	−1.04	−6.68	+2.59	+0.05	+0.06
3	352	−4.79	+2.21	−2.42	−0.95	−6.85	+2.19	+0.05	+0.05
6	362	+2.34	−1.33	+1.85	+0.31	+0.89	−3.11	−0.04	−0.02
7	348	+2.27	+3.76	+1.58	−1.09	+1.13	+0.53	−0.03	+0.06
8	368	+1.04	−0.68	+1.04	+0.03	−2.09	−0.88	+0.01	−0.02
9	350	−0.60	+1.13	−0.58	−0.98	−1.95	−0.32	0.00	−0.06
11	352	−0.33	+0.17	−0.18	+0.57	−1.49	+0.20	0.00	+0.05
12	368	−1.63	+2.06	−0.26	+0.08	−3.40	+0.60	0.00	+0.01
13	366	−3.62	+0.37	−0.08	+0.51	−2.66	−0.21	−0.01	0.00
14	350	+1.18	−0.99	−0.08	+0.99	+0.17	−2.02	+0.02	−0.05
15	356	−1.63	−2.33	+0.21	−1.25	−1.37	−4.39	−0.02	+0.01
16	364	+3.68	+2.94	−1.43	+0.37	+3.62	+0.63	+0.05	+0.01
17	348	+2.67	+1.64	−1.39	+1.82	+2.44	−1.10	+0.05	+0.03
18	354	−0.06	+5.51	+2.00	+0.85	+1.10	+1.61	+0.07	0.00
20	352	−0.38	+3.69	+2.09	+0.90	+0.76	+1.65	+0.07	0.00
23	362	−2.40	−0.88	+0.08	−0.80	−2.01	−2.60	−0.01	0.00
$\Sigma\lvert v\rvert/16$		2.0	2.1			2.4	1.5		
r.m.s.		2.4	2.6			3.1	1.9		
better, average/cases				+1.3/7	+0.6/10			+0.0/8	+0.0/8
worse, average/cases				−1.0/9	−1.0/6			−0.0/5	−0.0/4

of circular coverage within Set 6; the wobble beyond is due to the lopsidedness of the fixed data area. By comparison, Figure 5b shows the analogous curve computed with isostatic compensation: it straightens out much sooner.

TOPOGRAPHIC–ISOSTATIC DEFLECTIONS

Experimentation with some isostatic models for this area (Fischer, 1974), specifically with the Pratt-Hayford hypothesis and a series of density values and depths of compensation, has suggested that there may exist some compensation, but that it takes place further down rather than at the traditionally adopted depth of 113.7 km. The assumption of twice this depth, 227 km, has given smaller residuals. Although the underlying geophysical facts, if any, can be modeled in a number of different ways, this assumption was maintained here for the time being. Table 3 shows the residuals and the difference in the effect of the two data sets.

A comparison of the "improvement" columns in Tables 1 and 3 confirms the impression of Figure 5: the isostatically reduced deflections derive their full magnitudes from a much smaller data area; neither the enlarged area nor its lopsidedness have a significant effect on the stabilized value. This result conforms with an earlier finding (Chovitz and Fischer, 1959) that on a global scale the topography beyond a radius of about 450 km has a negligible effect on a deflection value under the assumption of the Pratt-Hayford isostatic theory (Fig. 6).

Table 3. Pratt-Hayford Isostatic Models, $\sigma = 2.4$
Residuals Based on Two Data Sets

	Depth of Compensation 113.7 km						Depth of Compensation 227 km					
	Set 5		Set 6		Improvement		Set 5		Set 6		Improvement	
Sta	v_ξ''	v_η''	v_ξ''	v_η''	$\Delta\lvert v_\xi\rvert''$	$\Delta\lvert v_\eta\rvert''$	v_ξ''	v_η''	v_ξ''	v_η''	$\Delta\lvert v_\xi\rvert''$	$\Delta\lvert v_\eta\rvert''$
1	−6.44	+2.94	−6.73	+2.65	−0.29	+0.29	−5.51	+3.43	−5.53	+2.98	−0.02	+0.45
3	−6.46	+2.21	−6.90	+2.24	−0.44	−0.03	−5.48	+2.75	−5.65	+2.64	−0.17	+0.11
6	+0.76	−3.10	+0.85	−3.09	−0.09	+0.01	+2.00	−2.42	+2.31	−2.38	−0.31	+0.11
7	+1.05	+0.69	+1.10	+0.59	−0.05	+0.10	+1.71	+0.66	+1.94	+0.37	−0.23	+0.29
8	−2.17	−0.90	−2.10	−0.86	+0.07	+0.04	−1.10	−0.42	−0.90	−0.28	+0.20	+0.14
9	−1.97	−1.17	−1.95	−0.26	+0.02	−0.09	−1.81	−0.63	−1.71	−0.88	+0.10	−0.25
11	−1.50	+0.34	−1.49	+0.25	+0.01	+0.09	−1.40	−0.12	−1.32	−0.35	+0.08	−0.23
12	−3.42	+0.57	−3.40	+0.61	+0.02	−0.04	−2.92	+0.69	−2.83	+0.84	+0.09	−0.15
13	−2.66	−0.29	−2.65	−0.21	+0.01	+0.08	−2.19	−0.04	−2.14	+0.24	+0.05	−0.20
14	+0.17	−1.88	+0.19	−1.97	−0.02	−0.09	−0.19	−2.59	−0.16	−2.84	+0.03	−0.25
15	−1.35	−4.55	−1.35	−4.40	0.00	+0.15	−0.95	−4.10	−0.94	−3.61	+0.01	+0.49
16	+3.73	+0.57	+3.67	+0.64	+0.06	−0.07	+2.63	+0.16	+2.46	+0.38	+0.17	−0.22
17	+2.61	−1.36	+2.49	−1.13	+0.12	+0.23	+1.78	−1.13	+1.56	−0.43	+0.22	+0.70
18	+1.28	+1.46	+1.17	+1.61	+0.11	−0.15	−0.24	+1.12	−0.52	+1.49	+0.28	−0.37
20	+0.94	+1.47	+0.83	+1.66	+0.11	−0.19	−0.61	+1.16	−0.90	+1.58	−0.29	−0.42
23	−2.00	−2.71	−2.00	−2.60	0.00	+0.11	−1.59	−2.40	−1.56	−2.03	+0.03	+0.37
Σ|v|/16	2.4	1.6	2.4	1.5			2.0	1.5	2.0	1.5		
r.m.s.	3.0	2.0	3.1	1.9			2.5	1.9	2.5	1.8		
better, average/cases					+0.1/11	+0.1/9					+0.1/11	+0.3/8
worse, average/cases					−0.2/5	−0.1/7					−0.2/5	−0.3/8

FURTHER REFINEMENTS

Figure 7 shows the residuals corresponding to Table 1, Set 6, and Figure 8 those of Table 3, Set 6, for 227 km depth of compensation. A comparison indicates that the isostatic compensation

helped particularly in the north, but made things much worse for the southern tip of the Kwajalein Island itself. Apparently, too much isostatic compensation has been applied for this island, which can be remedied by placing a small surload just north of it. It must be near enough for the desired effect, and small enough not to affect adversely the rest of the atoll. It is visualized, geophysically, as an intrusion of the denser basaltic oceanic crust (σ = 2.98 g/cm^3) into the volcanic core of the atoll (σ = 2.4 g/cm^3) with a density difference of +0.58 g/cm^3. Similarly, three other surloads were placed as shown in Figure 8, with a dramatic reduction of the residuals (Table 4 and Figure 8). The location and amount of these surloads was explored first by treating them as point masses representing limited slabs above the basaltic layer, which is assumed to begin at 6 km depth and is normally covered by about 1 km of sediments. The point mass computation was followed by computation for 0'.5 x 0'.5 columns for the extent of the slab with a height of 4 km, 2 km, 2 km, and 3 km, respectively; the difference in results was only a few tenths of seconds.

Table 4. Deflection Residuals From an Adopted Model Pratt-Hayford (227 km) and Four Surloads

	Data Set 6			Data Set 6	
Sta	v_ξ''	v_η''	Sta	v_ξ''	v_η''
1	−1.23	+1.69	13	−0.73	+0.77
3	−1.14	+1.93	14	−0.17	−0.65
6	+2.37	+0.94	15	+0.27	−1.90
7	−0.83	−1.62	16	+0.53	−0.03
8	−0.93	+0.68	17	+1.34	+0.64
9	−0.90	+0.12	18	−0.55	+0.56
11	−0.56	+0.86	20	−0.77	+0.46
12	−2.10	+1.25	23	−0.22	−1.10
			$\Sigma\|v\|/16$	0.9	0.9
			r.m.s.	1.1	1.1

This refinement of the density model for the atoll expresses the geophysical likelihood that the rock density is not uniform throughout, which may have something to do with the way this volcanic atoll was formed. From a purely computational viewpoint such refinements could be inserted locally to perfection, but that would defeat the purpose. To find a density model for predicting as yet unobserved deflection values the model must be geophysically plausible and regionally valid.

Variations of density could also be added successfully to the model represented in Figure 7. This has been done with data Set 5 (Fischer, 1974). While the details of the refinements will differ depending on what else has already been built into the density model, they may be equivalent descriptions of the same underlying reality. For example, the surplus density in the center of the atoll (Fig. 8) may be roughly equivalent to two density deficiencies flanking the atoll.

The density model represented by Figure 8 and Table 4 was tested against 16 newly observed deflections, with residuals shown in Table 5. Their magnitudes of less than 2" and of around 1" r.m.s. are certainly encouraging.

COMPUTATION WITH UNIVAC–1108

Computations for this project were done on the UNIVAC-1108* using the FORTRAN compiler language. Theoretically, the programing for the deflection computation was rather straightforward. Practically, though, there were a few difficulties such as conserving computer time and keeping track of the large amount of data used in the computations.

*Any mention herein of a commercial product does not constitute endorsement by the U.S. Government.

Table 5. Sixteen Test Points Pratt-Hayford (227 km) and Four Surloads

Sta	Observed Deflection ξ''	η''	Residuals v_ξ''	v_η''
2	−23.59	+11.69	−1.16	+1.29
4	−23.79	+ 6.95	−1.48	+1.32
5	−21.62	+11.79	−0.84	+1.11
10	+ 0.05	+21.11	−0.29	+0.35
19	+28.89	+10.49	−1.76	+0.57
21	+26.27	+10.14	−0.92	+0.34
22	+28.75	+11.16	−1.43	+1.00
24	−20.47	+17.73	−1.13	+1.59
25	−19.58	+13.75	+0.09	+1.88
26	−19.23	+16.74	−0.42	+0.68
27	−12.33	+19.80	+0.77	+0.73
28	− 4.50	+24.49	−0.14	−0.69
29	−11.01	−12.99	−1.42	+1.05
30	+ 2.54	+24.96	+0.69	+0.45
31	+26.93	− 2.39	−1.17	+1.38
32	+29.20	+ 6.88	−1.37	+1.87
		$\Sigma pvv/16$	0.9	1.0
		r.m.s.	1.1	1.1

The computation of each bathymetric value was accomplished by a subroutine, separate from the main program. This made it possible to have a different subroutine for each variation of the density model that was considered. This also made it easier to change back and forth between models without tampering with the main program.

A special effort had to be made to make the subroutines as efficient as possible because of the multiple effect any unnecessary calculation would have on the computer time. A subroutine had to be called about 20,000 times for each station, or once for each bathymetric value contribution. As it turned out, the CPU time to compute both deflection components averaged out to be 13 to 16 seconds per station. For example, it takes about 8.5 minutes of CPU time to compute 64 deflections, using about 20,000 bathymetric values.

The data were read from the various charts by inspection, using templates to divide the latitude-longitude grid into rectangular areas of different sizes, as mentioned earlier. The values were then placed eight on a card to be read and placed on tape. The latitude and longitude values at the upper left hand corner of each rectangle were used as the control point. The cards also contained the length (in minutes of arc) of a side of the squares represented on the card, the ϕ,λ position of the first value on the card, and a control variable in the column following each baythmetric value. During the computation, the control variable was checked before using each bathymetric value. If the variable was N, the value was ignored and the program moved on to the next value.

Using the control variable in this way was very useful during this project for two reasons: it made corrections easier and it enabled the replacement of any value representing a given rectangular area with a set of values for subdivisions into different sizes of rectangular areas.

SUMMARY AND CONCLUSIONS

The first impression that the visible distribution of land and water in the region of the atoll

would explain the major part of the large deflection values has proved correct: values larger than 20" have been reproduced with an r.m.s. error of 2" to 3". Further, simple assumptions about the density distribution, including isostatically compensated and uncompensated masses, have reduced this error to less than 1".5. More detailed assumptions could probably reduce this error even further.

The construction of a series of tentative density models for the area was guided by a set of initially available astrogeodetic deflections and tested against another set of deflections observed at a later date. While there were several successful models with different sets of small residuals, the real geophysical structure could not yet be clearly identified at that time. For example, models with and without isostatic compensation were both successful, because the effect of the compensation could be modeled also by density differences of reasonably placed uncompensated mass excesses or deficits, in more than one way. Geophysical interpretation will have to wait for further studies, supported by other geophysical evidence.

REFERENCES

Chovitz, B., and Fischer, I, The Influence of the Distant Topography on the Deflection of the Vertical, *Bull.Geod.* No. 54, 1959.

Fischer, I., Slopes and Curvatures of the Geoid from Gravity Anomalies by Electronic Computer, *J. Geophys. Res.*, vol. 71, No. 20, 4909, 1966.

Fischer, I., Deflections at Sea, *J. Geophys. Res.*, 1974 (in press).

Stubbs, A.R., Cartney, B.S., and Legg, J.G., Telesounding, A Method of Wide Swathe Depth Measurement, *Internat. Hydrographic Rev.*, vol. 51, No. 1, 1974.

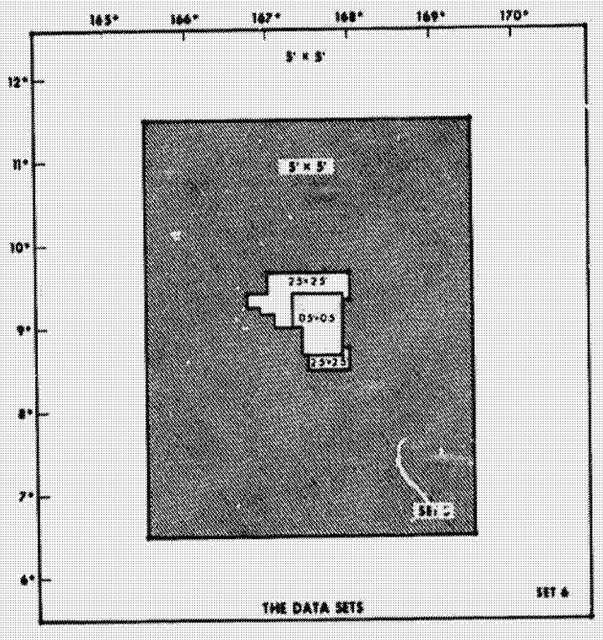

Figure 1

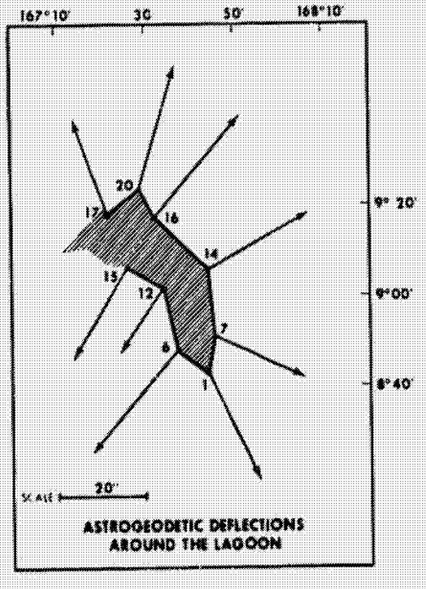

Figure 2

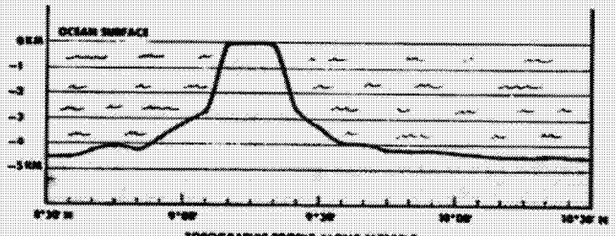

TOPOGRAPHIC PROFILE ALONG 167° 20' E

Figure 3

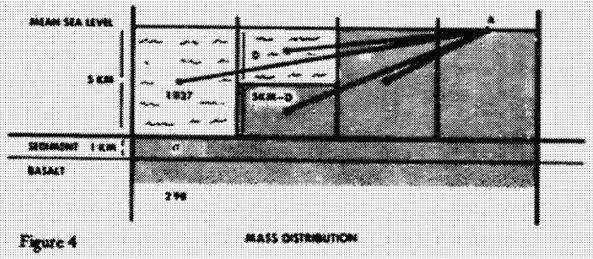

MASS DISTRIBUTION

Figure 4

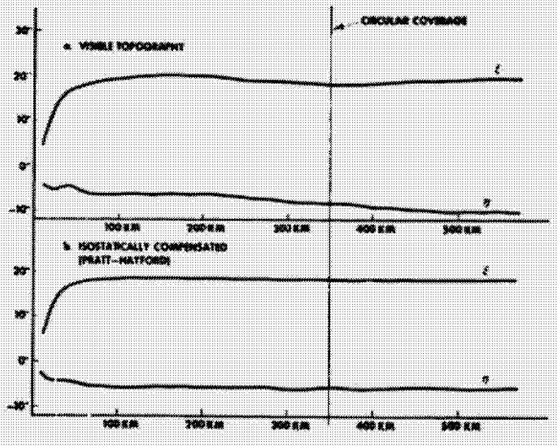

ACCRUAL OF DEFLECTION VALUES WITH DISTANCE (STATION 17)

Figure 5

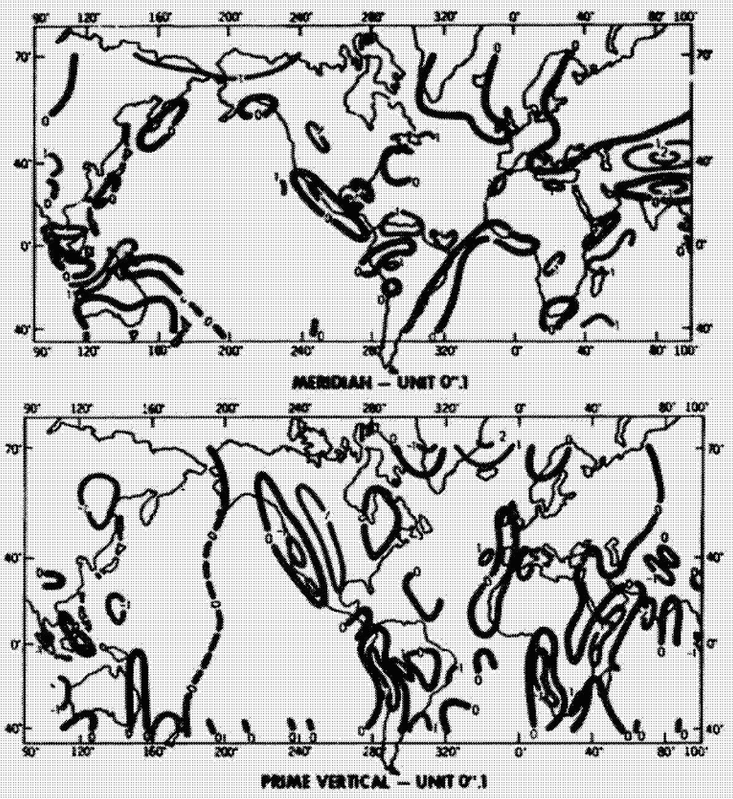
MERIDIAN — UNIT 0".1
PRIME VERTICAL — UNIT 0".1
INFLUENCE OF TOPOGRAPHY BEYOND 470 KM
ISOSTATIC REDUCTION: PRATT–HAYFORD 113.7 KM

Figure 6

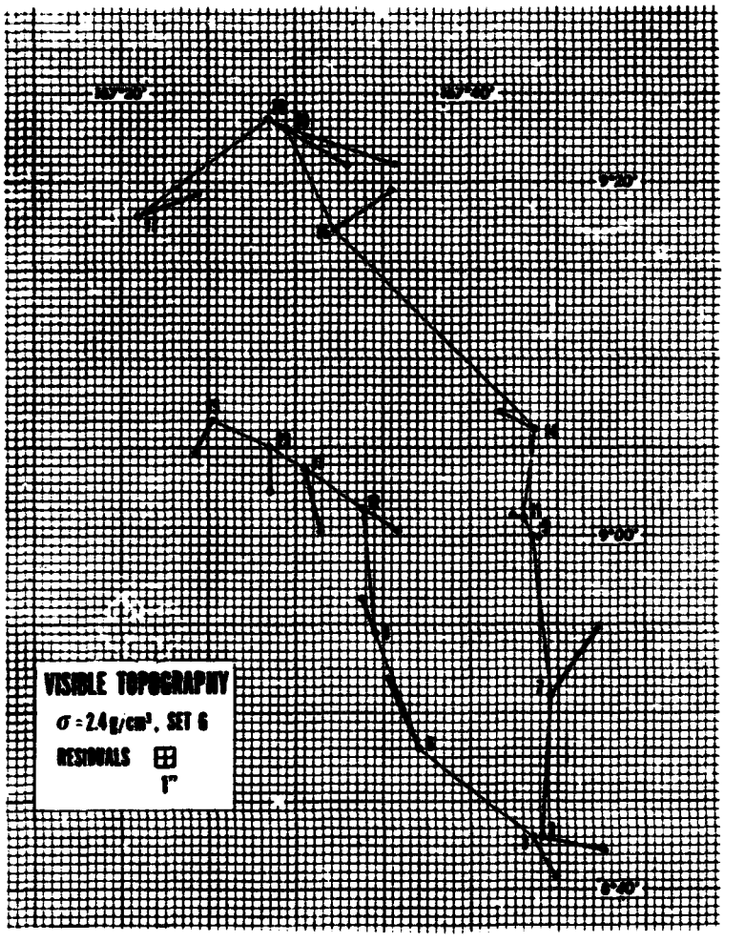

Figure 7

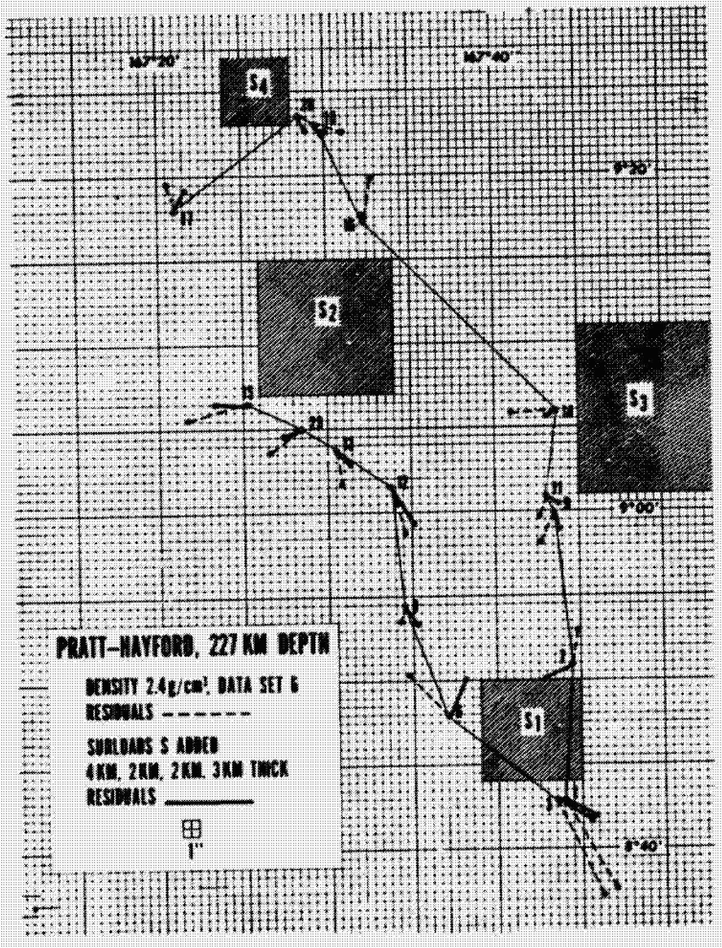
147°20'
147°40'
9°20'
9°00'
8°40'
S4
S2
S3
S1
PRATT–HAYFORD, 227 KM DEPTH
DENSITY 2.4 g/cm³, DATA SET 6
RESIDUALS - - - - - -
SURLOADS S ADDED
4 KM, 2 KM, 2 KM, 3 KM THICK
RESIDUALS ———
1"

Figure 8

OPERATIONAL RELIABILITY OF A CONVENTIONAL SATELLITE NAVIGATION SYSTEM IN BEAUFORT SEA GRAVITY STUDIES

E. F. Chiburis and Peter Dehlinger
Marine Sciences Institute
and Department of Geology and Geography
The University of Connecticut
Groton, Connecticut 06340

ABSTRACT

In conjunction with surface-ship gravity studies conducted in the Beaufort Sea, an analysis was made of ship positions obtained with a conventional satellite navigation system aboard a USCG icebreaker operating on the continental margin north of Alaska. Every possible fix was obtained during 1972 and 1973 field seasons to permit the calculation of accurate corrections to gravity measurements. Analyses were made of gravity anomaly misties at trackline intersections and of satellite fixes, indicating that routinely obtained navigation data are sufficient to determine anomalies within a one milligal uncertainty.

INTRODUCTION

A marine gravity program was conducted aboard USCG icebreakers on the continental margin of the Beaufort Sea, north of the Alaskan coastline, during the summers of 1972 and 1973. The principal purposes of the program have been to determine crustal and subcrustal structures across the continental margin and to relate them to the tectonic history of the Arctic Basin. Approximately 2000 reliable free-air gravity anomalies have been determined in an area extending eastward from Point Barrow to Barter Island (near the Alaskan-Canadian border) and from the coastline northward to about the 2000 m isobath. The program is being continued aboard an icebreaker during the summer of 1974.

Ship positioning was obtained with a satellite navigation system and, for part of the operation, with a ship course recorder for positioning between satellite fixes. The satellite fixes were analyzed in some detail for the purpose of making as accurate gravity reductions as possible. Although the fixes were not obtained for purposes of evaluating the navigation system itself, the analysis demonstrates the adequacy of routinely obtained ship-board fixes for deep ocean geophysical studies.

FIELD PROCEDURES

Continuous gravity measurements were made aboard the USCGC Glacier in conjunction with the Coast Guard's program, Western Beaufort Sea Ecological Cruise (WEBSEC). The purpose of WEBSEC was to establish certain marine environmental baselines in the vicinity of the Alaskan northslope. The scheduled WEBSEC tracklines generally suited our gravity requirements, particularly the long tracklines which were to be run perpendicular to the

coastline. Figure 1 shows tracklines made during 1972 and 1973 along which reliable gravity anomalies were calculated. The total number of WEBSEC tracklines are more extensive than those shown in Figure 1, but are located in the same general area.

The instruments used to measure gravity were LaCoste and Romberg stable-table surface-ship meter systems No. S-42 (1972) and No. S-51 (1973). The satellite navigation system was the AN/SRN-9 which is part of the Glacier regular navigation equipment. During the 1973 cruise, a course recorder linked to the ship's gyro system was operated to assist in the navigation reduction. The recorder has a resolution of approximately 1^{0}.

The ship maintained generally constant speeds and headings in open waters; along such constant velocity lines, reliable gravity measurements and corresponding Eotvos corrections were obtained. Numerous oceanographic stations were also occupied as part of WEBSEC, most of them in open water and each for periods of from a few hours to more than a day. Gravity was measured continuously while on station and drift of the ship was determined from satellite fixes. The resultant gravity measurements provided excellent anomaly values. On several occasions the ship was anchored at sea, the longest anchored station being occupied for about 20 hours. These anchored stations provided the most reliable gravity measurements and the most significant data for estimating the mean error of satellite fixes. On other occasions, the ship was secure in drifting ice for more than two days. Using a helicopter to transport a geodetic land meter between stations, a base-station tie was then obtained between gravity measured on the ice alongside the ship and the Woollard base station at Barrow. During these time periods, conventional gravity anomalies were also obtained. Frequently, the ship was underway in ice, during which gravity measurements were attempted. When breaking too heavy ice or when dodging floating ice, resultant accelerations were sometimes too large to provide reliable gravity measurements, and Eotvos corrections were sometimes too uncertain to permit reliable anomaly determinations. While gravity anomalies could not be calculated under such severe operating conditions, all available satellite fixes were nonetheless obtained then as well as under more favorable ship conditions.

Because satellite passes are more numerous at high latitudes than elsewhere, the fixes obtained during the program provide an unusual opportunity for the determination of the reliability of routine fixes. One of our gravity personnel assisted in rerunning the Doppler data aboard ship in an attempt to improve the quality of the fixes over otherwise routine calculated values, thus assuring that fix errors were minimized. Low-angle satellite passes were usually not accepted because of too few Doppler data; similarly, some high-angle passes were rejected because of too small Doppler shifts.

Satellite fixes were obtained under three different ship operating conditions: running, drifting, and anchored. The latter two involved on-station fixes for periods from a few hours to several days.

DATA REDUCTION AND EVALUATION

The criteria used for selecting gravity data from the continuous analog records are (1) to generally accept all data when operating in ice-free conditions, with anomalies determined from the records at about 10 minute intervals and, (2) to accept those data, when the ship was breaking or dodging ice, in which the recordings could readily be smoothed over intervals of several minutes (short-period gravity variations of less than

3-5 mgal). Gravity measurements were excluded which fluctuated on the order of tens of milligals; these data could not be smoothed because extraneous accelerations of long duration were included in the recordings, usually due to substantial ship maneuvering (backing, rapid course changes of long duration, stop and start, etc.). However, sea states were generally so calm in the area that all measurements, except when actually breaking ice, were made within acceptable acceleration limits.

Ship speeds were often less than 2 knots when operating in ice and 6 knots in open waters. At latitudes of 70^{0}-72^{0}N, the maximum Eotvos corrections (for easterly or westerly headings) are 5 and 15 mgal, respectively. Assuming errors of 0.25 km in navigation fixes (as discussed later), errors in Eotvos correction will be less than 0.5 mgal in ice and 1.5 mgal in open water. A larger source of anomaly error, however, is due to incorrect positioning in areas of steep gravity gradients.

The uncertainty in calculated gravity anomalies was determined from an analysis of misties at all available trackline intersections, totaling 86. Figure 2 shows the results of the mistie analysis. The misties range from 0.0 to 5.0 mgal, the mean mistie being 1.5 mgal. By distributing the mistie equally between two intersecting lines, the uncertainty in anomaly determination is 1.1 mgal, which includes the effects of meter reliability and of errors in navigation.

The mode of the misties is seen to be 1.0 mgal (Fig. 2); the 90th percentile 0.3 mgal (10% of the misties are less than 0.3 mgal); the 50th percentile or median mistie 1.3 mgal; and the 10th percentile 3.3 mgal (90% of the misties are less than 3.3 mgal). The misties are seen to be small, without exception, despite the fact that some of the intersections are located over steep gravity gradients (as large as 10 mgal/km in some areas). The navigation data are thus concluded to be quite reliable.

An estimate of the accuracy of routinely obtained satellite fixes is indicated in Fig. 3, where all 17 available fixes are plotted about the mean fix position for one anchored ship station. The mean error of the fixes is 0.25 km (800 ft), with a standard deviation about the mean position of 0.31 km. These errors indicate what can be expected from routine navigational data as available from the bridge logs. It should be pointed out, however, that the precision of fixes could usually be improved when our gravity personnel reduced the recorded Doppler data. Whether the improved precision amounted to a significant increase in accuracy would have to be separately evaluated.

While the ship was on station, the usually high drift rates due to water currents or wind required that gravity data be Eotvos corrected. Fig. 4 is an example of four selected drift profiles obtained with multiple fixes while the ship was "stopped". For comparison, the estimated mean navigation error is also shown on the figure. The observed drift is clearly much larger than the estimated position error. Gravity anomalies obtained at drifting positions thus include Eotvos corrections based on drift determined from the satellite fixes.

The majority of fixes were obtained while the ship was underway; these running fixes should involve slightly larger errors than the anchored fixes as a result of ship speed. However, at ship speeds of less than the 6 knots in open water, and less than the 2 knots in ice, the increased fix errors should be small. If the observed uncertainty in gravity anomaly were due entirely to errors in Eotvos correction, the maximum error in ship speed can be calculated from the well-known equation

$$\Delta g = 7.5\ (\Delta v_E)\ \cos\ \phi$$

where Δg is in mgal, Δv_E in knots, and ϕ is the latitude. For a mean anomaly uncertainty of 1.1 mgal and a latitude of 71°,

$$\Delta v_E = 0.45 \text{ knot} = 0.83 \text{ km/hr}$$

If fixes are obtained at half hour intervals, the total position error in the two adjacent fixes becomes 0.4 km. As not all of the uncertainty can be attributed to position errors, the maximum error in running fixes would be less than 0.4 km, and it may be nearly as small as that obtained at anchor (0.25 km).

Errors in gravity anomaly include the error due to the performance of the meter system, error in Eotvos correction, and error in assumed station location. The latter effect introduces two types of errors. The first is the effect of assuming an incorrect latitude (in a field of uniform gravitational potential) in the normal gravity formula used to calculate the gravity anomaly. This involves an error of 0.4 mgal/km in a north-south direction at high latitudes. The second applies to areas exhibiting gravity gradients where gravity at the apparent station is different from that at the place of actual measurement. Of these two sources of error, the first is due to using an incorrect value of normal gravity and the second to using both an incorrect "observed" value and an incorrect normal gravity value.

The anomaly error due to incorrect positioning in a field with a gravity gradient can be estimated. For reasonable values of 0.5 mgal in uncertainty in the meter system, 0.1 mgal as the error in the normal gravity formula for a north-south position error of 0.25 km, and 0.5 mgal as the uncertainty in Eotvos correction (in ice areas), the mean anomaly error Δd associated with incorrect positioning along a gravity gradient can be obtained from,

$$\Delta g = [(0.5)^2 + (0.1)^2 + (0.5)^2 + (\Delta d)^2]^{\frac{1}{2}} = 1.1 \text{ mgal uncertainty}$$

from which

$$\Delta d = 0.84 \text{ mgal.}$$

An error of 0.84 mgal, due to an incorrectly assumed position along a gravity gradient where position errors between adjacent fixes are taken as 0.4 km ($[(0.25)^2 + (0.25)^2]^{\frac{1}{2}}$), implies measurements in a gravity field with gradients of approximately 2 mgal/km. The largest gravity gradients in the area exceed 10 mgal/km. The maximum observed gravity mistie (5.0 mgal), assuming a navigation uncertainty of 0.25 km, corresponds to a gravity gradient of 8.5 mgal/km.

CONCLUSIONS

Observed fixes obtained with an AN/SRN-9 satellite navigation system under routine operating conditions aboard a surface ship in the Beaufort Sea have a mean error of 0.25 km, as determined from 17 successive fixes at an anchored position. The corresponding standard deviation about the mean position is 0.31 km. This accuracy is sufficient to provide gravity anomaly determinations, except for the effect of meter performance, within an uncertainty of one milligal.

ACKNOWLEDGMENTS

We gratefully acknowledge the cooperation and assistance of the U. S. Coast Guard, particularly the Office of Polar Operations and the officers and men of the USCGC Glacier. Appreciation is expressed to Oregon State University and to the Naval Oceanographic Office for loan of the gravity meters used to make the ship board measurements. This study has been supported in part by the Office of Naval Research under Contract N00014-68-A-0197-0002.

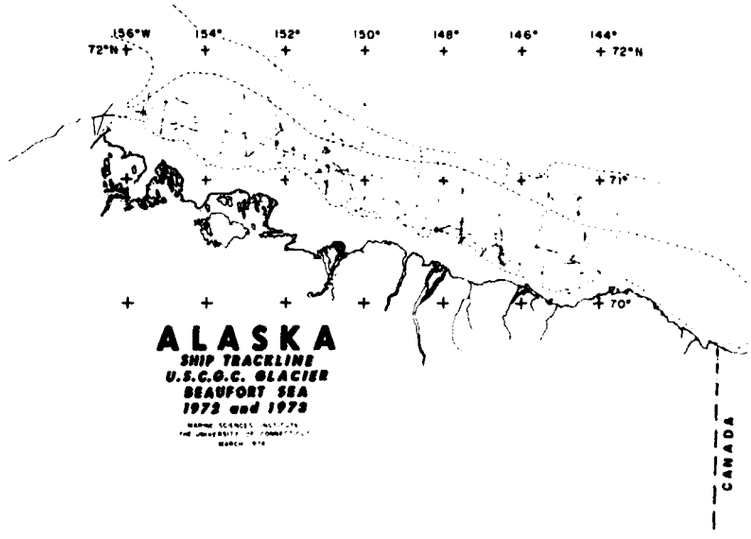

Figure 1. Ship tracklines along which gravity anomalies were calculated. Satellite fixes were obtained along these lines and at intermediate ship positions not shown.

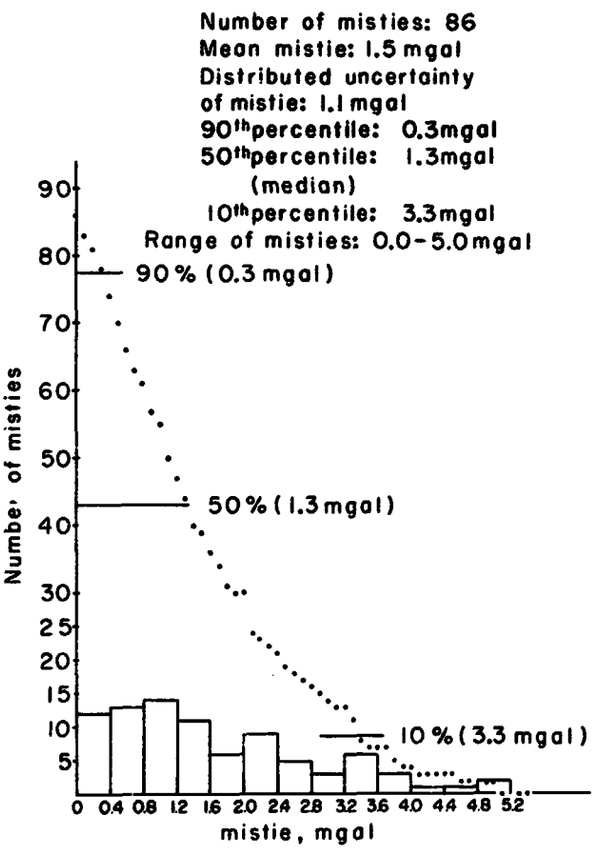

Figure 2. Discrete and cumulative distribution of free-air gravity anomaly misties at trackline intersections. Discrete interval, 0.4 mgal; cumulative interval, 0.1 mgal.

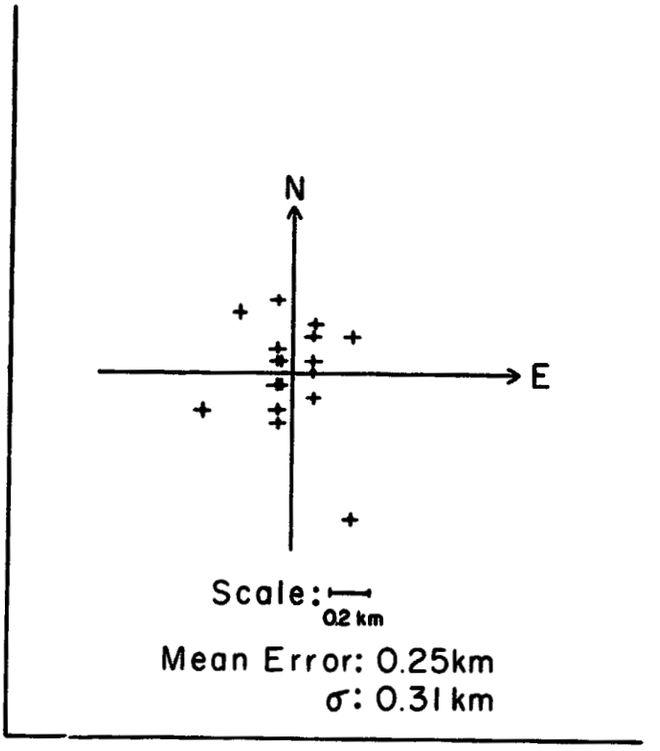

Figure 3. Multiple satellite fixes from a single anchored position. Positions plotted relative to the mean. Vertical and horizontal distances are to same scale.

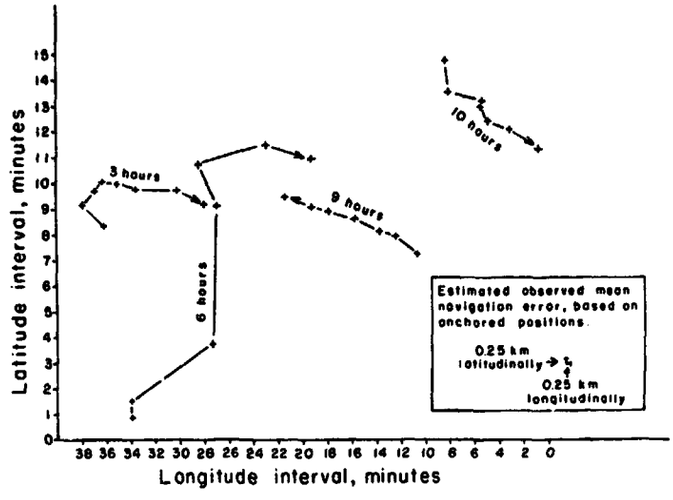

Figure 4. Multiple satellite fixes from four selected oceanographic station positions showing directions and durations of drift. Shown to scale are observed mean latitudinal and longitudinal navigation errors of 0.25 km.

EVALUATION OF OCEAN GRAVITY DATA

BILLY J. BOYER
DEFENSE MAPPING AGENCY AEROSPACE CENTER
RESEARCH DEPARTMENT
DOD GRAVITY SERVICES DIVISION

ABSTRACT

An investigation is made of the problems encountered in evaluating ocean gravity data received from various organizations. Statistical and graphical representations are developed to show problems caused by the divergence of the surveyed gravity data. Discrepancies noted are most pronounced when a vessel's track consists of a sequence of intersecting segments and particularly when different vessel's tracks intersect. Present techniques of evaluation and adjustment of ocean gravity surveys to unify the data into a compatible system are discussed.

INTRODUCTION

The Department of Defense (DOD) Gravity Library is located at the Defense Mapping Agency Aerospace Center (DMAAC) in St. Louis, Missouri. Established in July 1964, the Library is the official depository for all gravity information held by the Department of Defense. Complete library services are provided, including technical knowledge and guidance on gravimetry and evaluated gravity data.

The Gravity Library has acquired over 9,000,000 unique worldwide gravity observations and maintains an automated master file of over 4,000,000 selected evaluated gravity stations. As of February 1974, the Gravity Library had totally automated 4,304,468 gravity stations. Of these 65% or over 2,800,000 of these automated gravity stations are within the oceans. Figure 1 illustrates the growth of the gravity data on file at the DOD Gravity Library.

The sources of the gravity information the Gravity Library receives covers a broad spectrum of the scientific community, both national and international and governmental and private. Usual sources are US Naval Oceanographic Office, Defense Mapping Agency Topographic Center, National Oceanic and Atmospheric Administration (NOAA), geophysical companies engaged in oil and mining activities, universities and institutes involved in geodetic or geophysical research, state agencies, national geological or geodetic commissions, and foreign governments with whom we have formal exchange agreements.

As can be seen on the gravity data graphic, the holdings have increased by approximately 1,000,000 stations a year. This is the largest known single collection of gravity data in the world.

The basic problem with this enormous and diverse collection is the adjustment and evaluation of a large mass of heterogeneous gravity anomaly data. As was indicated earlier, the data is collected from a variety of sources, surveyed over a number of years, surveyed for different purposes, using a multitude of ships and equipment, and performed under ever-changing sea and weather conditions.

The evaluation of gravity data in the oceans presents many unique problems not encountered in evaluating land gravity data. On land, the systematic errors are primarily datum and scale differences which can generally be eliminated by semi-automatic or automatic methods. Because of the density and proximity of reference base stations, the errors present in land gravity data are generally easily identified. In ocean surveys even these systematic errors become difficult to identify and to eliminate primarily because of lack of control - both gravity and geodetic. Random errors are difficult to identify on land surveys and are even more difficult to isolate in ocean gravity surveys. On land extensive use of the Bouguer anomaly and trend analysis aids greatly in the evaluation of land gravity data. However, the use of the Bouguer anomaly in evaluating ocean data has proven to be of minimum value. It is considered by many authors that the introduction of the Bouguer reduction for the ocean conceals or masks the natural pattern of the gravity anomaly field.

The evaluation of diverse and large amounts of ocean gravity presents additional difficulties not realized in land gravity data. Principal of these is the probable error contribution resulting from inaccurate Eötvös corrections. The Eötvös correction (dg), accounts for the effect of the ship's course and speed and is generally computed by the formula:

$$dg = 7.5v \sin A \cos \phi$$

where V is the speed of the ship in knots, A is the ship's course or azimuth, and Ø is the latitude. In middle latitude, an east-west velocity of 1 mile per hour corresponds to a change in observed gravity of 5 milligals. With the development of modern sophisticated navigation systems, it is now possible to obtain the Eötvös correction within 1 or 2 milligal. However, most of the ocean data available was surveyed prior to development of improved navigation systems and contains large errors due to inaccurate Eötvös corrections.

Another source of error in ocean gravity is the inability to effectively eliminate cross-coupling. This cross-coupling error is caused by a coupling between the horizontal and vertical accelerations incident upon the gravimeter creating a bias in the recording of measured gravity. This error is removed by continuous computation during the actual survey and is difficult, if not impossible, to correct once the data is reduced and placed in the library system.

The Gravity Library does not receive all the measured input to calculate these corrections, therefore, the depth of investigations and analysis of their error contribution is hampered. However, with improved navigation and gravimeter systems, reliability and accuracy of later date surveys are being realized and the selection of preferred or control source data is considerably enhanced.

Still the task of developing a unified set of gravity values from various sets of gravity sources must be accomplished. Since gravity data, primarily in the form of gravity anomalies,

are used in many DOD scientific programs, the evaluation and unification process must eliminate any blunders and reduce the errors to a minimum.

ANALYSIS OF GRAVITY DISCREPANCIES AT TRACK INTERSECTIONS

The accuracy or at least the reliability of ocean gravity measurements can most easily be determined by comparing free air gravity anomaly values at track intersections. These comparisons made for individual surveys and between different surveys provide for analysis that guide selection of methods that will eliminate or reduce errors to a minimum.

This is a formidable task because of the large amount of survey track intersections in some areas and few or no survey track intersections in other areas.

As a sample of the track intersection discrepancies found, an analysis of the gravity discrepancies at track intersections in 848 - 1° x 1° areas in the Pacific Ocean is shown by the histogram in Figure 2. A total of 280 ship track intersections were analyzed. Track intersection discrepancies ranged from 9 to 150 milligals. The mean mis-tie of the 280 intersections is 13.6 milligals. The root mean square (RMS) discrepancy for all intersections was ± 24.3 milligals. A RMS of this magnitude is indicative of the presence of large systematic and/or random errors. These intersection analyses provide an example of the divergence of surface ship gravity measurements that have been surveyed over a number of years. Large unaccountable errors are identified and because it is impossible to attribute these errors to any single factor, some of the gravity data is initially unusable when evaluated in conjunction with later date surveys.

However, every effort is made to evaluate and adjust the maximum amount of gravity data. Various techniques and procedures are employed by the Gravity Library to achieve this goal.

Because of the quantity of data and the large number of sources, maximum use of automated processes is a necessity. As related earlier, all gravity data received by the Gravity Library is completely automated and coded to indicate the organization that performed the actual ship survey. This is extremely useful in the evaluation of data as it is received and in subsequent evaluation of new gravity survey data.

EVALUATION OF GRAVITY DATA IN A SELECTED AREA

In the initial stage of evaluating the combined surveyed gravity data in a selected area, a source plot is prepared using an automatic plotter. In addition to the source plot, all pertinent information including the organization that performed the survey, date, number of stations provided, and extent of the survey is furnished by the computer from a completely automated file reference library. This information can be furnished on an area by area basis. The source plot, which can be provided at any scale, shows all ship tracks with an individual code which represents the different sources in the selected area. For more recent surveys the track number when furnished by the surveying organization, are being included and can be annotated on the source plot. Figure 3 is an example of the source plot for a selected area.

The source plot shown in Figure 3 indicates four different surveys have been performed in the area with a total of 19

different tracks. These tracks produced 26 intersections and about 1228 miles of continuous data. Using this source plot annotated with track intersection discrepancies, a good example of the status of several ship gravity measurements is shown. The average unadjusted difference between tracks for all 26 intersections is 30.3 milligals. Of these, 54% are over 10 milligals. The maximum observed difference is 85 milligals. The highest intersection differences occurred along a single northeast by southwest line. It is readily seen that large unaccountable errors are present; however, the magnitude of the errors contributed by any specific survey cannot be definitely specified.

Since the Gravity Library does not normally receive navigation logs, ship logs, or sea state conditions at the time of the survey, it is difficult if not impossible to determine if the discrepancies are due to errors in navigation or gravity meter instrument or to inaccurate removal of computational errors such as the Eötvös effect.

Continuing the evaluation with the limited information relative to all the surveys in the area, the tracks are first inspected for systematic errors. Next, all unadjusted free air anomalies are contoured. Figure 4 is a contoured free air anomaly map of all sources for the selected area which shows unlikely gravity gradients. This initial contour map will show certain tracks to deviate significantly from the gravity trend or regional gravity field. Using this contour map information and source plot information, a preferred or control data source can generally be selected.

Few techniques are presently available to identify the exact magnitude of error; therefore, the most favored approach is to develop a smoothed free air gravity anomaly map after blunders are removed and inconsistencies and discrepancies between ship tracks are minimized. Care must be taken in using a smoothed free air contour map as the only criteria in determining the accuracy and reliability of a survey or a system of surveys. The insulating effect of the layer of water smooths out short wave length features and results in making it more difficult to identify low-amplitude anomalies along gravity survey lines.

The computer approach in which purely statistical analysis form the basis for evaluation and adjustment does not eliminate the need for geophysical investigations and decisions, but it does reduce the problem considerably.

GEOPHYSICAL INVESTIGATIONS

All available information is used in developing the smoothed gravity contour map. Principal data in this evaluation is water depth and ocean bottom topography information. Additionally, the use of free air gravity anomaly profiles has proven to be useful in the evaluation process. Figure 5 shows the comparison of the free air gravity anomalies profiles for two adjacent tracks. The two nearly coincident tracks also represent different surveys. It can be seen that the amplitude of the two gravity tracks is significantly greater and slightly broader. Although the gradient differs in magnitude, the trend of the anomalies are similar. Since the two tracks are not exactly coincident some of the differences in measured gravity are real. In this sample as in most of the ocean areas geophysical information is for the most part to general and regional in nature for fine detail adjustment of individual tracks. However, geophysical information can be and is used to evaluate the relative accuracy

of gravity profiles. As an example, gravity correlation analysis with available geophysical information can be used in identifying subtle changes in the gravity field due to the effect of local geologic variations in density or structure. The trained geophysicists should be prepared to know what to expect of the gravity field variations in areas of local irregularities such as seamounts, trenches, and the edge of the continental shelf. In these geophysically significant areas, abrupt changes in the gravity field may at first be interpreted as erroneous measurements in gravity. Conversely, the geophysicists should be aware of the form of the gravity field in the more regional geological and broad tectonic features such as an abyssal plain where smooth, non-varying gravity measurements along the profile should be expected.

For the two profiles in Figure 5, correlation with water depth does not aid in the resolution of the large gravity differences. The maximum difference between the two profiles is 77 milligals at a distance of 50-55 miles along the two tracks. The depth is approximately 4,600 meters throughout the length of the two tracks as determined from the only available bathymetric chart in the area. However, reliable depth information is extremely useful for detecting local irregularities such as seamounts, trenches, ridges and the edges of the continental shelf. Correlation of point or continuous gravity measurements with other surveyed geophysical parameters such as magnetic and heat flow have not been used successfully in evaluating and adjusting ocean gravity surveys. However, the local correlation between the ocean bottom topography and the free air anomalies permits a reliable estimation of the statistical characteristics and magnitude of the gravity field.

RESULTS OF EVALUATION AND ADJUSTMENTS

The results of the track intersection analysis and subsequent adjustments are shown on the contoured gravity anomaly map in Figure 6. The contours are smoothed out and indicate there is a good correlation with the ocean bottom topography. The high positive areas indicate anomalies which in fact consists of two prominent near surface features.

Before the data was adjusted in this sample area track intersection discrepancies ranged from 3 to 85 milligals. The RMS for all 26 intersections was $\pm$46.3 milligals with a mean mis-tie of 30.3 milligals. After eliminating the unusable portion of the data and making adjustment to the remaining tracks, the RMS for the track intersection discrepancies was reduced to $\pm$4.0 milligals.

Other procedures and methods have been developed to evaluate and adjust gravity data held by the DOD Gravity Library. Computer programs have been written for these methods that can process large quantities of data. However, these programs have not proved to be as valuable for ocean survey data as for land gravity data. One of these computer programs is the Common Station Comparison Program which generates a cross reference file of gravity stations from different sources that lie within a specified interval of each other. By comparing gravity anomalies at common and near common stations, the datum and scale differences between the various sources of data can be determined. Another computer program available is the Least Squares Adjustment of Gravity Sources which adjusts one gravity survey to the scale and datum of another. Common stations between two sources are analyzed and if a systematic relationship is evident, these values are used as input for the adjustment.

In developing these methods of evaluation, it is seen that these statistics computed in the computer programs describe the repeatability of the measured gravity, particularly during an individual survey, but not always the actual gravity or gravity anomalies.

Other authors have developed additional statistical methods to correct for systematic errors by making comparisons at line crossings; however, these methods have essentially treated data of a homogeneous survey and did not consider track data from several different surveys. Other limitations such as the requirement for evenly spaced data have further hampered the use of these statistical methods in our evaluation processes.

CONCLUSION

Although analyses of track intersections and subsequent adjustments does not guarantee complete elimination of errors, it does provide a means to unify large quantities of data with a limited amount of information. New and improved methods are being sought that will give greater reliability to this problem. In the last few years, emphasis has been on improvement and development of ocean gravimeters and stable platforms. Recent improvements and future development of improved navigation systems will make it possible to measure gravity with repeatability and accuracy of that presently achieved near shore. Until significant amounts of better quality gravity become available in the world's oceans, methods as previously described will continue to be required.

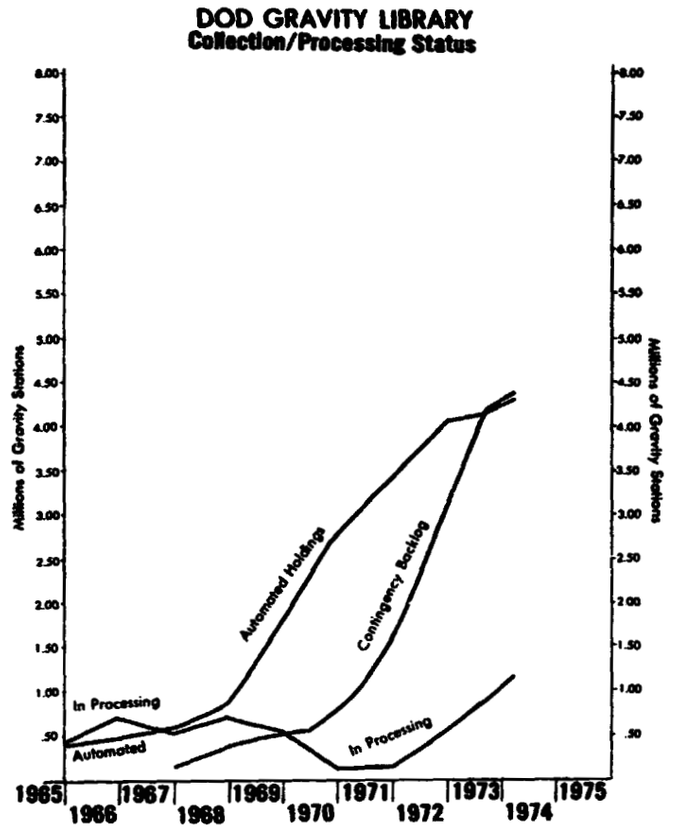

Figure 1. DOD Gravity Library Gravity Station Holdings

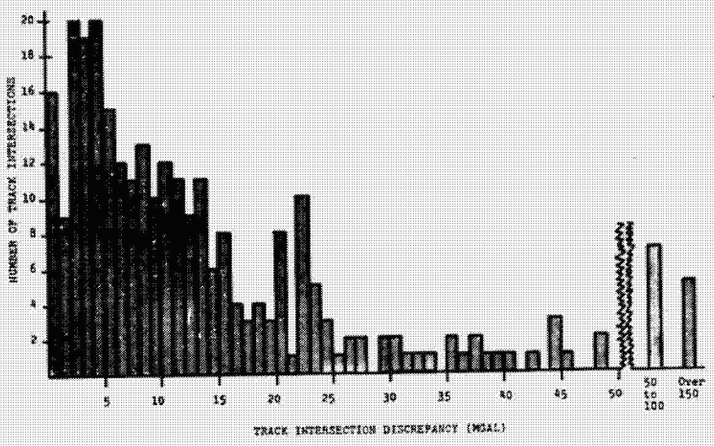

Figure 2. Histogram of the Discrepancies Between Gravity Measurements at Track Intersections of 848 One Degree Quadralaterals in the Pacific Ocean

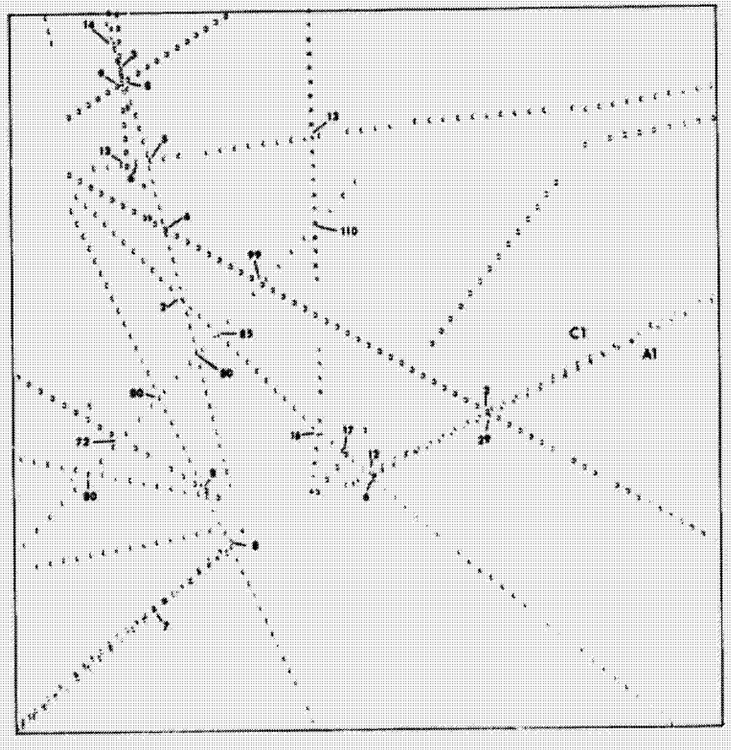

Figure 3. Gravity Data Source Plot of a Sample Area

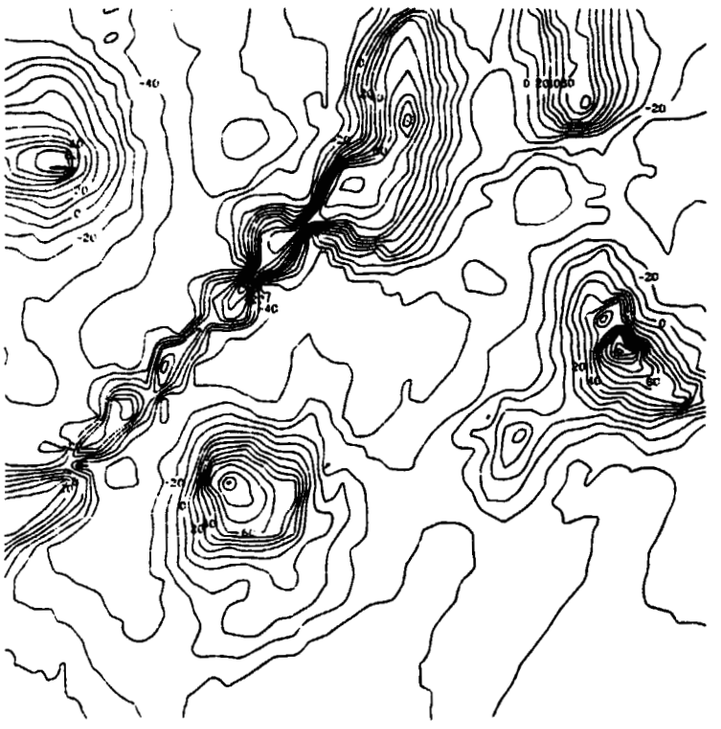

Figure 4. Contoured Free Air Anomaly Map of Sample Area Before Adjustment

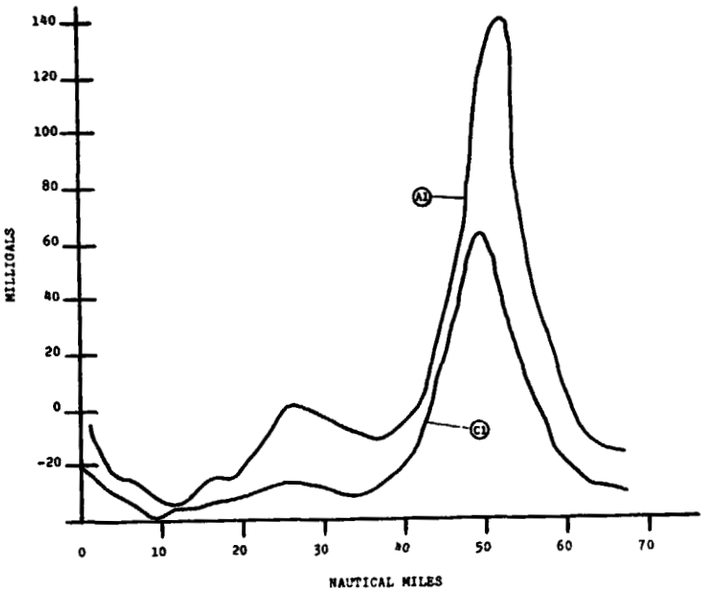

Figure 5. Comparison of Free Air Gravity Anomaly Profiles for Two Adjacent Tracks

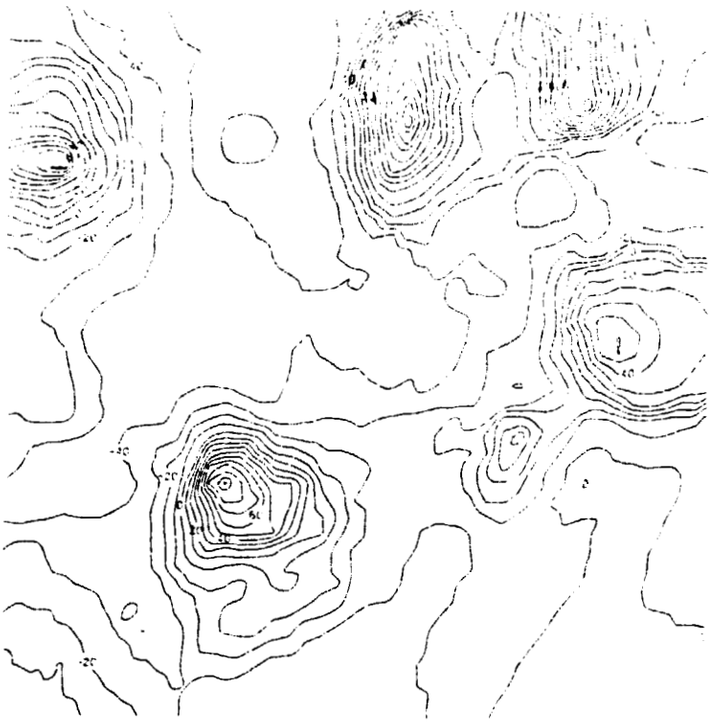

Figure 6. Contoured Free Air Anomaly Map of Sample Area After Adjustment

HEAVE MOTION ESTIMATION*

Thorgeir Palsson
The Analytic Sciences Corporation
Reading, Massachusetts 01867

Norman Melling
Naval Air Development Center
Warminster, Pennsylvania 18974

William F. O'Halloran, Jr.
The Analytic Sciences Corporation
Reading, Massachusetts 01867

Abstract

This paper describes the analysis and development of a filter for estimating the heave displacement of a survey ship using measurements obtained from an on-board gravity meter. The gravity meter is designed to measure the magnitude of gravity which changes slowly at the low speed of the ship. Vertical accelerations which occur at higher frequencies are also sensed but are suppressed by a low-pass filter, which is an integral part of the gravity meter. Using this instrument for sensing heave motion, therefore, runs counter to its design objectives. The heave accelerations and the associated displacement can, however, be recovered and separated from the gravity measurement by appropriate filtering of the gravity meter signal. Two filter designs are considered, i.e., a fixed gain Kalman type filter and a filter designed on the basis of frequency response. These designs are analyzed using statistical heave process models, which are used to simulate the heave acceleration to obtain the corresponding gravity meter measurements. The models are based on analysis of at-sea gravity meter data which were collected for this purpose. Statistics of the filter performances are included.

Introduction

The U. S. Navy has been actively engaged in developing instrumentation for use in oceanographic research. One such instrument is a heave displacement processor which can be used to correct errors in ocean depth measurements introduced by the vertical heave motion of the ship.

The heave displacement processor, developed for installation in late 1974 aboard the USNS Wyman, TAGS 34, will be used to provide on-line heave motion data in digital format. An onboard gravity meter located near the metacenter of the vessel provides a very accurate measure of the ship's vertical accelerations. Thus, it is not necessary to develop a special sensor as a part of the heave processor. The combined effects of acceleration and gravity are sensed by a temperature controlled accelerometer which is

* This work was performed in part under U. S. Navy Contract No. N00140-73-C-0642.

mounted on a gyro stabilized platform. The heave acceleration measurements, with 4 to 20 second periods, are attenuated by a simple low pass active filter, since the gravity meter is primarily designed to measure low frequency gravity anomalies. The filter is an integral part of the gravity meter, however, and must be accounted for in the design of the heave processor. The variations in the gravity measurements depend only on the ship's speed and can be regarded as a dc input in comparison with the heave acceleration frequencies.

The heave processor must therefore be capable of separating the heave acceleration from the effects of gravity in addition to compensating for the dynamic effects of the gravity meter filter. The required accuracy of the estimate is about 0.1 fathoms (0.6 ft) with a sampling interval of 0.1 seconds. Hardware specifications for the heave processor have been written as a result of the studies performed and a contract for its manufacture let by the Naval Air Development Center. The heave processor will consist of an analog active filter with a digital output signal.

The Heave Process Model

The heave motion of a ship is caused by buoyant forces due to ocean waves of varying amplitudes and frequencies acting on the ship's hull. It has been found that this motion can be described as a stationary random process whose characteristics depend on the sea state and the dynamic characteristics of the ship (Ref. 1). This means that the heave process can be mathematically modeled as a linear time invariant system (shaping filter) which is driven by uncorrelated noise. In the approach taken here the ocean dynamics and the ship's dynamics are considered as a single system, since the ship's dynamics are expected to be similar for a class of oceanographic vessels. In any event, it would probably be difficult to separately determine the ship's transfer function.

The shaping filter which was chosen to represent the heave acceleration dynamics consists of two cascaded second order systems given by the transfer function:

$$H(s) = \frac{s^3}{(s^2 + 2\zeta_1 \omega_1 s + \omega_1^2)(s^2 + 2\zeta_2 \omega_2 s + \omega_2^2)} \qquad (1)$$

This transfer function has been used previously to model vertical ship motion and has the appropriate property of being band limited. Thus, the natural frequencies of the transfer function, whose input is wideband noise, determine the bandwidth of the acceleration dynamics. The damping ratios can then be used to adjust the general shape of the frequency response as described later in this paper.

The transfer function of the gravity meter can be modeled as a first order lag:

$$F(s) = \frac{1}{\tau_g s + 1} \qquad (2)$$

where τ_g is the time constant of the filter which is used to attenuate the heave acceleration signal. The force of gravity, which is the primary input quantity to the gravity meter, can be modeled as a constant in comparison with the high frequency acceleration effects. Only the gravity anomaly residual must be considered if the nominal value of the gravity field is subtracted from the output of the gravity meter.

The total output of the gravity meter can then be realized in a state space configuration as shown in Fig. 1 by using the transfer functions of

Palsson
Melling
O'Halloran

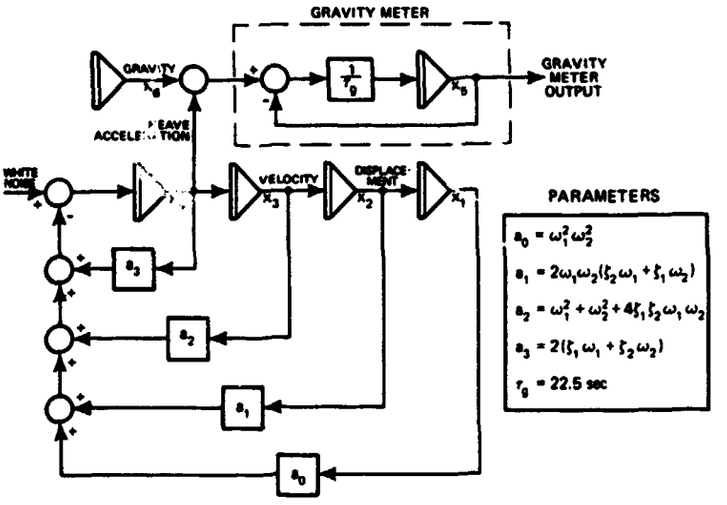

Figure 1. Realization of Heave Process and Gravity Meter Models

Eqs. (1) and (2). The constant residual gravity input is modeled as a random initial condition of an integrator. In this formulation, the heave acceleration, velocity and displacement appear as state variables as can be seen from Fig. 1. This form of the state equations is therefore very convenient for the analysis and simulation of the system.

The power spectral density of the gravity meter output due to the heave acceleration is easily obtained from the transfer functions of Eqs. (1) and (2) in the form:

$$\Phi_o(w) = \frac{Q \cdot \omega^6}{[(\omega_1^2 - \omega^2)^2 + 4\zeta_1^2\omega_1^2\omega^2][(\omega_2^2 - \omega^2)^2 + 4\zeta_2^2\omega_2^2\omega^2][\tau_g^2\omega^2 + 1]} \quad (3)$$

where Q denotes the power spectral density of the white noise input. This function is plotted in Fig. 2 for the design model values given in Table I, which were used before the at-sea heave data became available. The input noise strength of $Q = 0.9$ ft^2/sec^5 was chosen to give a heave displacement amplitude of 2.5 ft.

Heave Data Analysis

A number of runs of gravity meter data were recorded at sea in May of 1973 aboard the USNS Wyman in various sea states. The Wyman is a 2400 ton (285 feet) survey ship with a cruising speed of about 11 knots. The data consists of gravity meter output which was sampled at 0.1 sec intervals and recorded on magnetic tape with each run lasting about 20 minutes. The test conditions were recorded for each run in terms of windspeed and direction, and shipspeed and heading, as well as observed wave height and direction. The conditions during the data collection were calm to moderate with a maximum recorded windspeed of 22 knots and up to 7 ft wave heights.

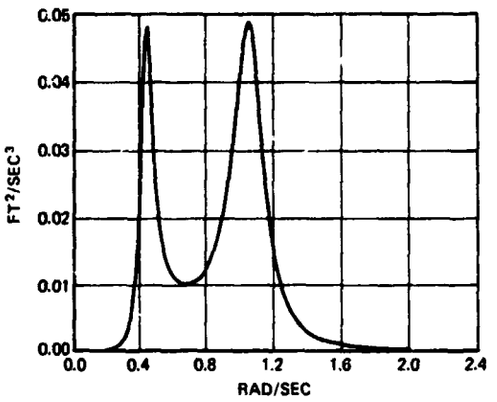

Figure 2. Power Spectral Density of Gravity Meter Output for Design Model

TABLE I

PARAMETER VALUES OF HEAVE PROCESS MODELS

PSD Model	Q (ft^2/sec^5)	ζ_1	ζ_2	ω_1 (rad/sec)	ω_2 (rad/sec)
Design Model	0.9	0.1	0.1	0.44	1.07
High Frequency Model	0.9	0.1	0.075	0.9	1.25
Low Frequency Model	0.9	0.15	0.25	0.5	1.0

Three data runs were selected for processing and comparison with the mathematical model. Segments of this data are shown in Fig. 3. Runs No. 1 and 2 contain relatively high frequencies whereas Run No. 3 is of somewhat lower frequency. These runs are representative of the spectrum of heave conditions encountered during the data collection and appear to have relatively stationary statistical properties. Each run was processed by Fast Fourier Transformation techniques in order to obtain its power spectrum.

The resulting power spectral densities are shown in Fig. 4, which also gives the adjusted power spectra of the mathematical process model. The spectra of Runs No. 1 and 2 are similar in appearance with peak energy in the neighborhood of 1.2 rad/sec and practically all the energy contained between 0.3 to 2.0 rad/sec, or periods from 3 to 20 sec. The spectrum for Run No. 3 is in the same general frequency band with most of the energy is at the lower end of the spectrum with peak energy around 0.5 rad/sec. It should be noted that these results include the effect of the gravity meter, i.e., the low pass prefilter. However, the heave acceleration power spectrum can be obtained if desired, since the transfer function of the prefilter is accurately unknown. These power spectra are also dependent on the dynamic characteristics of the ship as noted above and would consequently have to be modified for a ship of a different class.

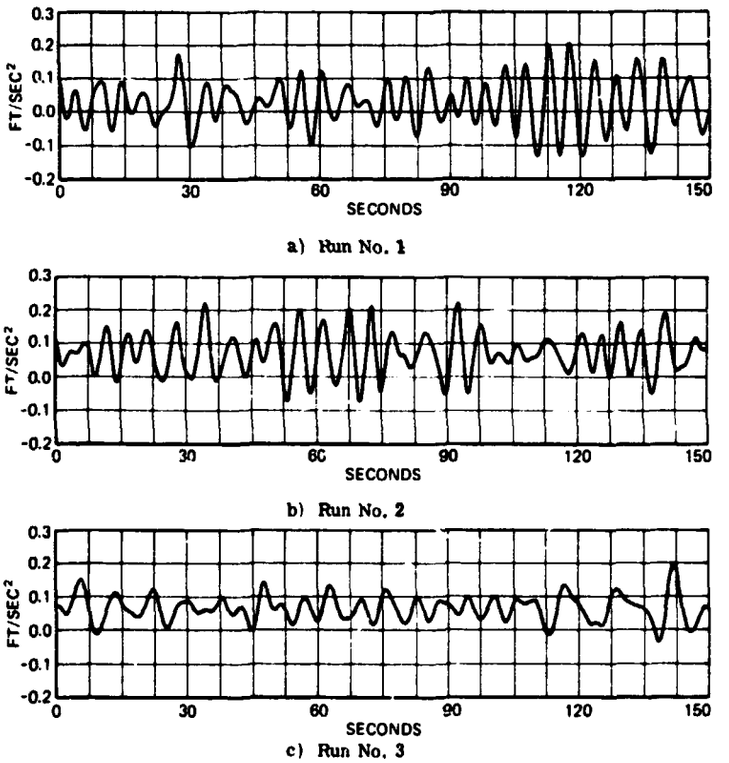

a) Run No. 1

b) Run No. 2

c) Run No. 3

Figure 3. Segments of Gravity Meter Output Data Taken At-Sea

Comparison of the PSD's of the design process model and the data in Figs. 2 and 4 respectively, indicates that the original design model parameters should be changed in order to obtain better agreement between the data and the mathematical model. For this purpose the natural frequencies and damping ratios of the model were adjusted by trial and error until a reasonably good agreement between the data and model spectra was achieved. Two sets of parameter values were obtained corresponding to the high frequency power spectra of Runs No. 1 and 2 on the one hand and the low frequency spectra of Run No. 3 on the other hand. The power spectra of the two resulting models have the same general shape as the corresponding PSD's of the data as can be seen from Fig. 4. The relatively low order of the model, however, limits the extent to which the variations of the data spectrum can be reproduced. The amplitude of the model power spectrum depends on the amplitude of the white noise input and can be adjusted to obtain any desired heave acceleration or displacement amplitude. The parameters of the three process models corresponding to Eq. (1) are summarized in Table I.

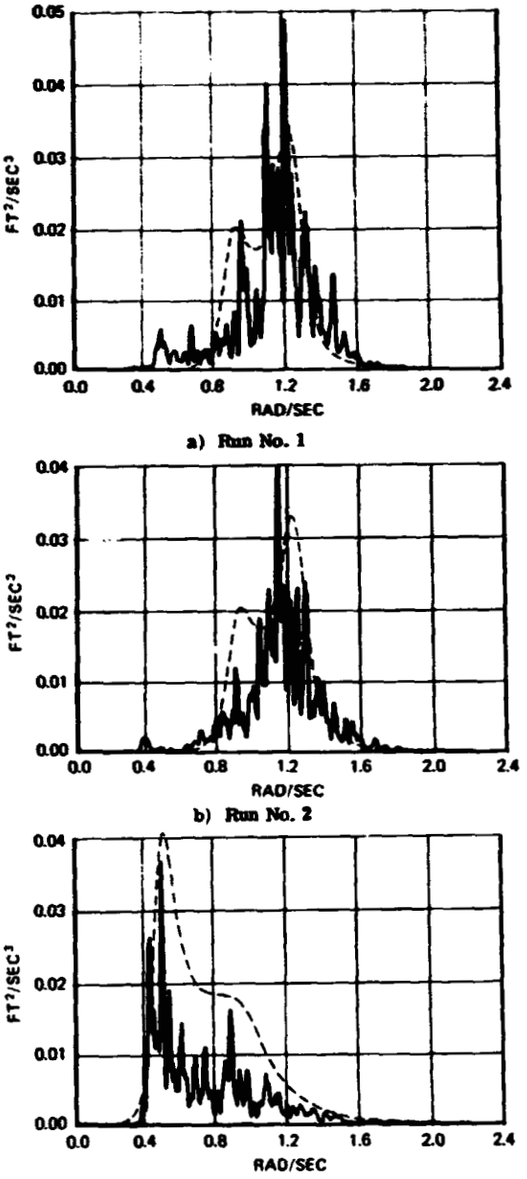

a) Run No. 1

b) Run No. 2

c) Run No. 3

Figure 4. PSD's of Gravity Meter Output for At-Sea Data (Solid Lines) and Adjusted Process Models (Dashed Lines)

Palsson
Melling
O'Halloran

Filter Design

The desired output of the heave filter is an estimate of the heave displacement, which is a double integral of the heave acceleration. In the absence of any disturbing inputs this objective could be achieved, in theory, by compensating for the dynamics of the gravity meter filter and integrating the resulting output twice. The initial conditions of the integrators, i.e., initial displacement and velocity, cannot be determined accurately, however, resulting in unstable computations of displacement. The infinite dc gain of the system would also result in a diverging heave displacement computation due to the nearly constant gravity input.

A more realistic approach consists of designing a transfer function which has the characteristics of a double integrator in the frequency band of interest, i.e., between 0.3 and 2.0 rad/sec, where heave acceleration is taken as the input variable. The break frequency of the gravity meter filter is 0.044 rad/sec which is substantially lower than the lowest frequency expected in the acceleration input. Its transfer function, therefore, has the characteristics of a single integrator in the frequency band of interest. The desired filter characteristics can then be obtained by adding a second integration in this frequency band and by reducing the dc gain to a very small value in order to eliminate the effect of the gravity residual. A transfer function which achieves this goal was suggested by the manufacturer of the gravity meter, Bell Aerospace Company:

$$G(s) = \frac{\tau_g s/\omega_f^2}{(\tau_g s + 1)\left(\frac{s^2}{\omega_f^2} + \frac{2\zeta_f}{\omega_f} s + 1\right)(\tau_f s + 1)} \tag{4}$$

where τ_g is the gravity meter filter time constant (22.5 sec) and:

$$\omega_f = 0.075 \text{ rad/sec}$$

$$\zeta_f = 0.5$$

$$\tau_f = 0.15 \text{ sec}$$

Any constant input is blocked by the numerator zero which in conjunction with the gravity meter filter and the damped second order mode provides the necessary double integration in the frequency band of the heave acceleration signal. The high frequency pole is added to attenuate noise but has essentially no effect on the signal.

The techniques of Kalman filtering offer another approach to the problem of estimating the heave displacement, as well as other states of the process, from the gravity meter output. The equation governing the estimate of the process states is then given by:

$$\dot{\underline{\hat{x}}} = F\underline{\hat{x}} + \underline{k}(z - \hat{x}_g) \tag{5}$$

where z is the gravity meter measurement:

$$z = x_g + v \tag{6}$$

and

$\hat{\underline{x}}$ = estimate of the (5 x 1) state vector $\underline{x}$ containing the heave process states and the gravity meter output

$\hat{x}_g$ = estimate of the gravity meter output x_g

v = uncorrelated measurement noise

$\underline{k}$ = (5 x 1) computed gain vector

The system matrix, F, can be obtained directly from the system realization in Fig. 1 as:

$$F = \begin{bmatrix} 0 & 1 & 0 & 0 & 0 \\ 0 & 0 & 1 & 0 & 0 \\ 0 & 0 & 0 & 1 & 0 \\ -a_0 & -a_1 & -a_2 & -a_3 & 0 \\ 0 & 0 & 0 & \frac{1}{\tau_g} & -\frac{1}{\tau_g} \end{bmatrix} \tag{7}$$

The gravity bias was not included as a state in the filter assuming that its effect could be subtracted separately. Addition of this state to the filter does not present any problem, however, but increases its order by one.

The gain vector was computed using the standard Kalman filter formulation by determining the steady-state solution of the Riccati equation (Ref. 2), because the filter is required to be time invariant. The parameter values and process noise variance of the design process model of Table I were used, since the at-sea heave data was unavailable at that time. The measurement noise intensity was varied resulting in several sets of gains. Table II gives three sets of gains and the corresponding measurement noise variances of which case No. 2 was chosen for further analysis. The performances of the two filter designs, i.e., the Bell filter and the Kalman filter, were then evaluated by simulation using the modified process models.

TABLE II
SETS OF CONSTANT GAINS FOR STEADY-STATE KALMAN FILTER

Parameter	Case No. 1	Case No. 2	Case No. 3
R (ft^2/sec^3)	4×10^{-4}	1×10^{-4}	2.5×10^{-5}
K_1 (sec)	-83.7	-135.3	-202.8
K_2	-3.4	-5.4	-5.6
K_3 (sec^{-1})	36.9	57.5	85.9
K_4 (sec^{-2})	31.9	76.0	167.4
K_5 (sec^{-1})	1.6	2.6	3.8

Simulation and Evaluation

The output of the heave filter is an estimate of the vertical displacement of the ship. It is therefore necessary to obtain an accurate reference heave displacement in order to be able to evaluate the error in the estimate of the filters. Unfortunately, no such reference exists for the gravity meter data described above since no independent displacement measurement was available. The only alternative is to use a digital computer simulation based on the heave process models of Table I and the dynamic filter equations. This makes it possible to generate both the filter outputs and the corresponding true heave displacement which is available as a state in the process model of Fig. 1. The driving noise was obtained by using a random number generator that gives a sequence of uncorrelated numbers with a normal distribution. The dynamic equations were then solved by using the system state transition matrix to propagate the system state forward in time.

The Bell and Kalman filters were compared by simulating their outputs using the design process model parameters of Table I. The rms error of the heave estimate was computed directly from the simulated results after initial transients in the system response had decayed. The simulation results showed that the steady-state Kalman filter could be expected to give about 30% better performance than the Bell filter, as can be seen from Table III. However, the Bell filter is simpler in design, since it only requires a third order transfer function (in addition to the dynamics of the gravity meter) whereas the Kalman filter is of fifth order. The Bell filter was therefore chosen for further development in view of the fact that its accuracy satisfies the design objectives.

The Bell filter was also tested by using the high and low frequency process models given by Table I with the results given by Table III. The low frequency model gives approximately the same percentage error result as the design model but the performance improves somewhat when the high frequency model is used.

A qualitative comparison of the mathematical heave model and the observed heave motion can be made by considering the two heave filter responses in Fig. 5. These represent the output (i.e., the estimated heave displacement) of the Bell filter using simulated and real gravity meter input data respectively. The time histories exhibit very similar dynamic characteristics, giving strong support to the validity of using the random process model to simulate the heave motion.

TABLE III

HEAVE FILTER SIMULATION RESULTS

Filter	Process Model	RMS Amplitude	RMS Error	Percent Error
Bell	Design Model	2.5 ft.	0.67 ft.	27%
Bell	High Frequency Model	2.7 ft.	0.63 ft.	23%
Bell	Low Frequency Model	2.2 ft.	0.61 ft.	28%
Kalman	Design Model	2.5 ft.	0.44 ft.	18%

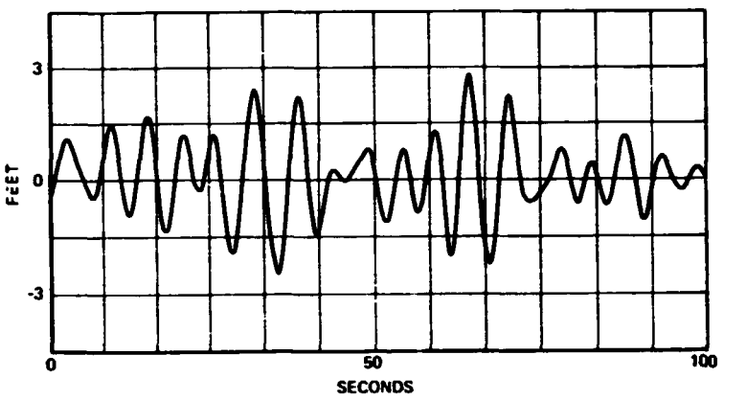

a) Simulated Gravity Meter Input Data

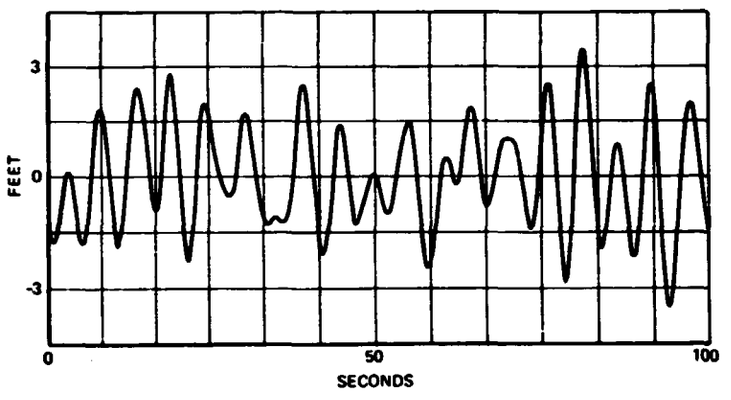

b) Real Gravity Meter Input Data

Figure 5. Heave Filter Outputs Using Simulated and Real Gravity Meter Data

The ability of the heave processor to estimate the heave amplitude with less than 0.1 fathom rms error clearly depends on the total heave displacement amplitude. Thus the design chosen for development can be expected to give satisfactory performance up to an amplitude of 3 ft (i.e., wave height of 6 ft) with some variation according to the frequency content of the heave motion. Thus, larger estimation errors have been observed at the lower end of the signal spectrum due to phase shift errors in the filter.

Conclusions

It has been found that a shipboard gravity meter can be used as a sensor for estimating the vertical displacement of a survey vessel. A relatively simple filter can be used to provide the required continuous on-line processing of the gravity meter data with an rms estimation error of about 25% of the total rms heave displacement amplitude. A more elaborate Kalman type filter could be used to improve this performance by about 30% at the cost of increased complexity in the filter design. The use of stationary random process models to simulate the heave dynamics of the vessel gave excellent agreement with data taken at-sea after adjustment of the model power spectral density to approximate the power spectrum computed from the data.

Acknowledgements

The authors would like to express their thanks to Mr. John DeMatteo and Mr. Mel Levrant of the Naval Air Development Center, Warminster, Pennsylvania, for their support and participation in this study. The assistance of Dr. David Porter of TASC, who performed most of the simulation work, is also gratefully acknowledged.

References

1. Newman, L. D. and Talwani, M., "Accelerations and Errors in Gravity Measurements on Surface Ships", Journal of Geophysical Research, Vol. 77, No. 23, August 1972.

2. Gelb, A. et. al., Applied Optimal Estimation, The M. I. T. Press, Cambridge, Mass. 1974.

RESOLUTIONS

The participants of the 1974 International Symposium on Applications of Marine Geodesy

reviewing the resolutions pertaining to marine geodesy made by IAPSO at its General Assembly in Bern, Switzerland, in 1967 and by IAG at its General Assembly in Moscow, USSR, in 1971, and

considering the contents of the scientific program held at Battelle Columbus Laboratories, Columbus, Ohio, in 1974,

recommend encouragement of the following:

(1) (a) Establishment of marine test sites or marine geodetic ranges suitable for the calibration and verification of precise geodetic and navigation methods,

(b) Conduct of "controlled-condition" experiments to determine the best accuracy attainable,

(c) Publication of results of such experiments.

(2) Continued studies on methods of determining the form of the geoid by satellite altimetry, taking oceanographic parameters into account

(3) Design and conduct of specific marine geodetic experiments and development of improved data-analysis techniques, to permit determination of tides, mean sea level, ocean surface heights above mean sea level, and sea floor spreading

(4) Development of astronomic instruments useable at sea to make possible geoid determination by astrogravimetric and astro-satellite techniques

(5) Establishment of geometric geodetic systems for determining marine boundaries and for positioning based upon existing technology, with the capability for improvement in accuracy with increasing need and improved technology

(6) Use of SI units in all reports, at least parenthetically

(7) Establishment of communication with users relative to their needs and accuracy requirements

(8) Development of space systems that would make possible better position determination at sea

(9) Continuation of efforts to increase the accuracy of position determination at sea by the optimum integration of different navigational aids,

and extend their appreciation to Battelle Columbus Laboratories for its hospitality and to the co-sponsors and associate sponsors, the organizing committee, and others who contributed to the success of the 1974 Symposium, and

suggest that another International Symposium be arranged in a few years (possibly 1977) to provide an opportunity for geodesists and marine scientists to discuss new developments in pertinent areas.

LIST OF PARTICIPANTS

J. Lynn Abbott
Scripps Institution of Oceanography
La Jolla, California 92037

William A. Allen
USAETL-Research Institute
Alexandria, Virginia 22314

David Anthony
Air Force Cambridge Research Labs
Bedford, Massachusetts 01776

Dr. John R. Apel
National Oceanic and Atmospheric Administration
Atlantic Oceanographic & Meteorological Labs
Miami, Florida 33149

John G. Baker
Del Norte Technology, Inc.
Sterling Park, Virginia 22170

S. Bakkelid
Norges Geografiske Oppmaling
Oslo, Norway

Emery I. Balazs
NOAA, NOS, NGS
Rockville, Maryland 20852

Dr. Angel A. Baldini
USAETL-Research Institute
Alexandria, Virginia 22314

R. W. Baltosser
Birdwell Division
Seismography Service Corp.
Tulsa, Oklahoma 74102

Dr. John Batch
Battelle-Columbus
Columbus, Ohio 43201

Major Larry D. Beers, USAF
Defense Mapping Agency
Washington, D. C. 20305

Charles W. Beierle
Defense Mapping Agency Aerospace Center
St. Louis, Missouri 63109

Joseph E. Bennett
Office of Naval Research
Arlington, Virginia 22217

Victor Benton
Interstate Electronics Corp.
Anaheim, California 92803

Harold D. Black
APO/John Hopkins University
Silver Spring, Maryland 20910

Jan Christiaan Blankenburgh
Royal Norwegian Council for Scientific Industrial Research
Continental Shelf Division
Hoffsveien 13, Oslo 2 Norway

B. R. Bowman
University of Hawaii
Honolulu, Hawaii

Bill J. Boyer
DMA Aerospace Center
St. Louis AFS, Missouri 63125

G. Brachet
Centre National D'Etudes Spatiales
Orge, France

Earl Brown
Marine Sciences Diretorate
Burlington, Ontario, Canada

Richard D. Brown
Computer Sciences Corp.
Silver Spring, Maryland 20910

P. Brunavs
Marine Sciences, Dept. of Environment
Ottawa, Ontario, Canada K1A OE6

George Bynum
Mobil Oil Corp.
Dallas, Texas 75221

Herman J. Byrnes
U.S. Naval Oceanographic Office
Washington, D. C. 20373

Andrew C. Campbell
U.S. Naval Oceanographic Office
Washington, D. C. 20373

M. Caputo
University of Bologna
Italy

Cloy N. Causey
Texaco
New York, New York 10017

D. J. Chalupka
Navships
Gaithersburg, Maryland 20760

William H. Chapman
U.S. Geological Survey
Annandale, Virginia 22003

Festus Charles
Land & Surveys Department
Trinidad & Tobago
West Indies

Davidson T. Chen
Naval Research Laboratory
Washington, D. C. 20375

Frank Christensen
Magnavox Research Laboratory
Torrance, California 90503

Dr. Edmund H. Christy, Jr.
Offshore Navigation, Inc.
Harahan, Louisiana 70183

M. H. Curlin
Lorac Service Corporation
Houston, Texas 77042

Edward M. Davin
NSF/Int'l. Decade of Ocean Explor.
Washington, D. C. 20550

Bruce W. Davis
Battelle-Columbus
Columbus, Ohio 43201

John De Matteo
Naval Air Development Center
Warminster, Pennsylvania 18974

R. S. Dietz
NOAA/Atlantic Oceanographic and
Meteorological Labs
Miami, Florida 33149

Inez Dimitrijevich
DMA Aerospace Center
St. Louis, Missouri 63118

Vojislav Dimitrijevish
DMA Aerospace Center
St. Louis, Missouri 63118

Joseph D. D'Onofrio
National Geodetic Survey
Rockville, Maryland 20852

B. C. Douglas
Wolf Research and Development
Riverdale, Maryland 20840

Joseph F. Dracup
National Geodetic Survey
Rockville, Maryland 20852

Marvin E. Drake
Sofar Station
F.P.O. New York 09560

Richard W. Earhart
Battelle-Columbus
Columbus, Ohio 43201

Irene Fischer
DMA Topographic Center
Washington, D. C. 20315

Dr. Eric Fischer
DMA Topographic Center
Washington, D. C. 20315

J. Ed French
RCA
Satellite Beach, Florida 32937

D. M. Fubara
Battelle-Columbus
Columbus, Ohio 43201

John S. Gitt
Westinghouse Electric Corporation
Annapolis, Maryland 21404

S. Gopalapillai
Battelle-Columbus
Columbus, Ohio 43201

Roger C. Gore
Aerospace Corporation
Torrance, California 90505

Stephan Grant
Canadian Hydrographic Service
Bedford Inst. of Oceanography
Dartmouth, Nova Scotia, Canada

Dr. Joseph Greenwood
University Inst. of Oceanography,
City University of New York
New York, New York 10453

Prof. Dr. Erwin Groten
Technical University Darmstadt
61 Darmstadt, Germany

Philippe Guerit
Centre National D'Etudes Spatiales
Bretigny-S/Orge, France 91.220

George Hadgigeorge
AFCRL
Bedford, Massachusetts 01876

C. William Hamilton
Battelle-Columbus
Columbus, Ohio 43201

Carl Hartdegen
Sofar Station
FPO New York, New York 09560

Ronald R. Hatch
Magnavox Research Labs
Torrance, California 90503

Ihor Havryluk
U.S. Steel Corporation
Pittsburgh, Pennsylvania 15230

Donald B. Heckman
AMF Sea Link
Alexandria, Virginia 22314

U. Heineke
Technical University Hanover
Nienburgerstr. 6
Hanover, West Germany

Thomas I. Hicks
U.S. Naval Weapons Lab
Dahlgren, Virginia 22448

Robert L. Hittleman
Hydro Products, A Tetra Tech Co.
San Diego, California 92121

Sandford R. Holdahl
NOAA, NOS, NGS
Rockville, Maryland 20852

Dr. James Hollinger
Naval Research Lab
Washington, D. C. 20375

Dave Howe
Satellite Positioning Corp.
Houston, Texas 77036

J. C. Husson
Centre National des Etudes Spatiales
Orge, France

Henry W. Ingram
Transcontinental Gas Pipe Line Corp.
Houston, Texas 77027

Dr. M. G. Johnson
NOAA
Rockville, Maryland 20852

Leonard S. Jones
Westinghouse Electric Corporation
Annapolis, Maryland 21404

J. H. Jorgenson
National Security Industrial Assn.
Washington, D. C. 20005

Joenil Kahar
Dept. of Geodesy, Inst. of Technology
Bandung, Indonesia

M. Asad Khan
NASA/Goddard Space Flight Center
Silver Spring, Maryland 20910

L. A. Kivioja
Survey & Mapping, Purdue University
Lafayette, Indiana 47907

Lung-Fa Ku
Environment Canada
Ottawa, Ontario, Canada K2B-6G4

Mark Kuhner
Battelle-Columbus
Columbus, Ohio 43201

Muneendra Kumar
The Ohio State University
Columbus, Ohio 43210

E. C. LaFond
Naval Undersea Center
International Assn. for the Physical
Sciences of the Ocean (IAPSO)
San Diego, California 92132

Katherine LaFond
Naval Undersea Center
IAPSO
San Diego, California 92132

Dr. Paolo Lanzano
Univ. of Manchester/US Naval Rsch.Lab
Washington, D. C. 20375

Alan R. Leeds
Lamont-Doherty Geological Observatory
Palisades, New York 10964

Michel Lefebvre
Centre National D'Etudes Spatiales
Athis Mons, France

Alfred Leick
The Ohio State University
Columbus, Ohio 43210

Clifford D. Leitao
NASA Wallops Flight Center
Wallops Island, Virginia 23337

Dr. Gordon Lill
National Ocean Survey, NOAA
Rockville, Maryland 20852

Herbert Ludwig
Technical University
Munich, West Germany

Kenneth V. Mackenzie
Naval Oceanographic Office
Washington, D. C. 20375

Dr. M. M. Macomber
DMA Hydrographic Center
Washington, D. C. 20390

Dr. Alexander Malahoff
Office of Naval Research
Arlington, Virginia 22217

James G. Marsh
NASA/Goddard Space Flight Center
Greenbelt, Maryland 20771

Ronald S. Mather
The University of New South Wales
Kensington, NSW, Australia 2033

Larry N. McAlister
AGU, ION, ACSM, SEG
Seiscom Delta, Inc.
Houston, Texas 77036

Walt McCandless
National Aeronautics and Space Administration
Washington, D. C. 20546

Dr. K. E. McConnell
University of Rhode Island
Kingston, Rhode Island 02881

D. L. McKeown
Canada Atl. OL/Bedford Inst. of Oceanography
Dartmouth, Nova Scotia, Canada

Daniel McLuskey
The Ohio State University
Columbus, Ohio 43210

Henry J. McManus
U.S. Naval Oceanographic Office
Washington, D. C. 20373

Norman Melling
Naval Air Development Center
Warminster, Pennsylvania 18974

Robert Mennella
Naval Research Laboratory
Washington, D. C. 20375

Ernest H. Metzger
Bell Aerospace Company
Buffalo, New York 14240

J. Clayton Mitchell
Dept. of Energy, Mines & Resources
Ottawa, Ontario, Canada K1A 0E9

Raymond B. Montgomery
Johns Hopkins University
Baltimore, Maryland 21218

Dr. Garth A. Morgan
Australian Embassy
Washington, D. C. 20036

Jim Morgan
Satellite Positioning Corp.
Houston, Texas 77036

Helmut Moritz
Technical University, Inst. of Physical Geodesy
Graz, Austria A-8043

A. George Mourad
Battelle-Columbus
Columbus, Ohio 43201

Foster Morrison
National Geodetic Survey
National Ocean Survey/NOAA
Rockville, Maryland 20852

Ivan I. Mueller
The Ohio State University
Columbus, Ohio 43210

John D. Mudie
Scripps Inst. of Oceanography
La Jolla, California 92037

Kenneth Nelson
DMAAC
St. Louis, Missouri 63118

Alvin W. Newberry
Jet Propulsion Laboratory
Pasadena, California 91103

David Nippert
Battelle-Columbus
Columbus, Ohio 43201

Dr. Vincent E. Noble
Naval Research Laboratory
Washington, D. C. 20375

Wm. F. O'Halloran, Jr.
Analytical Sciences Corporation
Reading, Massachusetts 01867

Wayne L. Olsen
DMA Hydrographic Center
Norfolk, Virginia 23511

Dr. Hyman Orlin
NOAA, NOS
Rockville, Maryland 20852

Roger T. Osborn
U.S. Naval Oceanographic Office
Suitland, Maryland 20689

John H. Ostrander
U.S. Naval Research Laboratory
Washington, D. C. 20375

John Overholt
Naval Oceanographic Office
Washington, D. C. 20373

Thorgeir Palsson
The Analytical Sciences Corporation
Reading, Massachusetts 01867

David W. Pasho
Global Marine Development, Inc.
El Segundo, California 90245

Julian K. Pawley
Teledyne Exploration Company
Houston, Texas 77036

Harvey Perlstein
Westinghouse Electric Corporation
Annapolis, Maryland 21404

Prof. Dr.-Ing. Horst Peschel
Technische Universitat Dresden
Dresden, GDR, East Germany

Lennart Pettersson
Rikets Allmanna Kartverk
Vallingby, Stockholm, Sweden S-162 10

M. Pieplu
Centre National D'Etudes Spatiales
Orge, France

R. Plugge
Martin Marietta
Denver, Colorado 80123

Donald E. Puccini
The Ohio State University
Columbus, Ohio 42210

Prof. Jacub Rais
National Surveys & Mapping
Jakarta, Indonesia

Prof. Dr.-Ing. Karl Ramsayer
Universitat Stuttgart
Sutttgart 1, West Germany

W. J. Rapatz
Dept. of Environment, Marine Sciences
Victoria, B.C., Canada

Richard Rapp
Dept. of Geodetic Science, OSU
Columbus, Ohio 43210

F. Alex Roberts
Chevron Oil Field Research Company
La Habra, California 90631

Dr. Al Robinson
Battelle-Columbus
Columbus, Ohio 43201

Jane V. Robinson
U.S. Naval Weapons Laboratory
Dahlgren, Virginia 22448

John F. Roeber, Jr.
U.S.C.G.
Bowie, Maryland 20715

John C. Rose
Hawaii Inst. of Geophysics,
University of Hawaii
Honolulu, Hawaii 96822

George T. Ruck
Battelle-Columbus
Columbus, Ohio 43201

Robert K. Selin
Defense Mapping Agency
Washington, D. C. 20305

John H. Satriano
Naval Air Development Center
Warminster, Pennsylvania 18974

Narendra K. Saxena
Dept. of Civil Engineering
University of Illinois
Urbana, Illinois 61801

Philip M. Schwimmer
Defense Mapping Agency
Washington, D. C. 20305

Prof. Dr.-Ing. Gunter Seeber
Institut fut Theoretische Geodasie
Hanover, Germany D3

Gabrielle Sewall
Marine Technology Society
Palo Alto, California 94301

A. Shapiro
Naval Research Laboratory
Washington, D. C. 20390

George W. Sheary III
Summa Corp., Ocean Mining Division
Houston, Texas 77011

William D. Siapno
Deepsea Ventures, Inc.
Gloucester Point, Virginia 23062

Tomas Soler
Dept. of Geodetic Science, OSU
Columbus, Ohio 43210

A. F. Spilhaus, Sr.
NOAA
Washington, D. C.

A. F. Spilhaus, Jr.
American Geophysical Union
Washington, D. C. 20036

Sam Stein
Sonatech, Inc.
Goleta, California 93017

James H. Straka
Pacific Missile Range
Point Mugu, California 93042

William B. Strange
NOAA-National Geodetic Service
Washington Science Center
Rockville, Maryland 20852

Jimmy C. Stribling
U.S. Naval Oceanographic Office
Washington, D. C. 20373

Hans U. Thurnheer
Gulf Research & Development Co.
Pittsburgh, Pennsylvania 15215

T. K. Treadwell
Texas A&M University
Dept. of Oceanography
College Station, Texas 77843

Carl Christian Tscherning
Danish Geodetic Institute
Ohio State University
Columbus, Ohio 43210

Leonard G. Turner
Division of National Mapping
Canberra, Act, Australia 2601

Enzo A. Uliana
Naval Research Laboratory
Washington, D C. 20375

U. A. Uotila
The Ohio State University
Columbus, Ohio 43210

Boudewijn H. W. van Gelder
Dept. of Geodetic Science, OSU
Columbus, Ohio 43210

Lt. Cdr. W. G. Van Gent
Netherlands Hydrographic Office
The Hague, Netherlands

Thomas J. Vogel
DMA Hydrographic Center
Washington, D. C. 20390

Dr. F. O. Vonbun
NASA/Goddard Space Flight Center
Greenbelt, Maryland 20771

J. H. M. Van Der Wal
Meetkundige Dienst Van De
Rijkswaterstaat
Delft, Holland

S. Vincent
Computer Sciences Corporation
Silver Springs, Maryland 20910

Donna M. Walls
Wolf Research & Development
Riverdale, Maryland 20840

Phil Ward
Texas Instruments, Inc.
Dallas, Texas 75238

A. B. Watts
Lamont-Doherty Geological Observatory
of Columbia University
Palisades, New York 10964

Dr. George C. Weiffenbach
Smithsonian Astrophysical Observatory
Cambridge, Massachusetts 02138

William T. Wells
Wolf Research & Development Corp.
Riverdale, Maryland 20840

Lt. James Wexler
NOAA, NOS
Rockville, Maryland 20852

Lumen E. Wilcox
DMA Aerospace Center
Manchester, Missouri 63011

Frank Williams
NASA Office of Applications/
Special Programs
Washington, D. C. 20546

Owen W. Williams
DMA/PR
Washington, D. C. 20305

George A. Zahn
Deepsea Ventures, Inc.
Gloucester Point, Virginia 23062

Robert E. Ziegler
DMA
Washington, D. C. 20315

Anthony Zuccaro
Naval Research Laboratory
Washington, D. C. 20375

INDUSTRIAL MEMBERS

American Bureau of Shipping
AMETEK
AMF Electrical Products
Baldt Anchor and Chain
Bechtel Corporation
Bendix Corporation
Bolt Beranek and Newman, Inc.
Calspan Corporation
Columbian Rope Company
Compass Publications, Inc.
Dames & Moore
Deepsea Ventures, Inc.
Delco Electronics GM Corporation
Dillingham Corporation
EDO Corporation
EG & G
El Paso Natural Gas Company
Environmental & Man
Exxon Company USA
FMC Corporation
Franklin Electric Company, Inc.
General Dynamics Corporation
General Electric
General Instrument Corporation
Gould Inc.
John T. Hepburn, Ltd.
Hermes Electronics, Ltd.
Honeywell, Inc.
Houston Natural Gas Corporation
Hydronautics, Inc.
ITT Cable-Hydrospace Division
J & J Marine Diving Company, Inc.
Lockheed Missiles & Space Company
The Magnavox Company
Mobil Oil Corporation
Murphy Pacific Marine Salvage Company
Ocean Data Systems, Inc.
Ocean Systems, Inc.
Oceanographic Consultants, Inc.
Operations Research, Inc.
Perry Oceanographics, Inc.
Plessey Environmental Systems
Raytheon Company
The Rochester Corporation
M. Rosenblatt & Son, Inc.
Seaward, Inc.
TRW Systems
Teledyne Hastings-Raydist
Transcontinental Gas Pipe Line Corp.
Tsurumi-Seiki Kosaku sho Company
Undersea Industries, Inc.
United States Steel Corporation
Westinghouse Electric Corporation
Wheeler Industries, Inc.

INSTITUTIONAL MEMBERS

U.S. Army Engineer Division
California Maritime Academy
Centre D'Etudes et de Recherches Techniques Sous-Marines
Chesapeake College
U.S. Coast Guard
Dept. of Transportation Library
Institute of Marine Science
International Association of Professional Divers, Inc.
Marine Sciences Directorate
Regional Marine Resources Council
University of Miami, Coral Gables
Naval Postgraduate School
University Institute of Oceanography
Oceanographic Commission of Washington
Sea Use Foundation
University of Southern California
Texas A & M University
Texas Coastal & Marine Council
Texas Offshore Terminal Commission

PATRON MEMBER

Alice Delamar

HONORARY MEMBERS

Dr. Paul M. Fye
Dr. J.H. Wakelin, Jr.
RAdm. E.C. Stephan, USN (Ret.)
Donald L. McKernan
Elmer P. Wheaton
Dr. John P. Craven
Dr. William E. Shoupp
David S. Potter